THÈSE

En vue de l'obtention du

DOCTORAT DE L'UNIVERSITÉ DE TOULOUSE

Délivré par :

Institut National Polytechnique de Toulouse (Toulouse INP)

Discipline ou spécialité :

Génie des Procédés et de l'Environnement

Présentée et soutenue par :

M. KASHIF NADEEM

le jeudi 19 mai 2022

Titre :

COMPLETE MECHANICAL MODEL OF A VERY LARGE SUBMERGED MEMBRANE BIOREACTOR

Ecole doctorale :

Mécanique, Energétique, Génie civil, Procédés (MEGeP)

Unité de recherche :

Laboratoire de Génie Chimique (LGC)

Directeur(s) de Thèse :

MME CLAIRE ALBASI

MME MARION ALLIET

Rapporteurs :

M. PETER VANROLLEGHEM, UNIVERSITE LAVAL

Membre(s) du jury :

M. GIORGIO MANNINA, UNIVERSITA DEGLI STUDI DI PALERMO, Président

M. ERKAN SAHINKAYA, Istanbul Medeniyet University, Membre

M. MATHIEU SPÉRANDIO, INSA TOULOUSE, Invité(e)

MME CLAIRE ALBASI, TOULOUSE INP, Membre

MME MARION ALLIET, TOULOUSE INP, Membre

M. SAM AZIMI, SIAAP, Membre

Keywords

Large-scale MBR, ASM3-BioP-EPS-SMP-RIS model, energy consumption, aeration model, fouling model, phosphorus removal, sensitivity analysis

Mots clés

BaM grande échelle, Modèle ASM3-BioP-EPS-SMP-RIS, dépense énergétique, modèle d'aération, modèle de colmatage, élimination du phosphore, analyse de sensibilité

ABSTRACT

Membrane bioreactors (MBRs) are successfully being adopted in super-large-scale (>100,000 $m^3.d^{-1}$) applications due to several advantages, mainly superior and consistent effluent quality. Moreover, the significant reduction in the membrane and operating costs has contributed to its wider acceptance. Despite their considerable evolution in the recent past and large-scale applications in municipal wastewater treatment, fouling and the cost associated with its mitigation are still hot topics and need the attention of researchers and academia to optimize and reduce the expense of MBR in the range of the conventional activated sludge process (CASP). Mathematical modeling is a great tool to explore the model-based optimization of operating costs associated with fouling mitigation strategies. For this, a comprehensive and integrated process model must be adapted, calibrated, and validated at a super-large-scale facility.

MBR involves complex interactions between biology and filtration, and its modeling is challenging without considering these interactions. In the recent past, integrated models have been developed and applied to MBRs, ranging from bench to pilot scales and rarely for full-scale facilities of capacity up to 15,000 $m^3.d^{-1}$. In this work, a super-large-scale MBR plant with a design capacity of 348,000 $m^3.d^{-1}$ is dynamically modeled to simulate the depollution and filtration-fouling processes.

The integrated model combines biochemical (ASM3-SMP-EPS-Bio-P, aeration, chemical precipitation), resistance in series (RIS) fouling, and energy sub-models. The comprehensive, integrated model is capable of simulating a) biological processes to describe the stoichio-kinetic activity of the biomass for carbon oxidation and nutrient removal (i.e., Nitrogen and Phosphorus) coupled with EPS-SMP production and degradation processes; b) the role of biological process aeration in carbon oxidation and nitrification under the influence of MLSS; c) the numerical balance of the volumes of the influent, effluent, sludge and all internal and external recirculation; d) coagulant addition inducing chemically enhanced phosphorus removal (CEPR) in addition to enhanced biological phosphorus removal (EBPR); e) fouling dynamics associated with synchronized filtration-relaxation, intermittent air-scouring and backwashing under the influence of transmembrane pressure (TMP), temperature, MLSS, and bound EPSs

concentration, and f) specific energy consumption. The model was calibrated using one-week data collected during the first experimental campaign and was validated against 92 days of data from the plant with and without the addition of $FeCl_3$.

The calibrated integrated model provided an acceptable correspondence for pollutants (COD, NO_x, NH_4, PO_4^{3-}, MLSS, EPSs, and SMPs) removal and prediction of the TMP, a direct indicator for fouling development. The model also successfully produced acceptable datasets not available from routine measurements, e.g., the evolution of the biomass and transformation of the pollutants in each reactor in series. Moreover, the model can provide detailed insights into reversible and irreversible fouling dynamics under the synchronized influence of multiple fouling abatement controls, including filtration-relaxation, intermittent air-scouring, and backwashing.

In order to be used to develop model-based controls and intelligent decision-making tools to optimize the functioning of the full-scale MBRs, particularly the air-scouring and activation and de-activation of the chemical washes to save energy and chemicals, this model would have to be validated in fouling conditions. Since it was not possible to test the limits of the model, the sensitivity analysis approach was investigated.

RÉSUMÉ

Les bioréacteurs à membrane (BaM) sont utilisés dans des applications de traitement des eaux usées à très grande échelle avec succès (>100 000 $m^3.d^{-1}$) en raison de plusieurs avantages, principalement une qualité d'effluent supérieure et constante. De plus, la baisse importante des couts des membranes et de leur exploitation a contribué à cette acceptation plus large, même sur ce marché économiquement sensible. Malgré leur évolution considérable dans un passé récent et les applications à grande échelle dans le traitement des eaux usées municipales, le colmatage des membranes et le coût associé à sa limitation sont encore des sujets d'actualité et nécessitent des travaux pour faire baisser les dépenses du BaM vers des valeurs comparables à celles des procédés classiques de traitement à boues activées (BAC). La modélisation mathématique est un excellent outil pour l'optimisation, fondée sur des modèles, des coûts d'exploitation associés aux stratégies de limitation du colmatage, en particulier l'aération de la membrane, qui est le principal facteur contribuant aux coûts énergétiques des BaM. Jusqu'ici le travail nécessaire d'adaptation calibration et validation d'un modèle intégré n'avait pas encore été mené sur une installation à très grande échelle.

Le BaM met en jeu des interactions complexes entre la biologie, la filtration et le colmatage, et sa modélisation est une tâche difficile en tenant compte de ces interactions. Dans le passé récent, des modèles intégrés ont été élaborés et appliqués aux BaM, principalement à l'échelle pilote, et rarement pour les installations à grande échelle de capacités allant jusqu'à 15 000 $m^3.d^{-1}$, et aucune étude de modélisation n'a été réalisée pour des installations à très grande échelle à ce jour. Dans ce travail, une usine concue sur la base d'un BaM à très grande échelle avec une capacité de traitement de 348000 $m^3.j^{-1}$ est modélisée dynamiquement pour simuler les processus de dépollution et de colmatage de la membrane. Le modèle intégré combine la biochimie (ASM3-SMP-EPS-Bio-P, aération et précipitation chimique), la résistance au colmatage en série (RIS) et les sous-modèles énergétiques. Le modèle intégré complet est capable de simuler a) les processus biologiques décrivant l'activité stoechico-cinétique de la biomasse pour l'oxydation du carbone et l'élimination des éléments nutritifs (c.-à-d. l'azote et le phosphore) couplés aux processus de production

et de dégradation des exo-polymères libres et liés; b) le rôle de l'aération pour le processus biologique dans l'oxydation et la nitrification du carbone sous l'influence des matières en suspension; c) le bilan matière sur les volumes des influents, des effluents, des purges et de toute recirculation interne et externe; d) l'ajout de coagulant pour l'élimination chimique améliorée du phosphore en plus d'une élimination biologique ; e) la dynamique de colmatage associée à la filtration-relaxation synchronisée, à l'air intermittent et au retro-lavage, sous l'influence de la pression transmembranaire (TMP), de la température, des MLSS et de la concentration en exopolymères liés, et f) de la consommation d'énergie spécifique en $kWh.m^{-3}$ ou $kWh.Kg^{-1}$, ainsi que de sa répartition entre usages. Le modèle a été étalonné à l'aide de données recueillies au cours d'une semaine de la première campagne expérimentale. Il a ensuite été validé par des données issues de 92 jours de fonctionnement avec et sans ajout de $FeCl_3$. De plus, une analyse de sensibilité a été utilisée pour déterminer les paramètres influents afin de faciliter l'étalonnage des sous-modèles et de démontrer la robustesse du modèle.

Le modèle intégré calibré a fourni une concordance acceptable pour l'élimination des polluants (DCO, NO_x, NH_4, PO_4^{3-}, MLSS, SPE et PGS), ainsi que la prédiction de la pression transmembranaire qui est un indicateur direct du développement du colmatage. Le modèle a aussi permis de compléter les jeux de données lorsque qu'elles étaient non-disponibles à partir de relevés de routine. p.ex. évolution de la biomasse et transformation des polluants dans chacun des réacteurs en série. De plus, le modèle est en mesure de fournir des renseignements détaillés sur la dynamique des colmatages réversible et irréversible, en tenant compte des différents moyens mis en œuvre pour les limiter. Le modèle peut être utilisé pour le développement d'opérations de contrôles commandes et outils d'aide à la décision afin d'optimiser le fonctionnement des BaM à grande échelle, en particulier la gestion de l'aération grosses bulles pour la limitation du colmatage ou la gestion des lavages chimiques dans un objectif d'optimiser les couts de l'énergie et des produits chimiques. Ce modèle devait être validé dans des conditions de colmatage avérées. Celles-ci étant relativement faibles, une approche par analyse de sensibilité a été menée, qui a permis de pointer les paramètres majeurs et de donner les limites de la robustesse du modèle. Elle a permis de conclure à l'utilité du modèle dans les objectifs fixés de son utilisation.

Table of Contents

List of Figures

List of Tables

Abbreviations

A/O	Anoxic - oxic
A^2/O	Anerobic-anoxic-aerobic
ANOs	Ammonia oxidizing organisms
ANN	Artificial neural network
ASM/ASMs	Activated sludge model(s)
ASM-1	Activated sludge model 1
ASM-2	Activated sludge model 2
ASM-2d	Activated sludge model -2, modified.
ASM-3	Activated sludge model 3
ASM-3-BioP	Modified ASM3 with Biological phosphorus removal
ARMA	Autoregressive moving average
ARX	Autoregressive exogenous
ATU	Allylthiorea
AAT	All at a time
A/MNN	Artificial/ neural network
BOD	Biological oxygen demand
BNR	Biological nutrient removal
BAF	Biological aerated filter
BAP	Biomass associated products
b/EPS	Bound /extra polymetric substances
BPC	Biopolymeric clusters
BIOS-R	Respirometer model
CASP	Conventional activate sludge process.
CEPR	Chemically enhanced phosphorus removal
CT	Capillary tube
CBA	Coarse bubble aeration
COD	Chemical oxygen demand
DPAOs	Denitrifying phosphorus accumulating organisms
DO	Dissolved oxygen
DAF	Dissolved air floatation
EPS	Extra polymetric substances
EBPR	Enhanced biological phosphorus removal
EEM	Excitation emission matrix
FS	Flat sheet
F/M	Food to microorganisms
FMs	Fuzzy Models
Fe	Ferric
FTIR	Fourier transform infrared spectroscopy.
FBA	Fine bubble aeration
GAOs	Glycogen accumulating organisms
GFC	Gel filtration chromatography
GSA	Global sensitivity analysis
HRT	Hydraulic retention time
HF	Hollow fiber
HLR	Hydraulic loading rate
INSA	Institut National des Sciences Appliquées de Toulouse
LB-EPS	Loosely bound EPS
LSTM	Long short-term memory

MLSS	Mixed liquor suspended solids
MLVSS	Mixed liquor volatile suspended solids
MBR/sMBR	Membrane bioreactor / submerged membrane bioreactor
MT	Multi-tubular
MLE	Modified Ludzack−Ettinger
MeOH	Metal hydroxide
MeP	Metal phosphate complex
MSRE	Mean square relative error
MATLAB	Matrix laboratory
MAPE	Mean absolute percentage error
MOCOPEE	Modélisation Contrôle et Optimisation des Procédés d'Epuration des Eau
NOB	Nitrate oxidizing bacteria
NSE	Nash-Sutcliffe efficiency
OHOs	Ordinary heterotrophic organisms
OTE	Oxygen transfer efficiency
ODE	Ordinary differential equations
ORP	Oxidation-reduction potential
OUR	Oxygen uptake rate
OTR	Oxygen transfer rate
OPEX	Operating cost
PFC	Pleated filter cartridge
PFCl	Polymeric ferric chloride
PAOs	Phosphate accumulating organisms
PCA	Principal component analysis
PHA	Polyhydroxyalkanoates
PID	Proportional integral derivative
PSD	Particle size distribution
PVDF	Polyvinylidene fluoride
PFD	Peak flow design
RIS	Resistance in series
RMSE	Root mean square error.
SAD	Specific aeration demand
SA	Sensitivity Analysis
SCADA	Supervisory control and data acquisition
SEM	Scanning electron microscope
SRT	Sludge retention time
SMP	Soluble microbial products
sN-DN	Simultaneous nitrification-denitrification
SW	Spiral wound
STOWA	Foundation for Applied Water Research
SAV-MBR	Seine Aval Membrane bioreactor
SEC	Specific energy consumption
SOTR	Standard oxygen transfer rate
TMP	Transmembrane pressure
TSS	Total suspended solids
TN	Total nitrogen
TKN	Total Khejdal nitrogen
TUDP	Technical University Delft
UAP	utilization associated products
UEC	Unit energy consumption
UCT	University Cape town
VBSA	Variance based sensitivity analysis
VFD	Variable frequency drive

Notations

A	Empirical constant used in aeration sub-model
As	Diffusers specific area
A_m	Active surface area of the membrane
a	Empirical constant in specific cake resistance equation
B	Empirical constant used in aeration sub-model
b	Empirical constant in specific cake resistance equation
c	Empirical constant in specific cake resistance equation
d	Empirical constant in specific cake resistance equation
αc	Specific cake resistance (measured)
$\alpha_{stickiness}$	Stickiness among sludge particle
e	Electrical charge
β_{dc}	Erosion rate coefficient
$\beta_{tension}$	Salinity tension correction factor
γ	Sludge compressibility
ω	Coefficient of correction of O_2 transfer associated with MLSS
ρ_{air}	Density of air
ρ_s	Density of sludge
ρ_w	Density of water
μ_s	Viscosity of sludge
μ_T	The viscosity of the sludge at given temperature
μ_p	Viscosity of permeate
η_m	Efficiency of motor
η_b	Efficiency of blower
η_p	Efficiency of pump
η_d	The efficiency of the diffusers
χ	Characteristics number used in aeration sub-model
C/N	Carbon to nitrogen ratio
C/P	Carbon to phosphorus ratio
C_∞	DO concentration of clean water.
$C_{\infty\text{-}20}$	DO concentration of clean water at 20 ^{0}C
C_d	Coefficient of drag
C*f*	The conversion factor for conversion of TSS to MLVSS
D_{imp}	Diameter of the impeller
d_p	Sludge particle size diameter
f	The porosity of the PVDF membrane
g	Gravitational constant
G	Shear intensity induced by coarse bubble aeration.
H_d	Depth of the diffuser
H_d	Dynamic head of the influent pump
J	Permeate flux
K_{La}	Oxygen transfer rate
M	Number of model parameters for sensitivity analysis
N	Total number of measurements
ns	Number of membrane sections
n	The base sample size for sensitivity analysis
N_r	Number of rotations
N_P	Power constant for mixer
N_d	Total number of diffusers
nP	Exponential constant for estimation of specific pore fouling

OTRf	Field oxygen transfer rate
p	TMP exponential coefficient
q_a	Coarse bubble aeration intensity
P_{atm}	Atmospheric pressure
P_i	Blower's inlet pressure
P_d	Blower's discharge pressure
PO_4^{3-}	Orthophosphate
Q_{inf}	Influent flow rate
Q_{air}	Process air flow rate
Q_{CB}	Coarse bubble aeration flow
Q_p	Permeate flow rate
Q_s	Sludge flow rate
Q_{CIP}	Flow of membrane cleaning agents
Q_{FeCl3}	Coagulant flow rate
Q_n	Normalized airflow per diffuser
R1	Recirculation from anoxic to pre-anoxic reactor
R2	Recirculation from aerobic to the anoxic reactor
R2	Recirculation from membrane aerated tank to the aerobic reactor.
R^2	Correlation coefficient
R_m	Membrane resistance
R_p	Pore fouling resistance
R_{sc}	Static cake resistance
R_{sc}	Dynamic cake resistance
R_T	Total filtration resistance
R_t	Total filtration resistance of one section
r_{sc}	The specific resistance of static cake
r_{dc}	The specific resistance of dynamic cake
r_p	Specific pore fouling resistance
r^2	Coefficient of determination
tf	Filtration time
T	Temperature
V_T	The volume of the aeration tank
V_f	Permeate volume at a given moment
X_{A-C}	Matrices of parameters space variability samples for SA
X_{O2}	Fraction of oxygen in air (%)

Statement of Original Authorship

The work in this thesis has not been previously submitted to meet the requirements for an award of doctoral degree at this or any other higher education institution. To the best of my knowledge and belief, the thesis contains no material previously published or written by another person except where due reference is made.

I also certify that this thesis is written by myself. Any support received in conducting the research and preparation of the thesis itself has been acknowledged individually.

Kashif NADEEM

19th May 2022, Toulouse

Acknowledgments

It is humbling to think of the number of people without whom this work would be nothing. I want to take this opportunity and express my sincere gratitude and appreciation to the following individuals and their institutions for their assistance in the completion of this dissertation:

- Mme. Claire ALBASI and Mme. Marion ALLIET for their consistent support and extraordinary guidance and supervision from the beginning to the end of this project. Both continuously encouraged me and were always willing and enthusiastic to assist in any possible way related to my research or administrative issues related to my research work.
- Mr. Jean BERNIER, Mr. Vincent JAUZIEN, Ms. Cécile CORNUT, and Ms. Queralt PLANA, for their support in data collection from the Seine Aval-MBR plant, analysis at SIAAP's lab and interpretation, and organizing and managing the experimental campaigns. It would not have been possible for me to conduct experimental campaigns without their support. I would extend my sincere thanks to Jean BERNIER for his supervision, data insights, and suggestions for improving the model's work. I appreciate their time and efforts in reviewing this dissertation and the manuscripts prepared for multiple knowledge contributions in journals, conferences, and seminars, particularly Mr. Vincent JAUZIEN and Mr. Sam AZIMI.
- Mr. Yannick Fayolle for his support in data analysis and interpretation.
- Mme Iréa TOUCHE for her help in refining and speeding up the MATLAB code and other IT team members in helping me from time to time in fixing my computational tools.
- Mr. Pascal FLOQUET and Mr. Rachid OURAT for their support and guidance in the sensitivity analysis of the model parameters and inputs.
- Administrative staff of the Laboratoire De Génie Chimique (LGC), including Patricia ULIANA, Brice VOUILLARMET, Daniele BUSCARY, and Christelle LABRUYERE.

- Higher Education Commission (HEC) of Pakistan, for its financial assistance. Furthermore, the logistics and administrative support of Campus France are also acknowledged.
- SIAAP, for its partial financing within the framework of the Mocopée program, and more particularly, Mr. Vincent ROCHER and Mr. Sam AZIMI for allowing me to access the plant database, for following my work with attention, and for reviewing the works before publication. I sincerely thank them for the means they made available to me regarding equipment and information.
- Reviewers and jury members - not only for their time but also for their intellectual contributions during the review and thesis defense. Special thanks are due to Prof. Peter VANROLLEGHEM (chair in water Quality modeling, Canada) and Prof. Giorgio MANNINA (University of Palermo, Italy) for their critical and detailed review of the thesis manuscript, which eventually helped in improving the quality of the final version. In addition, I would like to thank Prof. Mathieu SPÉRANDIO (LSBP-INSA Toulouse-France) and Prof. Erkan ŞAHİNKAYA (Istanbul Medeniyet University, Turkey) for sharing their observations and suggestions for improving the scientific quality of the work.
- I am also grateful to my research colleagues, including Jialu ZHU and Marcos OLIVEIRA FILHO, for their support in conducting the experimental work at SIAAP and to my lab fellows, especially Muhammad MUKHLIS ESHAMUDDIN and Manon GRANGER-DELACROIX for their moral support and to my other friends from Pakistan for their unconditional support during the time of the pandemic.

Lastly, I would be remiss in not mentioning my family, especially my wife, Aamena BATOOL, for her support in compiling the dissertation and helping in designing multiple diagrams and figures.

PART-I: PREAMBLE TO THESIS

Chapter 1: **General Introduction**

This section presents a brief on a fundamental understanding of the membrane bioreactor (MBR), global challenges, various configurations, applications, global markets scenarios, prospective growth in the global market, and future research directions.

1.1 INTRODUCTION

MBR is considered to be an intensified conventional activated sludge process (CASP) as it combines the features of low-pressure filtration technologies, especially ultra-filtration (0.01-0.5µm) and microfiltration (0.1 – 0.4µm); and suspended growth biological reactors and results in the elimination of tertiary treatments (Abdel-Fatah, 2018; Hai et al., 2018; Judd, 2010).

MBR technology is a mature and well established and is being extensively adopted in wastewater treatment; for municipal, commercial and industrial applications (Krzeminski et al., 2017; Burman and Sinha, 2018; Habib et al., 2017; Hamedi et al., 2021) because of number of advantages over CASP including: less space requirements (Zuthi et al., 2017; Kulesha et al., 2018; Xiao et al., 2019; Krzeminski et al., 2017), better process stability (Janus and Ulanicki, 2015), superior and constant supernatant quality (Krzeminski et al., 2017; Zuthi et al., 2017; Xiao et al., 2019; Hai et al., 2018; Habib et al., 2017), higher nutrient removal (Habib et al., 2017; Kulesha et al., 2018), higher heavy metal removal (Krzeminski et al., 2017), extended sludge retention time (Burman and Sinha, 2018; Habib et al., 2017), decoupling of hydraulic retention time (HRT) and sludge retention time (SRT) (Judd, 2008; Pimentel et al., 2015; Xiao et al., 2019), better control over solid inventory and SRT (Boyle-Gotla et al., 2014), less sludge production (Cadore et al., 2018; Burman and Sinha, 2018; Habib et al., 2017; Zuthi et al., 2017), concentrated biomass loading/higher mixed liquor suspended solid (MLSS) (Akhondi et al., 2017; Hai et al., 2018), simultaneous and improved nitrification/de-nitrification (Burman and Sinha, 2018; Judd, 2008), higher volumetric loadings, improved disinfection of supernatant through, higher removal of pathogenic bacteria and viruses (Judd, 2008; Krzeminski et al., 2017; Gabarrón et al., 2015),

potential degradation of specific refractory pollutant (Park et al., 2017, Dolar et al., 2012, Ma et al., 2018), supernatant re-use applications (Krzeminski et al., 2017; Habib et al., 2017; Gabarrón et al., 2015; Shen et al., 2015; Zhang et al., 2014), reduced GHG impact (Baresel et al., 2022), and larger possibility of automation and control (Makisha et al., 2018).

Despite all these leading edges over the CASP, the MBR technology is still struggling on many fronts, including limitations in oxygen transfer associated with higher biomass concentrations (Barreto et al., 2017), exorbitant loss of permeability due to fouling (Barreto et al., 2017; Hamedi et al., 2021; Kimura and Uchida, 2019); 30-34 % higher operational costs (Bertanza et al., 2017) due to energy consumption in aeration and pumping and chemical consumption in cleaning to counter the membrane fouling (Krzeminski et al., 2017; Li et al., 2019; Meng et al., 2017), higher investment (Xiao et al., 2019; Zhang et al., 2021), an increased tendency for foaming (Judd, 2010), sludge production with high dewatering requirements and yet higher costs for membrane replacement (Lo et al., 2015; Iglesias et al., 2017). All these disadvantages hamper the MBR for its broader applications and even penetration to the costs sensitive markets (Krzeminski et al., 2017; Mirbagheri et al., 2015).

In addition, membrane fouling induces transmembrane pressure (TMP) increase, which is evaluated to be the main trigger. In the recent past, several efforts have been dedicated to reducing and optimizing the cost of membrane aeration associated with membrane fouling mitigations, and still, no universal solution has been explored (Krzeminski et al., 2012, 2017).

1.2 VARIOUS CONFIGURATIONS OF MBRS

Different MBR configurations are available; depending upon the oxygen availability, permeate flow direction, placement of the membrane module, membrane geometry, and reactor configurations associated with recirculation directions. The submerged membrane bioreactor (SMBRs) is the most common, widely used in municipal applications and equally popular among researchers (Zhang et al., 2021).

MBRs usually target nitrogen and phosphorous simultaneously. For effective biological nutrient removal (BNR), several arrangements for oxic, anaerobic, and anoxic environments are used in various configurations (Monclús et al., 2010;

Vaiopoulou et al., 2007). For example, configurations such as modified Ludzack-Ettinger (MLE) process, A/O, A^2/O, University of Cape Town (UCT), Virginia Initiative Process (VIP), and Bardenpho process have been tried and tested for nutrient removal in MBR (Ahn et al., 2003; Ersu et al., 2010; Hai et al., 2018). All these configurations give different performances for BNR, and this is mainly because of the introduction of intermittent aeration (Wang, 2020) and re-circulations of the sludge from the aerobic to anaerobic (Daigger et al., 2010; Monclús et al., 2010) reactors, which impact the microbial community and stimulate competition among them for the substrate utilization. A detailed assessment of multiple MBR configurations for their effectiveness in nutrient removal is published as part of the peer-reviewed publication of this work, placed in **Annexure-A.**

Several submerged MBR technologies have now been commercialized with improved membranes and lower capital investment (Zhang et al., 2021). By 2010, at least seventy recognized manufacturers of MBR systems (Sutherland, 2010) were operational around the world, including Zenon-Zeeweed (General Electric), Memcor (Siemens), Asahi Kasei (Kubota OW), Memstar (United Envirotech), Mitsubishi (Mitsubishi Rayon Engineering), Puron (Koch Membrane Systems), Toray, Econity, Kolon & Para, and PentAir Xflow (Buer and Cumin, 2010; Hai et al., 2018; Judd, 2010) and competing for global supplies. The following section briefly presents different configurations used in commercially available systems for full-scale applications.

1.3 LARGE SCALE APPLICATION OF MBRS AND THEIR EVOLUTION

By 2005, around 2,200 MBR plants were globally operational (Mirbagheri et al., 2015). North America reported 219 MBR facilities treating municipal wastewater, with just 17 exceeding 10,000 $m^3.d^{-1}$ (Yang et al., 2006). Around 37 MBR plants with 5,000 $m^3.d^{-1}$ capacity were operational in 2008, while more than 800 commercial MBR WWTP were operational in Europe (Lesjean and Huisjes, 2008). As shown in **Fig. 1.1**, the installed capacity of the individual MBR jumped to the next level after every five years.

It has been reported that the size of the MBR plants has exponentially increased over the past few years and has crossed the individual plant installed capacity of

100,000 $m^3.d^{-1}$ (Xiao et al., 2019; Zhang et al., 2021), with the largest operational plants located in Stockholm (Sweden), Beijing (China), Guizhou (China) and Paris (France) having treatment capacities of 0.86 million $m^3.d^{-1}$, 0.78 million $m^3.d^{-1}$, 0.35 million $m^3.d^{-1}$ and, 0.348 million $m^3.d^{-1}$, respectively (Judd and Judd, 2018; Krzeminski et al., 2017).

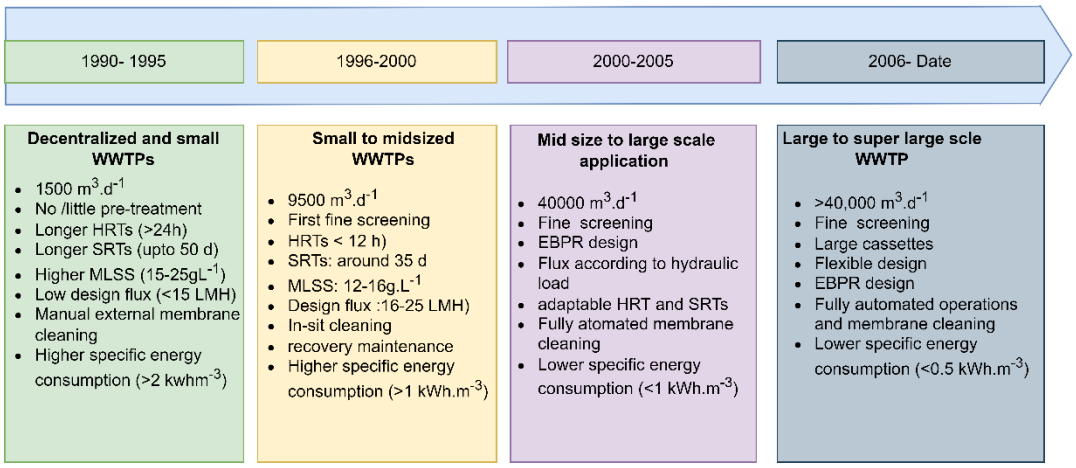

Fig. 1.1: MBR generations adopted and modified from Buer and Cumin (2010)

As of today, globally, there are around 62 super-large scales (>100,000 $m^3.d^{-1}$) MBR facilities contributing to the treatment of more than 11.4 million $m^3.d^{-1}$ of wastewater, with almost 60% of this treatment capacity located in China (Xiao et al., 2019; Zhang et al., 2021). Notably, most of these large-scale MBRs are used for municipal wastewater treatment, whereas industrial wastewater treatment MBRs are much smaller (Meng et al., 2017). Still, most of the MBR plants operational worldwide are medium- or small-scale in capacity.

1.4 MBR MARKET AND GROWTH DRIVERS

Since the mid-1990s, MBR plants have been installed at an exponential rate due to technological advances, e.g., lower operating costs with an immersed configuration as discussed in ***section 3.1*** and considerable reductions in the membrane cost (Zhang et al., 2021). As a result, the number and capacity of MBR installations continue to grow further, and the global size of the MBR market was valued at US$ 3.09 billion in 2020 and is further forecasted to reach US$ 5.48 billion by 2028 at a compound annual growth rate of 7.02% (Emergen, 2021). Worldwide, APAC (Asia-Pacific) is considered to have the highest MBR market growth in the world. **Fig. 1.2** summarizes

the MBR market growth by region during the period 2017-2024 (Market Research, 2022).

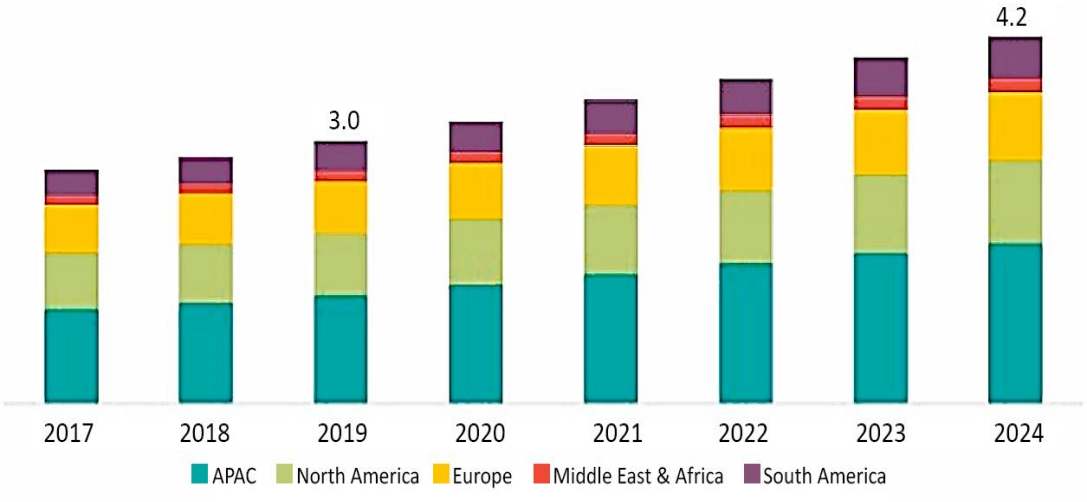

Fig. 1.2: MBR market value (US$) by region (Market Research, 2022).

Growing risk of water scarcity, ability of MBR to provide superior and consistent effluent quality, stricter regulation for effluent discharge, reducing investment costs, maturity and acceptance of the technology, and the opportunity to upgrade existing WWTPs are the key driving factor for broader applications and growing MBR market.

1.5 RESEARCH TRENDS

Keeping in view the growing commercial acceptance and large applications, dedicated and focused research is being carried out by academia and manufacturers. The economics of the MBR technology is linked to energy consumption, filtration efficiency (higher and consistent flux), and membrane replacement costs (Krzeminski et al., 2017). High energy consumption, operation costs, and fouling issues are still the dominant areas of research in the field of MBRs (Aslam et al., 2017; Krzeminski et al., 2017; Meng et al., 2017). As shown in **Fig. 1.3**, a chronological sequence of paper publishing, patent applications and large-scale MBR is presented, and it can be seen that by the end of 2021, the cumulative numbers of scientific publications and patents were 15,195 and 16,287, respectively.

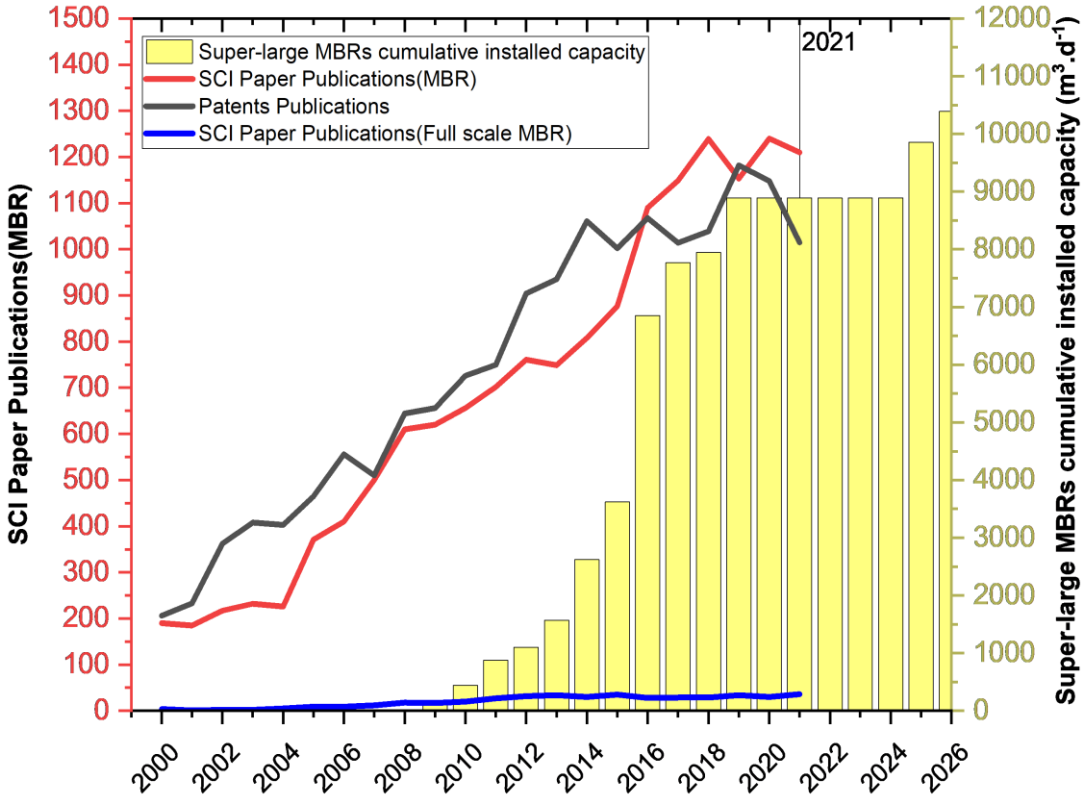

Fig. 1.3: MBR publications, patents, and full-scale engineering applications for the last 25 years (Scopus, April-2022)

The direction of research in the last two decades has been focused on applications, the development of novel configurations and the optimization of the MBRs. The optimization aims are to improve operational efficiency, improve performance for target pollutant removal, cut construction and operating costs, and reduce energy consumption in operations, especially air scouring. Membrane fouling control is an ongoing MBR research goal. Generally, novel fouling control, aeration, and intelligent air scour regulation systems are expected in the near future (Xiao et al., 2019; Zhang et al., 2021). The comprehensive review by Meng et al. (2017) also mapped the research needs beyond 2020, as shown in **Fig. 1.4**, with the focus on the development of the fouling controls system for full-scale applications and to reduce the specific energy demand, which is needed due to both environmental and economic concerns. Lower specific energy demand is expected with the construction of more super large-scale MBR facilities coupled with precise and automatic control of innovative aeration strategies based on analyses of pollutant removal and membrane fouling (Zhang et al., 2021).

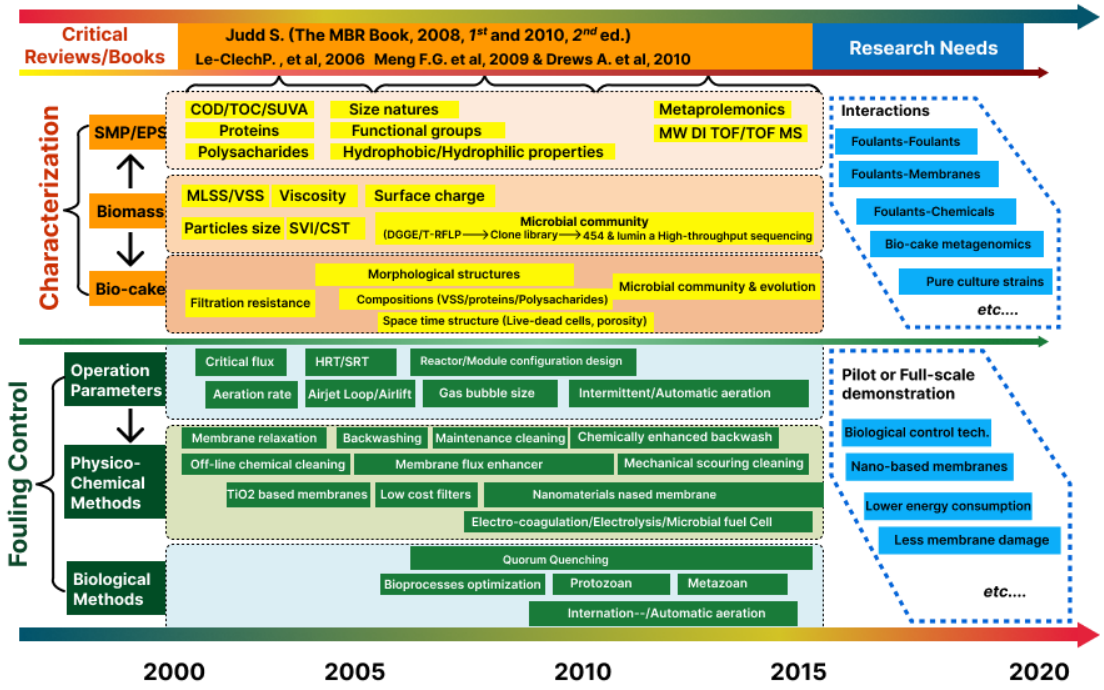

Fig. 1.4: Research needs for pilot and full-scale MBRs (Meng et al., 2017)

1.6 SUMMARY AND IMPLICATIONS

To sum up, MBR is an upgraded version of CASP that offers superior and consistent effluent quality with operating costs significantly reduced in the last decade, which is now almost comparable to CASP. As membrane modules gradually become cheaper, demands for the quality of treated effluent become more stringent, and the operation of MBRs gradually becomes more cost-effective, the market for MBRs in both industrial and municipal water grows. Further research is expected to reduce the specific energy consumption when coupled with a robust and intelligent fouling control system for full-scale applications.

PART-II: LITERATURE REVIEW

Chapter 2: Membrane Fouling in MBRs and its Control

Understanding the fouling mechanism is pertinent for the development of any mechanistic models for simulation of the fouling evolution in MBRs with time as well as in synchronization with the fouling control measures in place. This chapter presents the literature review on membrane fouling, factors that influence it, and the various types of fouling development mechanisms. It also presents a detailed review of the effects of the addition of the coagulant. Furthermore, several commercially available fouling control strategies are discussed in this chapter.

2.1 MEMBRANE FOULING

Understanding the fouling phenomenon is an essential requirement for developing the systems and strategies for the sustainable operations of the MBR. Fouling is the result of chemical and physical interactions happening between the mixed liquor and the membrane surface in a submerged membrane bioreactor (Krzeminski et al., 2017; Burman and Sinha, 2018). Therefore, the membrane and bioreactors cannot be studied in isolation while understanding the fouling mechanism in sMBR (Drews, 2010). Fouling can be described as a lumped effect of multiple factors resulting in gradual loss of the membrane permeability due to concentration polarization, deposition/adsorption of organic (including microbes and dead cells) and inorganic colloids (including metal salts added for chemical precipitation), and suspended matters within and onto the surface of the membrane (Krzeminski et al., 2017; Aslam et al., 2017; Boyle-Gotla et al., 2014; Azis et al., 2018). Loss of membrane permeability leads to a decline in permeate flux, higher TMP, aeration shear implementation; resulting in more energy consumption and frequent cleaning of the fouled membranes (Azis et al., 2018; Burman and Sinha, 2018; Drews, 2010; Zuthi et al., 2017). The permeability loss of the membranes may also be due to the sludging and clogging of the membranes modules and bundles (Drews, 2010). Membrane fouling is likely to contribute to the deterioration of supernatant quality and membrane performance and reduces the useful life of the membrane, which is estimated at around ten years (Cote et al., 2012), and results in enhanced operating costs.

The fouling process is explained in **Fig. 2.1**. Fouling is attributed mainly to the mechanisms simultaneously and interlinkingly happening in MBRs, including i) sorption of soluble micro-colloids inside the membrane pores, ii) pore plugging due to the deposition/adsorption of particles inside the membrane pores, iii) the formation of cake layer outside the membrane surface as a result of biomass deposition (Habib et al., 2017; Krzeminski et al., 2017; Shen et al., 2015; Zuthi et al., 2017).

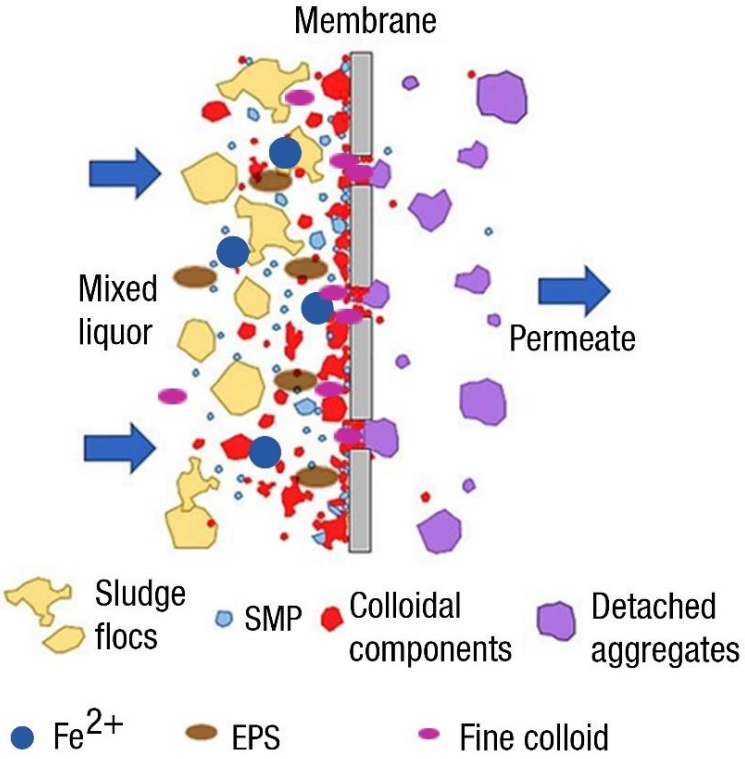

Fig. 2.1: Fouling phenomenon and fouled HF membrane

In recent publications, MLSS is reported to be the significant and poorly understood factor for membrane fouling as major foulants, including biofilm with extracellular polymeric substances (EPS), soluble microbial products (SMP) / organic compounds, colloids, particulates, dead cell debris, dissolved inorganic compounds, and sludge flocs; are parts of it and produced within due to biological and chemical processes (Habib et al., 2017; Iorhemen et al., 2016; Krzeminski et al., 2017; Oliver et al., 2008).

2.2 CLASSIFICATION OF THE MEMBRANE FOULING

Membrane fouling is classified in multiple ways, and there is no universally accepted and adopted approach. Based on the literature, fouling can be classified based on three

distinct approaches, i.e., i) flux recovery, ii) the location of fouling, and iii) fouling components.

2.2.1 Classification based on flux recovery

Reversible fouling is attributed to the formation of a sludge cake layer by loosely attached foulants which can be removed through physical means such as backwashing / relaxation (Di Bella et al., 2018; Drews, 2010; Meng et al., 2017). After physical cleaning, the flux can be recovered to an acceptable level. Due to the fact that the detachable foulants return to the mixed liquor during aeration scouring or backwashing, fouling is often referred to as recoverable. *Irreversible fouling* is linked to pores constriction caused by permanently attached foulants and can be removed through chemical cleaning or chemically enhanced backwashing (Di Bella et al., 2018; Drews, 2010); the flux cannot be recovered through physical means.

2.2.2 Classification based location of the fouling

The cake layer or external fouling is due to the formation of the layer on the membrane surface and is considered the major mechanism of fouling (Lee et al., 2018; Zuthi et al., 2017). The constituents of the MLSS, including proteins and polysaccharides, tend to form a gel layer on the membrane surface while colloids accumulate on the membrane surface and adsorb on the gel layer, leading to the gradual formation of a cake layer (Lee et al., 2018; Meng et al., 2009). This cake layer is reversible and can be removed through backwashing (Lee et al., 2018). Some of the colloidal constituents of MLSS having sizes smaller than the pores size get entrapped in the pores and cause plugging, which results in a substantial loss in porosity and permeability of the membrane. This type of plugging can only be removed through chemical cleaning (Lee et al., 2018). Clogging happens due to the agglomeration of solids (organic and inorganics) in the pores openings of the membrane and results in permeability loss. Clogging is attributed to the phenomenon of slugging (filling of membrane channels with solids) and braiding (accumulation of hairs and fibers on the membrane surface) or also known as ragging (Stefanski et al., 2011).

2.2.3 Classification based on biomass constituents

Depending upon the nature of fouling matter, fouling may be classified into three categories, i.e., i) biofouling, ii) organic fouling, and iii) inorganic fouling (Hai et al., 2018; Judd and Judd, 2018; Kulesha et al., 2018; Meng et al., 2017).

Biofouling is defined as the deposition, growth, and metabolism of undesirable micro-organisms (resulting in the formation of bound EPS and SMP) or flocs onto the membrane surface and the pores, leading to the development of the biofilm/bio-cake and membrane resistance increase, which results in severe fouling and a steep decline in flux (Aslam et al., 2017; Burman and Sinha, 2018; Busch et al., 2007; Janus and Ulanicki, 2015; Kulesha et al., 2018). Bio-cake formation is considered the main reason for fouling (Meng et al., 2009).

Organic fouling is described as the deposition and adsorption of soluble microbial SMPs and EPSs within the pores of the membrane and on the surface of the membrane, respectively (Ni et al., 2011; Meng et al., 2017; Drews, 2010). Organic fouling is considered a subset of biofouling (Burman and Sinha, 2018). It is caused by the formation of biofilm and attachment of colloidal organic and microbial substances on the membrane surface (Meng et al., 2017). In addition, synthetic organics, greases, oil, and surfactants present in the wastewater also accumulate on the membrane surface and result in membrane fouling (Kulesha et al., 2018). SMPs are responsible for the initial fouling of the membrane. The EPSs, being the major organic foulants, are responsible for prolonged fouling of the membranes, which may lead to irreversible fouling and eventually early replacement of the membrane (Meng et al., 2007; Wang et al., 2008). The effects of SMPs on membrane fouling are attributed to the factors such as i) SMPs concentrations in the mixed liquor, ii) membrane material, and iii) operational mode). In addition to fouling, SMPs are also responsible for effluent quality as the COD is linked with the formation of the SMPs (Ni et al., 2011). SMPs are low to high molecular weight compounds ranging between 0.5 -50 kDa. Due to their solubility potential, these can get into the pores of the membranes and get deposited onto the pores surface. Measurement and characterization of SMPs are still a challenge because of their unknown composition. As mentioned by Meng et al. (2017), the research on the role of SMPs on the membrane fouling has been of great interest but is still poorly understood (Meng et al. 2021). Similarly, Ni et al.(2011)

have recommended to explore the interaction between the SMPs and EPSs happening in the mixed liquor and on the surface of the fouled membrane due to the constant formation of SMPs associated with the release of EPSs. Inorganic fouling in the MBR occurs due to chemical and biological precipitation of mineral ions (Ca^{2+}, Mg^{2+}, Fe^{3+}, Al^{3+}, SO_4^{2-}, PO_4^{3-}, CO_3^{2-}, OH^-, etc.) and ionizable groups (COO^-, CO_3^{2-}, SO_4^{2}, PO_4^{3-}, OH^-) on the membrane surface. Mineral ions are accumulated on the membrane surface through entrapment in the gel layers (Wang et al., 2008). Inorganic mineral ionizable groups may cause fouling when precipitation occurs on the membrane due to hydrolysis and oxidation during the chemical process, such as coagulation (Iorhemen et al., 2016).

2.3 FACTORS AFFECTING THE MEMBRANE FOULING

Parameters responsible for membrane fouling can be grouped into different categories such as i) influent wastewater properties, ii) Biomass characteristics, iii) operating and hydrodynamic conditions, iv) membrane module and characteristics (Le-Clech et al., 2006; Akhondi et al., 2017; Deung Park, 2015; Meng et al., 2009). A classification of the factors affecting the MBR fouling is shown in **Fig. 2.2** (see Page.19.).

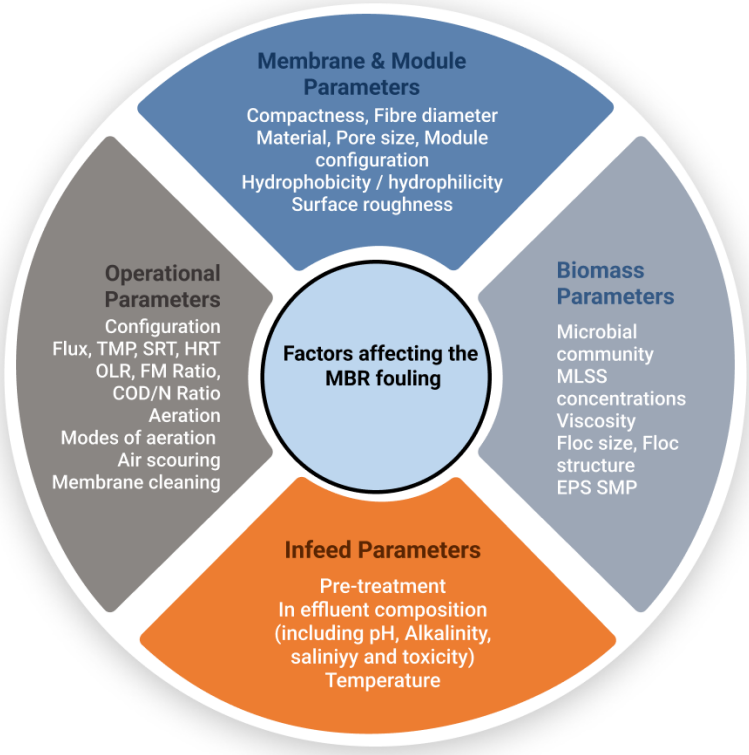

Fig. 2.2: Classification of the factors affecting the fouling in MBRs

Fouling in MBR is still poorly understood because of the several cross-boundary interactions happening among all four categories of factors and at various levels of the system, as explained by the interlinking chart in **Fig. 2.3.**

2.3.1 Mixed liquor characteristics

Activated sludge composition plays a crucial role in the development of fouling in MBRs. As it has already been discussed in the previous section, the MBRs are usually operated at higher solid concentrations and, therefore, fouling may be impacted. According to the literature review, several properties of the mixed liquor, such as MLSS concentration, viscosity, EPS/SMP concentrations, floc size, and structure, affect the fouling phenomenon and are necessary to better understanding mechanistic modeling of the MBRs. A synthesis of the mixed liquor properties affecting the membrane fouling is presented in **Table 2-1.**

Table 2-1: Effect of biomass properties on membrane fouling in MBRs

Sr#	*Mixed liquor Characteristics*	*Effect on Membrane Fouling*	*References*
1.	Mixed Liquor Suspended Solids (MLSS) Concentration-	MLSS concentration has a positive co-relation with the fouling rate.	(Bottino et al., 2009; Chang and Kim, 2005; Pan et al., 2010; Psoch and Schiewer, 2006; Trussell et al., 2007; Wu and Huang, 2009; Yigit et al., 2008)
		MLSS concentration has a negative co-relation with the fouling rate.	(Kornboonraksa and Lee, 2009; Rosenberger et al., 2006, 2005)
		MLSS concentration has little to no co-relation with the fouling rate.	(Le-Clech et al., 2003; Lesjean et al., 2005)
		Higher MLSS concentration induced faster membrane fouling by increasing the chances of sludge deposition on the membrane surface due to the presence of higher EPS and SMP concentrations.	(Lousada-Ferreira et al., 2010)
2.	Mixed liquor viscosity	Sludge viscosity is found to have a positive correlation with the fouling rate.	(Chae et al., 2006; Itonaga et al., 2004; Le-Clech et al., 2006; Moreau et al., 2009; Trussell et al., 2007)

Sr#	*Mixed liquor Characteristics*	*Effect on Membrane Fouling*	*References*
3	Extra polymeric substances (EPSs)	EPS concentration have a positive co-relation with the fouling rate	(Chae et al., 2006; Drews et al., 2006b; Xie et al., 2012)
	Polysaccharides	Only the polysaccharides fraction of the EPSs positively affected the fouling rate.	(Lesjean et al., 2009)
	Tightly bond EPS	Tightly bound EPS has more potential to foul the membrane than the loosely bound EPSs.	(Ramesh et al., 2007)
4	Soluble microbial products (SMPs)	SMPs contribute less to the fouling as compared to the EPSs.	(Ramesh et al., 2007)
		SMPs concentrations with MLSS concentrations exceeding 10 $g.L^{-1}$ did not have any effect on the membrane fouling. The optimal MLSS concentrations for MBR < 710 $g.L^{-1}$	(Lousada-Ferreira et al., 2010, Nadeem et al., 2022)
		The concentration of SMPs reduced as SRT increased and the rate of membrane fouling.	(Meng et al., 2009)
		SMPs are accumulated on the membrane surface, reducing the filterability, and thus increasing the fouling.	(Drews et al., 2006; Geng and Hall, 2007; X. Zhang et al., 2015)
6	Particle size	Generally, a decrease in floc size increased the membrane fouling; consequently, increase in floc size improved filtration. However, there are studies where an increase in the floc size (associated with coagulant addition) also results in a fouling increase (Nadeem et al., 2022). Furthermore, a decrease in the floc size reduced the viscosity of the sludge (Braak et al., 2017).	(Lin et al., 2011; Shen et al., 2015; Wang et al., 2011)
7	Filamentous bacteria	The higher concentrations of filamentous bacteria increased the viscosity of the sludge and caused bulking, which the severally increased cake resistance.	(Kim et al., 2013; Meng et al., 2017)

2.3.2 Influent composition and operational parameters

Influent composition and operating conditions include sludge retention time (SRT), hydraulic retention time (HRT), biological aeration or dissolved oxygen (DO) concentrations, temperature, permeate flux, and sequence and duration of backwashing or relaxation. Numerous studies have been conducted to determine the effect of MBR operational parameters on the membrane fouling, and the summary of these studies is presented in **Table 2-2**.

Table 2-2: Influent composition and operating parameters and their influence on MBR fouling

Sr#	*Influent Characteristics /operating parameters*	*Effect on Membrane Fouling*	*References*
1	Hydraulic retention time (HRT) and Sludge retention time (SRT)	Low HRTs and/or too long SRTs increased the fouling rate and reduced the filtration efficiency of MBRs. SRT of 20-30 days and HRT of 12-18 hours has been found optimum.	(Chae et al., 2006; Deng et al., 2015; Fallah et al., 2010; Guo et al., 2012; Huang et al., 2011; Jeong et al., 2010; Meng et al., 2009; Shariati et al., 2011; Villain and Marrot, 2013)
2	F/M ratio or organic loading rate	A higher F/M ratio increased the metabolic growth and EPS production, which increased the irreversible fouling.	(Dvořák et al., 2011; Khan et al., 2013; Liu et al., 2012; Meng and Yang, 2007)
		Low F/M reduced the cell growth and sludge deflocculating. A four-fold reduction in the F/M ratio resulted in 20 times decrease in the steady-state membrane fouling rate.	(Trussell et al., 2007)
3	Organic loading rate	Higher fouling rates with increased organic loading	(Johir et al., 2012 ; Tay et al., 2009)
4	C/N ratio	Low C/ N ration reduced the fouling rate	(B. Wu et al., 2012)
		A high C/N ratio improved the MBR performance by lowering the membrane fouling.	(Fu et al., 2009; Hao et al., 2016)
		A low C/N ratio reduced organic matter and nutrients removal efficiencies.	(Mannina et al., 2017, 2016)
5	Temperature	At lower temperatures, the production of EPS increased, known to impact fouling.	(Drews et al., 2006a; Guo et al., 2012; Ma et al., 2013; Van den Brink et al., 2011)
		The sludge settle-ability and filterability are reduced at low temperatures.	(Krzeminski et al., 2012)
6	Salinity	Higher salinity changes the sludge properties (like floc structure and size distribution changes) mainly due to changes in the microbial composition; SMP concentration also increased (see **Table 2-1**) as well as fouling.	(Di Bella et al., 2013)
		The sludge characteristics analysis showed that filtration resistance, SMP, and EPS gradually increased following the salinity increase from 0 to 35 $g \cdot L^{-1}$.	Xie et al.,2014

Sr#	*Influent Characteristics /operating parameters*	*Effect on Membrane Fouling*	*References*
		At high salt concentrations, pore blocking resistance increased, which increased membrane fouling. Biomass properties characterized by increased salinity had an impact on membrane filtration and fouling properties.	(Jang et al., 2013)
7	pH and alkalinity	Low pH values help in better flocculation and improved adsorption of EPS on the membrane surface. An increase in pH will result in higher fouling rates.	(Sweity et al., 2011; Wang et al., 2012)
		Too high concentration of alkalinity may increase the pH, which in turn will increase the fouling rate as well as increased deposition of Ca^{+} ions on the membrane surface, known as scaling problem.	(Arabi and Nakhla, 2008; Meng et al., 2009)
8	Biological aeration and DO concentration [Fine bubble (<2mm) aeration]	Higher aeration intensities can damage the floc structure by breaking them into smaller flocs, increasing their chances of depositing into the membrane pores, leaving the pores blocked and thus irreversible fouling.	(Deng et al., 2015; Deung Park, 2015; Ji and Zhou, 2006).
		Biological process is negatively affected at lower airflow rates which results in bio flocculation and cake layer formation through increasing EPS, SMP, and MLSS deposition on the membrane surface.	(Faust et al., 2014; Gao et al., 2011)
9	Air-scoring [coarse bubble (>2mm) aeration]	Higher aeration rates can mitigate membrane fouling in a specific scope. Increased aeration results in an increased EPS and SMP concentrations in mixed liquor and thus higher irreversible fouling. Furthermore, high aeration results in thinner, denser, and less permeable biofouling. Optimum SADm varies from system to system, and therefore, it is difficult to derive an optimum range.	(Braak et al., 2011; De Temmerman et al., 2014; Germain et al., 2005; Pourabdollah et al., 2014; Zhang et al., 2013)
		The effect of cyclic air-scouring on fouling is contradictory in the literature.	(Ding et al., 2016; Wu and He, 2012)

2.3.3 Membrane and module characteristics

Membrane material, pore size and distribution, surface charge, roughness, the geometry of membrane fibers, and hydrophilicity or hydrophobicity are the membrane characteristics responsible for fouling in isolation or interlinking. The summary of the

membrane and module properties affecting the fouling is summarized in **Table 2-3** below.

Table 2-3: Effects of membrane properties on fouling

Sr#	*Biomass Characteristics*	*Effect on Membrane Fouling*	*References*
1	Hydrophobicity/ Hydrophilicity	Hydrophobic membranes are more prone to higher fouling than hydrophilic membranes due to the interactions between feed water, microbial cells, and membrane materials. In hydrophobic membranes, higher rates of pores plugging occur, and higher amounts of polysaccharides and protein in SMP are rejected due to cake layer formation on the membrane surface, which results in a lower permeability. Ceramic membranes are hydrophilic; hence they foul less. Polymeric membranes are mostly hydrophobic and exhibit more fouling. Coating the hydrophilic material on the polymeric membrane's surfaces reduced the fouling.	(Nittami et al., 2014) . (Maximous et al., 2009) (Hofs et al., 2011; Jin et al., 2010; Mutamim et al., 2013) (Dolina et al., 2015). (Hamza et al., 2016)
2	Zeta potential	Higher zeta potential might mitigate fouling by inducing stronger electrostatic double layer and repulsive interactions.	(X. Zhang et al., 2015)
3	Surface charge	The membrane surface is usually negatively charged, and some cations from the sludge-like Ca^{+2} or Al^{3+} may react with the membrane surface and lead to fouling.	(Guglielmi and Andreottola 2010; Rana and Matsuura, 2010)
4	Surface roughness	Membranes with a rough surface are more prone to fouling, however, membranes with protruding fibers on the membrane surface act as antifouling.	(Elimelech et al., 1997; Guglielmi and Andreottola, 2010.) (Hashino et al., 2011) .
5	Pores size	In general, membrane pore size increases the tendency for the pore-blocking mechanism. However, it is totally linked with the membrane material.	(Guglielmi and Andreottola, 2010; Jin et al., 2010; Le-Clech et al., 2006; Van den Broeck et al., 2012) (Miyoshi et al., 2015)

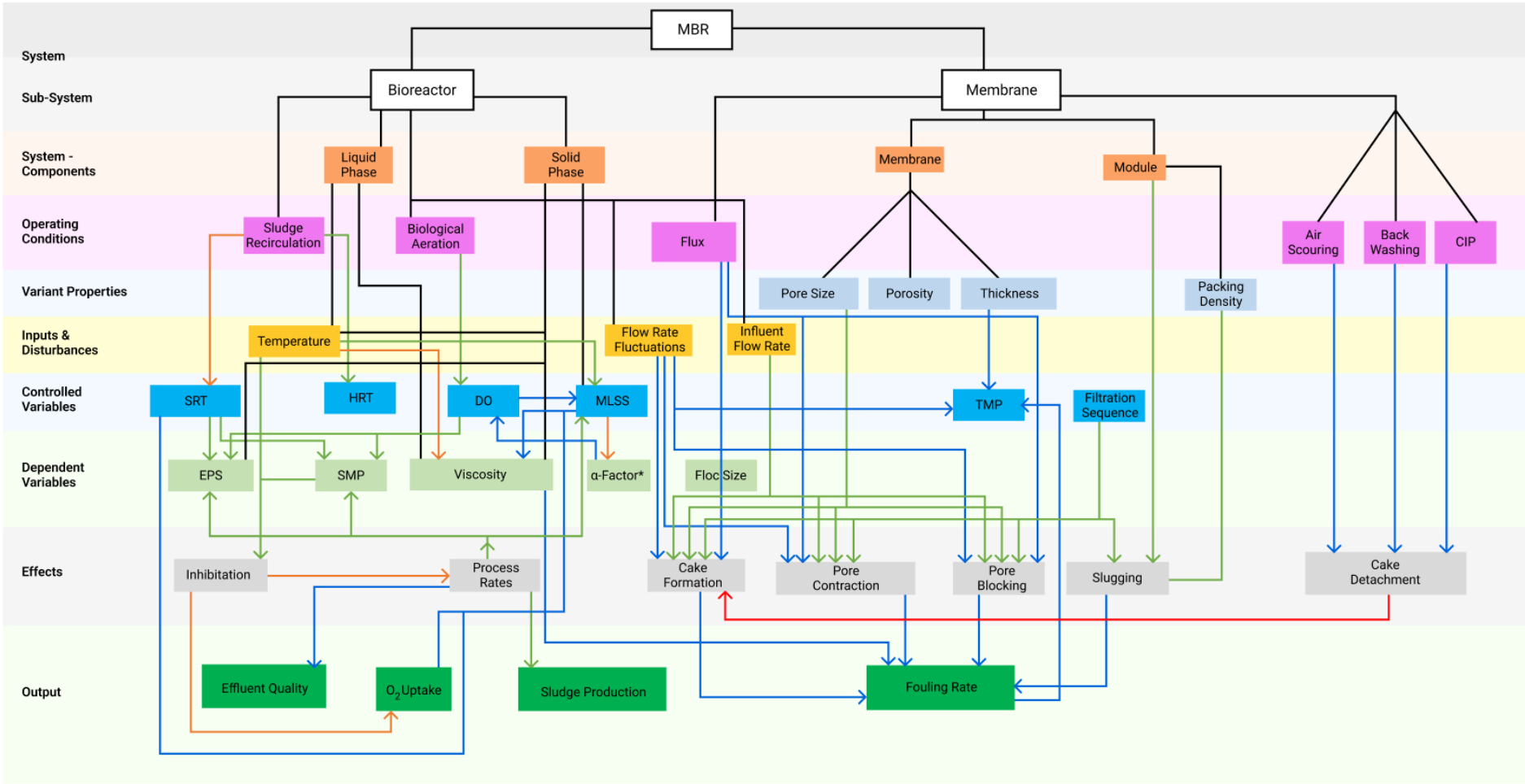

Fig. 2.3: Relationship between the various actors of the fouling phenomenon

Factors affecting the membrane fouling are diverse and cross-linking. The findings are contradictory, as presented in **Table 2-1**-**Table 2-3**. The synthesis of these effects and their interlinking are drawn in **Fig. 2.3.**

2.4 COAGULANT ADDITION FOR PHOSPHORUS REMOVAL AND MEMBRANE FOULING IN MBRS

In WWTP facilities, the coagulant is generally used to instill chemically enhanced phosphorus removal (CEPR). The CEPR in MBR is relatively different than CASP due to i) limited or no soluble phosphorus going with MBR effluent, and thus the metal carryover is comparatively less than CASP, or even negligible, ii) operation of MBRs at higher SRT and thus higher MLSS which improved the flocculation and coagulation potential of phosphorus iii) addition of the coagulant at the downstream of the process in case of MBR, and iv) interaction of metal ions with EPS and membrane surface that may cause or reduce membrane fouling, which is controversial in the literature. This section is dedicated to exploring the interaction of the coagulant addition with the mixed liquor and how it constitutes an overall role in membrane fouling.

The precipitant is usually added downstream of the CASP. In contrast, in the MBR systems, a coagulant is added in the mixed liquor before the filtration process or sometimes directly into the membrane tank (Gómez et al., 2013; Song et al., 2008). Therefore, the logistics and control of chemical additives, the dynamics, and the reliability of chemical P-removal are all more complicated in the MBR process than in CASP (Zhang et al., 2015). In addition to P-removal, the addition of precipitant (if dosed inadequately) into the MBR is likely to impact organic, inorganic, and biofouling (Hai et al., 2018; Meng et al., 2017). **Table 2-4** is dedicated to summing up the role of the coagulant in MBR for CEPR and fouling abatement / enhancement.

As discussed in the MBR fouling literature, inorganic fouling in MBRs is caused by bioprocesses and chemical precipitation of metal cations (e.g., Fe^{3+} and Al^{3+}) and physiological anions (e.g., PO_4^{3-} and SO_4^{2-}) onto the membrane (Iorhemen et al., 2017; Wang et al., 2008). Several studies investigated the addition of a small coagulant concentration into the MBR to control the membrane fouling. It reduced the extent of the TMP evolution, which is assumed to be attributed to the large-sized floc formation (formed due to neutralization); it also reduced organic concentration in the supernatant (reduction of organic fouling), limiting the pore blockage (Fan et al., 2007; Fleischer

et al., 2005; Koseoglu et al., 2008; Wu et al., 2006; Zhang et al., 2008). In addition, it has been perceived that an optimum coagulant addition decreases the compressibility of the sludge flocs, changes the particle size distribution (PSD), reduces the concentration of EPS (and thus the fouling), increases the porosity of the membrane-associated with sludge cake, and increases the MLSS filterability (Gómez et al., 2013; Song et al., 2008; Sun et al., 2019). Finally, it is assumed to pose an unknown risk to the membrane life when operated over extended periods (Gnirss et al., 2003) and requires further research.

As described by Song et al.(2008), the hydraulic resistance of the cake is influenced by the coagulant addition, and a noticeable reduction was observed with the addition of coagulant above 200 $mg.L^{-1}$. Usually, higher concentrations than the coagulant (*Fe/P in the range of 2-4*) are used for phosphorus removal. Therefore, the results of these studies might be insufficient to understand the trade-off between P-removal and membrane fouling. If the objective is complete P-removal, the Fe/P ratio is adjusted in the range of 1.5 and 4 (Sun et al., 2019; Takács et al., 2011; Z. Zhang et al., 2015). Thus, it is essential to look at different studies about P-removal and membrane fouling to conclude.

The coagulant (alum) addition enhanced membrane filtration performance and reduced fouling due to the incorporation of the colloidal solids into the flocs (later removed with sludge) rather than sticking onto the membrane surface (Fleischer et al., 2005). In a lab-scale study by Song et al. (2008), the effects of ferric chloride and alum addition were investigated on P-removal and membrane fouling. The authors found that the alum addition (13.3 mg Alum/mg P) resulted in 98% P-removal and reduced the specific cake resistance due to increased sludge particle size (from 45 µm to 57 µm). It was further found that the nitrification process was not impacted by the addition of $FeCl_3$, while the phosphorus was removed and the membrane fouling effectively controlled. However, the coagulant reduced the pH to almost half (≈3.4) of its initial value as the dose increased from 0 - 500 $mg.L^{-1}$.

In another lab-scale study, the addition of $FeCl_3$ (Fe/P ratio =2) successfully removed 99.7% of the phosphorus from the synthetic wastewater. It decreased the fraction of SMPs by 50% (having protein and carbohydrate sizes falling between 0.1-0.4 µm),

thus reducing the membrane fouling propensity due to increased floc size (Mishima and Nakajima, 2009). Another pilot-scale study by Yang et al. (2011) employing polymeric ferric chloride (PFC) revealed increased membrane fouling. The authors analyzed the cake using a three-dimensional excitation-emission matrix (EEM) and gel filtration chromatography (GFC). The study indicated that higher molecular weight organics (>1000 kDa) were the main contributors to membrane biofouling. Fourier transform infrared spectrum (FTIR) analysis further confirmed that these higher molecular weight organics were mostly proteins and polysaccharides, differently from Meng et al. (2017), wherein it was mainly polysaccharides. The same authors also observed the formation of a dense and nonporous gel layer onto the membrane surface with clusters of bacteria and biopolymers with the help of a scanning electron microscope (SEM). Besides, X-ray elemental diffractometric analysis revealed that ferric metal was the most prominent foulant responsible for inorganic fouling of the membrane.

Holba et al. (2012) investigated the effect of low coagulant concentration on P-removal and SMP production at pilot and full-scale. A fixed coagulant solution dose of 3.5 mg$FeSO_4.7H_2O.L^{-1}$, equivalent to 0.34 g.L^{-1} of Fe^{+2}, was used for all three systems (one pilot and two full-scales). A better P-removal efficiency (84.7%) with a 68% reduction of SMPs was observed in the pilot-scale plant. However, large load fluctuations and constant coagulant dosing in the full-scale plant caused unsatisfactory P-removal (*% age removal not reported by the authors*). In another pilot-scale MBR study by Wang et al. (2014), similar effects have been documented where the coagulant dosing required optimization to balance the enhanced P-removal and coagulant-driven membrane fouling. In another study, the addition of metal salt (i.e., $FeCl_3$) resulted in 89%–97% phosphorus removal efficiency and produced more sludge (Chae et al., 2015). In a lab-scale investigation by Sun et al. (2019), the addition of metal salt (20 mg$Al_2(SO_4)_3.L^{-1}$), equivalent to 3.15 g.L^{-1} of Al^{3+}, resulted in achieving over 90% phosphorus removal and reduced TMP (from 11.3 kPa.d^{-1} to 0.57 kPa.d^{-1}) due to a decline in EPS concentrations and in accumulated particles on the membrane surface, and also an increase in the particle size. The study by Asensi et al. (2019a) revealed that the addition of $FeCl_3$ (in neutralized conditions) linearly increased the floc size and resulted in a more compact floc structure. It also increased the settling properties of the sludge to an extent where the coagulant concentration

reached an optimum level; beyond this optimal concentration, the floc cannot retain the coagulant, and the settling properties are then negatively impacted. This suggests that while modeling the membrane fouling using phenomenological models, changes in the settling properties of the sludge due to the addition of the coagulant should not be ignored. Furthermore, if a model predicts the phenomena, it is a way to prove it. In another pilot-scale study by Gómez et al. (2013), the addition of 12.4 mg$FeCl_3.L^{-1}$ improved the phosphorus removal efficiency from 54.7% to 84.7%. The authors observed a reduction in SMPs concentration with the addition of the coagulant. The X-ray elemental diffractometric analysis of the cake layer found a significant increase in the Fe^{3+} concentration and a substantial contribution to inorganic fouling. The same authors further noticed that, at lower coagulant concentrations, it was not easy to ascertain the trade-off between the fouling reduced by the SMPs removal and Fe^{3+} deposition and the resulting inorganic fouling. The higher coagulant doses resulted in a significant pH decrease and precipitated TP present in the sludge, resulting in a lack of available phosphorus for PAO to grow and participate in the EBPR process. This becomes more pertinent for MBR systems, which are operated at higher biomass concentrations than CASP since the coagulant is added before recirculation.

Phosphorus is essential for microbial communities other than PAOs to participate in nitrification and de-nitrification processes (Daigger et al., 2010). Similarly, Zhang et al. (2015) found that the precipitant dosing lowered the irreversible membrane fouling with the Fe/P molar ratios < 1. However, phosphorus removal was compromised, and severe irreversible fouling (due to the Fe-rich gel layer) was observed with higher molar ratios due to the formation of Fe-SMPs complexes and amorphous ferric hydroxides (Fe/P >2). The severity of the membrane fouling was observed when the coagulant was dosed in the anoxic zone compared to dosing in the aerobic zone (much closer to the membrane). The authors further found that a molar ratio of 2 for Fe^{3+}/P successfully removed 99% of the phosphorus without impeding the nitrification and de-nitrification. However, it impacted the nitrification process significantly with a higher dose (molar ratio of 4) due to increased consumption of alkalinity associated with a decrease in the pH value to almost 4 and thus required the pH adjustment. Minimizing overall iron dosage is also important for cost reasons and to avoid unwanted side effects like membrane fouling.

Table 2-4: Coagulant addition for phosphorus removal and fouling

Sr. No.	*Reference*	*Wastewater*	*Scale*	*Configuration*	*Influent wastewater characteristics (mgL^{-1})*							*Coagulant Information*			*Total P-removal %*	*Effluent P mgL^{-1}*	*EPS/SMP/macro molecules*	*Fouling*
					TSS	*COD*	*TN*	*NH4*	*NO3-N*	*PO43-*	*TP*	*Coagulant*	*Molar Ratio Me/P*	*Optimum dose (mgL-1)*				
1	(Gnirss et al., 2003)	RW	Lab	A/O		998	70	41	0.4		10.5	GFH	2.12	40	99.0%	0.1	NC	NE
		RW	Pilot	A/O		740	61	43	~~		9.1	GFH	2.45	40	98.9%	0.1	NC	NE
2	(Adam et al., 2002)	RW	Lab	UCT		998	69.7	41.3	0.42		10.5	$FeCl_3$	1.3	25	99.5%	0.05	NC	NC
3	(Song et al., 2008)	SW	Lab			45	35.4				11.1	$AlCl_3$	1.51	30	98.0%	0.05	NC	↓
		SW	Lab			27	30.8				13.1	$FeCl_3$	1.28	30	98.0%		NC	↓
4	(Mishima and Nakajima, 2009)	SW	Lab	A/O		560						$FeCl_3$	1.0	2260	92.5%		↓	↓
		SW	Lab	A/O		25						$FeCl_3$	2.0	4520	99.7%		↓	↓
5	(Gómez et al., 2013)	RW	Pilot	A/O	130	250		49	1.4	4.6	4.7	$FeCl_3$	2.0	12.4	84.7%	0.7	↓	NC
6	(Yang et al., 2011)	RW	Pilot	A/O		196	20.5	18.5	1.2		2.9	PFC	2.4	12.5	91.0%	0.26	↓	↑
7	(Holba et al., 2012)	RW	Pilot	MLE	757	724		40.8		4.2	4.3	$FeSO_4$	0.5	3.5	84.7%		↓	NC
		RW	Full	MLE		1140		105			8.7	$FeSO_4$	0.2	3.5	85%		↓	NC
		RW	Full	MLE	155	655		73.4			14.5	$FeSO_4$	0.1	3.5			↓	NC
8	(Wang et al., 2014)	RW	Pilot	UCT		400	50	25			9	FeCl3	2		>96%	0.05	↓	↑
		RW	Pilot									$FeSO_4$	2		>96%	0.05	↓	↑
9	(Zhang et al., 2015)	SW	Lab	UCT		400	60	25			10	$FeCl_3$	4		99.8%	0.02	↓	↑
												$Fe_2(SO_4)_3$	2		99.6%	0.03	↓	↑
10	(Wu et al., 2015)	SW	Pilot	A/O		400	50				8	$AlCl_3$	2		95.2%	0.384	NC	NC
			Pilot									$FeCl_3$	2		96.7%	0.264	NC	NC
11	(Li et al., 2017)	RW	Lab			50	17	15			2	Ferric	5.6	20	80.3%	0.29	↓	↓
												$AlCl_3$	17.2	30	80.3%	0.33	↓	↓

Sr. No.	*Reference*	*Wastewater*	*Scale*	*Configuration*	*Influent wastewater characteristics (mgL^{-1})*							*Coagulant Information*			*Total P-removal %*	*Effluent P mgL^{-1}*	*EPS/SMP/macro molecules*	*Fouling*
					TSS	*COD*	*TN*	*NH4*	*NO3-N*	*PO43-*	*TP*	*Coagulant*	*Molar Ratio Me/P*	*Optimum dose (mgL-1)*				
12	(Lee et al., 2017)	SW	Lab	UCT		293	24.3	20.7	0.4		4.25	PAC	3.4		85.5%	0.62	↑	↑
13	(Li et al., 2018)	RW	Lab			360	28.5				6.35	$FeCl_3$	1.8	20	95.60 %	0.28	↓	↓
14	(Wu et al., 2019)	RW	Pilot	UCT						3.05		$Fe2(SO_4)_3$	2				↓	↓
15	(Sun et al., 2019)	RW	Lab	UCT		268.1	40.4	38.6			4.97	$AlCl_3$	2.3	10	85.40 %	0.73	↓	↓
16	(Ren et al., 2019)	SW	Lab	A/O		425	45	27.5			10	$Fe2(SO4)_3$	2		96.9%	0.31	NC	↓
													1		96.2%	0.38	NC	↓
17	(Alibardi et al., 2021)	RW	Full	A/O	338	579		26.9			9.18	$Fe2(SO_4)_3$	3.75	14	95%	0.46	NC	NC

Furthermore, the same authors found that lowering the phosphorus concentrations to 0.1- 0.2 $mgP.L^{-1}$ using higher coagulant doses did not inhibit nitrification. As reported by Philips et al. (2003), the harmful effects of the chemical coagulants (Fe^{2+} and Fe^{3+}) were blamed for suppressing nitrification and de-nitrification due to the toxicity induced by the metals. Some studies used dissolved air flotation (DAF) and biologically aerated filters (BAF) as post/pre-treatment to membrane filtration to improve the P-removal performance as well as to counter the inorganic fouling caused by metal deposition onto the membrane surface (Lee et al., 2016; Li et al., 2017). Similarly, Ren et al. (2019) reported the change in the microbial composition due to the addition of ferrous in a ceramic MBR with a molar ratio of 2. The authors found that the relative abundance of the aerobic denitrifying bacterial community "Zoogolea" increased consistently. While the population of other bacterial communities, including "Dechloromonas, Hyphomicrobium, and Thauera (anoxic denitrifying bacteria), Nitrospira (NOB) and Candidatus Accumulibacter (PAO) which is responsible for BioP-removal, is reduced sharply due to the toxic effects of iron dose on bacterial physiology.

A trade-off between coagulant dose, fouling, and phosphorus removal is reported differently for different studies, and hence further research is needed to explore the relationship between the type (cake formation, pore blocking, etc.) and quantum of the fouling induced (Loderer et al., 2015; Z. Zhang et al., 2015). The majority of the MBR studies summarized in **Table 2-4** are either lab-scale or pilot-scale units, whereas experiences with P-removal and fouling abatement/fouling increase are limited, implying that more research in this area is required.

Chemically enhanced phosphorus removal (CEPR) is a well-established yet poorly understood process because of the formation of unknown metal complexes and multiple pathways involved. P-removal in MBR differs from in CASP due to specificities involved in its functioning and the risk of fouling development (Mbamba et al., 2019; Sun et al., 2019). Moreover, the effect of MLSS concentration and floc size (smaller in MBRs) on CEPR performance should be investigated, considering the competing mechanism for MeP and MeOH production. Most of the bench-pilot scale studies have reported opposite trends for fouling and phosphorus removal, while experiences of phosphorus removal and fouling abatement/fouling increase are

limited. Dedicated research is needed to investigate how coagulant addition affects membrane fouling and how much and what kind of fouling is caused by the addition of coagulant.

2.5 FOULING MITIGATIONS

Several fouling control strategies have been developed and deployed, including:

- Reducing flux to under critical or low TMP (Gkotsis et al., 2014; Instituto Mexicano de Tecnología del Agua et al., 2015; Kimura and Uchida, 2019; Lee et al., 2018),
- Refining of infeed through fine screens (Krzeminski et al., 2017),
- mechanical cleaning sweeping and use of abrasive materials (Zuthi et al., 2017),
- Backwashing with the permeate (Akhondi et al., 2017; Aslam et al., 2017; Azis et al., 2018; Lee et al., 2018; Gkotsis et al., 2014; Di Bella et al., 2018) ,
- Relaxation or cyclic operation (Lee et al., 2018),
- Air scouring or enhanced shear (Akhondi et al., 2017; Aslam et al., 2017; Di Bella et al., 2018; Azis et al., 2018; Lee et al., 2018; Gkotsis et al., 2014),
- Chemical cleaning shear (Krzeminski et al., 2017; Akhondi et al., 2017; Aslam et al., 2017; 2018; Azis et al., 2018; Lee et al., 2018; Gkotsis et al., 2014; Meng et al., 2017a; Busch et al., 2007),
- Chemically enhanced backwashing,
- Sonication (Azis et al., 2018; Gkotsis et al., 2014),
- Mechanically assisted cleaning using granular media like activated carbon (Busch et al., 2007a; Krzeminski et al., 2017; Lee et al., 2018),
- Vibrations, rotations, and reciprocations (Krzeminski et al., 2017), electric field (Gkotsis et al., 2014; Krzeminski et al., 2017; Meng et al., 2017),
- Chemical modification of mixed liquor through the addition of coagulants, suspended particles, and carriers (Azis et al., 2018; Gkotsis et al., 2014; Krzeminski et al., 2017; Lee et al., 2018; Meng et al., 2017; Zuthi et al., 2017)
- Modification of membrane surface (with Nano-particles coating, patterning, grafting),
- Quorum quenching (Gkotsis et al., 2014; Krzeminski et al., 2017; Lee et al., 2018)

- Chemical reaction on the membrane surface (Gkotsis et al., 2014),
- Integration of advanced oxidations process with MBRs (Gkotsis et al., 2014; Krzeminski et al., 2017),
- Introduction of microbial fuel cells (Krzeminski et al., 2017),
- Use of patterned membranes, plasma treatment (Gkotsis et al., 2014),
- Systematic optimization of aeration and operational parameters (Meng et al., 2017a; F. Zuthi, 2014)

The above means for fouling abatement have been investigated and proved their effectiveness at the lab scale, while few of these are implemented in commercial-scale MBRs. In addition to the above control measurements, some other parameters have recently been studied, such as reactor design modification timing and intervals for filtration, backwashing, and /or relaxation are important along with the backwashing flow rates (Akhondi et al., 2017; Lee et al., 2018).

2.6 SUMMARY AND PROSPECTIVES

From the literature survey, it has been seen that extensive research has been dedicated to the understanding of the fouling phenomenon, dealing with a range of topics assessing the effects of various controlled variables (e.g., HRT, SRT, DO concentrations), and feed water characteristics like F/M ratio, COD/N/P ratio, temperature, pH, salinity, etc. Research has also been dedicated in the last decade to the development of fouling and/or mitigation strategies and the development of fouling control systems and characterization methodologies. The following points conclude the literature survey related to fouling and its control:

- Too low or high SRT may alter the sludge characteristics, such as the production of smaller sludge flocs and the release of higher concentrations of EPSs/SMPs which are more prone to intrude to the membrane pores and cause severe fouling. An optimum SRT of 20-40 days for synthetic wastewater has been suggested, while for real municipal wastewater, the recommended SRT value is 20-30 days. Some studies have reported the SRT value is between 20 and 50 days for real wastewater, depending on the size of the system and on the mode of operations.

- Short HRT (<10 hours) is found to be responsible for i) production of filamentous bacteria, ii) increase in MLSS concentration (high EPS/SMPs), iii) high sludge viscosity, and iv) development of thick and compact cake layer and thus more severe fouling. It has also been reported that high SMPs are produced and flocs with small sizes when dealing with synthetic wastewater containing toxic substances. An optimum HRT of more than 10 hours is suggested with the optimum SRT.

- Dissolved oxygen concentrations or aeration intensity are affected by the duration of aeration, position, diffuser type, and sludge viscosity. An optimum level of aeration is required as too high aeration may alter the sludge properties by altering the floc size (small flocs at high aeration intensities) and increase the release of the SMPs/EPSs. On the contrary, low aeration is unable to break the cake layer due to limited shear on the membrane surface and is unable to remove the cake layer. Similarly, an optimum temperature of between 15 and 30 C is required for membrane performance. At low temperatures, sludge properties are negatively affected, such as: changes in the viscosity, increased SMPs and EPSs concentrations, and the formation of smaller flocs. Similarly, too high temperature is also responsible for the poorer MBR performance.

- High organic loading (i.e., higher F/M ratio) increases the concentration of EPSs, which aggravates the membrane fouling. In contrast, under a low organic loading or F/M ratio, cell lysis may induce higher fouling due to the famine conditions and death of the microbes. The low COD/N ratio reduces the fouling rate as it increases the EPSs concentration, protein fraction, and sludge deposition on the membrane surface. At the same time, it has been found that a high COD/N ratio led to an elevated production SMPs. It has also been found that higher concentrations of nitrogen and phosphorus in the feedwater reduced the settle-ability, flocculation tendency, and dewater-ability and enhanced the release of SMPs, which cause higher fouling.

- Salinity is a crucial factor for fouling control in MBR. Higher salinity increased the density and viscosity, they lead to the release of the SMPs due to the incomplete degradation of organic substances and the release of cell contents

to protect microbial cells from salt toxicity, which thus may cause irreversible fouling.

- Asymmetric membranes with enhanced hydrophilicity, less surface roughness, higher zeta potential, and chosen pores sizes, also linked with the membrane material, have been suggested in the literature to control the fouling in the MBRs.

- Several fouling control techniques, including chemical, physical, physio-chemical, and biological (quorum quenching), are being used and studied. The addition of the chemicals may change the properties of the sludge and fouling behavior. A literature review has revealed that the addition of coagulant for CEPR has been controversial regarding fouling. Therefore, more dedicated research is needed to establish the precise contribution of the coagulant added for CEPR in fouling, especially at a full-scale.

Chapter 3: Operating Cost and Energy Consumption in Full Scale MBRs

This section examines peer and non-peer-reviewed published data to present state of the art on the operating costs of full-scale MBRs. This clarifies the global patterns of operating costs compared to the Seine Aval MBR. It also focuses into the energy consumption data distribution in the MBR process and the membrane air scouring, which is a hot topic for energy optimization studies, especially at the full-scale.

3.1 OPERATING COSTS OF FULL-SCALE MBRS

There is a dearth of data on detailed operating and energy consumption of full-scale MBR plants published in peer-reviewed papers. Gabarrón et al.(2014) surveyed three full-scale sMBR facilities (capacities varied in the range of 1,100 - 2,160 $m^3.d^{-1}$), equipped with HF membranes, and evaluated their global operational cost, which varied in the range of 0.46 - 0.57 €.m^{-3} or 0.52 - 0.64 US$.$m^{-3}$. A few more studies have recently been published with operating cost data from several full-scale facilities. As per the findings of the Iglesias et al. (2017), based on a detailed investigation of 14 MBRs with capacities in the range of 288–35,000 $m^3.d^{-1}$ located in multiple cities in Spain; the OPEX of the studied MBRs ranged from 0.23 to 0.51 US$.$m^{-3}$. Similarly, Xiao et al. (2019) published the findings of a survey focused on large-scale MBRs in China. The ranges of operating costs, energy consumption, and chemical costs of large-scale MBRs (10,000 $m^3.d^{-1}$) for municipal wastewater treatment in China are depicted in **Fig. 3.1**. According to the findings of this survey, when the membrane depreciation cost is not included, the operating cost is associated with energy consumption (40 %–60 %), chemical consumption (10%–30%), sludge disposal (5 %–15 %), labor costs (10 %–30 %) and others (5 %–20 %). The operating cost depends on the loading capacity of the MBR system, with larger hydraulic capacity and maximum utilization corresponding to a narrower distribution of operating costs. Overall, the operating cost is mainly in the range of 0.12–0.2 US$ m^{-3} for MBRs

commissioned in 2006–2014 and mainly in the range of 0.11–0.18 US$.m^{-3} for MBRs commissioned thereafter.

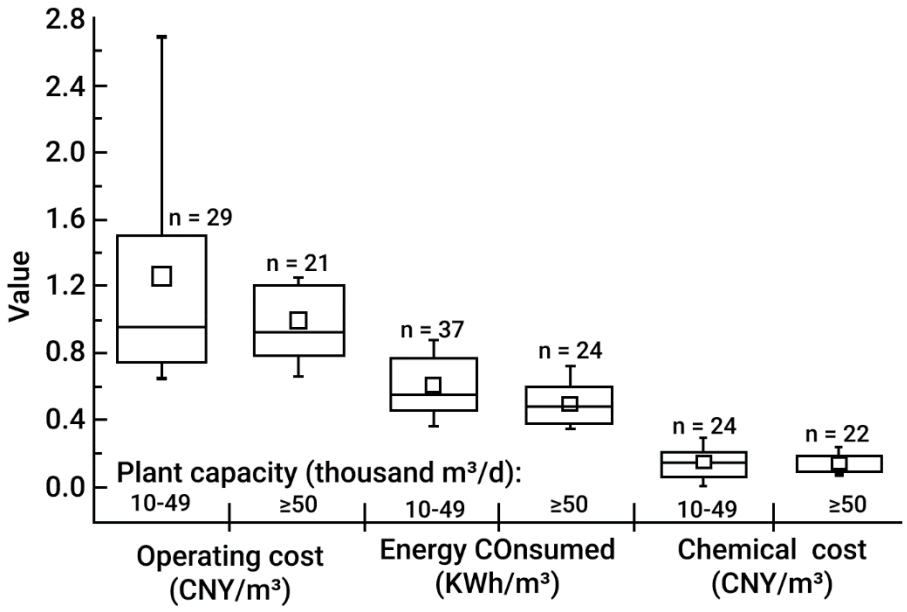

Fig. 3.1: Major operating costs in large scale MBRs (Xiao et al., 2019)

Operating costs of MBR (excluding membrane depreciation) could be comparable to those of CAS with tertiary treatment process with increasing effluent quality requirements (Brepols et al., 2010; Iglesias et al., 2017; Young et al., 2014). The model based study by Arif et al. (2020) for MBR and CASP with a capacity of 300,000 m^3.d^{-1} reported an operating cost of 0.43 US$.m^{-3} and 0.2 US$.m^{-3}. In summary, the MBRs still have a higher operating cost than the conventional CASP process but comparable with tertiary treatment.

3.2 ENERGY CONSUMPTION IN FULL-SCALE FACILITIES

As a general trend, the specific energy consumption tends to decrease when the size of the plant, the flow rate, or the served population equivalent (PE) increases, and the actual utilization of the hydraulic capacity of the plant is maximum or close to its peak flow design capacity (Gabarrón et al., 2014; Krzeminski et al., 2012). This is due to the ability to exploit economies of scale in larger systems, which results in larger but more efficient equipment, better performing automation and regulation, and, in many cases, more and better-trained personnel operating the plant. Barillon et al. (2013) found that hydraulic and organic loads are the most important operating parameters

influencing MBR energy efficiency. Most of the investigated MBR facilities are operated at lower loads, resulting in higher specific energy consumption due to the significant fraction of fixed energy consumption.

Typically, the processes and their associated energy spent on membrane operations include i) membrane aeration, ii) membrane feed pumps (supply), iii) sludge recirculation, iv) permeate extraction, v) backwash, and chemical cleaning pumps. Energy consumption associated with biological treatment processes such as aeration for biological purposes, propellers, and/or mixers is considered related to the biological treatment component. Other energy consumption required for plant operation is generally referred to as "the rest". This may include influent pumping, pre-treatment, sludge post-treatment, building heating, electricity for offices, and control systems.

Additionally, the components of the treatment plant included in the data considered for analysis should be verified, as different plants are designed differently and may incorporate additional processes not found in other plants. For example, post-treatment of activated sludge such as thickening, dewatering, or incineration may vary between locations. A comparison of the various MBRs is almost certainly incomplete without these details. Nonetheless, such information is frequently omitted, making it difficult to conduct a fair comparison. Most of the published studies have distributed the energy consumption data among different consumers and varied from study to study, making it hard to reasonably draw generic components.

3.2.1 Specific energy consumption

Energy cost in the MBRs contributes, on average, 48% of the total operating cost (Wang et al., 2020), out of which total aeration cost lies in the range of 40 -80% (Gabarrón et al., 2014; Kimura and Uchida, 2019; Sun et al., 2016; Xiao et al., 2019). According to the literature survey of peer-reviewed publications from the last decade, energy consumption in 25 full-scale facilities (1000- 20,000 $m^3.d^{-1}$) located in different geographical locations ranged between 0.46 - 2.2 $kWh.m^{-3}$ (Barillon et al., 2013; Gabarrón et al., 2014; Iglesias et al., 2017; Krzeminski et al., 2012). According to the most recent study from China, MBRs with treatment capacities ≥ 50 000 $m^3.d^{-1}$ cost 0.3–0.5 $kWh.m^{-3}$ for municipal wastewater (Zhang et al., 2021).

3.2.2 Energy consumption distribution by consumer

As per the analysis of the data collected from the literature survey and presented in **Fig. 3.2**, the share of membrane scouring to mitigate fouling varies in the range of 23-74 % (Park et al., 2015; Krzeminski et al., 2012; Barillon et al., 2013; Fenu et al., 2010c; Maere et al., 2011). In the recent past, several efforts have been dedicated to reducing and optimizing the cost of membrane aeration associated with the mitigation of membrane fouling. However, no definitive solution has been proposed (Krzeminski et al., 2017). The biological process aeration accounts for 1–40% of the total.

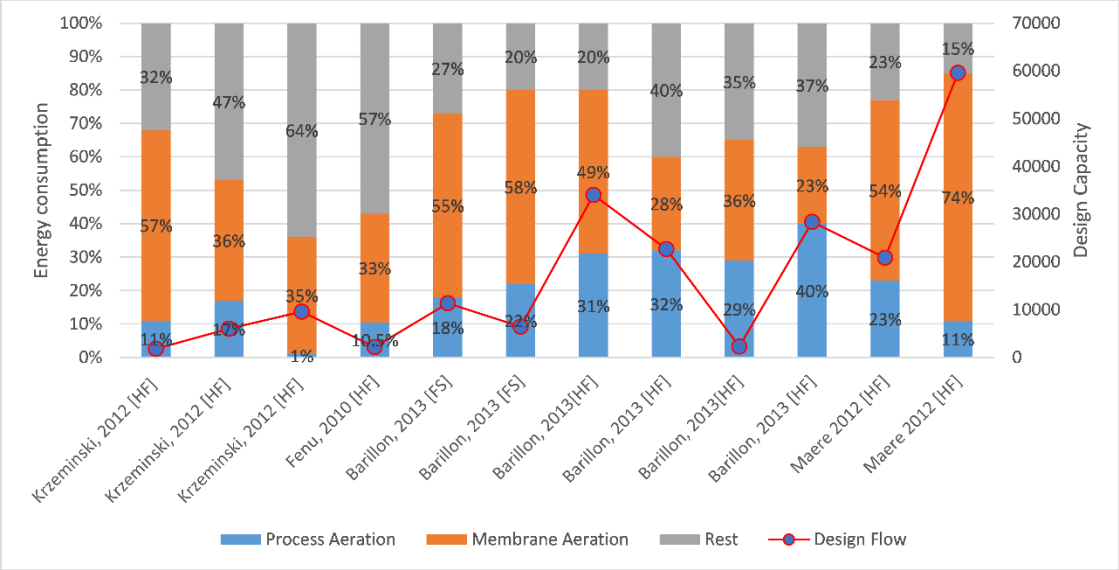

Fig. 3.2: Energy consumption distribution in full-scale MBRs

Data related to other energy consumers such as mixers, influent pumping, permeate production, chemical cleaning, permeate pumping, recirculation, foaming breaking, and coagulant addition sensors is not reported in all studies, making it difficult to compare their energy use with energy spent on aeration. Nonetheless, from the studies above, the part of mixing ranges from 7 to 43%. It ranges from 0.1 to 6% for permeate pumping and recirculation ranges from 6 to 22%.

3.3 SUMMARY AND IMPLICATIONS

Operational cost data, and in particular energy consumption data, from full-scale MBR facilities is scarce and not completely available in the public domain. Based on the available data from the full-scale MBR with design capacities in the range of 1000 - 20,000 $m^3.d^{-1}$ located in different geographical locations, the specific energy

consumed varied in the range of 0.46 - 2.2 $kWh.m^{-3}$. While MBRs with treatment capacities ≥ 50 000 $m^3 \cdot d^{-1}$ cost 0.3–0.5 $kWh \cdot m^{-3}$ for the municipal wastewater.

Data from limited peer-reviewed papers are generally available in the format of $kWh.m^{-3}$ and are rarely reported in the form of $kWh.kg^{-1}$ pollutants removed. The frequently used metric, i.e., $kWh.m^{-3}$ can be misleading, for comparisons of different regions, as systems with input wastewater of low pollution load would appear more efficient. Practical research should be dedicated to exploring the operational cost with a detailed breakup of the distribution of the various energy consumption units.

Chapter 4: Mathematical Modelling of MBRs

In most cases, the full-scale MBR plants are operated and maintained as per the recommendations and guidelines of the manufacturers, and further optimization is not usually practiced. In terms of time and resource requirements, modeling is a valuable tool for assessing and simulating the performance of various alternatives, providing knowledge on the mechanism occurring within the given system and affecting the performance of the MBR, resulting in a reduction in operational costs. The design, prediction, and control of MBR systems are greatly aided by calibrated and validated models that depict the MBR process. The advantages of MBR technology may be fully realized with the help of comprehensive and fully integrated models that are also useful in real-world applications.

This chapter presents models for individual (e.g., biological, filtration, and chemical processes) as well as integrated aspects of the MBR wherein several processes are interacting, and it is necessary to consider those aspects. The unmodified and modified ASMs applications to model biological processes in MBRs are discussed with reference to published works. Furthermore, models that describe the filtration and fouling phenomena in MBRs are presented with respect to their real applications at various scales.

4.1 MATHEMATICAL MODELS AND MODELING APPROACHES

A model is characterized by describing and depicting the properties in mathematical terms of systems functioning and associated events happening in reality (Stockburger, 1996). Nonetheless, a model does not contain every aspect of the real system because of the simplicity to be maintained and the number of aspects of the system under consideration. A model is the mathematical representation of a system in the form of multiple equations of various kinds and orders used to relate the inputs to outputs for the system being modeled. A well-defined mathematical model helps to accurately understand and predict the process evolution and analyze and manipulate it for process optimization for specific purposes, including nutrient removal optimization and energy

optimization. A model provides an alternative to laboratory scale, pilot scale, and even full-scale experiments, which are usually not possible in reality due to a number of limitations, including time and resource constraints, and to run experiments, especially at the full-scale.

Mathematical models can be divided into three distinct types (Truong-Meyer, 2012), i.e., i) mechanistic (white-box) approaches, which use chemical, physical and biological laws to describe a process; (ii) empirical (black-box) methods, which are based on empiricism and do not use laws; (iii) semi-empirical (grey-box) models, use both mechanistic and empirical knowledge (Gernaey and Sin, 2011; Robles et al., 2013; Sin and Al, 2021) as presented in **Fig. 4.1**. It means the more mechanistic the model is the greater is its explanatory power.

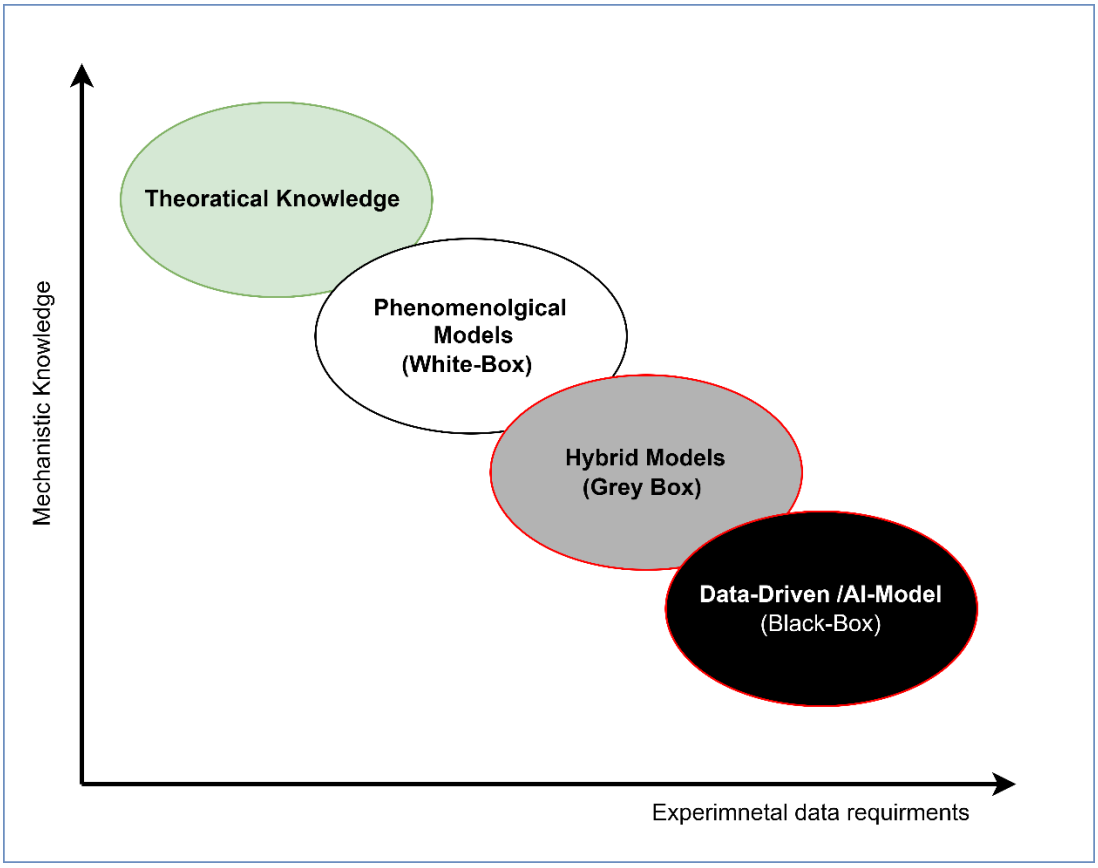

Fig. 4.1: Different types of models and their relative ranking (Truong-Meyer, 2012)

4.1.1 Empirical models

Data-driven models do not need any knowledge of the phenomena occurring in the system; by learning from input and output data, their parameters are adjusted in order

to predict the functioning of the system (Gernaey and Sin, 2011). Data-driven models have a structure of their own, but this is totally predetermined by the modeler in order to achieve the desired match and has nothing to do with the actual inner physical, biological, or chemical process knowledge. These are solely based on linear or non-linear correlations between inputs and outputs (Liang et al., 2006). This approach is preferable to the mechanistic method when the physical principles at the basis of the observed behavior are not clearly understood or when a mechanistic model is too complex or too difficult to calibrate. These models are often called *black-box models* when the inner model structure is totally inaccessible or grey-box models when a partial internal description is possible (Sin and Al, 2021). Several data-driven models are used to predict the effluent quality and develop robust and intelligent data-driven process control systems. For example, depending upon the mathematical approach, the most popular being the principal components analysis –PCA (Praus, 2019), autoregressive moving average –ARMA (Boyd et al., 2019), autoregressive exogenous –ARX with external input models (Jonsdottir et al., 2007), neural networks –NNs (Byliński et al., 2019), long short term memory - LSTM models (Wu et al., 2021; Yaqub et al., 2020) and fuzzy models –FMs (Nadiri et al., 2018; Suard et al., 2019) are widely used in wastewater process modeling. In all cases, the model structure is dependent on the method, and its dimensionality is selected through a compromise between model performance and computational complexity. This is generally accomplished by optimization (using algorithms, e.g., Bayesian) of the hyper-parameters of the model (Sin and Al, 2021).

4.1.2 Semi-empirical or hybrid models

Stochastic grey-box or hybrid models combine black-box models (e.g., artificial neural network-ANN) with trusted white-box model equations (Gernaey et al., 2004), with the objective of improving physical knowledge as explained in **Fig. 4.2**. The motivation behind the adaptability of the hybrid modeling in WWT process modeling is to improve the predictions of the first principles models, i.e., mechanistic ASMs or filtration models, and hence correct the errors/uncertainties present in the mass balances. Often, hybrid models are used to predict complex process phenomena, such as full-scale wastewater treatment plants. Anderson et al. (2000) integrated a white box model (ANN) to learn from the biological kinetic rates from the process data in the mechanistic model (ASM2d) using a parallel combination. The application of their

approach to a more complex problem involving phosphorus kinetics was not successful. Similarly, Lee et al. (2002) also designed a hybrid neural network based on a simplified mechanistic model (ASM1) and achieved much more accurate predictions with good extrapolation properties than purely mechanistic and data-driven approaches.

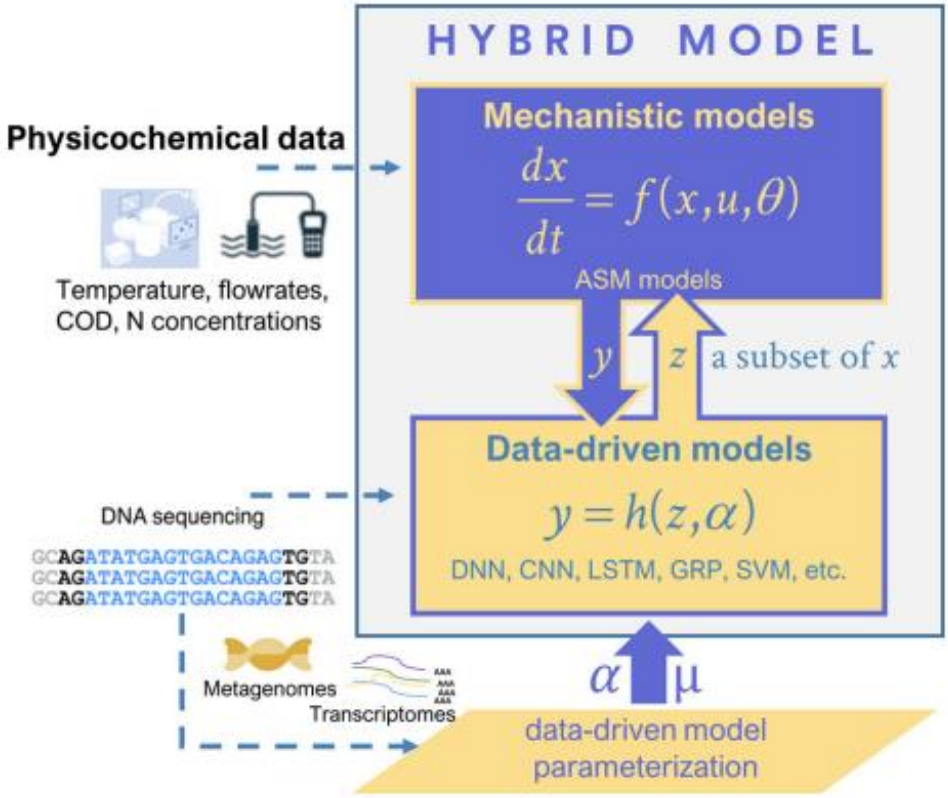

Fig. 4.2: Hybrid or grey-box models (Sin and Al, 2021)

In another work, Fang et al.(2010) used a serial combination to model the errors from a mechanistic model (ASM3-BioP) with a neural network to improve the predictions of effluent COD, NH_4, and PO_4^{3-}, similar to the application of extended Kalman filter to learn from the errors (Miron et al., 2017).

4.1.3 Phenomenological models

The most widely used wastewater treatment process modeling approach is phenomenological or mechanistic (Gernaey and Sin, 2011; Hvala and Kocijan, 2020). A mechanistic model uses equations that represent the phenomena occurring in the system. When solved, these models predict the behavior of the system. The

unquestionable advantage of this modeling approach is to gather knowledge about phenomena happening within the system.

4.1.3.1 Mechanistic biological models

The ASM family is a set of mathematical models in the form of algebraic and ordinary differential equations (ODEs) to kinetically describe the biological transformation of pollutants such as COD, nitrogen, and phosphorus, depending upon the type of ASM model; carried out by the micro-organisms. The biological processes are represented as biochemical reactions with stoichiometric relationships and kinetic equations based on Monod-type kinetics in a matrix format (commonly known as "Petersen" or "Gujer" matrix). A stoichiometric and composition matrix, a rate vector, and other information like units and names are all included in the matrix format. Gujer (1985) introduced the matrix notation, enabling modelers to communicate in a more ordered and organized manner for an easy implementation of the model in any computational system or software.

A couple of detailed reviews have been published during the last two decades, focusing on comparing the model structures, limitations, and differences among the processes such as hydrolysis, growth, and decay of organisms, including their limitations for phosphorus removal. The first detailed review was conducted by (Baetens, 2001), considering all the published models, metabolic and ASM (original and modified), and combinations till 2000. Following that, Gernaey et al., (2004) published a detailed review of the white-box kinetic models (ASM1, ASM2, ASM2/ASM2d, ASM3 TUDP, Barker & Dold's model, and ASM3-BioP) and discussed that how the objective of the modeling influences the model selection from the available range, data gathering, and model calibration. The authors addressed the grey box, black-box, and hybrid models and their potential applications in WWTPs, such as supervisory control system development. Following this, Hauduc et al. (2013) compared seven published models, including ASM1, ASM2d, ASM3, ASM3-BioP, ASM2d-TUD, Barkers & Dold's model, and UCTPHO^{+} using a structured approach and dealt with the difficulties in comparing models as highlighted by Baetens (2001).

These models are compared based upon several standard processes, including i) hydrolysis, ii) fermentation, iii) growth and decay of OHOs, iv) growth and decay of ANOs, v) growth and decay of PAOs, vi) storage of PHA and vii) storage of

polyphosphate. Following the works of Gernaey et al. (2004) and Hauduc et al. (2013), the mini-review of Zuthi et al. (2013) compared the five models (ASM2, ASM2d, TUDP, UCTPHO^{+}, and ASM3-BioP) which took into account the phosphorus removal for the CASP and MBR along with the advantages and disadvantages of these models. The referred studies may be consulted for a detailed understanding of ASM models.

All these models can be organized under three groups as presented in **Fig. 4.3**, i.e., i) models considering the role of denitrifying PAOs, ii) models without considering the role of denitrifying PAOs, and iii) models with the incorporation of the PAO and GAOs.

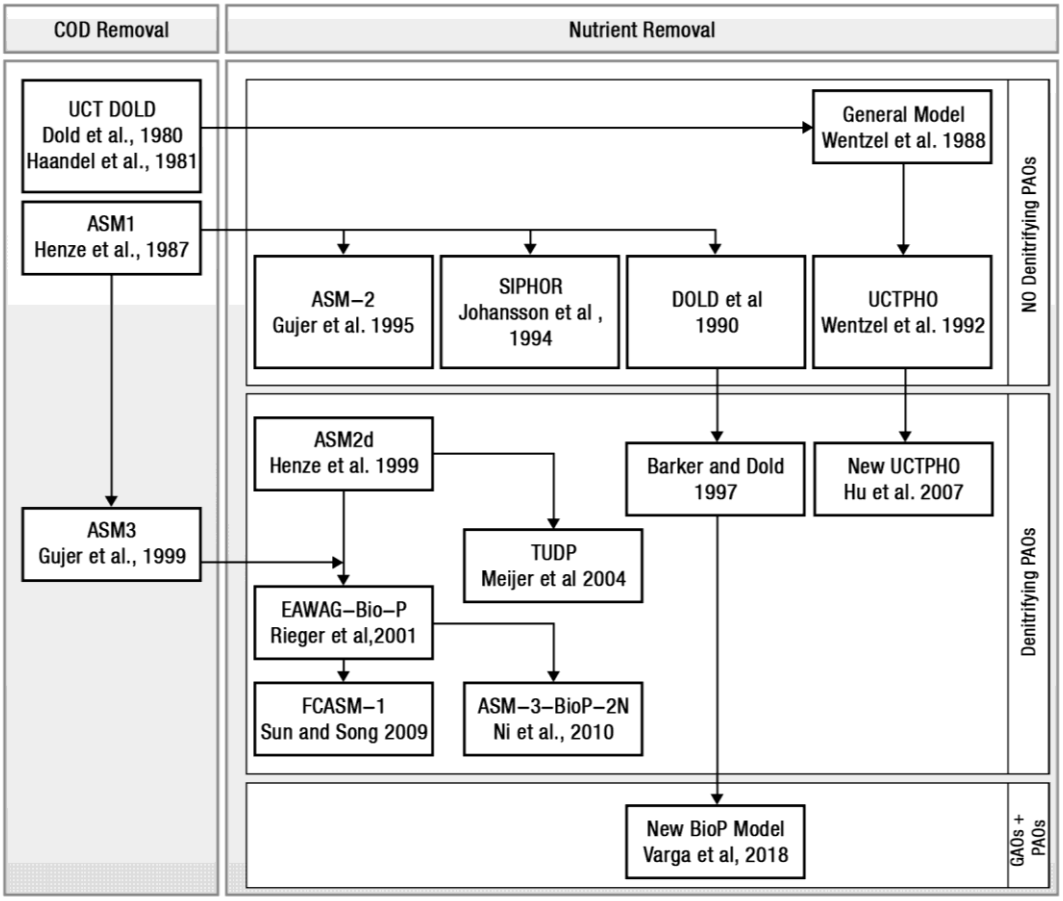

Fig. 4.3: Evolution and classification of the activated sludge models (Nadeem et al.,2022)

The applications of ASM are presumably meant for modeling the activated sludge processes operating conditions. These last ones are depend on the particular treatment process, varying within a typical range e.g., range of SRT 3-15 d, range of HRT 3-5 h,

and range of MLSS 1.5 - 4 $g.L^{-1}$ for completely mixed systems (Tchobanoglous et al., 2003). The following sections present the applications of the available unmodified and modified ASMs incorporating the SMPs and EPSs as major membrane foulants in the MBRs functioning.

4.1.3.2 Applications of ASMs to MBR

A detailed review by Fenu et al. (2010a), comprehensively presented the applications of the ASMs in MBRs, although no full-scale modeling study was carried out by that time. Therefore, the review did not address the concern of applying the ASMs to full-scale MBRs, but only to lab and bench scales.

Un-modified ASMs: Following section reports the major conclusions from the detailed review of Fenu et al. (2010a), in case ASMs are applied without incorporating the concepts of EPS/SMPs:

- The difference in the operational specificities (see **Table 4-2** *)* between CASP and MBR had the greatest impact on nitrification parameters. However, depending on the hydrodynamic and operational conditions of the MBRs, it is recommended to determine the kinetic parameters as a cohesive set for each new study.
- Denitrification rates and characteristics seemed identical in MBR and CASP, except for the dissolved oxygen half-saturation constant KOH, which describes oxygen toxicity in anoxic zones. This was due to the smaller floc size in MBRs compared to CASP.

Furthermore, based on the comprehensive review paper published as a separate study (Nadeem et al., 2022) under this Ph.D. work, it was concluded that ASMs could successfully simulate the BioP- removal in MBRs when fundamental differences in MBR functioning compared to CASP are considered (*refer to* ***section 4.2***). However, due to complete biomass retention in MBRs and especially the PAOs due to their increased size, several PAOs related model parameters required adjustments through calibration approaches. In some cases, batch tests were conducted to establish the stoichiometry of the PAOs and GAOs. Most of the studies considered calibrating the kinetic parameters, while a few studies even calibrated the stoichiometric parameters

as well, which seemed necessary to accommodate the effects due to different stoichiometric rates induced by the GAOs and PAOs competition for phosphorous uptake. In the absence of modeling experience from full-scale MBRs, Fenu et al. (2010a) suggested carrying out full-scale modeling studies to rule out the difference between lab-scale and full-scale applications. Considering the needs, Delrue et al. (2010) and Fenu et al. (2010a) contemporarily presented full-scale MBR modeling studies with ASM-1 and AM2d with plant capacities of 1,600 $m^3.d^{-1}$ and 5,000 $m^3.d^{-1}$, respectively.

Delrue et al. (2010) found AMS-1 suitable for modeling nitrogen removal in full-scale MBR (special precautions were taken), especially considering the biological tanks as completely mixed and the volume of the membrane tanks equal to zero with 100% solids retention and ignoring the fouling phenomenon. The validity of the model is limited to configuration and continuous DO setpoint < 1.5 $mg.L^{-1}$ allows simultaneous nitrification-denitrification (SN-DN). Despite complex configuring (recirculation, variation in tank filling, backwashes), the prediction of sludge production was accurate. The presence of two simultaneous aeration systems (fine and coarse bubbles) - a non-ideal mixing system and limitations in oxygen transfer made it challenging to predict the DO concentrations. The oxygen transfer coefficient was not calibrated but extracted through a long-term mass balance approach. SN-DN and non-ideal mixing required a high half-life saturation coefficient for nitrate up to 3.0 $gN.m^{-3}$ Autotrophic growth rate was found to be time-dependent.

Fenu et al. (2010c) calibrated the ASM2d model for oxygen transfer, nitrogen, and phosphorus removal as well as for aeration energy optimization. ASM2d model was adopted, and ASM parameters and the half-saturation coefficients were adjusted. A lower K_{OA_AUT} theoretically improved the aeration energy performance by increasing the O_2 mass transfer. It was found that a variation of the parameter from 0.5 (default) to 0.2 $mgO_2.L^{-1}$ yielded a very modest decrease in the aeration power consumption. At the same time, the TN removal increased significantly by 2.5%. The TN performance increase is significant despite the irrelevant energy saving since the O_2 mass transfer rate improvement applies to both fine and coarse bubble aeration systems. The phosphate removal could not be modeled successfully with ASM2d. The modeled PO_4 concentration in the effluent was higher than the observed values. The phosphate

accumulating organisms (PAOs) were outcompeted in the model since PHA could not be sufficiently stored, even though the storage rate was arbitrarily increased. The coarse bubbles provided for scouring purposes in the membrane chambers could potentially have a role in the biological process if a different process layout were used. Similarly, Daigger et al. (2010) modeled the Traverse city full-scale MBR plant with a capacity of 32,000 $m^3.d^{-1}$ and the Broad Run pilot plant using ASM2d. The publication provided no details about the model structure, calibration, and validation processes.

Maere et al. (2011) used ASM-1 as a basis to devise a benchmark simulation model, i.e., BSM-MBR, to simulate a full-scale MBR facility with a capacity of 1,800 $m^3.d^{-1}$ and a membrane surface area of 71,500 m^2, to evaluate operational and control strategies in terms of effluent quality and operating costs. Default kinetic and stoichiometric parameters were used to simulate COD, TSS, NH_4, and energy consumption in various processes, particularly in process aeration. Steady-state and dynamic simulations revealed that BSM-MBR, as expected, outperformed conventional BSM1 for effluent quality, mainly due to complete retention of solids and improved ammonium removal from extensive aeration combined with a higher biomass level. It is pertinent to mention that the simulation results were not validated with experimental data.

Gabarrón et al. (2015) used ASM2d in WEST simulation software to model a full-scale MBR with a capacity of 7,000 $m^3.d^{-1}$, and default kinetic and stoichiometric parameters were used for the system description, while the data from the experimental campaigns were used to calibrate and validate the model. The model was able to simulate the system for NO^{3-}–N, NH^{4+}–N, and TSS with accuracy, in terms of mean square relative error (MSRE) of 13%, 15%, and 1.5%, respectively. This demonstrated that the unmodified ASM could be applied to the full-scale system, subject to the availability of sufficient data from the plant SCADA system of the plant. In usual practice, it is not the case. The modelers may require additional data sets acquired through dedicated experimental campaigns, which are time-consuming and often costly.

Large fractions of flocs, bacteria, biopolymers such as polysaccharides, proteins, and organic colloids are mostly retained in the bioreactor of an MBR, which may

significantly affect biodegradation kinetics within the bioreactor. The ASM models do not specifically consider the impacts of these retained particles on the bio-kinetics. However, in MBR systems with typically low organic loads, the retained molecules may significantly affect the metabolic path allowing further use of carbon-based metabolites. Furthermore, ignoring SMP and EPS formation may lead to a general overestimation of true cellular growth rates, and this would severely underpredict the COD effluent concentrations (Fenu et al., 2010a; Jiang et al., 2009).

Applications of modified ASMs: this section presents the application of the modified ASMs in MBRs. Similar to applications of unmodified ASM, there is a dearth of full-scale modeling studies with modified ASMs.

Fenu et al. (2010c) used the ASM2d-SMP model originally developed by Jiang et al. (2008) to simulate the MBR part of a full-scale municipal hybrid MBR. The authors pointed out the defects in the utilization associated products (UAP) calibration protocols suggested by Jiang et al. (2008) and the poorly represented degradation kinetics of UAP. The UAP was found to be significantly more prevalent than the biomass associated products (BAP), and the SMP rejection rate of the membranes was found to be susceptible to influent dynamics. Employing a single fixed SMP retention factor (as most studies do) would thus appear inappropriate. The model was fairly able to describe SMP, COD, NH_4, and NO_3 measurements on a daily basis, but detailed dynamics and results were not available in the publication. Based on their findings, the authors concluded that the modeling of SMPs did not improve the predictions for nutrient removal, sludge production, or energy consumption. Fenu et al. (2010a) concluded that using ASMs extension with the EPSs/SMPs approach is appropriate only if the following goals are pursued:

- Integrated modeling with a focus on linking biology with membrane fouling
- Prediction of soluble chemical oxygen demand (COD), and
- Modeling systems with high SRTs.

Extending the ASMs with EPS-SMPs modules, without absolute necessity, makes the calibration cumbersome, especially in integrated models where a number of aspects of the process are considered altogether, and the structure of the model is already complex.

4.1.3.3 Mechanistic chemical precipitation models

Several chemical precipitation models were developed for phosphorus removal in wastewater systems, and very few of them have been adopted for precipitation modeling in CASPs and MBRs. The precipitation model commonly used in combination with ASMs is briefly discussed regarding its conceptualization and processes involved, application in MBR modeling, and the -phosphorus removal limitations.

ASM2d is mainly being used for modeling chemical P-removal in MBRs. Chemical precipitation models employ three main approaches: i) chemical equilibrium approach, ii) kinetic model approach, iii) combined chemical equilibrium-kinetic approach, and geo-chemical complexation (De Haas et al., 2000; Smith et al., 2008). These precipitation models are briefly reviewed for quick comparison in terms of processes considered, limitations, and their usefulness for coupling with the biological and filtration models in the MBR. **Table 4-1** presents a comparative summary of available chemical precipitation models, and further details could be assessed from a section of a review published under this Ph.D. work (Nadeem et al., 2022).

The literature review has revealed that chemical precipitation models now have improved the ability to predict the effluent phosphorus removal for even low concentrations. However, these are still unable to reliably describe the removal kinetics and impacts of the metal complex aging with higher SRTs. Not even a single study has been reported for their application and validation with the system operating at higher SRTs such as MBR. The most recent model (Hauduc et al., 2015) yet requires validation at full-scale. Furthermore, the models have not been tested to predict chemical phosphorus removal behavior in complex waters, where organics and other organisms could obstruct removal mechanisms**.** Improving the models' ability to explain these processes would result in more stable effluent phosphorus levels and chemical sludge output at lower coagulant dose rates, resulting in cost savings in chemical and sludge treatment.

Table 4-1: Comparative assessment of the chemical phosphorus removal models

	(Ferguson and Kina. 1977)	*(Luedecke et al., 1988)*	*(Briggs, 1996)*	*WEF,1998*	*IWA-ASM2d Model, 1999*	*(Smith et al., 2008)*	*(Hauduc et al., 2015)*
Modeling Approach							
Kinetic model					√		
Chemical equilibrium Model	√	√		√		√	√
Combined kinetic-equilibrium model			√				
Geo-chemical reaction modeling						√	√
System behavior (change in concentration over time)							
steady state	√	√		√		√	√
dynamic			√	√		√	√
Removal Mechanisms Considered							
hydrolysis		√	√				
dissociation		√	√				
precipitation		√			√		√
Co-precipitation	√		√	√		√	√
adsorption		√	√			√	
De-sorption			√				
surface complexation/aging							√
biological nutrient requirements			√				
dissolution			√				
Coagulants Considered							
Aluminum	√		√	√			
Ferric		√	√	√	√		√
Type of model concerning calculations							
Empirical	√	√	√				
Mechanistic					√	√	√
pH dependence	√	√	√				
Alkalinity Dependence							
Influence of Aging/surface consolidation							
Ability to Predict Low P-Concentration							
Limited	√	√	√				
Excellent				√	√		√
P-species Considered							
Orthophosphate	√		√	√	√		√
Total Phosphorus		√					
Influent P-Fractionation			√				

Further research is needed to explore the applicability of these precipitation models at full-scale MBRs operating at higher SRTs and with smaller floc size, generally undesirable for effective coagulation, and operating under higher shear induced by the coarse bubble aerations.

4.1.3.4 Mechanistic fouling models

The membrane performance in the MBR system, both qualitative and quantitative, usually decrease over time due to fouling resistances discussed in ***section 2.2***. Multiple stand-alone mechanistic models of membrane fouling that account for the combined impacts of the many distinct fouling resistances to the physical fouling phenomena are available, which could be classified into three different categories, i.e., i) empirical hydrodynamic model (Liu et al., 2003), ii) fractal permeation model (Meng et al., 2005), and iii) resistance in series (RIS) models (Li and Wang, 2006). Multiple reviews have thoroughly covered filtration and fouling models (Guo et al., 2012; Hamedi et al., 2021; Naessens et al., 2012; Ng and Kim, 2007). RIS is mainly used to explain the effect of various fouling processes on the membrane permeability (Naessens et al., 2012) and is therefore discussed here in terms of its applicability for modeling full-scale MBRs.

4.1.3.4.1 RIS fouling model

In the RIS model, membrane resistance to flux is calculated using Darcy's law (Choo and Lee, 1996), assuming that the osmotic pressure is negligible (see **Eq. 4.1**), while total membrane resistance is given by **Eq. 4.2.**

$$J = \frac{TMP}{\mu_p \cdot R_{total}} \quad 4.1$$

$$R_{total} = R_m + R_p + R_c \quad 4.2$$

The resistance R_m is the non-varying intrinsic resistance of the membrane typically determined by Darcy's law and refers to an initial state of the membrane, i.e., newly bought or newly cleaned. R_p is the pore fouling resistance caused by solute deposition inside the membrane pores, and this can be calculated by **Eq. 4.3** (Li and Wang, 2006).

$$R_p = r_p \times V_p \quad 4.3$$

Cake layer resistance (Rc) in **Eq. 4.2** can be calculated according to the **Eq. 4.4** proposed by Lee et al. (2002), where r_c is the specific cake resistance, V_p is the total

volume filtered, Am is the surface membrane filtration area, X_{TSS} is the total suspended solids, and k is a coefficient with value in the range of 0 - 1.

$$R_c = \frac{r_c \times k \times Vp \times XTSS}{Am} \quad 4.4$$

Cho et al. (2005) derived a logistic relationship (**Eq.** 4.5) among specific cake resistance, MLSS, bound EPS (bEPS), TMP and expressed the specific cake resistance (rc) as a function of bEPS, TMP, MLVSS, and viscosity (μ)

$$r_c = \frac{TMP}{\mu^2}\left(9.3E^{12} + 1.803E^{4}\left(1 - \left(-115\left(\frac{bEPS}{MLVSS}\right)\right)\right)^{36.66}\right) \quad 4.5$$

Later, Zarragoitia-González et al. (2008) modified the equation assuming bound EPS (bEPS) is associated with SMP and expressed the bEPS in terms of SMP concentration in the bioreactor (S_{SMP}) with an appropriate coefficient, and the modified **Eq. 4.6.**

$$r_c = \frac{TMP^{Pr}}{\mu^2} \times \left(a + b\left(1 - \exp\left(-c\left(\frac{S_{SMP}}{0.8 \times X_{TSS}}\right)\right)\right)^{d}\right) \quad 4.6$$

Where, a, b, c, d and p_r are empirical constants.

The advantages associated with the RIS model are that it accounts for cleaning cycles and characterizes fouling development over time with varying sludge concentrations, filtration fluxes, aeration intensities, and backwashing. Several MBR modeling studies have used the RIS approach to model reversible and irreversible fouling (Wintgens et al., 2003; Zarragoitia-González et al., 2008; Mannina et al., 2018; Gabarrón et al., 2014).

The specific cake resistance equation given by Cho et al. (2005) has been adopted by several researchers without re-determining its coefficients linked to the specificities of the MBR system under consideration. Especially, the EPS, SMP, and TMP are likely to vary from system to system and with variations in the sludge composition. It should also be taken into consideration that the system used by Cho et al. (2005) was a dead-end module and therefore was under direct pressure, while the membrane in the MBR module is not under direct pressure. The adopted values of the coefficient in the large

variety of studies change a lot (Mannina et al., 2018; Zarragoitia-González et al., 2008), and this presents a calibration challenge for the modelers.

The specific cake resistance equation proposed by Cho et al. (2005) is not universally applicable for all kinds of MBR systems (lab-full scale), especially considering the fact that the equation was developed for a lab-scale system, which is quite different from full-scale ones, with specific sludge characteristics and operating TMP. Furthermore, at the time when this equation was proposed, precise definitions for today's known variations of biopolymers such as EPSs, bound EPSs, loosely bound EPSs, extracted EPSs (eEPSs), free EPSs, bio-polymeric clusters (BPCs, i.e., group of SMPs and EPSs), and SMPs were not set up. Keeping in view of the recent understanding of the EPSs and SMPs, further experiments for expressing the specific cake resistance as a function of TMP, MLSS, SRT, F/M ratio, SMPs, EPSs, coagulant dose and rate of chemical cleaning is expected (Mannina et al., 2020).

4.2 CONSIDERATIONS FOR MECHANISTIC MBR MODELING

It is well understood that MBRs operate under different conditions than CASP and require a comprehensive understanding of the processes and adjustments in models initially developed for CASP to successfully simulate the transformation of pollutants and biomass evolution. The need for adjustments in ASMs' applicability to MBR is mainly attributed to: i) different microbial compositions leading to the calibration /re-adjustment of stoichiometric and kinetic parameters ii) higher biomass concentration leading to reduced oxygen transfer and uptake, iii) production of EPSs (linked to flocs) and SMPs (dissolved) and their accumulation onto the membrane surface iv) additional aeration involved in membrane scouring and re-circulation of oxygen saturated sludge from MBR to the aerated/unaerated zones, and v) the role of membrane filtration on nutrient removal (Fleischer et al., 2005; Hai et al., 2018; Judd, 2010; Maere et al., 2011; Verrecht et al., 2008). The comparison of these parameters for CASP and MBR is proposed in the tabulated format in **Table 4-2**.

Table 4-2: Consideration in applying ASMs to the MBRs process modeling

Parameter/Factor	***Conventional Activated Sludge***	***Membrane Bioreactor***
Microbial Composition	CASPs are operated at lower SRTs ranging between 4-15 days (Hai et al., 2018; Judd, 2010)	SRT of MBRs ranges between the same to three-time the CASP's ones (Hai et al., 2018). MBR promotes slow-growing micro-organisms such as nitrifiers and micro-organisms usually washed out in a CASP system while the membrane retains 100%.
MLSS	CASP is operated at MLSS concentrations ranging between 1500 to 3000 $g.m^{-3}$ (Hai et al., 2018)	MBRs are operated at higher MLSS concentrations ranging between 4000–15,000 $g.m^{-3}$ (Hai et al., 2018) and, therefore, lower F/M ratio. Higher MLSS, in combination with higher SRT, causes stress to the micro-organisms in an MBR, which requires more energy for cell maintenance and leaves less energy for cell production. Higher MLSS may induce the competitive advantage of GAOs over PAOs.
EPS/SMP	EPS/SMP produced in CASP are washed away and/or removed through sludge. EPS/SMPs are not considered in unmodified ASMs	Accumulation of the EPS/SMPs onto the membrane surface may affect the fouling and the biological process. EPS/SMP concentration in MBR sludge may differ from the CASP sludge due to different microbial communities and the F/M ratio.
Fine Bubble Aeration	Aeration is used for carbon matter degradation and nitrification conversion.	Aeration is used for carbon matter degradation and nitrification. However, due to higher MLSS concentration (unfavorable) and smaller floc size (favorable), mass transfer limitations have been reported

Parameter/Factor	*Conventional Activated Sludge*	*Membrane Bioreactor*
		differently in MBRs than in CAPs (Fenu et al., 2010a).
Coarse bubble aeration	Coarse bubble aeration is not involved.	In addition to fine bubble aeration, coarse bubble aeration aims at scrubbing the membrane surface to mitigate the membrane fouling. It creates turbulence and affects the floc size and mass transfer processes.
Separation	separation is carried out by the clarifiers (secondary), and the phenomenon is modeled through clarifier/settling models (Hai et al., 2018; Henze et al., 2008)	Separation is carried out by physical media (membrane). MBR requires a sub-model to simulate filtration–fouling phenomenon and retention of the soluble/dissolved fraction of COD and nutrients (Di Bella et al., 2008; Mannina et al., 2018).

4.3 INTEGRATED MBR MODELS AND THEIR APPLICATIONS

An integrated MBR model incorporates both the biological and filtration processes (Mannina et al., 2021), i.e., one that considers the reciprocal effect of MBR biology on membrane fouling. An integrated model requires a biological sub-model (ideally a suitable activated sludge model with an additional chemical precipitation module), a hydrodynamic sub-model (flow), a filtration-fouling sub-model, and an interface (via suitable variables) to fully connect these models. Sometimes, additional modules such as process aeration, COD fractionation, and pH general models are added based on the intended requirements and level of complexity. These integrated models are proved to better simulate/model the MBR system's behavior (Hamedi et al., 2021; Mannina et al., 2021).

In the last two decades, several efforts have been dedicated to developing an integrated model capable of simulating the bio-kinetic and filtration-fouling performance of MBR. However, the majority of these efforts are limited to bench-scale (<0.05 $m^3.d^{-1}$) and pilot-scale (<1 $m^3.d^{-1}$) systems (Di Bella et al., 2008; Janus, 2014; Y. Lee et al., 2002; Mannina et al., 2011; Sarioglu et al., 2017; Zarragoitia-González et al., 2008; Zuthi et al., 2017) while only a few integrated models have been developed for full-

scale (>10,000 $m^3.d^{-1}$) MBR systems (Gabarrón et al., 2015; Suh et al., 2013; Wintgens et al., 2003). Only, Gabarrón et al.(2015) successfully validated the ASM2d-RIS model with data from a full-scale facility of 15,000 $m^3.d^{-1}$, while studies by Wintgens et al. (2003) and Suh et al.(2013) were not validated.

To date, no study has been found for the super-large scale (≥100,000 $m^3.d^{-1}$) facilities (Nadeem et al., 2022) even though the total number of super-large scale facilities has now increased by over 62 (Xiao et al., 2019) with a cumulative treatment capacity over 10 million $m^3.d^{-1}$ (Xiao et al., 2019; Zhang et al., 2021). The following sections briefly assess several literature-based integrated model development attempts.

4.3.1 Integrated models state of the art

A detailed summary of several studies involving integrated MBR modeling is presented in **Table 4-3** with a comparative assessment of the size, bio-kinetic models, and its components, as well as considerations involved therein. In all these previously published integrated modeling studies, ASM1 is widely used as the bio-kinetic model for simulating the biological processes in MBRs, with EPS or EPS-SMP modules to describe the organic matter degradation and nitrification-denitrification as well as production and fate of SMPs and EPSs.

In order to integrate fouling in MBR in the simulation, Lee et al. (2002) combined an ASM1-SMP model from Lu et al. (2001) with a resistance-in-series fouling model. In this way, the authors considered MLSS an important factor for fouling. They considered the concentration of SMPs negligible compared to MLSS, thus ignoring the pore fouling, and largely focusing on cake resistance. The model of Lu et al. (2001) was not balanced in terms of COD (i.e., biomass loss (Mannina et al., 2011b)) and did not include the deep-bed filtration effect in the filtration model as used by Di Bella et al. (2008). Later, Zarragoitia-González et al.(2008) and Di Bella et al. (2008) contemporarily presented rigorous integrated models incorporating SMP and EPS production and their fate. Both models became the basis for today's improved integrated models from this onwards. The biological model (ASM1-EPS-SMP) presented by Zarragoitia-González et al.(2008) is based on the modified bio- kinetic models of Lu et al. (2001) and Cho et al. (2003) to mimic the carbon and nitrogen removal performance of MBR. In this model, the filtration process is modeled based on the approach proposed by Li and Wang (2006), and dynamic specific cake

resistance is modeled by considering the approach proposed by Cho et al. (2005). The model of Zarragoitia-González et al.(2008) takes into account the dynamic effects of sludge cake attachment/detachment from the membrane under the influence of filtration and coarse bubble aeration. The model, however, did not include the influence of backwashing (Mannina et al., 2021) and the role of the cake layer as filter media based on deep-bed theory to remove organics and soluble fractions of the pollutants (Cosenza et al., 2013). Furthermore, the bio-kinetic model was not calibrated nor validated except for the oxygen transfer coefficient (K_La), which was measured experimentally though kept constant throughout the simulation runs. In addition, it did not include the adverse effects of elevated sludge concentrations on aeration efficiency and did not take into account the potential mass transfer limitations associated with MBR (Insel et al., 2011; Naessens et al., 2012). Furthermore, the model did not satisfy the continuity check for COD due to imbalanced stoichiometry (Cosenza et al., 2013; Hamedi et al., 2021; Mannina et al., 2011b).

The model presented by Di Bella et al. (2008) involved the same bio-kinetic as the one included in the model of Zarragoitia-González et al. (2008), while the filtration model of Wang et al.(2006) is modified to incorporate the role of cake layer as filter media (deep-bed theory) to remove the fraction of the soluble COD. In addition, backwashing is used as a driving force for attachment and detachment of the cake layer from the membrane instead of coarse bubble aeration as used by Zarragoitia-González et al. (2008). The model, however, did not include the role of EPS or SMPs in biofilm/cake formation. The specific cake resistance is assumed to be constant and independent of the MLSS and EPS/SMP concentrations and thus unable to explore the mass transfer limitations of MBR at higher MLSS concentrations. In addition, the filtration flow rate distributed over the membrane surface is averaged, which is a significant approximation for submerged MBR with hollow fiber membranes transfer capacities. It also ignored the influence of aeration on cake detachment and attachment (Mannina et al., 2011b; Zuthi, 2014). Similar to Zarragoitia-González et al. (2008), the model of Di Bella et al.(2008) used fixed K_{La} and did not take into account the actual aeration flow rates. Although the bio-kinetic model was calibrated using a sensitivity analysis approach and was validated with the experimental data of MLSS, COD, NH_4-N, and N-NO_3 but lacked validation of the TMP and fouling profiles.

The model of Di Bella et al.(2008) was later improved by Mannina et al.(2011) by including the sectional approach to accommodate the uneven filtration distribution in hollow fiber membrane and replacing the model of Lu et al. (2001) with a modified bio kinetic-model of Jiang et al. (2008), taking into account, the effect of coarse bubble aeration. The model was calibrated using global sensitivity analysis and validated for COD, MLSS, NO_3-N, and total resistance. Similar to previous studies, the model did not consider the real aeration flow rates and used the fixed K_{La} value for the entire simulation period. Furthermore, the model was again based on the assumption of Cho et al.(2005), wherein the TMP in case of dead-end filtration is assumed to be influential for the specific cake resistance increase. In the case of SMBR, the membrane reactor is not under any direct pressure (Suh et al., 2013), and therefore this assumption may require re-consideration.

Thus far, the models lack capabilities to describe the biological nutrient removal in MBRs. In a bid to improve integrated models, the model proposed by Cosenza et al.(2013) incorporated the ASM2d-SMP bio-kinetic model proposed by Jiang et al. (2008) and the filtration models proposed by Di Bella et al. (2008) and Mannina et al. (2011b). This enabled the MBR to fully describe the nutrient removal capabilities and filtration mechanisms. Again, the model carried forward the limitations of the model proposed by Mannina et al. (2011b). Furthermore, the model did not consider the removal of ortho-phosphate (PO_4^{3-}) by chemical precipitation. Suh et al. (2013) used a modified ASM3-EPS-SMP model of Janus and Ulanicki (2010) for EPS and SMP generation and degradation, and they also integrated it with the RIS model of Wang et al. (2006) for membrane fouling simulation. The authors have still not considered the contribution of SMP to membrane fouling and have only considered the concentration of EPS according to the logistic equation originally proposed by Cho et al. (2005). The model was calibrated to the extent of the RIS model using sensitivity analysis. However, due to the unavailability of the data from the full-scale facilities, this adopted model was not validated.

Most recently, Lindamulla et al. (2021) presented an integrated model which combined the ASM-1 with the EPS model suggested by Janus and Ulanicki (2010) and the SMP model of Jiang et al. (2008) for bio-kinetic modeling of MBR. The fouling is modeled using the approach suggested by Zuthi et al. (2017), considering the SMP as a major

foulant. The model, however, did not consider the specificities associated with dynamic K_{La} and specific cake resistance. Furthermore, the model did not consider the effect of coarse bubble aeration and backwashing on the attachment-detachment of the cake. Neither did it account for the effect of filtration –relaxation sequencing, which is generally the case for all commercial MBRs. Therefore, this model could be used for a specific system but cannot be universally applied for full-scale facilities operating with multiple fouling abatement controls.

Almost all the above discussed models lacked energy consumption modeling, except for the Zarragoitia et al. (2009), wherein energy consumption only due to coarse bubble aeration is modeled as a function of TMP, filtration-idle time, aeration flow, and filtrate volume. The study by Suh et al. (2013) presented a mathematical model with ASM3-EPS-SMP bio-kinetic model borrowed from Janus (2014) and a filtration model by Li and Wang (2006). In this way, they have modified the specific cake resistance equation of Cho et al. (2005), assuming that the MBR is not under any pressure, unlike dead-end filtration, and therefore, replacing the TMP with a fixed coefficient without describing the approach to estimate and calibrate this newly introduced coefficient. Similarly, another study by Janus (2014) used the bio-kinetic ASM1-EPS-SMP model in combination with the fouling model of Wang et al. (2006). At the same time, the specific cake resistance is dynamically modeled as a function of EPS/MLVSS by modifying the original approach of Cho et al. (2005). In the studies of Suh et al. (2013) and Janus (2014), the formation of the SMP had no link with the irreversible fouling phenomenon. Moreover, the integrated models presented were not validated due to a lack of experimental data from full-scale facilities.

4.4 OPEN LICENSE AND COMMERCIAL SIMULATION SOFTWARE

The modelers have used various special-purpose simulation software, which is far less straightforward than the general-purpose simulation environments such as MATLAB / SIMULINK and spreadsheets. The most frequently used simulation software in simulation studies in academia and industry are: BioWin, GPS-X, SIMBA, WEST (previously EFOR), SUMO, and EAWAG's AQUASIM. Simulators like ASIM, STOAT, Lynx, and JASS are primarily used in academia for research and teaching purposes. The wastewater treatment industry is also using relatively new simulators like DESASS (design and simulation of activated sludge systems) and EPD

(EnviroProDesigner) to design and optimize WWTPs. The comparative assessment of these simulation software could be found in already published study (Nadeem et al., 2022). The choice of the simulation environment depends upon the modeler's familiarity with the coding languages. It also depends upon the complexity of the system being modeled and leverage to kept for the flexibility of adapting/developing new modules for unit processes.

Table 4-3: Features of the published integrated MBR modeling studies

References	*(Y. Lee et al., 2002)*	*(Wintgens et al., 2003a)*	*(Zarragoitia-González et al., 2008)*	*(Di Bella et al., 2008)*	*(Zarragoitia et al., 2009)*	*(Mannina et al., 2011b)*	*(Suh et al., 2013a)*	*(Cosenza Alida et al., 2013)*	*(Mannina et al., 2018)*	*(Janus, 2014b)*	*(Lindamulla et al., 2021)*
bench scale [< 0.05 $m^3.d^{-1}$]	√		√								
pilot Scale [≥ 0.05 ≤ 10 $m^3.d^{-1}$]				√	√			√	√		√
full scale [>10 m^3≤ 100,000 $m^3.d^{-1}$]		√					√			√	
Super-large scale [> 100,000 $m^3.d^{-1}$]			NO -SUPER-LARGE-SCALE MODELING STUDY TILL DATE								
membrane surface area [m^2]	--	--	0.3	0.93	2.5		28,000	0.93	1.4		0.273
Reactor Volume[m^3]	--	--	0.105	0.013	1.0	0.19	6000	0.616	-	0.2	0.19
MBR configuration		A/O	A/O	A/O	A/O	A/O	2-stage A/O	UCT	UCT	A/O	A/O
Wastewater [real or synthetic municipal]		Real	Real	Real	Real	Real	Real	Real	Real	real	Synthetic
activated sludge model	ASM1	ASM3	ASM1	ASM1	ASM1	ASM1	ASM3	ASM2d	ASM2d	ASM1	ASM1
modified with EPS /SMP	SMP		SMP-EPS	SMP	SMP-EPS	SMP	SMP-EPS	SMP	SMP	SMP	SMP-EPS
Number of additional processes	4	0	2	2	2	4	6	7	7	6	2
pollutants considered	C,N	C,N	C,N	C,N	C,N	C,N	C,N	C,N,P	C,N,P	C,N	C,N
dynamic/steady state (SS) simulation	dynamic	steady	dynamic	dynamic	dynamic	dynamic	dynamic	dynamic	dynamic	dynamic	dynamic
chemical precipitation of PO_4^{3-}											
sectional approach			√		√	√		√	√		
deep bed filtration (COD removal)				√		√		√	√		
Dynamic specific cake resistance			√		√	√	√	√	√	√	
specific cake resistance is related to bound EPS or soluble EPS (SMPs)			SMPs		SMPs	SMP	*bEPS*	SMPs	SMPs	bEPS	SMP
static cake layer resistance	√	√	√	√	√	√	√	√	√	√	√
dynamic cake layer resistance			√	√	√	√	√	√	√		
Pore fouling		√	√		√	√	√	√	√		√
effect of backwashing				√		√		√	√	√	
effect of intermittent coarse bubble aeration			√		√			√		√	
effect of aeration intensity			√		√	√	√	√	√	√	
effect of filtration-relaxation cycle			√	√	√	√	√	√	√	√	√

References	*(Y. Lee et al., 2002)*	*(Wintgens et al., 2003a)*	*(Zarragoitia-González et al., 2008)*	*(Di Bella et al., 2008)*	*(Zarragoitia et al., 2009)*	*(Mannina et al., 2011b)*	*(Suh et al., 2013a)*	*(Cosenza Alida et al., 2013)*	*(Mannina et al., 2018)*	*(Janus, 2014b)*	*(Lindamulla et al., 2021)*
full energy estimation model							√			√	
aeration model							√			√	
GHGs emission model									√		
Calibration protocol											
Stochastic (sensitivity analysis)				√		√	√	√	√		√
Heuristic											
No calibration	√	√	√		√					√	
Bio-kinetic sub-model validation				√		√		√	√		√
Filtration sub-model validation		√	√		√	√			√		√
Berkeley Madonna (BM), FORRTAN (F), R			BM	F	BM			F	R		
MATLAB/SIMULINK	√	√				√	√			√	
Commercial software											Aquasim

4.5 SUMMARY AND PERSPECTIVES

The literature review showed that the activated sludge models in standalone as well as in integrated configuration with mostly used RIS fouling models are validated and are successful in simulating the pollutants removal and fouling evolution of the MBR systems with design capacities in the range 0.3-7,000 $m^3.d^{-1}$. No study has been found for the super large-scale facilities (≥100,000 $m^3.d^{-1}$), even though the total number of super-large-scale facilities has increased now. Furthermore, most of the modeling studies have used rigorous calibration of the model parameters, including both heuristic and mechanistic (i.e., through sensitivity analysis tools), and the values of model parameters vary to a large extent, posing a difficulty in adapting the values for a new system.

Large-scale modeling studies should be carried out to explore the utility of the existing models and to use these validated models for the development of advanced controls for optimization of pollutant removal processes, fouling prediction, and automatic controls. Moreover, the comprehensiveness of the model should be improved by considering the incorporation of the sub-modules i.e., i) COD, N, and P fractions, ii) full-scale dynamic aeration based on the actual aeration system in place, iii) coagulant addition along with particle size distribution, iv) energetic consumption, vi) the contribution of coarse bubble aeration to the overall O2 supply in aerobic reactor, v) accurate hydraulic modeling to fully characterize the anaerobic/aerobic/anoxic reactors and vi) GHGs emissions modeling.

Chapter 5: **Objectives of Thesis**

Global and specific objectives of this thesis work are based on the gaps identified in the literature review presented heretofore and in alignment with the objectives of the umbrella program of SIAAP, i.e., "*Modélisation Contrôle et Optimisation des Procédés d'Epuration des Eau* (MOCOPEE) and are presented in this chapter.

5.1 GLOBAL OBJECTIVES

Global objectives are listed considering the overall contribution of this work in the domain of the MBR modeling.

5.1.1 Development of integrated and comprehensive model for full-scale MBR

The integrated model developed in this work aimed to link all the components of the MBR processes including biological processes (carbon oxidation and nutrient removal), oxygen supply for biological process, and diffusion limitation associated with the higher MLSS concentrations and diffusers fouling, filtration -fouling mechanisms and energy consumption associated with multiple energy consumption installations, and in particular air-scouring. The model is intended to simulate:

- Removal kinetics of COD, NH_4^+ and ideally NO_x and PO_4^{3-} with regards to activated sludge process variables in combination with filtration-fouling model
- Dynamic K_{La} based on the actual design of the aeration system and oxygen supply,
- TMP and total filtration resistance under the influence of filtration-relaxation, backwashing, and intermittent aeration mechanisms.
- Specific energy consumption and the bifurcation of the energy consumed by various unit operations.

5.1.2 Validation of the integrated model at a super large-scale

The measured data from the full-scale / super-large scale MBRs is relatively limited and is usually not maintained by the plant operator in line with the requirements of the modeling work. One of the global objectives of this work is to collect, treat and manage

the missing data sets (through experiments) required for validation of the model at a super large-scale.

5.2 SPECIFIC OBJECTIVES

The 3 specific objectives of this work are split into 1 operational and 2 scientific objectives:

- To develop a fully calibrated and validated model to be used as a basis for optimization and development of control systems for process improvement and consumption of energy and chemicals.
- To explore to what extent modeling of super-large scale is different than modeling a laboratory scale and pilot scale systems.
- To investigate the influence of the input and parameters uncertainties on model output.

PART-III: MATERIALS AND METHODS

Chapter 6: Seine Aval MBR Wastewater Treatment Plant

This chapter presents the general arrangements and specificities of the Seine Aval MBR wastewater treatment facility. It is the experimental data provider for the integrated modeling in the current work. It is a super large scale (>100,000 $m^3.d^{-1}$) facility, being one of its original characteristics. It includes the plant schematics, specifications of biological and membrane basins, hydraulic characteristics, and the overall *functioning* status of the plant. According to Petersen et al.(2002) and Rieger et al.(2012), plant design data are needed for model configuration and its successful calibration.

6.1 SEINE AVAL WASTEWATER TREATMENT PLANT

This MBR facility is a part of Europe's largest wastewater water treatment plant located on the Seine River at Achères-France and has been operational since 2017.

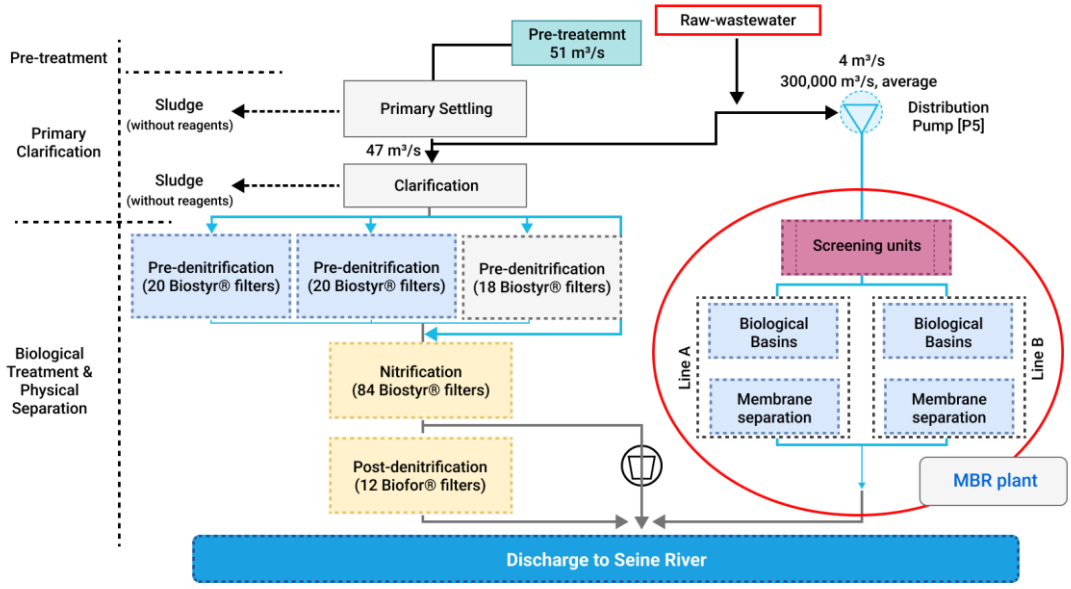

Fig. 6.1: Seine Aval wastewater treatment plant, Paris, adapted and modified from (SIAAP, 2014)

The Seine Aval wastewater treatment plant receives around 1.70 million $m^3.d^{-1}$ of municipal wastewater generated by approximately 70% of the Parisian population. From the total wastewater received at the Seine Aval plant, the MBR facility is currently handling around 200,000-328,000 $m^3.d^{-1}$(upper design limits of 4 $m^3.s^{-1}$ is only for 13 hours) of pre-treated influent, while the rest of it is being treated by the conventional processes as presented in **Fig. 6.1**. This work, however, concerns only MBR process, and does not include the conventional treatment processes.

The MBR feeding consists of settled wastewater from clarifiers, mixed with by-passed pre-treated wastewater, if necessary. The mixed influent is already sieved by 1 mm sized rotary screens to remove suspended and filamentous materials and by the way to protect the downstream membrane units from clogging. The MBR is composed of an activated sludge process used for the secondary treatment, and a solid-liquid separation is accomplished with *Zenon's ZeeWeed^{TM} 500D* braid-reinforced membranes. MBR plant is divided into two lanes. Each activated sludge treatment lane further consists of 3 biological reactors feeding 14 MBR tanks operating in parallel. The schematic of a single lane is presented in **Fig. 6.2** below, while the overall schematic of the facility is presented in **Fig. 6.3**.

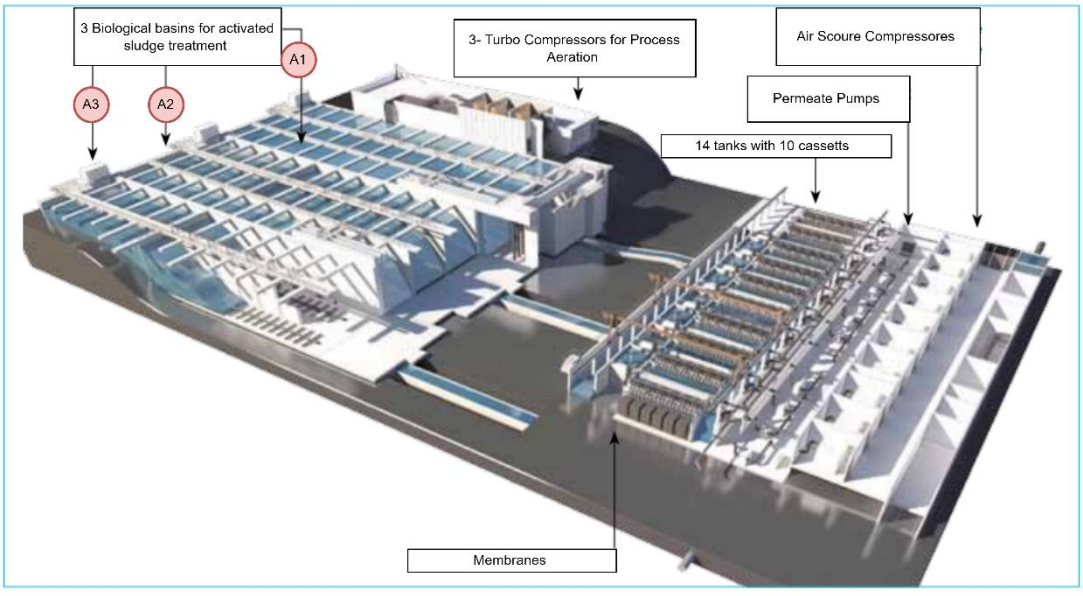

Fig. 6.2: Schematics of a single lane of the Seine Aval MBR (SIAAP, 2014)

6.2 ACTIVATED SLUDGE TREATMENT PROCESS CONFIGURATION

Each of the six biological reactors is designed in a modified University Cape Town (mUCT) configuration with pre-anoxic as the first zone (see **Fig. 6.4**). It helps in the removal of any residual nitrates coming from the recirculation streams as well as in the influent. This zone is not mixed. The second zone is the anaerobic zone, where biological phosphorous removal takes place without any oxygen supply. The anoxic zone is the third stage of the biological treatment, and denitrification takes place here. The last zone of the biological basin is the aerobic zone, where residual BOD is removed, and allows further nitrification. The total available volumetric capacity of a single bioreactor is 19,573 m^3, out of which 90% is normally used. A summary of the biological reactor configuration is given in **Table 6-1**.

Table 6-1: Volumetric distribution of biological reactors into zones

Zone	Unit vol per biological reactor (V) in m^3	Number of biological reactors (N)	Volume of each Zone (V×N) in m^3	Total volume of biological basin ((PA+AN+AX+AO) in m^3
Pre-Anoxic (PA)	373	6 (3 *in each line*)	2,238	117,438
Anaerobic (AN)	4,400		26,400	
Anoxic (AX)	6,000		36,000	
Aerobic (AO)	8,800		52,800	

6.2.1 Biological process aeration system

In wastewater treatment processes, biological process aeration introduces air into liquid, providing an aerobic environment for microbial degradation of organic matter. The purpose of biological process aeration is two-fold: 1) to supply the required oxygen for microorganisms metabolism, and 2) to provide mixing so that the microorganisms come into intimate contact with the dissolved air and suspended organic matter (Gebara, 1999).

The overall nominal flow throughput per tank is 14,000 $Nm^3.h^{-1}$. In the aerobic zone of each of the six biological reactors, there are 1,568 fine bubble diffusers installed on 17 ramps located at the bottom of the basin (see **Fig. 6.4**), leading to a nominal airflow rate of 9 $Nm^3.h^{-1}$.

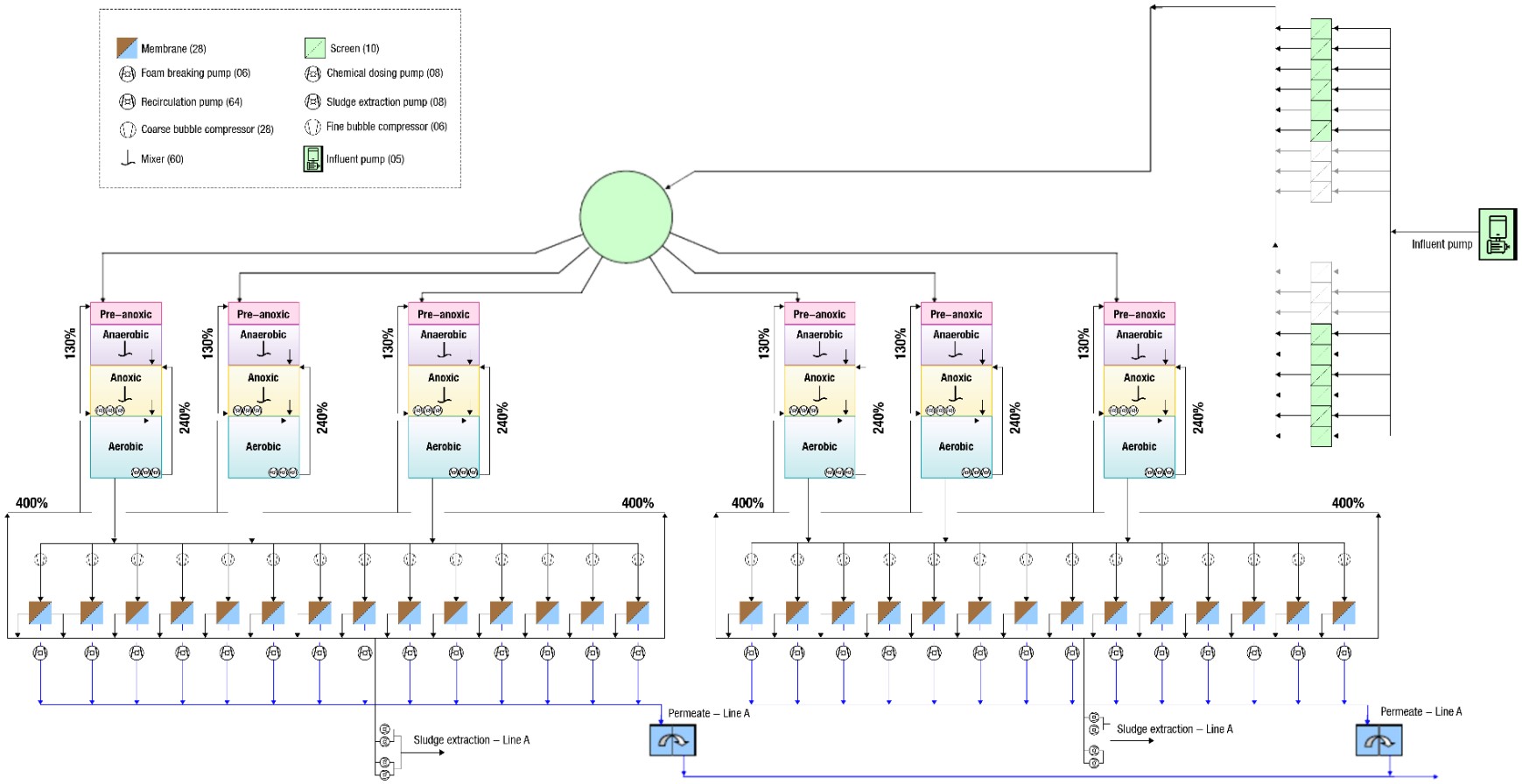

Fig. 6.3: Layout of the full-scale Seine Aval MBR facility

This configuration results in different dissolved oxygen concentrations in each of the four sub-zones of the aerobic with different oxygen transfer rates. The distribution summary of the diffusers in one bioreactor, as well as entire facility, is given in **Table 6-2**.

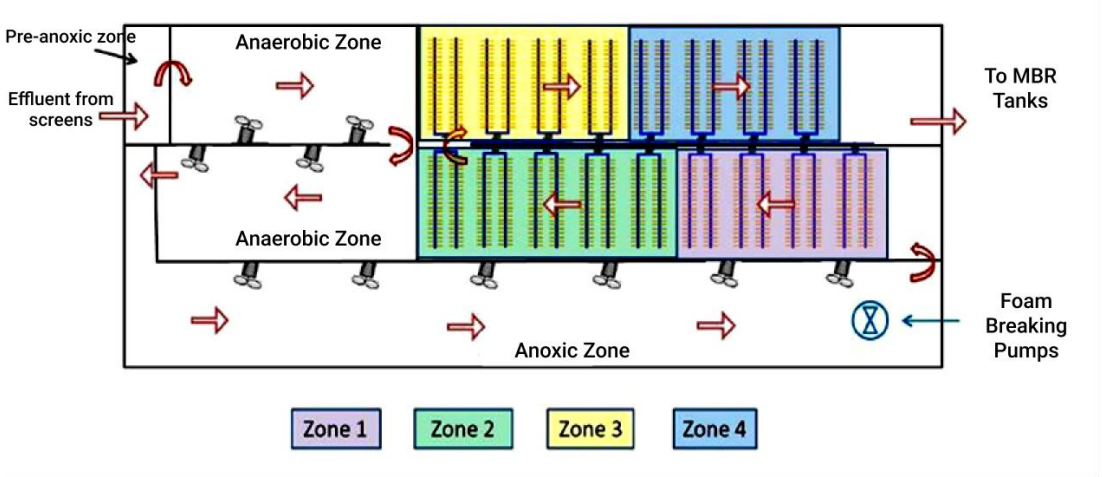

Fig. 6.4: Aeration system configuration in aerobic zones of the bioreactors

Biological nitrogen and phosphorus removal processes are sensitive to dissolved oxygen (DO) concentrations which means that the aeration system is required to be modeled with reasonable accuracy to show the system dynamics (Rieger et al., 2012).

Table 6-2: Distribution of air diffusers per biological basin and the entire facility

Zone	Surface Area (m^2)	Numbers of ramps (N)	Number of rackets per ramp (n)	Number of diffusers per racket (R)	No. of diffusers per bioreactor K1=(n×R)	Total diffusers K=K1×6
Zone -I	270	4	8	52	416	2,496
Zone -2	240	5	10	48	480	2,880
Zone -3	270	4	8	44	352	2,112
Zone -4	180	4	8	40	320	1,920
				Total diffusers	**1568**	**9,408**

The detailed information about the installed aeration system would be helpful in calibrating the model for nitrification and the EBPR process.

6.2.2 Coagulant addition for phosphorus removal

Municipal wastewater usually contains total phosphorus (TP) concentrations in the range 1− 20 mg.L^{-1} (Nadeem et al., 2022). EBPR performance of the full-scale MBR facilities is normally low, and chemically enhanced phosphorus removal (CEPR) is used to meet the stringent regulatory requirements. Coagulant dosing has been reported to decrease the membrane fouling if applied at low-to-moderate concentrations (Fe:P molar ratios < 1). However, much higher concentrations (Fe:P molar ratio in the range of 1.5−4.0) are needed when almost complete P-removal is the aim. Ferric chloride ($FeCl_3$) is efficient in removing phosphorus without affecting the microbiology in the sludge. Further details about the P-removal by CEPR process in MBR and factors affecting its performance can be found in work separately published (Nadeem et al., 2022) and is placed in **Annexure-A.**

There are two injection points for $FeCl_3$ at SAV MBR, as demonstrated in **Fig. 6.5**. The *primary injection* point is at the end of the anaerobic tank, while the *secondary injection* is at ¾ of the aerobic zone.

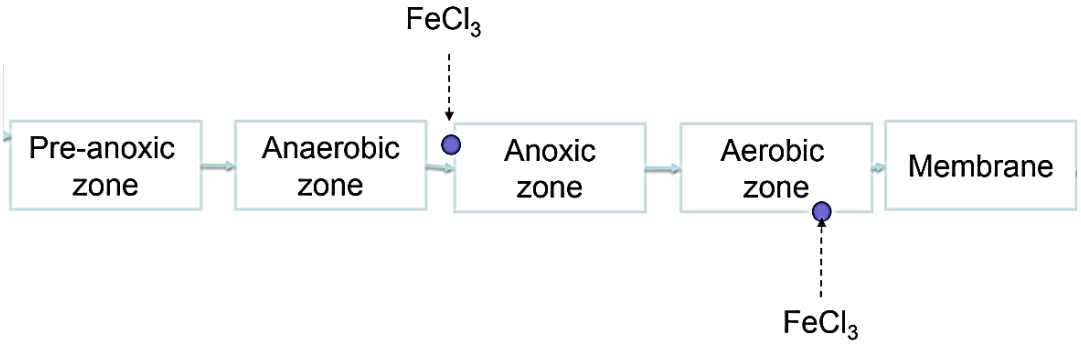

Fig. 6.5: Primary and secondary coagulant injection locations

Thus, each of the two activated sludge lanes has six (06) dosing pumps (3 for the primary injection and 3 for secondary injection), making it 12 coagulant dosing pumps for the entire facility. The metering pump flow rate is set in the range of 50-290 L.h^{-1}. The commercial solution of $FeCl_3$ with a purity of 41% is commonly used. The average injection rate is 23.3 mg$FeCl_3$.L^{-1} and this can increase up to 39.3 mg $FeCl_3$. L^{-1} during peak period.

6.2.3 Control systems

The plant is equipped with multiple control systems to regulate flow, biological process aerations, recirculation, and coagulant addition for Phosphorus removal. The following sections briefly present these controls.

6.2.3.1 Inflow control to the MBR facility

The instantaneous flow for the MBR facility is defined according to the incoming flow to the Seine Aval WWTP. It can vary between 1 and 4 $m^3.s^{-1}$, which is the maximum design capacity of the MBR facility (see **Table 6-3**). However, the maximum flow of 4 m^3 sec^{-1} is limited to 13 hours per 24-hour period.

Table 6-3: Inflow guidelines for the MBR facility at Seine Aval (SIAAP, 2016)

Flow rate at Sine Aval (Q_{SAV})	*MBR flow rate setpoint*
Q_{SAV}<7 m^3 sec^{-1}	1 $m^3.sec^{-1}$
7 $m^3.sec^{-1}$≤ Q_{SAV}<12 $m^3.sec^{-1}$	1.5 $m^3.sec^{-1}$
12 $m^3.sec^{-1}$≤ Q_{SAV}<14 $m^3.sec^{-1}$	2 $m^3.sec^{-1}$
14 m $.sec^{-1}$≤ Q_{SAV}<18 $m^3.sec^{-1}$	2.5 $m^3.sec^{-1}$
18 $m^3.sec^{-1}$≤ Q_{SAV}<21 $m^3.sec^{-1}$	3 $m^3.sec^{-1}$
21 $m^3.sec^{-1}$≤ Q_{SAV}<25 $m^3.sec^{-1}$	3.5 $m^3.sec^{-1}$
25 $m^3.sec^{-1}$≤ Q_{SAV}	4 $m^3.sec^{-1}$

6.2.3.2 Recirculation control

In order to achieve a sufficient biological nutrient removal, tanks in series (pre-anoxic, anaerobic, anoxic, and aerobic tanks) with conditions for the proliferation of

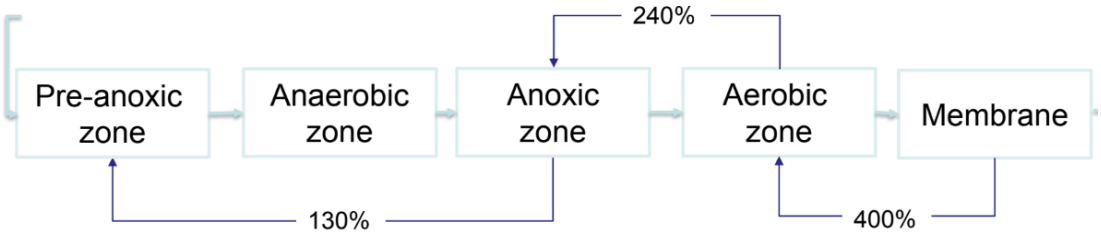

Fig. 6.6: Sludge recirculation scheme

autotrophs, heterotrophs, nitrifies-denitrifies, and phosphate accumulating organisms are required.

There are three different sludge mixing and recirculation among them. recirculation within each biological tank as explained in **Fig. 6.4** and **Fig. 6.6** and further explained below**.**

- The recirculation from anoxic zone to pre-anoxic zone: it represents 130% of the daily volumetric inflow. The sludge is returned to the pre-anoxic zone for removal of residual nitrates coming from the anoxic zone. The recirculation also contributes to develop the phosphorus accumulating organism (PAOs) and to reduce the phosphorus concentrations in the aerobic tank.
- The recirculation of mixed liquor from the aerated zone to the anoxic zone: it represents 240% of the daily volumetric inflow. It allows to eliminate the nitrate produced in the aerobic zone.
- The recirculation of membrane tanks to the aerobic zone: It generally represents 400% of the daily volume and allows recirculation of the nitrifying biomass but may vary depending upon the action of the MLSS control system. This recirculation also helps at maintaining a TSS concentration in the membrane tanks and is required to sweep the membrane surface. If the recirculation rate is too low, the MLSS in the membrane tank may increase rapidly, making the physical separation difficult and increasing fouling propensity. The main objective of the high recycle rate is to redistribute the sludge concentration and minimize the membrane fouling associated with higher MLSS concentrations. It is important to note that the recirculation of MLSS from the membranes zone to the aerobic zone may be fully saturated with high concentrations of DO varying in the order of 2 -6 $mg.L^{-1}$, depending upon the DO concentration from the sludge in the aerobic zone. This oxygen cannot be significantly controlled because the airflow provided by the air scour blowers is mandatorily required to provide a minimum shear across the surface of the membranes to mitigate the potential membrane fouling.

From the modeling point, recirculation flow information with MLSS concentrations is essential, and the gathered information has been used for model structure design and its further calibration.

6.2.3.3 Biological process aeration control

The aeration system installed at the SAV MBR has four aerated zones in the aerobic reactor (based on the different number of diffusers), with two different O_2 set points. The DO concentration is reported by two sensors installed at two different locations. Each zone has an airflow rate adjusted by a PID controller based on the O_2 setpoint. The controller has a manually selected setpoint. Under normal operation (i.e., continuous aeration), a secondary controller based on a setpoint on the effluent NH_4^+ measured online is used to modify, in a cascade mode, each O_2 setpoint in the aerobic tank with a correction factor. If the ammonia analyzer is not working, the manually selected O_2 setpoint is used without corrections. The PID controller for O_2 setpoint corrections using ammonia measurements and setpoints can be disabled manually.

The measured O_2 values used for control are the average measurements of the three aerated tanks (average per zone) of each lane. This implies that each activated sludge lane is controlled in a similar way and should receive a similar airflow rate. Lanes A and B could, however, be controlled differently if needed. If for some reason, the average measurement is not available, then the average value of the other process lane is used. If the average measurement is not available for both lanes, the influent ammonia loading rate measured online after the sieving/screening step is used, along with a lookup table provided by the supplier to decide on an airflow rate. If even that analyzer fails, then a default, constant aeration flow rate is used.

The PID controllers for airflow rates calculations using O_2 setpoints output results in % of air valve opening. These outputs are once again limited by a maximum and a minimum value. There is only one air flowrate measurement in each activated sludge lane, consisting of the combined air demand for zone-1 and zone-2.

There is also an option to use aeration in a sequential on/off mode. In this mode, the aeration is on, normally for around 120 minutes, and off for around 60 minutes. The DO related setpoint values used during the study period are given in **Table 6-4** as reference.

Table 6-4: Biological process aeration controller settings

Aeration control loop parameters	*Units*	*Before July 2018*	*July 18 -Nov 2019*
Sequenced aeration mode	ON		
Aeration time during sequenced aeration	Min	120	90
Non-aeration time during sequenced aeration	Min	60	60
O_2 setpoint in aerobic zone 1	$mgO_2.L^{-1}$	1.5	1.8
O_2 setpoint in aerobic zone 2	$mgO_2.L^{-1}$	0.8	1.2
Maximum value of the O_2 correction factor (NH_4^+ driven)	….	1.2	1.2
Minimum value of the O_2 correction factor (NH_4^+ driven)	….	0.8	0.8
NH_4^+ setpoint	$mgN.L^{-1}$	0.5	0.5

6.2.3.4 Coagulant addition control

Under normal operation, both injection points are in use and aeration turned on. The injected $FeCl_3$ volume/flowrate in the anoxic reactor is computed using a PID controller according to the influent wastewater flow rate. At the secondary injection point, the controller uses a second setpoint of the effluent PO_4^{3-} measured online to decide on a cascaded mode of the $FeCl_3$ flow rate setpoint. Each $FeCl_3$ setpoint has both a minimum and a maximum value.

Each of the commands of these injection points can be manually disabled. Also, each lane (A and B) can be operated differently, but each of the three bioreactors (inside A or B) is operated in the same way. The secondary injection point is also automatically disabled when there is no aeration in the aerobic tank. When some injection point is not available (i.e., involuntarily not in use), a simple **Eq.6.1** is used to increase the other injection setpoint.

$$Setpoint_{X,corrected} = Setpoint_{X,initial} \,.\, K_Y \,.\, Setpoint_{Y,initial} \qquad 6.1$$

Where X is the number of the available injection point, and Y is the number of the unavailable ones. K_2 is normally higher than one, and K_1 is lower than one. The reasoning for this is that the primary injection is considered more efficient than the secondary one. Note that when the aeration is off in the aerobic tank, the secondary injection point is unavailable, and the primary setpoint compensation is activated. Also, note that a second set of maximum and minimum setpoint values can be reached after compensation.

Table 6-5: Phosphorus removal control system setpoints

PO_4^{3-} control loop parameters	Units	Before July 2018	July 18 -Nov 2019
Primary $FeCl_3$ concentration	$mg.L^{-1}$	25	15
Primary coefficient (K_Y)	….	0.8	0.8
Maximum primary $FeCl_3$ concentration	$mg.L^{-1}$	30	20
Secondary coefficient (K_y)	….	1.5	1.5
Maximum secondary $FeCl_3$ concentration (before applying the secondary coefficient)	$mg.L^{-1}$	20	30
Maximum secondary $FeCl_3$ concentration (after applying the secondary coefficient)	$mg.L^{-1}$	30	30
Minimum secondary $FeCl_3$ concentration (before applying the secondary coefficient)	$mg.L^{-1}$	5	10
Default secondary $FeCl_3$ concentration	$mg.L^{-1}$	10	15
PO_4^{3-} setpoint	….	0.35	0.25

When the PO_4^{3-} analyzer is offline, the secondary injection point falls back to a manually selected $FeCl_3$ setpoint, similar to what is used for the primary one. The PO_4^{3-} related setpoint values used before and after 18th July 2018 are given in **Table 6-5**.

6.3 MEMBRANE FILTRATION

The SAV MBR facility has two membrane lanes with 14 tanks each (i.e., 28 Tanks in total) and is equipped with ZeeWeed™ 500D as shown in the **Fig. 6.7** with specifications provided in **Table 6-6.** Each of the tanks contains ten cassettes, and each cassette consists of 48 modules (see **Fig. 6.8**). In addition, 26 tubular diffusers (13 per half cassettes) are fed by two air ducts and permeate drawn out via a single duct.

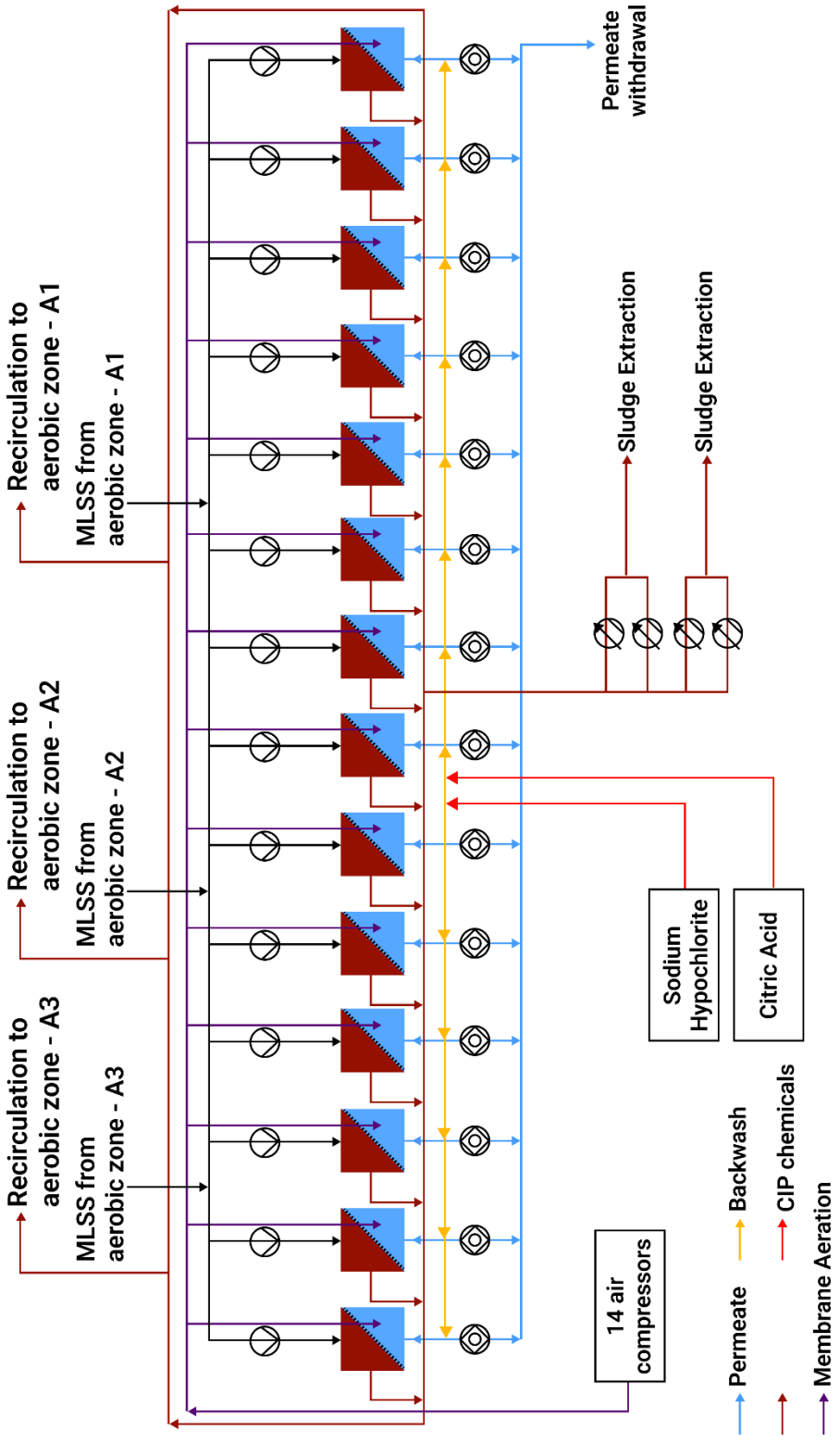

Fig. 6.7: Schematic of the 14 MBR tanks of lane-A operating in parallel

6.3.1 Functioning of the tanks

The sludge from the aerobic zones of each lane flows to the 14 membrane aerated tanks of the corresponding MBR lane, as shown in **Fig. 6.7**. The filtration cycle varies in the range of 7-15 minutes (adjusted to 11 minutes) and is regulated by the operator. Each tank can be individually programmed, automatically as well as manually (different operational sequences such as backwashing filtration, degassing cycle, maintenance cleaning, intensive recovery cleaning, tank emptying, rinsing, aeration sequencing, etc.)

Table 6-6: Specifications of ZeeWeed^{TM} 500D module

Parameter	Value
External/Internal diameter	1.9/0.8 mm
Filtration flux direction	Outside -in
Material	Polyvinylidene fluoride (PVDF)
Pore size	0.04 micron
Total surface area/module	34.4 m^2
Total Available surface area	462,336 m^2
Module Dimension (H×W×D)	2198×844×49 mm
Surface properties	Non-ionic & hydrophilic

Fig. 6.8: Module, cassettes, and single MBR tank

It takes 20 seconds for degassing, followed by eight filtration-relaxation cycles of 660 seconds and 45 seconds, respectively. The 8th relaxation cycle is extended by 35 seconds of backwashing. In total, it takes 5,695 seconds until the next de-gassing.

Considering that on each tank, there are ten membrane cassettes, the tanks are paired, and two compressors per pair are installed, the aeration cycles are operated as follows:

- **10/10 configuration:** when both compressors are operational, five cassettes on each tank are aerated simultaneously for 10 seconds (5 from one tank with one compressor and five from the coupled tank with the other compressor) with a relaxing period of 10 seconds while the other 5 cassettes of each tank are non-aerated. Thus, the cycles are about 20 seconds plus 5 seconds (approx.) required to open and close the valves.
- **10/30 configuration:** when only one compressor is operational, 5 cassettes in one tank are aerated for 10 seconds with a relaxing period of 30 seconds (while the other cassettes are non-aerated, 5 cassettes at a time). In this case, the entire cycle takes 40 seconds, plus 5 seconds (approx.) to open and close the valves. The aeration is operated in alternation within tanks, i.e., (1) aeration of 5 cassettes in tank-1, (2) aeration of 5 cassettes in tank-2, (3) aeration of the other five cassettes in tank-1, (4) aeration of the other five cassettes in tank-2.
- **Special configuration:** When a tank is at standby, it is aerated as its coupled tank, either operated like 10/30 or 10/10. However, when both coupled tanks are on standby, the aeration mode is automatically, 10/30 for energy savings.

Furthermore, backwashing is applied to remove part of the fouling, which is apparently not removed by the relaxation and/or air scouring. Backwashing involves permeate injection against the flow through the membranes for a programmed sequence that the operator could modify. This phase of backwashing may be replaced by a relaxation stage.

6.3.2 MLSS control in MBR tank

MLSS from the membrane tanks is re-circulated back to the aerobic zone of the biological tanks to maintain the MLSS concentrations and nitrification rates. The recirculation rate (R) concentration factor (K= $\frac{R+1}{R}$) is given by **Eq. 6.2**.

$$MLSS_{MBR} = K \times MLSS_{aerobic\ tank} \quad 6.2$$

Standard K values are given in **Table 6-7**, these values are used to prevent excessive accumulation of TSS in membrane tanks. The control loop of the feedback system regulates the K factor and keeps close the value fixed by the operator by altering the recirculation ratio. For this, the controller relies on the measurement of four TSS sensors.

Table 6-7: Setpoints for TSS regulation in MBR tank

	Unit	*Case-I*	*Case-II*	*Case-III*	*Case-IV*
Inflow to the membrane lines	$m^3.d^{-1}$	143,000	200,000	248,711	300,000
TSS concentration in Aerobic Zone	$g.L^{-1}$	7.0	7.0	8.0	7.2
Recirculation ratio	%	700	600	500	400
K values	-	1.14	1.17	1.2	1.25
TSS concentration in Membrane tanks	$g.L^{-1}$	8.0	8.2	9.6	9.0

With this MLSS control system in place, the following three scenarios are possible for regulation of K value:

i. If the TSS measurement in the membrane tank is equal to the set value, the pumps will continue pumping the MLSS at the same rate back to the aerobic zone.
ii. If the TSS measurement in the membrane tanks is higher than the pre-set value, the control system will increase the recirculation rate by increasing the pumping rate.
iii. If the TSS measurements in the membrane tanks is lower than the pre-set value, the control system will decrease the recirculation rate through decreasing the pumping rate.

6.3.3 Chemical Cleaning of the membrane

Two kinds of the chemical cleaning processes are used at the SAV MBR plant i.e., 1) maintenance cleaning (in-situ), which lasts about 2 hours per tank to prevent the risk of fouling and clogging, and ii) intensive cleaning (ex-situ), which lasts about 24 hours per tank to regenerate the filtering capacity of the membranes. The frequency and chemicals used in both kind of chemical cleaning process are given in **Table 6-8**.

Table 6-8: Description and frequency of the chemical washes

	Chemicals	Type of cleaning	Conc. (mg/L)	Frequency per tank	pH
Maintenance Cleaning (In-Situ)	Bleach	Organic	200	Twice per week	10.5 Max
	Acid	Mineral	1100	Once per week	2.5-3.5
Intensive Cleaning (Ex-Situ)	Bleach	Organic	1100	twice per year per tank	10.5 Max
	Acid	Mineral	2200	twice per year per tank	2.5-3.5

6.4 INSTALLED ENERGY CONSUMERS IN SAV MBR

The energy requirements in several processes of the MBR plant operations with fixed (i.e., mixers and foam breakers) and variables (influent pumping, fine and coarse bubble aeration, recirculation, permeate pumping, and backwashing). A list of such equipment and their installed power, along with necessary information is provided in **Table 6-9**. All these power consumers are used for energy consumption estimation and simulation.

Table 6-9: Energy consumers installed at Seine Aval MBR facility

Main process	Equipment	Functions/locations	Number of Units installed	Installed Power (kW)	Controls/state
Influent pumping	Submersible centrifugal pump	Influent pumping from station to MBR	04 01	1250	Variable frequency drive (VFD)/dynamic
Recirculation pumps	Submersible pump	Anoxic →pre-anoxic	18	90	VFD/ dynamic
		Aerobic –anoxic	18		VFD/ dynamic
		Membrane tank →aerobic	28		
Mixers/agitators	Horizontal axial mixers	Anaerobic reactor	24	288	Fixed speed
		Anoxic reactor	36	432	Fixed speed
Foam breaking/de-gasification	Foam breakers submersible motor.	Breaking of foam and removal of air in the anoxic zone	06	1080	Fixed speed

Main process	Equipment	Functions/locations	Number of Units installed	Installed Power (kW)	Controls/state
Dosing pumps	Lobe pumps	Coagulant addition in anoxic and aerobic tanks	12	384	Fixed speed
Fine bubble aeration	Centrifugal compressors	Biological process aeration	06	4650	VFD/ dynamic
Membrane scouring	lobe compressors	Fouling abatement control	28	2100	Fixed speed. dynamic
Permeate suction and backwashing	Lobe pumps	Permeate extraction and backwashing of the fouled membranes	28	21	Fixed speed
Sludge extraction	centrifugal pump	Extraction of sludge from the membrane tank	12	16	Variable frequency drive (VFD)/dynamic

6.5 SUMMARY

The Seine Aval MBR is a super-large-scale facility and is the 4th largest in the world with a peak flow design capacity of 348,000 $m^3.d^{-1}$ (not exceeding 4 m^3s^{-1} for 13 hours). Other important design aspects are summarized in **Table 6-10**. All these data were used for the configuration of the model as well as its calibration.

Table 6-10: Summary of the SAV-MBR design features

Design feature	units	Descriptions
Screen Size	mm	1.00
Number of process lanes	--	Two (02)
Number of ASP bioreactors in each lane	--	Three (03)
Bioreactor configuration type		Modified University Cape Town
Biological reactor's volume	m^3	117,438
Volumetric distribution of bioreactor	%	Pre-anoxic (1.79%); anaerobic (21.06%); anoxic (28.72%); aerobic (42.12%); MBR-bioreactor (6.32%)
Aeration system	--	Sub-surface aeration systems 9408 diffusers backed by 6 HOWDEN's blowers
Recirculation		Anoxic (130%); aerobic (240%); MBR-bioreactor (400%) and controlled by PID

Design feature	units	Descriptions
Membrane material	-	Polyvinylidene fluoride (PVDF)
Membrane pore size and surface properties	µm	0.04 (Non-ionic & Hydrophilic)
Membrane manufacturer & model	-	Zenon, hollow fiber (HF), ZeeWeed^{TM} 500D
Number of MBR lanes	--	Two (02)
Number of tanks in each lane	--	14
Number of cassettes in each tank	--	10
Number of modules in each cassette	--	48
Surface area of a single module	m^2	34.4
Surface area of a single Tank	m^2	16,512
Total membrane area	m^2	462,336
De-gassing, filtration-relaxation, and backwashing sequencing of MBR	-	20 seconds of degassing, followed by eight filtration-relaxation cycles of 660 seconds and 45 seconds respectively. 35 seconds of backwashing. In total, it takes 5,695 seconds until the next de-gassing.
Aeration -relaxation sequencing		10/10; 10/30 or can be programmed
Type of chemical cleaning		- Maintenance cleaning (2/week) - Recovery cleaning (2/week)

Chapter 7: Existing Data and Additional Experimental Campaigns

In addition to an accurate understanding of the functioning of the plant, sufficient and high-quality data is essential for the knowledge-based modeling and trustable quality of simulation results. Keeping this in mind, this chapter presents a comprehensive data set required for the configuration, calibration, and validation of an integrated MBR model for the Seine Aval plant. It also presents the approach used to collect, treat, and adjust multiple datasets collected from the supervisory control and data acquisition (SCADA) system and daily laboratory analysis data. In addition, a data-driven approach used to reduce the complexity of the plant layout is presented.

7.1 DATA REQUIREMENTS

Configuration, calibration, and validation of the phenomenological model required multiple data sets, including i) physical data related to plant design, ii) operational settings, iii) input data, iv) output data, and v) additional data sets related to bio-kinetics of the biomass. The physical data has already been presented ***Chapter 6:***. This chapter is dedicated to presenting and analyzing the input, operational, and output data sets and cleaning these before using them in the modeling work. Two kinds of data set from the available data were gathered. The first one-week long data set (13/05/2019-19/05/2019) was used for the steady-state and dynamic calibration of the model, and the other 3 months long (01/11/2018- 31/01/2019) were used for the long-term dynamic validation of the model. A third data set of 2 weeks duration (20/9/2020-04/10/2020) was also gathered to re-validate the integrated model.

7.2 DATA SOURCES AT SEINE AVAL MBR PLANT

Input data is available from two sources, i.e., i) routine laboratory measurements and ii) installed flow quantity and quality reporting sensors. The schematic of the data availability with respect to data sources is presented in **Fig. 7.1.**

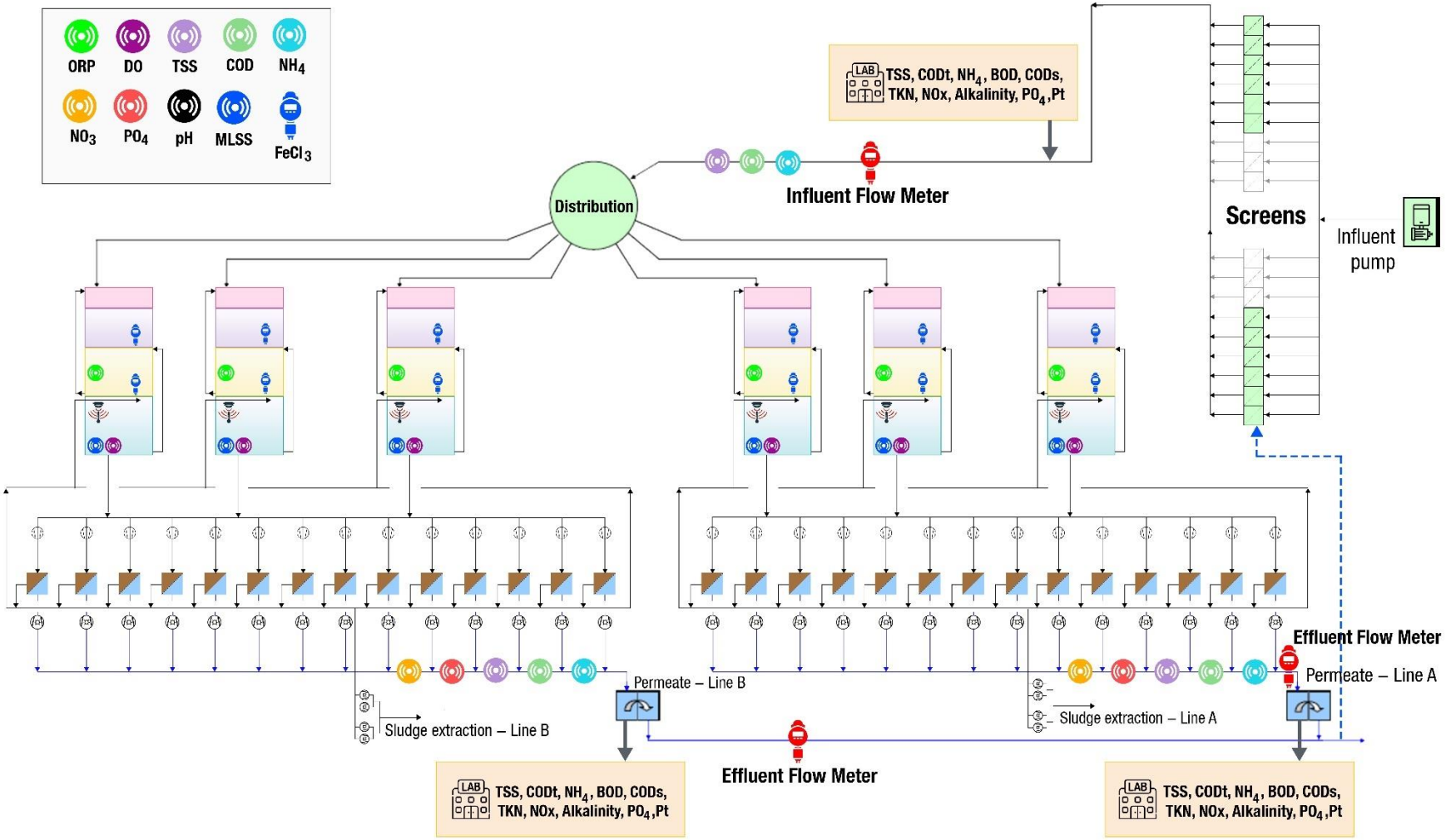

Fig. 7.1: Data sampling and sensors installation points

Monitoring data is available, whatever the measuring frequencies described in **Table 7-1**. All the data sets are not available with 15 minutes measurements frequencies. Furthermore, most of the process information is available from the aerobic tank, and very little is known about the processes happening in pre-anoxic, anaerobic, and anoxic reactors. In addition, almost all bio-kinetic models required COD in fractionated form. While, at SAV-MBR, data related to CODs and COD_{tot} is available only, and no information about the EPS and SMPs concentrations is available from the membrane and/or aerobic reactors.

Table 7-1: Available data and frequencies of measurements

Data type	*Parameters*	*Units*	*Measuring Locations*	*Measuring Frequency*		
				15 Minutes	*Daily*	*Weekly /Fortnightly*
Influent Flow	Q_{inf}	$m^3.d^{-1}$/ $m^3.h^{-1}$	P5	✓	✓	
Influent Quality (✓) Effluent Quality (※)	TSS	$mgTSS.L^{-1}$	After sieving Permeate of Lane-A and Lane-B	✓	✓※	
	COD_{total}	$mgO_2.L^{-1}$			✓※	
	COD_{sol}	$mgO_2.L^{-1}$			✓	
	BOD_5	$mgO_2.L^{-1}$			✓	
	TKN	$mgN.L^{-1}$			✓※	
	NH_4	$mgN.L^{-1}$		✓※	✓※	
	NO_3	$mgN.L^{-1}$		※	✓※	
	NO_2	$mgN.L^{-1}$			✓※	
	PO_4	$mgP.L^{-1}$		※	✓※	
	TP	$mgP.L^{-1}$			✓※	
	Alkalinity	$molHCO_3^{-1}$			✓※	
	pH			✓	✓※	
Process Conditions & Sludge Properties	$QFeCl_3$	$m^3.d^{-1}$/ $m^3.h^{-1}$	Anoxic & Anerobic	✓	✓	
	ORP	mV	Anoxic	✓		
	DO	$mgO_2.L^{-1}$	aerobic	✓		
	MLSS	$g.TSS.L^{-1}$	aerobic	✓		✓
	Temperature	C	aerobic	✓		
	Air consumption	$Nm^3.d^{-1}$/ $Nm^3.h^{-1}$	Aerobic	✓	✓	
	COD_{sol}	$mgO_2.L^{-1}$	Aerobic			✓
	Recirculation	$m^3.d^{-1}$/ $m^3.h^{-1}$	Tanks in series	✓	✓	
Extracted Sludge	VSS	$g.L^{-1}$	Sludge			✓
	DVM	%	Sludge			✓
	TTF	sec	Sludge			✓

Data type	*Parameters*	*Units*	*Measuring Locations*	*Measuring Frequency*		
				15 Minutes	*Daily*	*Weekly /Fortnightly*
	Q_{sludge}			✓	✓	
Membrane Filtration and sludge properties	Flux- Inst.	$L.m^{-2}.h^{-1}$		✓		
	Flux-Average	$L.m^{-2}.h^{-1}$		✓		
	TMP	mbar		✓		
	Permeability	$L^{-1}.m^{-2}.bar^{-1}$			✓	
	SADm	$m^3h^{-1}m^{-2}$			✓	
	Tanks in production	No.			✓	
	TSS	$g.L^{-1}$		✓		
	Chemical consumptions in cleaning	$L.d^{-1}$			✓	
	Number of tanks on 10/10 aeration-relaxation sequencing	No			✓	
	Number of tanks on 10/30 aeration-relaxation sequencing	No.			✓	
	Chemical washes	No.				✓

7.3 DATA TREATMENT AND ADJUSTMENTS

A four-tier approach suggested by Rieger et al. (2012) and presented in **Fig. 7.2** was adopted for the cleaning of the datasets. This section explains and presents the data cleaning and reconciliation procedure used for 3 months long data. The same procedure has been adopted for the other two data sets collected from the laboratory and SCADA system with standardized excel tools prepared under this work.

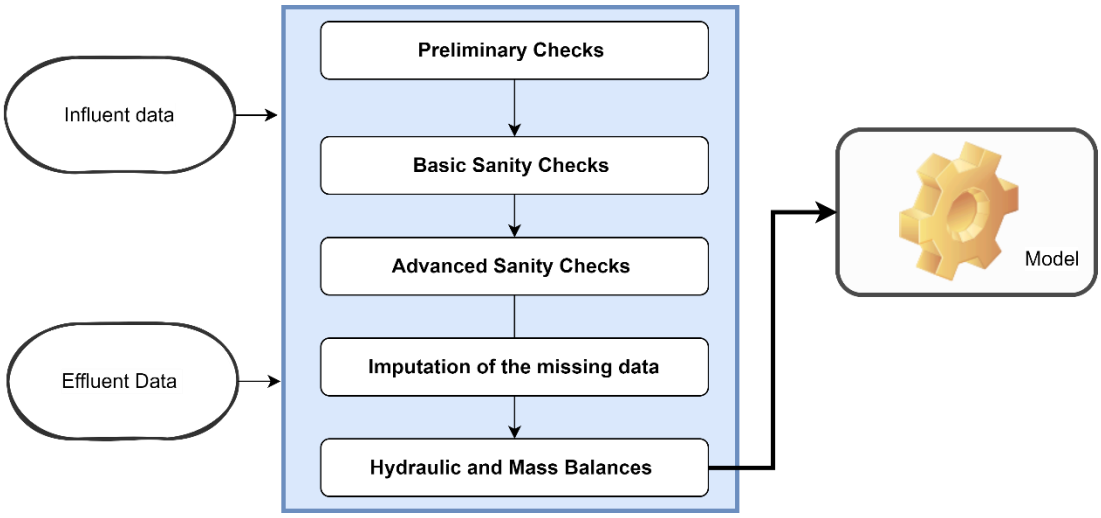

Fig. 7.2: Data cleaning and approach

7.3.1 Preliminary checks

Preliminary checks included the data visualization through time series and box plots, to see the trajectories of the mass flow and faults linked to sensor calibration, statistical outliers (beyond upper and lower quartiles in the box plots and time series analysis), and elimination of unjustified zero values. The information on the minimum detection limits for the sensors installed at SAV-MBR and the lab analysis methods being used at the SIAAP was helpful to rule out the possibility of data discrepancies. **Table 7-2** and **Table 7-3** respectively, summarizes the minimum detection limits of sensors installed at various locations of the plant and the detection limits of laboratory methods used in SIAAP laboratory. The errors related to sensors error as well as the statistical errors were eliminated from each of the data sets available from the sensors and/or laboratory analysis. As an example, influent NH_4 data is visualized using box plots and time series chart with minimum and maximum limits of the outliers and is presented in **Fig. 7.3.**

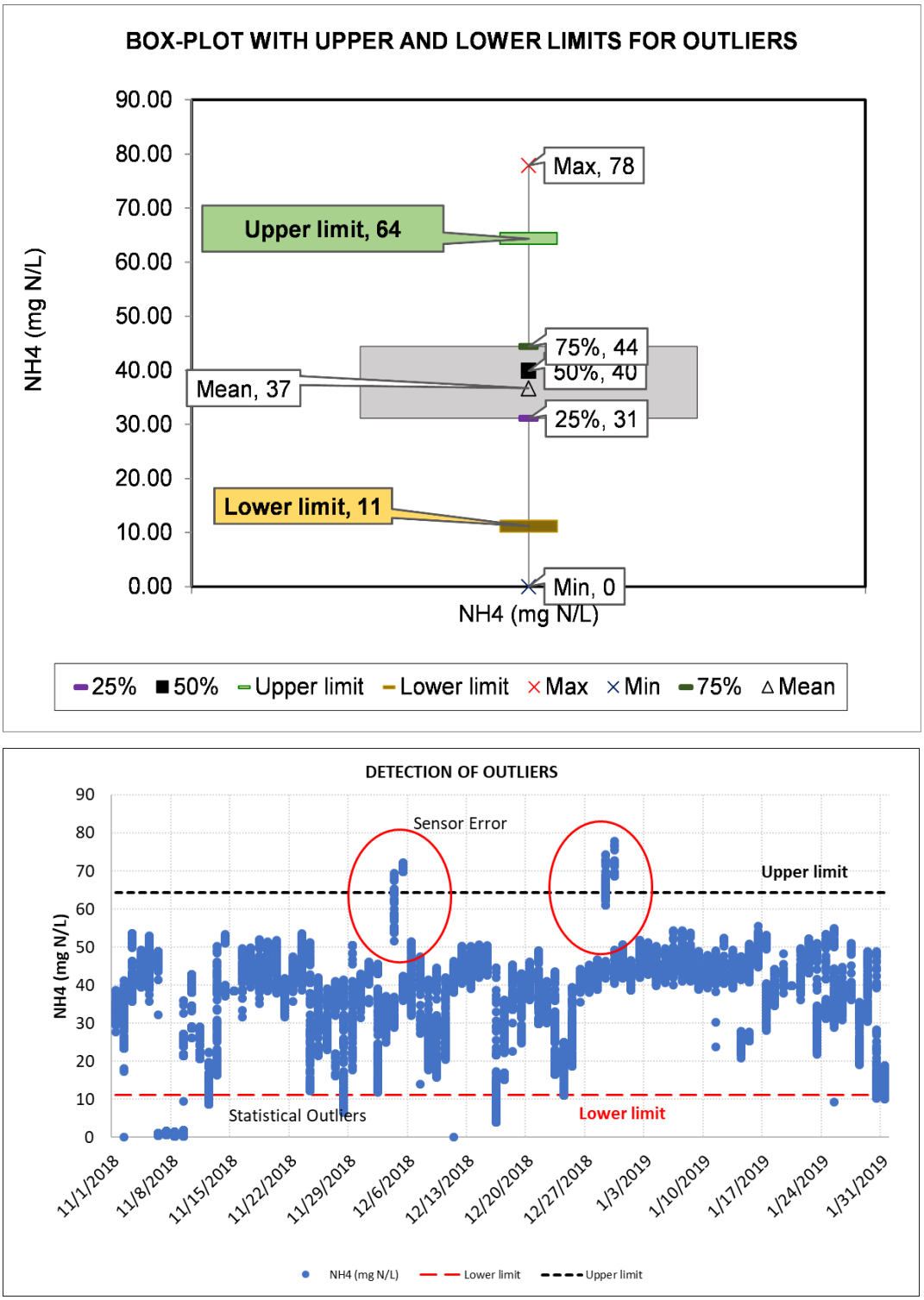

Fig. 7.3: Influent NH_4 data visualization for sensor error and statistical outlier detection

Table 7-2: Minimum and Maximum detection limits of the sensor installed at various locations of the SAV plant

Location of sensor	Measurement	Unit	Measuring Frequency	Range	Precision
Sieving Output	COD	$mgO_2.L^{-1}$	15 Minutes	0-600	1 $mgO_2.L^{-1}$
	TSS	$mg.L^{-1}$		0-500	Unspecified
	NH_4	$mg.L^{-1}$		0-100	3%±0.05 $mg.L^{-1}$
Anoxic Zone	ORP	mV	15 Minutes	50-500 (-ve)	Unspecified
	Temp	^0C		0-50	Unspecified
Aerobic Zone/ Recycle stream from aerobic to anaerobic	Diss. O_2	$mg.L^{-1}$	15 Minutes	0-10	± 2%
	TSS	$mg.L^{-1}$	15 Minutes	0-10	Without calibration < 5% of the measured data ± 0,01 FNU/NTU
Outlet of the MBR Tanks (Permeate Testing)- Each tank	Turbidity	NTU	15 Minutes	10^{-3} -10^3	± 0,008 FNU ±1 % of the measured data (0 – 10 FNU)
Outlet of the MBR Lane	NO_3	$mg.L^{-1}$	15 Minutes	0.1-100	± 0.1 $mg.L^{-1}$
	PO_4	$mg.L^{-1}$		0.05-15	2 % of the measured data + 0.05 $mg.L^{-1}$
	NH_4	$Mg.L^{-1}$		0.05-20	3 % of the measured data + 0.05 $mg.L^{-1}$
	Turbidity	NTU		10^{-3} -10^3	± 0,008 FNU ±1 % of the measured data (0 – 10 FNU)
	pH	--		0-14	Unspecified

7.3.2 Basic sanity checks

Basic sanity checks were further used to eliminate any discrepancies in the data. This was ensured by verifying simple relationships for each data sets of the influent and effluent (see **Fig. 7.4**). In case the logical relationship was not true for a given data, data entries for that specific day/time were removed.

Table 7-3: Minimum detection limits of the laboratory analysis methods at SIAAP

Measurement	Units	Location	Minimum Limit	Expanded Uncertainty
TSS	$mg.L^{-1}$	Influent & Effluent	2	15%
BOD_5	$mgO_2.L^{-1}$	Influent	3	15%
BOD_5 (permeate)	$mgO_2.L^{-1}$	Effluent	0.5	15%
COD	$mgO_2.L^{-1}$	Influent & Effluent	15	10%
TKN	$mgN.L^{-1}$	Influent & Effluent	1	5%
NH_4	$mgN.L^{-1}$	Influent & Effluent	0.25	10%
NO_2	$mgN.L^{-1}$	Influent & Effluent	0.02	10%
NO_3	$mgN.L^{-1}$	Influent & Effluent	0.25	10%
PO_4	$mgP.L^{-1}$	Influent & Effluent	0.05	10%
P_{tot}	$mgP.L^{-1}$	Influent & Effluent	0.20	10%
Alkalinity	°F	Influent & Effluent	2 – 40	Unspecified
pH		Influent & Effluent	2 - 12	Unspecified

The outliers observed for the phosphorus may be due to testing inaccuracies because in most of these cases the values for P_{tot} and PO_4^{3-} are the same.

Influent Quality Pragamatic Check					
Date	TKN>NH4	Ptot>PO4	COD_{tot}>BOD_5	CODtot>CODsol	Ntot = TKN+NO2+NO3
11/1/2018	TRUE	TRUE	TRUE	TRUE	TRUE
11/2/2018	TRUE	TRUE	TRUE	TRUE	TRUE
11/3/2018	TRUE	TRUE	TRUE	TRUE	TRUE
11/4/2018	TRUE	TRUE	TRUE	TRUE	FALSE
11/5/2018	TRUE	TRUE	TRUE	TRUE	FALSE
11/6/2018	NO Data				
11/7/2018					
11/8/2018	TRUE	TRUE	TRUE	TRUE	FALSE
11/9/2018	TRUE	TRUE	TRUE	TRUE	TRUE
11/10/2018	TRUE	TRUE	TRUE	TRUE	TRUE
11/11/2018	TRUE	TRUE	TRUE	TRUE	TRUE
11/12/2018	TRUE	TRUE	TRUE	TRUE	TRUE
11/13/2018	TRUE	TRUE	TRUE	TRUE	TRUE
11/14/2018	TRUE	TRUE	TRUE	TRUE	TRUE
11/15/2018	TRUE	TRUE	TRUE	TRUE	FALSE
11/16/2018	TRUE	TRUE	TRUE	TRUE	FALSE
11/17/2018	TRUE	TRUE	TRUE	TRUE	TRUE

Effluent Quality Pragamatic Check					
Date	TKN>NH4	Ptot>PO4	COD_{tot}>BOD_5	CODtot>CODsol	Ntot = TKN+NO2+NO3
11/1/2018	TRUE	TRUE	TRUE	TRUE	TRUE
11/2/2018	TRUE	TRUE	TRUE	TRUE	TRUE
11/3/2018	TRUE	TRUE	TRUE	TRUE	TRUE
11/4/2018	TRUE	TRUE	TRUE	TRUE	TRUE
11/5/2018	TRUE	TRUE	TRUE	TRUE	TRUE
11/6/2018	No Data				
11/7/2018					
11/8/2018	TRUE	FALSE	TRUE	TRUE	TRUE
11/9/2018	TRUE	FALSE	TRUE	TRUE	TRUE
11/10/2018	TRUE	TRUE	TRUE	TRUE	TRUE
11/11/2018	TRUE	TRUE	TRUE	TRUE	TRUE
11/12/2018	TRUE	TRUE	TRUE	TRUE	TRUE
11/13/2018	TRUE	FALSE	TRUE	TRUE	TRUE
11/14/2018	TRUE	FALSE	TRUE	TRUE	TRUE
11/15/2018	TRUE	FALSE	TRUE	TRUE	TRUE
11/16/2018	TRUE	FALSE	TRUE	TRUE	TRUE
11/17/2018	TRUE	FALSE	TRUE	TRUE	TRUE

Fig. 7.4: Basic sanity checks for influent and effluent data

7.3.3 Advanced sanity checks

Advanced sanity checks were used to further identify and remove the faulty data points. Mass load ratios are more relevant than individual pollutants concentrations because, they are less reliant on rain (Petersen et al., 2002; Rieger et al., 2012). Mass load ratios are

visualized through box plots and time series to identify and exclude the outliers. A single instance of the influent N_{tot}/COD_{tot} is presented in **Fig. 7.5** as an example.

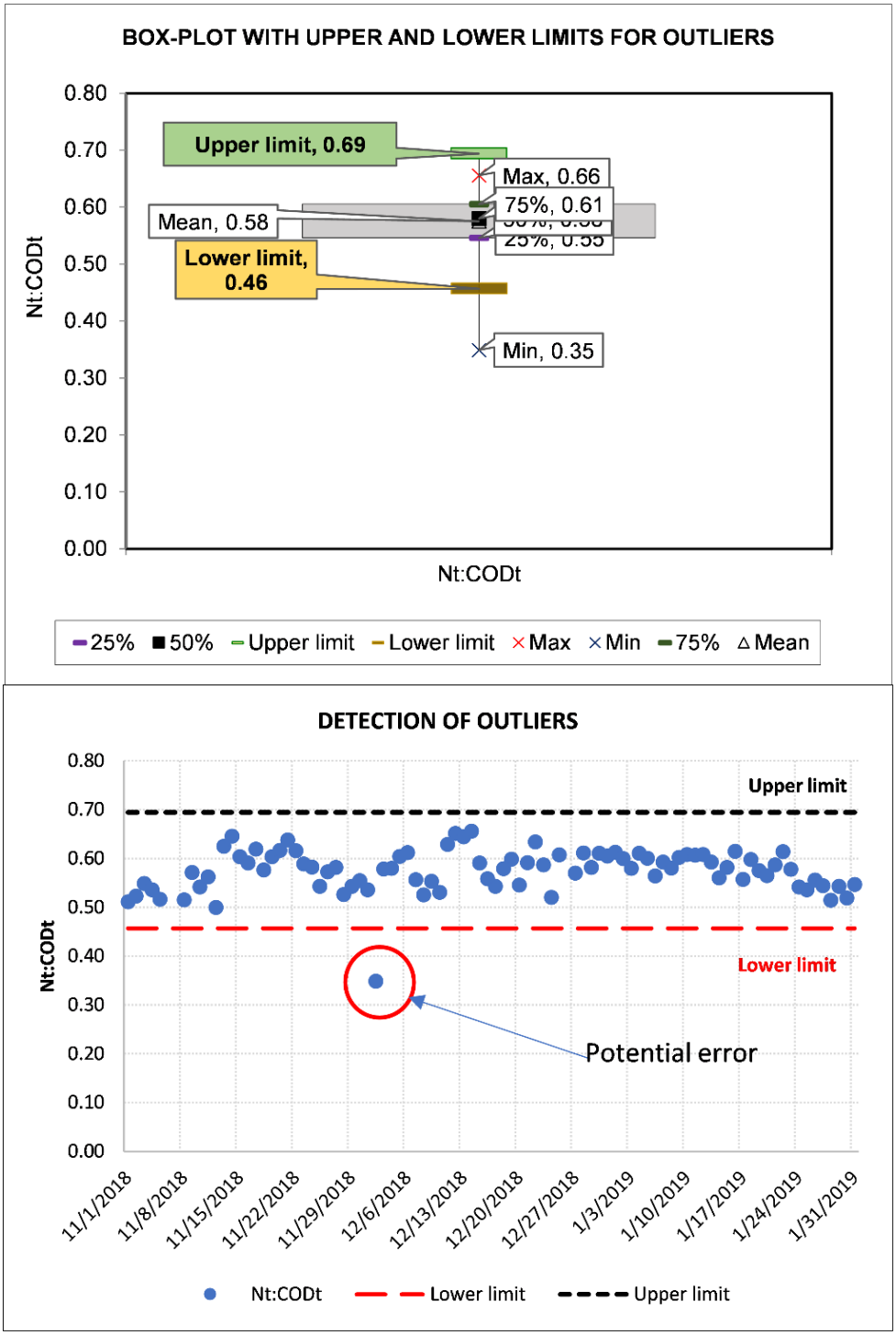

Fig. 7.5: N_{tot}: COD_t influent ratio with daily average data

7.3.4 Data Imputation

After removing the outliers identified in all previous 3 steps, the missing values were replaced by the moving averages of the last 3 days (daily data) for all the influent, effluent, and process data, with 24 hours moving average in case of 15 minutes sensor data.

7.3.5 Hydraulic and mass balancing

7.3.5.1 Hydraulic balance

As part of the hydraulic balance, data analysis was carried out on average daily flows for the 3 months data. The balance sheet is the sum of the inflow rates (influent, coagulant addition, chemicals for membranes cleaning) and the outflows (including permeate, sludge, and drain). The system boundary for the calculation of the hydraulic balance is shown in **Fig. 7.6**.

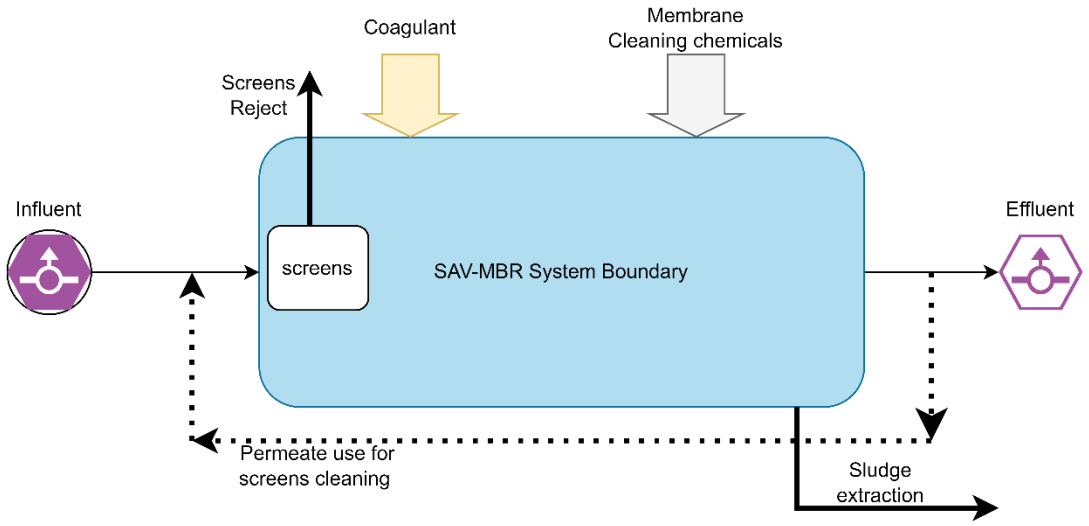

Fig. 7.6: boundary for the hydraulic balance of SAV MBR

It should be noted that the outflow rates for discharge materials at the screening areas are not known and are considered negligible compared to other flows. Similarly, permeate volumes used to clean the screens (up to 4% of the influent) and getting back to process are not included in the hydraulic balance. **Eqs 7.1 -7.2** represent the hydraulic balance at Seine Aval.

$$Q_{inf} + Q_{FeCl3} + Q_{CIP} = Q_P + Q_s \quad 7.1$$

Here,

Q_{inf}: influent flow rate ($m^3.d^{-1}$)

Q_{FeCl3} : Coagulant solution addition at anoxic and anerobic tanks (m^3d^{-1})

Q_{CIP} : Acetic acid and bleach consumption in in-situ membrane cleaning (m^3d^{-1})

Q_p: Permeate production rate ($m^3.d^{-1}$)

Qs: Sludge extraction rate ($m^3.d^{-1}$)

The balance is considered reasonably closed at 100 ± 10% (Rieger et al., 2012) while for the SAV-MBR, 3 months long data, the average balance is evaluated to be 102% with variations in the range of ± 4% without considering the influence of the rain and recirculated of the permeate to the screens for cleaning (see **Fig. 7.7**).

$$Hydraulic\ Balance\ (\%) = \frac{\sum Outflow\ rates}{\sum Inflow\ rates} \times 100 \quad 7.2$$

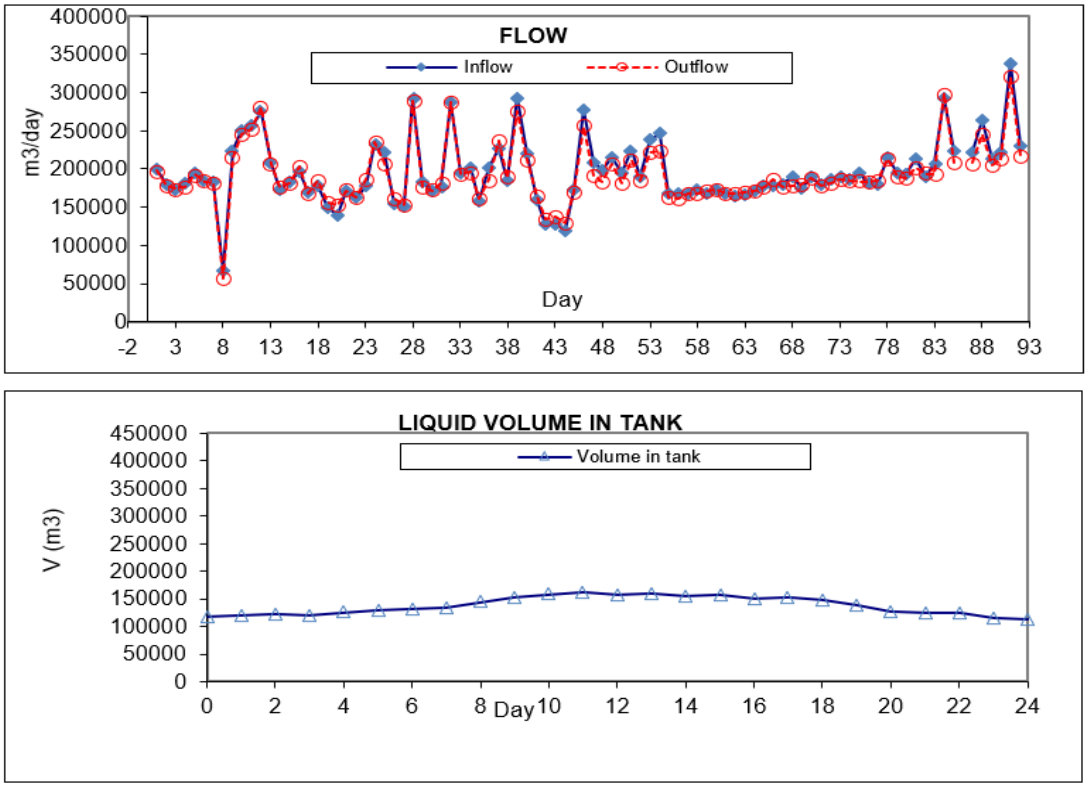

Fig. 7.7: Hydraulic balance for 3 months data

7.3.5.2 Mass balances

Since almost all activated sludge models are mass balance-based, feeding the balanced data would improve the accuracy of the simulations. Mass balances can also help identify systematic errors in wastewater treatment plant data sets (Petersen et al., 2002). The mass balances were carried out for COD, nitrogen (N), and phosphorus (P) for the entire SAV MBR system. These balances are carried out on flows averaged over long periods, at least three times the sludge retention time (Rieger et al., 2012), i.e., 92 days in the present case. Mass balance was calculated for all 92 days of average data, while the hydraulic balance was performed with daily flow datasets. The basic principle of the mass balance is described by the conservation **Eq.7.3.**

$$\text{Input} + \text{Reaction} = \text{Output} + \text{Accumulation} \qquad 7.3$$

Phosphorus balance: Phosphorus being the refractory wastewater component, is considered to conserve its mass as the influent, effluent, and sludge, leaving the MBR system to retain the mass and the phosphorus is not converted into any gaseous form. The balance is represented by **Eq. 7.4** . An excel-based tool was developed for phosphorus balancing, considering the balanced hydraulics achieved in ***section 7.3.5.1*** and the available influent and effluent concentrations from the daily laboratory measurements for 92 days. Though actual Phosphorus concentrations in the sludge being extracted were unknown (as the Phosphorus in the sludge is not measured at SIAAP), an average concentration of 110 $mg.L^{-1}$ for the period without the addition of coagulant and 140 $mg.L^{-1}$ for the period with coagulant addition was assumed (based on data available from other plants of SIAAP). It was later confirmed under dedicated experimental campaigns, presented in ***Chapter 9:***. As per the experimental campaigns, the average values in the extracted sludge varied in the range of 140-160 mgL^{-1}.

$$Q_{inf} \times C_{inf} = [Q_s \times C_s + Q_p \times C_p + V\frac{dTP}{dt}] \qquad 7.4$$

Where, C_{inf} is the concentration ($g.m^{-3}$) of TP in the influent; C_s is the concentration (gm^{-3}) of TP in sludge, and Cp is the concentration (gm^{-3}) of the TP in the effluent. The average

daily phosphorus balance varied between 70% and 109%. The outliers were removed and replaced with acceptable moving average values to bring the balance within the acceptable range of 100 ± 20%. Although the ideal acceptability is within the range of 100 ± 10% (Rieger et al., 2012), in the current case, the precise data for the phosphorus flow in the extracted sludge is not available for 92 days, and an average value is adopted. Therefore, the results obtained are said to be acceptable.

Oxygen consumption balance: On a 24-hour basis, the daily oxygen consumption of the entire plant was calculated using non steady-state mass balances for COD and total nitrogen (TN) by simplifying the approach suggested by Racault et al. (2011). The oxygen consumption balance is termed as "open" because several reactive flows are not measured. Indeed, a fraction of the flow is used to convert the pollutants into the gaseous phase i.e., CO_2, N_2, N_2O, etc. (see **Fig. 7.8**). This balance makes it possible to estimate the oxygen consumed to degrade the carbonaceous and nitrogenous organic matter. Oxygen consumption was calculated from measurements of overall oxygenation yields and operating parameters of the aeration system installed at the Seine Aval and presented in the ***Chapter 6:***

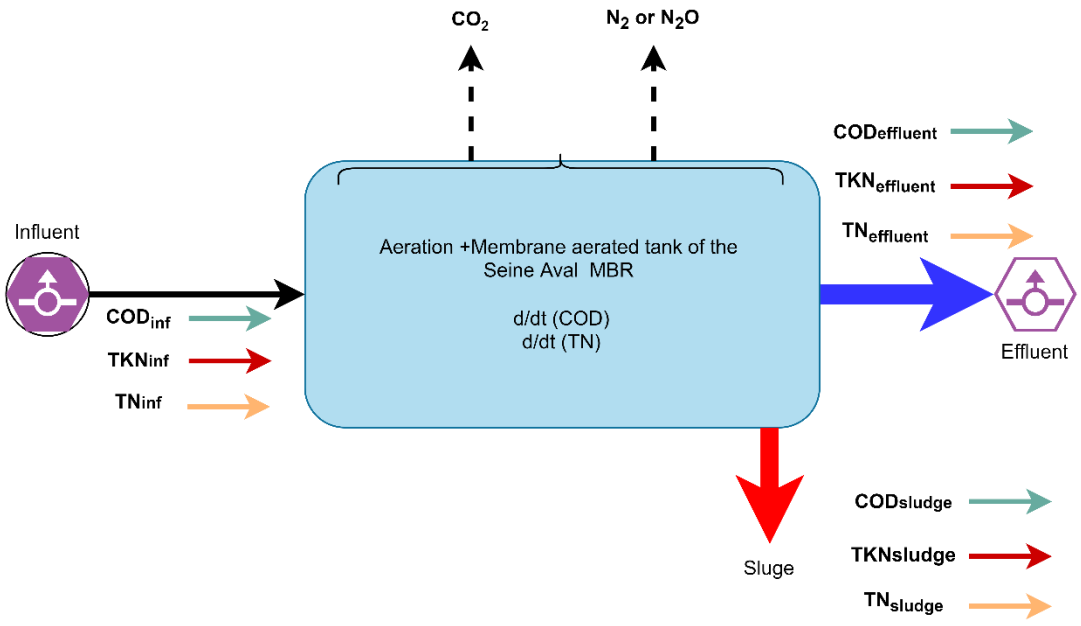

Fig. 7.8: Mass balance boundary and terms for COD and Nitrogen balance

The total oxygen consumption (OC_{tot}, $kgO_2.d^{-1}$) is calculated from the oxygen requirements for the oxidation of organic matter (OC_{COD}, kgO^2d^{-1}) and the treatment of nitrogen by nitrification (OC_{NOx}, $kgO_2.d^{-1}$) and by denitrification (OC_{DN}, $kgO_2.d^{-1}$). The overall balance of oxygen consumption is expressed in **Eq. 7.5**.

$$OC_{tot} = OC_{COD} + OC_{NOx} - OC_{DN} \quad 7.5$$

Considering the COD mass flow ($kgCOD.d^{-1}$), the oxygen consumption balance for degradation of the carbonaceous matter at SAV MBR in the aerobic zone is expressed as **Eq.7.6**. The oxygen consumed in nitrification process is estimated using **Eq. 7.7**, while for denitrification, it is estimated using **Eq. 7.8.**

$$OC_{COD} = COD_{influent} - COD_{sludge} - COD_{effluent} - V\frac{dCOD}{dt} \quad 7.6$$

It should be noted that, some of the organic matter in the shape of the particulate matter is removed at the screening stage, and due to the absence of any data about that extraction, it is not considered for COD balance.

$$OC_{NOx} = [TN_{influent} - TKN_{sludge} - TKN_{effluent} - V\frac{dTN}{dt}] \times 4.57 \quad 7.7$$

$$OC_{DN} = [TN_{influent} - TN_{sludge} - TN_{effluent} - V\frac{dTN}{dt}] \times 2.86 \quad 7.8$$

Since the TN, TKN, and COD_{tot} flows in the extracted sludge are not measured in routine at Seine Aval, these calculations are based on 3 days average values measured during the experimental campaign.

Once the total oxygen consumption (OC_{tot}) was estimated using **Eqs. 7.5-7.8,** the volumetric air consumption data available from the SCADA system of the SAV MBR,

was used for estimation of the daily mass of oxygen i.e., MO_2 ($kgO_2.d^{-1}$) transferred to the aeration basin by using **Eq. 7.9**

$$MO_2 = Q_{air} \times E_d \times \rho_{air} \times X_{O_2} \quad 7.9$$

Where, Q_{air} is the daily oxygen consumption ($Nm^3.h^{-1}$), E_d is the efficiency of the diffuser system installed at SAV per meter depth (5.1%) and X_{O2} is the fraction of the oxygen in the air (21%) and ρ_{air} is the density of the air (1.204 $kg.m^{-3}$) at 20 ^{0}C. Moreover, in these calculations, the quantity of oxygen injected into the membrane tank is assumed to be non-influential for biological processes and COD and N conversions.

Taking into account the estimated oxygen consumed (**Eq. 7.5**) and actual oxygen supplied (**Eq. 7.9**), the global oxygen balance was estimated using the **Eq. 7.10.**

$$O_2\ Balance\ \% = \frac{MO_2}{OC_{tot}} \times 100 \quad 7.10$$

The daily oxygen balance varied in the range 87- 137%. This variability of the oxygen balance might be associated with the air consumption in the MBR tank, which is not considered. In addition, data related to sludge COD and TKN were not available, and average values were used instead for entire 92 days.

In summary, the mass balances of phosphorus and oxygen consumption are not accurate but acceptable to an extent that is much better than the raw data. Indeed, the differences are reduced, and the averages tend towards 100±10%. However, these assessments are not complete because of the several hypotheses made for each stage of the reconciliation process due to the lack of available datasets, mainly related to extracted sludge (not measured in routine). However, adopting average TP and TN concentrations is not helpful for achieving accurate mass balance results due to large variations in the inlet wastewater.

7.4 EXPERIMENTAL CAMPAIGNS

In the previous chapter, it was explained that existing data from the SCADA system and routine laboratory measurements were collected and reconciled. However, these data were not sufficient for model configuration, steady- state/dynamic calibration, and validation

of the model. Dedicated experimental campaigns were carried out to compensate for the deficiencies in the available datasets in order to achieve higher simulation performance. This paragraph presents the methodologies adopted for the collection and analyses of the data applied to two experimental campaigns and their corresponding results. Experimental campaigns were carried out for the following objectives:

- To compensate for the missing datasets needed for mass balance analysis (discussed in the previous chapter).
- To establish initialization conditions for setting up the model and validate.
- To validate the steady state simulation of the model for each of the reactors.
- To understand the pollutants and biomass transformations, through their balances, within each of the reactors.

7.4.1 Targeted datasets

7.4.1.1 Pollutants removal profile each of bioreactor zone

The first experimental campaign (13/05/2019-19/05/2019) was designed to collect the influent and sludge samples for analysis from positions (S1-S8) marked in **Fig. 7.9,** while in the second experimental campaign (20/9/2020-04/10/2020), membrane permeate analysis was carried out instead of the extracted sludge. Several analytical methods have been used to determine the concentration of nutrients, organic matter, and suspended solids in the influent and effluent. Most of these methods applied are in accordance with the French standard based on EN-ISO regulations (see **Table 7-4**). Likewise, the non-standardized methodologies used are based on cited references and methodologies already published or established by commercial labs. Grab samples from the plant were collected, with proper labeling on pre-supplied bottles by Carso.

In order to analyze influent, effluent, and sludge, the samples during the first campaign, were prepared without filtration leading to unreliable results for soluble species due to on-going chemical and biological reactions within samples. While, in the 2nd experimental campaign, for the nitrates (NO_3^-), nitrites (NO_2^-), Ammonium (NH_4^+), and phosphates (PO_4), sludge samples were centrifuged at 5000 rpm for 15 minutes and the liquid was extracted and sent to the laboratory for further analysis.

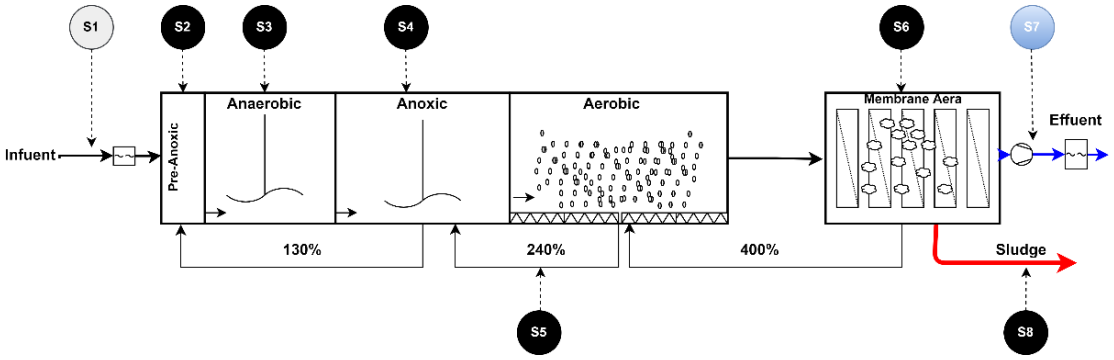

Fig. 7.9: Sampling locations during experimental campaigns

Table 7-4: Analytical methods used for the analysis of influent, effluent, and sludge

Analysis	Units	Sample type	Method	Standard's reference
TSS	$mg.L^{-1}$	Influent/Effluent	Gravimetric + filter-filtration (Whatman 934 AH)	NF EN 872
MLSS	$mg.L^{-1}$	Sludge		NF EN 872
BOD_5	$mgO_2.L^{-1}$	Influent/Effluent/sludge	Dilution and seeding method with allylthiourea (ATU) addition	NF EN ISO-5815-1
$BOD_{soluble}$	$mgO_2.L^{-1}$	Influent/Effluent/sludge	Dilution and seeding method with allylthiourea (ATU) addition (after filtration)	NF EN ISO-5815-1
COD	$mgO_2.L^{-1}$	Influent/Effluent/sludge	spectrophotometric	ISO 15705
	$mgO_2.L^{-1}$			
$COD_{soluble}$	$mgO_2.L^{-1}$	Influent/Effluent/sludge	spectrophotometric (after filtration)	ISO 15705
TKN	$mgN.L^{-1}$	Influent/Effluent/sludge	Distillation	NF EN 25663

Analysis	Units	Sample type	Method	Standard's reference
$TKN_{soluble}$	$mgN.L^{-1}$	Influent/Effluent/sludge	Distillation (after filtration)	NF EN 25663
NH_4^+	$mgN.L^{-1}$	Influent/Effluent/sludge	Continuous Flow Analysis (CFA)	NF EN ISO 11732
NH_4^+, soluble	$mgN.L^{-1}$	Influent/Effluent/sludge	CFA (after filtration)	NF EN ISO 11732
NO_3^-	$mgN.L^{-1}$	Influent/Effluent/sludge	CFA (after filtration)	NF EN ISO 13395
NO_2^-	$mgN.L^{-1}$	Influent/Effluent	CFA (after filtration)	NF EN ISO 13395
PO_4^{3-}	$mgP.L^{-1}$	Influent/Effluent	CFA (after filtration)	ISO 15681-2
TP	$mgP.L^{-1}$	Effluent/Effluent/sludge	Mineralization and spectrophotometric (Ganimede)	NF EN ISO 6878
MVSS	$mg.L^{-1}$	Influent/Effluent/sludge	Gravimetric	M_J004 (CARSO)
pH	-	Influent/Effluent/sludge	Electro-chemical	NF EN ISO 10523

7.4.1.2 Influent fractionation and biomass concentrations

Influent fractionation is a critical step in model calibration considering the form and complexity of MBR. A precise data about the influent components' fractionation is essential. A practical approach is to estimate the average fractions required by the biokinetic model used in this study. The hypothesis is that these ratios between the measured total compounds and their fractions are constant over time. However, these may change depending upon changes in the influent characteristics, and re-estimation of the influent fractions would be required in case of changes in the influent quality (Rieger et al., 2010). Since the ASM3-BioP-EPS-SMP model is used in this study, therefore COD fractionation is required by the model and is presented in the following sections.

Respirometry tests were carried out as per the procedure followed by the SIAAP using BIOS-R-respirometer (INSA, Toulouse-France) to estimate the soluble readily biodegradable (S_B) and slowly biodegradable particulate substrate (X_{CB}) fractions of COD. A wastewater to sludge ratio of 0.25 was used to estimate the volume of the wastewater and sludge for the COD fractionation experiment and was evaluated to be 1.9 L and 0.55 L, respectively. 50g ATU (Allylthiorea) was added to a 2.5 L reactor to inhibit nitrification during the specific investigation of heterotrophic substrate degradation. The respirometry monitored the DO concentration through the O_2 sensor installed in the reactor vessels. The respiration rate of the biomass was estimated from the decrease of the oxygen concentration in the BIOS-R vessel using **Eq. 7.11** below.

$$\frac{dO_2}{dt} = -OUR \tag{7.11}$$

Then by separately integrating the two decreasing OUR parts in the Respiro-graph and considering that only a part (1-Y_H) of the substrate is oxidized for energy and can be detected with the respirometer, one is finally able to determine X_{CB} (slowly biodegradable particulate substrate) and S_B (readily biodegradable substrate). Additional respirometry tests were carried out to estimate Y_H using the protocol of SIAAP, and it was evaluated to be 0.639 g O_2/gO_2.

$$S_B = \frac{1}{1 - Y_H} \int_0^{t1} OUR \left(\frac{V_{inf} + V_{sludge}}{V_{inf}} \right) \tag{7.12}$$

$$X_{CB} = \frac{1}{1 - Y_H} \int_{t1}^{t2} OUR \left(\frac{V_{inf} + V_{sludge}}{V_{inf}} \right) \tag{7.13}$$

The COD data from treated sludge at the aerobic reactor was used to estimate the soluble unbiodegradable (S_U) fraction, which is estimated to be around 90% of the COD in the aerobic reactor tank (STOWA protocol).

$$S_U = 0.90 \times COD_{sol} \tag{7.14}$$

$$X_U = COD_t - S_B - X_{CB-}S_U \quad 7.15$$

This data collection was performed on 1 sample for the first experimental campaign and on two samples for the second one.

7.4.1.3 Total and soluble extra polymeric substances

The analyses of total EPS and soluble EPS or SMP (Drews, 2010) in mixed liquor taken from anaerobic, aerobic, and membrane aerated reactors were carried out. EPS concentrations were quantified as glucose and proteins through Anthrone and Lowry methods, respectively (Raunkjær et al., 1994), and were then expressed as mg.CODL^{-1} using appropriate conversion factors adopted from Aquino & Stuckey (2004)**.** The analytical deviation for the Lowry method is 20% for the protein concentration ≤ 25 mgL^{-1} and 10% for the protein concentration $\geq$ 25 mg.L^{-1}, while for measurement of polysaccharides using the Anthrone method is about 10% (Stricot, 2008).

7.4.1.4 Specific cake resistance measurements

In order to measure the filtration resistance of the sludge cake, filtration experiments were performed with the dead-end filtration method to determine the order of magnitude of the specific sludge cake resistance.

Fig. 7.10: Experimental setup for measurement of specific cake resistance

The fouling potential of the sludge is tested in a system comprising a cylindrical filtration cell of 60 ml volume (Sartorius filtration pressure cell). A compressed air circuit makes it possible to work at constant pressure. The volume of filtered water is measured and recorded over time using an electronic balance, as shown in **Fig. 7.10.** The filtration surface is circular with a diameter of 45 mm.

Flow monitoring was done by the permeate weighing over time through automated data acquisition. The membranes used are cellulose nitrate filters (Sartorius Stedim) having 0.45µm pores. By following the evolution of the filtration through the representation of time / Volume as a function of Volume, it is possible to make a linear regression of the data and obtain the slope (Δ) of the line and to get the product α according to the **Eq. 7.16** below.

$$\alpha = \frac{2 \times \Delta \times TMP \times A^2}{C \times \mu} \qquad 7.16$$

With, C, the concentration of MLSS in the mixed liquor ($g.L^{-1}$), TMP the transmembrane pressure in Pa, A the membrane surface in m^2, and µ the dynamic viscosity of the permeate/water in Pa.s , α is the specific resistance of the deposit, expressed in $m.kg^{-1}$.

7.5 SUMMARY

The collected data were treated and reconciled for model configuration, calibration, and validation. Several steps were necessary: statistical and technical outliers, logical checks, and ratio checks, followed by data imputation and validation checks, including hydraulic and mass balance. However, missing datasets related to sludge quality were major impediments to meet the desired accuracy. In addition, available data from the SCADA system and routine laboratory measurements were not sufficient to initialize and calibrate the model due to missing data from the zones other than aerobic. Despite data reconciliation has largely helped in improving the quality of the data required for modeling, further experimentation was required to produce the missing data sets. Dedicated experimental campaigns were carried out to complete the missing data sets needed for calibration and validation of the model.

PART-IV: RESULTS & DISCUSSIONS

Chapter 8: Description and Structure of the Integrated MBR Model

This chapter describes the different sub-models of the processes chosen to demonstrate the integrated process dynamics of MBR for pollutants removal and their interactions with the fouling development, as well as the role of various fouling abatement controls in place at the SAV-MBR plant. Each sub-model is chosen based on the targeted objectives i.e., pollutants and considered phenomenon considering the SAV-MBR processes and design configurations.

8.1 SETTING UP THE INTEGRATED MODEL

This part presents the global approach of the modeling, pointing out the interactions of the sub-models presented in the following sections. The comprehensive, integrated model presented in this study is applied to a super-large scale MBR to simulate; a) biological processes through the description of the stoichio-kinetic activity of the biomass for carbon oxidation and nutrient removal coupled with EPS-SMP production and degradation processes; b) the role of biological process aeration in carbon oxidation and nitrification under the influence of MLSS; c) the numerical balance of the volumes of the influent, effluent, sludge wastage and all internal and external recirculation; d) coagulant addition inducing chemically enhanced phosphorus removal (CEPR) in addition to enhanced biological phosphorus removal (EBPR); e) fouling dynamics associated with synchronized filtration-relaxation, intermittent air-scouring and backwashing under the influence of transmembrane pressure (TMP), temperature, MLSS, and bound EPS concentration, and f) energy consumed by the various installations in the plant. The scheme of the integrated knowledge-based model is given in **Fig. 8.1**. It depicts the connectivity of various sub-models and the flow of information during the simulation run. The bio-kinetic sub-model transfers the real-time information of simulated X_{TSS} and X_{EPS} to the aeration sub-model to dynamically estimate the specific cake resistance required in

the filtration/fouling sub-model. Furthermore, the precipitation sub-model takes the volumetric addition of ferric chloride ($FeCl_3$) and transmits the processed information of metal hydroxide complex (MeOH) concentration to the bio-kinetic model. While the aeration sub-model considered the X_{TSS} information from the biological part of the model to provide an integrated model with real-time dynamic K_{La}. Finally, total energy consumption in the plant is modeled with the results from the integrated model. The details of each of the sub-models are given in the following sections.

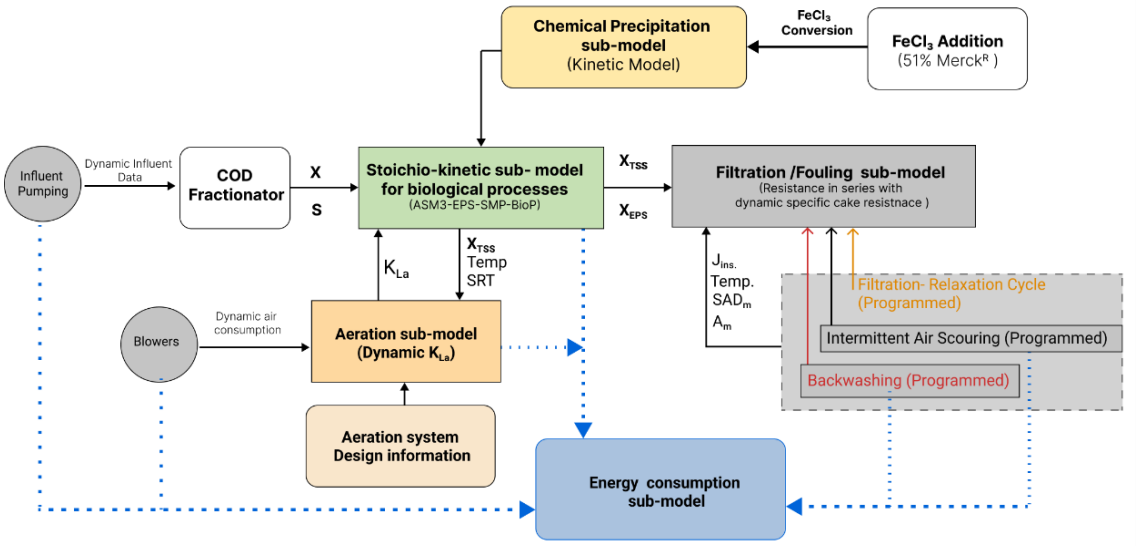

Fig. 8.1: Schematic of integrated MBR processes and energetic model

The model was coded in a MATLAB environment (Math Works, R2020a) due to the flexibility of configuration as per the requirements compared to commercial software (Gernaey et al., 2004). The simulations were run on a system with Intel (R) Core (TM) i5-7300 HQ CPU@2.5GHz and 4-logical processors specifications.

8.2 BIOKINETIC SUB-MODEL

The bio-kinetic sub-model presented in this work employed the coupling of models proposed by Fan et al. (2011) and Janus (2014) by considering pathways for the formation of SMPs, including substrate utilization, biomass decay, EPS hydrolysis, and consequently adapting and modifying the stoichiometric coefficient and rate expressions (Laspidou and Rittmann, 2002). In order to further enhance the nutrient removal modeling

capabilities of the bio-kinetic sub-model, the Bio-P removal module was borrowed from Rieger et al. (2001a) to describe the Bio-P removal as well as the denitrification carried out by the phosphate accumulating organisms (PAOs). Bio-P module was further extended by adding two chemical processes, i.e., precipitation and re-dissolution (Henze et al., 1999), to simulate the CEPR process.

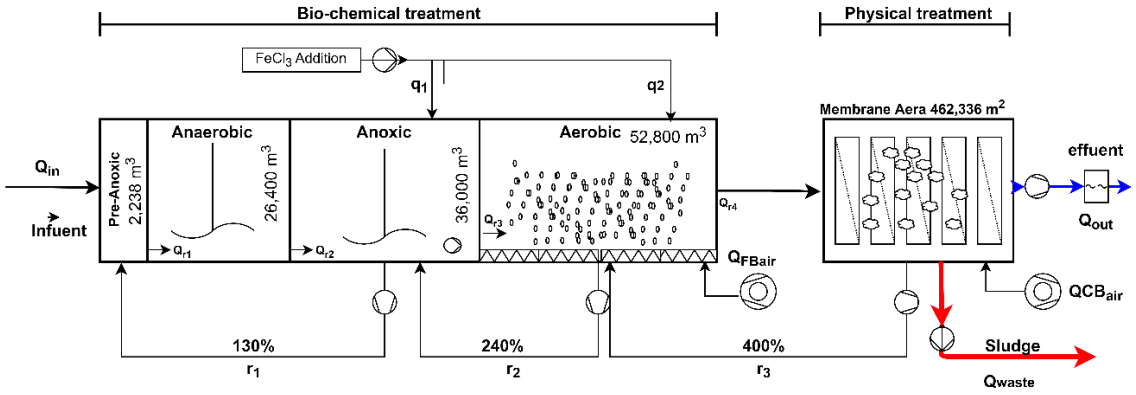

Fig. 8.2: simplified schematic of MBR used for model configuration

The model can describe the carbon oxidation, nitrification, de-nitrification, and bio-chemical phosphorus removal kinetics of the wastewater treatment process. The entire bio-chemical sub-model has collectively been termed "ASM3 EPS-SMP-P" in this thesis. The simplified layout of the SAV-MBR considered for the biokinetic model structuration is presented in **Fig. 8.2**.

Since the objective of this work is to simulate the carbon-oxidation, nitrification, denitrification, and phosphorus removal. IWA basic models ASM2d and ASM3 were subjectively compared, and ASM3 was chosen based on the following considerations:

- *Influent fractionation in ASM3 is relatively easier than in ASM2d, which is essential in full-scale applications due to the scarcity of information related to influent fractions.*
- *ASM3 is designed to be the core of several wastewater models (for example, EAWAG modules on biological phosphorus removal can be easily connected as well module for CEPR can be added) and to satisfy primarily the requirements of practical model applications (Henze et al., 1999; Petersen et al., 2003)*

- *Literature review revealed that ASM1 followed by ASM2d are widely used models in MBR studies at lab and full-scales. ASM3 (modified and unmodified) has been applied to pilot and full-scale systems but has never been validated at super-large scales.*

8.3 COMPONENTS OF THE BIOKINETIC SUB-MODEL

Bio-kinetic sub-model components are divided into soluble (S) and particulate (X). It has been assumed that particulate components are associated with the activated sludge, which can be concentrated by the membrane, and the soluble components can pass through the membrane surface. **Table 8-1** provides a short definition of the dissolved (bold) and particulate (normal) components of the bio-kinetic model.

Table 8-1: Definition of the bio-kinetic components concentrations

#	*Definition*	*Component*	*Units*
1	**Dissolved oxygen**	$\mathbf{S_{O2}}$	$gCODm^{-3}$
2	Particulate biodegradable organics	X_{CB}	$gCOD\ m^{-3}$
3	**Soluble biodegradable organics**	$\mathbf{S_B}$	$gCOD\ m^{-3}$
4	**Soluble Utilization Associated Products**	$\mathbf{S_{UAP}}$	$gCOD\ m^{-3}$
5	**Soluble Biomass Associated Products**	$\mathbf{S_{BAP}}$	$gCOD\ m^{-3}$
6	**Soluble undegradable organics**	$\mathbf{S_U}$	$gCOD\ m^{-3}$
7	**Ammonia ($NH_4^+ + NH_3$)**	$\mathbf{S_{NHx}}$	$gN\ m^{-3}$
8	**Nitrate and nitrite (NO_3^-, NO_2^-)**	$\mathbf{S_{NOx}}$	$gN\ m^{-3}$
9	**Dissolved nitrogen gas**	$\mathbf{S_{N2}}$	$gN\ m^{-3}$
10	Particulate undegradable organics	X_U	$gCOD\ m^{-3}$
11	Extra Polymeric Substances	X_{EPS}	$gCOD\ m^{-3}$
12	Ordinary heterotrophic organisms	X_{OHO}	$gCOD\ m^{-3}$
13	Storage compound in OHOs	$X_{OHO,Stor}$	$gCOD\ m^{-3}$
14	Autotrophic nitrifying organisms (NH_4^+ to NO_3^-)	X_{ANO}	$gN\ m^{-3}$
15	**Inorganic soluble phosphorus**	$\mathbf{S_{PO4}}$	$gP\ m^{-3}$
16	Phosphorus accumulating organisms	X_{PAO}	$gCOD\ m^{-3}$
17	Stored polyphosphates in PAOs	$X_{PAO,PP}$	$gP\ m^{-3}$
18	Stored poly-β-hydroxyalkanoate in PAOs	$X_{PAO,Stor}$	$gCOD\ m^{-3}$
19	**Alkalinity (HCO_3^-)**	$\mathbf{S_{HCO}}$	$mol\ HCO_3\ m^{-3}$
20	Total suspended solids	X_{TSS}	$gTSS\ m^{-3}$
21	Metal hydroxide compounds	X_{MeOH}	$g\ TSS\ (Fe)\ m^{-3}$
22	Metal phosphate compounds	X_{MeP}	$g\ TSS(Fe)m^{-3}$

8.3.1 Biokinetic sub-model presentation

Three groups of microorganisms i.e., heterotrophs (X_{OHOs}), autotrophs (X_{ANOs}), and phosphate accumulating (X_{PAOs}) organisms are relevant to several unknown parameters in each of the processes. The adapted and modified bio-chemical sub-model consisted of 22 state variables and 37 biochemical processes described by the Peterson matrix in **Table 8-2.** The process rate equations for each process are given in **Table 8-3**. The conservation factors for COD, nitrogen (N), phosphorus (P), electric charge (e), and TSS are also presented in **Table 8-3**. While, considering the size of the matrix, full expression of the stoichiometric parameters used in the matrix are given in **Annexure-B.** The use of a matrix simplified the presentation of stoichiometric, kinetic, and process rate equations in the simulation environment.

The elemental mass-balance of each transformation was checked by the approach suggested by Hauduc et al. (2010) to ensure the mathematical accuracy of the model. The mass balance was verified by using Eq. **8.1**.

$$\sum_{j=1}^{j=37} \sum_{k=1}^{k=22} \boldsymbol{\nu}_{j,k} \cdot \boldsymbol{i}_{l,k} = 0; l \in \{\text{COD}, \text{N}, \text{P}, \text{e}, \text{TSS}\} \qquad 8.1$$

Where $\boldsymbol{\nu}$ is the stoichiometric coefficient, $\boldsymbol{i}$ is the conversion factor for COD, N, P, electrical e, and TSS. The subscripts j, k, and l represent the Peterson matrix rows (processes), composition matrix column, and Peterson matrix columns (components), respectively. Furthermore, when implementing the bio-kinetic sub-model, the effect of temperature on the kinetic parameters was considered by applying the Arrhenius equation.

8.3.2 Hydraulic and mass balance sub-models

The hydraulic sub-model helps to ensure the volumetric balances of the flows in each of the reactors in series, considering influent flow, recirculation, and sludge wastage. The volumetric balances and hydraulic retention times of each of the reactors in series are based on the simplified scheme of the plant given in **Fig. 8.2**.

Table 8-2: Peterson Matrix to describe the stoichiometry and process kinetics of the bio-kinetic sub-model

No.	Processes (j)	1	2	3	4	5	6	7	8	9	10	11	12	13	14	15	16	17	18	19	20	21	22	*process rates*
		model components and their stoichiometry (i)																						
		S_{O2}	X_{CB}	S_B	S_{UAP}	S_{BAP}	S_U	S_{NHx}	S_{NOx}	S_{N2}	X_U	X_{EPS}	X_{OHO}	X_{OHO_Stor}	X_{ANO}	S_{PO4}	X_{PAO}	X_{PAO_PP}	X_{PAO_Stor}	S_{HCO}	X_{TSS}	X_{MeOH}	X_{MeP}	
p_1	Hydrolysis		-1	c_1			f_1	g_1								u_1				y_1	z_1			pr_1
p_2	Aerobic storage of $X_{OHO,Stor}$ based on S_B	a_2		-1				i_{N_SB}						m_2		i_{P_SB}				y_2	z_2			pr_2
p_3	Aerobic storage of $X_{OHO,Stor}$ based on S_{UAP}	a_3			-1			i_{N_SUAP}						m_3		i_{P_SB}				y_3	z_3			pr_3
p_4	Aerobic storage of $X_{OHO,Stor}$ based on S_{BAP}	a_4				-1		i_{N_SBAP}						m_4		i_{P_SB}				y_4	z_4			pr_4
p_5	Anoxic storage of $X_{OHO,Stor}$ based on S_B			-1				i_{N_SB}	h_5	$(-h_5)$				m_5		i_{P_SB}				y_5	z_5			pr_5
p_6	Anoxic storage of $X_{OHO,Stor}$ based on S_{UAP}				-1			i_{N_SUAP}	h_6	$(-h_6)$				m_6		i_{P_SB}				y_6	z_6			pr_6
p_7	Anoxic storage of $X_{OHO,Stor}$ based on S_{BAP}					-1		i_{N_SBAP}	h_7	$(-h_7)$				m_7		i_{P_SB}				y_7	z_7			pr_7
p_8	Aerobic growth of X_{OHO} based on S_B	a_8		c_8	d_8			g_8				j_8	k_8			u_8				y_8	z_8			pr_8
p_9	Aerobic growth of X_{OHO} based on S_{UAP}	a_9			d_9			g_9				j_9	k_9			u_9				y_9	z_9			pr_9
p_{10}	Aerobic growth of X_{OHO} based on S_{BAP}	a_{10}				e_{10}		g_{10}				j_{10}	k_{10}			u_{10}				y_{10}	z_{10}			pr_{10}
p_{11}	Aerobic growth of X_{OHO} based on $X_{OHO,Stor}$	a_{11}			d_{11}			g_{11}				j_{11}	k_{11}	m_{11}		u_{11}				y_{11}	z_{11}			pr_{11}
p_{12}	Anoxic growth of X_{OHO} based on S_B			c_{12}	d_{12}			g_{12}	h_{12}	$(-h_{12})$		j_{12}	k_{12}			u_{12}				y_{12}	z_{12}			pr_{12}
p_{13}	Anoxic growth of X_{OHO} based on S_{UAP}				d_{13}			g_{13}	h_{13}	$(-h_{13})$		j_{13}	k_{13}			u_{13}				y_{13}	z_{13}			pr_{13}
p_{14}	Anoxic growth of X_{OHO} based on S_{BAP}					e_{14}		g_{14}	h_{14}	$(-h_{14})$		j_{14}	k_{14}			u_{14}				y_{14}	z_{14}			pr_{14}
p_{15}	Anoxic growth of X_{OHO} based on $X_{OHO,Stor}$				d_{15}			g_{15}	h_{15}	$(-h_{15})$		j_{15}	k_{15}	m_{15}		u_{15}				y_{15}	z_{15}			pr_{15}
p_{16}	Growth of X_{ANO} (Nitrification)	a_{16}			d_{16}			g_{16}	$1/Y_{ANO}$			j_{16}			n_{16}	u_{16}				y_{16}	z_{16}			pr_{16}
p_{17}	Hydrolysis of X_{EPS}			c_{17}		e_{17}		g_{17}				-1								y_{17}	z_{17}			pr_{17}
p_{18}	Aerobic respiration of $X_{OHO,Stor}$	-1												-1							z_{18}			pr_{18}
p_{19}	Anoxic respiration of $X_{OHO,Stor}$								$-1/i_{NO3\_N2}$	$1/i_{NO3\_N2}$				-1						y_{19}	z_{19}			pr_{19}
p_{20}	Aerobic endogenous respiration of X_{OHO}	a_{20}				e_{20}		g_{20}			i_{20}	j_{20}	-1			u_{20}				y_{20}	z_{20}			pr_{20}
p_{21}	Anoxic endogenous respiration of X_{OHO}					e_{21}		g_{21}	h_{21}	$(-h_{25})$	i_{21}	j_{21}	-1			u_{21}				y_{21}	z_{21}			pr_{21}
p_{22}	Aerobic endogenous respiration of X_{ANO}	a_{22}				e_{22}		g_{22}			i_{22}	j_{22}			-1	u_{22}				y_{22}	z_{22}			pr_{22}
p_{23}	Anoxic endogenous respiration of X_{ANO}					e_{23}		g_{23}	h_{23}	$(-h_{23})$	i_{23}	j_{23}			-1	u_{23}				y_{23}	z_{23}			pr_{23}
p_{24}	Aeration	1																						pr_{24}
p_{25}	Storage of X_{PHA}			-1				i_{N_SB}								u_{25}		w_{25}	1	y_{25}	z_{25}			pr_{25}
p_{26}	Aerobic storage of X_{PP}	a_{26}														-1		1	x_{26}	y_{26}	z_{26}			pr_{26}
p_{27}	Anoxic storage of X_{PP}								h_{27}	$(-h_{27})$						-1		1	x_{27}	y_{27}	z_{27}			pr_{27}
p_{28}	Aerobic growth of X_{PAO}	a_{28}						$-i_{N\_XBio}$								$-i_{P\_XBio}$	1		x_{28}	y_{28}	z_{28}			pr_{28}

No.	Processes (j)	1	2	3	4	5	6	7	8	9	10	11	12	13	14	15	16	17	18	19	20	21	22	process rates
		model components and their stoichiometry (i)																						
		S_{O2}	X_{CB}	S_B	S_{UAP}	S_{BAP}	S_U	S_{NHx}	S_{NOx}	S_{N2}	X_U	X_{EPS}	X_{OHO}	X_{OHO_Stor}	X_{ANO}	S_{PO4}	X_{PAO}	X_{PAO_PP}	X_{PAO_Stor}	S_{HCO}	X_{TSS}	X_{MeOH}	X_{MeP}	
p_{29}	Anoxic growth of X_{PAO}							$-i_{N\_XBio}$	h_{29}	$(-h_{29})$						$-i_{P\_XBio}$	1		x_{29}	y_{29}	z_{29}			pr_{29}
p_{30}	Aerobic endogenous respiration of X_{PAO}	a_{30}						g_{30}			i_{30}					u_{30}	-1			y_{30}	z_{30}			pr_{30}
p_{31}	Anoxic endogenous respiration of X_{PAO}							g_{31}	h_{31}	$(-h_{31})$	i_{31}					u_{31}	-1			y_{31}	z_{31}			pr_{31}
p_{32}	Aerobic lysis of X_{PP}															1		-1		y_{32}	z_{32}			pr_{32}
p_{33}	Anoxic lysis of X_{PP}															1		-1		y_{33}	z_{33}			pr_{33}
p_{34}	Aerobic respiration of X_{PHA}	-1																	-1		z_{34}			pr_{34}
p_{35}	Anoxic respiration of X_{PHA}								h_{35}	$(-h_{35})$									-1	y_{35}	z_{35}			pr_{35}
p_{36}	Precipitation															-1				y_{36}	1.42	-3.45	4.86	pr_{36}
p_{37}	Redissolution															1				y_{37}	-1.42	3.45	-4.86	pr_{37}
Conservatives																								
1	COD	-1	1	1	1	1	1		i_{COD_NO3}	i_{COD_NO2}	1	1	1	1	1		1		1					
2	Nitrogen		i_{N_XCB}	i_{N_SB}	i_{N_SUAP}	i_{N_SBAP}	i_{N_SU}	1	1	1	i_{N_XU}	i_{N_XEPS}	i_{N_XBio}		i_{N_XBio}		i_{N_XBio}							
3	Phosphorus		i_{P_XCB}								i_{P_XU}		i_{P_XBio}		i_{P_XBio}		i_{P_XBio}						31/150.8	
4	Ionic/electrical charge							1/14	-1/14							-1.5/31		-1/31		-1				
5	TSS		i_{TSS_XCB}								i_{TSS_XU}	i_{TSS_XEPS}	i_{TSS_XBio}	$i_{TSS\_XOHO\_Stor}$	i_{TSS_XBio}		i_{TSS_XBio}	3.23	0.6		-1	1	1	

Table 8-3: Kinetic rate expressions for the ASM3-EPS-SMP-P biokinetic sub-model

Process	process rates expressions
pr_1	$q_{XCB\_SB\_hyd}$ * $\mathbf{Msat_{XCB\_XOHO\_KCB\_hyd}}$ * X_{OHO}
pr_2	f_{STO} * q_{SB_Stor} * $\mathbf{Msat_{SO2\_KO2\_OHO}}$ * $\mathbf{Msat_{SB\_KSB\_OHO}}$ * X_{OHO}
pr_3	f_{STO} * q_{SUAP} * $\mathbf{Msat_{SO2\_KO2\_OHO}}$ * $\mathbf{Msat_{UAP\_OHO}}$ * X_{OHO}
pr_4	f_{STO} * q_{SUAP} * $\mathbf{Msat_{SO2\_KO2\_OHO}}$ * $\mathbf{Msat_{BAP\_OHO}}$ * X_{OHO}
pr_5	f_{STO} * q_{SB_Stor} * nu_{OHO_AX} * $\mathbf{Minh_{SO2\_OHO}}$ * $\mathbf{Msat_{SNOx\_KNOx\_OHO}}$ * $\mathbf{Msat_{SB\_KSB\_OHO}}$ * X_{OHO}
pr_6	f_{STO} * q_{SUAP_stor} * nu_{OHO_AX} * $\mathbf{Minh_{SO2\_OHO}}$ * $\mathbf{Msat_{SNOx\_KNOx\_OHO}}$ * $\mathbf{Msat_{UAP\_OHO}}$ * X_{OHO}
pr_7	f_{STO} * q_{SBAP_stor} * nu_{OHO_AX} * $\mathbf{Minh_{SO2\_OHO}}$ * $\mathbf{Msat_{SNOx\_KNOx\_OHO}}$ * $\mathbf{Msat_{BAP\_OHO}}$ * X_{OHO}
pr_8	$(1-f_{STO})$ * μ_{OHO_Max} * $\mathbf{Msat_{SO2\_KO2\_OHO}}$ * $\mathbf{Msat_{SB\_KSB\_OHO}}$ * $\mathbf{Msat_{SNHx\_KNHx\_OHO}}$ * $\mathbf{Msat_{SHCO\_KAlk\_OHO}}$ * $\mathbf{Msat_{SPO4\_KPO4\_OHO}}$ * X_{OHO}
pr_9	$(1-f_{STO})$ * $\mu_{OHO\_SMP\_max}$ * $\mathbf{Msat_{SO2\_KO2\_OHO}}$ * $\mathbf{Msat_{UAP\_OHO}}$ * $\mathbf{Msat_{SNHx\_KNHx\_OHO}}$ * $\mathbf{Msat_{SHCO\_KAlk\_OHO}}$ * $\mathbf{Msat_{SPO4\_KPO4\_OHO}}$ * X_{OHO}
pr_{10}	$(1-f_{STO})$ * $\mu_{OHO\_SMP\_max}$ * $\mathbf{Msat_{SO2\_KO2\_OHO}}$ * $\mathbf{Msat_{BAP\_OHO}}$ * $\mathbf{Msat_{SNHx\_KNHx\_OHO}}$ * $\mathbf{Msat_{SHCO\_KAlk\_OHO}}$ * $\mathbf{Msat_{SPO4\_KPO4\_OHO}}$ * X_{OHO}
pr_{11}	μ_{OHO_Max} * $\mathbf{Msat_{SO2\_KO2\_OHO}}$ * $\mathbf{Msat_{SNHx\_KNHx\_OHO}}$ * $\mathbf{Msat_{XSTO\_XOHO\_qSB\_stor}}$ * $\mathbf{Msat_{SHCO\_KAlk\_OHO}}$ * $\mathbf{Msat_{SPO4\_KPO4\_OHO}}$ * X_{OHO}
pr_{12}	$(1-f_{STO})$ * μ_{OHO_Max} * $nu_{OHO_{AX}}$ * $\mathbf{Minh_{SO2\_OHO}}$ * $\mathbf{Msat_{SNOx\_KNOx\_OHO}}$ * $\mathbf{Msat_{SNHx\_KNHx\_OHO}}$ * $\mathbf{Msat_{SHCO\_KAlk\_OHO}}$ * $\mathbf{Msat_{SB\_KSB\_OHO}}$ * $\mathbf{Msat_{SPO4\_KPO4\_ANO}}$ * X_{OHO}
pr_{13}	$(1-f_{STO})$ * $\mu_{OHO\_SMP\_max}$ * nu_{OHO_AX} * $\mathbf{Minh_{SO2\_OHO}}$ * $\mathbf{Msat_{SNOx\_KNOx\_OHO}}$ * $\mathbf{Msat_{UAP\_OHO}}$ * $\mathbf{Msat_{SNHx\_KNHx\_OHO}}$ * $\mathbf{Msat_{SHCO\_KAlk\_OHO}}$ * $\mathbf{Msat_{SPO4\_KPO4\_ANO}}$ * X_{OHO}
pr_{14}	$(1-f_{STO})$ * $\mu_{OHO\_SMP\_max}$ * nu_{OHO_AX} * $\mathbf{Minh_{SO2\_OHO}}$ * $\mathbf{Msat_{SNOx\_KNOx\_OHO}}$ * $\mathbf{Msat_{BAP\_OHO}}$ * $\mathbf{Msat_{SNHx\_KNHx\_OHO}}$ * $\mathbf{Msat_{SHCO\_KAlk\_OHO}}$ * $\mathbf{Msat_{SPO4\_KPO4\_ANO}}$ * X_{OHO}
pr_{15}	μ_{OHO_Max} * nu_{OHO_AX} * $\mathbf{Minh_{SO2\_OHO}}$ * $\mathbf{Msat_{SNOx\_KNOx\_OHO}}$ * $\mathbf{Msat_{SNHx\_KNHx\_OHO}}$ * $\mathbf{Msat_{XOHO\_qSB\_stor}}$ * $\mathbf{Msat_{SHCO\_KAlk\_OHO}}$ * $\mathbf{Msat_{SPO4\_KPO4\_ANO}}$ * X_{OHO}
pr_{16}	μ_{ANO_Max} * $\mathbf{Msat_{SO2\_KO2\_ANO}}$ * $\mathbf{Msat_{SNHx\_KNHx\_ANO}}$ * $\mathbf{Msat_{SHCO\_KAlk\_ANO}}$ * $\mathbf{Msat_{SPO4\_KPO4\_ANO}}$ * X_{ANO}
pr_{17}	$q_{XEPS\_SBAP\_hyd}$ * $\mathbf{Msat_{XEPS\_hyd}}$ * X_{OHO}
pr_{18}	m_{Stor_Ox} * $\mathbf{Msat_{SO2\_KO2\_OHO}}$ * X_{OHO_Stor}
pr_{19}	m_{Stor_Ax} * $\mathbf{Minh_{SO2\_OHO}}$ * $\mathbf{Msat_{SNOx\_KNOx\_OHO}}$ * X_{OHO_Stor}
pr_{20}	m_{OHO_ox} * $\mathbf{Msat_{SO2\_KO2\_OHO}}$ * X_{OHO}
pr_{21}	m_{OHO_Ax} * $\mathbf{Minh_{SO2\_OHO}}$ * $\mathbf{Msat_{SNOx\_KNOx\_OHO}}$ * X_{OHO}
pr_{22}	m_{ANO_ox} * $\mathbf{Msat_{SO2\_KO2\_ANO}}$ * X_{ANO}
pr_{23}	m_{ANO_Ax} * $\mathbf{Minh_{SO2\_ANO}}$ * $\mathbf{Msat_{SNOx\_KNOx\_OHO}}$ * X_{ANO}
pr_{24}	K_{La} * $(S_{O2sat} - S_{O2})$
pr_{25}	$q_{PAO\_SB\_Stor}$ * $\mathbf{Msat_{SB\_KSB\_PAO}}$ * $\mathbf{Msat_{XPP\_XPAO\_Ks\_fPP\_PAO}}$ * $\mathbf{Msat_{SHCO\_KAlk\_PAO}}$ * X_{PAO}

Process	process rates expressions
pr26	$q_{PAO\_PO4\_PP} * \mathbf{Msat_{SO2\_KO2\_PAO}} * \mathbf{Msat_{SPO4\_KPO4\_PAO}} * \mathbf{Msat_{XPAO\_sto\_XPAO\_Kfstor\_PAO}} * \mathbf{Minh_{XPP\_XPAO\_KI\_fPP\_PAO}} * \mathbf{Msat_{SHCO\_KAlk\_PAO}} * X_{PAO}$
pr27	$q_{PAO\_PO4\_PP} * nu_{PAO} * \mathbf{Minh_{SO2\_PAO}} * \mathbf{Msat_{SNOx\_KNOx\_PAO}} * \mathbf{Msat_{SPO4\_KPO4\_PP}} * \mathbf{Msat_{SHCO\_KAlk\_PAO}} * \mathbf{Msat_{XPP\_XPAO\_Ks\_fPP\_PAO}} * \mathbf{Minh_{XPP\_XPAO\_KI\_fPP\_PAO}} * X_{PAO}$
pr28	$\mu_{PAO\_Max} * \mathbf{Msat_{SO2\_KO2\_PAO}} * \mathbf{Msat_{SNHx\_KNHx\_PAO}} * \mathbf{Msat_{SPO4\_KPO4\_PAO}} * \mathbf{Msat_{SHCO\_KAlk\_PAO}} * \mathbf{Msat_{XPAO\_sto\_XPAO\_Kfstor\_PAO}} * X_{PAO}$
pr29	$\mu_{PAO\_Max} * nu_{PAO} * \mathbf{Minh_{SO2\_PAO}} * \mathbf{Msat_{SNOx\_KNOx\_PAO}} * \mathbf{Msat_{SPO4\_KPO4\_PAO}} * \mathbf{Msat_{XPAO\_sto\_XPAO\_Kfstor\_PAO}} * \mathbf{Msat_{SHCO\_KAlk\_PAO}} * X_{PAO}$
pr30	$m_{PAO} * \mathbf{Msat_{SO2\_KO2\_PAO}} * X_{PAO}$
pr31	$m_{PAO} * nm_{PAO} * \mathbf{Minh_{SO2\_PAO}} * \mathbf{Msat_{SNOx\_KNOx\_PAO}} * X_{PAO}$
pr32	$b_{PP\_PO4} * \mathbf{Msat_{SO2\_KO2\_PAO}} * X_{PAO\_PP}$
pr33	$b_{PP\_PO4} * nb_{PP\_PO4} * \mathbf{Minh_{SO2\_PAO}} * \mathbf{Msat_{SNOx\_KNOx\_PAO}} * X_{PAO\_PP}$
pr34	$m_{PAO\_stor} * \mathbf{Msat_{SO2\_KO2\_PAO}} * X_{PAO\_Stor}$
pr35	$m_{PAO\_stor} * nm_{PAO\_stor} * \mathbf{Minh_{SO2\_PAO}} * \mathbf{Msat_{SNOx\_KNOx\_PAO}} * X_{PAO\_Stor}$
pr36	$q_{P\_pre} * S_{PO4} * X_{MeOH}$
pr37	$q_{P\_red} * X_{MeP} * (S_{HCO})/(K_{alk\_pre}+S_{HCO})$

Whereas, saturation and inhabitation terms used in the process rates calculations are as follows;

$$\mathbf{Msat_{SO2\_KO2\_OHO}} = \frac{S_{O2}}{(K_{O2\_OHO}+S_{O2})}; \mathbf{Msat_{SO2_{KO2_{OHO}}}} = \frac{S_B}{(K_{SB_{OHO}}+S_B)}; \mathbf{Msat_{UAP\_OHO}} = \frac{S_{SUAP}}{(K_{SUAP\_OHO}+S_{UAP})}; \mathbf{Msat_{SNHx\_KNHx\_OHO}} = \frac{S_{NHx}}{(K_{NHX\_OHO}+S_{NHx})}$$

$$\mathbf{Msat_{SNOx\_KNOx\_OHO}} = \frac{S_{NOx}}{(K_{NOx\_OHO}+S_{NOx})}; \mathbf{Msat_{BAP\_OHO}} = \frac{S_{BAP}}{(K_{BAP\_OHO}+S_{BAP})}; \mathbf{Msat_{SHCO\_KAlk\_OHO}} = \frac{S_{HCO}}{(K_{Alk\_OHO}+S_{HCO})}; \mathbf{Msat_{SPO4\_KPO4\_OHO}} = \frac{S_{SPO4}}{(K_{PO4\_OHO}+S_{PO4})}$$

$$\mathbf{Minh_{SO2\_OHO}} = \frac{K_{O2\_OHO}}{(K_{O2\_OHO}+S_{O2})}; \mathbf{Msat_{SO2\_KO2\_PAO}} = \frac{S_{O2}}{(K_{O2\_PAO}+S_{O2})}; \mathbf{Msat_{SB\_KSB\_PAO}} = \frac{S_B}{(K_{SB\_PAO}+S_B)}; \mathbf{Msat_{SNHx\_KNHx\_PAO}} = \frac{S_{NHx}}{(K_{NHx\_PAO}+S_{NHx})}$$

$$\mathbf{Msat_{SHCO_{KAlk_{PAO}}}} = \frac{S_{HCO}}{(K_{Alk_{PAO}}+S_{HCO})}; \mathbf{Msat_{SPO4_{KPO}}} = \frac{S_{PO4}}{(K_{PO4_{PAO_{nut}}}+S_{PO4})}; \mathbf{Msat_{SPO4\_PAO\_upt}} = \frac{S_{PO4}}{(K_{PO4\_PAO\_upt}+S_{PO4})}; \mathbf{Msat_{SNOx\_PAO}} = \frac{S_{NOx}}{(K_{NOx_{PAO}}+S_{NOx})};$$

$$\mathbf{Minh_{SO2\_PAO}} = \frac{K_{O2\_PAO}}{(K_{O2\_PAO}+S_{O2})}; \mathbf{Msat_{SPO4\_KPO4\_ANO}} = \frac{S_{PO4}}{(K_{PO4\_ANO}+S_{PO4})}; \mathbf{Msat_{SNHx\_KNHx\_ANO}} = \frac{S_{NHx}}{(K_{NHx\_ANO}+S_{NHx})}; \mathbf{Msat_{SO2\_KO2\_ANO}} = \frac{S_{O2}}{(K_{O2\_ANO}+S_{O2})}; \mathbf{Minh_{SO2\_ANO}} = \frac{K_{O2\_ANO}}{(K_{O2\_ANO}+S_{O2})};$$

$$\mathbf{Msat_{XPAO\_sto\_XPAO\_Kfstor\_PAO}} = \frac{(X_{PAO\_stor}/X_{PAO})}{\left(K_{fstor\_PAO}+(X_{PAO\_stor}/X_{PAO})\right)}; \mathbf{Msat_{XPP\_XPAO\_Ks\_fPP\_PAO}} = \frac{(X_{PAO\_PP}/X_{PAO})}{\left(f_{PP\_PAO\_Max}+(X_{PAO\_PP}/X_{PAO})\right)}; \mathbf{Msat_{XSTO\_XOHO\_qSB\_stor}} = \frac{(X_{OHO\_stor}/X_{OHO})}{\left(K_{fStor\_OHO}+(X_{OHO\_stor}/X_{OHO})\right)}$$

$$\mathbf{Minh_{XPP\_XPAO\_KI\_fPP\_PAO}} = \frac{\left(K_{S\_fPP\_PAO}-(X_{PAO\_PP}/X_{PAO})\right)}{\left(K_{I\_fPP\_PAO}+f_{PP\_PAO\_Max}-(X_{PAO\_PP}/X_{PAO})\right)}; \mathbf{Msat_{XCB\_XOHO\_KCB\_hyd}} = \frac{(X_{CB}/X_{OHO})}{\left(K_{XCB\_hyd}+(X_{CB}/X_{OHO})\right)};$$

The reactions described by the model were solved through a set of ordinary differential equations (ODEs) for a known initial concentration of pollutants in each of the tanks considered as reactor in series with assumed complete mixing. The differential **Eqs. 8.2-8.3**, describing the mass balances of the soluble and particulate components of the Peterson matrix for known compositions in the membrane aerated reactor, respectively, is presented as an example, respectively. These differential equations were then solved using $ODE15_s$ algorithm of the MATLAB. The values of the stoichiometric and kinetic parameters adopted from Fan et al. (2011), Janus (2013), and Rieger et al.(2012) are given in **Annexure-B.**

$$\frac{d}{dt}\left(C_{S_k}\right)=\frac{Q_{r4}\cdot C_{sk\,in}-\left(Q_{Eff}+Q_{inf}\cdot r_3+Q_w\right)\cdot C_{sk\,out}}{V_{MT}}+\sum_{k=1}^{n}\nu_{j,k}\cdot\rho_j \qquad 8.2$$

$$\frac{d}{dt}\left(C_{X_k}\right)=\frac{Q_{r4}\cdot C_{Xk\,in}-\left(Q_{inf}\cdot r_3+Q_w\right)\cdot C_{Xk\,out}}{V_{MT}}+\sum_{k=1}^{n}\nu_{j,k}\cdot\rho_j \qquad 8.3$$

Where; Q_{r4} is sludge flow ($m^3.d^{-1}$) to the membrane aerated reactor; S_{sk} and S_{Xk} are the concentration of the soluble and particulate components of the Peterson matrix respectively, the subscripts, 'in", "out" and "w" represent, influent, effluent and waste sludge respectively. The notation, $V_{j,k}$ represents the stoichiometric coefficient corresponding to the process "j" and component "k" of the Peterson matrix, while ρ_j represents the corresponding conversion rate by which each of the processes in the Peterson matrix is governed. The first terms on the left-hand side of both expressions reflect the accumulation process within the reactor, while the second terms describe the conversion rate of the given pollutant and thus its removal.

8.4 CHEMICAL PRECIPITATION SUB-MODEL

Chemically enhanced phosphorus removal is accomplished by adding $FeCl_3$ .Two chemical processes are adapted from ASM2d to empirically model the phosphorus precipitation with $FeCl_3$ and production of hypothetical complexes i.e., $Fe\,(OH)_3$ and $FePO_4$, by considering their reaction rates and stoichiometry. The precipitation and re-dissolution are assumed to be reverse processes, which are balanced at steady state according to **Eq. 8.4**,. At the same time, the concentration of $FeCl_3$, in terms of

available MeOH, is computed using **Eq. 8.5**. The ODEs related to the addition of $FeCl_3$ in the overall code are activated only if the coagulant is being added and the duration of which is specified.

$$FeCl_3 + PO_4^{3-} \rightleftharpoons FePO_4 \downarrow + 3Cl^- \quad 8.4$$

$$MeOH[gTSSm^{-3}] = \frac{Q_{FeCl_3} \times \rho \times \phi \times \left(\frac{M_{Me(OH)3}}{M_{FeCl3}} \right) \times 1000}{Q_S} \quad 8.5$$

Where; Q_{FeCl3} is the flow rate ($m^3.d^{-1}$) of the ferric chloride solution; ρ is the density of the $FeCl_3$, φ is the percentage purity of the solution (decimal), M_{Fe} is the molar mass of ferric (55.845 $g.mol^{-1}$), M_{FeCl3} is the molar mass of the ferric chloride (162.2 $g.mol^{-1}$), $M_{Me\,(OH)3}$ is molar mass of ferric hydroxide and Q_s is the flow rate of sludge in anoxic/aerobic reactor. The average Fe/ P molar ratio of 2.17 was calculated from data available for influent P-loading and $FeCl_3$ additions. It was found to be sufficient to reduce the PO_4^{3-} below set point and within the optimum range found in the literature (Nadeem et al., 2022)

The precipitation model adapted in this work is easy to implement and calibrate (due to the limited number of parameters), as concluded in the ***section 4.1.3.3***

8.5 AERATION SUB-MODEL

Fine bubble aeration allows maintaining a DO concentration for nitrification and organic carbon removal in the activated sludge process in the aerated zone of the MBR. A dynamic oxygen transfer coefficient ($K_L a$) is used, considering the actual airflow rates. The aeration sub-model is based on the theory developed by Boyle et al. (1989) with an extension to consider the correlation between αSOTE, SRT, tank geometry, and the airflow, proposed by Rosso et al.(2005). *This aeration sub-model is adapted and modified to estimate the dynamic $K_L a$ considering the actual airflow rate being provided by the blowers and taking into account the design configuration of the aeration system at SAV-MBR.*

Keeping in view the similar configurations of the aeration system in all the six biological basins and to simplify the aeration model complexity, it was hypothesized

that all aeration basins are operated on a single set point (2.5 g.m^{-3}). This assumption is also used to calculate a daily average dynamic K_La value considering the total airflow rates, the number of diffusers and their associated bubbling surface area, diffuser submergence, SRT, standard oxygen transfer efficiency (SOTE) of the installed aeration system, temperature of the sludge, MLSS concentrations, sludge density, and state of the diffusers (fouling).

As suggested by Rosso et al.(2005), the diffuser-specific area was adopted from the design specifications manual provided by the aeration system supplier of the SAV MBR plant. In this procedure, only the actual bubbling or active surface area was considered, and the normalized airflow per diffuser was calculated from **Eq. 8.6**.

$$Q_n = \frac{Q_{air}}{A_s \times N_d \times H_d} \qquad 8.6$$

Where: Q_n is the normalized air flow rate (sec^{-1}) per diffuser; Q_{air} is air flow rate (m^3 .sec^{-1}); A_s is the diffusers specific area (m^3); N_d is the number of the diffusers and H_d is submergence height (m) of the diffuser. Rosso et al.(2005) used characteristic number χ (days. sec) to group all operating parameters and calculated by **Eq. 8.7** below.

$$\chi = \frac{SRT}{Q_n} \qquad 8.7$$

Regression analyses of αSOTE as linear functions of *log* χ is presented by **Eq. 8.8** where, A and B are coefficient of regression analysis.

$$\alpha SOTE = A \times \log_{10}(\chi) - B \qquad 8.8$$

According to Boyle et al. (1989), diffuser submergence affects the oxygen transfer rate as depicted in the relationship **Eq. 8.9**. Where, α is an empirical factor (unit less) and SOTE is standard oxygen transfer efficiency (% per meter depth). The α value is known to be highly correlated with MLSS concentrations (Insel et al., 2011).

$$\alpha = \frac{\alpha SOTE}{SOTE \times H_d} \times 100 \qquad 8.9$$

Standard oxygen transfer rate (SOTR) at 20 ^{0}C and 1atm is given by the **Eq. 8.10**. Where, ρ_{air} is density of the air (kg.m^{-3}) and X_{O2} is fraction of oxygen in the air (%).

$$SOTR = Q_{air} \times \rho_{air} \times \frac{SOTE \times H_d}{100} \times \frac{X_{O_2}}{100} \quad 8.10$$

Field oxygen transfer rates (OTR_f) is the basic parameter used to quantify the ability of the aeration system to transfer oxygen into the water per unit of time, kgO_2.d^{-1}, while OTR_f is the total weight of oxygen from the input air which is transferred (dissolved) into the water. The OTR_f while taking into account the oxygen diffusion limitation and diffuser fouling (Boyle et al., 1989; Jenkins, 2013; Suh et al., 2013) can be given by **Eq. 8.11** below.

$$OTR_f = SOTR \times \theta^{T-20} \times \frac{(\beta_{tension} \times (C_\infty - C_L))}{C^*_{\infty 20}} \times \alpha_{oxygen} \times F_{diff\_fouling} \quad 8.11$$

Where $\beta_{tension}$ is the salinity surface tension correction factor, α_{oxygen} is the clean to process water correction factor, which is calculated from **Eq. 8.12,** Θ is the temperature correction factor for O_2 transfer, and $F_{diff\_fouling}$ is the correction factor for fouling of an air diffuser. While C_∞ is the DO saturation concentration for clean water in an aeration reactor, is calculated from **Eq. 8.13**. C_L is the required O_2 concentration (2.5 mg.L^{-1}) in the aerated tank. $C_{\infty 20}$ is the DO saturation concentration in clean water at 20 °C and 1 atm (gO_2m^{-3}).

$$\alpha_{oxygen} = \exp^{\omega \times XTSS} \quad 8.12$$

Where, ω is the α_{oxygen} factor exponent coefficient and X_{TSS} is the total suspended solid concentration of mixed liquor (g.L^{-1}). The dissolved oxygen saturation concentration for clean water in **Eq. 8.15** is calculated from **Eq. 8.13** :

$$C_\infty = 0.5 \times C_{\infty 20} \times \left(\frac{P_d}{P_{atm}} + \frac{O_{out}}{X_{O_2}} \right) \quad 8.13$$

Where, P_d is the pressure at the bottom of an aeration reactor which is calculated from **Eq. 8.14,** P_{atm} is the atmospheric pressure (101,300 Pa), and O_{out} is the percentage of oxygen in the air leaving the surface of an aerated reactor (%), which is calculated from **Eq. 8.15**.

$$P_d = \rho_s \times g \times H_d + P_{atm} \qquad 8.14$$

Where; ρ_s is the density of sludge (kg.m^{-3}), calculated using **Eq. 8.19** and g is the gravitational acceleration (9.81 m.s^{-2}).

$$O_{out} = X_{O2} \times (1 - SOTE \times H_{d \times} \alpha_{oxygen}) \qquad 8.15$$

Based on the actual calculated OTR_f, the dynamic K_{La} for the biologically aerated reactor is calculated using **Eq. 8.16** which is assumed to be the same for the membrane aerated reactor. While the K_{La} for non-aerated reactors is assumed to be close to zero.

$$K_{La} = \frac{OTR_f}{(\beta_{tension} \times C_\infty - C_L) \times V_T} \qquad 8.16$$

Where, V_T is the volume (m^3) of the aerated reactor. While other parameters have already been defined heretofore. The values of parameters used in aeration-sub model are summarized in **Table 8-4**.

Table 8-4: Values of parameters used in aeration sub-model

Symbol	description	unit	range	references
$f_{diff\_fouling}$	Correction factor for diffuser fouling	--	0.8 - 1	(Suh et al., 2013)
SOTE	standard oxygen transfer efficacy of diffuser	%	1.5 - 5	(Hai et al., 2018 ; Jenkins, 2013; Suh et al., 2013)
$\beta_{tension}$	Salinity surface tension correction factor	--	0.9 - 0.99	(Jenkins, 2013 ; Suh et al., 2013)
ρ_{air}	density of air	kg.m^{-3}	1.28	(El-Said et al., 2017)
ω	α_{oxygen} coefficient for O_2 transfer correction associated with X_{TSS} concentrations	--	0.046-0.087	(Germain et al., 2007; Krampe and Krauth, 2003; Muller et al., 1995)

8.6 FOULING SUB-MODEL

In this work, the resistance in series (RIS) model with the sectional approach proposed by Li and Wang (2006) is adopted to take into account the incremental development

of the fouling. *The RIS model is chosen over several available fouling models (see **section 4.1.3.4**) due to the fact that, it is likely the most complete, universally acceptable, easy to use, and able to more comprehensively describe the fouling evolution (Bella and Trapani, 2019).*

It has been hypothesized that the immersed membrane surface experiences non-uniform distribution of shear induced by the air scouring, resulting in uneven deposition of the cake layer and variable flux across the membrane surface. To accommodate this phenomenon, the membrane surface was assumed to be static and divided into 128 dimensionally (*i*,*j*) equal sections. In addition, the following modifications and assumptions were considered:

a) In addition to filtration and aeration mechanisms, intermittency of relaxation and coarse bubble aeration, as well as sequenced backwashing, were considered in synchronization with filtration-relaxation
b) Instead of static specific cake resistance (see **section 9.2.1.3**), dynamic specific cake resistance is considered.
c) Considering the low concentration of soluble EPS (or S_{MPs}, which is modeled as the sum of S_{UAP} and S_{BAP}) compared to X_{EPS} (<1% of the total EPS) and X_{TSS}, the S_{MPs} contribution to the development of the cake layer is ignored. The specific cake resistance, however, is linked to several other factors, including i) chemical properties of the foulants, TMP, MLSS concentration, the viscosity of the sludge, and X_{EPS} concentrations (Cho et al., 2005; Lee et al., 2002);
d) The effect of the chemical cleaning and coagulant addition on the particle size distribution and sludge properties is not considered. The coagulant addition impacts the fouling only by the increase of X_{TSS}
e) Effect of the cake layer as filter media to retain soluble COD is not considered.

Keeping in view the functional specificities of the Seine Aval MBR plant, the mathematical structure of the RIS model is presented in the following sections.

8.5.1. Net cake layer during filtration mode and under the influence of aeration

When MBR is in the filtration mode, the suspended flocs of sludge approach (X_{TSS}) the surface of the membrane under the force exerted by the permeate cross flow, however shear exerted by the coarse bubble aeration prevents sludge deposition onto

the membrane surface. Under these opposing forces, the net accumulation rate of the dynamic sludge cake ($\frac{d_{Mdc}}{dt}$) for each of the 128 sections is described by the conservation equation (**Eq. 8.17**). The first part of the equation describes the attachment rate of the sludge particles, from the deposit result probability leant on the effect of opposite drag forces for suction and lift force from aeration. It increases with the increase in permeate flux (J) and X_{TSS} concentration and decreases with the increase in transverse lift ($C_d . d_p$) and aeration shear intensity (G). The second part of the **Eq. 8.17** describes the rate of biomass detachment during the filtration process and under the influence of aeration, which is a function of the sludge stickiness ($\alpha_{stickiness}$), sludge compressibility (γ) and filtration time (t_f), permeate production per unit area of the membrane (V_f), erosion rate coefficient (β_{dc}) and the shear intensity. Therefore, at a given shear intensity, a stickier cake layer (associated with the higher α values) is more difficult to remove. Similarly, higher filtration time and compression coefficient also reduce the sludge detachment rates, thus increase the net cake layer accumulation.

$$\frac{dM_{dc(i)}}{dt} = \frac{24 X_{TSS} J^2}{24J + C_d . d_p G} - \frac{\beta_{dc}(1-\alpha_{stickness}) G M_{dc}^2}{\gamma V_f t_f + M_{dc}} \qquad 8.17$$

The sine curve expression proposed by Li and Wang (2006) is adopted to estimate the apparent shear intensity (G) for each of the membrane sections .

$$G(i) = \begin{cases} \left[0.1 + 0.45 \cdot \left(1 + \sin . \frac{(2\varepsilon_i - \varepsilon_a).\pi}{2\varepsilon_a}\right)\right] . \sqrt{\frac{\rho_s . g . q_a}{\mu_s}} ; \varepsilon_i < \varepsilon_a \text{.....(a)} \\ \sqrt{\frac{\rho_s . g . q_a}{\mu_s}} ; \varepsilon_i \geq \varepsilon_a \text{.....(b)} \end{cases} \qquad 8.18$$

First part of the **Eq. 8.18** (a) describes the distribution of shear in first 85 sections. Where, ε_i is the accumulated surface area of these (<85) fractions, while second part of **Eq. 8.18** (b) describes the shear on, ε_a which is membrane surface fractions (>85) with maximum shear intensity. Whereas ρ_s and μ_s are density (kg.m^{-3}) and viscosity (Pa.s) of the sludge, which can be estimated by **Eqs. 8.19-8.20,** respectively. While q_a (L.m^2.s^{-1}) is the specific aeration intensity given by **Eq.8.21**.

$$\rho_s = \rho_w \times 0.99959 \times \exp^{0.0004397 \times X_{TSS}} \quad 8.19$$

$$\mu_s = \mu_w \times 1.05 \times \exp^{0.08 \times X_{TSS}} \quad 8.20$$

$$q_a = \left[\frac{Q_{CB}}{A_m} \right] \quad 8.21$$

Where ρ_w is the density of the water (kg.m^{-3}), T is the temperature ($^{\circ}$C) of permeate, Q_{CB} is the airflow rate (L.sec^{-1}) and A_m is the surface area (m^2) of the membrane under operation at a given time.

8.5.2. Dynamic cake detachment under relaxation mode

The dynamic sludge cake layer is time-dependent, and it is assumed that it would probably be removed by the air scouring action during the relaxation stage of the cycle. The dynamic sludge cake layer is not further compressed during relaxation time and can proliferate in the absence of permeate suction. Li and Wang (2006) assumed at least a one-tenth reduction in the original value of compressibility coefficient (γ) under idle-cleaning mode. Therefore, the detachment part of **Eq.8.17** is modified to accommodate the cake influence of relaxation or idle cleaning cycle and the rate of stable sludge cake detachment ($\frac{d_{Msc}}{dt}$) is given by **Eq.8.22** below.

$$\frac{dM_{sc(i)}}{dt} = -\frac{\beta_{dc}(1-\alpha_{stickness})GM_{dc}^2}{0.1\gamma V_f + M_{dc}} \quad 8.22$$

8.5.3. Dynamic cake detachment due to backwashing

In addition to intermittent aeration and relaxation sequencing, a portion of the stable cake layer is detached during the backwashing cycle with a fixed flow rate which is scheduled after every seventh filtration-relaxation cycle in the considered SAV-MBR system. This means only detachment force caused by the sum of the local shears due to aeration and permeate backwashing is dominating. The detachment of the stable cake layer during the backwashing period is described by the coefficient of sludge detachment η_c and is given by **Eq.8.23** (Di Bella et al., 2008; Mannina et al., 2011b). The values of η_c varies between 0.9-0.9999 (Mannina et al., 2011b).

$$\frac{dM_{sc}}{d} = -\eta_c \cdot M_{sc} \quad 8.23$$

8.5.4. Total membrane filtration resistance and TMP

Total resistance (R_t) for each of the sections was divided into i) intrinsic resistance of the membrane (R_m), which was assumed to be constant and was estimated using the operational TMP and flux data for the period right after the ex-situ chemical wash and permeability recovery of the membrane, ii) Pore fouling resistance $(\mathrm{R_p})$ caused by the solute deposition into membrane pores, iii) dynamic sludge cake resistance (R_{dc}) or reversible fouling and iv) stable sludge cake (R_{sc}) and is given by **Eq.8.24**. Irreversible fouling was assumed to be the sum of R_m, $\mathrm{R_p}$ and R_{sc}. The fouling attributed to inorganic and concentration polarization due to the presence of cations naturally present in the municipal wastewater as well as produced during the addition of ferric chloride was not considered in the current model.

$$R_t(i) = R_m(i) + R_p(i) + R_{dc}(i) + R_{sc}(i) \quad 8.24$$

Pore fouling resistance $(\mathrm{R_p})$ caused by the deposition of the soluble (solute) fraction of the sludge onto membrane pores was considered to increase in proportion to permeate flux (J) and filtration time (t_f) and is given by **Eq.8.25.**

$$R_{p(i)} = r_p \times J_{(i)} \times t_f \quad 8.25$$

Where , $\mathrm{r_p}$ is specific pore fouling resistance of membrane ($\mathrm{m^{-1}}$) of the membrane, which was estimated using the **Eq. 8.26** originally developed by Wiesner and Aptel (1996) and later modified by Zuthi et al.(2017).

$$r_p = \frac{8 \times h_m}{f \times r^2} \times \exp^{n_p} \quad 8.26$$

Where, $\mathrm{h_m}$ is the thickness of the membrane (m), f is the porosity of the membrane (%); r is the radius of the pore (m), n_p is the exponential coefficient (unit-less). The resistances of the dynamic and stable sludge cake were assumed to be a function of

biomass accumulating on the membrane surface Li and Wang (2006), and was modeled using calculated by **Eqs.8.27-8.28**, respectively.

$$R_{dc(i)} = r_{dc} M_{dc(i)} \quad 8.27$$

$$R_{sc(i)} = r_{sc} M_{sc(i)} \quad 8.28$$

Where, r_{dc} and r_{sc} are the specific resistances per the mass of dynamic and stable sludge cakes, respectively, and both coefficients were assumed to be equal ($\therefore r_{dc} = r_{sc}$) as proposed by Zarragoitia-González et al.(2008) and later by Mannina et al. (2011b). In order to estimate the specific cake resistance of the sludge cake, Cho et al. (2005) introduced a dimensionless sigmoid relationship r_{dc} , MLVSS (mixed liquor volatile suspended solids), EPS (bound), and transmembrane pressure (*under dead-end filtration*). However, considering the fact the membrane in MBR module is not under the same pressure experienced by the membrane in dead-end filtration mode. Zarragoitia-González et al.(2008) modified the TMP influence by introducing an exponential factor ($C_{TMP} = TMP^p$) which helped to better estimate the cake compression under reduced direct pressure on the cake. Furthermore, MLVSS was modified to X_{TSS} (using a factor C_f for MLVSS/ MLSS ratio) to conveniently use the frequently measured data in full-scale facilities. The modified **Eq.8.29** is used to estimate the dynamic cake resistance.

$$r_{dc} = r_{sc} = \frac{C_{TMP}}{\mu_w^{\,2}} \cdot \left(a + b\left(1 - \exp\left(-c\left(\frac{X_{EPS}}{C_f \times X_{TSS}} \right) \right) \right) \right)^d \quad 8.29$$

Where, C_{TMP} is the coefficient of the transmembrane pressure, a, b, c, and d are empirical constants; μ_w is the viscosity of permeate (Pa.s); X_{EPS} is the concentration of total EPS (g.CODm^{-3}); and, X_{TSS} is the concentration of mixed liquor suspended solids (g. CODm^{-3}). The values of the empirical constants were adopted from Zarragoitia-González et al. (2008) with a slight modification in exponential parameter (p) to adjust the differences of the operating TMP in the dead-end filtration module and MBR system. Whereas C_f was adjusted by computing it from the available data of MLVSS and MLSS. The total sectional resistances are added as resistances in parallel according to the **Eq.8.30** below.

$$\frac{1}{R_T} = \sum_{i=1}^{n} \left(\frac{ns(i)}{Rt(i)} \right) \qquad 8.30$$

Where ns (i) is the surface of the i^{th} section of the membrane, n is a total number of sections (i.e., 128) and $R_t(i)$ is the total resistance of the i^{th} section while R_T is total resistance of the membrane area under consideration. Finally, TMP (**Eq. 8.31**) evolution is modeled using the Darcy's Law (Choo and Lee, 1996). The range of the values of several model parameters used by multiple researchers is summarised in **Table 8-5** . Most of the ranges of the parameters are wide. That can be interpreted through two linked assumptions : the first one points out disparities of situations and sludge caracterstics tha should be taken into account in the model's parameters, the second one focus on the inadequation to take int account multiple behaviors, of the model structure, due to its evolution (added and modified equations and constants along time)

$$TMP = \mu_W \times J \times R_T \qquad 8.31$$

Table 8-5: Range of the parameters and coefficients used in fouling sub-model

Symbol	description	unit	range	references
a	constant for specific cake resistance	Depending on C_{TMP}	1.16E3 - 9.3E12	(Cho et al., 2005; Cosenza et al., 2014; Cosenza Alida et al., 2013; Mannina et al., 2011a; Zarragoitia-González et al., 2008)
b	constant for specific cake resistance		1.36E4 - 8.7E06	
c	constant for specific cake resistance	gTSS.gCOD^{-1}	115 - 295.4	
d	constant for specific cake resistance	--	2.83 - 1427	
C_d	coefficient of the drag and lifting force	--	0.04 - 0.46	(González-Hernández and Jáuregui-Haza, 2021; Li and Wang, 2006; J. Wu et al., 2012; Zarragoitia-González et al., 2008)
C_{TMP}	TMP constant for specific cake resistance	Pa (or equivalent)	50 - 4179	(Mannina et al., 2011b; Suh et al., 2013)
d_p	MBR sludge particle diameter (without $FeCl_3$)	µm	5 - 240	(Iorhemen et al., 2016; Pechaud et al., 2015; Suh et al., 2013)
r_p	specific pore fouling resistance	m^{-2}	9.0E9 - 1.4E14	(Zarragoitia-González et al., 2008; Suh et al., 2013; Di Bella et al., 2008; Zuthi et al., 2017b)
r_m	Membrane intrinsic resistance	m^{-1}	1.0E11 - 1.2E12	(Li and Wang, 2006; Zarragoitia-González et al., 2008; Zuthi et al., 2017)

Symbol	description	unit	range	references
$\alpha_{stickiness}$	coefficient of sludge particles stickiness	--	0.113 - 0.67	(Di Bella et al., 2008; Li and Wang, 2006; Mannina et al., 2011b; Suh et al., 2013; J. Wu et al., 2012, 2012; Zarragoitia-González et al., 2008)
β_{dc}	erosion coefficient of dynamic sludge cake	--	0.00035 – 0.01	(Di Bella et al., 2008; Li and Wang, 2006; Mannina et al., 2011b; Suh et al., 2013; J. Wu et al., 2012; Zarragoitia-González et al., 2008)
β_{sc}	erosion coefficient of static sludge cake	--	0.00035 – 0.01	
γ	compression coefficient for sludge cake	$kg.m^{-3}.s^{-1}$	2.0E-5 – 3.0E-3	(Di Bella et al., 2008; Li and Wang, 2006; Mannina et al., 2011b; Suh et al., 2013; J. Wu et al., 2012; Zarragoitia-González et al., 2008)
η_{bw}	Efficiency of backwashing	%	90 -100	(Di Bella et al., 2008; Li and Wang, 2006; Mannina et al., 2011b)

8.7 ENERGY SUB-MODEL

The energy requirements in several process of the MBR plant operations with fixed (i.e., mixers and foam breakers) and variables power consumers such as influent pumping, fine and coarse bubble aeration, recirculation, permeate pumping and backwashing is simulated. A list of installed of energy consumers with necessary information is provided in **Table 6-9** . The approach to model energy consumption by each of these devices is described in the following sub-sections.

8.6.1. Influent pumping

A simplified equation (**Eq 8.32**.) borrowed from Gernaey et al. (2006), and Zoungrana et al. (2020) was modified and used to model the power uptake by the submersible centrifugal pumps. Input data of the active number of pumps in a given time is considered.

$$P5_{[kw]} = \frac{\rho \times g \times H_d \times Q_{\inf}}{3.6 \times 10^6 \times \eta_p \times \eta_m} \qquad 8.32$$

Where P_5 is the pump power uptake (kW), Q_{inf} is the volumetric flow of the fluid through the pump ($m^3.h^{-1}$), ρ is the density of the wastewater being pumped to MBRs (1000 $kg.m^{-3}$), g is the gravitational acceleration (9.81 $m.s^{-2}$); η_p is the efficiency of the pump (decimal) and η_m is the efficiency of the motor (*decimal*). The power (kW)

data was then converted to energy consumed (kWh) by multiplying it with an operating time.

8.6.2. Sludge mixing

The agitators are used in the anoxic and an anaerobic zone for continuous mixing of the mixed liquor. Although these are fixed energy consumers, however for the purpose of the modeling, **Eq.8.33** is adopted to estimate the power uptake at given rotations of the agitator, P_{Mixer} (Pechaud et al., 2021; Tanguy and Thibault, 2002).

$$P_{Mixer[kW]} = \frac{\rho_s \times N_p \times N_r^{\,3} \times D_{imp}^{\,5}}{1000} \qquad 8.33$$

Where, N_r is the rotation speed of the mixer (s^{-1}); N_p is the power constant provided by the supplier (KSB®), D_{imp} is the diameter (m) of the impeller of the mixer.

8.6.3. Process and membrane aeration

The biological process and membrane aeration power consumption are modeled using **Eq.8.34** modified from Jenkins (2013). However, while modeling biological process aeration, the efficiency of the variable frequency drive motors is considered as well.

$$P_{CBA[kW]} = 0.006755 \times \frac{Q_{air} \times P_i \times \left[\left(\frac{P_d}{P_i}\right)^{0.283} - 1\right]}{\eta_b \times \eta_m} \qquad 8.34$$

Where, Q_{air} is the blower inlet flow rate ($m^3.h^{-1}$), P_i and P_d are the blower inlet and discharge pressure (psia), respectively. While η_b is the efficiency of the blower.

8.6.4. Pumping energy consumption in recirculation and sludge extraction

The energy consumed by the submersible pump in internal and external recirculation is modelled by using **Eq.8.35** below.

$$P_{recir-pumps[kw]} = \frac{1}{t_1 - t_0} \int_{t0}^{t1} (Q_{r1} \times f_{anox} + Q_{r2} \times f_{aero} + Q_{r3} \times f_{mem} + Q_w \times f_{waste}) \times dt \qquad 8.35$$

Where $f_{anox}, f_{aero}, f_{mem}$ and f_{waste} are the pumping energy factors for anoxic re-circulation, aerobic-recirculation, membrane recirculation, and sludge extraction. The values of $f_{anox}, f_{aero}, f_{mem}$ and f_{waste} estimated using regression analysis of the data for sludge recirculated/pumped and the energy consumed.

8.6.5. Permeate pumping

In addition to the above discussed energy consumptions, MBRs have additional consumption in permeate extraction as effluent ($P_{permeate}$) and it was modeled using **Eq.8.36** (Judd, 2010) below.

$$P_{Peramate}[kW] = \frac{1}{t_1 - t_0}\int_{t_0}^{t_1}\left(\frac{TMP_s \times Q_p(t)}{3600 \times \eta_p}\right).dt \qquad 8.36$$

WhereTMP_s is the simulated transmembrane pressure (kPa), Q_p is the effluent flow rate ($m^3.h^{-1}$), and η_p is the efficiency (decimal) of permeate extraction pump. The summary of the several parameters used in the energy sub-model is given in **Table 8-6.**

Table 8-6: Range of the multiple parametric values used in energy sub-model

Symbol	Description	unit	range	references
f_{Anx}	energy uptake factor anoxic recirculation	--	0.0002 - 0.13	(Gabarrón et al., 2015b; Hai et al., 2018a; Krzeminski et al., 2012; Mannina et al., 2020; Suh et al., 2013a)
f_{Aer}	energy uptake factor aerobic recirculation	--		
f_{mem}	energy uptake factor membrane recirculation	--		
N_p	power number for mixers	--	0.3 - 5	(Alleyne et al., 2014; Pechaud et al., 2015)
g	gravitational constant	$m.s^{-2}$	9.81	
n	constant for air	--	0.283	parameters with universally accepted values
ρ_w	density of the water	$kg.m^{-3}$	1000	
P_{atm}	Atmospheric pressure adjusted to plant location	Pa	1.03E5	
R	gas constant	$J.mol^{-1}K^{-1}$	8.314	
η_{pump}	influent pump efficiency	%	70 - 90	(Jenkins, 2013)
η_{motor}	influent pump motor efficiency	%	70 - 90	
η_{bf}	fine bubble aeration turbo blower efficiency	%	70 - 90	(Jenkins, 2013; Mannina et al., 2020; Suh et al., 2013)
η_{bc}	coarse bubble aeration turbo blow efficiency	%	70 - 90	
ρ_{air}	density of air	$kg\ m^{-3}$	1.28	(El-Said et al., 2017)

8.8 CALIBRATION PROTOCOL

8.7.1. Calibration of the Biokinetic sub-model

In this work, values of kinetic and stoichiometric parameters of the bio-chemical model have been used in the range reported in the literature and calibrated by Fan et al.(2011), Janus (2013) and Rieger et al. (2001), along with some adjustments in the values of the stoichiometric parameters to reach the balanced "Peterson" matrix. Few parameters were adjusted using the heuristic approach to realistically simulate the biological processes for P-removal. Later, sensitivity analysis was carried out to explore the influential parameters for parameter screening using Morris screening (stage-1) with dynamic simulations and to adjust the most influential parameters to improve the model fit, if required, followed by manual calibration.

The experimental data of the influent COD fractionation, concentration of X_{OHO} and X_{ANO} were also used to calibrate the model in a steady state. Furthermore, measured data of the state variables from each reactor in series helped to improve the model's accuracy. In addition, dynamic K_La calibration was used to further improve the dynamic simulation.

8.7.2. Calibration of the fouling sub-model

The available values of the coefficients used in the fouling sub-model varies a lot, as demonstrated in several modelling studies, and this presented a calibration challenge in this work. In order to explore the most influential parameters and to reduce the calibration effort due to the wide range of the available parameters, sensitivity analysis was carried out considering the range of the values found in several studies (see **Table 8-5**). After exploring the most sensitive model parameters, the values of the influential parameters were manually adjusted, considering RMSE as an objective function.

8.7.3. Indicators for performance evaluation of model

In order to evaluate the accuracy of the model with respect to a particular variable, root mean square error (RMSE) and coefficient of determination (R^2) were used for all measured state variables of the bio-kinetic and energy model. At the same time, mean absolute percentage error (MAPE) was also used for fouling sub-model to evaluate its

performance for TMP and total resistance. The **Eqs.8.37-8.39** were used to estimate the model prediction accuracy.

$$RMSE = \sqrt{\frac{1}{N}.\sum_{j=1}^{N}\left(y_{obs(t_j)} - y_{sim(t_j)}\right)^2} \quad 8.37$$

$$R^2 = 1 - \frac{\sum_{j=1}^{N}\left(y_{obs(t_j)} - y_{sim(t_j)}\right)^2}{\sum_{j=1}^{N}\left(y_{sim(t_j)} - \bar{y}_{obs(t_j)}\right)^2} \quad 8.38$$

$$MAPE = \frac{100}{N}.\left|\frac{y_{obs_{(tj)}} - y_{sim_{(tj)}}}{y_{obs_{(tj)}}}\right| \quad 8.39$$

Where N is total number of measurements,y_{obs} and y_{sim} are the observed and simulated data at given time (t_j), while $\bar{y}_{obs}$ is the mean of the observed data.

8.9 SUMMARY

An integrated MBR process model was set up in MATLAB environment-based plant design. The integrated model combined the biochemical (ASM3-EPS-SMP-P) and resistance in series (RIS) filtration models. The biochemical part of the model considered the stoichio- kinetic activity of the biomass for carbon, nitrogen, and phosphorus removal. The filtration part of the model covered the fouling dynamics due to intermittent air scouring synchronized with filtration-backwashing cycles and also considered the influence of temperature, flux, TMP, and biomass characteristics, i.e., MLSS and EPSs concentrations. Furthermore, the aeration model based on the actual design of the diffused air aeration system installed for SAV-MBR and considering the oxygen diffusion limitations due to higher MLSS concentration was adopted to calculate the real oxygen transfer rate. In addition, the energetic consumption model was set up to estimate the real energetic consumption and specific energy consumption estimations.

Chapter 9: Reconciled Data and Results of the Experimental Campaigns

This chapter presents the results of the data cleaning and analysis as well the experimental campaigns executed to compensate for the missing data and further to fully depict and understand the functioning of the system.

9.1 RECONCILED DATASETS FOR CALIBRATION AND VALIDATION

As explained earlier, three datasets from the SCADA system were retrieved, treated, and reconciled using the methodologies explained in ***Chapter 7:***. Among the large amount of data that have been collected and treated, this section presents a summary of relevant datasets based on the reconciled data.

9.1.1 Data sets for steady state and dynamic calibration

The SCADA data collected during the week-long experimental campaign (13/05/2019-19/05/2019) was treated and reconciled. A summary of the data is presented in **Table 9-1** and **Table 9-2**.

Table 9-1: Characteristics of influent and effluent data used for model calibration

Parameter	Notation	Units	Influent			Effluent		
			Avg.	Max	Min	Avg.	Max	Min
Total Suspended Solids	TSS	$mgTSS.L^{-1}$	150	224	49	<2		
Biological Oxygen Demand	BOD_5	$mgO_2.L^{-1}$	152	186	86	2.9	3.7	1.7
Chemical Oxygen Demand	COD_t	$mgO_2.L^{-1}$	385	458	225	15	16	15
COD soluble	CODs	$mgO_2.L^{-1}$	133	140	121	-	-	-
Total Khejdal Nitrogen	TKN	$mgN.L^{-1}$	262	56	49	2	3	1
Ammonium	NH_4-N	$mgN.L^{-1}$	32.7	42.6	19.8	0.5	0.9	0.3
Nitrite	NO_2^-	$mgN.L^{-1}$	0.11	0.13	0.01	0.04	0.10	0.02

Parameter	Notation	Units	Influent			Effluent		
			Avg.	Max	Min	Avg.	Max	Min
Nitrate	NO_3^-	$mgN.L^{-1}$	0.25	0.30	0.23	11.9	14.7	7.9
Ortho-Phosphorus	PO_4^{3-}	$mgP.L^{-1}$	2.9	3.4	1.7	2.3	4.0	0.2
Total Phosphorus	P_{tot}	$mgP.L^{-1}$	4.9	5.7	3.1	2.4	4.1	0.2
Alkalinity	HCO_3^-	$mg.L^{-1}$	214	260	157	112	168	101
pH	pH		7.7	7.9	7.5	7.9	7.9	7.8
COD/BOD		--	2.6	3.50	2.09	-	-	-
COD/N		--	7.8	8.8	6.6	-	-	-
COD/P	-	--	77.9	86.4	77.9	-	-	-

Table 9-2: Sludge characteristics and operational settings for model calibration

Parameter	Unit	Average	Max.	Min.
Flow rate	$m^3.d^{-1}$	188,373	206,574	163,272
Sludge extraction	$m^3.d^{-1}$	3568	3746	3389
Permeate production	$m^3.d^{-1}$	202,015	226,097	188,586
MLSS- Aerobic Zone	$g.L^{-1}$	5.45	5.62	5.35
MLSS -membrane aerated zone	$g.L^{-1}$	5.46	5.62	5.28
Dissolved oxygen (DO)	$mg.L^{-1}$	1.21	1.58	0.78
Hydraulic retention time (HRT)	hours	16.05	18.43	14.56
Sludge retention time (SRT)	days	35.15	36.98	33.46
Temperature (aerobic tank)	^0C	18.83	19.56	17.52
Specific aeration demand (SADm)	$L.h^{-1}.m^{-2}$	131.13	140.80	125.6
Instantaneous flux	$L.\ h^{-1}.m^{-2}$	22.95	24.12	21.62
Transmembrane pressure (TMP)	Pa	5318	6016	4872
Aeration sequencing	min/min		10/10-10/30	
Backwash flow rate	$L.h^{-1}.m^{-2}$	36		
$FeCl_3$ addition	$mg.L^{-1}$	0	0	0

9.1.2 Datasets for long term dynamic model validation

Table 9-3 presents the characteristics of the raw, settled, and influent wastewaters for periods with (01/11/18-15/12/18) and without (16/12/18- 31/01/2019) addition of coagulant ($FeCl_3$), used for the model validation. While **Table 9-4** presents the summary statistics of the flow and operational parameters based on the analysis of the three months of data collected from the plant.

The COD/N ratio of influent is one of the most critical parameters for the wastewater nitrogen removal process because it directly affects functional microorganism populations, including autotrophic ammonium (–N) oxidizing and heterotrophic denitrifying bacteria. Considering the low COD/N ratio of the primary treated wastewater, raw influent is mixed with settled water in a 40/60 ratio to adjust the COD/N ratio in the range of 7-7.7, optimally required for enhanced nitrogen removal.

Table 9-3: Characteristics of influent and effluent data used for model validation

Parameter	Notation	Units	wastewater and MBR influent			Effluent	
			raw wastewater	settled wastewater	MBR feed Influent	without $FeCl_3$ addition	with $FeCl_3$ addition
Total Suspended Solids	TSS	$mgTSS.L^{-1}$	243.6 ± 67.8	112.8 ± 31	141.7 ± 36.9	2.00	2.00
Biological Oxygen Demand	BOD_5	$mgO_2.L^{-1}$	188.6 ± 37.1	n.m.	139.8 ± 35.9	2.3 ± 0.8	2.7 ± 1
Chemical Oxygen Demand	COD_t	$mgO_2.L^{-1}$	469.8 ± 98.3	276 ± 75.6	345.3 ± 82.5	15.2 ± 0.6	15.8 ± 1.3
COD soluble	CODs	$mgO_2.L^{-1}$	n.m.	n.m.	124.6 ± 37.2	47 + 0.45	45 + 0.67
Total Khejdal Nitrogen	TKN	$mgN.L^{-1}$	53.2 ± 9.9	40.2 ± 12.3	47.5 ± 10.0	1.5 ± 0.5	1.5 ± 0.4
Ammonium	NH_4-N	$mgN.L^{-1}$	54.9 ± 10.2	40.8 ± 11.8	34.3 ± 8.2	0.5 ± 0.3	0.6 ± 0.3
Nitrite	NO_2^-	$mgN.L^{-1}$	n.m.	n.m.	0.2 ± 0.2	0.06 ± 0.03	0.07 ± 0.03
Nitrate	NO_3^-	$mgN.L^{-1}$	n.m.	n.m.	1.0 ± 0.9	12.4 ± 3.1	10.2 ± 1.8
Ortho-Phosphorus	PO_4^{3-}	$mgP.L^{-1}$	2.93 ± 0.6	2.4 ± 0.7	2.9 ± 0.6	2.4 ± 0.7	0.3 ± 0.4
Total Phosphorus	P_{tot}	$mgP.L^{-1}$	5.62 ± 1.0	4.1 ± 1.2	4.9 ± 0.9	2.5 ± 0.8	0.4 ± 0.4
Alkalinity	HCO_3^-	$mg.L^{-1}$	n.m.	n.m.	220 ± 51	118 ± 21	122 ± 15
pH	pH	-	7.6 ± 0.1	7.6 ± 0.1	7.9 ± 0.1	7.9 ± 0.1	7.9 ± 0.1
COD/BOD			2.4 - 2.5	n.m.	2.4 - 2.5		
COD/N	-	-	8.6 - 9.0	6.7 - 7.1	7.0 - 7.7	n.m.	n.m.
COD/P	-	-	80.4 - 85.8	66.3 - 69.1	65.7 – 73.7	n.m.	n.m.

Table 9-4: Flow, sludge characteristics, and operational settings for model validation

Parameter	Unit	Average	Maximum	Minimum
Flow rate	$m^3.d^{-1}$	197,933	311,536	122,492
Sludge extraction	$m^3.d^{-1}$	3688	5681	815
Permeate production	$m^3.d^{-1}$	189,084	315,988	56,146
MLSS- Aerobic Zone	$g.L^{-1}$	5.07	6.92	4.50
MLSS -membrane aerated zone	$g.L^{-1}$	5.08	6.65	4.30
Dissolved oxygen (DO)	$mg.L^{-1}$	1.70	6.90	0.09
Hydraulic retention time (HRT)	hours	14	22	9

Parameter	Unit	Average	Maximum	Minimum
Sludge retention time (SRT)	days	29	43	21
Temperature	^0C	16.57	19.10	11.15
Specific aeration demand (SADm)	$L.h^{-1}.m^{-2}$	191.05	238.71	131.18
Instantaneous flux	$L.h^{-1}.m^{-2}$	27.21	53.96	10.55
Transmembrane pressure (TMP)	Pa	5204	13261	1647
Aeration sequencing	min/min		10/30	10/10
Backwash flow rate	$L.h^{-1}.m^{-2}$	36	-	-
$FeCl_3$ addition	$mg.L^{-1}$	30.73	54.94	4.241

Results presented in **Table 9-3** revealed that the plant amicably removes the BOD and COD with their removal efficiencies of 98.6% and 96.6%, respectively. The nitrification and de-nitrification efficiencies without coagulant addition are 97.2% and 79.2%, respectively.

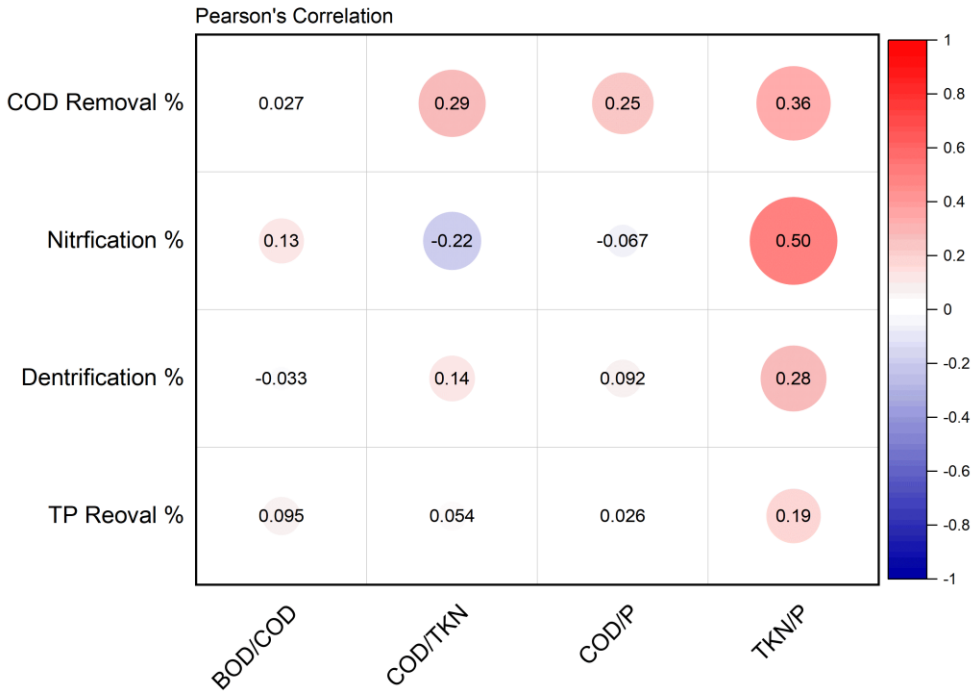

Fig. 9.1: Correlation of influent ratios and removal efficiencies based on 3 months data analysis

Phosphorus removal without coagulant addition was limited to 55.5%, while after addition (after 16/12/2018 until 31/01/2019) of coagulant it jumped to 92.8%. This low removal efficiency pointed out the underrated role of the anaerobic reactor for the biological removal of phosphorus. This might be associated with a fixed anoxic-anaerobic recirculation ratio, irrespective of the influent P load. **Table 9-4** presents the

summary statistics of the flow and operational parameters based on the analysis of the three months data collected from the plant. It was also examined that the efficiencies for COD removal, nitrification, denitrification, and phosphorus removal were not dependent on influent concentration. Only the TKN/P ratio was found to be influential for nitrification and denitrification processes, as presented in **Fig. 9.1**.

9.1.3 Datasets for dynamic model re-validation

Another dataset was collected from SAV during the 2nd two weeks long experimental campaign (20/9/2020-04/10/2020) and was treated and reconciled. A summary of the data is presented in **Table 9-5** and **Table 9-6**.

Table 9-5: Characteristics of influent and effluent data used for re-validation

Parameter	Notation	Units	Influent			Effluent		
			Avg.	Max	Min	Avg.	Max	Min
Total Suspended Solids	TSS	$mgTSS.L^{-1}$	87	160	48	2	2	2
Biological Oxygen Demand	BOD_5	$mgO_2.L^{-1}$	53	58	45	2.5	3.2	2.1
Chemical Oxygen Demand	COD_t	$mgO_2.L^{-1}$	213	280	144	15.2	16.1	15
COD soluble	CODs	$mgO_2.L^{-1}$	75	102	48	--	--	--
Total Khejdal Nitrogen	TKN	$mgN.L^{-1}$	-	-	-	2.1	3.2	1.2
Ammonium	NH_4-N	$mgN.L^{-1}$	27.8	40.7	15.1	0.33	1.16	0.01
Nitrite	NO_2^-	$mgN.L^{-1}$	0.20	0.39	0.02			
Nitrate	NO_3^-	$mgN.L^{-1}$	0.68	1.39	0.25	7.77	11.49	4.66
Ortho-Phosphorus	PO_4^{3-}	$mgP.L^{-1}$	1.2	1.6	0.7	0.78	1.92	0.09
Total Phosphorus	P_{tot}	$mgP.L^{-1}$	2.76	4.82	0.97	2.1	3.6	0.1
Alkalinity	HCO_3^-	$Mg.L^{-1}$	-	-	-	-	-	-
pH	pH		7.6	7.9	7.3	-	-	-
COD/BOD		--	2.94	3.35	2.48			
COD/N		--	7.35	9.36	5.06			
COD/P	-	--	89.9	186.0	47.0			

Table 9-6: Sludge characteristics and operational settings for model re-validation

Parameter	Unit	Average	Max.	Min.
Flow rate	$m^3.d^{-1}$	216,921	297,548	129,771
Sludge extraction	$m^3.d^{-1}$	3591	4765	2839
Permeate production	$m^3.d^{-1}$	213,330	294,364	126,648
MLSS- Aerobic Tank	$g.L^{-1}$	4.69	4.95	4.40
MLSS -membrane aerated tank	$g.L^{-1}$	4.68	4.94	4.43
Dissolved oxygen (DO)	$mg.L^{-1}$	1.58	3.30	0.38
Hydraulic retention time (HRT)	hours	14.57	23.18	10.11
Sludge retention time (SRT)	days	36	44	26
Temperature (aerobic tank)	^0C	21.31	23.75	18.35
Specific aeration demand (SADm)	$L.h^{-1}.m^{-2}$	184.62	211.16	158.93
Instantaneous flux	$L.h^{-1}.m^{-2}$	29.26	38.14	19.56
Transmembrane pressure (TMP)	Pa	7224	9896	4242
Aeration sequencing	min/min		10/10-10/30	
Backwash flow rate	$L.h^{-1}.m^{-2}$		36	
$FeCl_3$ addition	$mg.L^{-1}$	0	0	0

Fig. 9.2 provides a comparison of the datasets used validation/re-validation in reference to the calibration dataset. It can be seen that most of the operational parameters of the validation dataset do not vary in large extent from the data used for calibration.

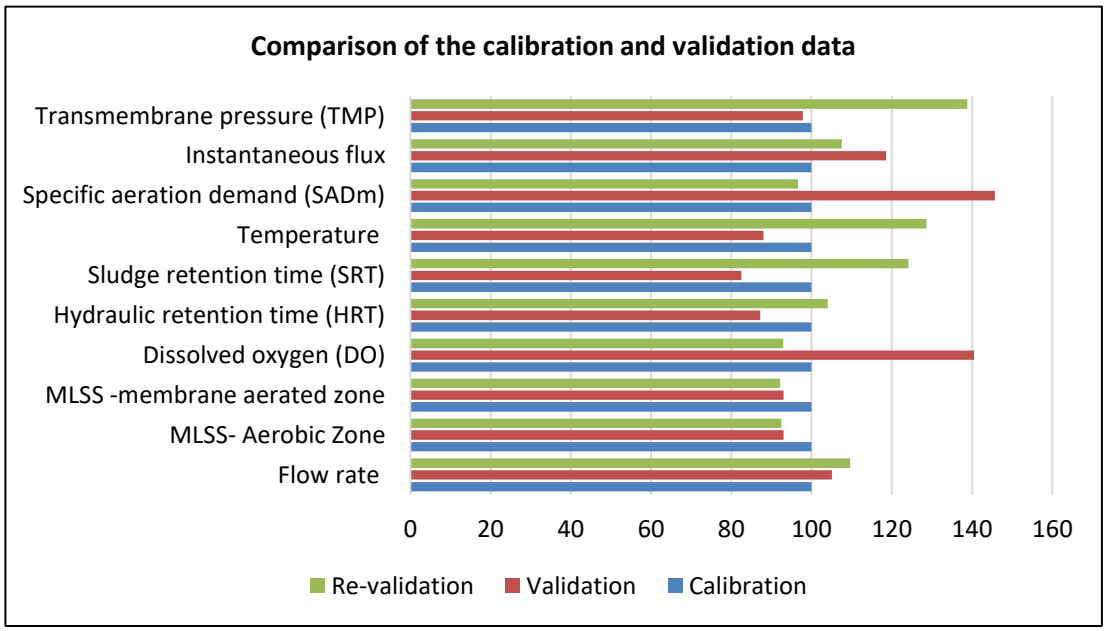

Fig. 9.2: Comparison of the data sets used for calibration, validation, and re-validation

However, DO concentrations in validation stage are 40% higher, compared to calibration data. This is probably linked to higher coarse bubble aeration (SADm) at higher inflow and flux. Higher TMP during the revalidation stage is likely due higher inflow and operations at elevated SRT. Temperature variations are relevant to weather conditions. This comparison will be helpful for understanding of the model results and interpretations thereof (***Chapters 10-12***).

9.1.4 Data-Driven simplification of the plant layout

The layout of the SAV -MBR facility was simplified to reduce the complexity of the model and to reduce the computational cost by considering the following conditions:

a) The design of each of the six activated sludge bioreactors, configuration (mUCT) with the identical dimensions of the pre-anoxic, anaerobic, anoxic, and aerobic zones

b) Similar recirculation flow (i.e., fixed 1.3 and 2.4 for anoxic and aerobic recirculation and variable membrane recirculation within the same range)

c) Operational process conditions in the aerobic zones (MLSS, DO, ORP, Temp), was found to be almost similar.

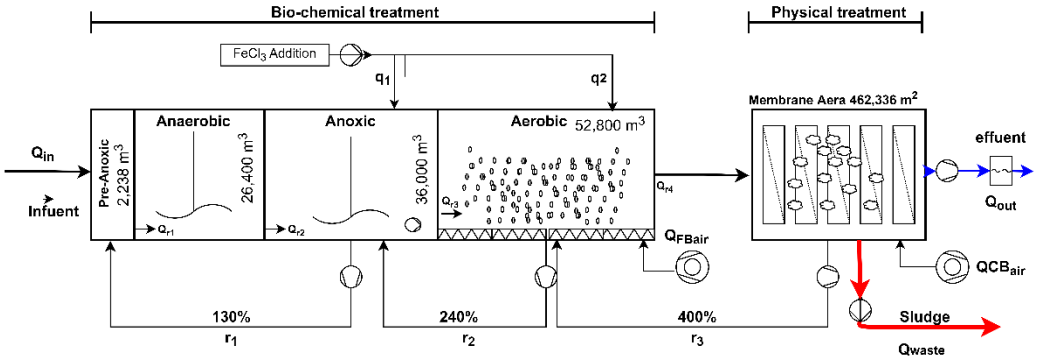

Fig. 9.3: Simplified schemas of the SAV-MBR

9.2 RESULTS OF THE EXPERIMENTAL CAMPAIGN

9.2.1 Pollutants profile in each of the reactors

During the first experimental campaign, the samples were taken on 3 consecutive days from 13/05/2019 to 15/05/2019. Summary results of pollutants with averages and standard deviations from mean during the 1st experimental campaign are given in **Table 9-7** and for 2nd experimental campaign in **Table 9-8.** The **Fig. 9.4 (a & b)**

presents the MLSS and MLVSS transformation at various stages of the plant. The MLVSS results refer to the activity of the activated sludge. The MLVSS over MLSS concentrations ratio in an MBR represents the organic components in the sludge and variations in this ratio indicate a change in the biomass composition.

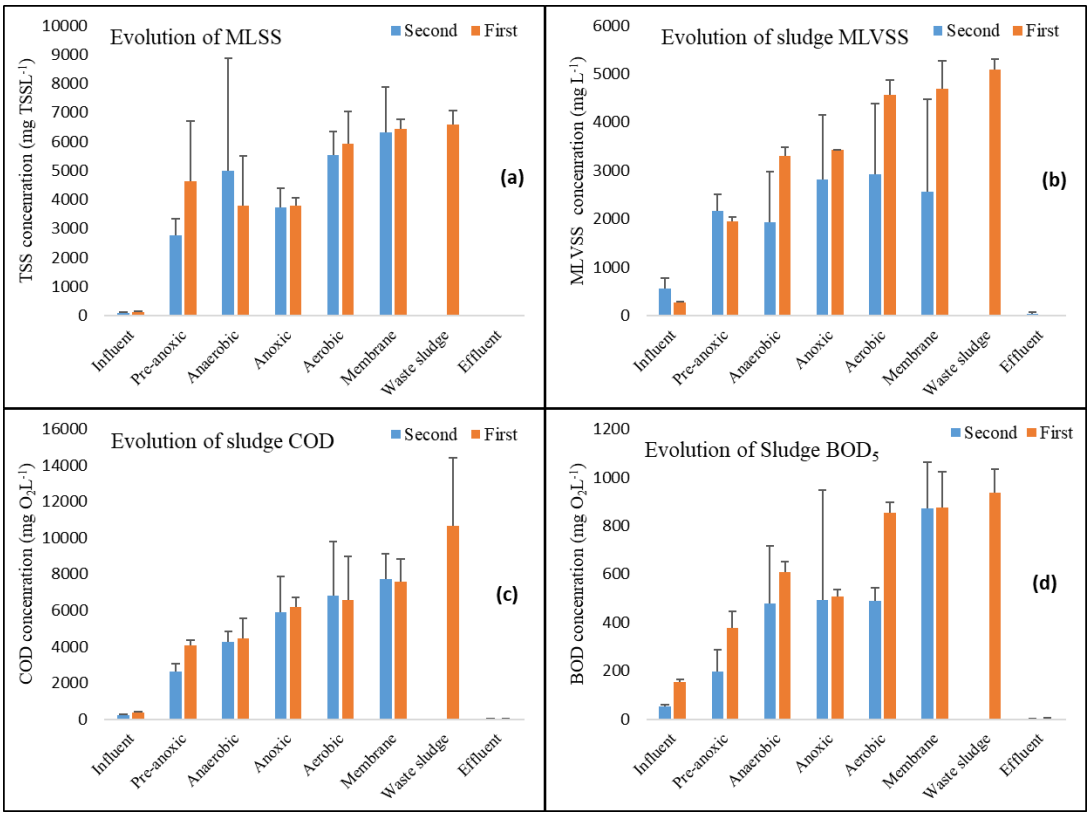

Fig. 9.4: Evolution of sludge COD, BOD_5, MLSS and VSS in the SAV MBR

The MLVSS/MLSS ratio of the influent was 4.45 which reduced to 0.60, 0.62,0.82,0.85, and 0.56 in the activated sludge of pre-anoxic, anerobic, anoxic, aerobic, and membrane aerated reactors, respectively (**Fig. 9.4** c-d). These results agree with the finding of other studies at full-scale, wherein the MLVSS/MLSS ratio remained constant at approximately 0.63-0.75 (Philippe et al., 2013; Rosenberger et al., 2000).

Table 9-7: Summary of the influent, effluent, and sludge at various stages of the process during 1st experimental campaign

Parameter	Unit	Influent		Pre-anoxic		Anaerobic		Anoxic		Aerobic		Membrane		Waste sludge		Effluent	
		Avg.	Std	Avg.	Std.Dev.	Avg.	Std.Dev	Avg.	Std.Dev	Avg.	Std.Dev	Avg.	Std.Dev	Avg.	Std.Dev	Avg.	Std.Dev
TSS/MLSS	$mg.L^{-1}$	**126**	30	**3235**	825	**2655**	625	**3793**	282	**5225**	655	**6435**	321	**6590**	490	**2**	0
BOD_5	$mgO_2.L^{-1}$	**153**	9	**377**	68	**607**	46	**507**	29	**853**	45	**873**	149	**937**	99	**2.5**	1.5
$BOD_{soluble}$	$mgO_2.L^{-1}$	**68.0**	2.8	**6.0**	1.0	**0.0**	0.0	**3.0**	0.0	**0.0**	0.5	**0.0**	0.5	**0.0**	0.0	**0**	0
COD_{total}	$mgO_2.L^{-1}$	**372**	38	**4073**	302	**3683**	403	**6207**	502	**6563**	740	**6730**	210	**7965**	25	**15.2**	2.1
$COD_{soluble}$	$mgO_2.L^{-1}$	**148**	2	**42**	8	**31**	1	**33**	1	**33**	5	**41**	11	**42**	12	**0**	0
MVSS	$mg.L^{-1}$	**275**	20	**1946**	88	**3305**	181	**3422**	15	**4559**	310	**4688**	584	**5083**	226	**0**	0
TKN	$mgN.L^{-1}$	**53**	6	**201**	8	**285**	69	**332**	19	**370**	44	**471**	20	**413**	98	**2.1**	0.25
NH_4	$mgN.L^{-1}$	**41**	4	**24.8**	2.7	**11.3**	1.4	**10.4**	1.4	**1.6**	0.4	**1.7**	0.4	**1.5**	0.3	**0.3**	0.02
N_{total}	$mgN.L^{-1}$	**53**	6	**201**	8	**285**	69	**332**	19	**370**	44	**472**	20	**414**	98	**10**	3.56
NO_3	$mgN.L^{-1}$	**<1**		**0.3**	0.1	**0.3**	0.1	**0.4**	0.1	**0.3**	0.2	**0.4**	0.1	**0.9**	0.6	**7.77**	4.3
NO_2	$mgN.L^{-1}$	**<1**		**0.0**	0.0	**0.0**	0.0	**0.0**	0.0	**0.0**	0.0	**0.0**	0.0	**0.0**	0.0	**0.01**	0
P_{total}	$mgP.L^{-1}$	**4.7**	0.7	**53.3**	4	**64**	14	**107.3**	13	**114.6**	21.5	**132**	12	**129.2**	43.6	**2.1**	0.16
PO_4	$mgP.L^{-1}$	**3.0**	0.4	**25.6**	2.5	**28.8**	5.7	**22.5**	1.6	**20.6**	3.5	**20.2**	1.5	**20.2**	1.9	**0.78**	0.21
pH	-	**7.6**		**7.3**	0.05	**7.1**	0.05	**7.2**	0.1	**7.1**	0.1	**7.3**	0.2	**7.1**	0.0	**0.1**	7.6

Note: Values in red colors were found unreliable.

Table 9-8: Summary of the influent, effluent, and sludge at various stages of the process during 2nd experimental campaign

Parameter	Unit	Influent		Pre-anoxic		Anaerobic		Anoxic		Aerobic		Membrane		Effluent	
		Avg.	Std.Dev	Avg.	Std.Dev	Avg.	Std.Dev	Avg.	Std.Dev	Avg.	Std.Dev	Avg.	Std.Dev	Avg.	Std.Dev
TSS/MLSS	$mg.L^{-1}$	82.61	28.88	2773	580	4998	3876	3737	661	5537	819	6323	1561	3.6	0
BOD_5	$mgO_2.L^{-1}$	52.66	6.80	197	89	477	239	493	454	490	52	870	192	<2	0
$BOD_{soluble}$	$mgO_2.L^{-1}$	35.33	8.74	0.0	0.0	3.3	0.0	3.0	0.0	3.3	0.6	3.0	0.1	<2	0
COD_{total}	$mgO_2.L^{-1}$	208	47.20	2612	452	4237	625	5877	2008	6793	3000	7743	1370	31	0
$COD_{soluble}$	$mgO_2.L^{-1}$	75.45	16.22	34	20	30	1	30	1	30	1	31	1	47	22.6
MVSS	$mg.L^{-1}$	556.00	213.33	2165	339	1937	1045	2818	1338	2930	1462	2570	1897	71.3	44.5
TKN	$mgN.L^{-1}$	64.99	15.98	177	37	199	16	232	67	302	102	214	87	1.83	1.88
NH_4	$mgN.L^{-1}$	27.62	8.37	23.8	4.8	18.9	3.9	8.9	2.1	3.0	1.7	2.6	1.6	2.30	0.15
NO_3	$mgN.L^{-1}$	0.68	0.29	3.0	1.5	2.0	0.2	6.1	6.1	10.0	7.9	13.2	9.4	15.67	3.06
NO_2	$mgN.L^{-1}$	0.20	0.09	0.1	0.0	0.1	0.0	0.1	0.1	0.1	0.0	0.1	0.0	0.18	0.12
P_{total}	$mgP.L^{-1}$	2.70	1.38	69.7	19.9	102.5	27.3	101.7	33.1	104.1	14.9	140.2	43.3	0.52	0.28
PO_4	$mgP.L^{-1}$	1.17	0.25	24.4	10.1	19.5	8.3	7.6	2.8	5.6	4.0	2.0	1.1	0.40	0.42
pH	-	7.30	0.10	7.0	0.15	6.9	0.12	7.0	0.1	6.9	0.1	7.0	0.1	7.3	0.2

Similarly, the COD/BOD ratio of the influent was 3.18, which increased to 12.02, 8.09,12.08.10.77 for pre-anoxic, anerobic, anoxic, aerobic, and membrane aerated reactors, respectively (refer to **Fig. 9.4** c &d).

Fig. 9.5 shows the transformation of COD_{sol} and BOD_{sol} in the system. It can be seen that the major fraction of the soluble COD is consumed in the various reactors of ASP and is uniformly distributed in all reactors, and is helpful for the membrane (MBR) to produce an effluent with lower and stable total COD (≤15 $mg.L^{-1}$).

While soluble BOD is readily transformed after entering into the pre-anoxic reactor, its values remain ≤5 $mg.L^{-1}$ all along the line until the membrane aerated reactor.

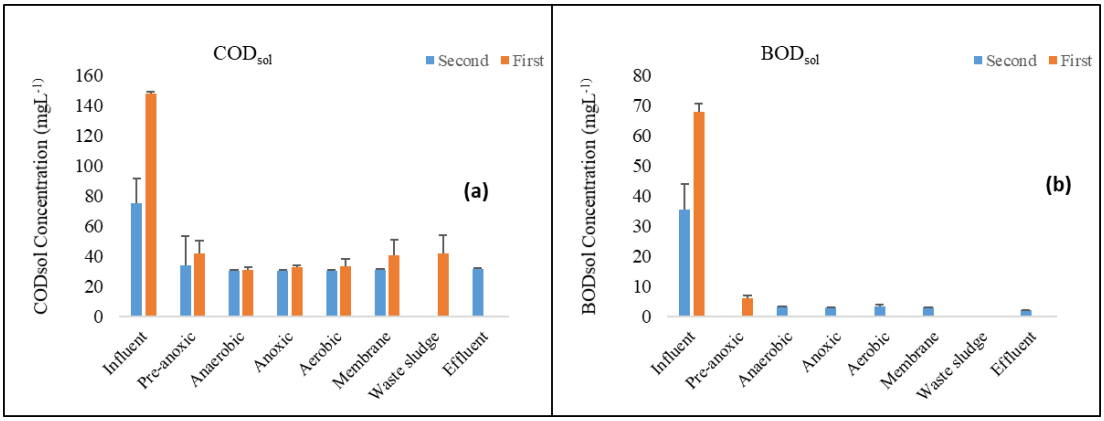

Fig. 9.5: Concentration of soluble BOD and COD in SAV-MBR

Experimental campaigns revealed that the biological processes consume around 90-100% of the soluble BOD. Similarly, the biological process can remove 80-90% of the soluble COD, and 10- 20% is retained by the membrane. Thus, it could be concluded that the COD removal is mainly due to activated sludge, while the membrane is greatly helpful in achieving a higher and more consistent COD removal efficiency.

In the MBR systems, nitrogen is removed via various stages and various mechanisms (Mao et al., 2020). Nitrogen compounds in the influent may either be assimilated by the sludge (stored in biomass) or transformed to gaseous nitrogen by the nitrification–denitrification process (Tchobanoglous et al., 2003). Sludge waste may remove the cell-assimilated nitrogen, and the gaseous nitrogen would escape from the MBR into the atmosphere. The residual nitrogen compounds stay in the wastewater and are discharged along with the effluents of the MBR system. According to Henze et al.

(2008b), the presence of nitrogen in the biomass is estimated at around 10% of the total weight of the biomass.

The performance of nitrogen transformation in the entire system is shown in **Fig. 9.6**. The influent NH_4 concentration accounted for 52-72% of the total nitrogen, it dropped gradually in the aerobic reactor (93% reduction) to a concentration of 2.3 $mg.L^{-1}$ depicting the presence of sufficient nitrifying bacteria which helped in nearly complete nitrification (**Fig. 9.6** c). However, NO_3^- concentration in the effluent was evaluated to be around 14.11 mgL^{-1}, which is 88% of the TN, suggesting incomplete denitrification.

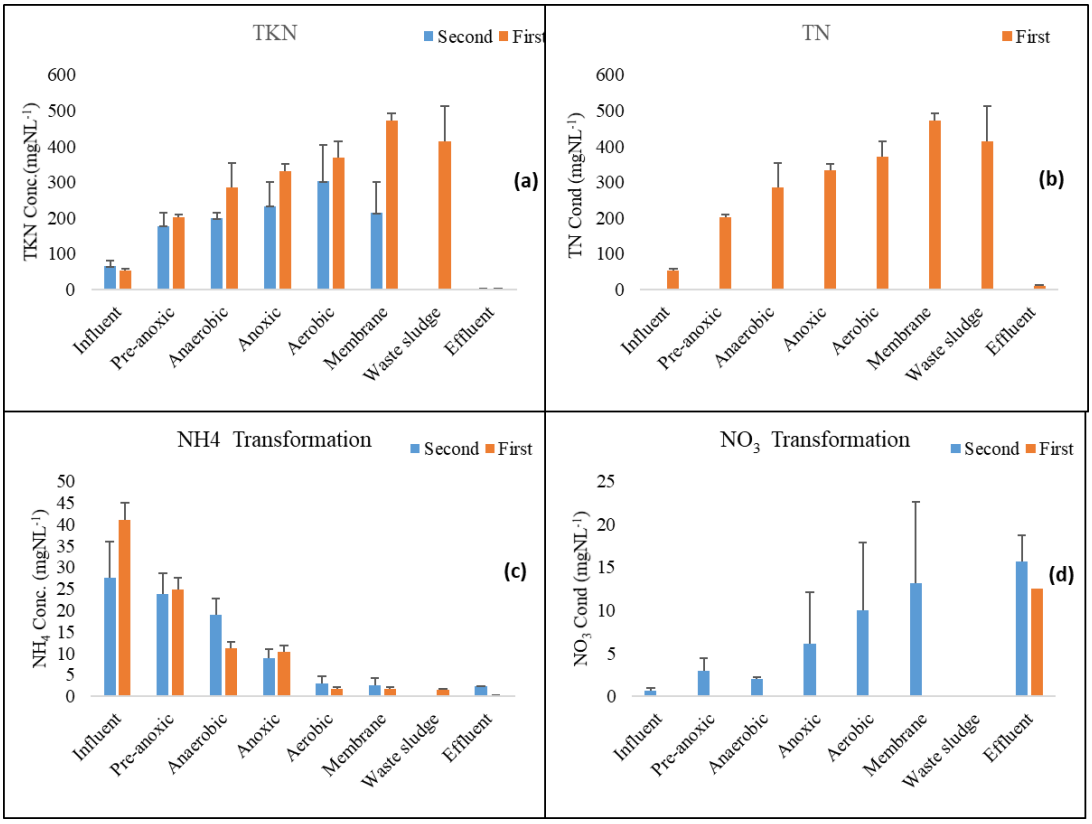

Fig. 9.6: Evolution of concentrations of nitrogen in different stages of the MBR

The transformation and removal of the total and orthophosphate are depicted in **Fig. 9.7**. The phosphate concentration is decreasing while the total concentration of the TP is increasing (i.e., TP/PO_4 dropped to 0.01 from 0.43).

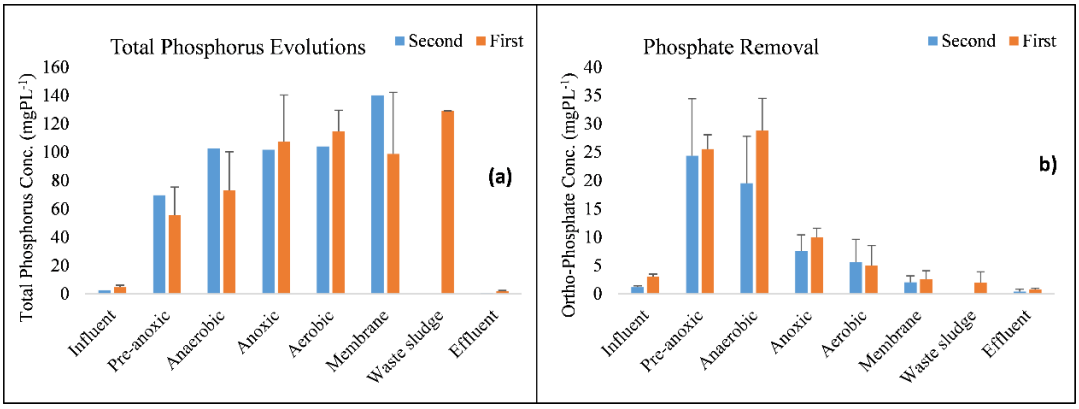

Fig. 9.7: Evolution of concentrations of phosphorus in different stages of the MBR

This is due to the fact that most of the TP is retained in the sludge by the membrane, depicting the functioning of the EBPR and/or CEPR processes. A relatively higher influent COD/P ratio of 77.03 was observed, which is quite higher than the required optimal range of 29-45 (Nadeem et al., 2022) for successful EBPR. This situation could be the possible explanation for this not sufficient removal rate before the coagulant addition.

9.2.1.1 COD fractions and biomass

According to the average of three experiments, COD fraction S_U, S_B, X_{CB}, and X_U were evaluated to be 9.3%, 31.9%, 47.9% and 10.9%, respectively. COD contribution associated with the active biomass is often neglected in the influent, which may contribute up to 15% (or more) of the total COD (Sperandio and Paul, 2000). The results in comparison with other municipal wastewater COD fractionation studies are presented in **Table 9-9** below. All the obtained values are in the literature ranges. Furthermore, 79% of the total fraction is biodegradable.

Table 9-9: COD fractions of the influent and comparison with other studies

S_U	S_B	X_{CB}	X_U	Reference
% COD fractions of municipal wastewater				
9.3	**31.9**	**47.9**	**10.9**	**This work**
7-11	10-20	53-60	7-15	(Kappeler and Gujer, 1992)
4	9	77	10	(Sözen et al., 1998)
2.2-6	50-61.7	22-34.4	8-16.2	(Płuciennik-Koropczuk et al., 2017)
8-10	20-25	60-65	5-7	(Ekama et al., 1986)
6.7	33.4	44	15.9	(Ignatowicz, 2019)

In addition to COD fractions, respirometry experiments helped in the estimation of the autotrophic and heterotrophic biomass in the aerobic reactor as well as their yield coefficients. Based on two respirometry experiments conducted during the experimental campaign, the heterotrophic (X_{OHO}) and autotrophic biomass (X_{ANO}) were evaluated to be 1,442 mg COD.L^{-1} and 338 mgCOD.L^{-1}, respectively.

9.2.1.2 EPS and SMPs concentration

The analytical results for EPS measurement are presented in **Fig. 9.8**. The average concentration of total EPS in the sludge was estimated to be around 988 mgCOD.L^{-1} with only <1% of the soluble fraction, also known as SMPs.

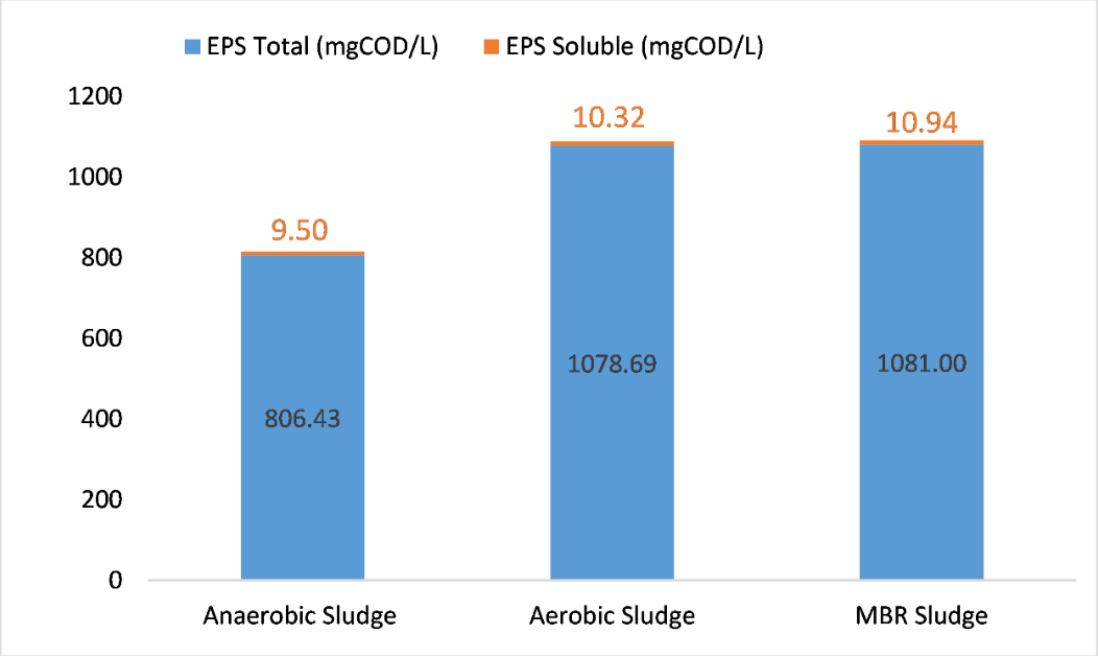

Fig. 9.8: Total and soluble EPS concentrations in the sludge

9.2.1.3 Specific cake resistance

Specific cake resistance increases linearly with increase in the TMP with Pearson's correlation coefficient of 0.983, indicating a significant compressibility of the deposited cake. (**Fig. 9.9**)

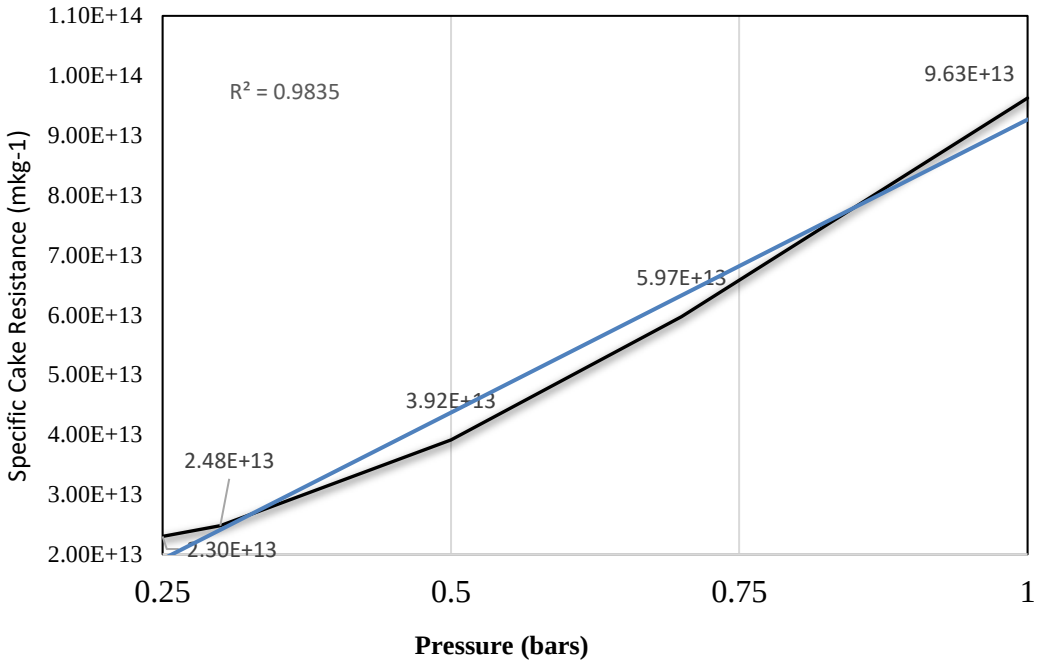

Fig. 9.9: Variation of specific cake resistance with increasing pressure

9.3 SUMMARY

Detailed analysis of the three months data revealed that the plant is functioning well for COD, BOD, and TSS, with removal efficiencies of 98.5%, 96.6% and 98.5%, respectively. The nitrification and de-nitrification efficiencies without coagulant addition are determined to be 97.2% and 79.2%, respectively. While Phosphorus removal without the addition of coagulant was limited to 55.5%, after addition of coagulant it increased to 92.8%.

Experimental campaigns essentially helped in producing the required datasets for configuration, initialization, steady-state, and dynamic calibration, and validation. Data sets related to COD fractions, heterotrophic and autotrophic biomass concentrations, EPS and SMP (as soluble EPS), as well as pollutants profiles within each of the reactors in series were collected during the experimental campaigns. In addition, the experimental campaign helped to precise the carbon, nitrogen, and phosphorus transformation from the entrance to the exit of the plant as well as the evolution of the biomass. This information is not monitored at SAV-MBR and is generally not available in the published literature, especially from the full-scale facilities, and probably would be different for each type of reactor configuration.

Chapter 10: Calibration and Validation of Sub-Models of Reactive Part

This chapter presents the methodology adopted for calibrating the sub-models used in the reactive part, with and without the addition of the coagulant. To ease the reading of this chapter, these will be referred to as biokinetic sub-models. Data from the experimental campaign, combined with the plant design data (see ***Chapter 6:***) and influent and process parameters gathered from the SCADA system (see ***Chapter 9:***), was used for steady state and dynamic calibration. Furthermore, three months of historic data (summary presented in **Table 9-3**) were used to validate the biokinetic models. In addition, the model was re-validated with data from the 2nd experimental campaign (with 15 days of data from the SCADA system). The overall objective of this chapter is to present a comprehensive and fully calibrated and validated phenomenological model capable of simulating the biological treatment performances of the SAV-MBR in terms of COD, nitrogen, and phosphorus (via EBPR and CEPR) removal processes. It also aims to simulate the X_{TSS} and X_{EPSs} concentrations required by the fouling sub-model for dynamic computation of the specific cake resistance and, more globally, the filtration performance (see ***Chapter 11:***).

10.1 STEP-WISE CALIBRATION PROCESS

The optimal set of stoichiometric and kinetic parameters for the biological sub-model may be different and specific for various systems, owing to the differences in environmental conditions, influent characteristics, reactor configuration, operating conditions, and biomass populations (Petersen et al., 2003; Zhu et al., 2015). The BIOMATH protocol , adapted for calibration of the bio-kinetic sub model after the influent characterization, was applied in accordance with the STOWA protocol (Rieger et al., 2012). The calibration strategy is presented in **Fig. 10.1**. The calibration process is divided into 8 steps (or 5 stages), simulation starts from step 5, while steps prior to this are essential preparatory steps.

Target definition: As stated in ***Chapter 5:,*** the target of the calibration process is to obtain a model capable of dynamically describing the carbon, nitrogen, and

phosphorus removal processes of an MBR. The biokinetic sub-model was expected to realistically describe the carbon-oxidation, nitrification, denitrification, oxygen dynamics, and evolution of the X_{TSS} and X_{EPS} concentrations. Based on the literature survey results, the targeted acceptable model fitness for COD, NH_4, NO_X, PO_4, and MLSS in terms of R^2 was set at ≥ 0.70 (Benedetti et al., 2008; Sin et al., 2011:Wang et al., 2017).

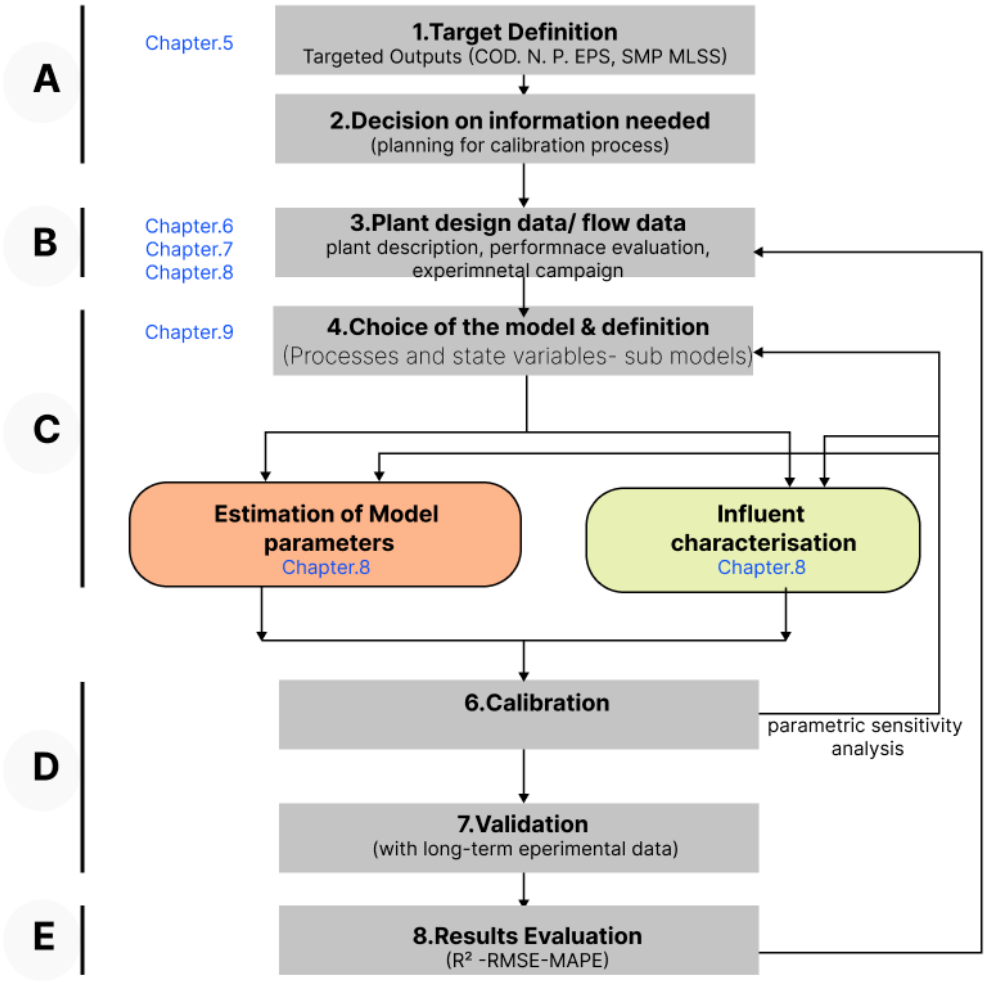

Fig. 10.1: Procedure for calibration of the biokinetic sub-model

Decision about information needed for calibration: This step included everything related to the calibration process planning, such as type of experimental data requirements, measuring frequencies, number, and locations of samples, and selection of standard methods for influent/sludge sample characterization.

Plant design data and flow characterization: This step included a collection of information related to i) plant design and process description (see ***Chapter 6:***), ii)

Existing data collection and analysis of the MBR performance (see methodology for data collection in ***Chapter 7:***), and iii) experimental campaigns to analyses the pollutants and biomass evolution (see ***Chapter 9:***). Data collected from full-scale facilities are often used, but the amount and quality need reconciliation, referring to the procedures suggested by Rieger et al.(2010).

Choice of the model/ sub-models: This included selecting the suitable ASM model to simulate the targeted pollutants with a description of the sub-model considered in the model structure for mass transfer (aeration) and chemical precipitation (see ***Chapter 8:***). This step also included influent fractionation and estimation of the biomass concentration in aerated sludge (see ***section 9.2)***

Pre-calibration: In order to reduce the calibration effort, some of the model parameters were determined experimentally and were fixed while the calibration was focused on the rest of the parameters: Heterotrophic yield coefficients, $Y_{Stor\_OHO\_Ox}$, and $Y_{SB\_Stor\_OX}$ were adjusted based on fitting of the measured (*through respirometry experiments*) and modeled oxygen uptake rate (OUR), while μ_{OHO_max}, K_{SB_OHO} and q_{SB_Stor} were set to their default. Furthermore, the yield coefficient of autotrophic biomass (X_{ANO}) was determined using their measured concentration (via respirometry) and modeled OUR fitted manually by adjusting the Y_{ANO} while keeping the μ_{ANO_max} and K_{NHx_ANO} to their default values.

10.2 SIMULATION AND CALIBRATION

Steady-state simulations were run with a one-week average flow rate, process conditions, influent composition, and the sludge composition data from the first experimental campaign. The steady state simulation was intended for the following purposes:

- To identify the proper initialization conditions of the state variables of the biokinetic sub-model for all the tanks in series, i.e., pre-anoxic, anerobic, anoxic, aerobic, and membrane aerated tanks,
- To verify whether the subset of the parameters measured and adapted from the literature is sufficient to proceed further for dynamic simulation or not?

- To determine whether the proposed model could simulate all the tanks in series, given the limited information and data sets available for pre-anoxic, anerobic and anoxic tanks.

Based on the literature (Rieger et al., 2010; Sperandio and Paul 2010), the concentration of the active biomass (X_{OHO}, X_{ANO}, and X_{PAO}) in the influent was assumed to be 4.2% of the total COD in the model, and their values are given in **Table 10-1**, along with the values of the composition of the other components in the influent.

Table 10-1: Influent composition for steady-state simulations

Component	*Symbol*	*Units*	*Value*	*Source*
Inert soluble organic	**S_U**	$gCOD.m^{-3}$	0.045×COD	Estimated
Readily biodegradable organics	**S_B**	$gCOD.m^{-3}$	0.276×COD	Measured
Slowly biodegradable organics	X_{CB}	$gCOD.m^{-3}$	0.508×COD	Measured
Inert particulate organics	X_U	$gCOD.m^{-3}$	0.1154×COD	Measured
Soluble utilization associated products	**SUAP**	gCOD.m-3	0.00002×COD	Assumed
Soluble biomass associated products	**SBAP**	gCOD.m-3	0.00002×COD	Assumed
Ammonium	**S_{NHx}**	$gN.m^{-3}$	41.0	Measured
Dissolved nitrated and nitrites	**S_{NOX}**	$gN.m^{-3}$	0.42	Measured
Dissolved nitrogen gas	**S_{N2}**	$gN.m^{-3}$	1.00	Assumed
Extra polymeric substances	X_{EPS}	$gCOD.m^{-3}$	0.00002×COD	Assumed
Ordinary heterotrophic organisms	X_{OHO}	$gCOD.m^{-3}$	0.0415×COD	Assumed
Storage compound in OHOs	X_{OHO_stor}	$gCOD.m^{-3}$	0.0115×COD	Assumed
Autotrophic nitrifying organisms (NH_4^+ to NO_3^-)	X_{ANO}	$gCOD.m^{-3}$	0.0002×COD	Assumed
Inorganic soluble phosphorus	**S_{PO4}**	$gP.m^{-3}$	3.0	Measured
Phosphorus accumulating organisms	X_{PAO}	$gCOD.m^{-3}$	0.0002×COD	Assumed
Stored polyphosphates in PAOs	X_{PAO_stor}	$gCOD.m^{-3}$	0.00002×COD	Assumed
Stored poly-β-hydroxyalkanoate in PAOs	X_{PAO_PP}	$gP.m^{-3}$	0.0001	Assumed
Alkalinity (HCO_3^-)	**S_{HCO}**	$molHCO_3^-$	4.0	Measured
Total suspended solids	X_{TSS}	$gTSS.m^{-3}$	126	Measured
Metal hydroxide compounds	X_{MeOH}	$gTSS.m^{-3}$	0.000001	Assumed
Metal phosphate compounds	X_{MeP}	$gTSS.m^{-3}$	0.000001	Assumed

For stoichiometric and kinetic parameters, except $Y_{Stor\_OHO\_Ox}$, $Y_{SB\_Stor\_OX}$ and Y_{ANO}, default values were used as a starting point and then adjusted manually with other selected parameters to obtain a reasonable (R^2> 0.70) fit of the averaged measured data values of the pollutants transformation in all reactors in series. The values of parameters thus calibrated are given in **Table 10-2**. Considering that the averaged measured data of the sludge and effluent for COD_{tot}, COD_{sol}, TP and X_{TSS} were fitted

reasonably (i.e., above threshold R^2) by the simulated results, the averaged measured and simulated results within the tanks are presented in **Table 10-3**. The state variables used in the model were lumped in terms of COD_{sol}, COD_{part}, COD_{tot} TKN, and TP using **Eqs. 10.1-10.5**.

$$COD_{sol} = S_U + S_b + S_{UAP} + S_{BAP} \quad 10.1$$

$$COD_{part} = X_{CB} + X_U + X_{EPS} + X_{OHO} + X_{OHO\_stor} + X_{ANO} + X_{PAO} + X_{PAO\_stor} \quad 10.2$$

$$COD_{tot} = COD_{sol} + COD_{part} \quad 10.3$$

$$TKN = S_{NHx} + S_B \cdot iN_{SB} + iN_{XU} \cdot X_U + iN_{XCB} \cdot X_{CB} + iN_{X_{Bio}} \cdot (X_{OHO} + X_{ANO} + PAO) \quad 10.4$$

$$TP = S_{PO4} + S_B \cdot iP_{SB} + iP_{XU} \cdot X_U + iP_{XCB} \cdot X_{CB} + iP_{X_{Bio}} \cdot (X_{OHO} + X_{ANO} + PAO) + X_{PP} \quad 10.5$$

Based on Morris screening, a fitting goodness criterion (i.e., $R^2 \geq 0.7$) between the observed data and simulation results was used to estimate parameter subset suitability for steady-state and dynamic simulations.

Table 10-2: ASM3-EPS-SMP-Bio-P model parameter values used for steady state and dynamic calibration

#	Notation	Units	*Default*	Estimated /Calibrated
1	$Y_{SB\_OHO\_OX}$		0.681	**0.67***
2	$Y_{Stor\_OHO\_Ax}$		0.54	0.59
3	$Y_{SB\_Stor\_OX}$		0.85	**0.81***
4	Y_{ANO}	$gCOD.L^{-1}$	0.24	**0.241***
5	q_{SB_Stor}	d^{-1}	5.0	6.0
6	K_{NHx_OHO}	$gN.m^{-3}$	0.01	0.02
7	u_{ANO_Max}	d^{-1}	1-1.8	1.70
8	K_{O2_ANO}	$gN.m^{-3}$	0.50	0.20
9	K_{NHx_ANO}	$gN.m^{-3}$	1.00	0.20
10	$q_{PAO\_PO4\_PP}$	d^{-1}	1.50	2.0
11	u_{PAO_Max}	d^{-1}	1.0	0.40
12	$q_{PAO\_SB\_Stor}$	d^{-1}	6.0	8.0

*Note: The values in bold are measured using a respirometry experiment and fitting the OUR for X_{OHOs} and X_{ANOs}

Table 10-3: Averaged measured and simulated results of the calibrated ASM3-EPS-SMP-P model using steady-state collected data from SAV-MBR during 1st experimental campaign.

Measured/ Observed	Pollutant	Pre-Anoxic	Anaerobic	Anoxic	Aerobic	Membrane Aerated
		1st Experimental campaign (CARSO data)				
Obs.	COD_{tot}	4626±2080	3042±481	4363±813	5981±902	6653±202
Sim.	$gCOD.m^{-3}$	**2589**	**2513**	**4214**	**5848**	**7193**
Obs.	S_{NOX}	-	-	-	-	-
Sim.	$gN.m^{-3}$	**0.09**	**0.002**	**0.42**	**11.66**	**12.55**
Obs.	S_{NHX}	-	-	-	-	-
Sim.	$gN.m^{-3}$	**24.6**	**26.03**	**13.38**	**0.24**	**0.05**
Obs.	S_{PO4}	-	-	-	-	-
Sim.	$gP.m^{-3}$	**4.23**	**20.78**	**7.07**	**2.4**	**2.1**
Obs.	TP	53±4	64.5±14.7	107±13	114±21	132±12.18
Sim.	$gP.m^{-3}$	**57**	**48**	**90**	**128**	**159**
Obs.	X_{TSS}	2523±1211	2655±625	4038±877	5225±655	5573±1009
Sim.	$g.m^{-3}$	**1836**	**1856**	**3203**	**4483**	**5520**

Noted: measured data is based upon an average of 3 samples.

The simulated results for particulate species, i.e., COD_{tot}, X_{TSS}, and TP, were found within the range of the measured concentrations within each tank, as shown in **Table 10-3**. The reliable results for soluble species were not available from the 1st experimental campaign and, therefore, could not be compared with the simulated data for all reactors in series. The simulated concentrations of NOx, NH_4^+, and PO_4^{-3} in the MBR tank were found within the range of the effluent concentrations measured at the exit of the membrane aerated tank. Therefore, these results were acceptable, and the model was further considered for dynamic simulations.

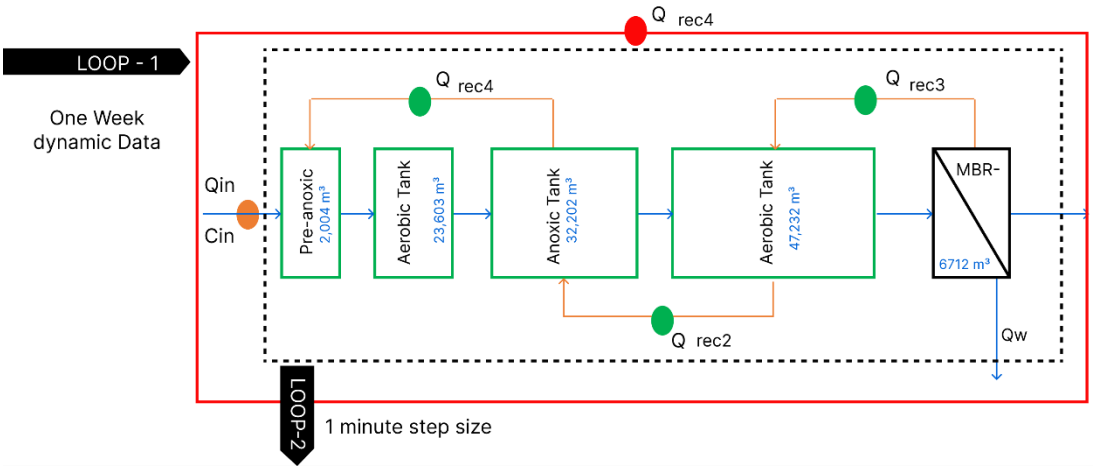

Fig. 10.2: Scheme for plant-wide dynamic simulations

A dynamic calibration process was carried out using the steady state calibrated model, with data sets from the SCADA system for one week, i.e., 13th May 2019 until 18th May 2019. The values of the state variables obtained in steady state simulations and validated later were used as initialization for dynamic simulations. The dynamic influent, operating conditions (including the actual aeration, recirculation ratios among different reactors and temperatures) and actual design of the system were considered for the dynamic simulation. The dynamic simulation procedure is shown in **Fig. 10.2**. The loop-1 uploads the dynamic data to the MATLAB program, while loop-2 simulates the reactors in series with a step size of 1 minute and runs for 24 hours.

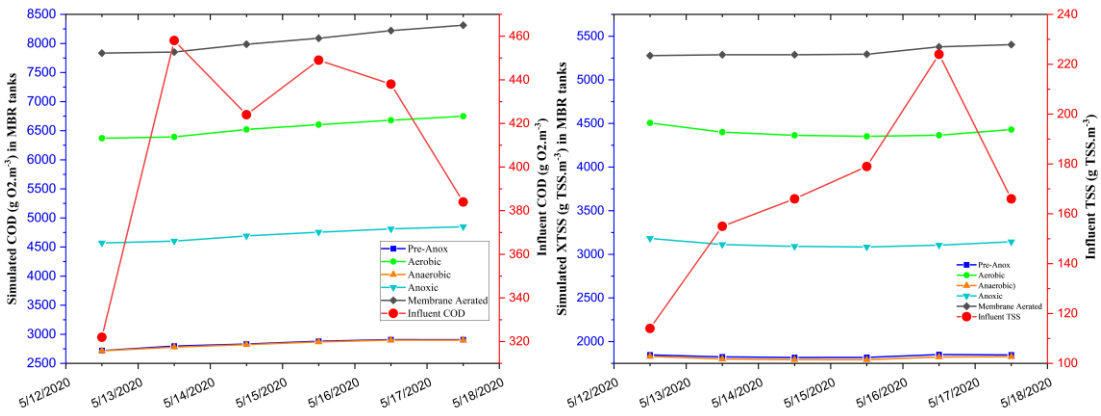

Fig. 10.3: Dynamically simulated COD_{tot} and X_{TSS} concentrations (left) through various zones of the bioreactor, with experimental influent COD_{tot} and X_{TSS} concentrations (right)

Fig. 10.3 illustrates the simulated concentrations of the COD_{tot} and X_{TSS} through various zones of the biological reactor and the influent concentration of the COD_{tot} and

X_{TSS}. COD_{tot} and X_{TSS} concentrations increase along the process with an increase in the influent COD and TSS concentrations.

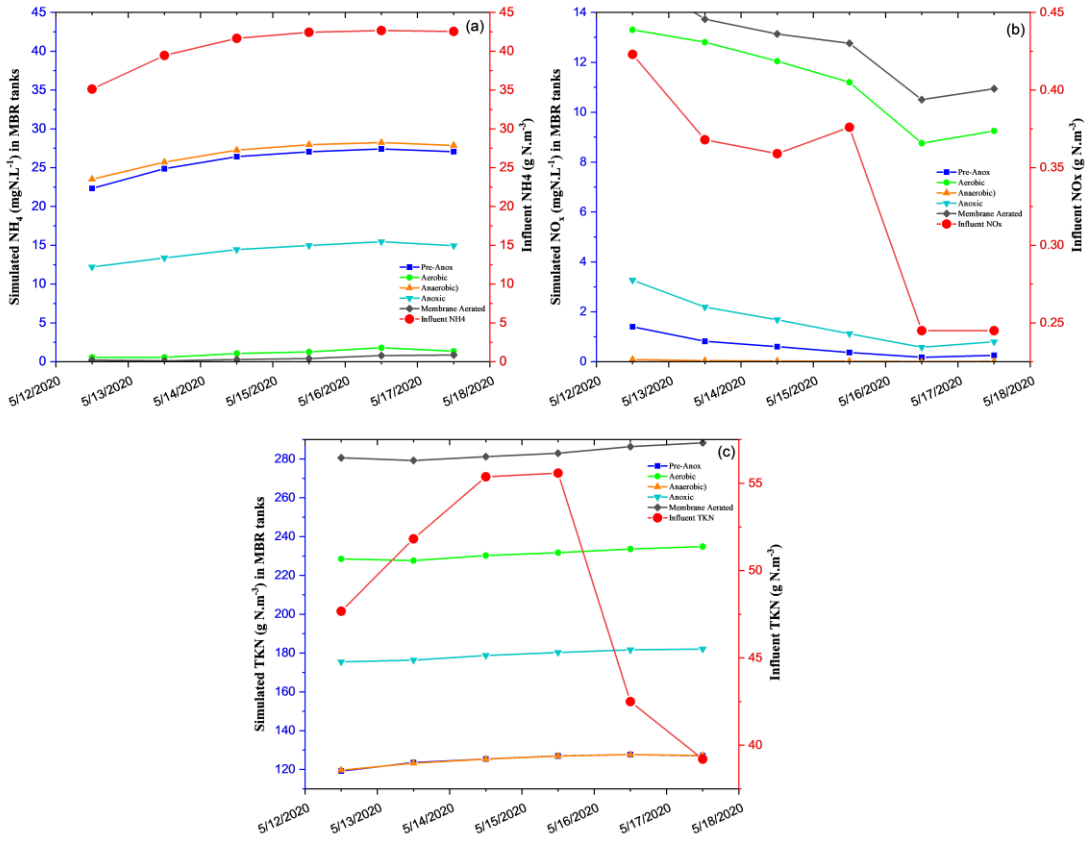

Fig. 10.4: Dynamically simulated NH_4^+(a), NO_X(b) and TKN(c) concentrations flow through various zones of the bioreactor, with experimental influent NH_4^+ NO_X and TKN concentrations

Fig. 10.4 presents the concentration of NH_4, NO_X, and TKN, while **Fig. 10.5** presents the concentration of PO_4 and TP through the various zone of the bioreactor. As already stated, the concentration of soluble species of nitrogen and phosphorus within each zone of the reactors could not be measured during the experimental campaign. Therefore, it was not possible to validate the simulated results for each of these zones. However, sufficient data for the effluent concentration was available at the outlet of the membrane tank to validate the dynamic calibration.

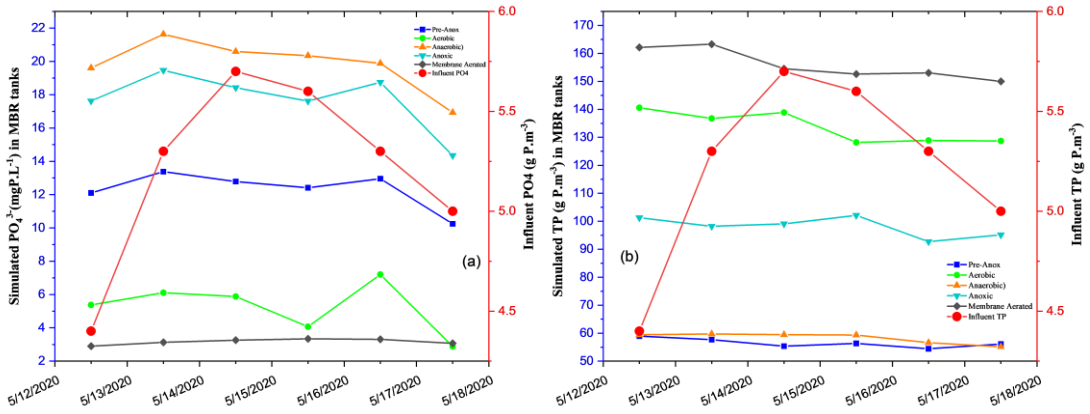

Fig. 10.5: dynamically simulated PO_4^{3-} (a) and TP (b) concentrations (left axis) flow through various zones of the bioreactor, with experimental influent PO_4^{3-} and TP concentrations (right axis).

Fig. 10.6 shows that the model is able to sufficiently simulate the effluent COD with RMSE of 1.27 mg.L^{-1} and with a coefficient of determination R^2 value of 0.83. This is higher than the set target ≥ 0.7, and therefore, the calibration of the COD was accepted.

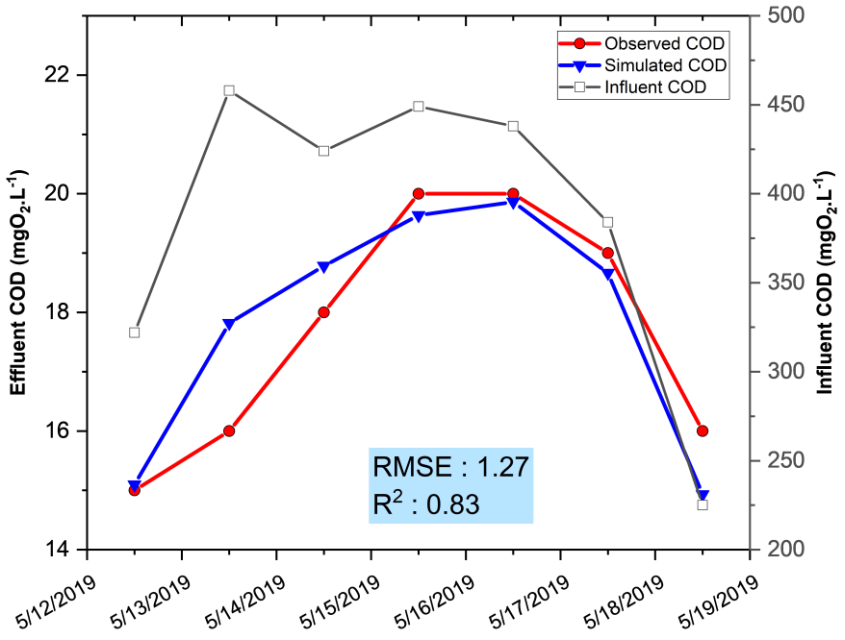

Fig. 10.6: Model calibration results for dynamically simulated effluent COD

Similarly, the model was able to simulate with a sufficient accuracy the NH_4^+ and NO_x concentrations with RMSE of 0.122 mg.L^{-1} and 1.14 mg.L^{-1}, respectively (**Fig. 10.7**). The model fitness for NH_4^+ and NO_x in terms of R^2 was evaluated at 0.96 and 0.856, respectively, and therefore, calibration was acceptable.

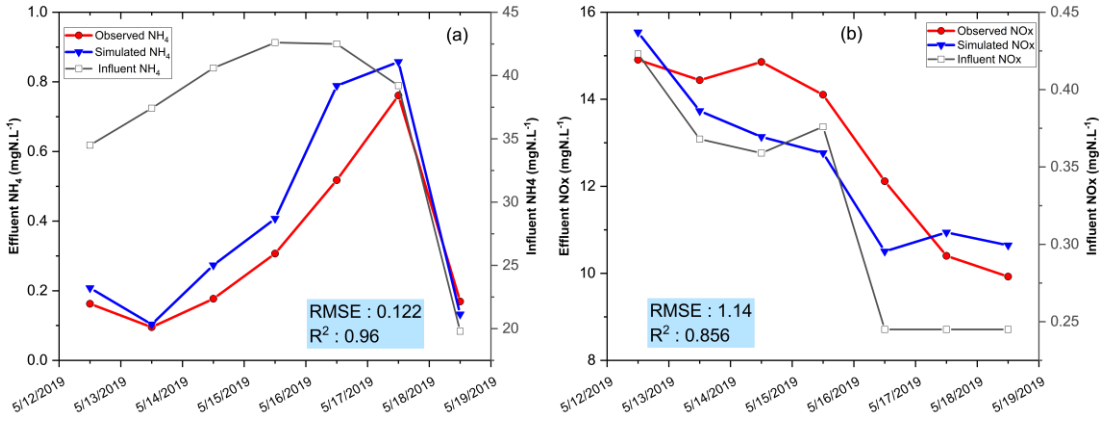

Fig. 10.7: Model calibration results for dynamically simulated effluent NH_4^+ (a) and NO_x (b) concentrations

Fig. 10.8 (a) shows that the model is able to describe the PO_4 removal performance with RMSE of 0.15 $mg.L^{-1}$ and R^2 value of 0.97. Similarly, **Fig. 10.8** (b) presents the simulated and observed X_{TSS} concentration in the membrane aerated tank. The model amicably simulated the X_{TSS} concentration with RMSE of 65 $mg.L^{-1}$ and with R^2 value of 0.81.

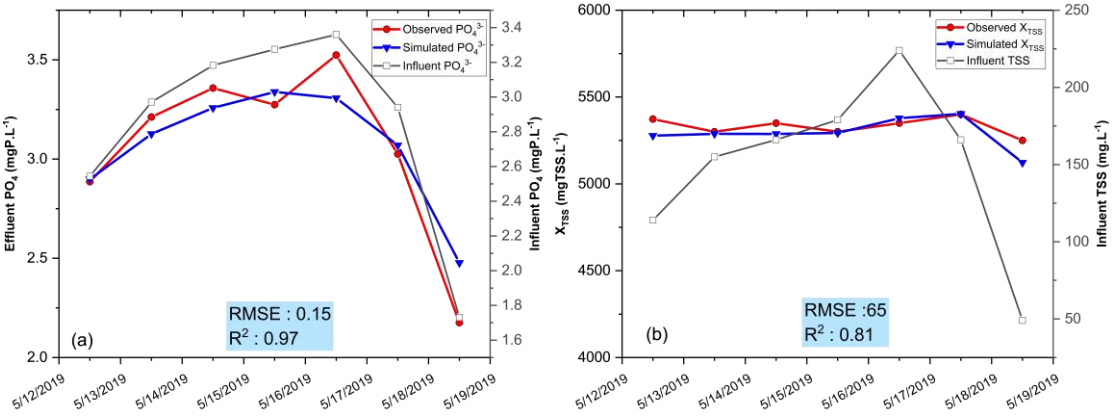

Fig. 10.8: Calibration results for dynamically simulated effluent PO_4 (a) and X_{TSS}(b)

These observations indicated that the calibrated model performed well. The stoichiometric and kinetic parameters subset acquired through calibration may be used to validate the model with data sets from a different period.

10.3 SENSITIVITY ANALYSIS OF THE BIOKINETIC SUB-MODEL

Morris Method: Parameter screening has been carried out to assess the influence of the stoichiometric and kinetic parameters on the model responses, namely the COD, NO_x, NH_4^+, PO_4^{3-} and X_{TSS}, in a dynamic state. For this, the global sensitivity analysis

(GSA) method, "*Morris Screening*", was used due to its low computational cost among other time-consuming GSA methods (Król et al., 2019; Pianosi et al., 2016; Ruano et al., 2011). The Morris method evaluates the so-called distribution of *Elementary Effects (EE)* of each model parameter to model outputs/responses, from which basic statistics are computed to derive sensitivity information. The parameters are changed over their entire range of defined uncertainty. It computes the partial derivatives (PDs) of the model at evenly distributed points (often called "resolution levels") within input ranges, and these derivatives are then averaged out. Morris's method gives 2 indicators related to sensitivity analysis; one is the sensitivity measures mean (μ), which reflects the main effect of the parameter on the output, and the other is the standard deviation of the EE (σ). It describes the interaction with other parameters or the nonlinear effects. A high standard deviation indicates that a factor is interacting with others because its sensitivity changes across the variability space. For a model with K number of parameters, where x =(x_1, x_2,...,x_K) is a vector of parameter values mapped onto the unit hypercube, and y(x) is the model output evaluated at point x. The elementary effect of parameter k can be given by **Eq.10.6** .

$$EE_k = \frac{Y(x1, x2, \ldots, xk + \Delta, \ldots, xK) - Y(x1, x2, \ldots, xK)}{\Delta} \qquad 10.6$$

Where Δ, the grid jump, is chosen such that x+Δ is still in the specified domain of parameter space; Δ is a value in $\frac{1}{1-p}$,…, $1 - \frac{1}{1-p}$ where p is the number of resolution levels that partitions the model parameter space into a uniform grid of points at which the model can be evaluated. The grid constructs a finite distribution of size $p^{K-1}\times[p-\Delta(p-1)]$ elementary effects per input parameters.

For "n.p" number of elementary effects associated with the k^{th} parameter sampled from the finite distribution of EE_k, the mean of the elementary effects can be given by **Eq.10.7.**

$$\sigma_k = \sqrt{\frac{1}{np}\sum_{r=1}^{np}\left(EE_k^r - \mu_k\right)^2} \qquad 10.7$$

The second statistical summary of interest is standard deviation of the EE associated with the k^{th} parameter from all the trajectories and is given by **Eq.10.8**.

$$\sigma_k = \sqrt{\frac{1}{np}\sum_{r=1}^{np}\left(EE_k^r - \mu_k\right)^2} \qquad 10.8$$

Where, np is the number of trajectories associated with the k^{th} parameter, r is the number of resolution levels, and k is number of parameters.

Particular choices and setting for GSA: Latin hypercube (LH) sampling strategy with radial design is used due to higher efficiency than other sampling techniques (Pianosi et al., 2016). In the LH-radial sampling strategy, the variations Δi are all taken starting from the same (randomly selected) point in the input space.

The minimum and maximum values for each parameter were determined by considering the variability limit of ±20% from the default or estimated value in this work. The sampling strategy builds "r" trajectories in the input space, each composed of a number of model parameters (K) + 1 point. The starting point of each trajectory is randomly selected over a uniform grid, and the subsequent K points are obtained by moving one factor at a time of a fixed amount Δ so that each trajectory allows for evaluating one EE per factor. The number of trajectories is selected in the range of 5-20 (Morris, 1991; Campolongo et al., 2007), and the resolution level (p) of the hyper-grid is fixed in the range of 4 -8 (Pianosi et al., 2015). In this work, the values of r and p were selected as 10 and 4, respectively. The final number of model evaluations was equal to r×(K+1) for one week-long dynamic simulation. For each simulation run, the simulation output was compared with daily measured data, calculating the NSE to further perform the sensitivity analysis. A MATLAB based tool developed by Pianosi et al.(2015) was used in this work, while bootstrapping was used to analyze the convergence of the EEs with respect to a number of model evaluations.

The Morris sensitivity measures (normalized between 0-1) for each response variable are shown in **Fig. 10.9**. The parameters in each sub-group are ranked according to the maximum overall efficiency of the model (i.e., minimum NSE). The ranking of the model parameter is helpful in their selection for calibration in order of their priority. Furthermore, Morris's screening can be used as a pre-step before moving to a detailed quantitative, sensitive analysis to reduce the high computational cost of variance-based sensitivity analysis (VBSA) methods.

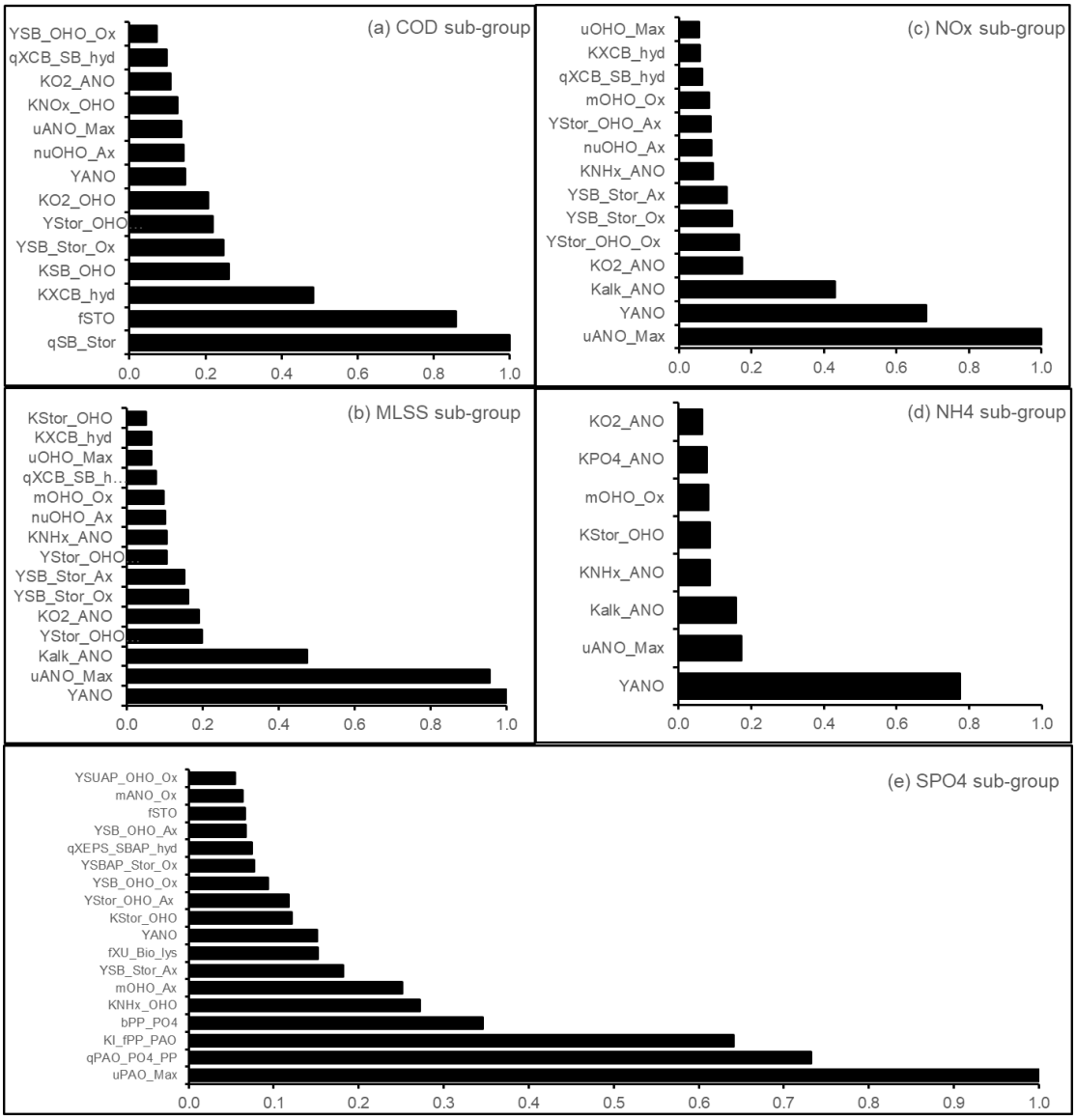

Fig. 10.9: Morris's method of sensitivity measure (normalized mean of elementary effects) for COD, X_{TSS}, NH_4^+, NO_x, and PO_4^{3-}

10.4 VALIDATION OF THE BIO-KINETIC SUB-MODEL

For validation of the bio-kinetic model, another data set was used (*details given in* ***Chapter 9:*** *and summaries in* **Table 9-3-Table 9-4**). The system was initialized with state variable concentrations acquired in the calibrated stage. As stated already, there was no $FeCl_3$ addition from 1st November 2018 until 15th December 2018. $FeCl_3$ addition started on 16th December 2018. The ODEs related to the chemical precipitation model were activated only after 16th December 2018. The default kinetic parameters related to chemical precipitation were then calibrated by the hit and trial method. The dynamically simulated results for effluent DO, COD, NO_X, NH_4^+, PO_4^{3-}

and X_{TSS} concentrations within the membrane aerobic reactor were validated with the experimental data for the same period.

Fig. 10.10 shows simulated and measured DO concentrations in the aerobic tank. The accuracy of the model in terms of RMSE is evaluated at 0.23 $mg.L^{-1}$, which is quite poor, as confirmed by the R^2 equal to 0.67, which demonstrated that the model could be further improved.

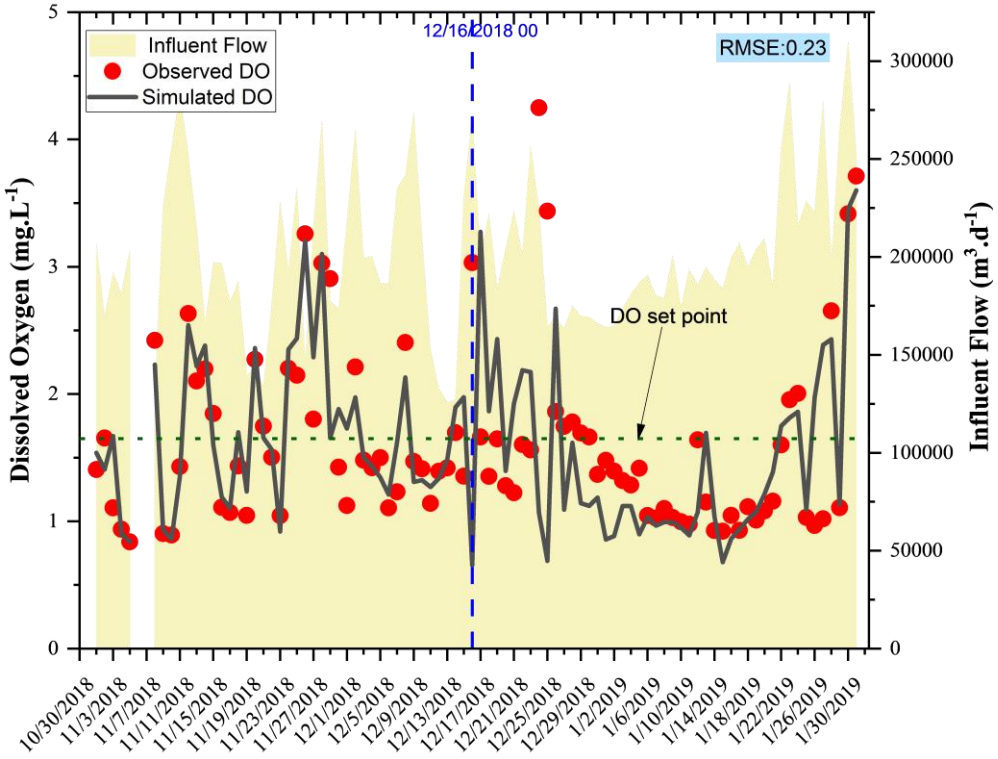

Fig. 10.10: Dynamically simulated and observed DO concentration in the aerobic zone of the reactor.

This might be associated with the fact that the intermittency of the aeration (see **Table 6-4**) is not considered for the biological process aeration model in this work. This slightly poor validation is linked to adopted values of several model parameters, especially the coefficient A and B in **Eq. 8.8** is adjusted based on a heuristic approach, and a more sophisticated calibration approach may help in further improvement. **Fig. 10.11** shows the simulated and observed effluent COD (right) and total COD load (left-area plot). Overall, the model was sufficient in predicting the COD profile with RMSE values of 3.12. Although, the model fit in terms of R^2 is poor (0.36) due to the unavailability of the observed data below 15 $mg.L^{-1}$, which is the minimum detection

limit of the standard method used by the plant operator. The model provides an opportunity for the plant operators to produce effluent COD data even below the laboratory detection limits and the COD profile within each of the reactors in series. Similarly, as shown in **Fig. 10.12** (a,b), the model could simulate the de/nitrification processes with RMSE values for NOx and NH_4^+ of 1.76 and 0.294 and with an acceptable R^2 values of 0.671 and 0.709, respectively.

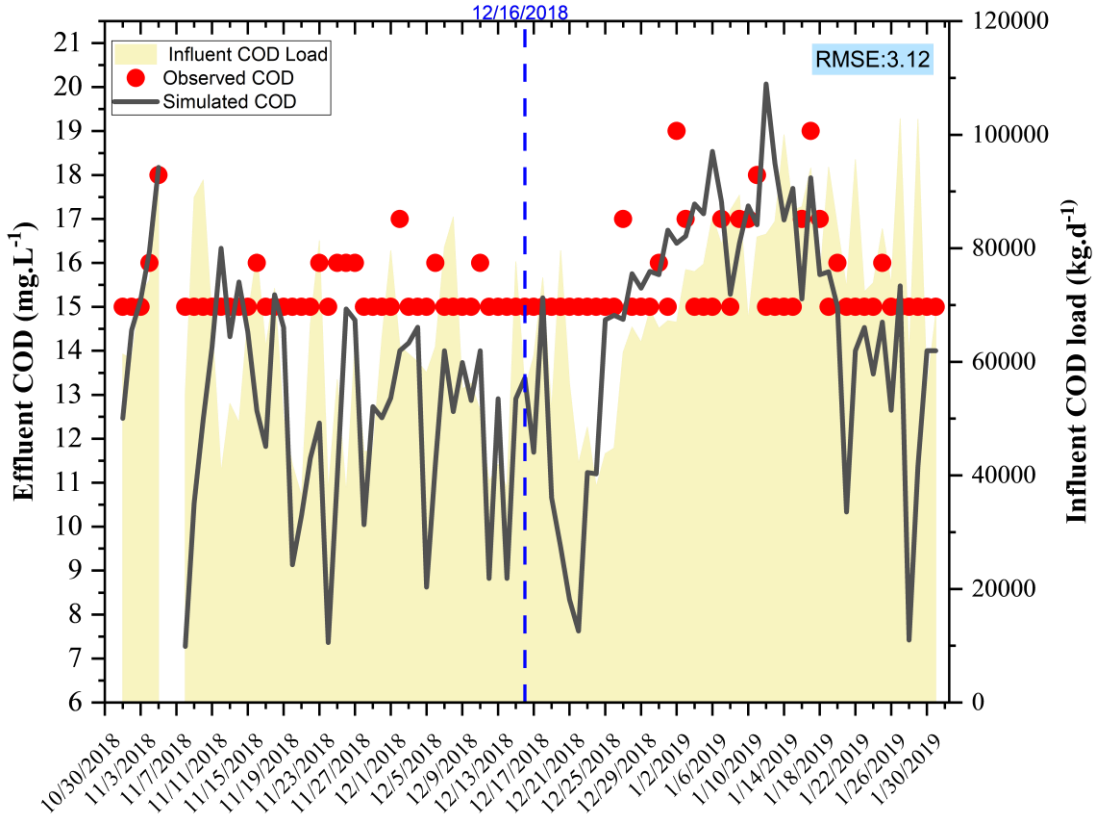

Fig. 10.11: Dynamically simulated and measured effluent COD concentrations in the effluent

Fig. 10.12(b) shows a significant decrease in NO_X concentrations after adding $FeCl_3$, which is probably linked to alkalinity consumption/precipitation or accumulation of ferric hydroxide in the MLSS, resulting in a pH drop to some extent. Another probable reason for this could be the existence of anoxic micro-zones in the center of larger sludge flocs that allows denitrification happening in traditional way (Nguyen et al., 2010; Yang et al., 2009). Guo et al., (2010) got the similar results with addition of Poly ammonium chloride.

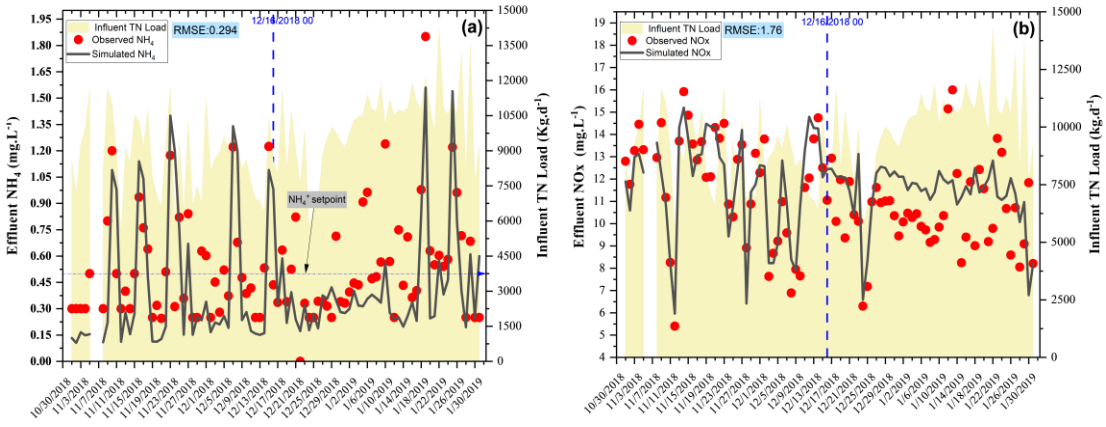

Fig. 10.12: Simulated and observed NH_4 (a) and NOx (b) concentration of the effluent

The default values of the kinetic parameters i.e., "K_pre" and "K_red" of the chemical precipitation model, could not sufficiently simulate the CEPR.

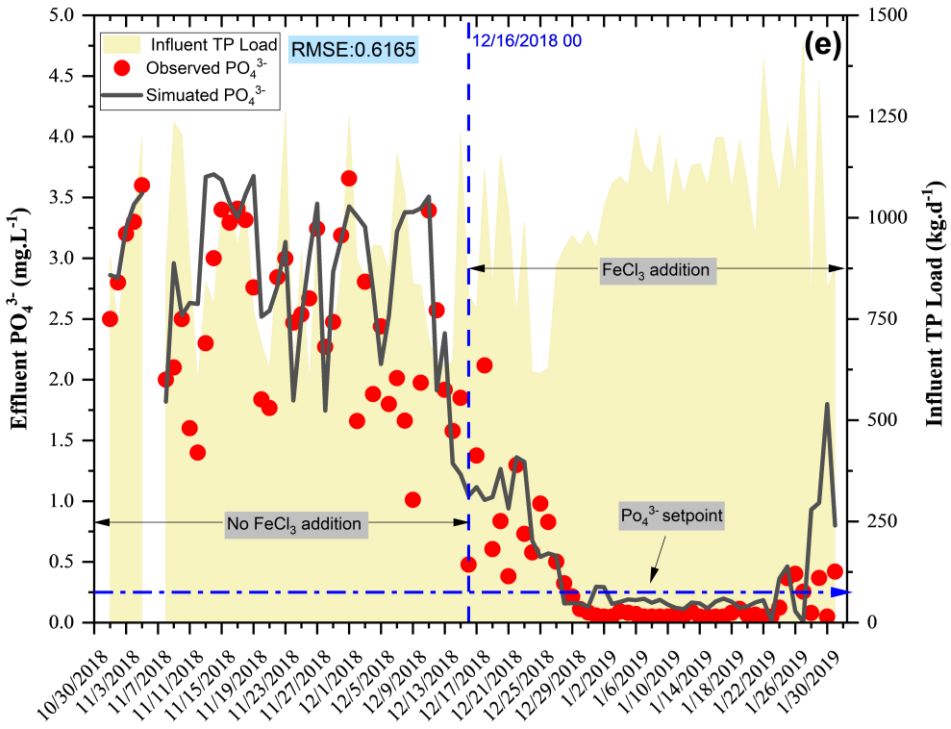

Fig. 10.13: Dynamically simulated and measured effluent PO_4^{3-}

Therefore, these two parameters were calibrated by changing the K_pre from 1 to 6 m^3 g[Fe (OH)].d^{-1}. The value of the K_red was automatically changed while conserving the relationship, i.e., K_red= 0.6× K_pre (Henze et al., 1999). **Fig. 10.13** presents the model performance for simulation of ortho-phosphate removal. It could be seen that the model is accurate enough to predict the biological phosphorus removal (before

$FeCl_3$ addition) as well as the lumped biological and chemical precipitation (after $FeCl_3$ addition with Fe/P molar ratio of 2.17) with an overall RMSE and R^2 values of 0.61 and 0.931, respectively.

Fig. 10.14 shows the simulated and observed X_{TSS} concentration profiles in the aerobic tank. The model fairly simulated the X_{TSS} with RMSE and R^2 values of 383 $mg.L^{-1}$ and 0.88, respectively. SMPs and EPSs concentrations within each reactor in series were also simulated; however, due to the unavailability of the observed data from the full-scale facility, the simulated results could not be validated.

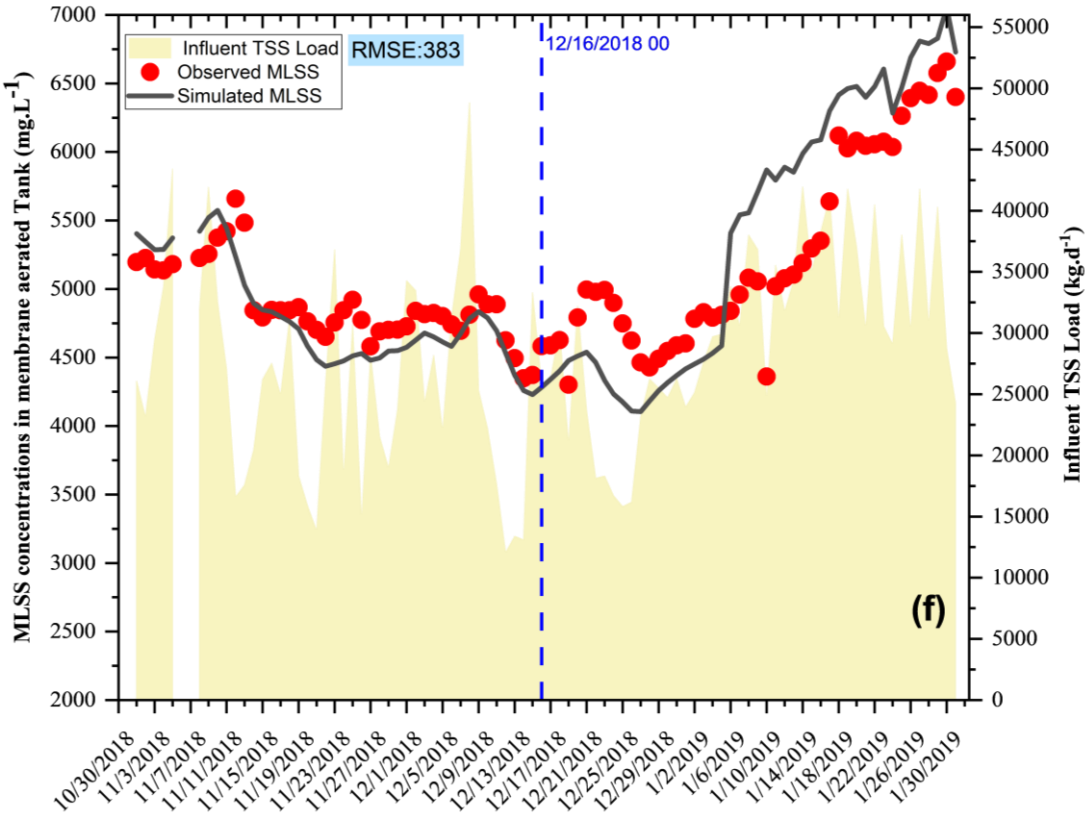

Fig. 10.14: Dynamically simulated and observed X_{TSS} concentrations in the membrane aerated tank

10.5 CONSOLIDATED VALIDATION OF THE BIO-KINETIC MODEL

In order to re-validate the biokinetic sub-model, another dataset for two weeks was acquired (see *section **9.1.3***). The initialization conditions in each of the tanks were adjusted as per the data gathered from the 2nd experimental campaign and mass

balances of the particulates (see **Table 9-8**). Based on the findings of sensitivity analysis and results of validation stage, a set of stoichiometric and kinetic parameters obtained from the calibration was adapted, and the same values were then used in the re-validation stage. No $FeCl_3$ addition was carried out during the re-validation period. The daily dynamic data acquired from the SCADA system was used for dynamic simulations.

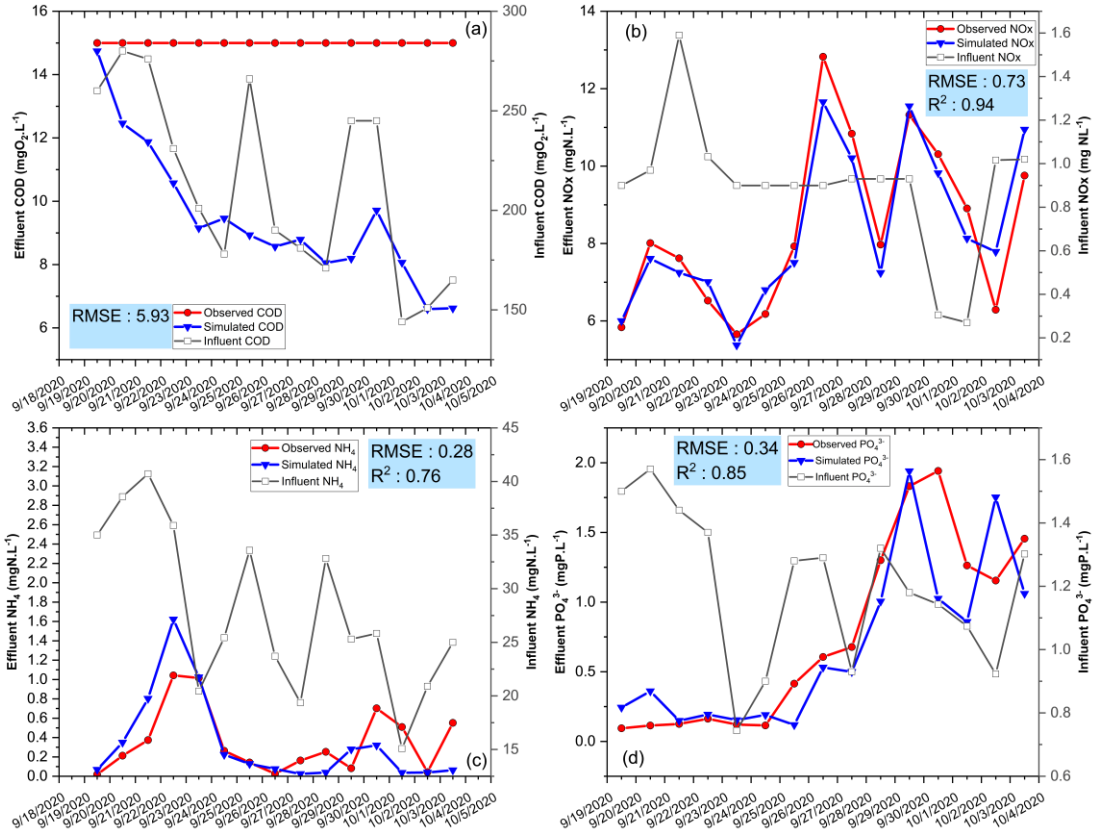

Fig. 10.15:Simulated and observed effluent profiles of COD (a), NOx (b), NH_4^+ (c), and PO_4^{3-} (d) for second consolidated validation of bio-kinetic model.

The simulated and observed effluent profiles for COD, NOx, NH_4^+ and PO_4^{3-} are shown in **Fig. 10.15** with RMSE values of 5.95 (a bit higher due to the fact the observed COD data below 15 $mg.L^{-1}$ is not available since below the detection limit), 0.73, 0.76, and 0.85 respectively. This shows that the model is sufficient to describe the pollution removal performance of the MBR at a super large-scale.

10.6 SUMMARY AND PERSPECTIVES

The ASM3-EPS-SMP model adapted and modified in this work can predict the dynamic variety of the influent soluble biodegradable organic matter, which is

considered soluble inert organic matter by the standard ASM3 is hardly treated. The model was calibrated with a data set from the 1st experimental campaign. In addition to 3 stoichiometric parameters measured through respirometry, 9 additional kinetic parameters were manually adjusted to improve the model fitness (see **Table 10-2**). The model was then validated with two different data sets. The calibrated and validated model is capable of successfully predicting the behavior of super large-scale MBR and provides the profile of the routinely measured pollutants, i.e., DO, COD, NH_4^+, NO_X, X_{TSS}, and PO_4^{3-} with an acceptable level of accuracy. Besides, it also provides EPS and SMPs flow concentrations which are not usually measured in full-scale facilities due to tedious and expensive experimentation. Obtaining these last data is expected towards an improvement in the filtration model accuracy.

Chapter 11: Calibration and Validation of Fouling Sub-model

This chapter presents the results of the filtration sub-model calibration, a sensitivity analysis of the model factors, and the validation of the model. In addition, an exploratory study has been proposed to interpret the results while relating the findings of the full-scale fouling assessment with the already published and comprehensively presented literature survey in ***section 2.3***. Furthermore, the validation results of the fouling-sub model with three new data sets for the full-scale and for a single tank are presented.

11.1 FOULING SUB-MODEL CONNECTIVITY

The fouling sub-model is provided with real-time MLSS and X_{EPS} concentrations simulated for the membrane-aerated tank as shown in **Fig. 11.1**. These two data series are then used to estimate the real-time specific cake resistance (static and dynamic).

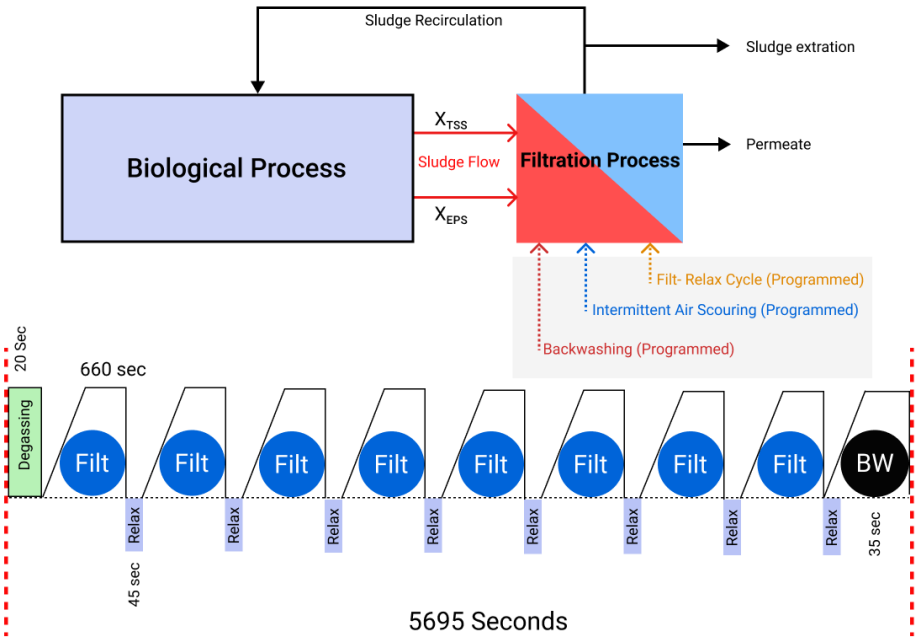

Fig. 11.1: Fouling sub-model connectivity with the biokinetic model (top) and filtration (filt), relaxation (relax), backwashing (BW), and degasification cycle at the SAV-MBR (bottom).

In addition, other data sets include the average instantaneous flux of the operating tanks (at real temperature), sludge temperature (to consider the effect on sludge viscosity), operating surface area of the membranes (considering the number of tanks in operation at a given moment) specific coarse bubble aeration rate and TMP for initialization. Furthermore, the Zenon system's operating parameters related to filtration relaxation, degasification, and backwashing durations were considered (see ***section 6.3***) as per the data retrieved from the SCADA system. Indeed, the Zenon's ZeeWeed 500D is equipped with an intermittent aeration system which could be operated either on 10/10 (10 seconds aeration 10 second no-aeration) or 10/30 configuration and is manually programmable by the operators. Available configuration data from all twenty-eight tanks made it possible to calculate the average operating configuration (i.e., relaxation time).

11.2 PRE-CALIBRATION

11.2.1 Viscosity as a function of temperature and MLSS

An increase in temperature leads to a decrease in the dynamic viscosity of the permeate and may lead to modifying the membrane fouling. In order to avoid the interference of the temperature effect on MBR fouling, non-linear regression between viscosity and temperature has been established by several researchers (Busch et al., 2007b; Huisman, 1996; Judd, 2010; Psoch and Schiewer, 2008; Rosenberger et al., 2006) and given in **Table 11-1**.

Table 11-1: Relationships to describe the effect of temperature on permeate viscosity

Mathematical Relationship	*Reference*
$\mu_T = \mu_w \cdot \frac{0.000479}{(T+42.5)^{1.5}}$	(Huisman, 1996)
$\mu_T = \mu_w \times e^{-0.0239\times(T-20)}$	(Rosenberger et al., 2006)
$\mu_T = \mu_w \times 1.78 e^{-0.041\times T^{0.875}}$	(Busch et al., 2007b)
$\mu_T = \frac{\mu_w \times 1.78}{1+0.0337\times T+0.000221\times T^2}$	(Psoch and Schiewer, 2008)
$\mu_T = \mu_w \times 1.025^{(20-T)}$ *; for T≤20 ^{0}C*	(Judd, 2010)
$\mu_T = \mu_w \times 1.033^{(20-T)}$ *; for T≥ 20 ^{0}C*	

Fig. 11.2 shows the results obtained from the different relationships described in **Table 11-1**. All these relationships provide similar results within a range of 0-40 ^{0}C, expect the one derived by Judd (2010), especially beyond 20 ^{0}C.

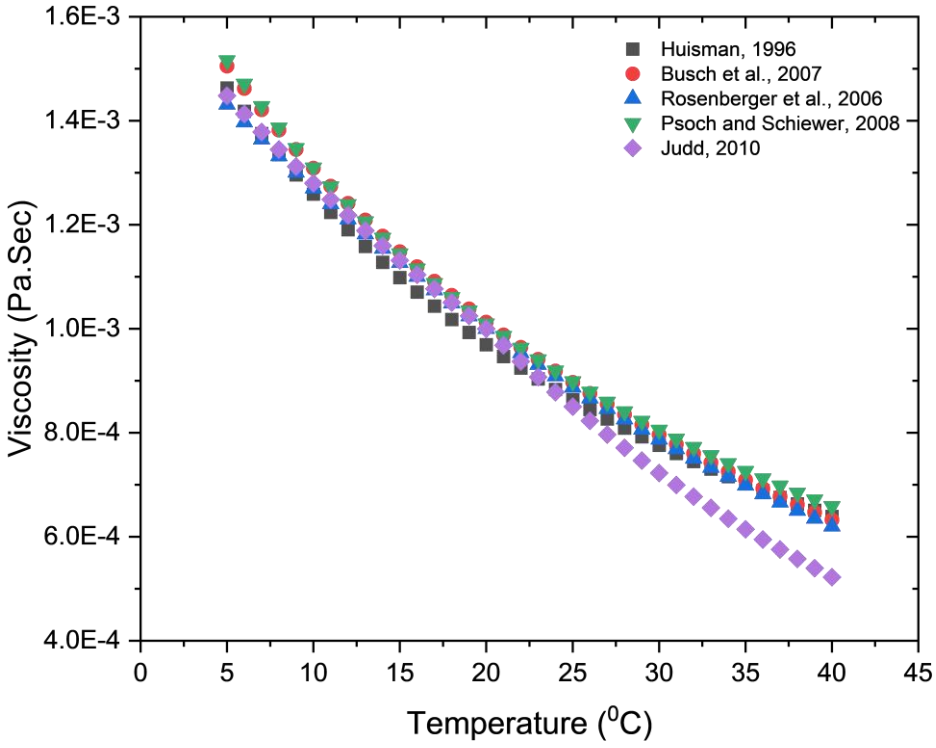

Fig. 11.2: Variations of viscosity with temperature between 5 and 40 ^{0}C considering different relationships found in the literature

Multiple simulations were run with relationships explained in **Fig. 11.2** and RMSE was monitored. After testing all relationships and their influence on the model performance, the one suggested by Busch et al.(2007b) provided least RMSE and was used for subsequent calibration of the fouling model.

Similarly, sludge viscosity is one of the influential factors for fouling (see ***section 2.3.1***), along with the temperature and X_{TSS} concentration. The sludge has a higher viscosity than permeate due to increased frictional forces caused by suspended particles in motion associated with aeration and/or mixing (Drews, 2010). Many viscosity models have been successfully applied to analyze the rheology of the sludge suspensions, as discussed in the detailed review by Ratkovich et al.(2013). While the higher suspended solids concentration and aeration (shear) in activated sludge suspensions in MBRs affect the viscosity of the mixed liquor, other rheological parameters such as yield stress, non-Newtonian flow characteristics, and thixotropic

behavior are typically overlooked. In this way, activated sludge is considered a Newtonian fluid but with a viscosity higher than water. The literature shows that several exponential and linear correlations between dynamic viscosity of the sludge were introduced (Krauth and Staab, 1993; Meng and Yang, 2007; Ng and Kim, 2007), and their mathematical expressions are given in **Table 11-2**.

Table 11-2: Relationship between sludge viscosity and MLSS

Mathematical Relationship	*Reference*
$\mu_s = 1.05 \times \mu_w \times e^{0.08 \times X_{TSS}}$	(Krauth and Staab, 1993)
$\mu_s = 0.909 \times \mu_w \times e^{0.0861 \times X_{TSS}}$	(Meng and Yang, 2007)
$\mu_s = 1.61 \times \mu_w \times e^{0.07 \times X_{TSS}}$	(Ng and Kim, 2007)
$\mu_s = 0.1488 \times X_{TSS} + 1.036$	(Xing et al., 2001)

The exponential expressions proposed by Krauth and Staab (1993) and Meng and Yang (2007) behaved almost in a similar manner, while the expression of Ng and Kim (2007) resulted in higher viscosity than the other two at the same X_{TSS} concentration. The linear correlation expressions derived by Xing et al. (2001) resulted in a totally different scenario, where the increase of the X_{TSS} concentration linearly increased the sludge viscosity. Considering this variation, the expression by Krauth and Staab (1993) was retained for onward calibration of the model as it has also been adapted by several other modelers (Mannina et al., 2011b; Zarragoitia-González, 2009) for modeling MBR systems, and this helped to improve the model fit. **Fig. 11.3** depicts the influence of varying the X_{TSS} concentration (1-25 $g.L^{-1}$) and temperature of the sludge (1-25 ^0C).

However, the exponential correlations presented in **Table 11-2** do not capture the underlying mechanics of fluid movement, as they are based solely on empirical data. These relations were primarily developed for CASP with lower solids concentrations having lower mixing and recirculation energy requirements. In contrast, MBR systems are more likely to have greater requirements. Therefore, the models may not represent the actual rheology of the sludge, and model of the activated sludge rheological properties is a complex step linked with the highly complex nature of the activated sludge suspensions (Ratkovich et al., 2013). The change in the viscosity of the sludge

also influenced sludge density, which is modeled by the expression used by Busch et al. (2007b) and Zarragoitia-González (2009) given as **Eq. 11.1.**

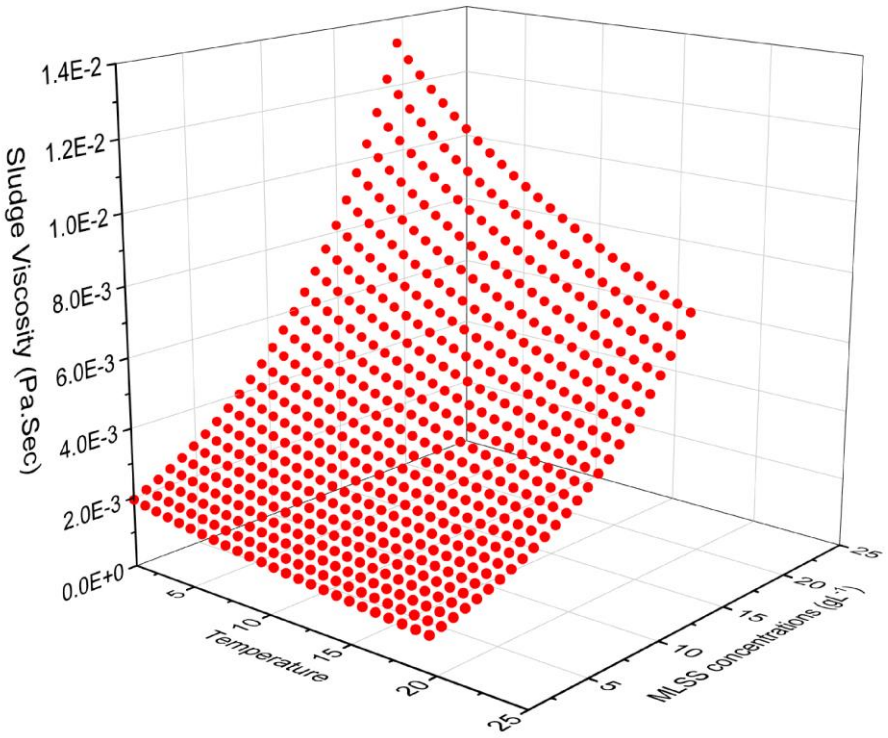

Fig. 11.3: Sludge viscosity under the influence of varying MLSS and temperature

$$\rho_s = \mu_T \times 0.99959 \times e^{0.0004397 \times X_{TSS}} \qquad 11.1$$

11.2.2 Dependence of specific cake resistance on EPS and MLSS

Although the results of different research investigations on the relationship between EPSs content in activated sludge and specific cake resistance have not yet been conclusive, it is widely accepted that the specific cake resistance is affected by EPSs and MLSS concentrations, as used in the studies of Cho et al.(2005), Zarragoitia-González (2009), and Ahmed et al.(2007). As explained in ***section 8.6,*** the logistic expression used by Cho et al.(2005) and later modified by Zarragoitia-González et al. (2008) is adopted to model the dynamic specific cake resistance with MLSS and EPSs data, simulated by the bio-kinetic part of the model. **Fig. 11.4** demonstrates that the specific cake resistance is influenced by EPSs and MLSS concentration, and beyond

certain limits (EPS ~280 mgCOD.L^{-1} and MLSS ~ 5.7 g.L^{-1}) there is no more influence on the specific cake resistance.

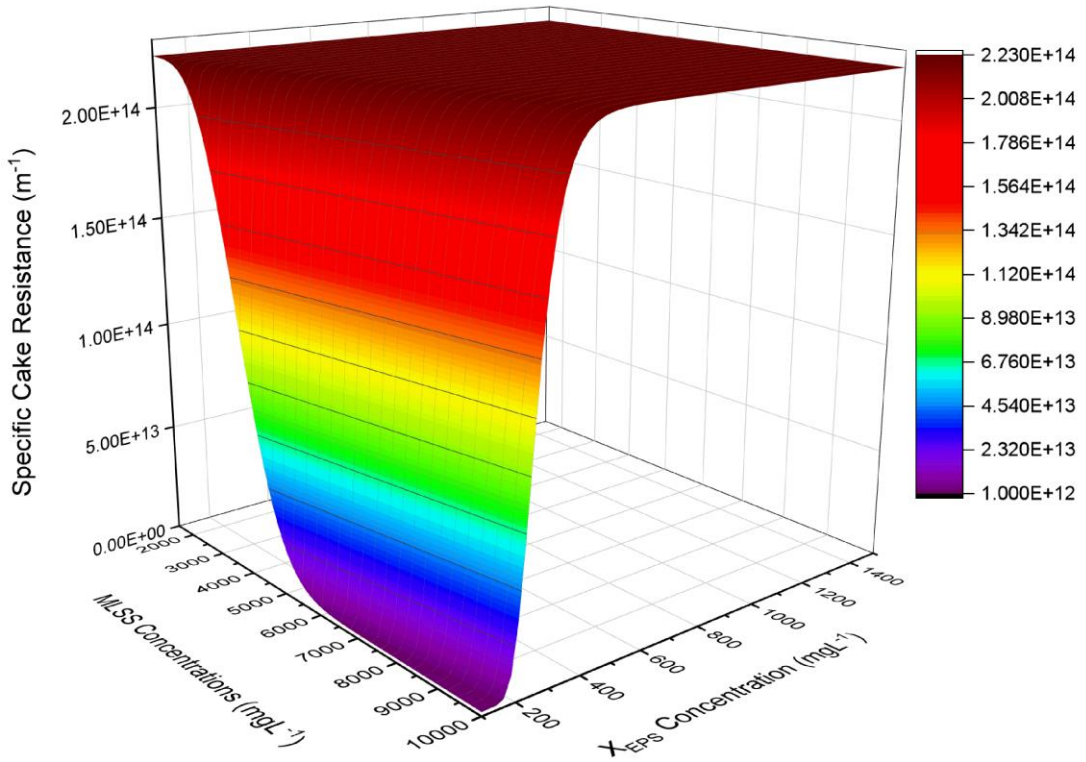

Fig. 11.4: Specific cake resistance under the influence of MLSS and X_{EPS} with default empirical parameters (with three months average TMP of 52 mbar)

11.3 SENSITIVITY ANALYSIS AND CALIBRATION OF FOULING SUB-MODEL

The fouling sub-model has fifteen model parameters, as listed in **Table 8-5**, with the values calibrated by multiple researchers in MBR studies. The values of these parameters vary within a large range, especially for empirical constants (i.e., 'a', 'b', and 'd'), specific pore fouling resistance (r_p), membrane resistance (R_m), the erosion coefficient of dynamic sludge cake (β_{dc}), the compression coefficient for sludge cake (γ) and coefficient of sludge particles stickiness ($\alpha_{stickiness}$). This presented a challenge for robust calibration of the model parameters. Global sensitive analysis (GSA) was then used to identify the most influential parameters to reduce the calibration effort as well the response of the model. The basic purpose of the variance-based GSA is i) to rank (or to prioritize parameters) aiming at generating the ranking of the input factors according to their relative contribution to the output variability and ii) to screen or to

fix a list of non-influential parameters, if any, which have a negligible influence on the output variability and iii) to map the ranges of the parameter variability space that produces significant, i.e., extreme, output values.

In order to compute the sensitivity indices of the fouling sub-model parameters, all parameters were regarded as stochastic and are therefore associated with a probability distribution within a defined range (see **Table 8-5**). From this defined input variability space, samples were randomly drawn using the 'All-[parameters]-At-a-Time' (AAT) method for a base sample of n=3,000 input combinations. First, two independent input samples, X_A and X_B, are built as a matrix of dimensions (n,M). Then, a matric X_C of dimension (n.M, M) is generated by recombination of the samples in X_A and X_B; X_C is composed of M blocks Xc_i (i=1,….M), each block being a (n,M) matrix whose columns are taken from the X_B matrix, except the i^{th} column, which is taken from the X_A matrix. Three corresponding model outputs i.e., Y_A, Y_B, and Y_C were calculated with the objective function "NSE" as scalar outputs. The total number of model evaluations for approximating the main and total effect indices is [N= n.(M+2)]. Then, the estimation of the main and total effects according to the approximation strategy described by Saltelli et al. (2010) was carried out. The convergence analysis was performed by using the bootstraps technique provided in the MATLAB based sensitivity analysis tool (Pianosi et al., 2015).

For each of the 15 model parameters, the first-order sensitivity index (or main effect) and the total-order sensitivity (or total effect) were computed using dynamic simulations and actual flux, membrane area, temperature, and SAD_m input data varying every 15 minutes. The former measures the direct contribution to the output variance from individual variations of a factor and is commonly used for ranking parameters, while the latter measures the overall contribution from both individual variations and through interactions with other factors and is used for screening the parameters (Pianosi et al., 2016). Available TMP data at 15 minutes frequency was used to compute the objective function and calibrate the fouling sub-model.

As shown in **Fig. 11.5** (a), first-order sensitivity indices for the fouling sub-model parameters show that the compression coefficient (γ or "gamma") for the dynamic sludge cake was found to be slightly influential on the membrane fouling (i.e., TMP)

along with the both empirical constants of dynamic specific cake resistance, i.e., aR and pR.

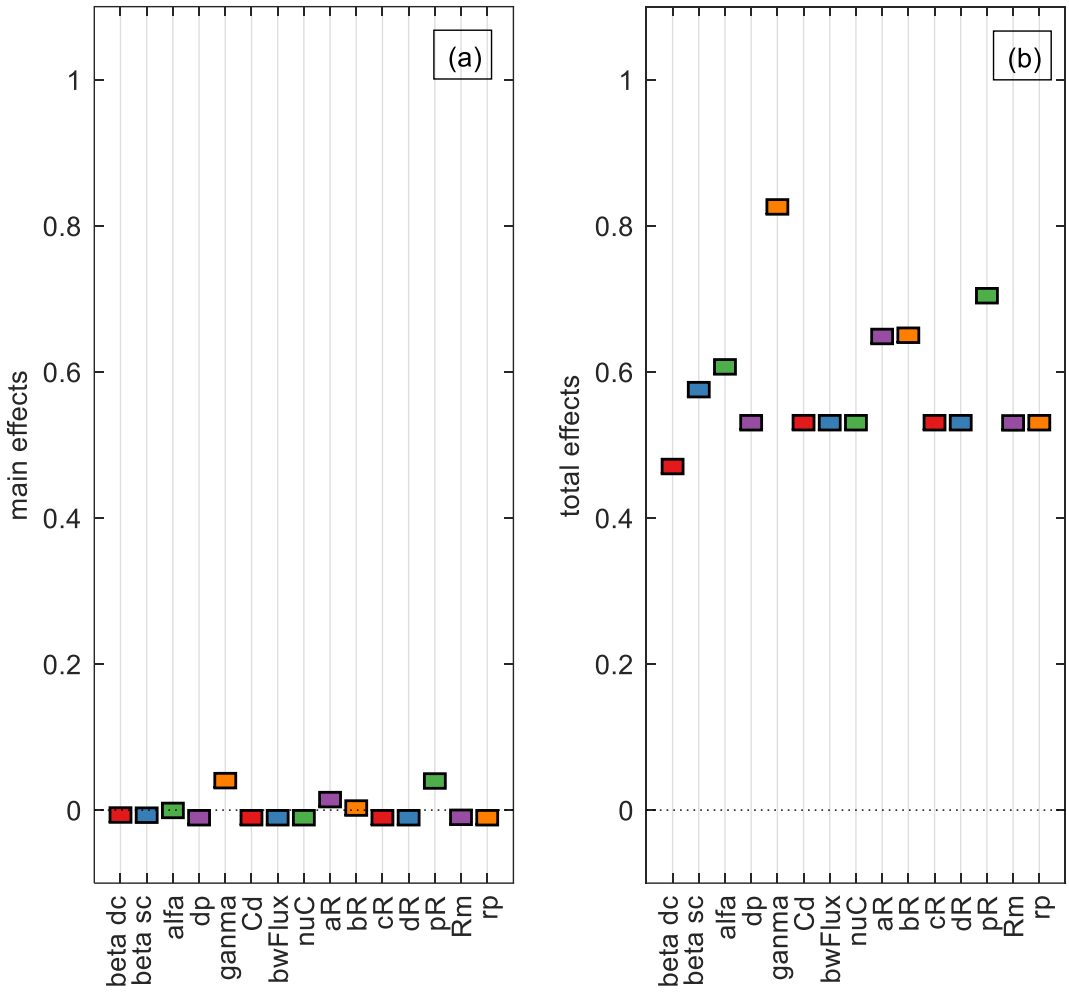

Fig. 11.5: Sensitivity indices calculated using the VBSA method a) main effects indices and b) total effect indices with 51,000 model evaluations.

Variations in individual parameters negligibly contributed to the variation in the TMP. It can be seen that some of the first-order sensitivity indices are negative, even after 51,000 model evaluations. However, the sensitivity indices could still be used and interpreted as suggested by Sarrazin et al. (2017).

As VBSA-based indices are numerical approximations of their theoretical values (between 0 and 1), and when approximation errors are large, the sum of the exact values and approximation error might be lower than zero, and this is mainly associated with a smaller sample size (Sarrazin et al., 2017). Increasing the sample size further may help in eliminating the approximation error but with the higher computational

costs (Pianosi et al., 2016). For the total sensitivity indices, parameters "gamma", "pR", "aR", "bR ", "alfa" and "beta_sc" were found significantly higher than the main effect sensitivity indices, as shown in **Fig. 11.5** (b). This means these 6 parameters have a significant effect on the simulated TMP, not only through their individual effects but also through interactions.

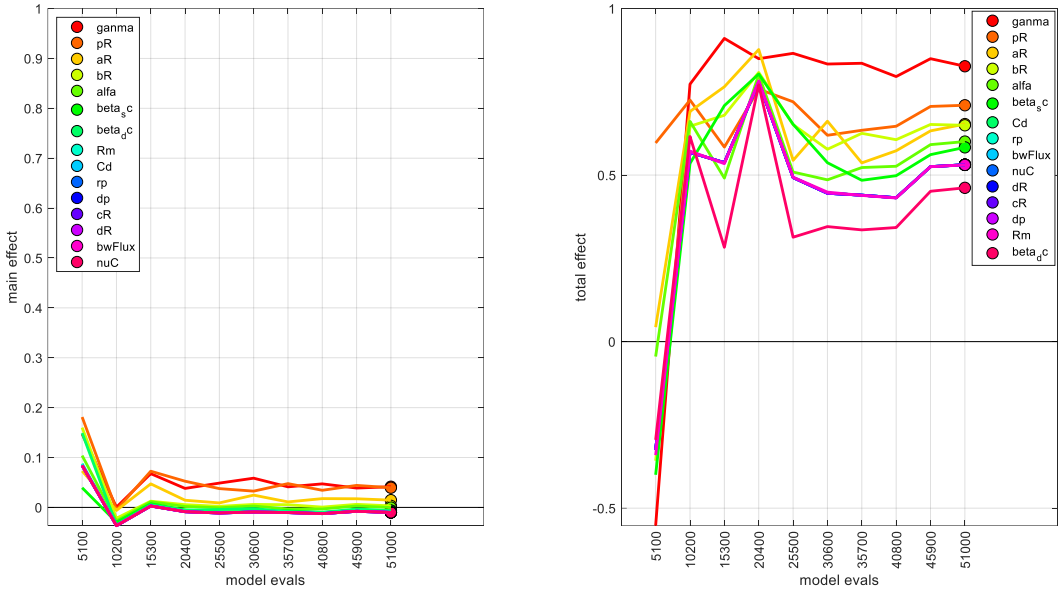

Fig. 11.6: Convergence plots of the (a) main and (b) total effects sensitivity indices using bootstrapping method

The remaining 9 parameters have total and interaction effects indices in their lower ranges and therefore have small effects, considering both direct and indirect interactions. The convergence analysis shows that the main effects (or *factor prioritization convergence*) have mostly converged. In contrast, the total effects had not yet converged and required an extension of the sample size. Therefore larger sample size would be needed as suggested in the literature (Saltelli et al., 2008; Sarrazin et al., 2016). The lack of convergence could be due to high non-linearities in the fouling sub-model and very large variations of the parametric values (see **Table 8-5**). Therefore, an approximate sample size required for convergence (*screening*) has not been explored further due to precision gain versus high computational cost ratio considerations.

11.3.1 Dynamic simulations and calibration of fouling sub-model

The calibration was performed with a dataset gathered during the first experimental campaign (i.e., 13/05/2019-19/05/2019). Dynamic simulations were performed to achieve the lowest possible MAPE and RMSE values.

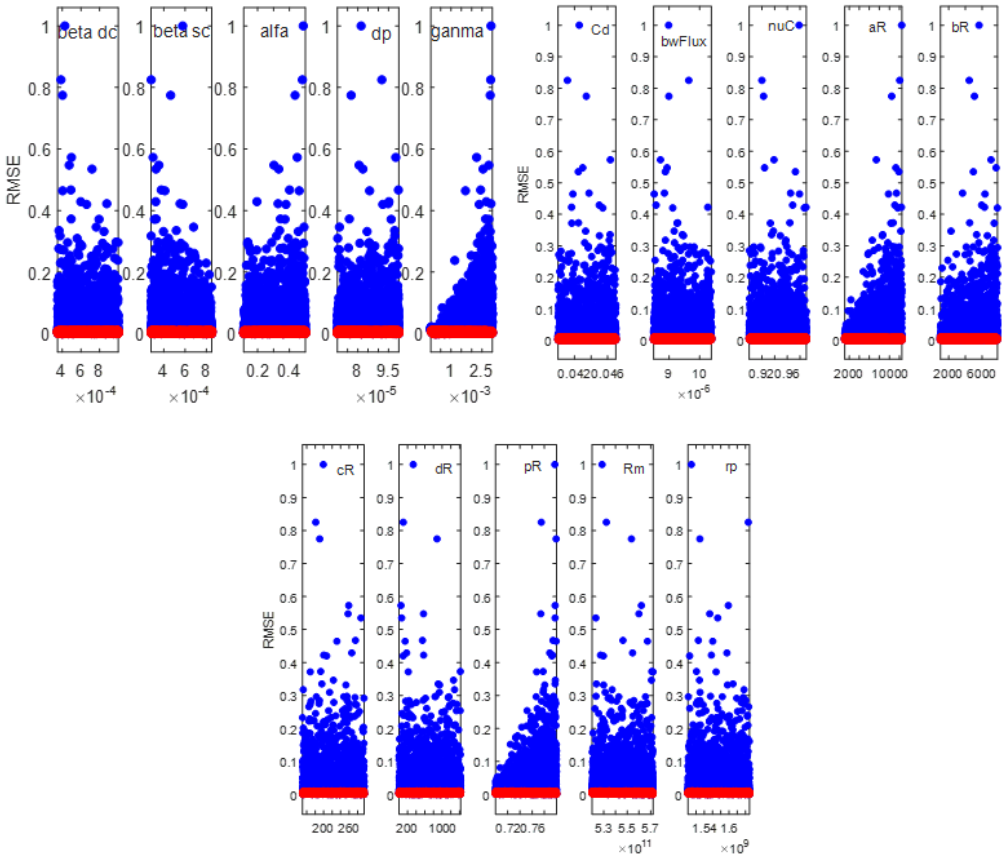

Fig. 11.7: Scatter plots of fouling sub-model parameters values as a function of RMSE, with highlighted 'behavioral parameterizations (simulations with poorer RMSE)' in red color with 3000 model evaluations.

The first-order sensitivity indices from the VBSA help in ranking the parameters in their order of influence on the fouling sub-model output (i.e., TMP). The values of influential parameters, i.e., “gamma” “pR” “aR” “bR”, “alfa”, and “beta_sc” were slightly adjusted within the range reported in the literature and given in **Table 8-5**. These selected model parameters are difficult to measure, system-dependent, and are not uniquely quantified in the literature. Based on the generalized likelihood uncertainty estimation (GLUE) scatter plots with values of the parameters as function of RMSE as shown in **Fig. 11.7**. The values of the calibrated model parameters are given in **Table 11-3**.

The dynamic simulations helped to evaluate the fluctuating cake mass, the static and dynamic cake resistances, the TMP, and the total fouling resistance.

Table 11-3: Calibrated values of fouling sub-model parameters

Symbol	Description	Unit	Value
aR	constant for specific cake resistance	--	1156.2
bR	constant for specific cake resistance	--	136001
cR	constant for specific cake resistance	--	172.4
dR	constant for specific cake resistance	--	150.9
C_d	coefficient of the drag and lifting force	--	0.041
pR	constant for specific cake resistance	--	0.72
d_p	MBR sludge particle diameter (without $FeCl_3$)	m	0.00010
r_p	specific pore fouling resistance	m^{-1}	Estimated
Rm	Membrane intrinsic resistance	m^{-1}	Estimated
$\alpha_{stickiness}$	coefficient of sludge particles stickiness	--	0.50
β_{dc}	erosion coefficient of dynamic sludge cake	--	0.00035
β_{sc}	erosion coefficient of static sludge cake	--	0.00028
γ	compression coefficient for sludge cake	$kg.m^{-3}.s^{-1}$	2.50E-05
η_{bw}	Efficiency of backwashing	%	98

Fig. 11.8 shows the dynamic deposition of the mass onto the surface of the membrane. It can be seen that no significant static deposit of the mass was found for one week.

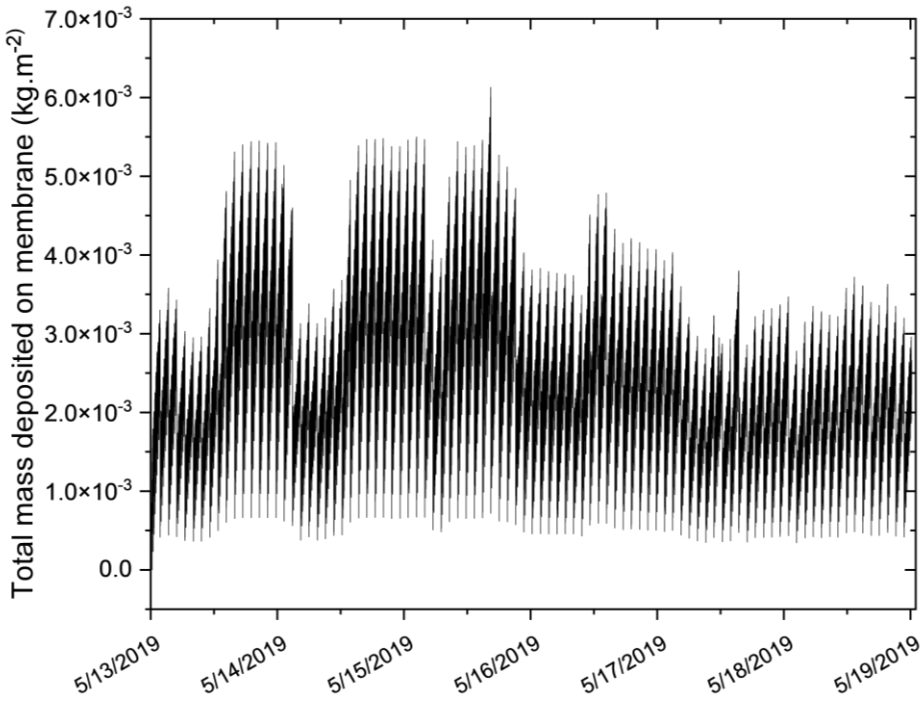

Fig. 11.8: One-week simulated deposition of the mass onto membrane surface under the influence of filtration-relaxation, backwashing, and intermittent aeration.

The hydrodynamic conditions at the vicinity of a membrane surface govern the deposition of the mass and air-scouring shear stress remains the main trigger to control consistent deposition. The temporal fluctuation in the shear stress affected cake detachment, in additional to fluctuating operating flux (linked with the influent flow). The large spikes in the graph reflect dynamicity of the mass deposition under fast varying conditions.

The model results can reflect long-term cake development and residual fouling associated with the mass deposition on the membrane surface. However, validation of the mass deposition is challenging due to the fast dynamics associated with multiple fouling abatement operations, i.e., filtration relaxation, aeration sequencing, backwashing. Consequently, non-existence of any residual mass on the membrane surface for long term is observed.

Similarly, **Fig. 11.9** depicts the evaluation of the static (a) and dynamic (b) cake resistances over a period of 1 week with depiction of the one-complete degassing to degassing cycle (sub-figures). Static resistance plot (a) is zoomed in further to reflect the simultaneous effect of the fouling accumulation and the wash-off phenomenon on the static resistance. The incremental steps indicate the fouling development during the filtration-relaxation cycles (under the influence of sequenced aeration), which mathematically results from the residual of the dynamic resistance. The backwash step seems effective in a large removal of the deposited mass

Dynamic resistance plot in **Fig. 11.9**(b) depicts the incremental of the temporal cake on the membrane surface. Each of the spike in the zoomed plot reflects the increase of the fouling (in the presence of the sequenced aeration) and get back near original level after activation of the relaxation.

The observed and simulated data for TMP and total resistance evolution for one week is presented in **Fig. 11.10**. The mean absolute percentage error (MAPE) for TMP and total resistance was 4.34% and 9.32%, respectively, with an acceptable R^2 values of 0.975 and 0.72, respectively, demonstrating the acceptability of the model calibration. The simplification of simulation process (i.e., simulating 28 tanks as a single unit) lead to a discrepancy between observed and simulated TMP with an appearance of peaks with simulated data as shown in **Fig. 11.10**(a). This is due to the fact that the observed TMP data are averaged of 28 tanks operating in tandem. The experimental data are also averaged in 15 minutes frequency where temporal fluctuations of individual tanks are lost in the statistical averaging and are not reflected precisely. Whereas simulated

data is available in high frequency with one second time interval, for filtration as well as aeration, and therefore fast dynamics in simulated data present peaks, especially at higher TMP.

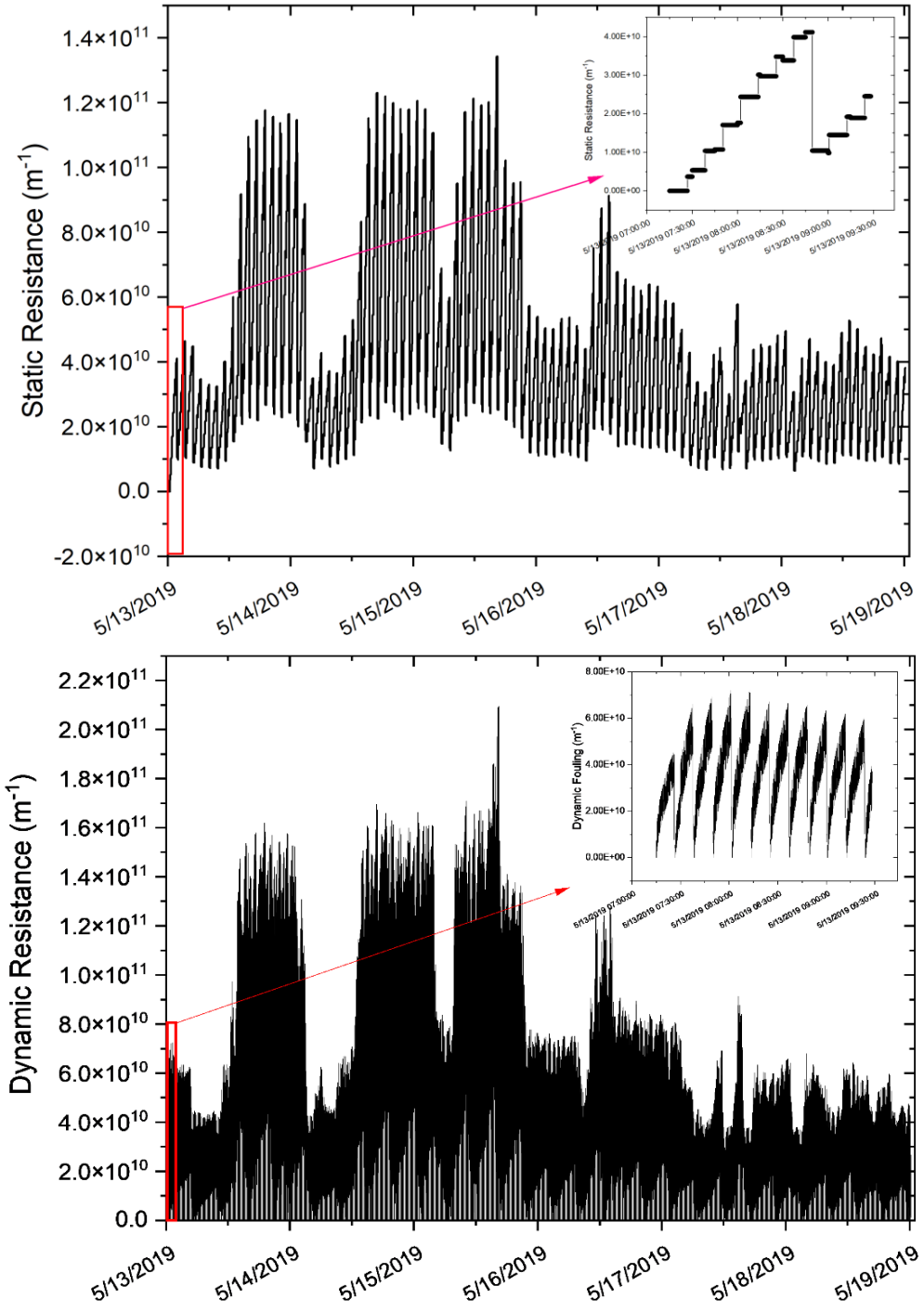

Fig. 11.9: Evolution of static (top) and dynamic (bottom) sludge cake resistance under the influence of fouling abatement controls in place at SAV-MBR

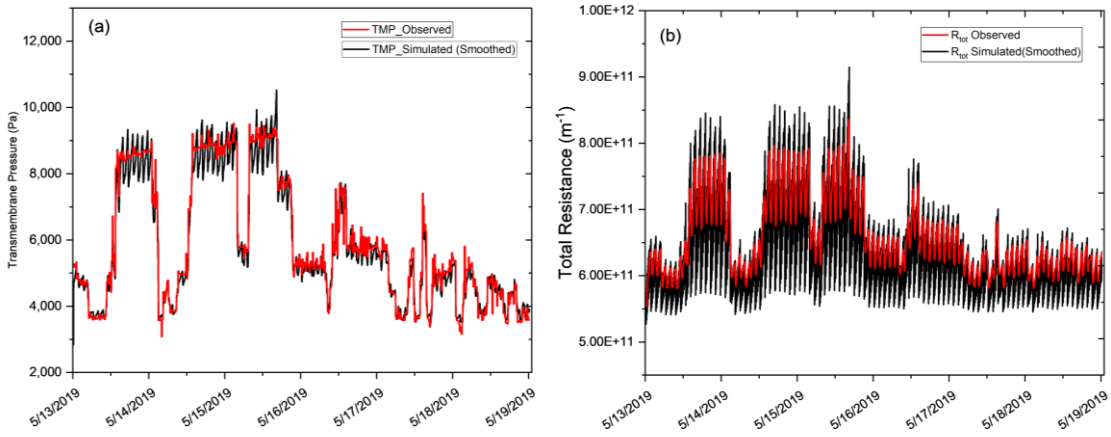

Fig. 11.10: Simulated and observed fouling sub-model outputs a) TMP and b) total filtration resistance for the calibration stage.

The extent of variation between the measured and observed total resistance is higher as compared to the TMP. This is probably due to the difference in the approaches considered for adjustment of temperature effect in calculation of the viscosity in the model and for SAV-MBR data.

11.4 MODEL VALIDATION WITH OF 90 DAYS DATA

Some data related to the number of membrane tanks in operation and the aeration intensity were unavailable for the first 10 days of the dataset used for validation, i.e., from 1st to 10th November 2018. Therefore, these days were not considered for the fouling sub-model and simulations for the remaining 83 days were run, i.e., 11/11/2018 until 31/1/2019. The data available in 15 minutes format for the number of tanks in operation in a given time, aeration intensity, filtration-relaxation sequencing, aeration sequencing, backwash time, backwash flow rate, instantaneous flux, MLSS, X_{EPS} and temperature were considered. The observed and simulated data for TMP and resistance in series evolution for one day is presented in **Fig. 11.11**,a) and b), respectively. The mean absolute percentage error (MAPE) for TMP and total resistance are 5.11% and 7.13%, respectively with an acceptable R^2 values of 0.971 and 0.749 respectively demonstrating that the calibrated model performs well to fairly simulate the fouling evolution with time.

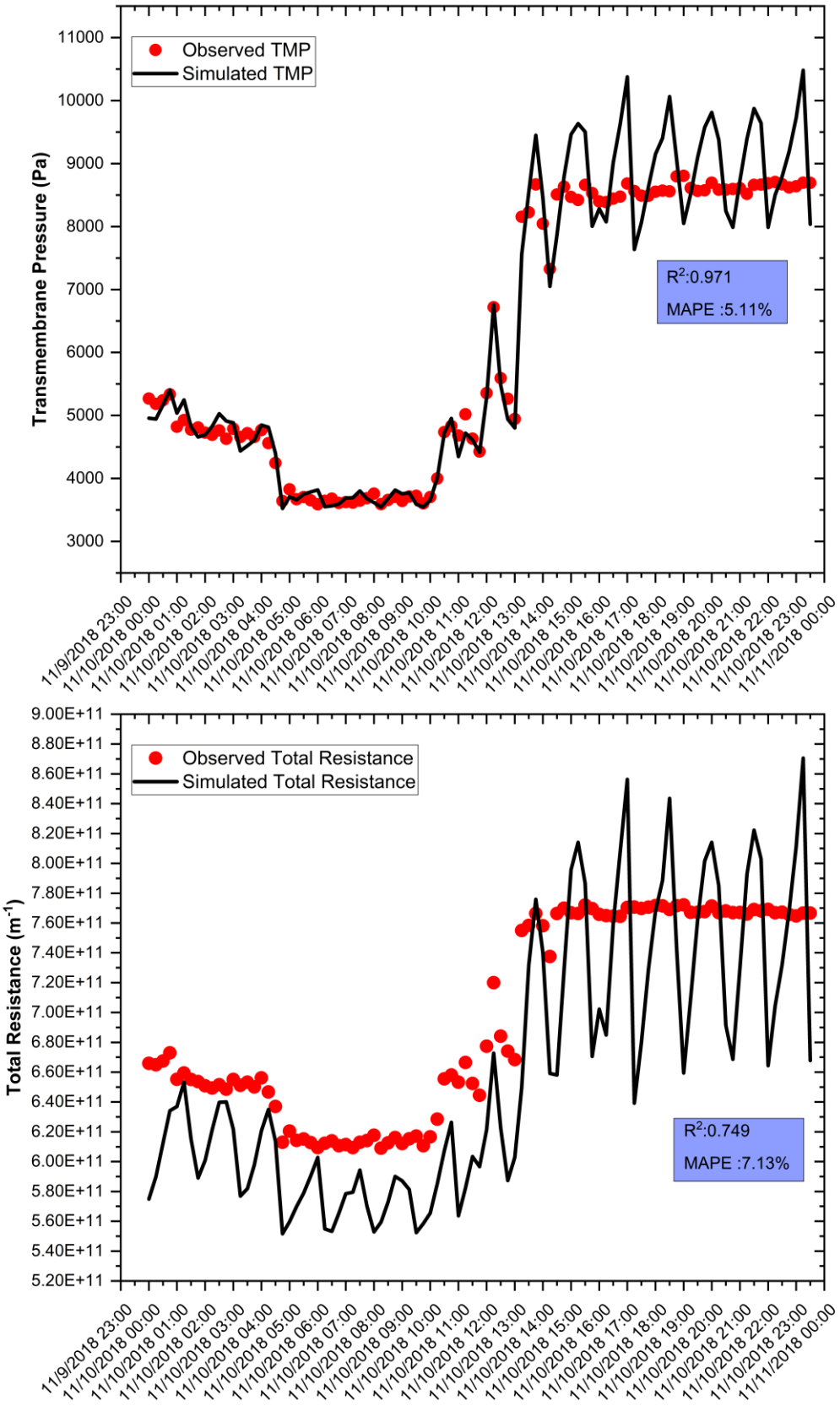

Fig. 11.11: Observed and model simulated data for (a) TMP evolution profile of on-day, (b) Total resistance evolution profile of one day

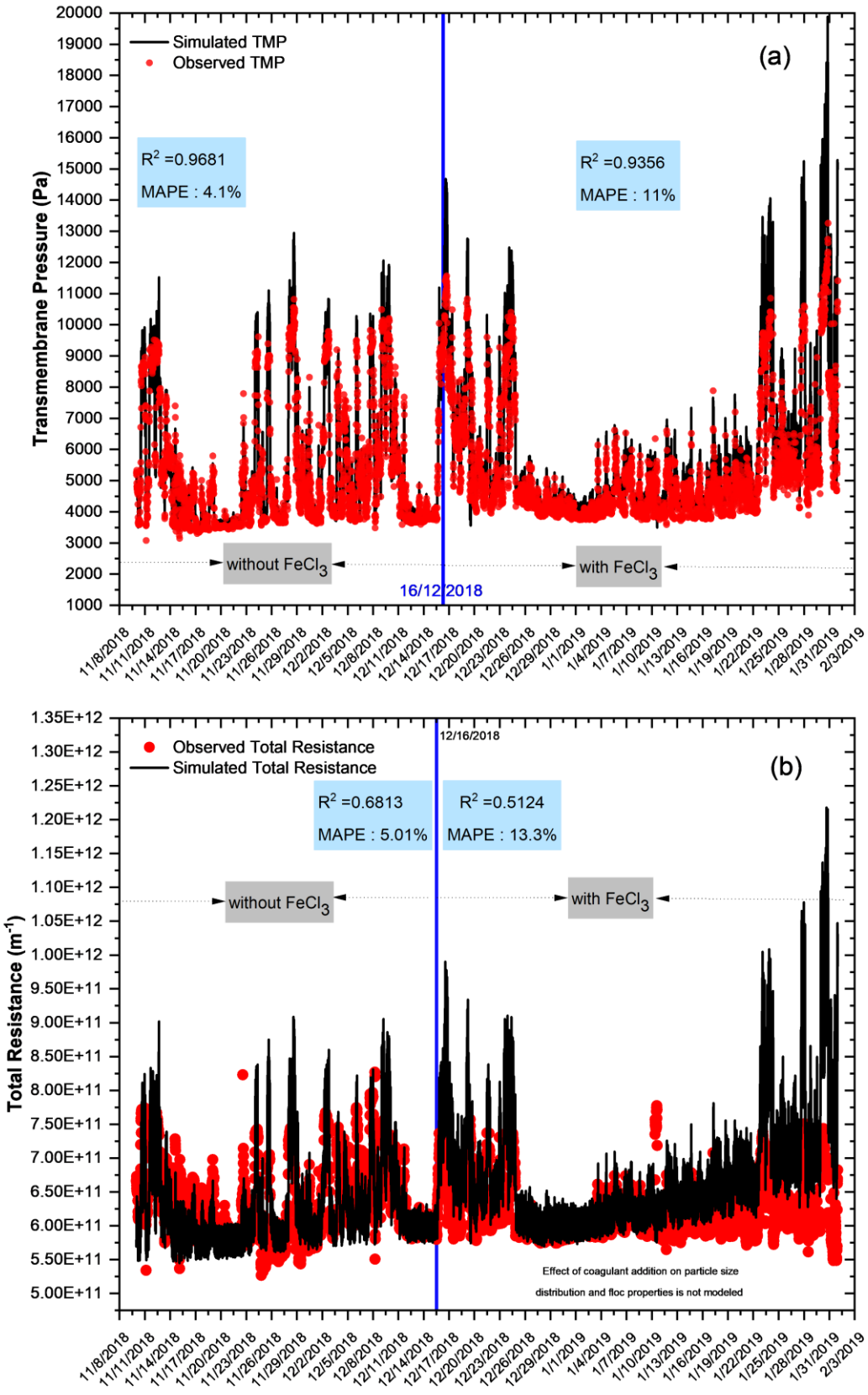

Fig. 11.12: Observed and model simulated data for (a) TMP evolution profile from 11/10/2018 until 31/1/2019 and (b) Total resistance evolution profile form 11/10/2018 until 31/1/2019

The simulations were then extended for the entire 83 days and the simulated results for TMP and total resistance in comparison with the observed ones are presented in **Fig. 11.12**. It can be seen in **Fig. 11.12** (a) that the TMP prediction accuracy of the model during the period 11/11/2018 until 16/12/2018 (i.e., without the addition of the coagulant) was pretty much stable with MAPE of 4.1% and R^2 value of 0.986 which is almost within the range of 1-day simulation results. However, the MAPE increased to 11% after the addition of $FeCl_3$, but the R^2 value dropped to 0.935. Similarly, the MAPE and R^2 values for total resistance were 5.01% and 0.68 respectively, before adding the coagulant (see **Fig. 11.12** (b)). However, MAPE increased to 13.3% after coagulant addition and the R^2 value reduced to 0.512. An explanation found in the literature that the addition of $FeCl_3$, which linearly increases the floc size and results in a compact floc structure, as investigated by (Asensi et al., 2019a). This suggested that the changes in the filtration properties of the sludge due to the addition of coagulant should be considered, which is not the case in the current work.

Some adjustments into the specific cake resistance (see **Eq. 8.29**) considering the other factors such as the influence of SMPs, particle size evolution, particle size distribution (PSD), or stickiness of the flocs associated with the addition of coagulant, may help to improve the better prediction of the specific cake resistance and thus the static and dynamic cake layer resistance.

In addition, the current model does not include the effect of chemical cleaning (in-situ and ex-situ, *see **section 6.3.3***) to remove the irreversible pore-fouling resistance, which linearly increases with time. Moreover, uncertainties in the measured inputs of the fouling sub-models could be a probable cause for the variations in the model output. A dynamic sensitivity analysis considering the model factors and inputs altogether could be fruitful in assessing the robustness of the models and their responsiveness to the variations in the inputs.

Furthermore, influent properties such as C/N ratio, pH, alkalinity (mol HCO_3^-) and operating parameters including organic loading rate ($kgCOD.m^{-3}.d^{-1}$), SRT (day), sludge temperature (^0C), DO concentration ($mg.L^{-1}$), ferric addition ($Kg.Fe.d^{-1}$), MLSS ($g.L^{-1}$) and operating flux ($L.m^{-2}h^{-1}$) were analyzed to explore their influence on the fouling (in terms of permeability decline). The correlation analysis revealed that the

permeability is highly negatively correlated with the flux (-0.93) and moderately negatively correlated with MLSS concentration (-0.38) in both MBR lanes.

The correlation between ferric addition and permeability appeared to be linked with DO concentrations, as shown in **Fig. 11.13**. Therefore, no absolute correlation could be established and this still remained inconclusive (Nadeem et al., 2022). Similar to the results, the role of the DO (see **Table 2-2**) and Ferric addition towards fouling abatement/ promotion is not conclusive in the literature.

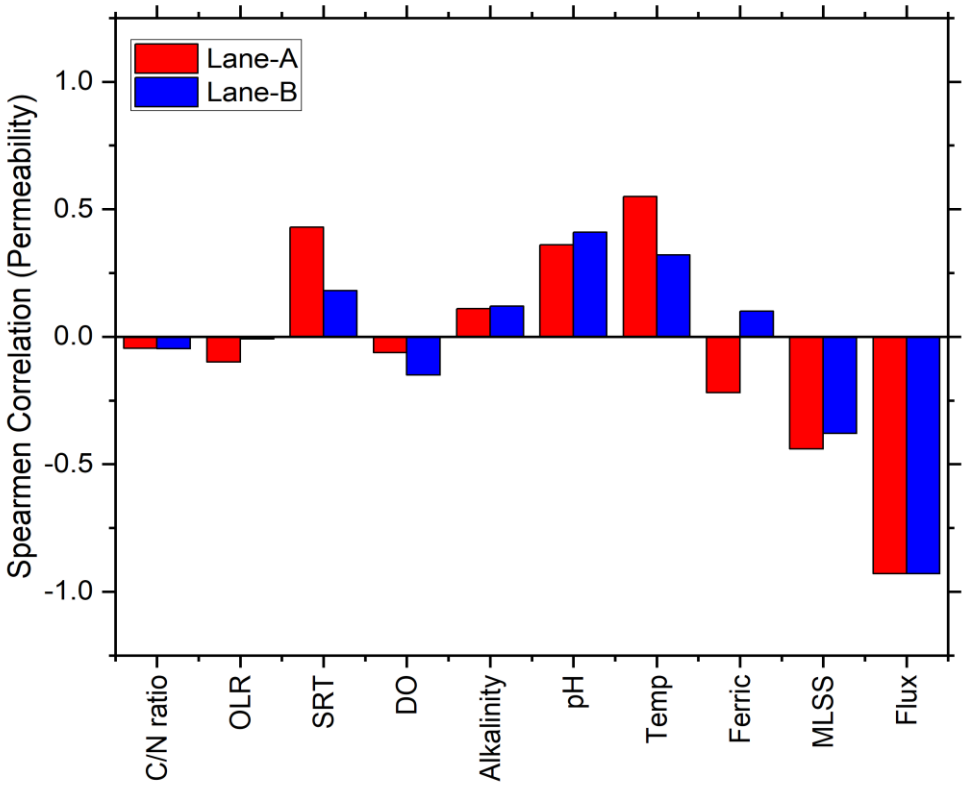

Fig. 11.13: Correlation between the permeability and other variables

SRT and pH, temperature, and alkalinity appeared to be positively correlated with permeability.

11.4.1 Re-validation with 2 weeks data at full-scale

In order to re-validate or test the integrated model at full scale, the operating membrane surface of 28 tanks, average instantaneous flux, temperature, and simulated MLSS and EPSs concentrations has been considered. No coagulant addition was carried out

during this testing period. The membrane total resistance was estimated from observed TMP, flux, and temperature data (using Darcy's law), and minimum value of total resistance is adapted for a period between two chemical washes. For each known chemical wash, the initialization values are updated based on the data for that specific period. As shown in **Fig. 11.14**, the simulated TMP fitted reasonably well with the measured TMP with MAPE and R^2 values of 6.09% and 0.964, respectively.

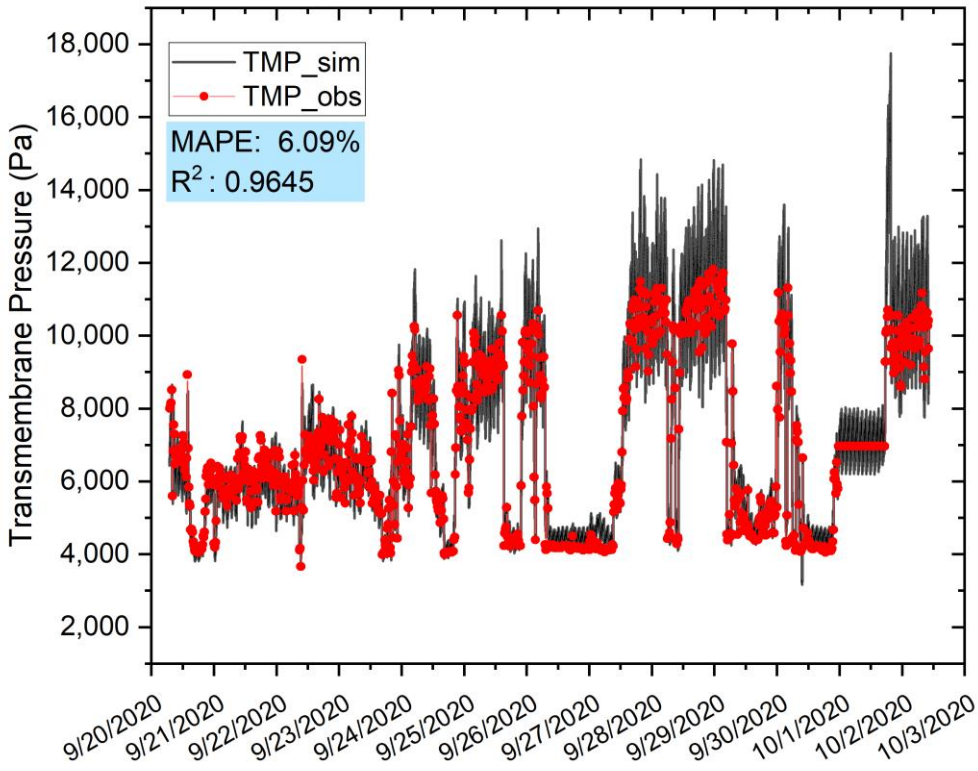

Fig. 11.14: Observed and simulated TMP with data from the 2nd experimental campaign

11.4.2 Validation of model with data from a single tank

All datasets tried heretofore showed negligible to no fouling, as shown in **Fig. 11.15**. The TMP increased linearly with almost perfect correlation with increased flux, and no TMP jump could be identified. The slope of the fitted fouling sub-model was almost the same for the data used for calibration and validation (**Fig. 11.15**a-b). For the re-validation period (**Fig. 11.15**c), the slope slightly increased from 2.66 to 3.01, depicting some fouling development. Although the fouling sub-model predicted the

TMP fairly well, the fouling model needs further test up for systems with prominent fouling.

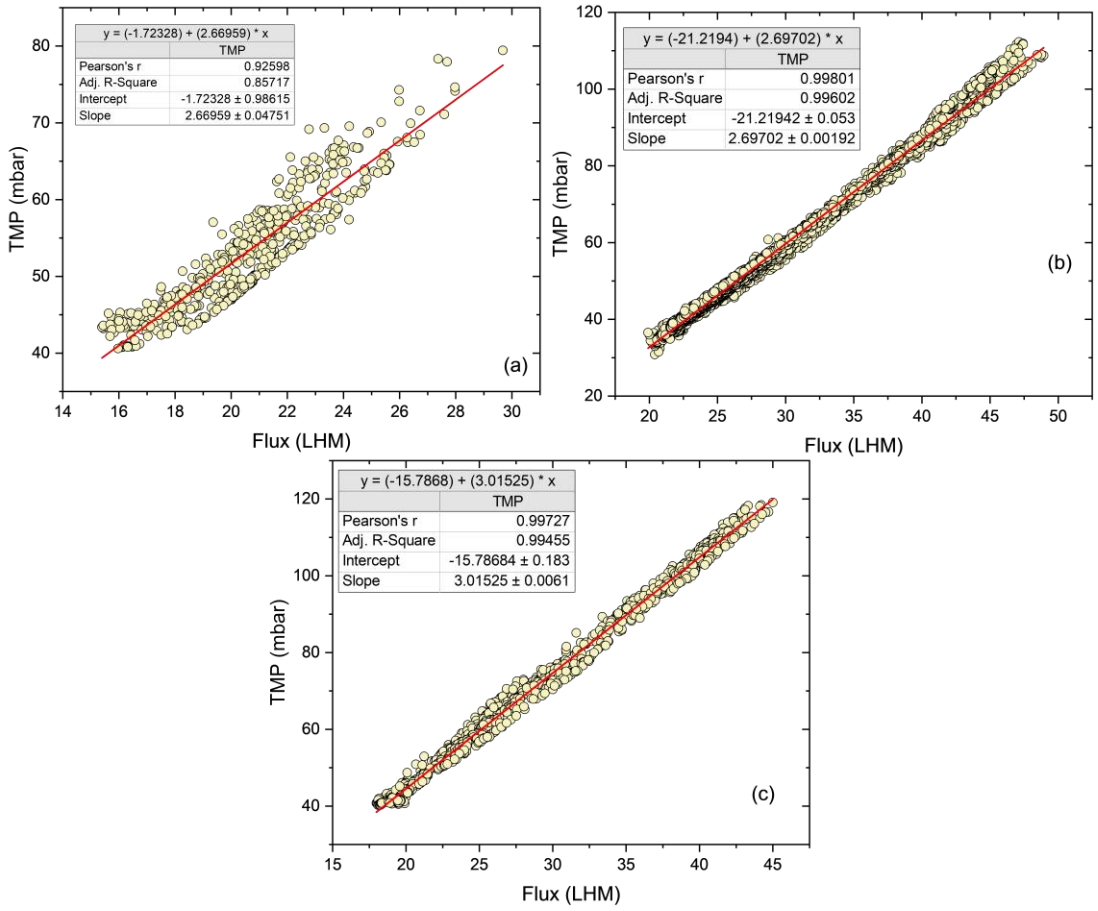

Fig. 11.15: Flux as a function of TMP for a) calibration period, b) validation period and c) re-validation period.

In a bid to test the model with data with prominent fouling, the permeability of all 28 tanks was investigated from November 2018 until December 2019. Only one tank (8A) was found with considerable permeability decline between two ex-situ chemical washes. It can be seen in **Fig. 11.16** that the permeability dropped from 562 $L.h^{-1}.m^{-2}.bar^{-1}$ to 318 $L.h^{-1}.m^{-2}.bar^{-1}$ starting from 1st Jan 2019 until 9th April 2019 (38% decline).

In order to simulate one tank, the measured MLSS (from a sensor installed in the MBR tank) and fixed X_{EPS} concentration (400 $mgCOD.L^{-1}$) along with the measured instantaneous flux at the actual temperature, aeration intensity, programed intermittency of aeration (10/10), backlashing and filtration-relaxation cycles, for the

8A-tank was used to simulate TMP using fouling sub-model as a stand-alone component.

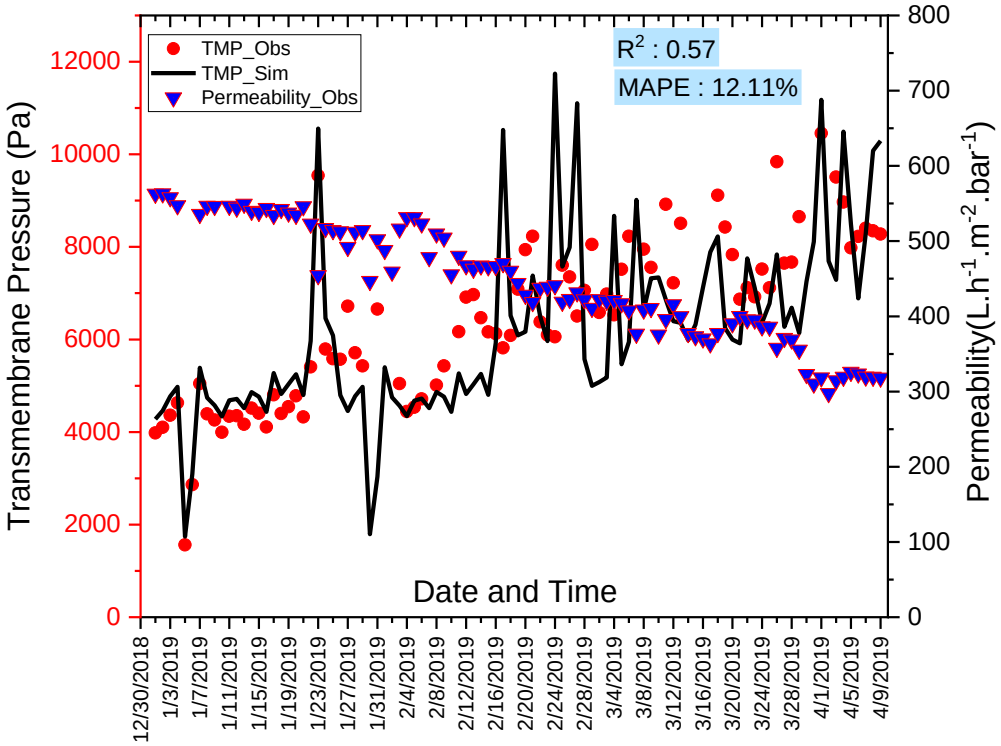

Fig. 11.16: Daily simulated and measured TMP of a single tank (8A) for a 4-month period

All model parameters were kept at their default values (set in this work during calibration and validation stages), except the "pR" which was adjusted to 0.68 instead of 0.72: this calibration deemed necessary owing to the size of the one tank versus the full-scale. For full-scale simulation, several simplifications were made, e.g., averaging the fluxes, air scouring rates, and relaxation times for all 28 tanks. The model simulates the TMP trend reasonably well with MAPE and R^2 values of 12.11% and 0.57, respectively. The decline in prediction accuracy is attributed to the fact that the X_{EPS} concentration is kept constant through the simulations. In addition, the daily average air scouring rate is used because high frequency (15 minutes) data were not available.

It seemed that the fouling sub-model is capable of simulating systems with higher fouling tendencies. Although, modeling one tank alone is not a true representation of the super-large-scale system (>100,000 $m^3.d^{-1}$). However, with this validation, it could

be projected that modeling all 28 tanks in parallel using their individually programmed configurations could help to improve the model performance and utility.

11.5 SUMMARY AND PERSPECTIVES

The selected filtration sub-model provided a reasonable level of prediction accuracy at the lowest computational cost and with a minimum amount of effort required for calibration. This model can be successfully applied to describe the membrane fouling-filtration process provided that the operating conditions, such as instantaneous filtration fluxes, mixed liquor suspended solids (MLSS), EPSs, and TMPs fall within the technical norms applied at SAV-MBR or any other HF-equipped full-scale facility. The fouling sub-model is validated with filtration data showing negligible to minimum fouling. Additional validation of the model would be required with data from super-large-scale facilities showing higher fouling tendencies. Therefore, it is difficult to ascertain the accuracy of the model under different operating conditions and higher fouling tendencies at full scale. Testing the fouling sub-model at the level of one tank (*with a membrane surface of 16,512 m^2*) with significant fouling, it provided a reasonable TMP prediction accuracy.

A few of the following limitations of the fouling sub-model require further consideration for a better understanding of the fouling phenomenon in full-scale applications:

a) The chemically enhanced backwashing (in-situ cleaning) is effective in removing a significant share of the irreversible, i.e., pore fouling (Hai et al., 2018a; Judd, 2010), and this effect should be incorporated into the fouling sub-model for improved accuracy.
b) The membrane surface in the current work is assumed to be static, while HF membrane fibers are flexible and moving under the influence of shear produced by the air scouring. HF membranes enjoy the added benefit of their loosely bound fibers, which preliminary studies have shown to help reduce the membrane fouling (Liu et al., 2016; Yeo et al., 2007). This effect could be considered while modeling the MBR systems with HF membranes. Furthermore, the applicability of the model with immersed flat sheet (FS) membranes should be explored in future works as flat sheet membranes are also being used at a large scale (>10,000 $m^3.d^{-1}$).

c) Particle size distribution and stickiness of particles are impacted by the addition of a coagulant (Nadeem et al., 2022). This effect should be taken into account when modeling MBR facilities using coagulant for CEPR.
d) The specific cake resistance equation proposed by Cho et al. (2005) is not universally applicable for all kinds of MBR systems (lab-full scale). Furthermore, at the times, when this equation was proposed, precise definitions for today's known variations of biopolymers such as EPSs, bound EPSs, loosely bound EPSs, extracted EPSs (eEPSs), free EPSs, bio-polymeric clusters (BPC i.e., group of SMP and EPS), and SMPs were not set up. Keeping in view the recent understanding of EPSs and SMPs, further experiments for expressing the specific cake resistance as a function of TMP, MLSS, SRT, F/M ratio, SMP, EPSs, coagulant dose, and rate of chemical cleaning is required.
e) The colloidal fraction of COD can be added into the filtration model (Wu et al., 2001). Considering this, it would be interesting to develop a biological model and then further link it with the impacts of the coagulant addition to explore the inorganic irreversible fouling associated with it.

The fouling sub-model in the stand-alone configuration is computationally robust and super-fast and, therefore, could be used as a tool to simulate the weekly in-situ chemical cleaning and bi-annual ex-situ-chemical cleaning for each of the membrane tanks. Furthermore, the fouling sub-model is a basic tool for analyzing the effects of changing the aeration sequencing and aeration intensity on fouling development.

Chapter 12: Energy Consumption at SAV MBR & Validation of Energy Sub-model

Energy consumption in wastewater treatment involves multiple forms of energy such as electrical, manual, fuel, and chemical, as classified by Singh et al. (2012). However, this chapter presents findings of the electrical energy audit of the SAV MBR facility and validation of the energy consumption sub-model with simulations based on data set from 11th Nov 2018 until 31st Jan 2019. Furthermore, it presents the energy consumptions distribution among various consumption items, including pumping, aeration, mixing, etc. In addition, it gives the energy consumed in terms of kWh.m^{-3} as well as kWh.kg^{-1} pollutants (COD, N, and P) removed or transformed, and further explores the relationships between the energy consumption, the pollutants removal performances, and the hydraulic loading of the system.

12.1 DATA COLLECTION

The electrical energy consumption in wastewater treatment facilities is influenced by multiple factors, including influent flow, pollutants loading in the influent (BOD or COD, TSS, N and P concentrations), the utility of the operating loading rate of the plant (Gurung et al., 2018; Longo et al., 2019), dilution of pollutant loads, especially during storm seasons when infiltration/inflow reaches to its maximum as investigated by Vaccari et al.(2018). A most common practice used to compare electrical energy demand is in terms of kWh.m^{-3} treated or kWh per person; however, this could be highly misleading as it assumed that pollutants concentrations in the influent do not differ significantly among the wastewater treatment facilities. It is more likely that large volumes of wastewater are received by the WWTPs due to unexpected factors such as storm water flow and melting of ice to the sewerage system that could possibly offer apparent energy discount due to higher denominator in the calculation of the kWh.m^{-3}. A more sensible metric to measure the financial sustainability of any wastewater treatment facility is suggested by comparing electrical energy consumption

in terms of units of the pollutants removed, for example, $kWh.kg^{-1}$ removed (Bodik and Kubaska, 2013; Longo et al., 2019) than unit energy consumption per cubic meter treated ($kWh.m^{-3}$).

12.2 ANALYSIS OF ENERGY DATA

Analysis of energy consumption is critical to exploring energy-saving regimes. In order to study the current energy consumption trends, 3 months of data of influent loading, process conditions and energy consumption were collected, processed, and treated to remove statistical outliers.

Daily energy consumption data from dynamic energy consumers were available for i) influent pumping (P5), ii) recirculation from anoxic to pre-anoxic (R1), iii) recirculation from aerobic to anoxic (R2), iii) biological process aeration (FBA), iv) membrane scouring (CBA) and permeate pumping (ePP). Energy consumed by the several fixed consumption item was estimated using the installed capacity information (*see* ***section 6.4***) from the operator, while energy consumed in recirculation of the influent from membrane aerated rector to the aerobic reactor and effluent pumping was estimated using the mathematical approach described in ***section 8.7***

As shown in **Fig. 12.1**, energy consumed in influent pumping (a), anoxic recirculation, (d) aerobic recirculation (e), and permeate pumping (f) is highly correlated with the influent flow rate with Pearson's correlation coefficient (r^2) of 0.88, 0.86, 0.84 and 0.81, respectively. Energy consumed in biological process aeration did not have any correlation ($r^2 \sim 0.001$) with the influent flow rate, as shown in **Fig. 12.1**(b). This is probably due to a controller system in place, which regulates the DO concentration around a fixed set-point by adjusting the airflow rates through a variable frequency drive (VFD) compressor and associated with the intermittency of the fine bubble aeration. Moreover, this could be associated with the aeration system, equipped with energy-efficient fine-bubble diffusers and highly efficient compressors. Set-point adjustment and actual oxygen consumption depend upon the influent COD, TN, and TP load, which varies from day to day and within 24 hours. It can be seen in **Fig. 12.1**c that the air consumption is likely to increase with the increase in COD/N and COD/P ratios. However, membrane air scouring was partially correlated with influent flow rate with R^2 value of 0.62.

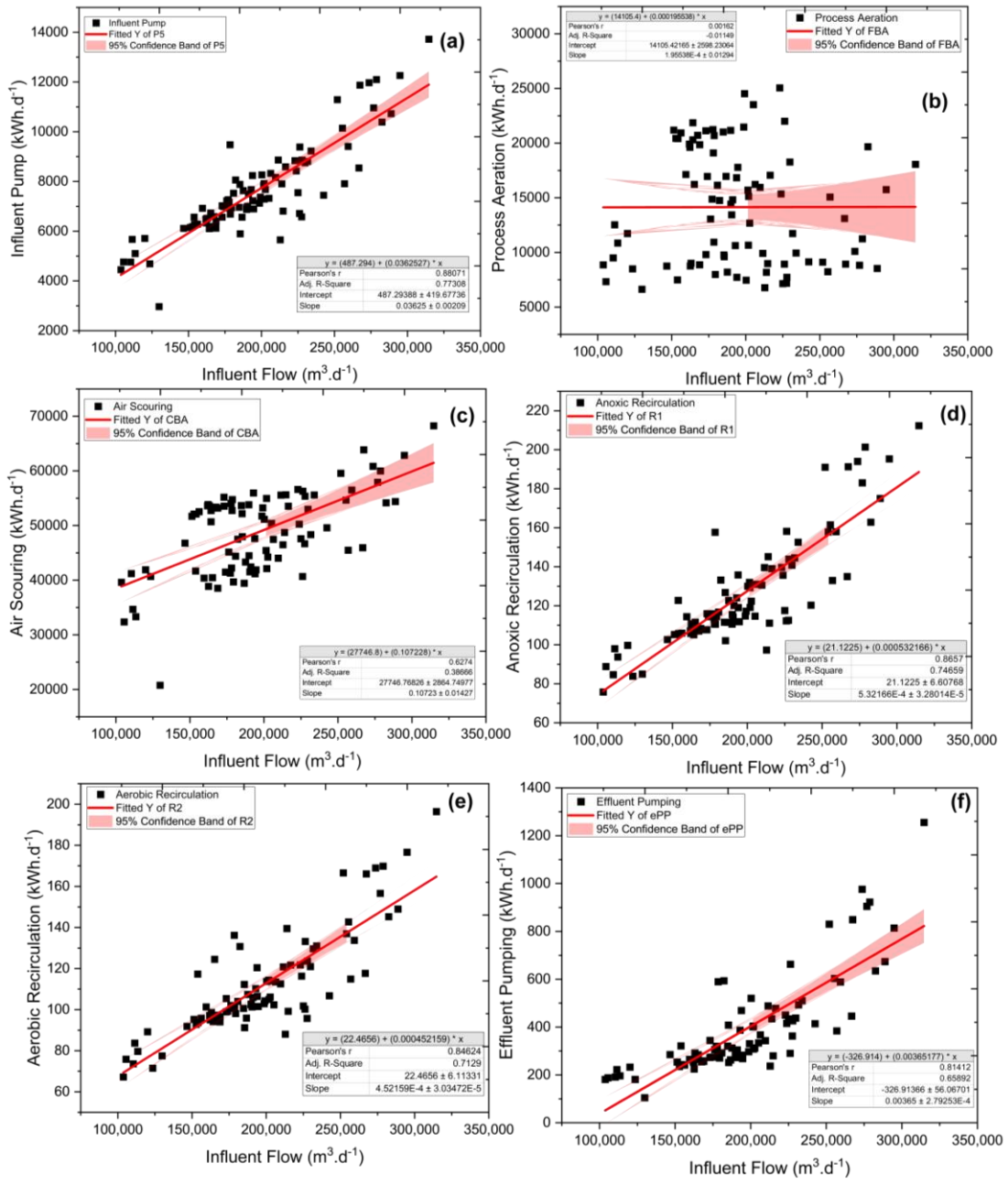

Fig. 12.1: Dynamic energy consumption and its relations with influent flow

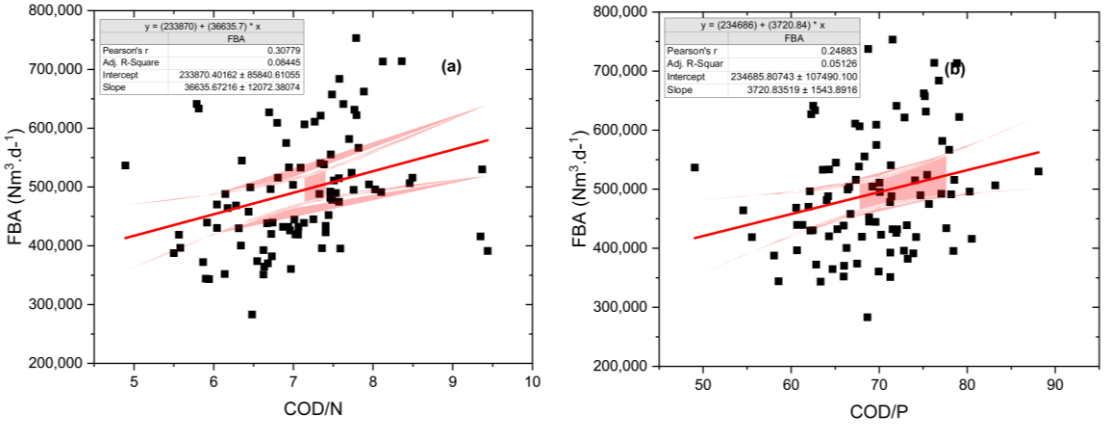

Fig. 12.2: Influent loading and aeration requirements

12.2.1 Specific energy consumption by flow

The specific energy consumption by volumetric flow rate without any optimization was calculated using **Eq. 12.1**. It varied between 0.35 and 0.74, and the average is evaluated to be 0.47 kWh.m^{-3}, which falls under the reported range of large-scale facilities.

$$SE_{(kWh.m^{-3})} = \frac{\text{Total energy consumption } (kWh.d^{-1})}{\text{Permeate Produced } (m^3.d^{-1})} \qquad 12.1$$

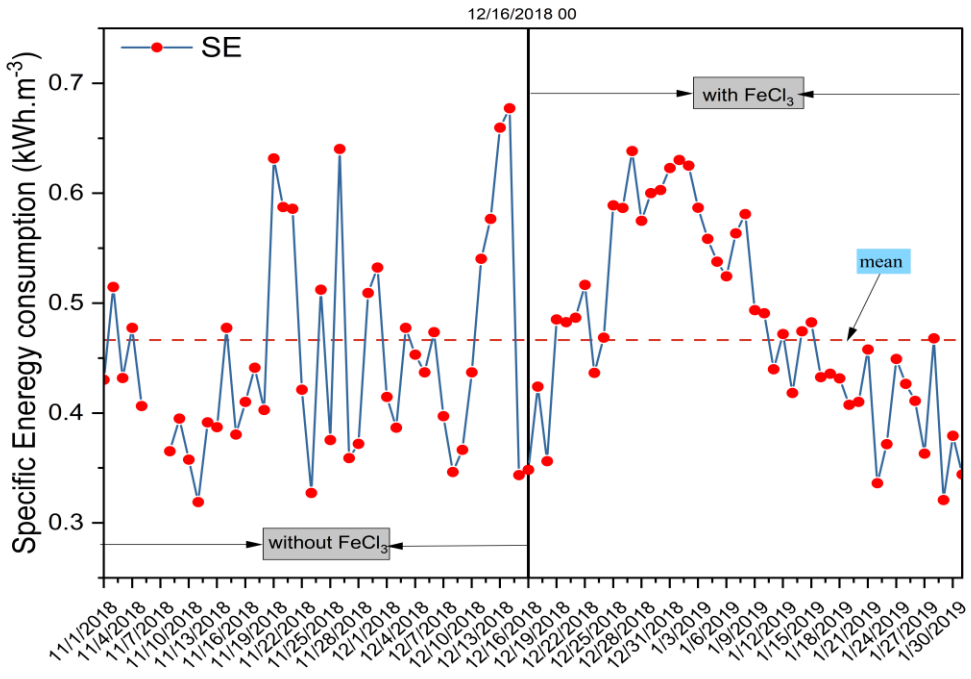

Fig. 12.3: Specific energy consumption by volumetric flow rate

According to the literature survey (**Table 12-1**), energy consumption in 25 full scale facilities (1000- 20,000 $m^3.d^{-1}$) located in different geographical locations ranged in between 0.46 - 2.2 $kWh.m^{-3}$ (Barillon et al., 2013; Gabarrón et al., 2014; Iglesias et al., 2017a; Krzeminski et al., 2012). According to the most recent study from China, MBRs with treatment capacities ≥50,000 $m^3.d^{-1}$ costed 0.3–0.5 $kWh.m^{-3}$ for municipal wastewater (Zhang et al., 2021).

Table 12-1: Review of the specific energy consumption in globally operated MBRs

Sr.No.	Flow rate (m^3d^{-1})	Country	Specific Energy	Reference
1	9,464	US	1.59	(Krzeminski et al., 2012)
2	2,990	US	0.66	(Krzeminski et al., 2012)
3	7,500	US	1.35	(Barillon et al., 2013)
4	4,420	France	1.12	(Barillon et al., 2013)
5	15,600	France	1.30	(Barillon et al., 2013)
6	1,560	France	0.86	(Barillon et al., 2013)
7	6,250	France	1.34	(Krzeminski et al., 2012)
8	2,000	Denmark	0.9	(Krzeminski et al., 2012)
9	2,700	Denmark	1.36	(Krzeminski et al., 2012)
10	1,820	Denmark	1	(Krzeminski et al., 2012)
11	12,000	Italy	0.85	(Krzeminski et al., 2012)
12	5,250	Italy	0.6	(Krzeminski et al., 2012)
13	16,000	Denmark	0.9	(Krzeminski et al., 2012)
14	8,544	Denmark	1.5	(Krzeminski et al., 2012)
15	5,520	Belgium	0.62	(Krzeminski et al., 2012)
16	6,000	Netherland	0.75	(Krzeminski et al., 2012)
17	4,150	UK	1.98	(Krzeminski et al., 2012)
18	2,000	Spain	0.898	(Iglesias et al., 2017)
19	1,400	Spain	0.86	(Iglesias et al., 2017)
20	3,750	Spain	1.95	(Iglesias et al., 2017)
21	1,880	Spain	0.79	(Iglesias et al., 2017)
22	1,575	Spain	0.9	(Iglesias et al., 2017)
23	2,116	Spain	0.46	(Iglesias et al., 2017)
24	20,000	Spain	0.534	(Iglesias et al., 2017)
25	1,320	Spain	1.1	(Iglesias et al., 2017)
26	1,100	Spain	0.714	(Iglesias et al., 2017)
27	5520	Belgium	0.64	(Fenu et al., 2010d)

Data presented in **Table 12-1** provided a poor correlation (0.02) between the design flow and $kWh.m^{-3,}$ suggesting using of other metrics, better suitable to describe the

electrical energy consumption dependency considering the characteristics of the influent to be treated.

12.2.2 Unit energy consumption

The unit energy consumption (UEC) calculated based on the inflow rate ignores the change in the concentration of the wastewater pollutants. It leads to the different unit energy efficiencies in an energy audit, and this is prominent from the fact that the standard deviation in $kWh.m^{-3}$ values for three months data is almost negligible (see **Table 12-2**). Therefore, UEC expressed as [$kWh.kg^{-1}$ pollutant removed] more accurately reflects the energy efficiency of WWTP and is consequently adopted here to benchmark energy consumption as a function of COD, TN, and TP removed. The UEC for pollutants is calculated as the ratio between daily energy consumption and daily pollutant removal rate, using **Eqs**. **12.2-12.3** below.

$$UEC_{kg^{-1}\,pollutant\ removed} = \frac{\text{Total Energy Consumption}\,(kWh.d^{-1})}{\text{Pollutant Removed}\,(kg.d^{-1})} \qquad 12.2$$

$$\text{Pollutant Removed}_{kg.d^{-1}} = (S_0 - S)_{g.L^{-1}} \times \text{Influent Flow Rate}_{(m^3.d^{-1})} \qquad 12.3$$

Where S_0 and S are the initial and final concentrations of the pollutants in $g.L^{-1}$.

Table 12-2: Summary of the UEC per kg COD and nutrients removal

	Specific energy consumption			
	$kWh.m^{-3}$	**$kWh.kg^{-1}$ COD removed**	**$kWh.kg^{-1}$ TN removed**	**$kWh.kg^{-1}$ TP removed**
Before $FeCl_3$	0.45	1.56	14.78	252.71
After $FeCl_3$	0.48	1.47	13.14	109.43

As can be seen in **Table 12-2** the standard deviation of UEC is higher than that of unit energy consumption by flow rate ($kWh.m^{-3}$), it is due to that the daily variation in wastewater quality. The average energy consumption in terms of $kWh.kg^{-1}$ COD removed for SAV-MBR was found to be 1.51, which is higher than CASP (Christoforidou et al., 2020; Gurung et al., 2018; Li et al., 2021) wherein varied in the range of 0.74-1 $kWh.kg^{-1}$ COD. High UEC in MBR is likely due to higher sludge viscosity associated with higher MLSS and active biomass, limiting aeration rates and

resulting in increased energy consumption (Nywening and Zhou, 2009; Verrecht et al., 2008). A most recent study by Li et al. (2021) explored the UEC at full scale MBR facilities in China and found values in the range of 1.043–2.698 kWh.kg^{-1} COD, which is higher than CASP. Results from the SAV-MBR lie in this reported range from full-scale facilities. Addition of $FeCl_3$ slightly reduced (6%) the UEC and daily fluctuations were marginally reduced, explained in **Fig. 12.4** below.

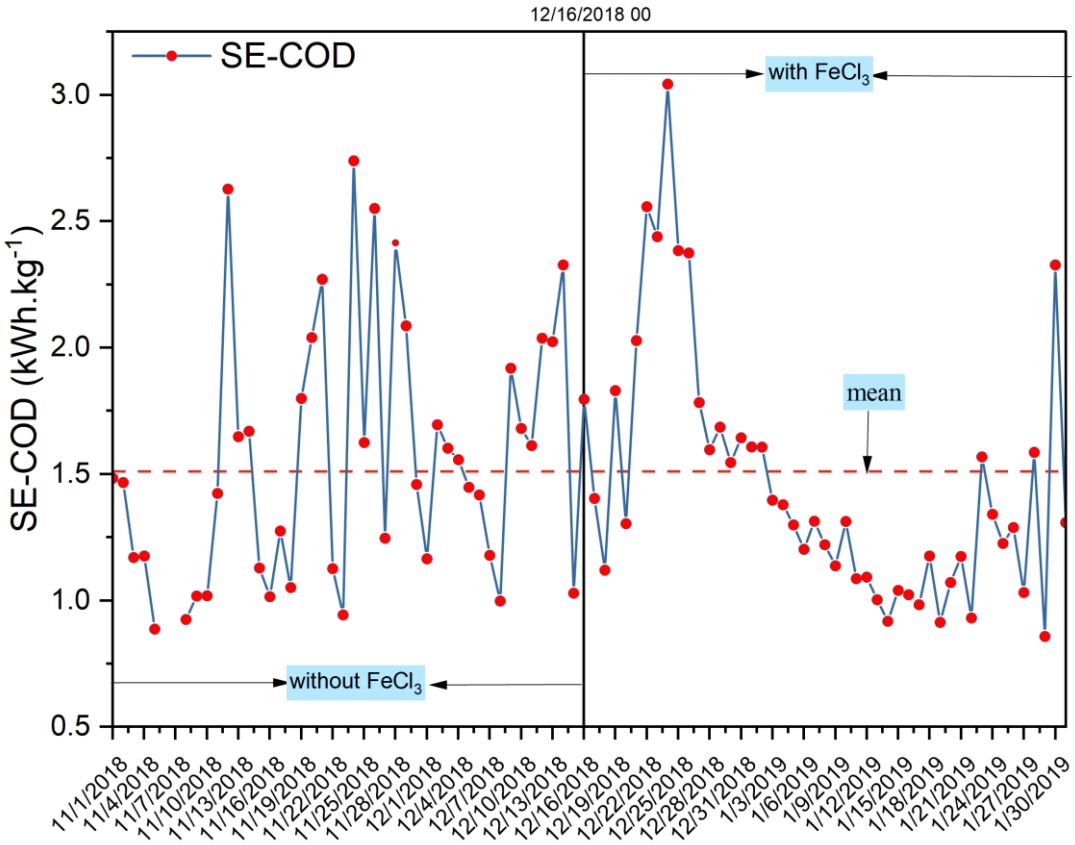

Fig. 12.4: Unit energy consumption per kg COD removed

Not enough data is reported in the literature to compare the energy consumption per kg of nutrient removal. Keeping in view the limitation of the data, it has been reported that the cost of TP removal in MBR is higher than CASP (Nadeem et al., 2022), mainly due to higher aeration in the biological process. The average removal cost of P-removal in MBR varies from 39.8 to 480 US$.Kg^{-1} depending on influent load, plant configuration, aeration intensity, and removal efficiencies. While, in CASP, it costs between 13.30- 101 US$.kg^{-1} (Arif et al., 2020; Bashar et al., 2018; Iglesias et al., 2017a; Jiang et al., 2005). Three months data analysis revealed that the UEC_{TN} varied in the range of 7.39-35.83, with an average of 13.92 kWh.kg^{-1}TN removed. It can be

seen in **Fig. 12.5**a, that UEC_{TN} marginally improved (11%) after the addition of coagulant (see **Table 12-2**). Similarly, the average UEC_{TP} was found to be 177.88 kWh.kg^{-1}TP removed with high variations in the range of 63-1233 kWh.kg^{-1}TP (see **Fig. 12.5**b).

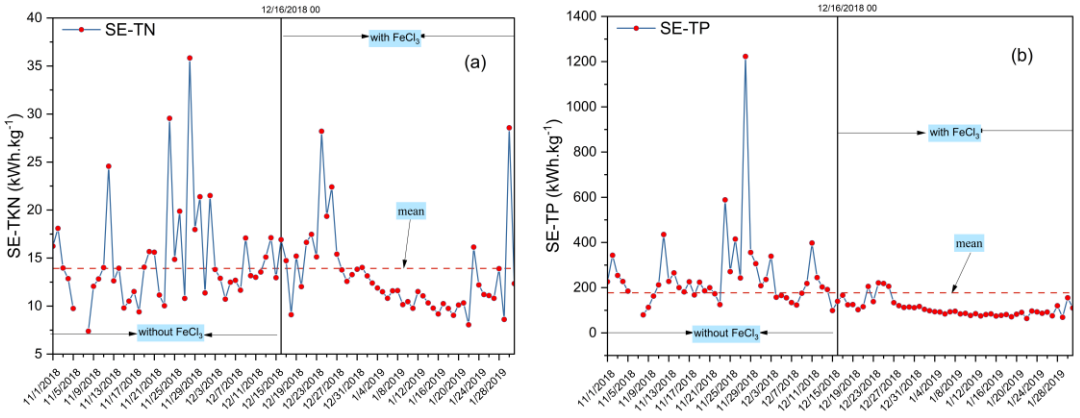

Fig. 12.5: Unit energy consumption per kg nutrient removal

12.2.3 Components of specific energy

Energy consumption distribution can be based on kWh.m^{-3} or kWh.Kg^{-1} pollutant removed. Since most of the literature data is available in terms of kWh.m^{-3} and therefore, it would be helpful to use kWh.m^{-3} as a basis to bifurcate the specific energy and for identification of the contributors.

As shown in **Fig. 12.6**, the membrane scouring is found to be the largest energy consumer at SAV-MBR, being 55.4%; the energy consumed by mixers, biological process aeration and influent pumping is 17%, 16.1% and 8.6%, respectively. The remaining 5.9% is consumed by other processes, including foam-breaking, recirculation, permeate extraction, sludge extraction, and coagulant addition.

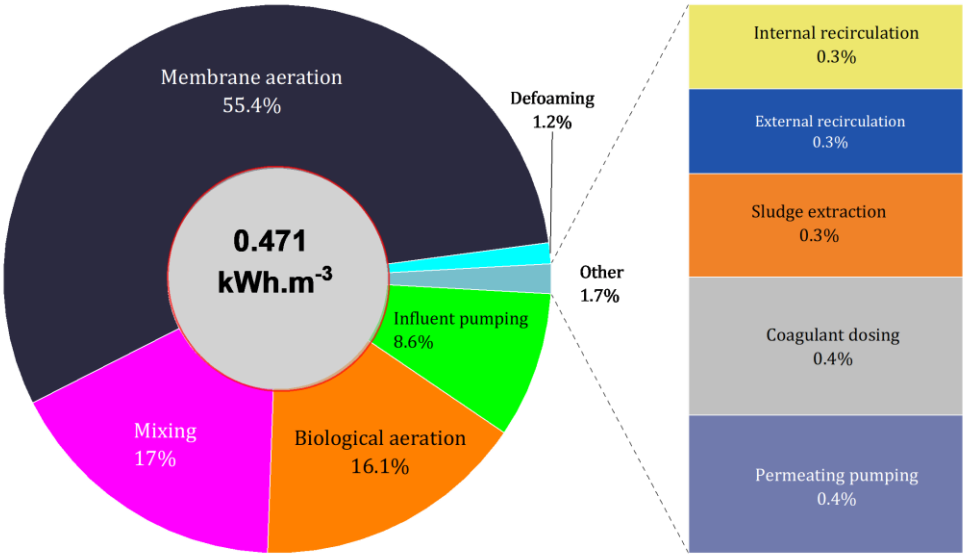

Fig. 12.6: Energy consumption distribution of Seine Aval MBR plant

12.3 OPERATIONAL LOADING RATE AND EFFLUENT QUALITY

Given the daily variation in flow rates, the design flow rate for WWTPs is based on the peak flow rate. Under normal situations, the hydraulic loading rate (HLR) is generally less than 100% of the design flow rate, which can be calculated using **Eq. 12.4**. However, on stormy/rainy days, the flow rate may exceed the design flow rate, and by-pass arrangements are required.

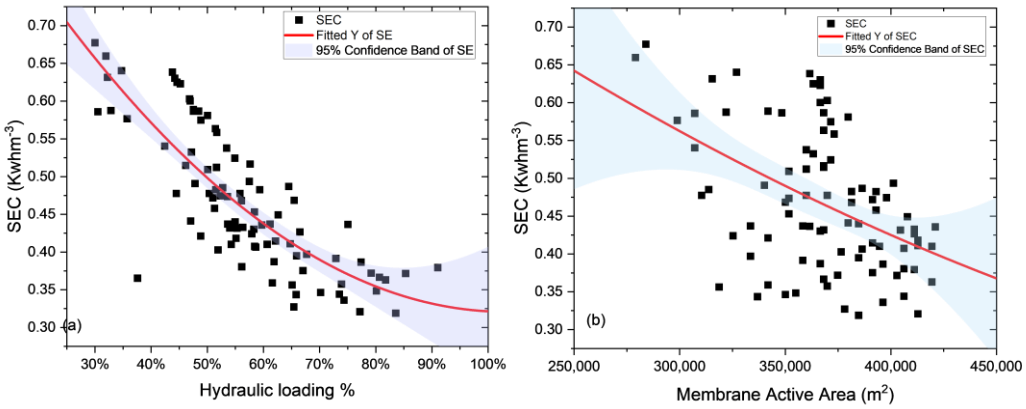

Fig. 12.7: SEC as a function of hydraulic loading rate and active membrane area

Considering the fact that the SAV-MBR has a PFD capacity of 14,500 $m^3.h^{-1}$, while 3-months data analysis revealed that on average around 55% of the hydraulic loading capacity is being utilized. This infers that, if the facility is operated close to design capacity, specific energy consumption will reduce to around 0.34 $kWh.m^{-3}$ (see

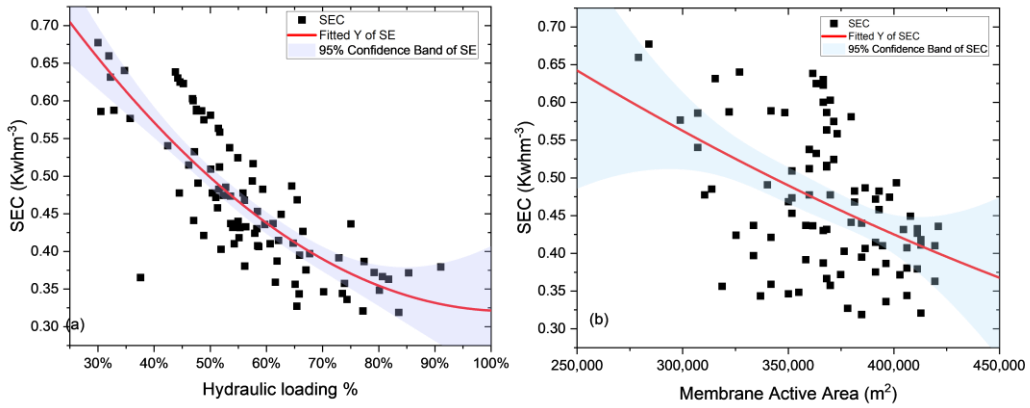

Fig. 12.7a).

This is due to the fact that the energy consumed by some devices such as agitators, foam breaking pumps, membrane aeration, and chemical cleaning of the membranes is not proportional to the volumes of the permeate production. Influent pumping (P5) and recirculation (R1-R2) were found to have a linear relation with energy consumption with R^2 values of 0.88 and 0.84, respectively.

$$\text{HLR} = \frac{\text{Actual influent flow rate } (m^3.d^{-1})}{\text{Design Capacity } (m^3.d^{-1})} \qquad 12.4$$

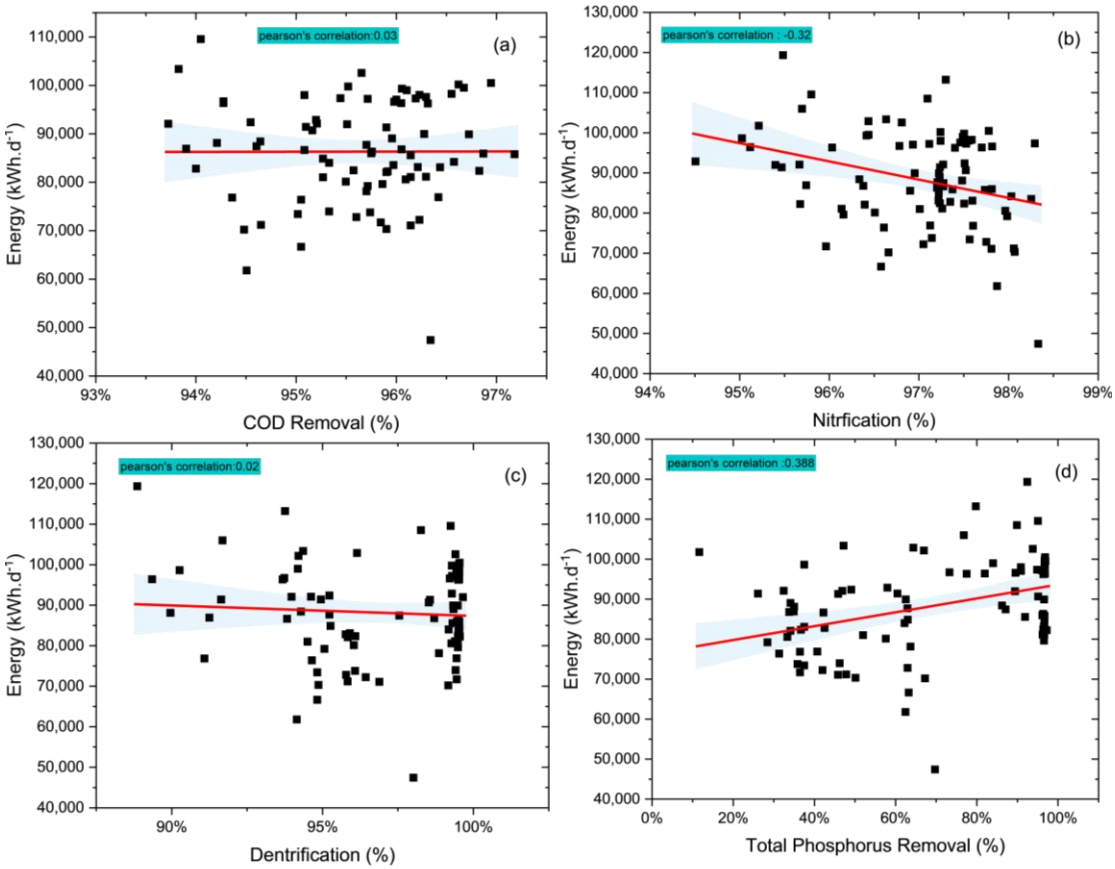

Fig. 12.8: Energy consumption as a function of effluent quality

Similarly, SEC values reduced with an increase in the active surface of the membrane (tanks in production in a given time), as shown in

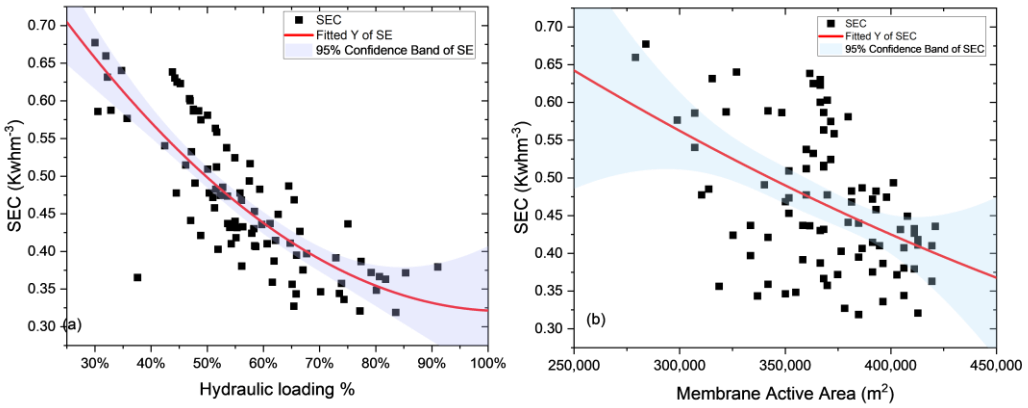

Fig. 12.7b.

Considering the availability of an energy and effluent data set from SAV- MBR, further analysis was performed to explore the window for future model-based energy optimization projects. **Fig. 12.8** shows that there is no significant correlation between

the specific energy consumption and efficiencies for COD removal (a), nitrification (a) denitrification (c), and total phosphorus removal (d).

This implies that an energy-saving program might be established for SAV-MBR without direct impact on effluent quality. Similar results are concluded by Verrecht et al.(2010) for a small scale MBR wherein they estimated 23% energy saving without compromising the effluent quality.

12.4 VALIDATION OF THE ENERGY-SUB MODEL

As stated earlier, the data from 11th Nov 2018 until 31st Jan 2019 were used to validate the energy sub-model. The energy consumed by the dynamic consumers, i.e., influent pumps, recirculation pumps (anoxic and aerobic), fine bubble aeration compressors, and coarse bubble aeration compressors, was estimated using the numerical approach discussed in ***section 8.7***. The simulated results compared with the measured energy consumption data are given in **Fig. 12.9.**

Energy consumed by the permeate suction pumps and membrane recirculation was also estimated by the numerical approach. However, due to the unavailability of the measured data from these two processes, simulated results were not validated. Whereas energies consumed by mixers, foam breaking pumps, and chemical dosing pumps were considered constant and were calculated from the installed capacity and operational working hours.

The overall energy consumed by all devices installed in the facility was simulated and compared with measured data from 11/10/2018 until 31/1/2019. **Fig. 12.10** depicts that the model amicably predicted the energy consumption with R^2 and RMSE values of 0.945 and 0.02, respectively.

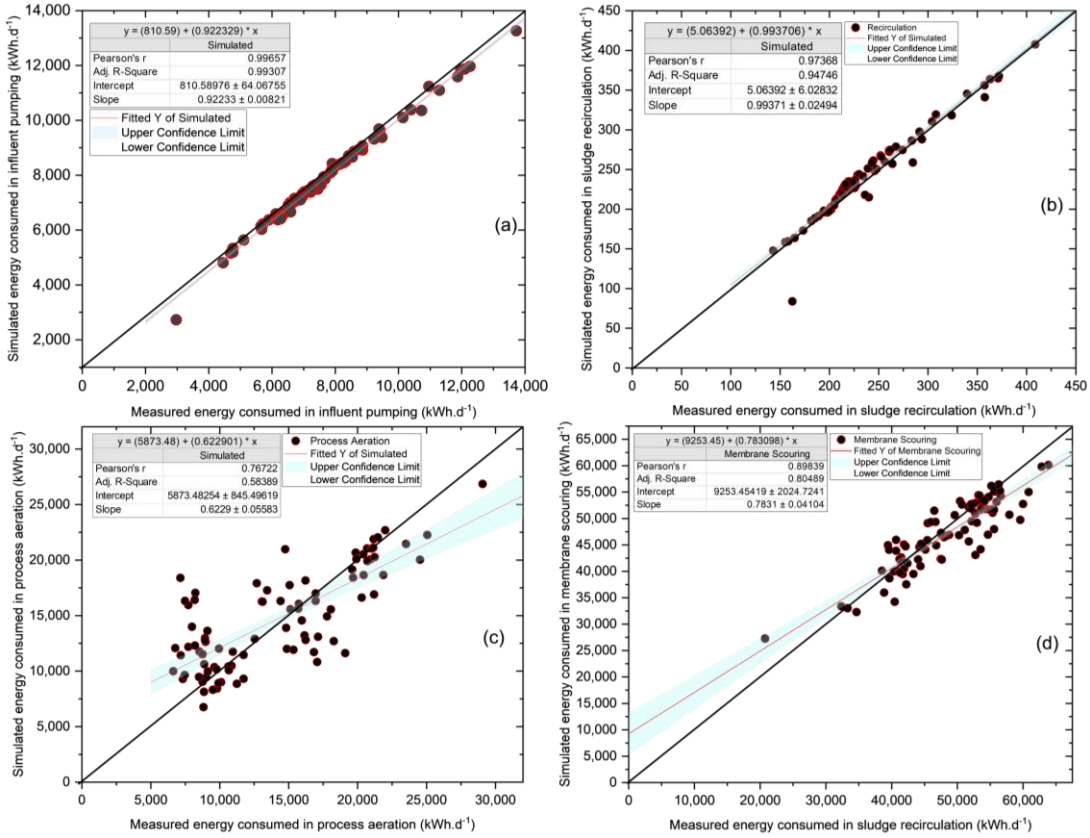

Fig. 12.9: Simulated energy consumption as a function of measured energy consumption in a) influent pumping, b) internal recirculation i.e., anoxic, and aerobic recirculation, c) biological process aeration, and d) membrane air-scouring.

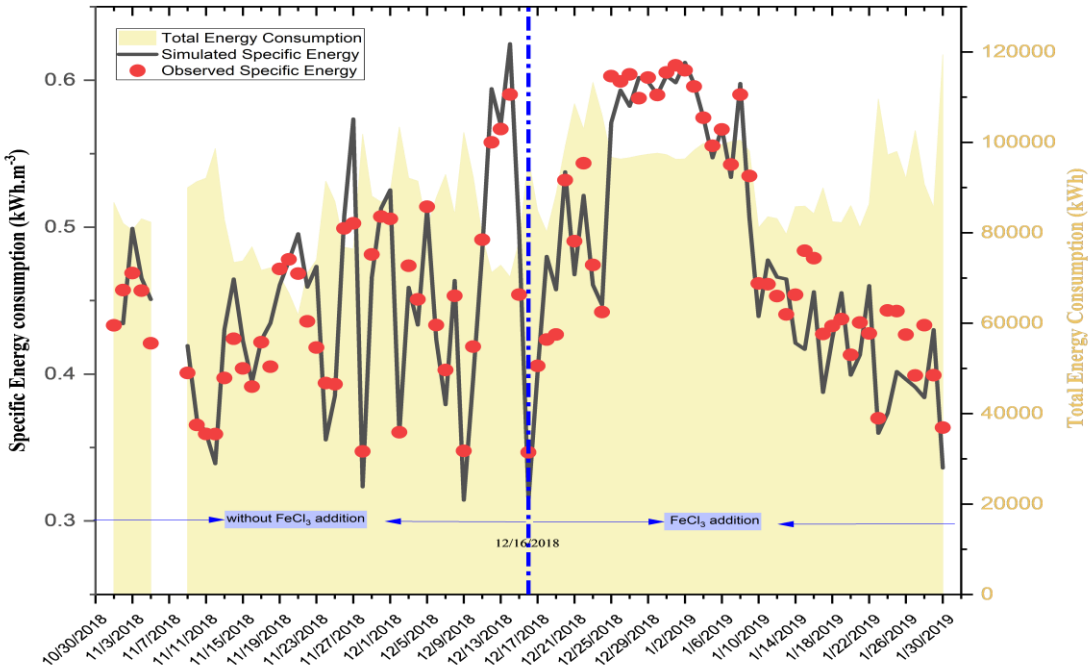

Fig. 12.10: Measured and simulated specific energy consumption

Specific energy consumption between 21/12/2018 and 1/6/2019 was significantly higher than rest of the period. A plausible reason for this peculiarity is the less influent rate and working and reduced number of tanks in operation (aeration is kept on during the non-operating periods).

12.5 SUMMARY AND PERSPECTIVES

The design flow rate of MBR, hydraulic loading rate (%), and influent pollutants (COD, TP, TN) concentrations have the most impact on the unit energy metric ($kWh^{-1}.m^3$ or $kWh.kg^{-1}$). Based on the analysis of the data and results presented in this chapter, the following conclusions can be derived:

- The specific energy consumption at SAV-MBR in terms of conventionally used metric was evaluated to be 0. 471 $kWh.m^{-3}$, which is reasonable, and falls on the lower side of the reported range of full-scale facilities data.

- Unit energy consumed for COD removal was evaluated to 1.56 $kWh.kg^{-1}$ which is higher than CASP but within the range for full-scale MBR facilities. Similarly, unit energy consumption for TN and TP removal was 13.92 $kWh.kg^{-1}$ and 177.88 $kWh.kg^{-1}$, respectively.

- On average, the Seine Aval MBR plant is operated with around 55% of the designed hydraulic load capacity, resulting in higher specific energy requirements. This is reduced to 0.34 $kWh.m^{-3}$ when the plant is operated close to its PFD design. Furthermore, specific energy consumption was found to be highly correlated with an active surface area of the membrane, i.e., number of tanks operating at a given moment.

- Membrane scouring is the single largest contributor to energy requirements with a share of 55.4%, and this presents an opportunity to significantly reduce the overall energy costs in full-scale MBRs. The other large energy consumers were mixing, biological process aeration, and influent pumping, with a share of 17%, 16.1%, and 8.6%, respectively, while the remaining 5.9% is consumed by other allied processes.

- No significant correlation between the specific energy consumed and efficiencies for COD removal, nitrification rate, denitrification rate, and total

phosphorus removal was found. This indicated the potential for energy saving without significantly impacting the quality of the effluent.

- The energy sub-model amicably simulated energy consumed in influent pumping, recirculation, process aeration, and membrane. The overall simulated specific energy consumption fitted excellently against observed data, with R^2 and RMSE values of 0.945 and 0.02, respectively.

Chapter 13: Exploratory Dynamic Sensitivity Analysis of the Model Inputs

Typically, conventional sensitivity analysis in wastewater modeling is used to rank the model parameters based on their sensitivity indices, and this knowledge is then used to reduce the calibration effort. In general, steady-state simulations explore the influence of changing the parametric values within a defined sampling method (one parameter at a time or all parameters at a time) within a specific range. Practically, the activated sludge process is a transient system and largely depends upon the influent composition, biological composition, and process conditions. In CASP, the parameter sensitivities may change with time due to evolving biology, changing inputs, or environment (e.g., temperature). Therefore, the calculation methods for the steady state cannot be an accurate reflection of reality. Dynamic sensitivity analysis could evaluate the influences on model responses due to variations of model parameters, initial conditions, and independent variables or time-dependent model inputs. The main difficulty in investigating the dynamics of systems under consideration is the infinite dimension due to the time-dependent inputs and high computational costs. The causes and effects of dynamic influent inputs, coupled with environmental conditions (e.g., temperature), have not been explored yet, particularly in the wastewater modeling field.

This work is dedicated to presenting an exploratory approach for analyzing the influence of dynamic variation of the inputs, environmental and process conditions using the deep learning-based black-box model. The approach is expected to be useful for interpretation and explanations of the fast-changing dynamics of the system and their influence on the model output. This chapter is presented mainly in two parts i.e., 1) deep-learning model development, training, and validation, and ii) using the trained model for dynamic sensitivity assessment of the model inputs on the output. The approach is being explored to reduce the computational time in sensitivity analysis as really high computation cost is experienced in conventional sensitivity analysis approaches. The model adaptation, structure and optimization are only briefly

discussed as the main objective is to explore the utility of the black-box models for dynamic sensitivity analysis.

13.1 SURROGATE MODEL AND UNCERTAINTY ANALYSIS

MBR is a complex biological system with a nonlinear behavior (Yaqub et al., 2020) due to multiple interactions between biology and membrane (Naessens et al., 2012) as well linked with significant variations in the influent flow and composition (Langeveld et al., 2012).

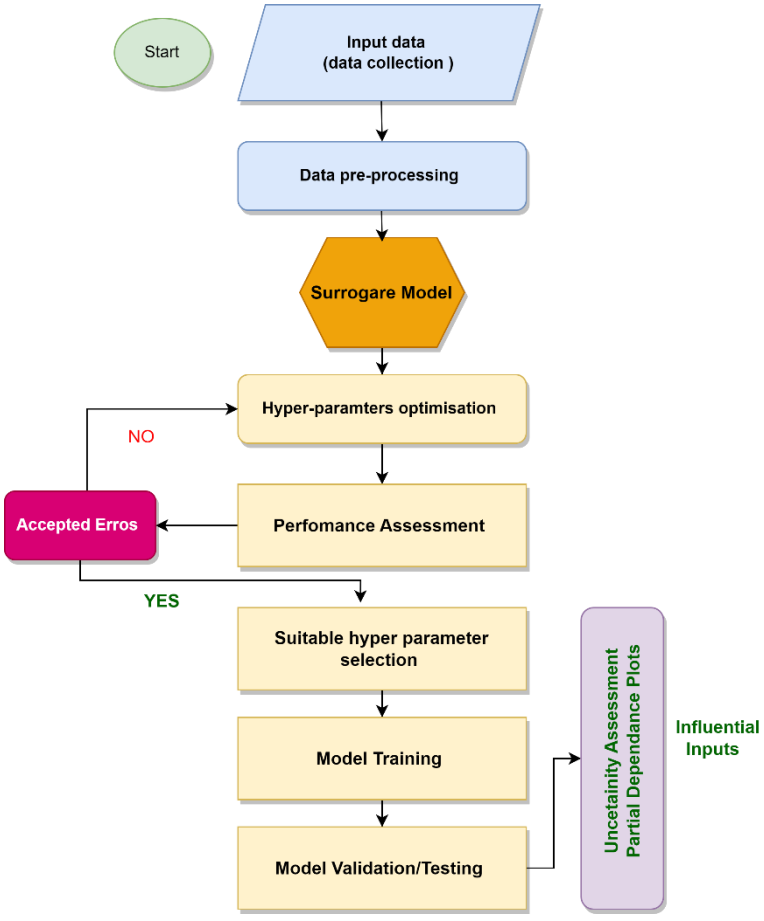

Fig. 13.1: Methodology for model development and uncertainty assessment

Conventional local and global sensitivity analysis (SA) approaches for phenomenological models take stoichiometric and kinetic parameters into account to explore their best-fitting values to reduce the calibration effort. Another SA can consider the influence of fluctuating influent variables, processes, and environmental conditions, keeping stoichiometric and kinetic parameters constant. To explore this "dual" sensitivity analysis (parameters and functioning conditions) which is an

emerging field to explore, a drastic reduction of the computational cost is necessary, which requires innovative approaches. Alternatives can be found in data-driven surrogates or black-box models. Several black-box models, discussed in ***section 4.1.1***, can be used in wastewater treatment modeling.

In this work, bi-directional long short-term memory (LSTM), the recurrent neural network, is used because its forward and backward hidden units are combined with linking the inherently connected context of the past and the future data signals. LSTM architecture accepts its data as a series of timestamps; each can be associated with many features/inputs. Moreover, the LSTM model is a recurrent neural network trained to resolve the gradient vanishing problem using the backpropagation algorithm (Wang et al., 2019). This work develops two LSTM models, i.e., 1) LSTM to predict effluent quality, and ii) LSTM to predict the TMP. A general methodology for the development of LSTM based models and their application for uncertainty assessment of the inputs is explained in **Fig. 13.1**.

13.2 LSTM FOR EFFLUENT QUALITY PREDICTION

13.2.1 Data pre-processing for the prediction of effluent composition

Data preparation before feeding a model is essential in machine learning techniques. A 15-minute interval of data from the sensors installed at various locations of the SAV-MBR plant (**see Fig. 7.1**) has been chosen and summarized in **Table 13-1**. This choice, different from the one of the knowledge-based models (daily lab data), has been made to produce a sufficient number of data sets for developing the methodology (despite the discrepancy of both data sets, as explained in ***section 7.2***). The errors or missing values were interpolated using forward filling interpolation. Any data leakage was avoided by forward filling from methods such as linear interpolation or even mean. The data was then clipped to remove outliers. These outliers were determined using the 5^{th} and 95^{th} percentiles of the data for each input. The preliminary data analysis aided the identification of trends, patterns, and anomalies of the dataset, which is an essential step in modeling. The randomization of the dataset affects LSTM models, particularly when nonlinear activation functions are used.

Therefore, the inputs and outputs datasets were normalized using the sci-kit-learn library's "MinMaxScaler" (Pedregosa et al., 2011) pre-processing class. This helped in speeding up the learning process and resulted in faster convergence. The predicted

values were converted to their original values before passing to the surrogate model for sensitivity analysis.

Table 13-1: Summary Statistics of the un-normalized dataset used for effluent quality LSTM

#		Units	Mean	Standard Deviation	Minimum	Maximum
Influent characteristics and operating parameters						
1	Q_{inf}	$m^3.h^{-1}$	7934	3387	1.2	15674
2	TSS	$g.m^{-3}$	99.5	28.6	5.3	173
3	COD_in	$g.m^{-3}$	217.9	134.0	1.2	500.3
4	NH_4-in	$g.m^{-3}$	36.7	12.4	0.2	77.9
5	P_in	$g.m^{-3}$	1.8	1.3	0.1	6.9
6	ORP	mV	-92.6	46.7	-302.7	28.3
7	Temp	°C	16.9	1.5	11.2	20.1
8	MLSS	$g.m^{-3}$	5054	632	50	6900
Output parameter						
1	COD_out	$g.m^{-3}$	11.2	3.3	1.3	21.2
2	P_out	$g.m^{-3}$	1.4	1.2	0.1	4.3
3	NH_4_out	$g.m^{-3}$	0.4	0.5	0.0	4.5

Note: n = 8774

Lastly, correlation among the input parameters using a Pearson's correlation coefficient (PCC) was estimated to measure the association between variables based on the covariance method. The PCC among the various inputs was checked and was found linearly independent within acceptable limits of < 0.80 (Dixon et al., 2016) for all parameters (see **Fig. 13.2**). The dataset was divided into three main streams; the first was used for model training (70%), and the second (20%) and the third (10%) were used for model validation and testing, respectively.

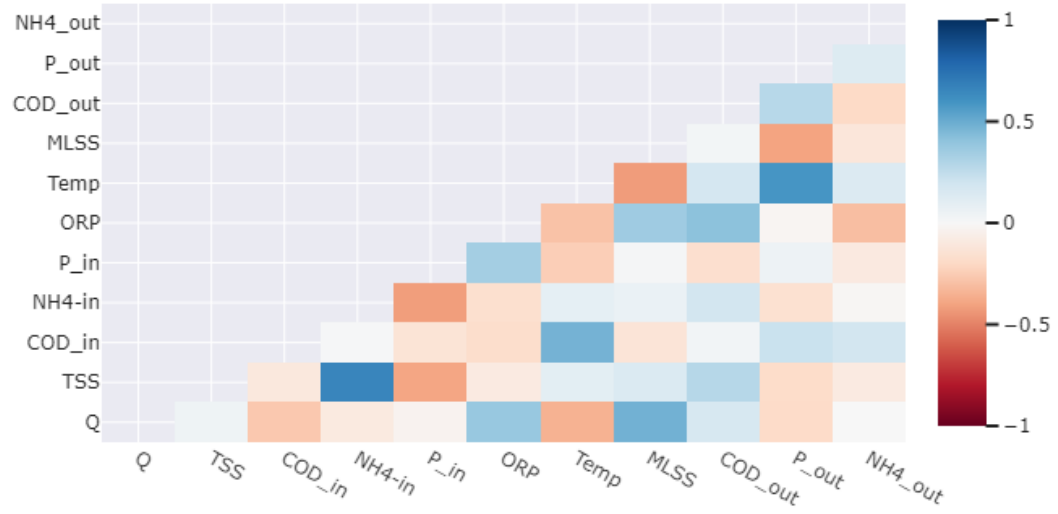

Fig. 13.2: Pearson's correlation coefficients of the input-response data sets for LSTM intended for effluent quality prediction.

13.2.2 Model structure for the prediction of effluent composition

The code used the sequential structure of the "TensorFlow Keras" (Abadi et al., 2016; Shukla and Fricklas, 2018; Tensor Flow, 2022) to create the model. The model comprised three LSTM layers, where the number of LSTM units decreases by half at each layer. The first two layers returned the whole sequences of values to pass into the subsequent layer. Each layer contained a recurrent dropout layer which applies dropout in a manner that is effective with the LSTM model. After the LSTM layers, the model had a dense and final activation layer. The dense layer matched the output dimensions of the model. The structural details of the LSTM intended for effluent quality prediction models are given in **Annexure-C** (Table C.1). The model was optimized using the "Adam" optimizer (Kingma and Ba, 2014). The learning rate (i.e., hyper-parameter in optimization algorithm is related to MSE used with values in the range of 0-1) had an exponential decay function. This choice ensured the effective, consistent convergence of the model. Additionally, when optimizing the model, the method of "gradient clipping" was applied. This clipping avoided exploding gradients and infinity values allowing a better convergence of the model. For activation, the model used a linear activation function. This function ensures that the outputs are distributed uniformly when scaled into a 0 to 1 range. With a different activation function such as sigmoid, the results may have favor values near 0 or 1, which would then scale and produces outputs with far less variance, sometimes constant.

13.2.3 Hyper parameters optimization and model training for the prediction of effluent composition

Bayesian hyper-parameter optimization (Nguyen, 2019) was used to ensure the effective convergence of the model. The implementation uses the "*scikit-optimization*" library (Louppe, 2017; Pedregosa et al., 2011; scikit, 2020). It builds a probability model of the objective function and uses it to select the most promising hyper-parameters to evaluate the actual objective function. In the Bayesian optimization process, distributions of the hyper-parameters are generated first with the specified ranges. It then creates a generalized version of the model function. This function accepts any configuration of parameters within the distributions and develops a model. In the second step, a sample from the hyper-parameter space is taken. With this sample, a model is trained, and the performance is measured. The samples are then combined

into a *surrogated/black-box* model based on Gaussian processes to optimize the hyper-parameter space. The hyper-parameters of the architected model were then optimized. These optimized values were then used for the training of model the model with 70% of the total loaded data. The previous step size was manually adjusted to 10, considering the best results. This study used the mean-square error (MSE) as a model performance evaluation indicator. The MSE values range from 0 to 1, and lower values indicate a good correlation between the experimental and model prediction.

13.2.4 Model validation and testing for the prediction of effluent composition

The calibrated model was then provided with unseen/new data for validation and testing. Using optimized parameters, the model produced optimal results without over or under-fitting. A good fit between the observed and predicted results can be achieved if the value of the MSE is close to zero.

The observed and predicted effluent COD, PO_4^{3-}, and NH_4^+ are plotted in **Fig. 13.3-Fig. 13.5,** respectively. The average MSE values were 0.045, 0.086, and 0.078 for COD, $PO4^{3-}$, and NH_4^+, respectively. The results are good and acceptable to proceed further for using the model for uncertainty assessment

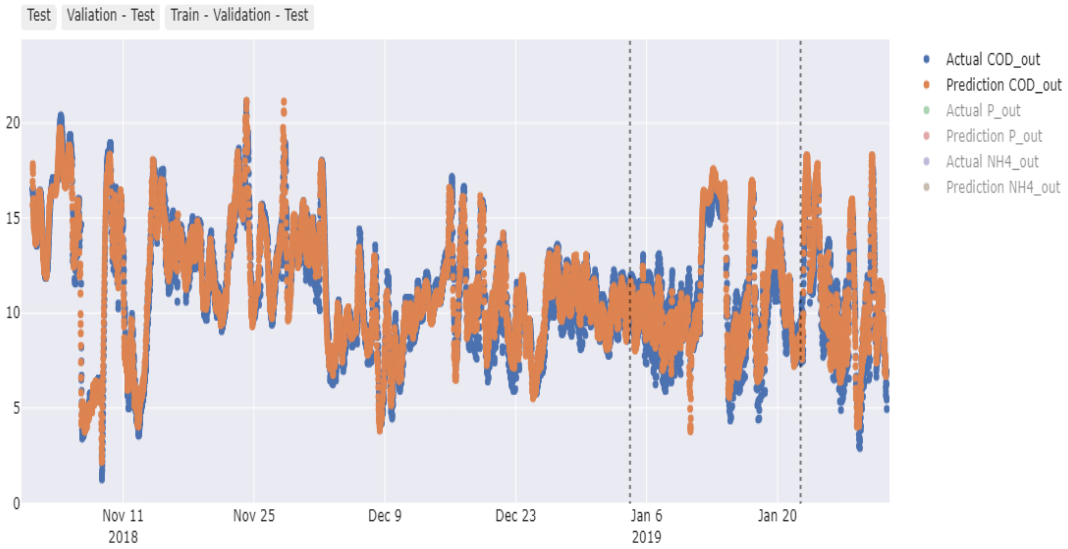

Fig. 13.3: Observed and predicted effluent COD ($g.m^{-3}$) for training phase (1st Nov 2918-5th Jan 2019), validation phase (6th Jan to 22nd Jan 2019), and testing phase (23rd Jan-30th Jan 2019).

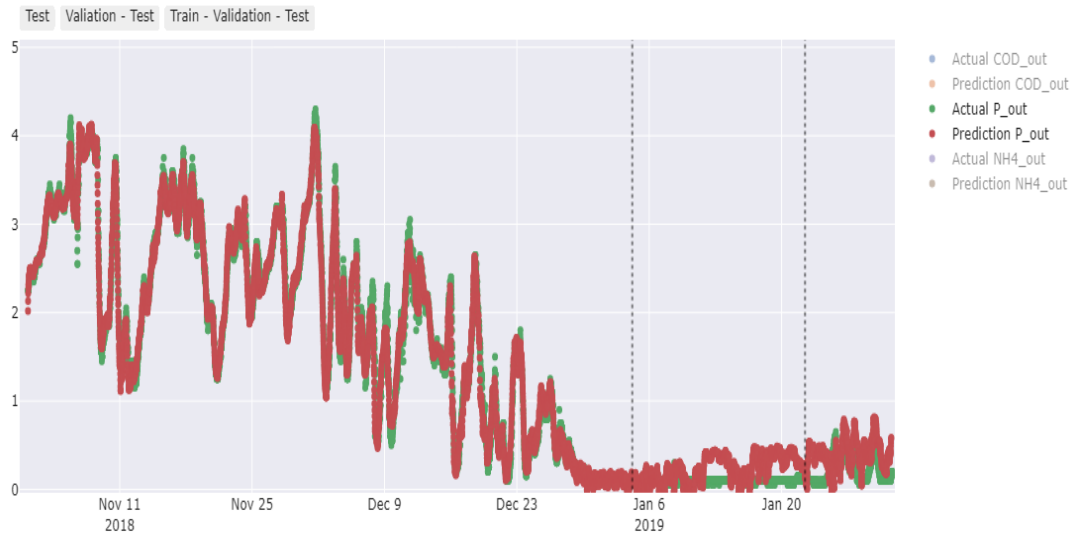

Fig. 13.4: Observed and predicted effluent PO_4^{3-} ($gP.m^{-3}$) for training phase (1st Nov 2918-5th Jan 2019) validation phase (6th Jan to 22nd Jan 2019) and testing phase (23rd Jan-30th Jan 2019).

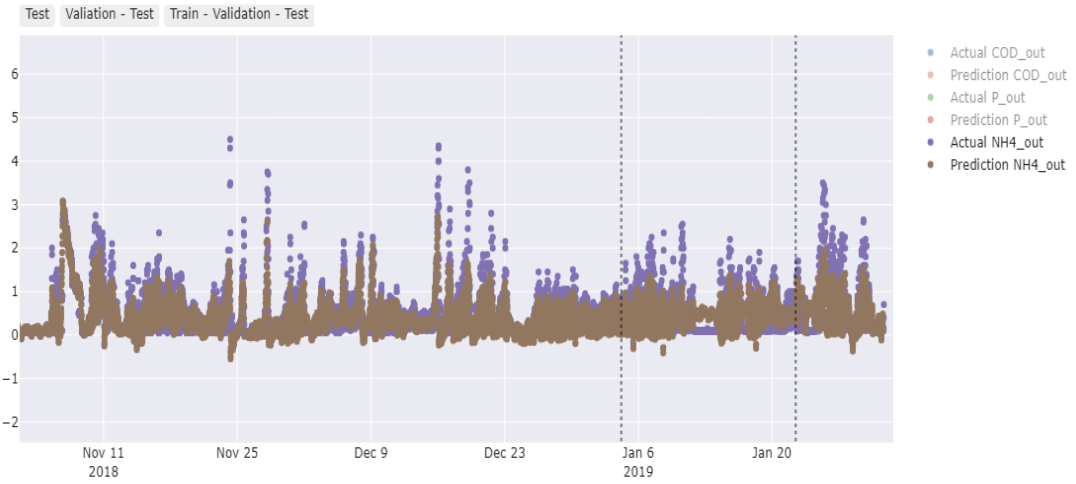

Fig. 13.5: Observed and predicted effluent NH_4^+ ($g.Nm^{-3}$) for training phase (1st Nov 2918-5th Jan 2019), validation phase (6th Jan to 22nd Jan 2019), and testing phase (23rd Jan-30th Jan 2019).

13.2.5 Data pre-processing & hyper parameters optimization for filtration

The data processing approach presented in ***section 13.2.1*** is used in the LSTM intended for TMP prediction. A statistical summary of un-normalized data used in this LSTM is given in **Table 13-2.**

Table 13-2: Summary statistics of the un-normalized dataset used for TMP prediction model

		Mean	Standard Deviation	Minimum	Maximum
Flux	LMH	22.2	1.99	16.9	25.5
MLSS	$g.m^{-3}$	5065.4	627.71	2300.0	6900.0
Temp.	^0C	16.6	1.38	11.2	19.3
SADm	LMH	53.6	7.07	37.1	66.3
TMP	mbar	52.6	18.60	30.8	132.6

Note: (n = 7939).

As shown in **Fig. 13.6**, no highly correlated parameters were found; thus, the data sets could be used for LSTM modeling. The model was trained with 70% of the data. Bayesian hyper-parameter optimization was carried out to select a set of most suitable parameters with minimum MSE (as an objective function) for 100 searches. In the default mode, the previous 10-step sliding window was used to predict the next value for TMP. The optimized values of the hyper-parameters(i.e., parameters used to control learning of the model e.g. learning rate), including batch size, minimum last step, gradient clipping, dropout rate, number of LSTM units, number of layers, and learning decay rate were used for the auto generated model. This automated optimization helped to converge the model in minimum time and significantly reduced calibration effort (compared to manual adjustment of the hyper-parameters).

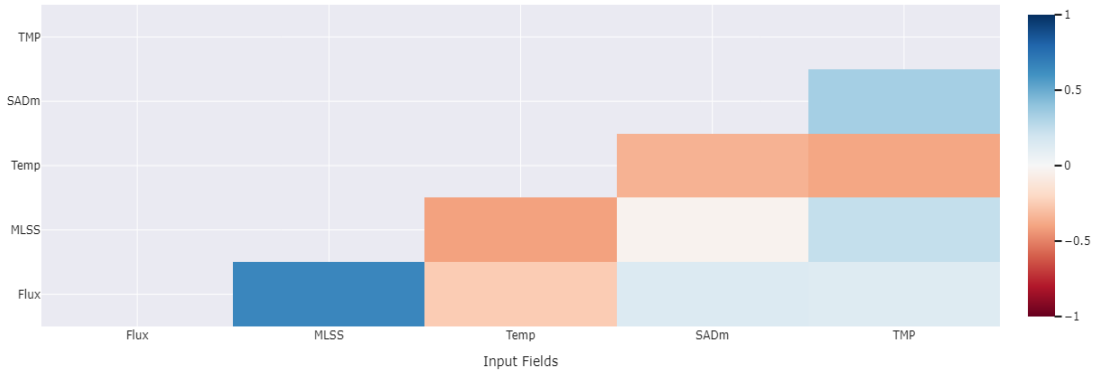

Fig. 13.6: Pearson's correlation coefficients of the input-response data sets for LSTM intended for TMP prediction.

Similar to the LSTM model used for effluent prediction, there are two bi-directional LSTM layers and one dense layer with one output. Further model structure is given at **Annexure -C** (Table C.2).

13.2.6 Model validation & testing for filtration

The trained and optimized model was then provided with another dataset (the next 20% for validation and the last 10 % for testing) to predict the TMP. The MSE was 0.0046, and R^2 value was 0.9074. The results are fairly well, suggesting the useability of the model for uncertainty assessment.

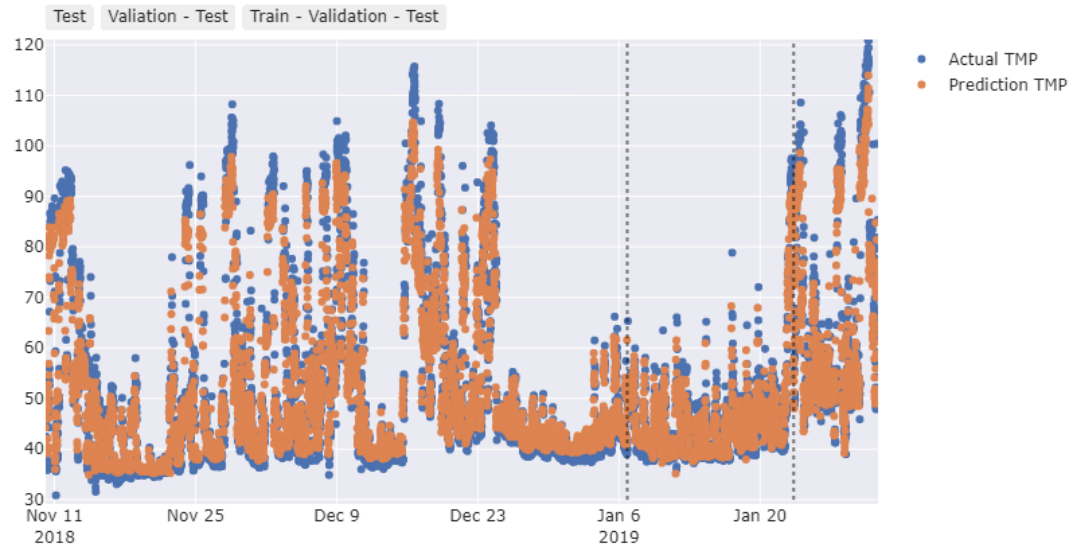

Fig. 13.7: Observed and predicted TMP for training period (10th Nov 2018- 5th Jan 2019), Validation period (6th Jan - 22nd Jan 2019), and testing period (23rd Jan- 30th jan 2019).

As shown in **Fig. 13.7**, the model is accurate enough to track the TMP profile. Therefore, the application of LSTM-based neural networks can be used for SA.

13.3 SENSITIVITY ANALYSIS

Once the accuracy of the black-box models was confirmed (with R^2 >0.80), the influence of the parameter was estimated individually on each of the response variables of the two LSTM models presented in the above sections. Several local and global approaches are available to assess the sensitivity contribution and interpretability: Global approaches including Partial Dependence Plots (PDP) and Individual Conditional Expectation (ICE), while local approaches, LIME (local interpretable model-agnostic explanations) and SHAP (SHapley Additive exPlanations), provide justifications for a single instance and have local fidelity (Friedman, 2001). A partial dependence analysis was chosen to describe the contribution of the individual parameters in the overall model response. The PDP adjusts one input parameter

(maximum two due to dimensionality constraints) for predicting the output, while the other inputs are kept to their original values; the ICE is the curve of the mean values of the PDP (Friedman, 2001; Jalali et al., 2020). This plot discovers the linear, monotonic, or nonlinear relationship between the predicted response and the selected input variables.

A sample of partial dependence plot of TMP with MLSS as a response variable is shown in **Fig. 13.8**.. From the ICE plot can be seen that the TMP proportionally increases with an increase in the MLSS concentrations. However, the behavior of the PDP is heterogenous with the MLSS concentrations lower than 5 $g.L^{-1}$. This shows that, apart from the MLSS, there are other unknown actors that influence the TMP evolution.

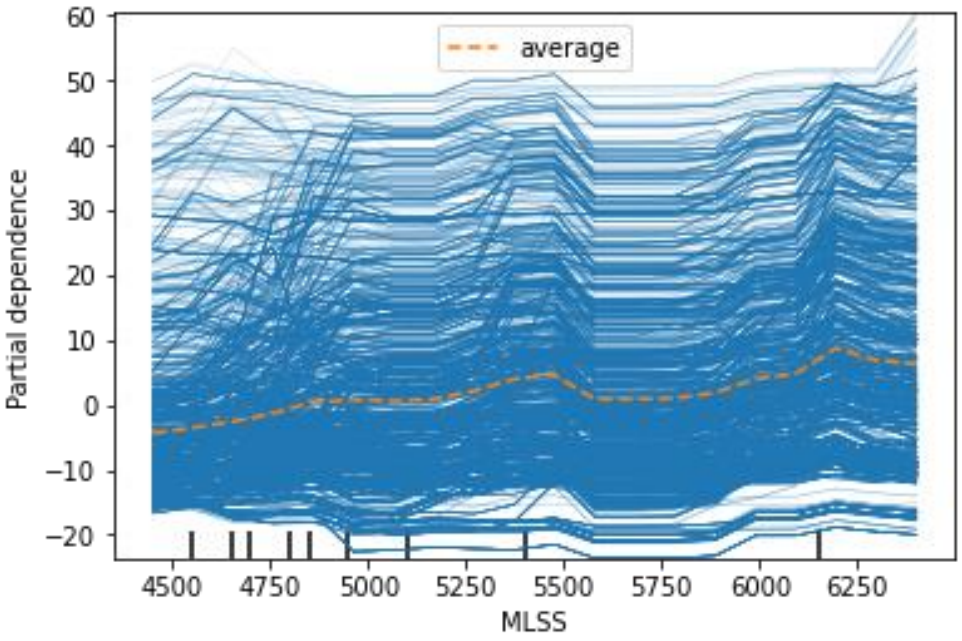

Fig. 13.8: An example of PDP (in blue) and ICE plot (dotted orange line) for TMP (Pa) function of MLSS ($g.m^{-3}$) (sample size: 5000)

SA of the effluent composition model in the **Fig. 13.9**, ICE curves for the predicted effluent PO_4^{3-} concentration on essential variable are presented.

Similarly, with increasing MLSS concentration, PO_4^{3-} concentration in the effluent decreases due to the uptake by the EBPR (consumption by biomass) or chemical precipitation (Nadeem et al., 2022). Other parameters, including TSS, COD, ORP, influent phosphorus (P_in), and NH_4, are likely not to influence the phosphorus removal prediction performance of the model.

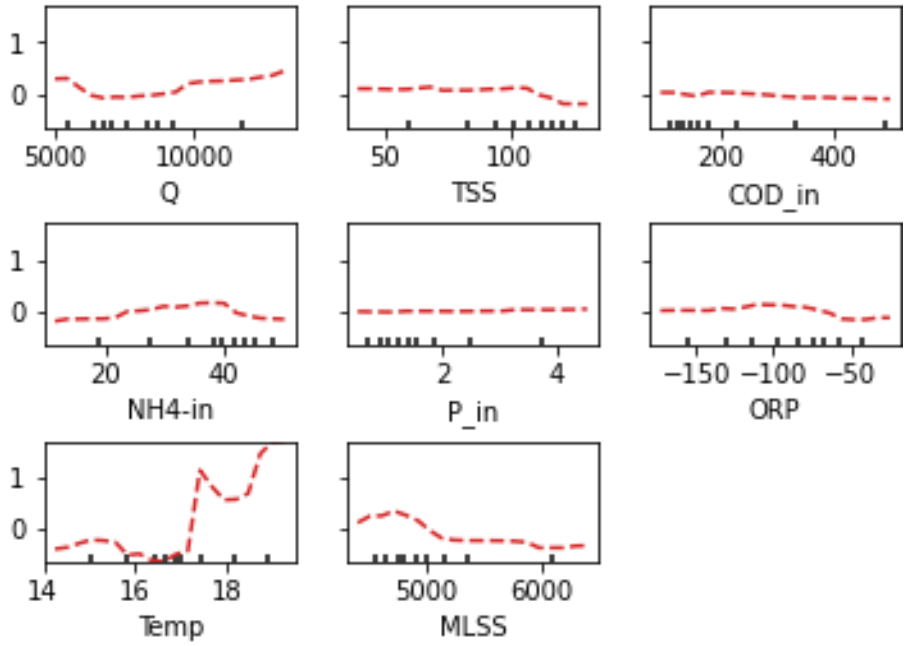

Fig. 13.9: ICE plots of effluent PO_4^{3-} concentration on essential variables (the pikes on the x-axis represented the fractile of target feature values and reflected the data density).

The results showed that phosphorus removal efficiency decreases by the increase in the temperature. Highest P-removal performance is achieved under 18 C^0 for SAV-MBR, representing the activation of the PAOs and maximum uptake rate at higher temperature. Similar results are reported by multiple researchers (Baetens et al., 1999; Liau et al., 2015; Sayi-Ucar et al., 2015), where higher P- removal at a temperature ranging between 10-17.5C and found inconsistencies at high temperatures around $40C^0$.

Fig. 13.10 presents the ICE plots of effluent NH_4^+ concentration on the influent and operational parameters. Particulate components, including influent TSS, MLSS, and COD concentrations, do not influence nitrification. While the increase in influent NH_4^+ load (linked to flow rates) and the decrease of ORP lead to reduced partial nitrification (i.e., higher NH_4^+ concentration). The influence of P_in, and Temp are less obvious.

Fig. 13.11 shows the ICE plots of the effluent COD concentration on inputs and process parameters. Since COD effluent mainly contains the soluble degradable fraction while the rest is retained by the membrane and therefore are shallow variations. This makes it difficult to conclude from the model results precisely.

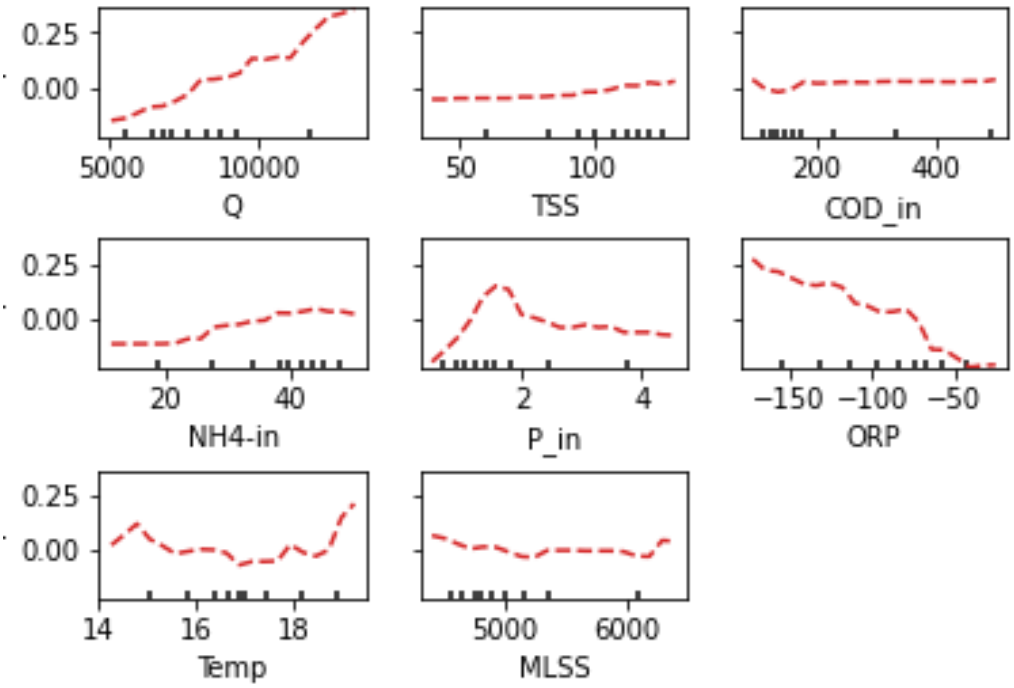

Fig. 13.10: ICE plots of effluent NH_4^+ on essential variables (the pikes on the x-axis represented the fractile of target feature values and reflected the data density).

It can be noticed that effluent COD is lower with increased MLSS concentration which is consistent with literature i.e. more biomass and better COD removal.

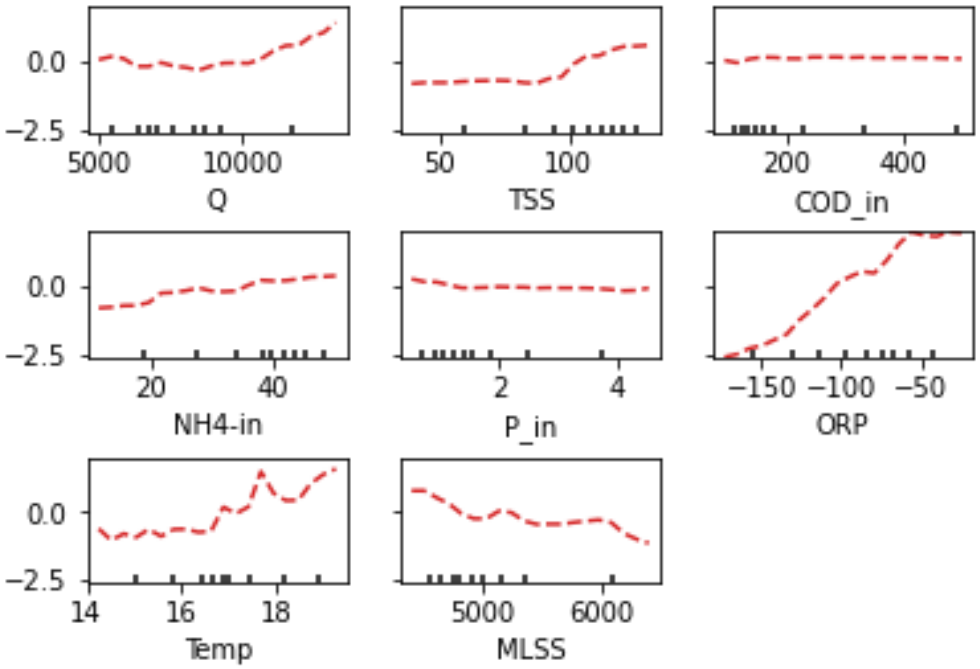

Fig. 13.11: ICE plots of effluent COD concentration on essential variables (the pikes on the x-axis represented the fractile of target feature values and reflected the data density).

13.3.1 SA of Filtration LSTM model

The LSTM used for TMP prediction is based on four inputs: flux, MLSS, temperature, and specific aeration demand (SADm). **Fig. 13.12** presents the model's response, with variations in each information. The influence of the flux variations on TMP is negligible and remains constant between the operating flux range of 16.9 and 25.5 LMH. According to established knowledge, after a minimum value, increasing the MLSS concentration increases the TMP (see ***section 2.3.1***). Similarly, an increase in the temperature results in a reduction of the TMP.

The literature has reported that the sludge settleability and filterability are reduced, and EPS production is increased at low temperatures (see ***section 2.3.2***). The response of SADm is non-linear as an increase in the SADm until 52 LHM increased the TMP, and after that, the further increase resulted in lowering the TMP. This is in accordance with the findings of Zhang et al. (2013b), wherein higher aeration intensity improved the membrane fouling in a specific scope. It is reported that with increasing aeration intensity, the quantity of EPS in suspension increased, and thus the irreversible fouling resistance. This approach of analyzing uncertainty can give numerous results that give qualitative information that still needs to be analyzed.

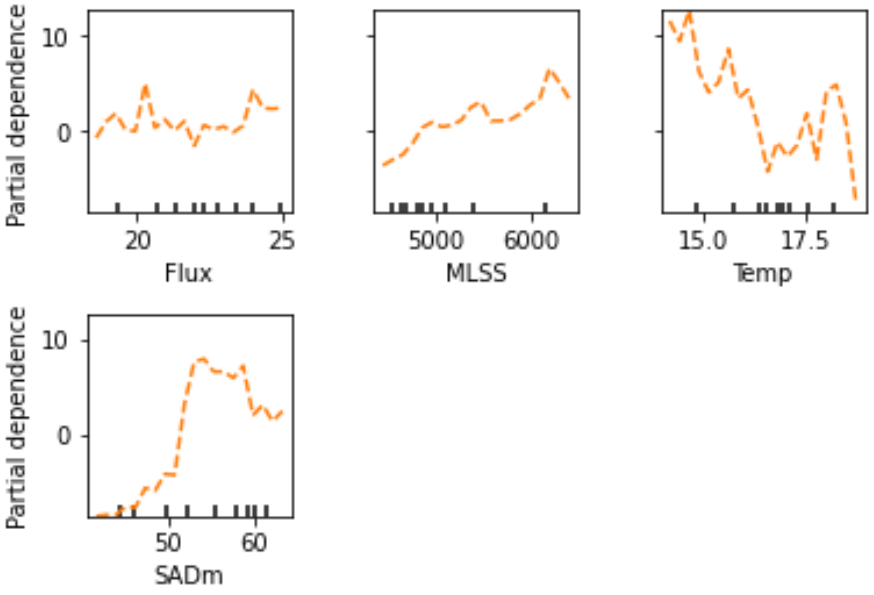

Fig. 13.12: ICE plots of TMP on essential variables (the pikes on the x-axis represent the fractile of target feature values and reflect the data density).

13.4 SUMMARY AND PERSPECTIVES

The proposed LSTM model successfully captured the nonlinear behavior of the SAV-MBR system in wastewater treatment with much less convergence time than the knowledge-based model. As a result, the use of LSTM-based neural networks in wastewater treatment plants may help in developing a sensitivity analysis methodology, since the machine learning model offers an opportunity to overcome the computational cost challenges posed by conventional uncertainty and sensitivity analysis methods. The preliminary results obtained for SA confirmed what is already known about the dependency of the response variables on the input data (for example huge effect of low temperature on TMP) and gave a mathematical tool to quantify these dependencies. Since it is a vast domain to explore, the answer about the robustness of the knowledge-based filtration model is yet pending as there is not sufficient data to confirm the fouling, but it opened new insights for further exploration of the field. Such results of SA may help to complete the knowledge about the implied phenomena, thanks to quantification. These results showed that this approach is a promising tool to manage the dynamic sensitivity analysis.

PART-V: CONCLUSION & PERSPECTIVES

Chapter 14: **Conclusions and Perspectives**

This chapter presents the general conclusions drawn from this thesis and perspectives and suggestions to conduct future research.

14.1 CONCLUSIONS

MBRs offers high and consistent effluent quality, but on the other hand, their energy consumption is relatively higher than CASP's, and its operational management is more complex too. These two major drawbacks are related to the fouling (including clogging) of the membranes. Available fouling abatement measures in commercial-scale systems, especially, air-scouring, consume high energy, as extensively discussed in the literature review (see ***Chapter 3:***). Mathematical models provide an opportunity to simulate and investigate the membrane fouling associated with the interactions between biological and filtration. A successfully calibrated and validated model, especially at a large-scale, can be helpful to explore the optimum operating conditions for fouling reduction and, consequently, save the air-scouring energy by using the calibrated and validated with good prediction accuracy. The literature review (***Chapter 4:)*** revealed that several integrated mathematical models have been developed in the last two decades. All these were validated at lab-pilot scale facilities, and no study has been carried out at a super-large scale, even though the number of super-large-scale facilities is growing.

In this work, a comprehensive, integrated MBR model is developed, presented, elaborated and validated with the operational data from the globally 4th largest submerged MBR plant with a peak flow design capacity of 348,000 $m^3.d^{-1}$ and equipped with hollow fiber membranes. The bio-chemical part of the model considered the stoichio-kinetic activity of the biomass for carbon, nitrogen, and phosphorus removal by using the ASM3-EPS-SMP-BioP model with dynamic aeration and chemical precipitation modules. A resistance in series (RIS) fouling model was used to simulate the TMP and total resistance. The model considers the membrane intrinsic resistance, with the development of pore fouling resistance, dynamic and static cake layer resistances under the influence of filtration-relaxation cycles, periodic backwashing, and synchronized aeration sequencing. The model allowed the

simultaneous modeling of biological activities such as biomass growth, nitrification, denitrification, phosphorus uptake, and chemical precipitation under the influence of coagulant addition, as well as membrane fouling phenomena, including cake attachment and detachment under the shear induced by the coarse bubble aeration and TMP evolution over time. The major conclusions are as follows:

14.1.1 Biological sub-model

The biokinetic part of the integrated model was calibrated and validated using chosen data sets, despite the scale and the complexity of the system. Thanks to initial fractionation of the influent, the model can sufficiently simulate the general behavior of the MBR for pollutants removal. The main conclusions related to the biological sub-model are following:

- Influent COD fractionation and estimation of yield coefficients of X_{OHO} and $X_{ANO,}$ greatly helped in calibration. In addition to measured $Y_{SB\_stor\_Ox}$, $Y_{stor\_OHO\_Ox}$ and Y_{ANO}, 9 additional kinetic parameters were manually adjusted within a range found in the literature, to improve the model fit up to an acceptable level (R^2>0.7).
- The biological sub-model was able to predict the effluent COD, NH_4^+, NO_x (nitrates & nitrites), PO_4^{3-} and MLSS concentrations within acceptable RMSE
- The biological process model beneficially serves to provide reasonable estimation for SMPs and EPSs concentrations in the supernatant of the MBR, avoiding time consumption and expensive measurements.
- The validated biological model could be used as a basis for activated sludge process optimization with model-based controls for aeration, recirculation (or MLSS control), and coagulation addition.
- In order to gauge the uncertainty of the bio-kinetic-model parametric values, global sensitivity analysis (GSA), was further carried out to rank the biokinetic model parameters in their order of priority to achieve maximum model performance. The GSA was done for each of the model output, i.e., i) COD, ii) NO_X, iii) NH_4^+, iv) PO_4^{3-}, v) MLSS, iv) EPS and v) SMPs. The results of GSA are given **Fig. 10.9**

14.1.2 Filtration-fouling sub-model

Filtration-fouling sub-model can simulate the fouling phenomena at the super large-scale facility, where no abnormal/severe fouling was detected, with a reasonable level of accuracy, low computational cost, and minimum efforts for calibration. Major conclusions related to fouling sub-model are as following:

- Implementation of the RIS model considering the complexity of the system and multiple fouling abatement measures in place at the SAV-MBR (i.e., sequenced filtration -relaxation, backwashing, coupled with an intermittent air-scouring) gave a complete and realistic picture of the process behavior. This is largely helpful in visualizing the effect of these fouling control means on cake attachment and detachment from the cake layer.
- TMP prediction by the model for entire plant is accurate: without the addition of the coagulant, the prediction was pretty much stable with MAPE of 4.1%. Similarly, MAPE for total resistance was 5.01% before the addition of the coagulant. After coagulant addition, MAPE for total resistance increased to 13.3%, probably due to a more compact floc structure and an increase in stickiness among sludge particles.
- Variance based global sensitivity analysis revealed that six parameters (i.e “gamma”, “pR”, “aR”, “bR “, “alfa” and “beta_sc”) out of 16 were found scientifically sensitive parameters.

14.1.3 Energy sub-model

- The simulated specific energy consumption excellently reproduced the observed data, with R^2 and RMSE values of 0.945 and 0.02, respectively. The specific energy consumption was evaluated as 0.471 $kWh^{-1}.m^{-3}$ which is reasonable and falls on the lower side of the reported range of full-scale facilities data (see ***Chapter 12:***).
- Membrane scouring is the single largest contributor to energy requirements with a share of 55.4%This presents an opportunity to significantly reduce the overall energy costs in full-scale MBRs. The other large energy consumers were mixing, biological process aeration, and influent pumping, with a share of 17%, 16.1%, and 8.6%, respectively, while other allied processes. remaining 5.9% is consumed by other

- The integrated and comprehensive model presented in this work may be used as a digital twin and shall be useful for the process engineers and the plant operators in optimizing the process parameters and in predicting the effluent quality, membrane fouling, and energetic consumption.

14.2 PERSPECTIVES

- Fouling sub-model is validated with filtration data showing negligible to minimum fouling. Additional validation of the model with data from the super-large-scale facilities showing higher fouling tendencies would enhance the robustness of the sub-model and enlarge the range of its application. Therefore, it is difficult to ascertain the accuracy of the model with the totally different operating conditions and higher fouling tendencies at full scale. Since each of the tanks is individually programmed for aeration intensity and sequencing (i.e., working of compressors) and chemical cleaning (in-situ and ex-situ), extending the fouling sub-model for each of the tanks would increase its prediction accuracy. Generally, all tanks do not experience the same level of fouling and simulating them one by one instead of an average in data handling, may provide the desired level of accuracy.

- Further research is needed to improve the filtration sub-model with the incorporation of the in-situ and ex-situ chemical cleaning effects; this would be easier in the case of tanks simulated one by one as proposed above. To further improve the filtration sub-model, when coagulation addition is considered, its effect on particle size distribution and stickiness of the MLSS should be explored as these are directly associated with the specific cake resistance.

- The parameters included in the filtration models vary in larger range, and this might be associated with their dependency on the concentration of the major foulants, including EPSs, SMPs, X_{TSS}, and colloidal components. This may vary depending upon the design (including the reactor configuration), the scale of the plant, and the operating conditions of the given MBR system. This needs to be further verified by operating the MBR system under different operating conditions such as MLSS concentrations, aeration intensity, and backwashing

frequency etc. To develop a systematic approach to estimate the specific parameters of the system model may thereby reduce calibration efforts.

- In the current mode, the influence of the temperature and MLSS concentrations have been considered to model the sludge viscosity, and the magnitude of the shear exerted onto the membrane surface. The influence of high aeration shear on the rheological properties of the sludge may be investigated and incorporated into the fouling model. It would be helpful for the management of the large bubbles, thanks to the ability of the model to accurately predict the relaxation effects.
- EPSs and SMPs parameters are usually not measured in routine at full-scale facilities, and high frequency data required for the purpose of modeling are not available. It is therefore, suggested to explore the utility of the commonly measured parameters such as soluble or colloidal COD. For this, the empirical correlation may be established between the concentrations of the soluble or colloidal components and the concentration of the EPSs or SMPs in the membrane bioreactor.
- The membrane surface in the current work is assumed to be static while HF membrane fibers are flexible and moving under the influence of shear produced by the air scouring. HF membranes enjoy added benefit of their loosely bound fibers which preliminary studies have shown to be helpful in reducing the membrane fouling. This effect could be considered while modeling the MBR systems with HF membranes. Furthermore, the applicability of the model with immersed flat sheet (FS) membrane should be explored in future works as flat sheet membrane are also being used at large scale (>35,000 $m^3.d^{-1}$), and their market share is growing.
- Membrane bioreactor (MBR) is a transient system and largely depends upon the influent composition, biological composition, and process conditions. In MBR, the model parameter sensitivities may change with time due to evolving biology, changing inputs, or environment (e.g., temperature). The work has shown the feasibility and interest of dynamic sensitivity analysis approach to evaluate the influence of time varying inputs on the model outputs.

A dynamic sensitivity analysis, in more than one dimension (2 or more parameters at a time) will help to consider the dynamic inputs and process conditions altogether for assessment of the uncertainty and robustness of the MBR dynamic integrated model involving both biology and swiftly changing conditions in the filtration process.

References

Abadi, M., Barham, P., Chen, J., Chen, Z., Davis, A., Dean, J., Devin, M., Ghemawat, S., Irving, G., Isard, M., 2016.: A system for large-scale machine learning, in 12th USENIX symposium on operating systems design and implementation (OSDI 16). pp. 265–283.

Abdel-Fatah, M.A., 2018. Nanofiltration systems and applications in wastewater treatment: Review article. Ain Shams Engineering Journal 9, 3077–3092. https://doi.org/10.1016/j.asej.2018.08.001

Adam, C., Gnirss, R., Lesjean, B., Buisson, H., Kraume, M., 2002. Enhanced biological phosphorus removal in membrane bioreactors. Water Science and Technology 46, 281–286. https://doi.org/10.2166/wst.2002.0606

Ahmed, Z., Cho, J., Lim, B.-R., Song, K.-G., Ahn, K.-H., 2007. Effects of sludge retention time on membrane fouling and microbial community structure in a membrane bioreactor. Journal of Membrane Science 287, 211–218.

Ahn, K.-H., Song, K.-G., Choa, E., Cho, J., Yun, H., Lee, S., Me, J., 2003. Enhanced biological phosphorus and nitrogen removal using a sequencing anoxic/anaerobic membrane bioreactor (SAM) process. Desalination, Desalination and the Environment: Fresh Water for all 157, 345–352. https://doi.org/10.1016/S0011-9164(03)00415-6

Akhondi, E., Zamani, F., Tng, K.H., Leslie, G., Krantz, W.B., Fane, A.G., Chew, J.W., 2017. The performance and fouling control of submerged hollow fiber (HF) systems: A Review. Applied Sciences 7, 765. https://doi.org/10.3390/app7080765

Alibardi, L., Vale, P., Bajón Fernández, Y., 2021. Full-scale trials to achieve low total phosphorus in effluents from sewage treatment works. Journal of Water Process Engineering 40, 101981. https://doi.org/10.1016/j.jwpe.2021.101981

Alleyne, A.A., Xanthos, S., Ramalingam, K., Temel, K., Li, H., Tang, H.S., 2014. Numerical investigation on flow generated by invent mixer in full-scale wastewater stirred tank. Engineering Applications of Computational Fluid Mechanics 8, 503–517. https://doi.org/10.1080/19942060.2014.11083303

Anderson, J.S., McAvoy, T.J., Hao, O.J., 2000. Use of hybrid models in wastewater systems. Industrial & Engineering Chemistry Research 39, 1694–1704. https://doi.org/10.1021/ie990557r

Aquino, S.F., Stuckey, D.C., 2004. Soluble microbial products formation in anaerobic chemostats in the presence of toxic compounds. Water Research 38, 255–266.

Arabi, S., Nakhla, G., 2008. Impact of calcium on the membrane fouling in membrane bioreactors. Journal of Membrane Science 314, 134–142. https://doi.org/10.1016/j.memsci.2008.01.037

Arif, A.U.A., Sorour, M.T., Aly, S.A., 2020. Cost analysis of activated sludge and membrane bioreactor WWTPs using CapdetWorks simulation program: Case study of Tikrit WWTP. Alexandria Engineering Journal 59, 4659–4667. https://doi.org/10.1016/j.aej.2020.08.023

Asensi, E., Alemany, E., Duque-Sarango, P., Aguado, D., 2019a. Assessment and modelling of the effect of precipitated ferric chloride addition on the activated

sludge settling properties. Chemical Engineering Research and Design 150, 14–25. https://doi.org/10.1016/j.cherd.2019.07.018

Asensi, E., Zambrano, D., Alemany, E., Aguado, D., 2019b. Effect of the addition of precipitated ferric chloride on the morphology and settling characteristics of activated sludge flocs. Separation and Purification Technology 227, 115711. https://doi.org/10.1016/j.seppur.2019.115711

Aslam, M., Charfi, A., Lesage, G., Heran, M., Kim, J., 2017. Membrane bioreactors for wastewater treatment: A review of mechanical cleaning by scouring agents to control membrane fouling. Chemical Engineering Journal 307, 897–913. https://doi.org/10.1016/j.cej.2016.08.144

Azis, K., Malioka, M., Ntougias, S., Melidis, P., 2018. Membrane fouling monitoring in a submerged membrane bioreactor. Proceedings 2, 653. https://doi.org/10.3390/proceedings2110653

Baetens, D., 2001. Enhanced Biological Phosphorus Removal: Modelling and experimental design gestimuleerde biologische fosfaatverwijdering: modelbouw en experimenteel ontwerp, Ph.D. dissertation, Universiteit Gent.

Baetens, D., Vanrolleghem, P.A., Van Loosdrecht, M.C.M. and Hosten, L.H., 1999. Temperature effects in bio-P removal. Water science and technology, 39(1), pp.215-225. https://doi.org/10.1016/S0273-1223(98)00787-2

Barillon, B., Ruel, S.M., Langlais, C., Lazarova, V., 2013. Energy efficiency in membrane bioreactors. Water Science and Technology 67, 2685–2691. https://doi.org/10.2166/wst.2013.163

Barreto, C.M., Garcia, H.A., Hooijmans, C.M., Herrera, A. and Brdjanovic, D., 2017. Assessing the performance of an MBR operated at high biomass concentrations. International Biodeterioration & Biodegradation, 119, pp.528-537. https://doi.org/10.1016/j.ibiod.2016.10.006

Bashar, R., Gungor, K., Karthikeyan, K.G., Barak, P., 2018. Cost effectiveness of phosphorus removal processes in municipal wastewater treatment. Chemosphere 197, 280–290. https://doi.org/10.1016/j.chemosphere.2017.12.169

Bella, G.D., Trapani, D.D., 2019. A brief review on the resistance-in-series model in membrane bioreactors (MBRs). Membranes 9, 24. https://doi.org/10.3390/membranes9020024

Benedetti, L., Batstone, D.J., De Baets, B., Nopens, I., Vanrolleghem, P.A., 2008. Global sensitivity analysis of biochemical, design and operational parameters of the Benchmark Simulation Model no. 2.

Bertanza, G., Canato, M., Laera, G., Vaccari, M., Svanström, M., Heimersson, S., 2017. A comparison between two full-scale MBR and CAS municipal wastewater treatment plants: techno-economic-environmental assessment. Environmental Science and Pollution Research 24, 17383–17393. https://doi.org/10.1007/s11356-017-9409-3

Bodik, I., Kubaska, M., 2013. Energy and sustainability of operation of a wastewater treatment plant. Environment Protection Engineering 39, 15--24.

Bottino, A., Capannelli, G., Comite, A., Mangano, R., 2009. Critical flux in submerged membrane bioreactors for municipal wastewater treatment. Desalination, Engineering with Membranes 245, 748–753. https://doi.org/10.1016/j.desal.2009.02.047

Boyd, G., Na, D., Li, Z., Snowling, S., Zhang, Q., Zhou, P., 2019. Influent forecasting for wastewater treatment plants in North America. Sustainability 11, 1764. https://doi.org/10.3390/su11061764

Boyle, W.C., Craven, A., Danley, W., Rieth, M., 1989. Oxygen transfer studies at the Madison Metropolitan Sewerage District facilities. retrieved from https://nepis.epa.gov/Exe/ZyPURL.cgi?Dockey=300035MP.TXT on 20th March 2022

Boyle-Gotla, A., Jensen, P.D., Yap, S.D., Pidou, M., Wang, Y., Batstone, D.J., 2014. Dynamic multidimensional modelling of submerged membrane bioreactor fouling. Journal of Membrane Science 467, 153–161. https://doi.org/10.1016/j.memsci.2014.05.028

Baresel, C., Jingjing, Y.A.N.G., Niclas, B.O.R.N.O.L.D., Kåre, T.J.U.S., Linda, K.A.N.D.E.R.S. and Klara, W.E.S.T.L.I.N.G., 2022. Direct GHG emissions from a pilot scale MBR-process treating municipal wastewater. Advances in Climate Change Research, 13(1), pp.138-145. https://doi.org/10.1016/j.accre.2021.09.006

Braak, E., Alliet, M., Schetrite, S., Albasi, C., 2011. Aeration and hydrodynamics in submerged membrane bioreactors. Journal of Membrane Science 379, 1–18. https://doi.org/10.1016/j.memsci.2011.06.004

Brepols, C., Schäfer, H., Engelhardt, N., 2010. Considerations on the design and financial feasibility of full-scale membrane bioreactors for municipal applications. Water Science and Technology 61, 2461–2468.

Briggs, T.A., 1996. Dynamic Modelling of Chemical Phosphorus Removal in the Activated Sludge Process. Master's Thesis, School of Graduate Studies, McMaster Univ., Hamilton, Ontario, Canada.

Buer, T., Cumin, J., 2010. MBR module design and operation. Desalination 250, 1073–1077. https://doi.org/10.1016/j.desal.2009.09.111

Burman, I., Sinha, A., 2018. A Review on membrane fouling in membrane bioreactors: Control and mitigation, in: Gupta, T., Agarwal, A.K., Agarwal, R.A., Labhsetwar, N.K. (Eds.), Environmental Contaminants: Measurement, modelling and control, energy, environment, and sustainability. Springer Singapore, pp. 281–315. https://doi.org/10.1007/978-981-10-7332-8_13

Busch, J., Cruse, A., Marquardt, W., 2007a. Run-to-run control of membrane filtration processes. AIChE Journal 53, 2316–2328. https://doi.org/10.1002/aic.11221

Busch, J., Cruse, A., Marquardt, W., 2007b. Modeling submerged hollow-fiber membrane filtration for wastewater treatment. Journal of Membrane Science 288, 94–111. https://doi.org/10.1016/j.memsci.2006.11.008

Byliński, H., Sobecki, A., Gębicki, J., 2019. The use of artificial neural networks and decision trees to predict the degree of odor nuisance of post-digestion sludge in the sewage treatment plant process. Sustainability 11, 4407.

Cadore, Í.R., Silva, M.K. da, Pollo, L.D., Tessaro, I.C., Cadore, Í.R., Silva, M.K. da, Pollo, L.D., Tessaro, I.C., 2018. Wastewater treatment in a pilot-scale submerged membrane bioreactor: study of hydrodynamics under constant operating pressure. Brazilian Journal of Chemical Engineering 35, 51–61. https://doi.org/10.1590/0104-6632.20180351s20160416

Campolongo, F., Cariboni, J., Saltelli, A., 2007. An effective screening design for sensitivity analysis of large models. Environmental Modelling & Software 22, 1509–1518.

Chae, S.-R., Ahn, Y.-T., Kang, S.-T., Shin, H.-S., 2006. Mitigated membrane fouling in a vertical submerged membrane bioreactor (VSMBR). Journal of Membrane Science 280, 572–581. https://doi.org/10.1016/j.memsci.2006.02.015

Chae, S.-R., Chung, J.-H., Heo, Y.-R., Kang, S.-T., Lee, S.-M., Shin, H.-S., 2015. Full-scale implementation of a vertical membrane bioreactor for simultaneous removal of organic matter and nutrients from municipal wastewater. Water 7, 1164–1172. https://doi.org/10.3390/w7031164

Chang, I.-S., Kim, S.-N., 2005. Wastewater treatment using membrane filtration—effect of biosolids concentration on cake resistance. Process Biochemistry 40, 1307–1314. https://doi.org/10.1016/j.procbio.2004.06.019

Cho, J., Ahn, K.-H., Seo, Y., Lee, Y., 2003. Modification of ASM No.1 for a submerged membrane bioreactor system: including the effects of soluble microbial products on membrane fouling. Water Science and Technology 47, 177–181. https://doi.org/10.2166/wst.2003.0644

Cho, J., Song, K.-G., Ahn, K.-H., 2005a. The activated sludge and microbial substances influences on membrane fouling in submerged membrane bioreactor: unstirred batch cell test. Desalination 183, 425–429.

Cho, J., Song, K.-G., Ahn, K.-H., 2005b. The activated sludge and microbial substances influences on membrane fouling in submerged membrane bioreactor: unstirred batch cell test. Desalination 183, 425–429.

Choo, K.-H., Lee, C.-H., 1996. Membrane fouling mechanisms in the membrane-coupled anaerobic bioreactor. Water Research 30, 1771–1780.

Christoforidou, P., Bariamis, G., Iosifidou, M., Nikolaidou, E., Samaras, P., 2020. Energy benchmarking and optimization of wastewater treatment plants in Greece, in: Environmental Sciences Proceedings. Multidisciplinary Digital Publishing Institute, p. 36.

Cosenza, A., Mannina, G., Neumann, M.B., Viviani, G., Vanrolleghem, P.A., 2013. Biological nitrogen and phosphorus removal in membrane bioreactors: model development and parameter estimation. Bioprocess Biosyst Eng 36, 499–514. https://doi.org/10.1007/s00449-012-0806-1

Cosenza, A., Mannina, G., Vanrolleghem, P.A., Neumann, M.B., 2014. Variance-based sensitivity analysis for wastewater treatment plant modelling. Science of The Total Environment 470–471, 1068–1077. https://doi.org/10.1016/j.scitotenv.2013.10.069

Cosenza Alida, Bella Gaetano Di, Mannina Giorgio, Torregrossa Michele, Viviani Gaspare, 2013. Biological nutrient removal and fouling phenomena in a University of Cape Town membrane bioreactor treating high nitrogen loads. Journal of Environmental Engineering 139, 773–780. https://doi.org/10.1061/(ASCE)EE.1943-7870.0000667

Cote, P., Alam, Z. and Penny, J., 2012. Hollow fiber membrane life in membrane bioreactors (MBR). Desalination, 288, pp.145-151. https://doi.org/10.1016/j.desal.2011.12.026

Daigger, G.T., Crawford, G.V., Johnson, B.R., 2010a. Full-scale assessment of the nutrient removal capabilities of membrane bioreactors. Water Environment Research 82, 806–818.

De Haas, D.W., Wentzel, M.C., Ekama, G.A., 2000. The use of simultaneous chemical precipitation in modified activated sludge systems exhibiting biological excess phosphate removal-Part 1: Literature review. Water SA 26, 439–452.

De Temmerman, L., Maere, T., Temmink, H., Zwijnenburg, A., Nopens, I., 2014. Salt stress in a membrane bioreactor: Dynamics of sludge properties, membrane

fouling and remediation through powdered activated carbon dosing. Water Research 63, 112–124. https://doi.org/10.1016/j.watres.2014.06.017

Delrue, F., Choubert, J.M., Stricker, A.E., Spérandio, M., Peuchot, M.M., Racault, Y., 2010. Modelling a full scale membrane bioreactor using Activated Sludge Model n°1: challenges and solutions. Water Science and Technology 62, 2205.

Deng, L., Guo, W., Ngo, H.H., Zuthi, Mst.F.R., Zhang, J., Liang, S., Li, J., Wang, J., Zhang, X., 2015. Membrane fouling reduction and improvement of sludge characteristics by bioflocculant addition in submerged membrane bioreactor. Separation and Purification Technology 156, 450–458. https://doi.org/10.1016/j.seppur.2015.10.034

Deung Park, H., 2015. Principles of membrane bioreactors for wastewater treatment, First. Ed. CRS Press, Taylor and Francis Group, NW.

Di Bella, G., Di Trapani, D., Judd, S., 2018. Fouling mechanism elucidation in membrane bioreactors by bespoke physical cleaning. Separation and Purification Technology 199, 124–133. https://doi.org/10.1016/j.seppur.2018.01.049

Di Bella, G., Di Trapani, D., Torregrossa, M., Viviani, G., 2013. Performance of a MBR pilot plant treating high strength wastewater subject to salinity increase: Analysis of biomass activity and fouling behaviour. Bioresource Technology 147, 614–618. https://doi.org/10.1016/j.biortech.2013.08.025

Di Bella, G., Mannina, G., Viviani, G., 2008. An integrated model for physical-biological wastewater organic removal in a submerged membrane bioreactor: Model development and parameter estimation. Journal of Membrane Science 322, 1–12.

Di Trapani, D., Di Bella, G., Mannina, G., Torregrossa, M., Viviani, G., 2015. Effect of C/N shock variation on the performances of a moving bed membrane bioreactor. Bioresource Technology 189, 250–257. https://doi.org/10.1016/j.biortech.2015.03.143

Ding, A., Liang, H., Li, G., Derlon, N., Szivak, I., Morgenroth, E., Pronk, W., 2016. Impact of aeration shear stress on permeate flux and fouling layer properties in a low pressure membrane bioreactor for the treatment of grey water. Journal of Membrane Science 510, 382–390.

Dixon, S.L., Duan, J., Smith, E., Von Bargen, C.D., Sherman, W., Repasky, M.P., 2016. AutoQSAR: an automated machine learning tool for best-practice quantitative structure–activity relationship modeling. Future Medicinal Chemistry 8, 1825–1839. https://doi.org/10.4155/fmc-2016-0093

Dolina, J., Dlask, O., Lederer, T., Dvořák, L., 2015. Mitigation of membrane biofouling through surface modification with different forms of nanosilver. Chemical Engineering Journal 275, 125–133. https://doi.org/10.1016/j.cej.2015.04.008

Dolar, D., Gros, M., Rodriguez-Mozaz, S., Moreno, J., Comas, J., Rodriguez-Roda, I. and Barceló, D., 2012. Removal of emerging contaminants from municipal wastewater with an integrated membrane system, MBR–RO. Journal of hazardous materials, 239, pp.64-69.

https://doi.org/10.1016/j.jhazmat.2012.03.029

Drews, A., 2010. Membrane fouling in membrane bioreactors—Characterisation, contradictions, cause and cures. Journal of Membrane Science 363, 1–28. https://doi.org/10.1016/j.memsci.2010.06.046

Drews, A., Lee, C.-H., Kraume, M., 2006a. Membrane fouling - a review on the role of EPS. Desalination 200, 186–188. https://doi.org/10.1016/j.desal.2006.03.290

Drews, A., Vocks, M., Iversen, V., Lesjean, B., Kraume, M., 2006b. Influence of unsteady membrane bioreactor operation on EPS formation and filtration resistance. Desalination, International Congress on Membranes and Membrane Processes 192, 1–9. https://doi.org/10.1016/j.desal.2005.04.130

Dvořák, L., Gómez, M., Dvořáková, M., Růžičková, I., Wanner, J., 2011. The impact of different operating conditions on membrane fouling and EPS production. Bioresource Technology 102, 6870–6875. https://doi.org/10.1016/j.biortech.2011.04.061

Ekama, G.A., Dold, P.L., Marais, G. v. R., 1986. Procedures for Determining Influent COD Fractions and the Maximum Specific Growth Rate of Heterotrophs in Activated Sludge Systems. Water Science and Technology 18, 91–114. https://doi.org/10.2166/wst.1986.0062

Elimelech, M., Xiaohua Zhu, Childress, A.E., Seungkwan Hong, 1997. Role of membrane surface morphology in colloidal fouling of cellulose acetate and composite aromatic polyamide reverse osmosis membranes. Journal of Membrane Science 127, 101–109. https://doi.org/10.1016/S0376-7388(96)00351-1

El-Said, M., Bhuse, V., Arendsen, A., 2017. An empirical study to investigate the effect of air density changes on the DSRC performance. Procedia computer science, complex adaptive systems conference with theme: Engineering cyber physical systems, CAS October 30 – November 1, 2017, Chicago, Illinois, USA 114, 523–530. https://doi.org/10.1016/j.procs.2017.09.025

Emergen, R., 2021. Membrane bioreactor market by system configuration (external, submerged), by membrane type (flat sheet, hollow fiber, multi-tubular), by application (industrial wastewater treatment, municipal wastewater treatment), and by region, forecasts to 2027 https://www.emergenresearch.com/industry-report/membrane-bioreactor-market (2021) received 6th September 2021.

Ersu, C.B., Ong, S.K., Arslankaya, E., Lee, Y.-W., 2010. Impact of solids residence time on biological nutrient removal performance of membrane bioreactor. Water Research 44, 3192–3202. https://doi.org/10.1016/j.watres.2010.02.036

Falahati-Marvast, H., Karimi-Jashni, A., 2020. A new modified anoxic-anaerobic-membrane bioreactor for treatment of real wastewater with a low carbon/nutrient ratio and high nitrate. Journal of Water Process Engineering 33, 101054. https://doi.org/10.1016/j.jwpe.2019.101054

Fallah, N., Bonakdarpour, B., Nasernejad, B., Alavi Moghadam, M.R., 2010. Long-term operation of submerged membrane bioreactor (MBR) for the treatment of synthetic wastewater containing styrene as volatile organic compound (VOC): Effect of hydraulic retention time (HRT). Journal of Hazardous Materials 178, 718–724. https://doi.org/10.1016/j.jhazmat.2010.02.001

Fan, F., Zhou, H., Husain, H., 2007. Use of chemical coagulants to control fouling potential for wastewater membrane bioreactor processes. Water Environment Research 79, 952–957. https://doi.org/10.2175/106143007X194329

Fan, J., Ding, Y., Qiu, Z., Li, W., Lu, S., 2011a. Development of mechanistically based model for simulating soluble microbial products generation in an aerated/non-aerated SBR. Bioprocess Biosystems Engineering 34, 1151. https://doi.org/10.1007/s00449-011-0566-3

Fang, F., Ni, B.-J., Xie, W.-M., Sheng, G.-P., Liu, S.-G., Tong, Z.-H., Yu, H.-Q., 2010. An integrated dynamic model for simulating a full-scale municipal wastewater treatment plant under fluctuating conditions. Chemical Engineering Journal 160, 522–529. https://doi.org/10.1016/j.cej.2010.03.063

Faust, L., Temmink, H., Zwijnenburg, A., Kemperman, A.J.B., Rijnaarts, H.H.M., 2014. Effect of dissolved oxygen concentration on the bioflocculation process in high loaded MBRs. Water Research 66, 199–207. https://doi.org/10.1016/j.watres.2014.08.022

Fenu, A., Guglielmi, G., Jimenez, J., Spèrandio, M., Saroj, D., Lesjean, B., Brepols, C., Thoeye, C., Nopens, I., 2010a. Activated sludge model (ASM) based modelling of membrane bioreactor (MBR) processes: A critical review with special regard to MBR specificities. Water Research 44, 4272–4294. https://doi.org/10.1016/j.watres.2010.06.007

Fenu, A., Guglielmi, G., Jimenez, J., Spèrandio, M., Saroj, D., Lesjean, B., Brepols, C., Thoeye, C., Nopens, I., 2010b. Activated sludge model (ASM) based modelling of membrane bioreactor (MBR) processes: A critical review with special regard to MBR specificities. Water Research 44, 4272–4294. https://doi.org/10.1016/j.watres.2010.06.007

Fenu, A., Roels, J., Wambecq, T., De Gussem, K., Thoeye, C., De Gueldre, G., Van De Steene, B., 2010c. Energy audit of a full scale MBR system. Desalination 262, 121–128. https://doi.org/10.1016/j.desal.2010.05.057

Fenu, A., Roels, J., Wambecq, T., De Gussem, K., Thoeye, C., De Gueldre, G., Van De Steene, B., 2010d. Energy audit of a full scale MBR system. Desalination 262, 121–128. https://doi.org/10.1016/j.desal.2010.05.057

Ferguson, J.F., King, T., 1977. A model for aluminum phosphate precipitation. Water Pollution Control Federation 49, 646–658.

Ferrero, G., 2011. Development of an air-scour control system for membrane bioreactors, Ph.D. Dissertation, University of Girona, Spain.

Fleischer, E.J., Broderick, T.A., Daigger, G.T., Fonseca, A.D., Holbrook, R.D., Murthy, S.N., 2005. Evaluation of membrane bioreactor process capabilities to meet stringent effluent nutrient discharge requirements. Water Environment Research 77, 162–178. https://doi.org/10.2175/106143005X41735

Friedman, J.H., 2001. Greedy function approximation: A gradient boosting machine. Annals of Statistics pp.1189–1232.

Fu, Z., Yang, F., Zhou, F., Xue, Y., 2009. Control of COD/N ratio for nutrient removal in a modified membrane bioreactor (MBR) treating high strength wastewater. Bioresource Technology 100, 136–141. https://doi.org/10.1016/j.biortech.2008.06.006

Gabarrón, S., Dalmau, M., Porro, J., Rodriguez-Roda, I., Comas, J., 2015a. Optimization of full-scale membrane bioreactors for wastewater treatment through a model-based approach. Chemical Engineering Journal 267, 34–42. https://doi.org/10.1016/j.cej.2014.12.097

Gabarrón, S., Ferrero, G., Dalmau, M., Comas, J., Rodriguez-Roda, I., 2014. Assessment of energy-saving strategies and operational costs in full-scale membrane bioreactors. Journal of Environmental Management 134, 8–14. https://doi.org/10.1016/j.jenvman.2013.12.023

Gao, D., Fu, Y., Tao, Y., Li, X., Xing, M., Gao, X., Ren, N., 2011. Linking microbial community structure to membrane biofouling associated with varying dissolved oxygen concentrations. Bioresource Technology. 102, 5626–5633. https://doi.org/10.1016/j.biortech.2011.02.039

Gebara, F., 1999. Activated sludge biofilm wastewater treatment system. Water Research 33, 230–238. https://doi.org/10.1016/S0043-1354(98)00210-3

Geng, Z., Hall, E.R., 2007. A comparative study of fouling-related properties of sludge from conventional and membrane enhanced biological phosphorus removal processes. Water Research 41, 4329–4338. https://doi.org/10.1016/j.watres.2007.07.007

Germain, E., Nelles, F., Drews, A., Pearce, P., Kraume, M., Reid, E., Judd, S.J., Stephenson, T., 2007. Biomass effects on oxygen transfer in membrane bioreactors. Water Research 41, 1038–1044. https://doi.org/10.1016/j.watres.2006.10.020

Germain, E., Stephenson, T., Pearce, P., 2005. Biomass characteristics and membrane aeration: Toward a better understanding of membrane fouling in submerged membrane bioreactors (MBRs). Biotechnology and Bioengineering 90, 316–322. https://doi.org/10.1002/bit.20411

Gernaey, K., Nopens, I., Vrecko, D., Alex, J., Dudley, J., 2006. An updated proposal for including further detail in the BSM2 PE calculation. Internal BSM2 taskgroup document.

Gernaey, K., Sin, G., 2011. Wastewater treatment models, in: Comprehensive Biotechnology. Elsevier.

Gernaey, K.V., van Loosdrecht, M.C.M., Henze, M., Lind, M., Jørgensen, S.B., 2004a. Activated sludge wastewater treatment plant modelling and simulation: state of the art. Environmental Modelling & Software, Environmental Sciences and Artificial Intelligence 19, 763–783. https://doi.org/10.1016/j.envsoft.2003.03.005

Gernaey, K.V., van Loosdrecht, M.C.M., Henze, M., Lind, M., Jørgensen, S.B., 2004b. Activated sludge wastewater treatment plant modelling and simulation: state of the art. Environmental Modelling & Software, Environmental Sciences and Artificial Intelligence 19, 763–783. https://doi.org/10.1016/j.envsoft.2003.03.005

Gkotsis, P., Banti, D., Peleka, E., Zouboulis, A., Samaras, P., 2014. Fouling isues in membrane bioreactors (MBRs) for wastewater treatment: Major mechanisms, prevention, and control strategies. Processes 2, 795–866. https://doi.org/10.3390/pr2040795

Gnirss, R., Lesjean, B., Adam, C., Buisson, H., 2003. Cost effective and advanced phosphorus removal in membrane bioreactors for a decentralised wastewater technology. Water Science and Technology 47, 133–139. https://doi.org/10.2166/wst.2003.0638

Gómez, M., Dvořák, L., Růžičková, I., Wanner, J., Holba, M., Sýkorová, E., 2013a. Influence of phosphorus precipitation on permeability and soluble microbial product concentration in a membrane bioreactor. Bioresource Technology 129, 164–169. https://doi.org/10.1016/j.biortech.2012.11.052

Gómez, M., Dvořák, L., Růžičková, I., Wanner, J., Holba, M., Sýkorová, E., 2013b. Influence of phosphorus precipitation on permeability and soluble microbial product concentration in a membrane bioreactor. Bioresource Technology 129, 164–169. https://doi.org/10.1016/j.biortech.2012.11.052

González Hernández, Y., Jáuregui Haza, U.J., Albasi, C., Alliet, M., 2014. Development of a Submerged Membrane Bioreactor simulator: a useful tool for teaching its functioning. Education for Chemical Engineers 9, 32–41. https://doi.org/10.1016/j.ece.2014.03.001

González-Hernández, Y., Jáuregui-Haza, U.J., 2021. Improved integrated dynamic model for the simulation of submerged membrane bioreactors for urban and hospital wastewater treatment. Journal of Membrane Science 624, 119053. https://doi.org/10.1016/j.memsci.2021.119053

Guglielmi, G. and Andreottola, G., 2010. Selection and design of membrane bioreactors in environmental bioengineering. In Environmental Biotechnology (pp. 439-516). Humana Press, Totowa, NJ.

Gujer, W., 1985. Ein dynamisches Modell fu¨ r die Simulation vonkomplexen Belebtschlammverfahren. Habilitationsschrift, ETH Zurich.

Guo, W., Ngo, H.-H., Li, J., 2012. A mini review on membrane fouling. Bioresource Technology, 122, 27–34. https://doi.org/10.1016/j.biortech.2012.04.089

Guo, W., Ngo, H.H., Vigneswaran, S., Dharmawan, F., Nguyen, T.T. and Aryal, R., 2010. Effect of different flocculants on short-term performance of submerged membrane bioreactor. Separation and Purification Technology, 70(3), pp.274-279.

https://doi.org/10.1016/j.seppur.2009.10.003

Gurung, K., Tang, W.Z., Sillanpää, M., 2018. Unit energy consumption as benchmark to select energy positive retrofitting strategies for Finnish wastewater treatment plants (WWTPs): a case study of Mikkeli WWTP. Environmental Processes 5, 667–681.

Habib, R., Asif, M.B., Iftekhar, S., Khan, Z., Gurung, K., Srivastava, V., Sillanpää, M., 2017. Influence of relaxation modes on membrane fouling in submerged membrane bioreactor for domestic wastewater treatment. Chemosphere 181, 19–25. https://doi.org/10.1016/j.chemosphere.2017.04.048

Hai, F.I., Yamamoto, K., Lee, C.-H., 2018a. Membrane biological reactors: theory, modeling, design, management, and applications to wastewater reuse. IWA Publishing.

Hamedi, H., Mohammadzadeh, O., Rasouli, S., Zendehboudi, S., 2021. A critical Review of biomass kinetics and membrane filtration models for membrane bioreactor systems. Journal of Environmental Chemical Engineering 106406. https://doi.org/10.1016/j.jece.2021.106406

Hamza, R.A., Iorhemen, O.T., Tay, J.H., 2016. Occurrence impacts and removal of emerging substances of concern from wastewater. Environmental Technology & Innovation 5, 161–175. https://doi.org/10.1016/j.eti.2016.02.003

Hao, L., Liss, S.N., Liao, B.Q., 2016. Influence of COD:N ratio on sludge properties and their role in membrane fouling of a submerged membrane bioreactor. Water Research 89, 132–141. https://doi.org/10.1016/j.watres.2015.11.052

Hashino, M., Katagiri, T., Kubota, N., Ohmukai, Y., Maruyama, T., Matsuyama, H., 2011. Effect of surface roughness of hollow fiber membranes with gear-shaped structure on membrane fouling by sodium alginate. Journal of Membrane Science 366, 389–397. https://doi.org/10.1016/j.memsci.2010.10.025

Hauduc, H., Rieger, L., Oehmen, A., Loosdrecht, M.C.M. van, Comeau, Y., Héduit, A., Vanrolleghem, P.A., Gillot, S., 2013. Critical review of activated sludge modeling: State of process knowledge, modeling concepts, and limitations. Biotechnology and Bioengineering 110, 24–46. https://doi.org/10.1002/bit.24624

Hauduc, H., Rieger, L., Takács, I., Héduit, A., Vanrolleghem, P.A., Gillot, S., 2010. A systematic approach for model verification: application on seven published activated sludge models. Water Science and Technology 61, 825–839. https://doi.org/10.2166/wst.2010.898

Hauduc, H., Takács, I., Smith, S., Szabo, A., Murthy, S., Daigger, G.T., Spérandio, M., 2015. A dynamic physicochemical model for chemical phosphorus removal. Water Research 73, 157–170. https://doi.org/10.1016/j.watres.2014.12.053

Henze, M., Gujer, W., Mino, T., Matsuo, T., Wentzel, M.C., Marais, G. v. R., Van Loosdrecht, M.C.M., 1999. Activated sludge model No.2d, ASM2D. Water Science and Technology 39, 165–182. https://doi.org/10.2166/wst.1999.0036

Henze, M., van Loosdrecht, M.C., Ekama, G.A., Brdjanovic, D., 2008. Biological wastewater treatment. IWA publishing.

Hernández, Y.G., Haza, U.J.J., Albasi, C., Alliet, M., 2016. Understanding the influence of operating parameters through in silico optimization of energy consumption of submerged membrane bioreactor for urban wastewater treatment. Desalination and Water Treatment 57, 16363–16375. https://doi.org/10.1080/19443994.2015.1081631

Hofs, B., Ogier, J., Vries, D., Beerendonk, E.F., Cornelissen, E.R., 2011. Comparison of ceramic and polymeric membrane permeability and fouling using surface water. Separation and Purification Technology 79, 365–374. https://doi.org/10.1016/j.seppur.2011.03.025

Holba, M., Plotěný, K., Dvořák, L., Gómez, M., Růžičková, I., 2012a. Full-scale applications of membrane filtration in municipal wastewater treatment plants. CLEAN – Soil, Air, Water 40, 479–486. https://doi.org/10.1002/clen.201000398

Huang, Z., Ong, S.L., Ng, H.Y., 2011. Submerged anaerobic membrane bioreactor for low-strength wastewater treatment: Effect of HRT and SRT on treatment performance and membrane fouling. Water Research 45, 705–713. https://doi.org/10.1016/j.watres.2010.08.035

Huisman, L., 1996. Rapid filtration. Department of Civil Engineering. Delft University of Technology, Delft 52.

Hvala, N., Kocijan, J., 2020. Design of a hybrid mechanistic/Gaussian process model to predict full-scale wastewater treatment plant effluent. Computers & Chemical Engineering 140, 106934. https://doi.org/10.1016/j.compchemeng.2020.106934

Iglesias, R., Simón, P., Moragas, L., Arce, A., Rodriguez-Roda, I., 2017a. Cost comparison of full-scale water reclamation technologies with an emphasis on membrane bioreactors. Water Science and Technology 75, 2562–2570.

Iglesias, R., Simón, P., Moragas, L., Arce, A., Rodriguez-Roda, I., 2017b. Cost comparison of full-scale water reclamation technologies with an emphasis on membrane bioreactors. Water Science and Technology 75, 2562–2570. https://doi.org/10.2166/wst.2017.132

Ignatowicz, K., 2019. Analysis of COD fractions in raw wastewater flowing into small and large wastewater treatment plants. Journal of Ecological Engineering 20.

Insel, G., Hocaoğlu, S.M., Cokgor, E.U., Orhon, D., 2011. Modelling the effect of biomass induced oxygen transfer limitations on the nitrogen removal performance of membrane bioreactor. Journal of Membrane Science 368, 54–63. https://doi.org/10.1016/j.memsci.2010.11.003

Instituto Mexicano de Tecnología del Agua, Estrada-Arriaga, E.B., Mijaylova Nacheva, P., García-Sánchez, L., Instituto Mexicano de Tecnología del Agua, Universidad Nacional Autónoma de México, 2015. Effect of mixed liquor volatile suspended solids on membrane fouling during short and long-term

operation of membrane bioreactor. Ingeniería y Ciencia 11, 137–155. https://doi.org/10.17230/ingciencia.11.21.7

Iorhemen, O.T., Hamza, R.A., Tay, J.H., 2017. Membrane fouling control in membrane bioreactors (MBRs) using granular materials. Bioresource Technology, Special Issue on Challenges in Environmental Science and Engineering, CESE-2016 240, 9–24. https://doi.org/10.1016/j.biortech.2017.03.005

Iorhemen, O.T., Hamza, R.A., Tay, J.H., 2016. Membrane bioreactor (MBR) technology for wastewater treatment and reclamation: Membrane Fouling. Membranes (Basel) 6. https://doi.org/10.3390/membranes6020033

Itonaga, T., Kimura, K., Watanabe, Y., 2004. Influence of suspension viscosity and colloidal particles on permeability of membrane used in membrane bioreactor (MBR). Water Science Technology 50, 301–309.

Jalali, A., Schindler, A., Haslhofer, B., Rauber, A., 2020. Machine learning interpretability techniques for outage prediction: A comparative study, in: PHM Society European Conference. pp. 10–10.

Jang, D., Hwang, Y., Shin, H. and Lee, W., 2013. Effects of salinity on the characteristics of biomass and membrane fouling in membrane bioreactors. Bioresource technology, 141, pp.50-56.
https://doi.org/10.1016/j.biortech.2013.02.062

Janus, T., 2014a. Integrated Mathematical Model of a MBR Reactor Including Biopolymer Kinetics and Membrane Fouling. Procedia Engineering, 12th International Conference on Computing and Control for the Water Industry, CCWI2013 70, 882–891. https://doi.org/10.1016/j.proeng.2014.02.098

Janus, T., 2013. Modelling and simulation of membrane bioreactors for wastewater treatment. Ph.D. Dissertation, De Montfort University- Leicester, UK.

Janus, T., Ulanicki, B., 2015. Interface model between the bioreactor and the membrane in a membrane bioreactor for wastewater treatment. Procedia Engineering 119, 1338–1347. https://doi.org/10.1016/j.proeng.2015.08.973

Janus, T., Ulanicki, B., 2010. Modelling SMP and EPS formation and degradation kinetics with an extended ASM3 model. Desalination 261, 117–125.

Jenkins, T.E., 2013. Aeration control system design: a practical guide to energy and process optimization. John Wiley & Sons.

Jeong, E., Kim, H.-W., Nam, J.-Y., Ahn, Y.-T., Shin, H.-S., 2010. Effects of the hydraulic retention time on the fouling characteristics of an anaerobic membrane bioreactor for treating acidifi ed wastewater. Desalination and Water Treatment 18, 251–256. https://doi.org/10.5004/dwt.2010.1781

Ji, L., Zhou, J., 2006. Influence of aeration on microbial polymers and membrane fouling in submerged membrane bioreactors. Journal of Membrane Science 276, 168–177. https://doi.org/10.1016/j.memsci.2005.09.045

Jiang, F., Beck, M.B., Cummings, R.G., Rowles, K., Russell, D., 2005. Estimation of costs of phosphorus removal in wastewater treatment facilities: adaptation of existing facilities. Water Policy Working Paper 11, 2005.

Jiang, T., Myngheer, S., De Pauw, D.J.W., Spanjers, H., Nopens, I., Kennedy, M.D., Amy, G., Vanrolleghem, P.A., 2008. Modelling the production and degradation of soluble microbial products (SMP) in membrane bioreactors (MBR). Water Research 42, 4955–4964. https://doi.org/10.1016/j.watres.2008.09.037

Jiang, T., Sin, G., Spanjers, H., Nopens, I., Kennedy, M.D., van der Meer, W., Futselaar, H., Amy, G., Vanrolleghem, P.A., 2009. Comparison of the

Modeling Approach between Membrane Bioreactor and Conventional Activated Sludge Processes. Water Environment Research 81, 432–440. https://doi.org/10.2175/106143008X370377

Jin, L., Ong, S.L., Ng, H.Y., 2010. Comparison of fouling characteristics in different pore-sized submerged ceramic membrane bioreactors. Water Research 44, 5907–5918. https://doi.org/10.1016/j.watres.2010.07.014

Johir, M.A.H., Vigneswaran, S., Sathasivan, A., Kandasamy, J., Chang, C.Y., 2012. Effect of organic loading rate on organic matter and foulant characteristics in membrane bio-reactor. Bioresource Technology, Special issue on the Challenges in Environmental Science and Engineering 113, 154–160. https://doi.org/10.1016/j.biortech.2011.12.002

Jonsdottir, H., Nielsen, H.A., Madsen, H., Eliasson, J., Palsson, O.P., Nielsen, M.K., 2007. Conditional parametric models for storm sewer runoff. Water Resources Research 43. https://doi.org/10.1029/2005WR004500

Judd, S., 2010. The MBR book: principles and applications of membrane bioreactors for water and wastewater treatment. Elsevier.

Judd, S., 2008. The status of membrane bioreactor technology. Trends in Biotechnology 26, 109–116. https://doi.org/10.1016/j.tibtech.2007.11.005

Judd, S., Judd, C., 2018. Largest MBR Plants (Over 100 MLD)—Worldwide. The MBR site: https://www. thembrsite. com/largest-membrane-bioreactor-plants-worldwide/(accessed 26 November 2018).

Kappeler, J., Gujer, W., 1992. Estimation of kinetic parameters of heterotrophic biomass under aerobic conditions and characterization of wastewater for activated sludge modelling. Water Science and Technology 25, 125–139.

Khan, S.J., Ilyas, S., Zohaib-Ur-Rehman, 2013. Impact of nitrogen loading rates on treatment performance of domestic wastewater and fouling propensity in submerged membrane bioreactor (MBR). Bioresource Technology, Challenges in Environmental Science and Engineering (CESE-2012) 141, 46–49. https://doi.org/10.1016/j.biortech.2013.03.196

Kim, M., Sankararao, B., Lee, S., Yoo, C., 2013. Prediction and identification of membrane fouling mechanism in a membrane bioreactor using a combined mechanistic model. Industrial & Engineering Chemistry Research 52, 17198–17205. https://doi.org/10.1021/ie402056r

Kimura, K., Uchida, H., 2019. Intensive membrane cleaning for MBRs equipped with flat-sheet ceramic membranes: Controlling negative effects of chemical reagents used for membrane cleaning. Water Research 150, 21–28. https://doi.org/10.1016/j.watres.2018.11.030

Kingma, D.P., Ba, J., 2014. Adam: A method for stochastic optimization. arXiv preprint arXiv:1412.6980.

Kornboonraksa, T., Lee, S.H., 2009. Factors affecting the performance of membrane bioreactor for piggery wastewater treatment. Bioresource Technology 100, 2926–2932. https://doi.org/10.1016/j.biortech.2009.01.048

Koseoglu, H., Yigit, N.O., Iversen, V., Drews, A., Kitis, M., Lesjean, B., Kraume, M., 2008. Effects of several different flux enhancing chemicals on filterability and fouling reduction of membrane bioreactor (MBR) mixed liquors. Journal of Membrane Science 320, 57–64. https://doi.org/10.1016/j.memsci.2008.03.053

Krampe, J., Krauth, K., 2003. Oxygen transfer into activated sludge with high MLSS concentrations. Water Science and Technology 47, 297–303. https://doi.org/10.2166/wst.2003.0618

Krauth, K.H., Staab, K.F., 1993. Pressurized bioreactor with membrane filtration for wastewater treatment. Water Research 27, 405–411.

Król, P., Gallina, A., Lubieniecki, M., Uhl, T., Żaba, T., 2019. Sensitivity analysis of a municipal wastewater treatment plant model, in: MATEC Web of Conferences. EDP Sciences, p. 05010.

Krzeminski, P., Leverette, L., Malamis, S., Katsou, E., 2017. Membrane bioreactors – A review on recent developments in energy reduction, fouling control, novel configurations, LCA and market prospects. Journal of Membrane Science 527, 207–227. https://doi.org/10.1016/j.memsci.2016.12.010.

Krzeminski, P., van der Graaf, J.H.J.M., van Lier, J.B., 2012. Specific energy consumption of membrane bioreactor (MBR) for sewage treatment. Water Science and Technology 65, 380–392. https://doi.org/10.2166/wst.2012.861

Kulesha, O., Maletskyi, Z., Ratnaweera, H., 2018. State-of-the-art of membrane flux enhancement in membrane bioreactor. Cogent Engineering 5, 1–30. https://doi.org/10.1080/23311916.2018.1489700

Langeveld, J.G., Clemens, F.H.L.R., van der Graaf, J.H.J.M., 2012. Interactions within the wastewater system: Modeling of Sewer Processes 1–11. https://doi.org/10.1061/40644(2002)295

Laspidou, C.S. and Rittmann, B.E., 2002. A unified theory for extracellular polymeric substances, soluble microbial products, and active and inert biomass. Water research, 36(11), pp.2711-2720.

Le-Clech, P., Chen, V., Fane, T.A.G., 2006. Fouling in membrane bioreactors used in wastewater treatment. Journal of Membrane Science 284, 17–53. https://doi.org/10.1016/j.memsci.2006.08.019

Le-Clech, P., Jefferson, B., Judd, S.J., 2003. Impact of aeration, solids concentration and membrane characteristics on the hydraulic performance of a membrane bioreactor. Journal of Membrane Science 218, 117–129. https://doi.org/10.1016/S0376-7388(03)00164-9

Lee, D.S., Jeon, C.O., Park, J.M., Chang, K.S., 2002. Hybrid neural network modeling of a full-scale industrial wastewater treatment process. Biotechnology and Bioengineering 78, 670–682. https://doi.org/10.1002/bit.10247

Lee, E.-J., An, A.K., Kim, H.-S., 2017. Effects of coagulant with different basicity on membrane-based biological treatment for removing phosphorus. Journal of Coastal Research 79, 65–69. https://doi.org/10.2112/SI79-014.1

Lee, E.-J., Kim, H.-S., Jang, A., 2016. Application of dissolved air flotation (DAF) with coagulation process for treatment of phosphorus within permeate of membrane bioreactor (MBR). Desalination and Water Treatment 57, 9043–9050. https://doi.org/10.1080/19443994.2015.1057034

Lee, K., Yu, H., Zhang, X., Choo, K.-H., 2018. Quorum sensing and quenching in membrane bioreactors: Opportunities and challenges for biofouling control. Bioresource Technology 270, 656–668. https://doi.org/10.1016/j.biortech.2018.09.019

Lee, Y., Cho, J., Seo, Y., Lee, J.W., Ahn, K.-H., 2002. Modeling of submerged membrane bioreactor process for wastewater treatment. Desalination 146, 451–457. https://doi.org/10.1016/S0011-9164(02)00543-X

Lesjean, B., Ferre, V., Vonghia, E., Moeslang, H., 2009. Market and design considerations of the 37 larger MBR plants in Europe. Desalination and Water Treatment 6, 227–233. https://doi.org/10.5004/dwt.2009.648

Lesjean, B., Huisjes, E.H., 2008. Survey of the European MBR market: trends and perspectives. Desalination 231, 71–81.

Lesjean, B., Rosenberger, S., Laabs, C., Jekel, M., Gnirss, R., Amy, G., 2005. Correlation between membrane fouling and soluble/colloidal organic substances in membrane bioreactors for municipal wastewater treatment. Water Science and Technology 51, 1–8. https://doi.org/10.2166/wst.2005.0615

Li, J., Tang, W.Z., Gu, L., 2021. Energy efficiency assessment of China wastewater treatment plants by unit energy consumption per kg COD removed. Environmental Technology 0, 1–15. https://doi.org/10.1080/09593330.2021.1969596

Li, P., Liu, L., Wu, J., Cheng, R., Shi, L., Zheng, X., Zhang, Z., 2019. Identify driving forces of MBR applications in China. Science of The Total Environment 647, 627–638. https://doi.org/10.1016/j.scitotenv.2018.07.412

Li, R., Wang, X., Li, X., 2018. A membrane bioreactor with iron dosing and acidogenic co-fermentation for enhanced phosphorus removal and recovery in wastewater treatment. Water Research 129, 402–412. https://doi.org/10.1016/j.watres.2017.11.035

Li, X., Liu, Y., Liu, F., Liu, A., Feng, Q., 2017. Comparison of ferric chloride and aluminum sulfate on phosphorus removal and membrane fouling in MBR treating BAF effluent of municipal wastewater. Journal of Water Reuse and Desalination 7, 442–448. https://doi.org/10.2166/wrd.2016.151

Li, X., Wang, X., 2006a. Modelling of membrane fouling in a submerged membrane bioreactor. Journal of Membrane Science 278, 151–161. https://doi.org/10.1016/j.memsci.2005.10.051

Li, X., Wang, X., 2006b. Modelling of membrane fouling in a submerged membrane bioreactor. Journal of Membrane Science 278, 151–161.

Liang, S., Song, L., Tao, G., Kekre, K.A., Seah, H., 2006. A modeling study of fouling development in membrane bioreactors for wastewater treatment. Water environment research 78, 857–864.

Liau, K.F., Shoji, T., Ong, Y.H., Chua, A.S.M., Yeoh, H.K., Ho, P.Y., 2015. Kinetic and stoichiometric characterization for efficient enhanced biological phosphorus removal (EBPR) process at high temperatures. Bioprocess Biosyst. Eng. 38, 729–737.

https://doi.org/ 10.1007/s00449-014-1313-3.

Lin, H.J., Gao, W.J., Leung, K.T., Liao, B.Q., 2011. Characteristics of different fractions of microbial flocs and their role in membrane foulingH. J. Lin et al.Characteristics of different fractions of microbial flocs in membrane fouling. Water Sci Technol 63, 262–269. https://doi.org/10.2166/wst.2011.047

Lindamulla, L.M.L.K.B., Jegatheesan, V., Jinadasa, K.B.S.N., Nanayakkara, K.G.N., Othman, M.Z., 2021. Integrated mathematical model to simulate the performance of a membrane bioreactor. Chemosphere 284, 131319. https://doi.org/10.1016/j.chemosphere.2021.131319

Liu, R., Huang, X., Sun, Y.F., Qian, Y., 2003. Hydrodynamic effect on sludge accumulation over membrane surfaces in a submerged membrane bioreactor. Process Biochemistry 39, 157–163. https://doi.org/10.1016/S0032-9592(03)00022-0

Liu, X., Wang, Y., Waite, T.D., Leslie, G., 2016. Fluid Structure Interaction analysis of lateral fibre movement in submerged membrane reactors. Journal of Membrane Science 504, 240–250. https://doi.org/10.1016/j.memsci.2015.12.056

Liu, Y., Liu, H., Cui, L., Zhang, K., 2012. The ratio of food-to-microorganism (F/M) on membrane fouling of anaerobic membrane bioreactors treating low-strength

wastewater. Desalination 297, 97–103. https://doi.org/10.1016/j.desal.2012.04.026

Lo, C.H., McAdam, E., Judd, S., 2015. The cost of a small membrane bioreactor. Water Science and Technology 72, 1739–1746. https://doi.org/10.2166/wst.2015.394

Loderer, C., Gahleitner, B., Woerle, A., Fuchs, W., 2015. Dynamic filtration—influence of different precipitation agents on the filtration performance using an inside-out filtration module. Desalination and Water Treatment 53, 940–950. https://doi.org/10.1080/19443994.2013.846235

Longo, S., Mauricio-Iglesias, M., Soares, A., Campo, P., Fatone, F., Eusebi, A.L., Akkersdijk, E., Stefani, L., Hospido, A., 2019. ENERWATER – A standard method for assessing and improving the energy efficiency of wastewater treatment plants. Applied Energy 242, 897–910. https://doi.org/10.1016/j.apenergy.2019.03.130

Louppe, G., 2017. Bayesian optimization with scikit-optimize. In PyData Amsterdam.

Lousada-Ferreira, M., Geilvoet, S., Moreau, A., Atasoy, E., Krzeminski, P., van Nieuwenhuijzen, A., van der Graaf, J., 2010. MLSS concentration: Still a poorly understood parameter in MBR filterability. Desalination 250, 618–622. https://doi.org/10.1016/j.desal.2009.09.036

Lu, S.G., Imai, T., Ukita, M., Sekine, M., Higuchi, T., Fukagawa, M., 2001. A model for membrane bioreactor process based on the concept of formation and degradation of soluble microbial products. Water Research 35, 2038–2048.

Luedecke, C., Hermanowicz, S.W., Jenkins, D., 1988. Precipitation of ferric phosphate in activated sludge: a chemical model and its verification, in: Water Pollution Research and Control Brighton. Elsevier, pp. 325–337.

Lyko, S., Wintgens, T., Al-Halbouni, D., Baumgarten, S., Tacke, D., Drensla, K., Janot, A., Dott, W., Pinnekamp, J., Melin, T., 2008. Long-term monitoring of a full-scale municipal membrane bioreactor—Characterisation of foulants and operational performance. Journal of Membrane Science, A special Issue on Membrane Reactors & Bioreactors 317, 78–87. https://doi.org/10.1016/j.memsci.2007.07.008

Ma, Z., Wen, X., Zhao, F., Xia, Y., Huang, X., Waite, D., Guan, J., 2013. Effect of temperature variation on membrane fouling and microbial community structure in membrane bioreactor. Bioresource Technology 133, 462–468. https://doi.org/10.1016/j.biortech.2013.01.023

Ma, J., Dai, R., Chen, M., Khan, S.J. and Wang, Z., 2018. Applications of membrane bioreactors for water reclamation: micropollutant removal, mechanisms, and perspectives. Bioresource Technology, 269, pp.532-543.
https://doi.org/10.1016/j.biortech.2018.08.121

Maere, T., Verrecht, B., Moerenhout, S., Judd, S., Nopens, I., 2011. BSM-MBR: A benchmark simulation model to compare control and operational strategies for membrane bioreactors. Water Research 45, 2181–2190. https://doi.org/10.1016/j.watres.2011.01.006

Makisha, N., Saveliev, O., Katella, S., 2018. Cost aspects of membrane bioreactors for wastewater treatment. IOP Conference Series: Earth and Environmental Science 177, 012037. https://doi.org/10.1088/1755-1315/177/1/012037

Mannina, G., Alliet, M., Brepols, C., Comas, J., Harmand, J., Heran, M., Kalboussi, N., Makinia, J., Robles, Á., Rebouças, T.F., Ni, B.-J., Rodriguez-Roda, I., Victoria Ruano, M., Bertanza, G., Smets, I., 2021. Integrated membrane bioreactors modelling: A review on new comprehensive modelling framework.

Bioresource Technology 329, 124828. https://doi.org/10.1016/j.biortech.2021.124828

Mannina, G., Capodici, M., Cosenza, A., Di Trapani, D., 2016. Carbon and nutrient biological removal in a University of Cape Town membrane bioreactor: Analysis of a pilot plant operated under two different C/N ratios. Chemical Engineering Journal 296, 289–299. https://doi.org/10.1016/j.cej.2016.03.114

Mannina, G., Cosenza, A., Ekama, G.A., 2018. A comprehensive integrated membrane bioreactor model for greenhouse gas emissions. Chemical Engineering Journal 334, 1563–1572. https://doi.org/10.1016/j.cej.2017.11.061

Mannina, G., Cosenza, A., Vanrolleghem, P.A., Viviani, G., 2011a. A practical protocol for calibration of nutrient removal wastewater treatment models. Journal of Hydroinformatics 13, 575–595. https://doi.org/10.2166/hydro.2011.041

Mannina, G., Di Bella, G., Viviani, G., 2011b. An integrated model for biological and physical process simulation in membrane bioreactors (MBRs). Journal of Membrane Science 376, 56–69. https://doi.org/10.1016/j.memsci.2011.04.003

Mannina, G., Ekama, G.A., Capodici, M., Cosenza, A., Di Trapani, D., Ødegaard, H., 2017. Moving bed membrane bioreactors for carbon and nutrient removal: The effect of C/N variation. Biochemical Engineering Journal 125, 31–40. https://doi.org/10.1016/j.bej.2017.05.005

Mannina, G., Ni, B.-J., Ferreira Rebouças, T., Cosenza, A., Olsson, G., 2020a. Minimizing membrane bioreactor environmental footprint by multiple objective optimizations. Bioresource Technology 302, 122824. https://doi.org/10.1016/j.biortech.2020.122824

Mannina, G., Pandey, A., Larroche, C., Ng, H.Y., Ngo, H.H., 2020b. Current developments in biotechnology and bioengineering: advanced membrane separation processes for sustainable water and wastewater management-case studies and sustainability analysis. Elsevier.

Mao, X., Myavagh, P.H., Lotfikatouli, S., Hsiao, B.S., Walker, H.W., 2020. Membrane bioreactors for nitrogen removal from wastewater: A review. Journal of Environmental Engineering 146, 03120002. https://doi.org/10.1061/(ASCE)EE.1943-7870.0001682

Market Research, 2022. Membrane bioreactor market by membrane type (hollow fiber, flat sheet, multi-tubular), system configuration (submerged, external), application (municipal wastewater treatment and industrial wastewater treatment), Region - global forecast to 2026.(consulted on 2022.09.20 - https://www.marketsandmarkets.com/Market-Reports/membrane-bioreactor-market-484.html?gclid=CjwKCAjwyaWZBhBGEiwACslQo-GRbi0QTZ5i0qRgSkpL2UDbSdvtwgLZTHx86CMl0IUSstvOW45v8xoCkD8QAvD_BwE)

Maximous, N., Nakhla, G., Wan, W., 2009. Comparative assessment of hydrophobic and hydrophilic membrane fouling in wastewater applications. Journal of Membrane Science 339, 93–99. https://doi.org/10.1016/j.memsci.2009.04.034

Mbamba, C.K., Lindblom, E., Flores-Alsina, X., Tait, S., Anderson, S., Saagi, R., Batstone, D.J., Gernaey, K.V., Jeppsson, U., 2019. Plant-wide model-based analysis of iron dosage strategies for chemical phosphorus removal in wastewater treatment systems. Water Research 155, 12–25.

Meng, F., Chae, S.-R., Drews, A., Kraume, M., Shin, H.-S., Yang, F., 2009. Recent advances in membrane bioreactors (MBRs): Membrane fouling and membrane

material. Water Research 43, 1489–1512. https://doi.org/10.1016/j.watres.2008.12.044

Meng, F., Yang, F., 2007. Fouling mechanisms of deflocculated sludge, normal sludge, and bulking sludge in membrane bioreactor. Journal of Membrane Science 305, 48–56. https://doi.org/10.1016/j.memsci.2007.07.038

Meng, F., Zhang, H., Li, Y., Zhang, X., Yang, F., 2005. Application of fractal permeation model to investigate membrane fouling in membrane bioreactor. Journal of Membrane Science 262, 107–116.

Meng, F., Zhang, H., Yang, F., Liu, L., 2007. Characterization of Cake Layer in Submerged Membrane Bioreactor. Environmental Science & Technology 41, 4065–4070. https://doi.org/10.1021/es062208b

Meng, F., Zhang, S., Oh, Y., Zhou, Z., Shin, H.-S., Chae, S.-R., 2017a. Fouling in membrane bioreactors: An updated review. Water Research 114, 151–180. https://doi.org/10.1016/j.watres.2017.02.006

Meng, F., Zhang, S., Oh, Y., Zhou, Z., Shin, H.-S., Chae, S.-R., 2017b. Fouling in membrane bioreactors: An updated review. Water Research 114, 151–180. https://doi.org/10.1016/j.watres.2017.02.006

Meng, S., Wang, R., Zhang, K., Meng, X., Xue, W., Liu, H., Liang, D., Zhao, Q. and Liu, Y., 2021. Transparent exopolymer particles (TEPs)-associated protobiofilm: A neglected contributor to biofouling during membrane filtration. Frontiers of Environmental Science & Engineering, 15(4), pp.1-10.

Mirbagheri, S.A., Bagheri, M., Boudaghpour, S., Ehteshami, M., Bagheri, Z., 2015. Performance evaluation and modeling of a submerged membrane bioreactor treating combined municipal and industrial wastewater using radial basis function artificial neural networks. Journal of Environmental Health Science and Engineering 13, 17. https://doi.org/10.1186/s40201-015-0172-4

Miron, M., Frangu, L., Caraman, S., 2017. Actuator fault detection using extended Kalman filter for a wastewater treatment process 2017, presented in 21st International conference on system theory, control and computing (ICSTCC).pp. 583–588. https://doi.org/10.1109/ICSTCC.2017.8107098

Mishima, I., Nakajima, J., 2009. Control of membrane fouling in membrane bioreactor process by coagulant addition. Water Science and Technology 59, 1255–1262. https://doi.org/10.2166/wst.2009.090

Miyoshi, T., Yuasa, K., Ishigami, T., Rajabzadeh, S., Kamio, E., Ohmukai, Y., Saeki, D., Ni, J., Matsuyama, H., 2015. Effect of membrane polymeric materials on relationship between surface pore size and membrane fouling in membrane bioreactors. Applied Surface Science 330, 351–357. https://doi.org/10.1016/j.apsusc.2015.01.018

Verrecht, B., Maere, T., Benedetti, L., Nopens, I. and Judd, S., 2010. Model-based energy optimization of a small-scale decentralized membrane bioreactor for urban reuse. Water Research, 44(14), pp.4047-4056.

Monclús, H., Sipma, J., Ferrero, G., Rodriguez-Roda, I., Comas, J., 2010. Biological nutrient removal in an MBR treating municipal wastewater with special focus on biological phosphorus removal. Bioresource Technology 101, 3984–3991. https://doi.org/10.1016/j.biortech.2010.01.038

Moreau, A.A., Ratkovich, N., Nopens, I., van der Graaf, J.H.J.M., 2009. The (in)significance of apparent viscosity in full-scale municipal membrane bioreactors. Journal of Membrane Science 340, 249–256. https://doi.org/10.1016/j.memsci.2009.05.049

Morris, M.D., 1991. Factorial sampling plans for preliminary computational experiments. Technometrics 33, 161–174.

Muller, E.B., Stouthamer, A.H., van Verseveld, H.W. van, Eikelboom, D.H., 1995. Aerobic domestic wastewater treatment in a pilot plant with complete sludge retention by cross-flow filtration. Water Research 29, 1179–1189.

Mutamim, N.S.A., Noor, Z.Z., Hassan, M.A.A., Yuniarto, A., Olsson, G., 2013. Membrane bioreactor: Applications and limitations in treating high strength industrial wastewater. Chemical Engineering Journal 225, 109–119. https://doi.org/10.1016/j.cej.2013.02.131

Nadeem, K., Alliet, M., Plana, Q., Bernier, J., Azimi, S., Rocher, V., Albasi, C., 2022a. Modeling, simulation and control of biological and chemical P-removal processes for membrane bioreactors (MBRs) from lab to full-scale applications: State of the art. Science of The Total Environment 809, 151109. https://doi.org/10.1016/j.scitotenv.2021.151109

Nadiri, A.A., Shokri, S., Tsai, F.T.-C., Asghari Moghaddam, A., 2018. Prediction of effluent quality parameters of a wastewater treatment plant using a supervised committee fuzzy logic model. Journal of Cleaner Production 180, 539–549. https://doi.org/10.1016/j.jclepro.2018.01.139

Naessens, W., Maere, T., Nopens, I., 2012. Critical review of membrane bioreactor models – Part 1: Biokinetic and filtration models. Bioresource Technology 122, 95–106. https://doi.org/10.1016/j.biortech.2012.05.070

Ng, A.N.L., Kim, A.S., 2007. A mini review of modeling studies on membrane bioreactor (MBR) treatment for municipal wastewaters. Desalination 212, 261–281. https://doi.org/10.1016/j.desal.2006.10.013

Nguyen, V., 2019. Bayesian optimization for accelerating hyper-parameter tuning, in 2019 IEEE Second International Conference on Artificial Intelligence and Knowledge Engineering (AIKE). IEEE, pp. 302–305.

Nguyen, T.T., Guo, W., Ngo, H.H. and Vigneswaran, S., 2010. A new combined inorganic–organic flocculant (CIOF) as a performance enhancer for aerated submerged membrane bioreactor. Separation and purification technology, 75(2), pp.204-209.
https://doi.org/10.1016/j.seppur.2010.07.010

Ni, B.-J., Rittmann, B.E., Yu, H.-Q., 2011. Soluble microbial products and their implications in mixed culture biotechnology. Trends in Biotechnology 29, 454–463. https://doi.org/10.1016/j.tibtech.2011.04.006

Nittami, T., Tokunaga, H., Satoh, A., Takeda, M., Matsumoto, K., 2014. Influence of surface hydrophilicity on polytetrafluoroethylene flat sheet membrane fouling in a submerged membrane bioreactor using two activated sludges with different characteristics. Journal of Membrane Science 463, 183–189. https://doi.org/10.1016/j.memsci.2014.03.064

Nywening, J.-P., Zhou, H., 2009. Influence of filtration conditions on membrane fouling and scouring aeration effectiveness in submerged membrane bioreactors to treat municipal wastewater. Water Research 43, 3548–3558.

Oliver, P., Rodríguez, R., Udaquiola, S., 2008. Water use optimization in batch process industries. Part 1: design of the water network. Journal of Cleaner Production 16, 1275–1286. https://doi.org/10.1016/j.jclepro.2007.06.012

Pan, J.R., Su, Y., Huang, C., 2010. Characteristics of soluble microbial products in membrane bioreactor and its effect on membrane fouling. Desalination 250, 778–780. https://doi.org/10.1016/j.desal.2008.11.040

Park, H.-D., Chang, I.-S., Lee, K.-J., 2015. Principles of membrane bioreactors for wastewater treatment. CRC Press.

Park, J., Yamashita, N., Park, C., Shimono, T., Takeuchi, D.M. and Tanaka, H., 2017. Removal characteristics of pharmaceuticals and personal care products: Comparison between membrane bioreactor and various biological treatment processes. Chemosphere, 179, pp.347-358.
https://doi.org/10.1016/j.chemosphere.2017.03.135

Pechaud, Y., Fayolle, Y., Duran, C., Pageot, S., Gillot, S., 2015. Biological floc size measurement for shear stress evaluation in full-scale aeration tanks, in 12th International Conference on Gas-Liquid & Gas-Liquid-Solid Reactor Engineering (GLS12). p. 4.

Pechaud, Y., Pageot, S., Goubet, A., Duran Quintero, C., Gillot, S., Fayolle, Y., 2021. Size of biological flocs in activated sludge systems: Influence of hydrodynamic parameters at different scales. Journal of Environmental Chemical Engineering 9, 105427. https://doi.org/10.1016/j.jece.2021.105427

Pedregosa, F., Varoquaux, G., Gramfort, A., Michel, V., Thirion, B., Grisel, O., Blondel, M., Prettenhofer, P., Weiss, R., Dubourg, V., Vanderplas, J., Passos, A., Cournapeau, D., Brucher, M., Perrot, M., Duchesnay, É., 2011. Scikit-learn: Machine Learning in Python. Journal of Machine Learning Research 12, 2825–2830.

Petersen, B., Gernaey, K., Henze, M., Vanrolleghem, P.A., 2003. Calibration of activated sludge models: A critical review of experimental designs. Biotechnology for the environment: Wastewater treatment and modeling, Waste Gas Handling 101–186.

Petersen, B., Vanrolleghem, P.A., Gernaey, K., Henze, M., 2002. Evaluation of an ASM1 model calibration procedure on a municipal–industrial wastewater treatment plant. Journal of Hydroinformatics 4, 15–38. https://doi.org/10.2166/hydro.2002.0003

Philippe, N., Stricker, A.-E., Racault, Y., Husson, A., Sperandio, M., Vanrolleghem, P., 2013. Modelling the long-term evolution of permeability in a full-scale MBR: Statistical approaches. Desalination 325, 7–15.

Philips, S., Rabaey, K., Verstraete, W., 2003. Impact of iron salts on activated sludge and interaction with nitrite or nitrate. Bioresource Technology 88, 229–239. https://doi.org/10.1016/S0960-8524(02)00314-0

Pianosi, F., Beven, K., Freer, J., Hall, J.W., Rougier, J., Stephenson, D.B., Wagener, T., 2016. Sensitivity analysis of environmental models: A systematic review with practical workflow. Environmental Modelling & Software 79, 214–232. https://doi.org/10.1016/j.envsoft.2016.02.008

Pianosi, F., Sarrazin, F., Wagener, T., 2015. A Matlab toolbox for Global Sensitivity Analysis. Environmental Modelling & Software 70, 80–85. https://doi.org/10.1016/j.envsoft.2015.04.009

Pimentel, G.A., Dalmau, M., Vargas, A., Comas, J., Rodriguez-Roda, I., Rapaport, A., Vande Wouwer, A., 2015. Validation of a simple fouling model for a submerged membrane bioreactor. IFAC-Papers Online, 8th Vienna International Conference on Mathematical Modelling 48, 737–742. https://doi.org/10.1016/j.ifacol.2015.05.031

Płuciennik-Koropczuk, E., Jakubaszek, A., Myszograj, S., Uszakiewicz, S., 2017. COD fractions in mechanical-biological wastewater treatment plant. Civil and Environmental Engineering Reports 24, 207–217.

Pourabdollah, M., Torkian, A., Hashemian, S.J., Bakhshi, B., 2014. A triple fouling layers perspective on evaluation of membrane fouling under different scenarios of membrane bioreactor operation. Journal of Environmental Health Science and Engineering 12, 1–11.

Praus, P., 2019. Principal component weighted index for wastewater quality monitoring. Water 11, 2376.

Psoch, C., Schiewer, S., 2008. Long-term flux improvement by air sparging and backflushing for a membrane bioreactor, and modeling permeability decline. Desalination 230, 193–204.

Psoch, C., Schiewer, S., 2006. Anti-fouling application of air sparging and backflushing for MBR. Journal of Membrane Science 283, 273–280. https://doi.org/10.1016/j.memsci.2006.06.042

Racault, Y., Stricker, A.-E., Husson, A., Gillot, S., 2011. Monitoring the variations of the oxygen transfer rate in a full-scale membrane bioreactor using daily mass balances. Water Science and Technology 63, 2651–2657. https://doi.org/10.2166/wst.2011.146

Ramesh, A., Lee, D.J., Lai, J.Y., 2007. Membrane biofouling by extracellular polymeric substances or soluble microbial products from membrane bioreactor sludge. Applied Microbiology Biotechnology 74, 699–707. https://doi.org/10.1007/s00253-006-0706-x

Rana, D., Matsuura, T., 2010. Surface modifications for antifouling membranes. Chemical Reviews. 110, 2448–2471. https://doi.org/10.1021/cr800208y

Ratkovich, N., Horn, W., Helmus, F.P., Rosenberger, S., Naessens, W., Nopens, I., Bentzen, T.R., 2013. Activated sludge rheology: a critical review on data collection and modelling. Water Research 47, 463–482.

Raunkjær, K., Hvitved-Jacobsen, T., Nielsen, P.H., 1994. Measurement of pools of protein, carbohydrate and lipid in domestic wastewater. Water Research 28, 251–262. https://doi.org/10.1016/0043-1354(94)90261-5

Ren, B., Li, C., Zhang, X., Zhang, Z., 2019. Fe(II)-dosed ceramic membrane bioreactor for wastewater treatment: Nutrient removal, microbial community and membrane fouling analysis. Science of the Total Environment 664, 116–126. https://doi.org/10.1016/j.scitotenv.2019.02.019

Ren, Baoyu, Li, C., Zhang, X., Zhang, Z., 2019. Fe(II)-dosed ceramic membrane bioreactor for wastewater treatment: Nutrient removal, microbial community and membrane fouling analysis. Science of The Total Environment 664, 116–126. https://doi.org/10.1016/j.scitotenv.2019.02.019

Rieger, L., Gillot, S., Langergraber, G., Ohtsuki, T., Shaw, A., Takacs, I., Winkler, S., 2012. Guidelines for using activated sludge models. IWA publishing.

Rieger, L., Koch, G., Kühni, M., Gujer, W., Siegrist, H., 2001. The EAWAG Bio-P module for activated sludge model No. 3. Water Research 35, 3887–3903.

Rieger, L., Takács, I., Villez, K., Siegrist, H., Lessard, P., Vanrolleghem, P.A., Comeau, Y., 2010. Data reconciliation for wastewater treatment plant simulation studies—planning for high-quality data and typical sources of errors. Water Environment Research 82, 426–433.

Robles, A., Ruano, M.V., Ribes, J., Seco, A., Ferrer, J., 2013. A filtration model applied to submerged anaerobic MBRs (SAnMBRs). Journal of Membrane Science 444, 139–147.

Rosenberger, S., Evenblij, H., te Poele, S., Wintgens, T., Laabs, C., 2005. The importance of liquid phase analyses to understand fouling in membrane assisted activated sludge processes—six case studies of different European

research groups. Journal of Membrane Science 263, 113–126. https://doi.org/10.1016/j.memsci.2005.04.010

Rosenberger, S., Laabs, C., Lesjean, B., Gnirss, R., Amy, G., Jekel, M., Schrotter, J.-C., 2006. Impact of colloidal and soluble organic material on membrane performance in membrane bioreactors for municipal wastewater treatment. Water Research 40, 710–720. https://doi.org/10.1016/j.watres.2005.11.028

Rosenberger, S., Witzig, R., Manz, W., Szewzyk, U., Kraume, M., 2000. Operation of different membrane bioreactors: experimental results and physiological state of the micro-organisms. Water Science and Technology 41, 269–277. https://doi.org/10.2166/wst.2000.0659

Rosso, D., Iranpour, R., Stenstrom, M.K., 2005. Fifteen Years of Offgas Transfer Efficiency Measurements on Fine-Pore Aerators: Key Role of Sludge Age and Normalized Air Flux. Water Environment Research 77, 266–273.

Ruano, M.V., Ribes, J., Ferrer, J., Sin, G., 2011. Application of the Morris method for screening the influential parameters of fuzzy controllers applied to wastewater treatment plants. Water Science and Technology 63, 2199–2206. https://doi.org/10.2166/wst.2011.442

Saltelli, A., Annoni, P., Azzini, I., Campolongo, F., Ratto, M., Tarantola, S., 2010. Variance based sensitivity analysis of model output. Design and estimator for the total sensitivity index. Computer physics communications 181, 259–270.

Saltelli, A., Ratto, M., Andres, T., Campolongo, F., Cariboni, J., Gatelli, D., Saisana, M., Tarantola, S., 2008. Global sensitivity analysis: the primer. John Wiley & Sons.

Sarioglu, M., Sayi-Ucar, N., Cokgor, E., Orhon, D., Van Loosdrecht, M.C.M., Insel, G., 2017. Dynamic modeling of nutrient removal by a MBR operated at elevated temperatures. Water Research 123, 420–428.

Sayi-Ucar, N., Sarioglu, M., Insel, G., Cokgor, E.U., Orhon, D., van Loosdrecht, M.C.M., 2015. Long-term study on the impact of temperature on enhanced biological phosphorus and nitrogen removal in membrane bioreactor. Water Res. 84, 8–17.

https://doi. org/10.1016/j.watres.2015.06.054

Sarrazin, F., Pianosi, F., Wagener, T., 2017. An introduction to the SAFE Matlab Toolbox with practical examples and guidelines, in: Sensitivity analysis in earth observation modelling. Elsevier, pp. 363–378.

Sarrazin, F., Pianosi, F., Wagener, T., 2016. Global Sensitivity Analysis of environmental models: Convergence and validation. Environmental Modelling & Software 79, 135–152.

scikit, 2020. scikit-optimize, Sequential model-based optimization in Python. URL https://scikit-optimize.github.io/stable/

Shariati, S.R.P., Bonakdarpour, B., Zare, N., Ashtiani, F.Z., 2011. The effect of hydraulic retention time on the performance and fouling characteristics of membrane sequencing batch reactors used for the treatment of synthetic petroleum refinery wastewater. Bioresource Technology 102, 7692–7699. https://doi.org/10.1016/j.biortech.2011.05.065

Shen, L., Lei, Q., Chen, J.-R., Hong, H.-C., He, Y.-M., Lin, H.-J., 2015. Membrane fouling in a submerged membrane bioreactor: Impacts of floc size. Chemical Engineering Journal 269, 328–334. https://doi.org/10.1016/j.cej.2015.02.002

Shukla, N., Fricklas, K., 2018. Machine learning with TensorFlow. Manning Greenwich.

SIAAP, 2016. Manuel général : Présentation de l'usine SAV.

SIAAP, 2014. Modernisation du traitement biologique, Seine Aval,

Sin, G., Al, R., 2021. Activated sludge models at the crossroad of artificial intelligence—A perspective on advancing process modeling. npj Clean Water 4, 1–7. https://doi.org/10.1038/s41545-021-00106-5

Sin, G., Gernaey, K.V., Neumann, M.B., van Loosdrecht, M.C. and Gujer, W., 2011. Global sensitivity analysis in wastewater treatment plant model applications: prioritizing sources of uncertainty. Water research, 45(2), pp.639-651.

Singh, P., Carliell-Marquet, C., Kansal, A., 2012. Energy pattern analysis of a wastewater treatment plant. Applied Water Science 2, 221–226.

Smith, S., Takacs, I., Murthy, S., Daigger, G.T., Szabo, A., 2008. Phosphate complexation model and its implications for chemical phosphorus removal. Water Environment Research 80, 428–438.

Song, K.-G., Kim, Y., Ahn, K.-H., 2008. Effect of coagulant addition on membrane fouling and nutrient removal in a submerged membrane bioreactor. Desalination 221, 467–474.

Sözen, S., Çokgör, E.U., Orhon, D., Henze, M., 1998. Respirometric analysis of activated sludge behaviour—II. Heterotrophic growth under aerobic and anoxic conditions. Water Research 32, 476–488.

Sperandio, M., Paul, E., 2000. Estimation of wastewater biodegradable COD fractions by combining respirometric experiments in various So/Xo ratios. Water Research 34, 1233–1246.

Stefanski, M., Kennedy, S., Judd, S., 2011. The determination and origin of fibre clogging in membrane bioreactors. Journal of Membrane Science 375, 198–203. https://doi.org/10.1016/j.memsci.2011.03.047

Stockburger, D.W., 1996. Introductory statistics: Concepts, models, and applications (1996). URL: http://www. psychstat. smsu. edu/introbook/sbk00. htm.

Stricot, M., 2008. Bioréacteurs à membranes à configuration externe : Influence de la configuration du procédé sur la structuration des matrices biologiques et le colmatage des membranes. Toulouse, INSA.

Suard, E., Fayolle, Y., Guerin, S., Jones, H., Guillaume, S., Rocher, V., Albasi, C., Alliet, M., Gillot, S., 2019. Statistical modelling of a semi-industrial scale membrane bioreactor using fuzzy inference methods. Presented at the 9th International Water Association (IWA) Membrane Technology Conference & Exhibition for Water and Wastewater Treatment and Reuse IWA-MTC, p. 2.

Suh, C., Lee, S., Cho, J., 2013a. Investigation of the effects of membrane fouling control strategies with the integrated membrane bioreactor model. Journal of Membrane Science 429, 268–281. https://doi.org/10.1016/j.memsci.2012.11.042

Suh, C., Lee, S., Cho, J., 2013b. Investigation of the effects of membrane fouling control strategies with the integrated membrane bioreactor model. Journal of Membrane Science 429, 268–281. https://doi.org/10.1016/j.memsci.2012.11.042

Sun, C., Leiknes, T., Weitzenböck, J., Thorstensen, B., 2010. Salinity effect on a biofilm-MBR process for shipboard wastewater treatment. Separation and Purification Technology 72, 380–387. https://doi.org/10.1016/j.seppur.2010.03.010

Sun, G., Zhang, C., Li, W., Yuan, L., He, S., Wang, L., 2019. Effect of chemical dose on phosphorus removal and membrane fouling control in a UCT-MBR. Frontiers of Environmental Science & Engineering 13, 1–11.

Sun, J., Liang, P., Yan, X., Zuo, K., Xiao, K., Xia, J., Qiu, Y., Wu, Q., Wu, S., Huang, X., Qi, M., Wen, X., 2016. Reducing aeration energy consumption in a large-scale membrane bioreactor: Process simulation and engineering application. Water Research 93, 205–213. https://doi.org/10.1016/j.watres.2016.02.026

Sutherland, K., 2010. The rise of membrane bioreactors. Filtration & Separation 47, 14–16.

Sweity, A., Ying, W., Ali-Shtayeh, M.S., Yang, F., Bick, A., Oron, G., Herzberg, M., 2011. Relation between EPS adherence, viscoelastic properties, and MBR operation: Biofouling study with QCM-D. Water Research 45, 6430–6440. https://doi.org/10.1016/j.watres.2011.09.038

Takács, I., Johnson, B.R., Smith, S., Szabó, A., Murthy, S., 2011. Chemical P removal–from lab tests through model understanding to full-scale demonstration, in: Proceedings of the 11th IWA Specialised Conference on Design, Operation and Economics of Large Wastewater Treatment Plants. pp. 101–108.

Tanguy, P.A., Thibault, F., 2002. Power Consumption in the Turbulent Regime for a Coaxial Mixer. The Canadian Journal of Chemical Engineering 80, 601–603. https://doi.org/10.1002/cjce.5450800423

Tay, J.-H., Liu, Y., Tay, S.T.-L., Hung, Y.-T., 2009. Aerobic granulation technology, in: Advanced Biological Treatment Processes. Springer, pp. 109–128.

Tchobanoglous, G., Burton, F.L., Stensel, H.D., 2003a. Metcalf & Eddy wastewater engineering: treatment and reuse. International Edition. McGrawHill 4, 361–411.

Tchobanoglous, G., Burton, F.L., Stensel, H.D., 2003b. Metcalf & Eddy wastewater engineering: treatment and reuse. International Edition. McGrawHill 4, 361–411.

Tensor Flow, 2022. Module: tf.keras. URL https://www.tensorflow.org/api_docs/python/tf/keras

Truong-Meyer, X.-M., 2012 Modélisation en génie des procédés. Ed. Techniques Ingénieur.

Truong-Meyer, X.-M., 2012b. Modélisation en génie des procédés. Ed. Techniques Ingénieur.

Trussell, R.S., Merlo, R.P., Hermanowicz, S.W., Jenkins, D., 2007. Influence of mixed liquor properties and aeration intensity on membrane fouling in a submerged membrane bioreactor at high mixed liquor suspended solids concentrations. Water Research 41, 947–958. https://doi.org/10.1016/j.watres.2006.11.012

Vaccari, M., Foladori, P., Nembrini, S., Vitali, F., 2018. Benchmarking of energy consumption in municipal wastewater treatment plants–a survey of over 200 plants in Italy. Water Science and Technology 77, 2242–2252.

Vaiopoulou, E., Melidis, P., Aivasidis, A., 2007. An activated sludge treatment plant for integrated removal of carbon, nitrogen and phosphorus. Desalination, Ninth Environmental Science and Technology Symposium 211, 192–199. https://doi.org/10.1016/j.desal.2006.02.092

van den Brink, P., Satpradit, O.-A., van Bentem, A., Zwijnenburg, A., Temmink, H., van Loosdrecht, M., 2011. Effect of temperature shocks on membrane fouling in membrane bioreactors. Water Research 45, 4491–4500. https://doi.org/10.1016/j.watres.2011.05.046

Van den Broeck, R., Van Dierdonck, J., Nijskens, P., Dotremont, C., Krzeminski, P., van der Graaf, J.H.J.M., van Lier, J.B., Van Impe, J.F.M., Smets, I.Y., 2012. The influence of solids retention time on activated sludge bioflocculation and

membrane fouling in a membrane bioreactor (MBR). Journal of Membrane Science 401–402, 48–55. https://doi.org/10.1016/j.memsci.2012.01.028

Verrecht, B., Judd, S., Guglielmi, G., Brepols, C., Mulder, J.W., 2008a. An aeration energy model for an immersed membrane bioreactor. Water Research 42, 4761–4770.

Verrecht, B., Judd, S., Guglielmi, G., Brepols, C., Mulder, J.W., 2008b. An aeration energy model for an immersed membrane bioreactor. Water Research 42, 4761–4770.

Villain, M., Marrot, B., 2013. Influence of sludge retention time at constant food to microorganism's ratio on membrane bioreactor performances under stable and unstable state conditions. Bioresource Technology 128, 134–144. https://doi.org/10.1016/j.biortech.2012.10.108

Wang, K., Qi, X., Liu, H., 2019. Photovoltaic power forecasting-based LSTM-Convolutional Network. Energy 189, 116225. https://doi.org/10.1016/j.energy.2019.116225

Wang, L.-L., Wang, L.-F., Ren, X.-M., Ye, X.-D., Li, W.-W., Yuan, S.-J., Sun, M., Sheng, G.-P., Yu, H.-Q., Wang, X.-K., 2012. pH Dependence of Structure and Surface Properties of Microbial EPS. Environnemental Science Technology. 46, 737–744. https://doi.org/10.1021/es203540w

Wang, Q., Wang, Z., Wu, Z., Han, X., 2011. Sludge reduction and process performance in a submerged membrane bioreactor with aquatic worms. Chemical Engineering Journal 172, 929–935. https://doi.org/10.1016/j.cej.2011.07.004

Wang, S., Zou, L., Li, H., Zheng, K., Wang, Y., Zheng, G., Li, J., 2020. Full-scale membrane bioreactor process WWTPs in East Taihu basin: Wastewater characteristics, energy consumption and sustainability. Science of The Total Environment 723, 137983. https://doi.org/10.1016/j.scitotenv.2020.137983

Wang, X., Ratnaweera, H., Holm, J.A., Olsbu, V., 2017. Statistical monitoring and dynamic simulation of a wastewater treatment plant: A combined approach to achieve model predictive control. Journal of Environmental Management 193, 1–7. https://doi.org/10.1016/j.jenvman.2017.01.079

Wang, Y., 2020. Intermittently Aerated MBR for Nutrients Removal and Phosphorus Recovery, in: Wang, Y. (Ed.), Development of Novel Bioelectrochemical Membrane Separation Technologies for Wastewater Treatment and Resource Recovery, Springer Theses. Springer, Singapore, pp. 43–79. https://doi.org/10.1007/978-981-15-3078-4_3

Wang, Y., Tng, K.H., Wu, H., Leslie, G., Waite, T.D., 2014. Removal of phosphorus from wastewaters using ferrous salts – A pilot scale membrane bioreactor study. Water Research 57, 140–150. https://doi.org/10.1016/j.watres.2014.03.029

Wang, Z., Wu, Z., Yin, X., Tian, L., 2008. Membrane fouling in a submerged membrane bioreactor (MBR) under sub-critical flux operation: Membrane foulant and gel layer characterization. Journal of Membrane Science 325, 238–244. https://doi.org/10.1016/j.memsci.2008.07.035

Wang, Z., Wu, Z., Yu, G., Liu, J., Zhou, Z., 2006. Relationship between sludge characteristics and membrane flux determination in submerged membrane bioreactors. Journal of Membrane Science 284, 87–94. https://doi.org/10.1016/j.memsci.2006.07.006

Wiesner, M.R., Aptel, P., 1996. Mass transport and permeate flux and fouling in pressure-driven processes. Water Treatment Membrane Processes 4.1-4.30.

Wintgens, T., Rosen, J., Melin, T., Brepols, C., Drensla, K., Engelhardt, N., 2003. Modelling of a membrane bioreactor system for municipal wastewater treatment. Journal of Membrane Science 216, 55–65. https://doi.org/10.1016/S0376-7388(03)00046-2

Wu, B., Yi, S., Fane, A.G., 2012. Effect of Substrate Composition (C/N/P ratio) on Microbial Community and Membrane Fouling Tendency of Biomass in Membrane Bioreactors. Separation Science and Technology 47, 440–445. https://doi.org/10.1080/01496395.2011.621503

Wu, H., Ikeda-Ohno, A., Wang, Y., Waite, T.D., 2015. Iron and phosphorus speciation in Fe-conditioned membrane bioreactor activated sludge. Water Research 76, 213–226. https://doi.org/10.1016/j.watres.2015.02.020

Wu, H., Wang, Y., Ikeda-Ohno, A., Miller, C.J., Waite, T.D., 2019. Impact of ferrous iron dosing on iron and phosphorus solids speciation and transformation in a pilot scale membrane bioreactor. Environmental Science: Water Research and Technology 5, 1400–1411. https://doi.org/10.1039/c9ew00225a

Wu, J., Chen, F., Huang, X., Geng, W., Wen, X., 2006. Using inorganic coagulants to control membrane fouling in a submerged membrane bioreactor. Desalination 197, 124–136. https://doi.org/10.1016/j.desal.2005.11.026

Wu, J., He, C., 2012. Effect of cyclic aeration on fouling in submerged membrane bioreactor for wastewater treatment. Water Research 46, 3507–3515. https://doi.org/10.1016/j.watres.2012.03.049

Wu, J., He, C., Zhang, Y., 2012. Modeling membrane fouling in a submerged membrane bioreactor by considering the role of solid, colloidal and soluble components. Journal of Membrane Science 397–398, 102–111. https://doi.org/10.1016/j.memsci.2012.01.026

Wu, J., Huang, X., 2009. Effect of mixed liquor properties on fouling propensity in membrane bioreactors. Journal of Membrane Science 342, 88–96. https://doi.org/10.1016/j.memsci.2009.06.024

Wu, X., Han, H., Qiao, J., 2021. Data-Driven Intelligent Warning Method for Membrane Fouling. IEEE Transactions on Neural Networks and Learning Systems 1–12. https://doi.org/10.1109/TNNLS.2020.3041293

Xiao, K., Liang, S., Wang, X., Chen, C., Huang, X., 2019a. Current state and challenges of full-scale membrane bioreactor applications: A critical review. Bioresource Technology 271, 473–481. https://doi.org/10.1016/j.biortech.2018.09.061

Xiao, K., Liang, S., Wang, X., Chen, C., Huang, X., 2019b. Current state and challenges of full-scale membrane bioreactor applications: A critical review. Bioresource Technology 271, 473–481. https://doi.org/10.1016/j.biortech.2018.09.061

Xie, W.-M., Ni, B.-J., Seviour, T., Sheng, G.-P., Yu, H.-Q., 2012. Characterization of autotrophic and heterotrophic soluble microbial product (SMP) fractions from activated sludge. Water Research 46, 6210–6217. https://doi.org/10.1016/j.watres.2012.02.046

Xie, K., Xia, S., Song, J., Li, J., Qiu, L., Wang, J. and Zhang, S., 2014. The effect of salinity on membrane fouling characteristics in an intermittently aerated membrane bioreactor. Journal of Chemistry, 2014.

https://doi.org/10.1155/2014/765971

Xing, C.-H., Qian, Y., Wen, X.-H., Wu, W.-Z., Sun, D., 2001. Physical and biological characteristics of a tangential-flow MBR for municipal wastewater treatment.

Journal of Membrane Science 191, 31–42. https://doi.org/10.1016/S0376-7388(01)00472-0

Yang, Shuai, Fenglin Yang, Zhimin Fu, and Ruibo Lei. "Comparison between a moving bed membrane bioreactor and a conventional membrane bioreactor on organic carbon and nitrogen removal." Bioresource technology 100, no. 8 (2009): 2369-2374.
https://doi.org/10.1016/j.biortech.2008.11.022

Yang, W., Cicek, N., Ilg, J., 2006. State-of-the-art of membrane bioreactors: Worldwide research and commercial applications in North America. Journal of Membrane Science 270, 201–211.

Yang, X.-L., Song, H.-L., Chen, M., Cheng, B., 2011. Characterizing membrane foulants in MBR with addition of polyferric chloride to enhance phosphorus removal. Bioresource Technology 102, 9490–9496. https://doi.org/10.1016/j.biortech.2011.07.105

Yaqub, M., Asif, H., Kim, S., Lee, W., 2020. Modeling of a full-scale sewage treatment plant to predict the nutrient removal efficiency using a long short-term memory (LSTM) neural network. Journal of Water Process Engineering 37, 101388. https://doi.org/10.1016/j.jwpe.2020.101388

Yeo, A.P.S., Law, A.W.K., Fane, A.G. (Tony), 2007. The relationship between performance of submerged hollow fibers and bubble-induced phenomena examined by particle image velocimetry. Journal of Membrane Science 304, 125–137. https://doi.org/10.1016/j.memsci.2007.07.039

Yigit, N.O., Harman, I., Civelekoglu, G., Koseoglu, H., Cicek, N., Kitis, M., 2008. Membrane fouling in a pilot-scale submerged membrane bioreactor operated under various conditions. Desalination, Selected Papers Presented at the 4th International IWA Conference on Membranes for Water and Wastewater Treatment, 15-17 May 2007, Harrogate, UK. Guest Edited by Simon Judd; and Papers Presented at the International Workshop on Membranes and Solid-Liquid Separation Processes, 11 July 2007, INSA, Toulouse, France. Guest edited by Saravanamuthu Vigneswaran and Jaya Kandasamy 231, 124–132. https://doi.org/10.1016/j.desal.2007.11.041

Young, T., Smoot, S., Peeters, J., Côté, P., 2014. Cost-effectiveness of membrane bioreactors treatment system for low-level phosphorus reduction from municipal wastewater. Water Practice and Technology 9, 316–323. https://doi.org/10.2166/wpt.2014.033

Zarragoitia, A., Schetrite, S., Jáuregui-Haza, U.J., Lorain, O., Albasi, C., 2009. Optimization of Wastewater Filtration Process in Submerged Membrane Bioreactors: Applicability of a Dynamic Model to Scale Up., in: de Brito Alves, R.M., do Nascimento, C.A.O., Biscaia, E.C. (Eds.), Computer Aided Chemical Engineering, 10th International Symposium on Process Systems Engineering: Part A. Elsevier, pp. 1545–1550. https://doi.org/10.1016/S1570-7946(09)70648-0

Zarragoitia-González, A., 2009. Desarrollo de modelos dinamicos para la simulacion y optimizacion de biorreactores con membrana sumergida para el tratamiento de aguas residuales, Ph.D. Dissertation Université de Toulouse.

Zarragoitia-González, A., Schetrite, S., Alliet, M., Jáuregui-Haza, U., Albasi, C., 2008. Modelling of submerged membrane bioreactor: conceptual study about link between activated slugde biokinetics, aeration and fouling process. Journal of Membrane Science 325, 612–624.

Zhang, C.H., Dong, Y.Y., Sun, H.J., 2013a. Effect of Aeration Intensity on Membrane Fouling of Non-Woven Fibers-MBR, Advanced Materials Research, pp. 1695–1698.

Zhang, H., Sun, B., Zhao, X., Gao, Z., 2008. Effect of ferric chloride on fouling in membrane bioreactor. Separation and Purification Technology 63, 341–347.

Zhang, J., Xiao, K., Liu, Z., Gao, T., Liang, S., Huang, X., 2021. Large-Scale Membrane Bioreactors for Industrial Wastewater Treatment in China: Technical and Economic Features, Driving Forces, and Perspectives. Engineering 7, 868–880. https://doi.org/10.1016/j.eng.2020.09.012

Zhang, X., Yue, X., Liu, Z., Li, Q., Hua, X., 2015. Impacts of sludge retention time on sludge characteristics and membrane fouling in a submerged anaerobic–oxic membrane bioreactor. Applied Microbiology and Biotechnology 99, 4893–4903. https://doi.org/10.1007/s00253-015-6383-x

Zhang, Y., Zhang, M., Wang, F., Hong, H., Wang, A., Wang, J., Weng, X., Lin, H., 2014. Membrane fouling in a submerged membrane bioreactor: Effect of pH and its implications. Bioresource Technology 152, 7–14. https://doi.org/10.1016/j.biortech.2013.10.096

Zhang, Z., Wang, Y., Leslie, G.L., Waite, T.D., 2015. Effect of ferric and ferrous iron addition on phosphorus removal and fouling in submerged membrane bioreactors. Water Research 69, 210–222. https://doi.org/10.1016/j.watres.2014.11.011

Zhu, A., Guo, J., Ni, B.-J., Wang, S., Yang, Q., Peng, Y., 2015. A Novel Protocol for Model Calibration in Biological Wastewater Treatment. Scientific Reports 5, 8493. https://doi.org/10.1038/srep08493

Zoungrana, A., Türk, O.K., Çakmakci, M., 2020. Energy coverage of ataköy-ambarlı municipal wastewater treatment plants by salinity gradient power. Journal of Water Process Engineering 38, 101552. https://doi.org/10.1016/j.jwpe.2020.101552

Zuthi, F., 2014. New mathematical models of biomass viability and membrane fouling in a membrane bioreactor, Ph.D. Thesis, University of Technology, Sydney, Australia.

Zuthi, M.F.R., Guo, W., Ngo, H.H., Nghiem, D.L., Hai, F.I., Xia, S., Li, Jianxin, Li, Jixiang, Liu, Y., 2017a. New and practical mathematical model of membrane fouling in an aerobic submerged membrane bioreactor. Bioresource Technology 238, 86–94. https://doi.org/10.1016/j.biortech.2017.04.006

Zuthi, M.F.R., Guo, W.S., Ngo, H.H., Nghiem, L.D., Hai, F.I., 2013. Enhanced biological phosphorus removal and its modeling for the activated sludge and membrane bioreactor processes. Bioresource Technology 139, 363–374. https://doi.org/10.1016/j.biortech.2013.04.038

ANNEXURES

Annexure -A	Review Paper: Modeling, simulation, and control of biological and chemical P-removal processes for membrane bioreactors (MBRs) from lab to full-scale applications: State of the art
Annexure-B	Full expression of the stoichiometric parameters used in Peterson matrix and their default and calibrated values
Annexure-C	LSTM models structure

ANNEXURE-A

Review Paper: Modeling, simulation, and control of biological and chemical P-removal processes for membrane bioreactors (MBRs) from lab to full-scale applications: State of the art

Science of the Total Environment 809 (2022) 151109

Contents lists available at ScienceDirect

Science of the Total Environment

journal homepage: www.elsevier.com/locate/scitotenv

Review

Modeling, simulation and control of biological and chemical P-removal processes for membrane bioreactors (MBRs) from lab to full-scale applications: State of the art

Kashif Nadeem [a], Marion Alliet [a], Queralt Plana [b], Jean Bernier [b], Sam Azimi [b], Vincent Rocher [b], Claire Albasi [a,*]

[a] Laboratoire de Génie Chimique, Université de Toulouse, CNRS, INPT, UPS, Toulouse, France
[b] Parisian Sanitation Public Service (SIAAP), Direction Innovation, 92700 Colombes, France

HIGHLIGHTS

- P-removal employing combined EBPR and chemical precipitation are successful in MBRs.
- Bio-kinetic models appeared to be successful in simulating the P-removal in MBRs.
- Specificities of MBR functioning require peculiar parameters for these models.
- EBPR instability at full-scale due to incomprehension of micro-organisms role.
- P-removal modeling studies at full/super-large scale MBRs are required.

GRAPHICAL ABSTRACT

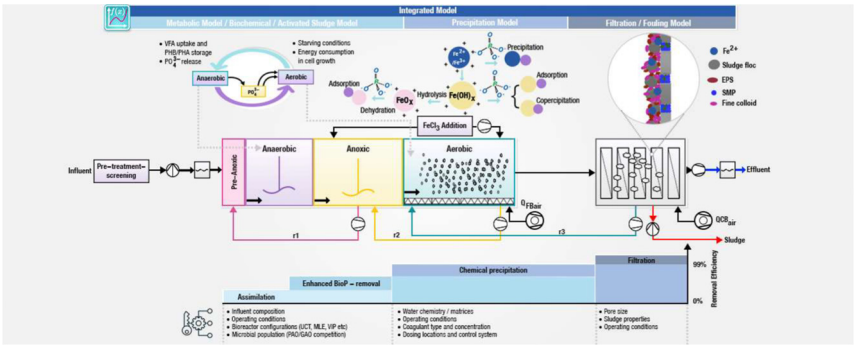

ARTICLE INFO

Article history:
Received 2 August 2021
Received in revised form 16 October 2021
Accepted 16 October 2021
Available online 22 October 2021

Editor: Qilin Wang

Keywords:
MBR
Phosphorus
Modeling
EBPR
Precipitation models
Super large-scale

ABSTRACT

Phosphorus (P) removal from the domestic wastewater is required to counter the eutrophication in receiving water bodies and is mandated by the regulatory frameworks in several countries with discharge limits within 1-2mgPL^{-1}. Operating at higher sludge retention time (SRT) and higher biomass concentration than the conventional activated sludge process (CASP), membrane bioreactors (MBRs) are able to remove 70–98% phosphorus without addition of coagulant. In full-scale facilities, enhanced biological phosphorus removal (EBPR) is assisted by the addition of metal coagulant to ensure >95% P-removal. MBRs are successfully used for super-large-scale wastewater treatment facilities (capacity >100,000 m^{3}d^{-1}). This paper documents the knowledge of P-removal modeling from lab to full-scale submerged MBRs and assesses the existing mathematical models for P-removal from domestic wastewater. There are still limited studies involving integrated modeling of the MBRs (full/super large-scale), considering the complex interactions among biology, chemical addition, filtration, and fouling. This paper analyses the design configurations and the parameters affecting the biological and chemical P-removal in MBRs to understand the P-removal process sensitivity and their implications for the modeling studies. Furthermore, it thoroughly reviews the applications of bio-kinetic and chemical precipitation models to MBRs for assessing their effectiveness with default stoichiometric and kinetic parameters and the extent to which these parameters have been calibrated/adjusted to simulate the P-removal successfully. It also presents a brief overview and comparison of seven (7) chemical precipitation models, along with a quick comparison of commercially available simulators. In addition to advantages associated with chemical precipitation for P-removal, its role in changing the relative abundance of the microbial community responsible for P-removal and denitrification and

* Corresponding author.
E-mail addresses: kashif.nadeem@toulouse-inp.fr (K. Nadeem), marion.alliet@ensiacet.fr (M. Alliet), AZIMI@siaap.fr (S. Azimi), Vincent.ROCHER@siaap.fr (V. Rocher), claire.albasi@ensiacet.fr (C. Albasi).

https://doi.org/10.1016/j.scitotenv.2021.151109

the controversial role in fouling mitigation/increase are discussed. Lastly, it encompasses several coagulant dosing control systems and their applications in the pilot to full-scale facilities to save coagulants and optimize the P-removal performance.

Contents

Nomenclature

ANO	autotrphic nitrite-oxidizing bacteria;
AOB	ammonia oxidizing bacteria;
A/O	anoxic-oxic;
A^2/O	anaerobic–anoxic-oxic;
AnMBR	anaerobic MBR;
ASMs	activated sludge models;
ATP	adenosine triphosphate;
AFO	amorphous ferric oxyhydroxide;
ASF	active site factor
ANN	artificial neural network;
BOD	biological oxygen demand;
BEMR	bioelectrical membrane bioreactor;
BNR	biological nutrient removal;
BAF	biologically aerated filter
CASP	conventional activated sludge process;
CPP	chemical precipitation process;
C/N	carbon to nitrogen ratio;
COD	chemical oxygen demand;
DAF	dissolved air floatation;
DNN	deep learning neural network;
DNN-GP	dual N/denitrification (Gao-PAOs)
DO	dissolved oxygen;
DPAOs	denitrifying PAOs;
eFAST	extended fourier amp. Sensitivity test
EPS	extra polymeric substances;
EU	European Union;
EEM	excitation emission matrix;

EQI	effluent quality index;
EBPR	enhanced biological P-removal;
F/M ratio	food to micro-organism ratio;
FTIR	Fourier transformed infrared spectrum;
GAOs	glycogen accumulating organisms;
GFC	gel-filtration chromatography;
HRT	hydraulic retention time;
HF	hollow fiber;
HSG	hochschulgruppe;
HFO	hydrous ferric oxides;
KOH	DO half-saturation coefficient;
MeP	metal phosphate
IWA	International Water Association
MeOH	metal hydroxide
MBR	membrane bioreactor
MLSS	mixed liquor suspended solids
MT	multi-tubular
MABR	membrane aerated bioreactor
MMBR	microalgae membrane bioreactor
MLE	modified Luzack-Ettinger
ML	mixed liquor
NOB	nitrite-oxidizing bacteria
OHO	ordinary heterotrophic organisms
OH^-	hydroxyl radical
OCI	operating cost index
PO_4^{3-}	orthophosphate
PI	proportional integral
PID	proportional–integral–derivative
PFC	polymeric ferric chloride
PAOs	phosphate accumulating organisms
PHA	polyhydroxyalkanoates
PHB	poly-hydroxybutyrate
PSD	particle size distribution
RM	real municipal wastewater
RIS	resistance in series
sMBR	submerged MBR
SCM	surface complexation model
SRT	sludge retention time
SMP	soluble microbial products
SAM	sequencing anoxic-anaerobic membrane
SEM	scanning electron microscope
SM	synthetic municipal wastewater
SRC	standardized regression coefficient
SCADA	supervisory control & data acquisition
TP	total phosphorous
TSS	total suspended solids
TMP	transmembrane pressure
TUDP	Technical University of Delft phosphorus
UCT	University Cape Town
VIP	Virginia institute process
VFA	volatile fatty acids
WWTPs	wastewater treatment plants(s)
WEF	Water Environment Federation

1. Introduction

1.1. Phosphorus removal regulation context

Rapid urbanization, coupled with industrial and agricultural sector growth, has increased nutrients in the effluent of wastewater treatment plants (WWTPs) and thus in the receiving water bodies. Higher nutrients concentrations exceeding the minimum permissible limits, among which phosphorus, is largely responsible for eutrophication. It deteriorates the aquatic environment due to excessive algal growth and depleting oxygen, making water habitat unsuitable for marine life. Depending upon the flow and fraction of extraneous domestic wastewater, phosphorous (P) concentrations range between 1 and 20 $mgP_{tot}L^{-1}$, and vary seasonally from region to region (Gray, 2004; Henze et al., 2008; Sayi-Ucar et al., 2015). Release of phosphorus above 0.1–0.2 $mgP_{tot}L^{-1}$ in running water and 0.005–0.01 $mgP_{tot}L^{-1}$ in stagnant water is highly assistive for eutrophication (Omwene et al., 2018; Rahman et al., 2016). Therefore, majority of the countries have set their national regulatory discharge limits in the range of 1–2 $mgP_{tot}L^{-1}$ with few exceptions such Japan and Belarus (Table A.1). Generally, effluent discharge limits are set based upon total phosphorus (TP) concentration. Since eutrophication is predominantly caused by the bioavailable fraction of phosphorus (phosphate, PO_4^{3-}), it is necessary to determine the permissible values of these bioavailable forms (Preisner et al., 2020). Keeping this in view, it is anticipated that many countries will introduce more stringent regulatory measures in the upcoming years, and the existing WWTPs might require upgradation to meet the required discharge limits.

1.2. Phosphorus in wastewater and its removal by treatment processes

The primary sources of phosphorus in the domestic wastewater are households (van Puijenbroek et al., 2019) with human excreta contributing about 30–50% while Gomes de Quevedo and da Silva Paganini (2016) reported that detergents are the main contributors with 20–80% of the phosphorus load. Generally, TP in wastewater is classified based upon its physical characteristics into soluble (can pass through 0.45 mm filter) and particulate fractions (Gu et al., 2011). Different analytical approaches have been developed for better characterizing the phosphorus including colorimetry, digestion, acid hydrolysis and particle size distribution (Gu et al., 2011; van Nieuwenhuijzen et al., 2004). In order to better choose the technology, unit operations and appropriate configurations for TP removal from the wastewater, a comprehensive understanding of the phosphorus fractions is essential (Gu et al., 2011; Yu et al., 2021). In a detailed fractionation approach, TP can be studied under a total of 17 fractions. Among these, 6 can be directly measured from wastewater samples while the remaining 11 could be calculated from the results of 6 different analyses (Gu et al., 2011; Reynolds & Davies, 2001) as depicted in Fig. 1. There is no standardized and universally accepted approach for classifying the phosphorus fractions and there is urgent need to address this issue along with the standardizing notations of each fraction and corresponding testing method (Rosario et al., 2021). For convenience, TP is generally classified into three major classes i.e. orthophosphate (PO_4^{3-}), polyphosphate (Poly-P) and organic phosphate. According to Rossle and Pretorius (2001), orthophosphate (PO_4^{3-}) is the most abundant in domestic wastewater and constitute about 70–90% in the raw and settled wastewater while other fractions are limited to 10–30% of the total phosphorus.

The phosphorus concentration in raw municipal wastewater tends to change due to lifestyle, urbanization, and industrial development. It has been estimated that around 3 million tons (Mt)/annum is lost as human waste, and only 1.3 Mt /year is treated by the WWTPs (Van Vuuren et al., 2010). Different technologies target a particular fraction of the phosphorus via chemical, biological, or combined treatment processes (Gu et al., 2011). Majority of the commercially available technologies can remove about 30% of the BioP, but high costs remain a major challenge (Ramasahayam et al., 2014). Furthermore, Phosphorus is a limited and non-renewable mineral resource. Globally, around 20 Mt/annum of phosphorus is mined, and due to this increasing consumption, phosphorus availability is projected to hit the low availability limits by the next 50–100 years, and the peak is expected to occur by 2034 (Azizi, 2018; Cordell et al., 2009). This emphasizes the recovery of phosphorus from the wastewater, which is estimated to be sufficient to meet 15–20% of the global phosphorus demand (Cordell et al., 2009). Keeping this view, Sweden has introduced regulatory criteria to recover 75% of the phosphorus from the WWTPs (Bashar et al., 2018).

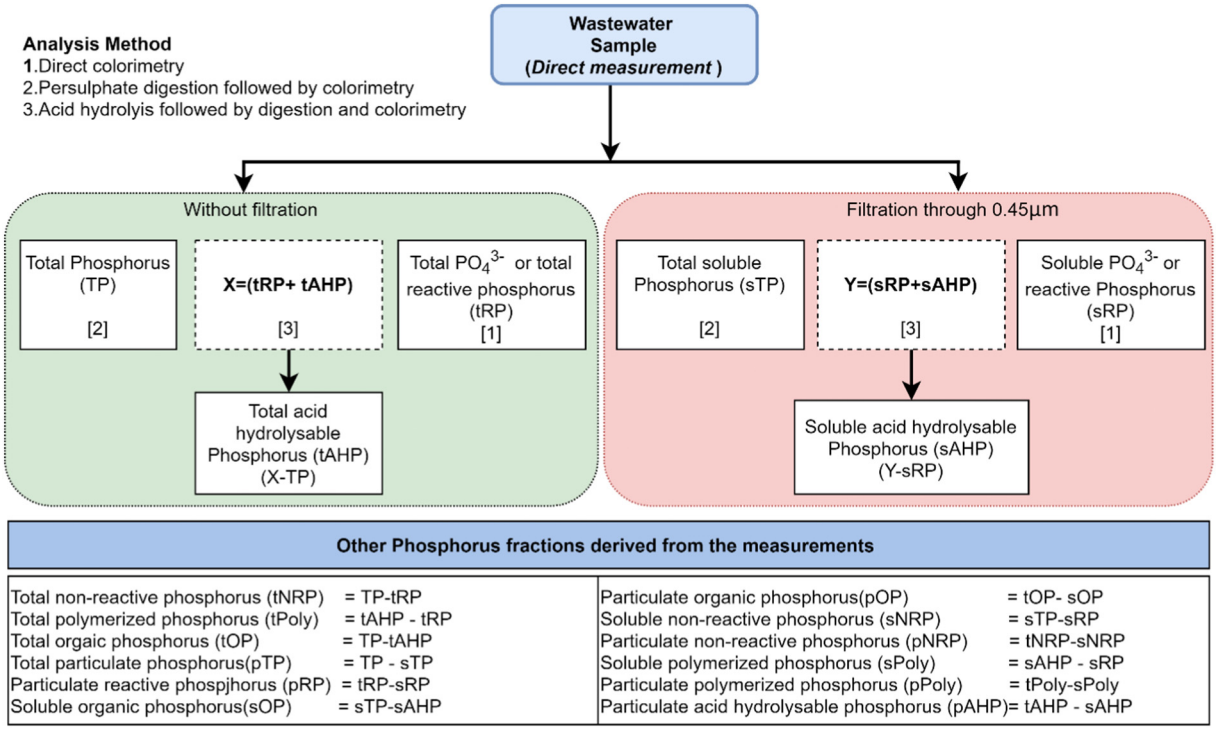

Fig. 1. Fractions of phosphorus in wastewater (modified from Gu et al., 2011).

Phosphate removal before discharging can be accomplished using various treatment methods such as physio-chemical, biological, and combinations thereof (Hai et al., 2018; Henze et al., 2008). Biological treatment is commonly used for domestic wastewater treatment at large-scale WWTP. Generally, BioP-removal efficiencies varied from 58.2% to 93.9% for full-scale EBPR facilities (Bunce et al., 2018; Zhang et al., 2011) and this large variations is mainly due to the varying high COD/P ratio (28.6–196.2) in the domestic influents. While, for bench sale studies the P-removal efficiencies are reported up to 99% (Bunce et al., 2018; Denisova et al., 2020).

In the last two decades, MBRs have extensively been adopted in wastewater treatment for municipal and industrial applications (Judd, 2010; Krzeminski et al., 2017). The MBR system is superior over conventional activated sludge process (CASP) regarding its compactness (up to 50% less footprint), robustness, better and consistent permeate quality with excellent solids retention (less sludge production), increased volumetric loading due to operation at higher sludge retention time (SRT), independence from hydraulic retention time (HRT), better disinfection, biomass enrichment and flexibility of the process (Hai et al., 2018; Judd, 2010; Xiao et al., 2019). According to Meng et al. (2012), there were more than 2500 MBRs operating globally by 2013 and number was growing with a growth rate of 10.5%. As of today, globally there are around 62 super-large scales (>100,000 m^3d^{-1}) MBR facilities contributing to the treatment of more than 10 million $m^3.day^{-1}$ of wastewater (Xiao et al., 2019). Given its commercial success, the global size of the MBR market was valued at US$ 3.09 billion in 2020 and is forecasted to reach US$ 5.48 billion by 2028 at a compound annual growth rate of 7.02% (Emergen, 2021). The present article aims to establish a state of the art of the modeling, simulation and control of super-large scale MBR for P-removal.

1.3. Scientific context

Literature screening in the current work found that the earlier reviews on P-removal are focused on either identifying the factors affecting P-removal in wastewater (Mulkerrins et al., 2004), micro-organisms and pathways involved (Ahmed, 2012), or emerging technologies (Guo et al., 2014). Similarly, very few reviews are dedicated to assessing the applicability of the ASMs (modified/unmodified) for nutrient removal in full-scale CASP/MBRs (Fenu et al., 2010; Naessens et al., 2012a, 2012b; Ng and Kim, 2007). The Scopus database was explored with key terms for the P-removal in MBRs and for modeling studies conducted from 2000 onwards. A total of 240 publications were found, including 18 publications related to P-removal modeling in MBRs. Each of these publications was further analyzed, as depicted in Fig. 2, constituting the basis of this review article. Furthermore, also based on Scopus data, 442 patents have been granted in the domain of P-removal in submerged MBR and 82% of these are registered in the US. They are reported in Fig. 2. Their number evolution is similar to the one of publications.

Most of these reviews are focused on CASP and/or general P-removal in wastewater, and none of these reviews is comprehensive enough to address all aspects of biological and chemical P-removal and its modeling in MBRs. Modeling approaches have been used to optimize MBRs ranging from the lab scale to full scale (Ferrero et al., 2011; Verrecht et al., 2008). However, very few publications have been dedicated to assessing and optimizing full scale MBR plants for P-removal in particular. There is no published study devoted to modeling and optimizing the super-large scale MBR for P-removal.

Based on the articles considered in this review, the MBRs are able to achieve 70 – 99 % P-removal with optimum operational settings and by maintaining sufficient substrate for the phosphorus accumulating organisms (PAOs) for their normal growth (Abegglen et al., 2008; Ersu et al., 2010; Silva et al., 2012; Smith et al., 2014). Although, better performance is reported for the MBR systems as compared to CASP but P-removal in MBRs is still difficult (especially in wastewater with low F/M ratio) because of its functional specificities (e.g., longer SRT and decoupled HRT). It is also expensive as compared to CASP due to excessive recirculation between aerobic/anoxic and anaerobic zones (mixing in the anaerobic zone) requiring extra energy and thus additional operational cost (Daigger et al., 2010; Lee et al., 2009; Sun et al., 2013). A recent study conducted at full-scale MBR facilities estimated P-removal specific energy consumption as high as 71.0 $kWh(kgP_{tot})^{-1}$ (Wang, 2020). The cost of P-removal in MBR is higher than CASP mainly

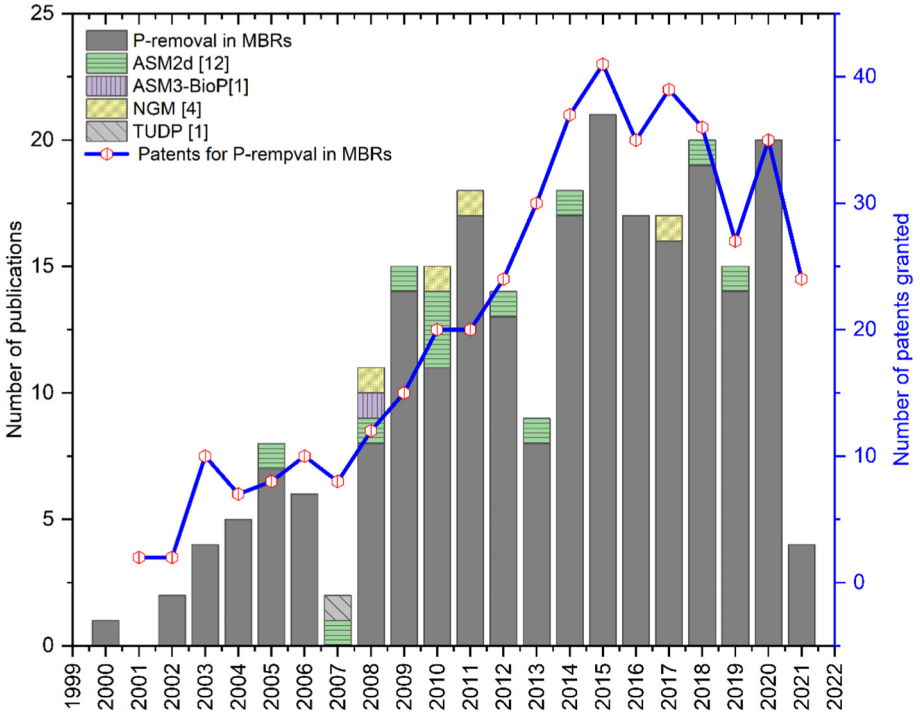

Fig. 2. Number of publications related to P-removal and modeling in MBRs.

due to higher aeration. The average removal cost of 1 kg P-removal in MBR varies from 39.8 to 480 US$ depending on influent load, plant configuration, aeration intensity and removal efficiencies. While, in CASP it costs between 13.30 and 101 US$/kg (Arif et al., 2020; Bashar et al., 2018; Iglesias et al., 2017). Generally, the super-large-scale MBR plants are operated as per the manufacturers' recommendations, and there has been limited research on their optimization for the nutrient removals.

This review focuses on assessing the applications of the existing mathematical models for biological and chemical P-removal in CASP and their applicability in MBRs ranging from pilot to full-scale. Section 2 includes a brief summary of the BioP-removal process in MBR compared to CASP, followed by an in-depth discussion on the role of various reactor configurations and their P-removal performance along with detailed discussion on factor affecting the P-removal in MBRs. Section 2.5 dedicated for assessing the applicability of the existing mathematical models for biological phosphorus removal. It also presents a summary of the MBRs specificities to be considered for their modeling. Furthermore, section 3 presents chemical P-removal process, factors affecting the chemical P-removal and its modeling using the existing models. The role of coagulants as a medium for chemical P-removal and fouling development or mitigation is also discussed in this section. Section 4 is dedicated to the role of various control systems used to optimize the P-removal in CASPs and MBR and corresponding operational cost reduction. Finally, the article concludes along with knowledge gaps and future research directions.

2. Biological phosphorous removal processes and its modeling

2.1. Enhanced biological P-removal (EBPR) in MBRs

P-removal process involves inducing phosphate incorporation into total suspended solids (TSS) and removing them via precipitation or filtration (Kim and Chung, 2014). Usually, a P_{tot}/TSS fraction of 2–5% is essential for BioP-removal in CASP, while this can be as high as 6–10% in MBR (Abegglen et al., 2008; Adam et al., 2002; Choi et al., 2011). This incorporation is generally accomplished through biological and chemical processes and combinations (Wilfert et al., 2015). No sharp limits exist between these methods to differentiate their performance when used in conjunction. For example, it has been observed that during the EBPR process, a significant part of the compound is chemically precipitated by the action of metal ions that were natural constituents of the wastewater (Wang et al., 2014). A carefully designed enhanced biological P-removal (EBPR) process may remove over 85–99% of phosphorus (i.e. Adam et al., 2003; Ramasahayam et al., 2014) and could even reduce the phosphorous concentration to less than 0.1 $mgPL^{-1}$ with the addition of external carbon source (Gnirss et al., 2003; Henze et al., 2008). The chemical precipitation processes can enhance the treatment efficiency of the biological WWTPs (Adam et al., 2003; Henze et al., 2008). However, it has the disadvantages of high chemical costs, chemical handling, storage requirements, increased chemically enriched sludge production, and subsequent sludge handling and disposal costs (Bunce et al., 2018; Chae et al., 2015). Stringent regulatory pressure and tight discharge limits have forced the WWTPs manufacturers and operators to develop and deploy efficient technologies to reduce the phosphorous discharge into water bodies (Gu et al., 2011; Vohla et al., 2011; Wadood and Sarmad, 2012).

MBRs can sufficiently remove the nutrient from the domestic wastewater and usually provide better results than CASP. Combining the EBPR with the MBR process reduces the reactor volume while achieving similar P-removal performance (Adam et al., 2003; Judd, 2010). MBR with 100% solids retention and chemical precipitation features could be a useful technology for phosphorus recovery, and further research should be dedicated to exploring the opportunities for P recovery. The understanding of the MBR functioning for the nutrient removal (P and N) is essential to design and optimize the P-removal through model based approaches. The experimental studies about the P-removal performance (along with the N removal) help to understand the process knowledge and to prepare a set of guidelines for a better adaptation of the available phosphorous models for the MBR.

2.2. MBR configurations and treatment sequence for P-removal

Traditionally, MBR is configured as submerged/immersed or side stream. In a submerged/immersed (sMBR) system, a membrane module

is installed within the bioreactor, and the treated effluent is withdrawn via negative pressure/vacuum. Air scouring is typically used to counter the cake layer formation, which can further be assisted through additional means such as filtration-relaxation sequencing, aeration sequencing and backwashing (Burman and Sinha, 2018; Hai et al., 2018). While, for the side stream configuration, the membrane is external to the bioreactor, and cake layer formation is mainly inhibited due to cross-flow-velocity (Hai et al., 2018; Judd, 2010). Novel configurations of the sMBR are based on an anti-fouling mechanism, such as a fixed-film membrane aerated biofilm reactor (MABR), bio-electrochemical MBR (BEC-MBR) or electrically-induced MBRs, microalgae membrane bioreactor (MMBR) which are yet being explored at the lab/pilot scale have not been included in this review. This review only focuses on sMBR along with the reactor configurations adopted for P-removal.

Several reactor configurations involving plug flow or strict compartmentalization, such as modified Ludzack-Ettinger (MLE), anoxic-oxic (A/O), anaerobic-anoxic-oxic (A^2/O), University Cape Town (UCT), modified UCT, Virginia institute process (VIP), and Bardenpho/modified Bardenpho with multiple stages processes, have been tried and tested for nutrient removal (Ahn et al., 2003; Ersu et al., 2008; Ersu et al., 2010; Hai et al., 2018; Monclús et al., 2010; Vaiopoulou et al., 2007; Zhang, 2020). The BioP-removal performance in this configurations mainly depends upon how the anaerobic reactor is maintained and protected from the nitrates interferences by controlling the internal recirculation. Table B.1 provides a brief description of each of the BioP-removal system configuration along with its advantages and disadvantages (Daigger et al., 2010; Fleischer et al., 2005; Hai et al., 2018). The roles of various zones involved in these configurations and dominating fractions of the microbial communities in these zones is summarized in Table B.2. The following section is dedicated to assess the performance of different configurations for BioP-removal in MBRs with capacity ranging from 0.01 to 45,000 $m^3.d^{-1}$.

Recycling oxygen-saturated mixed liquor from the membrane zone to the unaerated zone (anoxic/anaerobic) negatively impacts the denitrification process. Thus, the abundance of nitrates reduces the P-removal performance since the occurrence of anaerobic conditions is less likely at higher recirculation ratios. An increase in the recirculation ratio leads to higher effluent NO_3-N and PO_4^{3-} concentrations (Fleischer et al., 2005). This is due to the fact that denitrification and P-removal processes compete for the same carbon source as demonstrated by another study (Maere et al., 2011). Different recirculation arrangements and rates from the MBR tank to upstream reactors result in lower/higher MLSS upstream of the membrane tank, also responsible for nutrients removal (Dold et al., 2010). In the last 2 decades, several attempts have been made to improve the BioP-removal efficiency of MBR by modifying the conventional configurations and developing the novel ones with focus on: i) reduced nitrates interferences ii) reduced recirculation iii) simultaneous denitrification and EBPR and iv) reduced overall footprint of the reactor.

Early studies of Adam et al. (2003) and of Lesjean et al. (2003) evaluated the effect of pre and post denitrification on P-removal in UCT configuration. A lab-scale study of Adam et al. (2003) found similar P-removal (99% with coagulant addition) performances in both cases while lower recirculation was required in post–denitrification mode from MBR to aerobic zone. Similarly, the pilot-scale studies of Lesjean et al. (2003, 2005) found identical P-removal performances in both pre- and post-denitrification modes without external carbon source addition. The recirculations in the study of Lesjean et al. (2003) were same as of Adam et al. (2003) and in both studies precipitation was used to lower the effluent phosphorus below 0.1 $g \cdot m^{-3}$. Another pilot scale study (Fleischer et al., 2005) compared the nutrient removal performance of three configurations with multi-stage Bardenpho process. The 5-stage configuration was comparatively effective in BioP-removal, however it was unable to meet the required effluent discharge standard without addition of coagulant. The recirculation of oxygen-saturated mixed-liquor from the MBR tank to an anaerobic zone through the aerobic zone proved successful in improving P-removal. However, the proposed configuration involved multiple recirculation streams associated with higher flow rates, resulting in increased footprint and recirculation cost. In another study dedicated to evaluating different MBR configurations, Ersu et al. (2008) evaluated five different configurations (three modified A^2/O and two A/O). The modified A^2/O configuration with 300% recirculation of the MBR sludge (3 times the influent flow) to anaerobic zone and 100% permeate recirculation to anoxic resulted in higher P-removal efficiency (> 88%). However, recirculation of the permeate may not be an economical choice since energy consumption in MBR is already slightly higher than in CASPs (Krzeminski et al., 2017; Xiao et al., 2019). Another study (Lee et al., 2009) evaluated the UCT and modified UCT (with step feed to anoxic zone) configurations with weak domestic wastewater (low F/M ratio) and found that modified UCT-configuration provided better P-removal (> 70%) than UTC (40%). The authors concluded that feeding weak wastewater directly to the anoxic zone provided enough substrate to the denitrifiers to remove nitrates, and this resulted in improved P-removal performance of the MBR. Based upon the findings of these two full scale facilities with 4–5 stages Bardenpho process, Daigger et al. (2010) provided guidelines for designing MBR configurations to achieve the P-removal below regulatory level including: i) membrane recirculation flow should be directed to the aerobic zone, ii) intense mixing at the inlets of the anaerobic and anoxic zones, iii) consistent internal recirculation flow rates to maintain the desired MLSS distribution and iv) carefully controlled metal salt addition in proportion to the phosphorus remaining after biological removal. The study of Holba et al. (2012) presented a comparative assessment of three MLE configurations. The highest P-removal efficiency was achieved with 2-stage MLE having single internal recirculation from aerobic to anoxic zone and with addition of coagulant. The study of Corsino et al. (2020) evaluated the nutrient removal performance of pre-denitrification A/O configuration with recirculation of 500% (5 times of the influent flow) from aerobic to anoxic tank. The authors found that the novel layout is capable to remove 97% of the phosphorus with addition of external carbon source and without addition of coagulant.

Several efforts have been devoted to develop an innovative MBR with intermittent aeration and recirculation to provide anaerobic and anoxic conditions for proliferation of PAOs and to maximize the P-removal. The study of Ahn et al. (2003) proposed an innovative modification to MLE process by introducing an intermittently sequencing anoxic/anaerobic zone to alternate the anoxic conditions for denitrification and anaerobic conditions for phosphorus release. Anoxic conditions were imposed for 1 h after every 3 h, and anaerobic conditions lasted for two hours with no recirculation. During the anoxic stage, a recirculation ratio of 600% was maintained. This modified MLE improved the P-removal efficiency (93%) without coagulant addition and at much lower recirculation rates as compared to conventional MLE. Similarly, Zhang et al. (2006) investigated a cyclic aerobic, anoxic/anaerobic reactor for improved nutrient removal while reducing the number of recirculation streams, complexity and footprint of the system. The proposed configuration successfully removed 90% of the phosphorus without addition of coagulant and carbon source and even at low COD/TKN ratio with anaerobic-aerobic cycle time of 40 min and 120 min respectively. In another study, Ahmed et al. (2007) evaluated the impact of internal recirculation (IR) in sequencing anoxic/anaerobic membrane bioreactor (SAM). The authors found highest BioP-removal performance (55%) when the IR rate set to 2.5 times of the influent flow. The study of Yuan et al. (2008) introduced an innovative MBR with alternating anoxic and anaerobic environments for improved denitrification and P-removal. The proposed reactor consisted of a continuously aerated MBR and an alternating anaerobic and anoxic zone in two separate bioreactors. Controlling the recirculation flow from aerobic zone by control valves to either of these two bioreactors, anoxic and anaerobic conditions were implemented in two single tanks alternately. The authors found higher P-removal (> 94%)

without addition of carbon source and coagulant. However, the P-removal efficiency was found highly correlated to recirculation cycle time which may vary depending upon the influent load.

MLE and 4-stage Bardenpho configurations offer limited to moderate BioP-removal due to absence of the anaerobic zones essential for growth and proliferation of the PAOs responsible for phosphate consumption and therefore coagulant addition is required to eliminate the phosphorus below the regulatory limits. While, A/O or Pho-redox configuration provided moderate to high P-removal performances depending upon, operational conditions, influent characteristic, introduction of sequencing anaerobic/anoxic conditions and controlled intermittent recirculation. A^2/O, 5-stage Bardenpho (with anaerobic as influent receiving zone), step-feed Bardenpho, UCT, MUCT and VIP configurations offer high to excellent BioP-removal performances. Table 1 depicts that the majority of the full-scale MBR facilities are equipped with MLE configuration and similar results have been documented by Pellegrin et al. (2015). This is due to fact that the CASPs with MLE configuration were upgraded to MBRs (Itokawa et al., 2014).

Bardenpho is the second widely used configuration at full-scale MBR facilities. Whereas, UCT and MUCT configurations are widely used for research studies at bench and pilot scales mostly with synthetic wastewater. This presents an opportunity to conduct more studies in this domain to fully assess the capabilities of innovative MBR configurations for simultaneous carbon and nutrient removal as required by the MBRs in majority of the cases in full-scale applications. Apart from the design configurations, P-removal in MBR is also affected by several other factors discussed in detail in Section 2.3.

2.3. Factors affecting the BioP-removal in MBR

In order to improve the P-removal mechanism as well as its prediction by mathematical model, a comprehensive understanding of the parameters affecting the BioP-removal is essential. There are limited numbers of MBR specific publications documenting the effect of SRT, HRT, feed composition and availability of VFA, DO concentrations, various recirculations, bacterial community (including PAOs/GAOs), alkalinity, pH, temperature, and other associated process and design parameters for BioP-removal. It is established that the BioP-removal in CASPs and the modified CASPs (such as MBR) are critically sensitive to various parameters such as SRT (Mulkerrins et al., 2004; Tchobanoglous et al., 2002; Wang et al., 2015). Since MBR is an extended version of the CASP replacing the secondary clarifiers by the membranes to retain 100% suspended solids, thus providing superior P-removal than CASP (Cho et al., 2005). Factors affecting the P-removal process in MBRs have been analyzed considering the various configurations of the WWTPs ranging from lab to large-scale applications from the reviewed publications.

2.3.1. Feed characteristics

COD is a limiting factor for the BioP-removal in the MBR process. It serves as a substrate for the microbial community (specifically PAOs) and can impede the removal efficiency if not available in the required concentration (Kapagiannidis et al., 2012; Park et al., 2019). For MBRs, a minimum COD/P ratio of 40–45 is required for effective P-removal (du Toit et al., 2007). Low PO_4^{3-} concentration in the influent resulted in higher P-removal efficiency in MBR. It was also found that increasing

Table 1
P-removal performance of various MBR configurations.

Configuration	Plants assessed	Wastewater type	Capacity ($m^3.d^{-1}$)	Influent TP ($g \cdot m^{-3}$)	BOD/TKN ratio	SRT (days)	HRT (hours)	Coagulant addition	P-removal (%)	Reference
2-stage MLE	1	Municipal	0.50	4.2	17.75***	40–45	16	YES	83	Holba et al., 2012
	7	Municipal	125–2140	2.7–4.1	1.1–3.5	n.a.	10–40	NO	50–68	Itokawa et al., 2014
	2	Municipal	1000-4200	2.90	0.1–1.1	n.a.	10–40	YES	65–92	Itokawa et al., 2014
	5	Municipal	1100–16,000	2.8–4.9	1.7–2.6*	37–45	8–9.2	YES	89–97	Chae et al., 2015
	1	Municipal	7000	7.0	4.30*	n.a.	n.a.	NO	60	Gabarrón et al., 2015
2-stage MLE (SAM)	1	Synthetic	0.01	3.66	6.52*	70	n.a.	NO	93	Ahn et al., 2003
3-stage MLE (cascade)	1	Municipal	6520	3.9	7.90*	14–21	3.5–5	NO	78	Fenu et al., 2010
	1	Municipal	60	7.8	10.86***	30–75	42	YES	45.9	Holba et al., 2012
	1	Municipal	30	10.6–18.3	8.9***	30–55	34	YES	27	Holba et al., 2012
A2/O	1	Synthetic	0.264 (1)	11.4	6.92	25	14	NO	59.1	Ersu et al., 2008
	1	Synthetic	0.264 (2)	11.4	6.92	25	14	NO	88.1	Ersu et al., 2008
	1	Synthetic	0.264 (5)	11.4	6.92	25	14	NO	58.7	Ersu et al., 2008
	1	Synthetic	0.083	5.5	5.25*	n.a.	10	YES	90–95	Banu et al., 2009
	1	Municipal	~45,000	3.3	7.87**	25	17	YES	93.9	Wang et al., 2018
	2	Municipal	500–2400	8.0	7.20**	18	n.a.	NO	74	Yılmaz et al., 2020
4-stage Bardenpho	1	Municipal	75	5.5	3.8	27	27	YES	99.45	Fleischer et al., 2005
5-stage Bardenpho	1	Municipal	42,000	5.4	6.5*	14	12.6	YES	99.07	Daigger et al., 2010
Step-feed Bardenpho	1	Municipal	33,000	8	5.95	10	8.9	YES	99.13	Daigger et al., 2010
A/O (Sequencing)	1	Synthetic	0.024–0.072	4	3.4–28	n.a.	7.3–22	NO	90	Zhang et al., 2006
A/O (sequencing)	1	Synthetic	0.096	6	10***	20	9.6	NO	94.1	Yuan et al., 2008
A/O (SAM)	1	Synthetic	0.01	5.7	7.09	50	8	NO	55	Ahmed et al., 2007
A/O/Phoredox	1	Municipal	30	20	5.1–10.5	n.a.	72	NO	70–90	Abegglen et al., 2008
A/O (modified)	1	Synthetic	0.264 (3)	11.4	6.92	25	14	NO	44.6	Ersu et al., 2008
A/O (modified)	1	Synthetic	0.264 (4)	11.4	6.92	25	14	NO	42.7	Ersu et al., 2008
A/O (Modified)	1	Synthetic	0.103	11–12.4	11–13.3	35–40	14.4–24	NO	97	Corsino et al., 2020
UCT	2	Municipal	0.01	8.4–10.5	10–14	15	18–21	YES	99	Adam et al., 2003
	2	Municipal	0.01–0.122	3–7.5	4.5–5.5	15–26	11–18	YES	90	Lesjean et al., 2005
	1	Synthetic	lab-scale	8.8	7.97*	35	5	NO	39.8	Lee et al., 2009
	1	Municipal	3–4.2	3.63◇	5.7	15–22.6	n.a.	NO	80	Monclús et al., 2010
	1	Municipal	0.616	4	1.93	n.a.	15.4	NO	60	Cosenza et al., 2013
	1	Municipal	19–26	5.39	4.67	20	7	NO	94.1	Smith et al., 2014
	1	Synthetic	0.012	4.7	7.07*	25	18	NO	82	Sun et al., 2019
	1	Synthetic	0.012	4.63	6.5*	25	18	YES	95	Sun et al., 2019
MUCT [step feed]	1	Synthetic	lab-scale	8.2	7.46*	37	5	NO	72.5	Lee et al., 2009
MUCT (sequencing)	1	Synthetic	0.011	8.2–11.3	4.3–5.2*	15	11–13	NO	75.2	Zhang et al., 2009
Modified VIP	1	Municipal	32,000	6.2	5.11	7.8	n.a.	YES	93.87	Daigger et al., 2010

* COD/TN ratio.
** BOD/TN ratio.
*** COD/NH_4-N, ◇PO_4^{3-}.

the influent PO_4^{3-} from 20 to 80 mgL^{-1} increased the sludge production from 2 to 6.2% (Choi et al., 2011). A recent A^2/O MBR study has investigated that high P-removal (82.6%) can be achieved with a low C/P ratio (29) and relatively high nitrate (5.6 NO_3-N mgL^{-1}) concentration (Falahati-Marvast and Karimi-Jashni, 2020) by the combination of assimilation and EBPR processes. Sometimes despite having a favorable COD/P ratio, P-removal is still compromised due to overloading and consequent decay of PAOs due to limited aeration (Abegglen et al., 2008). In the study of Oehmen et al. (2007) it was found that a COD/P ratio lower than 50 mgCOD/mgP favors the growth of GAOs, and the same was experienced by Monclús et al. (2010) in their UCT type MBR pilot plant.

Theoretically, 7–12 mg of VFAs are required to remove 1 mg of PO_4^{3-} through EBPR in CASP, and this VFA/PO_4^{3-} can be high as 20 depending upon the soluble fraction of COD in municipal wastewater (Al-Atar, 2007; Janssen et al., 2002; Monti et al., 2007; Mulkerrins et al., 2004). Typically municipal wastewater is VFA deficient, while MBR operated at high MLSS/higher SRT would require an external carbon source (ethanol) in the anaerobic zone or side stream P-recovery unit for effective P-removal (Monti et al., 2007).

Typically, a BOD/P ratio of 20 is considered a minimum requirement for better P-removal efficiencies in MBR studies dealing with municipal wastewater (Adam et al., 2003), However, this could go as higher as 45 and are still favorable for biological P-removal (Fleischer et al., 2005). It has been validated under a study (Wang, 2020) conducted to evaluate the nutrient removal performance of 11 full-scale MBR facilities located in China wherein the BOD/P ratio was found in the range of 12.22–36.94, and eight MBR facilities performed good P-removal due to the BOD/P ratio > 20. However, an external carbon source was still essential for total nitrogen removal.

In addition to COD/P or BOD/P, it was investigated that a low COD/N ratio between 5.3 and 7.3 resulted in satisfactory P-removal (Wang et al., 2015), while in a more recent study, it is found that low C/N ratio decreased P-removal (Mannina et al., 2020). A lower BOD/TKN ratio may result in poor denitrification and remaining nitrates, thus negatively impacting the overall nutrient removal capabilities of MBR. External addition of carbon source in these systems become essential (Fleischer et al., 2005). Several studies with PAOs have also confirmed that elevated concentrations of nitrite negatively affect phosphorus uptake activities of PAOs under both aerobic and anoxic conditions (Saito et al., 2004). When there is limited nitrate availability, ordinary heterotrophic organisms (OHOs) outcompete PAOs for nitrate, and there is a low impact on the EBPR process.

From all these considerations, it may be concluded that the optimum range of COD/P is around 40 and C/N in between 5.3 and 7.3. MBR is adapted to treat wastewater with high P and N contents with COD/TN/TP ratio in the range of 100/28.5/1.16–100/11/0.87 compared to conventional limit of 100/5/1 (Ersu et al., 2008), This is probably explained by the fact that the total bacteria and nitrogen-cycling groups in the MBR sludge are different than CASP (Wan et al., 2011).

2.3.2. MLSS concentration and P-removal in MBR

MBR operates at quite high MLSS concentrations (4000–15,000 $g \cdot m^{-3}$), which lowers the oxygen transfer rate due to increased viscosity and increase aeration expense (Judd, 2010). Thus, an adjustment in the oxygen transfer coefficient is needed for MBR modeling studies (Germain et al., 2007; Insel et al., 2011). Furthermore, sludge mass is disproportionate through the reactor length as the MLSS concentration in the downstream zone (membrane tank) is higher as compared to upstream zones of the MBR, and this is regulated through excessive inter-reactor recirculation to achieve uniform MLSS concentrations for better biological nitrogen and P-removal (Ramphao et al., 2005). Several studies found that the higher MLSS concentration had little to no effect on P-removal kinetics. Thus, parameters used for ASMs could be applied to MBR systems (Adam et al., 2003; Holakoo et al., 2005; Parco et al., 2007). It was further concluded that the complete solids retention by the membrane might change the microbial population and thus impact the growth kinetics (Parco et al., 2007). Another study found that P-removal was positively affected by increasing the MLSS concentration to a certain level (7 g/L optimum), and beyond this, P-removal was negatively impacted possibly because of the higher fraction of the dead biomass due to higher SRT (Wang et al., 2015).

Besides, it has been further investigated that the SMPs inhibit the anaerobic uptake of PAOs in CASP (Ichihashi et al., 2006). It was also later observed and confirmed by Jiang et al. (2009) for MBR with two batch tests. The results were similar to the previously experienced in case of CASP. Based on these results, the authors recommended to design and to operate MBRs at lower SRTs to avoid the production and accumulation of the SMPs onto the membrane surface. This inference is based upon only two tests and it is therefore advised to conduct more studies to explore the relationship between the SMPs and P-removal performance of the membrane, while keeping in mind the role of SMP in membrane fouling, and the role they could play in P retention (Gao et al., 2004).

2.3.3. Microbial communities and P-removal in MBRs

Autotrophic nitrifying bacteria and heterotrophic bacteria (GAOs respiring nitrates) compete for their growth under the same operating conditions while it is commonly accepted that the level of BioP-removal is directly proportional to the number of PAOs present in the system. EBPR is a tailored process for BioP-removal based upon PAOs property of intracellular accumulation of phosphate in poly-phosphate (Poly-P) form under cyclic anaerobic-aerobic (mainly anaerobic). Accumulated phosphorous is then carried away with the extracted sludge (Lesjean et al., 2003) as presented in Fig. 3. Since PAOs can store excess phosphorus in the form of polyphosphate (poly-P) granules in their bacterial cells after their metabolic demand would be satisfied. Whereas, P-removal by the assimilation phenomenon (which takes place only during growth process) by non-PAO biomass is limited to 15–30% (Lesjean et al., 2009; Monclús et al., 2010; Ramasahayam et al., 2014). The COD serves as a substrate for the growth of PAOs, providing them volatile fatty acids (VFAs) for consumption and synthesis of the poly-hydroxybutyrate (PHB while PHA when considering the role of only specific PAO class known as “Candidatus Accumulibacter phosphatis”) by releasing phosphorus and degrading the glycogen under anaerobic conditions. In the second step, phosphorus is taken up by the PAOs at higher rates in the presence of the excess oxygen provided for the oxidation of the PHBs/PHA with an injection of the influent at the anaerobic zone (Mulkerrins et al., 2004; Zhang et al., 2018). In order to meet the required phosphorus discharge target through relying only upon the proliferation of PAOs is not practiced (PAO communities remain very low) and even hardly possible for the large-scale MBR facilities (de-Bashan and Bashan, 2004).

In addition to phosphate uptake under aerobic environment by the PAO, it is also consumed by the DPAO (Kishida et al., 2006) in the anoxic environment where they consume nitrates and enhances the overall P-removal efficiencies. In addition to the aerobic zone in the MBR process, the membrane is intensively aerated to avoid fouling issues. This aeration also improved the P-removal efficiency as no P-release occur during the effluent production, unlike CASP. Furthermore, complete retention of solids in MBR helps to reduce the TP concentration in the effluent (Monti et al., 2006).

Other carbon growing micro-organism like GAOs also consume VFAs without contributing to P removal. GAOs found in pilot and full scale EBPR system are reported to cause nutrient limited conditions due to higher consumption of substrate available for proper proliferation of PAO organisms (Oehmen et al., 2007; Silva et al., 2012). MBRs are generally operated at higher SRTs (> 20 days) and low F/M ratio, which creates starvation conditions for micro-organisms resulting in inactivation or even death of PAOs and thus reduces sludge activity (Han et al., 2015; Yilmaz et al., 2007). Minimizing the GAOs concentration in the EBPR

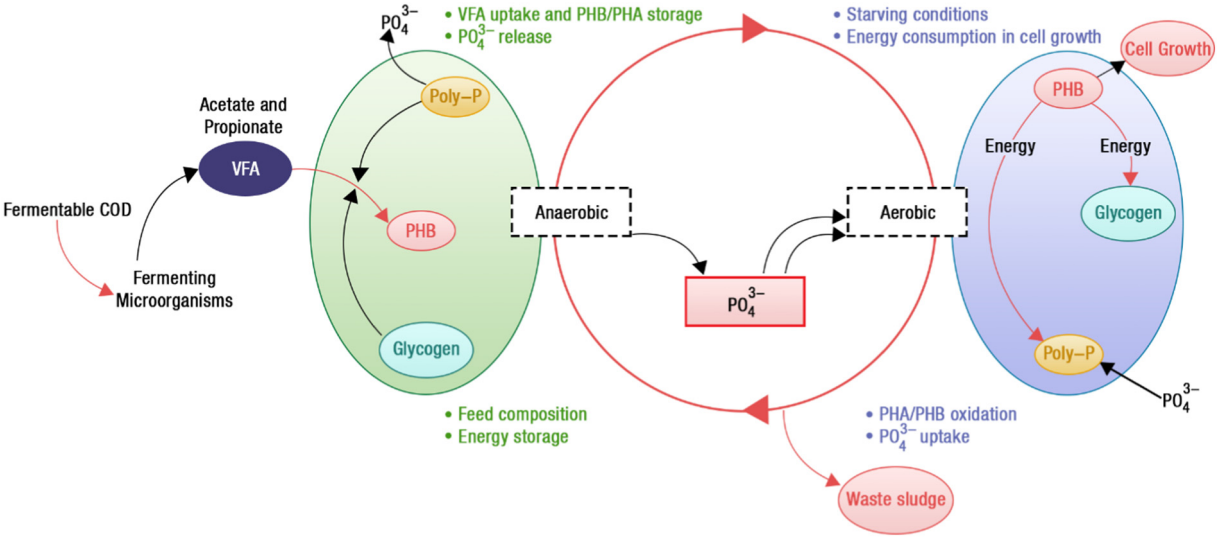

Fig. 3. PO_4^{3-} removal by the EBPR process under anaerobic/aerobic environment.

process in MBR may result in achieving higher P-removal efficiencies in the laboratory and pilot-scale systems.

Most of the studies at the laboratory and pilot scale systems have demonstrated that minimizing the GAOs concentration in the EBPR process in MBR resulted in achieving higher P-removal efficiencies. On the contrary, another study conducted at full-scale investigated the role of PAOs and GAOs for P-removal and concluded that GAOs do not appear to be a problem. Explanation of this could be due to the presence of competing DPAOs. It is, therefore, essential to rethink the PAO-GAO interaction for full-scale plants (Stokholm-Bjerregaard et al., 2017).

Furthermore, there is a conflict between the factors that govern nitrifying bacteria and PAOs. Nitrifiers (GAOs) have a slow growth rate and need a longer SRT (> 5 days)) to grow, while the PAOs favor a shorter SRT ranging between 3 and 5 days (Onnis-Hayden et al., 2011). A longer SRT in MBRs means low net PAO biomass growth and thus limited phosphorus storage in new cell material and the system. PAOs need to be exposed to alternating anaerobic and aerobic conditions and thus are favored through the recycle streams, while the nitrifiers are maintained in the aerobic tank. Findings of the available studies have concluded that the type and amount of carbon source, pH, and temperature significantly affect the balance between PAOs and GAOs (Song et al., 2008).

Higher PAOs and DPAOs concentration help to achieve higher P-removal efficiency in MBR (Cho et al., 2005). It has been found that PAOs concentration in municipal wastewater varies from 0 to 1% of total COD (Sun et al., 2013), while in the sludge, the concentration of the PAO can be up to 7–10% of the total biomass (Mao et al., 2015; Silva et al., 2012). The PAOs can store up to 0.17 gP/gTSS, which is comparatively much higher than what can be typically stored in the sludge mass (0.015 gP/gTSS) (Henze et al., 2008). In a UCT–type, MBR operated with weak and strong wastewater to analyze the phosphorus uptake in an anoxic zone. DPAOs played a vital role in phosphorous removal, along with nitrogen. The removal rate in the anoxic zone was higher for high strength wastewater than weak wastewater and thus indicated that up to 40% phosphorus could be removed through P-uptake (Lee et al., 2009).

The roles of GAOs and PAOs have been studied for CASP full-scale plants, but studies for full-scale MBR with higher SRT are still missing. SRT and carbon sources seem to be determinant parameters in previous studies.

In the early interpretation of the EBPR, the *Acinetobacter* was considered as the only class of PAOs responsible for accumulating phosphorus in WWTPs (Barnard et al., 2017). By the late 1990s, understanding of the EBPR expanded, and it was found that the microbial class "Candidatus Accumulibacter phosphatis" are primary organisms responsible for PAO characteristics (Liu et al., 2019). Several mathematical models; including, ASM2/ASM2d, TUDP, Barker and Dold's, and UCTPHO$^{+,}$ are based upon the functional working of "*Candidatus Accumulibacter phosphatis*" for P-removal (Hauduc et al., 2013; Ni et al., 2010) and competition between the PAOs and GAOs is not considered. The study of Mielczarek et al. (2013) investigated 28 Danish EBPR based WWTPs and reported that 27% of the PAOs are "*Tetrasphaera*". Similarly, Stokholm-Bjerregaard et al. (2017) studied 19 full-scale EBPR based WWTPs and found similar results to Mielczarek et al. (2013) with "*Tetrasphaera*" as the most abundant PAO accounting for 10.7% of the total active biomass. The most recent research conducted on 32 full-scale wastewater facilities located in 12 different countries found that "*Tetrasphaera*" is the most abundant (Nielsen et al., 2019) and confirmed the findings of the previous studies conducted on a full-scale. Apart from the *Accumulibacter, Acinetobacter,* and *Tetrasphaera*; other genera of PAOs are *Aeromonas*, *Enterobacter, Moraxella, Klebsiella, and Pseudomonas* (Mielczarek et al., 2013; Stokholm-Bjerregaard et al., 2017).

At lab-scale, mainly "*Candidatus Accumulibacter phosphatis*" were found, whereas at full-scale, *Tetrasphaera* were the most abundant microbial community. This could affect the mechanisms of P-removal at these different scales and their modeling and therefore require further research and improvements in the ASM models as far as the role of PAOs is concerned.

2.3.4. Sludge retention time and P-removal in MBRs

SRT may influence the sludge characteristics, such as viscosity, biomass concentration, microbial community's composition, floc size, viscosity, and cell surface properties (Hocaoglu et al., 2011). The effect of SRT on P-removal in MBRs is still conflicting in the literature. It was initially believed that BioP-removal is difficult to achieve at higher SRTs as experienced in MBR; however Adam et al. (2003) first demonstrated that P-removal could be achieved in MBR operating at even higher SRTs with influent having a higher VFA/P ratio.

Some other studies have reported even superior (> 90%) BioP-removal at longer SRTs (25–75 days) in MBR systems with and without sequencing anoxic/anaerobic functioning (Ahn et al., 2003; Cho et al., 2005; Ersu, 2006). As such, there may be an optimum SRT needed for nutrient removal in an MBR. The evaluation of full-scale MBR facilities showed unexpected high BioP-removal operating at higher SRTs and technically not designed for EBPR. No explanation was provided for this peculiar behavior (Silva et al., 2009). Higher SRTs helped in lowering the rate of phosphate release during PHA storage (Adam et al., 2003;

Nopens et al., 2007; Rosenberger et al., 2000; Sun et al., 2019) and thus negatively affecting the P-removal due to higher growth of AOB (higher NO_2 production) which lead to compromise the functioning of heterotrophic non-PAOs and PAOs as explained by Mannina et al. (2020). Whereas Lesjean et al. (2009) found that higher EBPR in MBR can be achieved even at higher SRT. Based on these conflicting studies, it can be assumed that others parameters are more impacting than SRT, and it is difficult to ascertain the role of SRT in P-removal in MBRs.

2.3.5. Hydraulic retention time and P-removal in MBRs

There are limited studies focused on documenting the effect of anaerobic and anoxic HRTs on P-removal in MBRs. The study presented by Cho et al. (2005) evaluated the performance of a sequencing anoxic/anaerobic MBR through varying HRTs and flux. The authors found higher P-removal at shorter anaerobic HRTs (1 h) due to higher substrate loading. The same authors further found that, the membrane fouling increased with increasing flux linked with shorter HRT. Another study (Monclús et al., 2010) supported the same argument wherein insufficient anaerobic HRT (0.921–2.05 h) reduced the conversion of readily biodegradable substrates to stored PHA and negatively impacted the P-removal due to reduced activity of PAOs for phosphate accumulation.

In another study (Song et al., 2008), the effect of change in HRT on P-removal in MBR was evaluated. The authors found that shorter HRT between anoxic and anaerobic induced a higher F/M ratio and increased biomass yield activity, especially in denitrification rate, which then improved P-removal efficiency. Similarly, Brown et al. (2011) reported that an optimal anaerobic HRT (2 h) is needed for PAOs to actively uptake the phosphate and PHA and use it as an energy source. While, Sun et al. (2013) found better P-removal efficiency with an overall higher HRT (11.6 h) and with anaerobic HRT (3.3 h). Most recently, a lab-scale MBR treating domestic wastewater has been investigated at higher HRT (9.6 h) and resulted in higher P-removal (Sözüdoğru et al., 2021). While, in another recent study (Falahati-Marvast and Karimi-Jashni, 2020), it has been found that P-removal in A^2/O-MBR slightly improved with reduction of aerobic HRT from 12 h to 6 h, presumably due to an increased biomass concentration at constant F/M ratio and under controlled temperature. The aerobic HRT does not seem to impact the P-removal, although it be must be maintained within a 6–12 h. While increasing anaerobic HRT (within range of 2–6 h) improved the P-removal to a certain limit where denitrification (by DPAOs) would be favored.

2.3.6. Effect of temperature on P-removal in MBRs

There are conflicting results from various studies documenting the effects of temperature on P-removal. A temperature ranging between 10 and 25 °C resulted in better P-removal, and inconsistencies have been found at high temperatures around 40 °C (Liau et al., 2015; Sayi-Ucar et al., 2015). Another study confirmed that beyond 90% P-removal could be achieved with 10 °C operating temperature (Wei et al., 2012). According to another study, PAOs are lower-range mesophiles or psychrophiles and are predominated only at 20 °C or lower temperature ranges. While on the other hand, GAOs are somewhat mid-range mesophilic organisms with an optimum temperature between 25 °C and 32.5 °C (Panswad et al., 2003).

2.3.7. Dissolved oxygen concentration and P-removal in MBR

To strike a balance between the required oxygen supply for nitrifiers in the aerated tank and creating an enabling environment for PAOs, a DO level of 2 mgL^{-1} is recommended (Hai et al., 2018). It has been found that too low (0.4–0.6 mgO_2L^{-1}) and too high (2.0–2.4 mgO_2L^{-1}) DO concentration has adverse effects on P-removal in MBR (Roberts, 2020). Similarly, Smith et al. (2014) found improved P-uptake in the aerobic reactor with DO concentration maintained at 2 mgL^{-1}. Another study (Fu et al., 2009) with A/O-MBR demonstrated that a concentration of 2.5 mgO_2L^{-1} is enough to remove almost 90% of the phosphorous. At concentration lower than 2.5 mgO_2L^{-1}, PHB stored in PAOs could not be decomposed effectively because of DO deficiency in the aerobic tank. Thus, no enough adenosine triphosphate (ATP) was produced, which led to the restraint of excessive phosphorus uptake of the continuous PHB accumulation in PAOs. On the other hand, when the DO level was higher (2–2.4 mgL^{-1}), a higher concentration of nitrate was sent back to an anaerobic tank creating a competitive environment for denitrifies (GAOs and DPAOs) and PAOs, thus limiting the P-removal efficiency (Yuan et al., 2012). In contrast, Nopens et al. (2007) found that the optimal P-removal can be achieved at a concentration of 0.5 mgL^{-1} which also correspond to lower nitrates which are known inhibitory agents. It has also been investigated that too low DO concentration (0.3 mgL^{-1}) in the aerated MBR zone triggered the uncontrolled growth of filamentous micro-organism (Insel et al., 2014). Another study evaluated no considerable effect of DO concentration (1–4.1 mgO_2L^{-1}) on biological P-removal without ascertaining the role of PAOs and GAOs (Sayi-Ucar et al., 2015).

A DO concentration between 0.4 and 2.0 mgL^{-1} is found an optimum range for P-removal above 80%. At the same time, there is disagreement for higher and lower concentrations from this optimum value. However, the choice for maintaining the DO level depends upon several other factors such as feed characteristics, target removal performance for COD and nitrogen, and the cost of biological aeration. Further assessment of the role of DO concentration at full-scale MBR facilities may help understand its role in EBPR. A summary of several factors affecting the P-removal in MBR is given in Table 2. The summarized results reflect that further research is needed to explore and verify the conflicting studies, especially at the full-scale.

2.4. Mathematical modeling of MBRs

It is well understood that MBRs operate under different conditions than CASP and requires a comprehensive understanding of the processes and adjustments in models initially developed for CASP to successfully simulate the phosphorous removal process in MBRs. The need for adjustments in ASMs' applicability to MBR is mainly attributed to: i) different microbial composition leading to the calibration of stoichiometric and kinetic parameters ii) higher biomass concentration leading to reduced oxygen transfer and uptake, iii) production of EPSs (linked to flocs) and SMPs (dissolved) and their accumulation onto the membrane surface iv) additional aeration involved in membrane scouring and recirculation of oxygen saturated sludge from MBR to the aerated/unaerated zones and v) the role of membrane filtration on nutrient removal (Fleischer et al., 2005; Hai et al., 2018; Judd, 2010; Maere et al., 2011; Verrecht et al., 2008). The comparison of these parameters for CASP and MBR is proposed as tabulated format in Table 3.

In a detailed review article, Fenu et al. (2010) discussed the adaptation of the for ASM models to the MBR with and without modifications. The unmodified ASMs required adjustments of nitrification related parameters, e.g., dissolved oxygen half-saturation coefficient (KOH), which was assumed to be attributed to smaller floc size in MBR, which eases the O_2 transfer. For modified ASM, extension with EPS/SMPs is justified if the modeling objective is to study higher SRT, linking the biology with the filtration, and with the necessity of predicting soluble COD in bulk. Otherwise, it makes the calibration process cumbersome and challenging to calibrate EPS/SMP-related parameters. It was further proposed to undertake full-scale studies to rule out the difference in lab-scale to full-scale models' applications. P-removal was briefly touched, taking into account five relevant studies, and no specific conclusion was derived due to the dearth of studies and insufficient available data. Albeit, it was suggested to explore the biological P-removal kinetics through additional research. Another comprehensive review on MBR modeling was conducted by Naessens et al. (2012a, 2012b). However P-removal aspect is not discussed. Most recently, based on earlier review on integrated MBR modeling, IWA task group has proposed best practices to be adopted to model MBR taking into account key process

Table 2
Summary of the factors affecting the P-removal in MBRs.

Factor	Parameters	Impact on P-removal	Optimum range	Reference
Influent characteristics	PO_4 loading	Higher BioP-removal at lower influent PO_4 concentrations.	2 –20 $gTP \cdot m^{-3}$	Choi et al., 2011; Monclús et al., 2010
	COD/P ratio	Higher C/P ratio positively impacts the P-removal. While lower C/P ratio lead to unstable conditions required to achieve maximum P-removal. A lower C/P ratio may result in higher nutrients (P&N) removal in the absence of nitrates interference.	29–45	Al-Hashimia et al., 2013; du Toit et al., 2007; Kapagiannidis et al., 2012; Monclús et al., 2010; Wang, 2020 Falahati-Marvast and Karimi-Jashni, 2020
	BOD/P ratio	Higher BOD/P results in higher BioP-removal	12.33–45	Adam et al., 2003; Fleischer et al., 2005; Wang, 2020
	COD/N ratio	A low COD/N ratio negatively impacts Phosphorus removal.	5.3–7.3	Hu et al., 2014; Lee et al., 2015; Mannina et al., 2018
	Nitrite concentration	Higher concentrations of nitrite negatively affect PAOs under both aerobic and anoxic condition	< 1 g NO_3. m^{-3}	Liu et al., 2011; Roberts, 2020; Saito et al., 2004; Sin et al., 2008
MLSS concentrations	MLSS concentration	Little or no effect on BioP-removal kinetics	<7 g TSS $.m^{-3}$	Adam et al., 2003; Holakoo et al., 2005; Parco et al., 2007
		BioP-removal is positively impacted by increasing the MLSS concentration up to an optimum concentration of 7 g/m^3		Wang et al., 2015
	EPS concentration	Higher EPS concentrations result in higher BioP-removal due to the fact that EPS act as a phosphorus reservoir (*approximately 5–10% of phosphorus in sludge is reserved in the EPS*)	20–130 $gCOD \cdot m^{-3}$	Adoonsook et al., 2019; Cloete and Oosthuizen, 2001; Zhang et al., 2013
	SMP concentration	SMPs inhibit the luxury BioP-uptake by PAOs in the anaerobic reactor	24–86 $gCOD \cdot m^{-3}$	Gao et al., 2004; Ichihashi et al., 2006; Jiang et al., 2009
Microbial community	PAOs & GAOs concentration	High PAO concentration resulted in higher BioP-removal in a MBR model based study.	7–10% of total biomass concentration	Jadhao and Dawande, 2012; Mao et al., 2015; Silva et al., 2012
	PAOs class and relative abundance	In full-scale WWTPs, PAOs class "Tetrasphaera" is found in abundance with relative fraction ranges between 10.7% and 27% of the total PAOs population.	10.7%—27% of the PAOs population	Mielczarek et al., 2013; Nielsen et al., 2019
Sludge retention time	SRT	Longer SRT and high MLSS/MLVSS concentration in MBR may induce a competitive advantage for GAOs over the PAOs, thus negatively impacting the BioP-removal performance. Longer SRTs positively impact the P-removal in MBRs. Especially when the system worked without sludge withdrawals	15–40 days	Ersu et al., 2010; Han et al., 2015; Hu et al., 2014; Lee et al., 2009; Nopens et al., 2007; Sun et al., 2019; Wang et al., 2015 Adam et al., 2002, 2003; Ahn et al., 2003; Ersu, 2006; Ersu et al., 2010; Mannina et al., 2020; Silva et al., 2012; H.-M. Zhang et al., 2006
Hydraulic retention time	Anaerobic HRT	An optimal anaerobic HRT is needed for BioP-removal without impacting the nitrogen removal. Higher anaerobic HRT helps in higher BioP-removal	2–2.9 h	Brown et al., 2011 Cho et al., 2005; Monclús et al., 2010
	Aerobic HRT	Reduction in aerobic HRT (12 h to 6 h) slightly improved the BioP-removal performance due to increase biomass at the constant FM ratio.	3–6 h	Ahmed, 2012; Falahati-Marvast and Karimi-Jashni, 2020; Sun et al., 2019
	Total HRT	Higher and stable BioP-removal efficiencies could be achieved at HRT lower than 10 h.	<10 h	Falahati-Marvast and Karimi-Jashni, 2020; Sözüdoğru et al., 2021; Sun et al., 2013
	Temperature	Better BioP- removal at a temperature ranging between 10-25C and inconsistencies at high temperatures around 40C	10–25 °C	Liau et al., 2015; Sayi-Ucar et al., 2015
Dissolved oxygen concentrations	DO concentration	BioP-removal was found independent of the DO concentrations. Higher DO concentration of 2.5 mgL^{-1} resulted in higher BioP-removal. Optimum DO (0.4–2.5 mgL^{-1}) is required for higher BioP-removal efficiency, and concentration above 2–2.4 resulted in decreasing the P-removal performance. Too low DO concentration (0.3 mgL^{-1}) can help filamentous bacteria grow and counteract BioP-removal	0.4–2.5 gO_2 m^{-3}	Sayi-Ucar et al., 2015 Fu et al., 2009 Downing et al., 2014; Hai et al., 2018; Nopens et al., 2007; Roberts, 2020; Smith et al., 2014; Yuan et al., 2012 Insel et al., 2014

indicators such as effluent quality index (EQI), membrane fouling, aeration, operating costs index (OCI), energy consumption, and mitigation of GHG emissions (Mannina et al., 2021).

MBR involves complex interactions which are taking into account through several combined modeling ways among i) biological processes, ii) membrane filtration – fouling phenomenon, and iii) hydrodynamics (Naessens et al., 2012a, 2012b; Ng and Kim, 2007). ASMs did not address the oxygen transfer/diffusion phenomenon, and aeration models were later developed and used as sub-models for MBR modeling studies (Delrue et al., 2010; Hocaoglu et al., 2011; Insel et al., 2011; Verrecht et al., 2008; Zarragoitia-González et al., 2008). Few integrated models have also been developed, taking into account the biological processes, filtration, fouling, and flow dynamics (Di Bella et al., 2008; Janus, 2014; Suh et al., 2013; Zarragoitia-González et al., 2008), but these still require validation at full-scale MBR plants. Their advantage for our purpose is to be available as a set of models where P-removal mechanisms may be integrated, with their impacts on other main variables. P-removal can be accomplished by biological reaction and chemical precipitation. Therefore different models can be classified with respect to biological (metabolic, ASMs, and the combination thereof) and chemical P-removal mechanisms.

2.5. Modeling and simulation of BioP-removal in MBRs

Mathematically, the BioP-removal process can be described either by i) metabolic model, ii) activated sludge models-ASM or iii) coupling of metabolic and ASM models, e.g., TUDP (Baetens, 2001; Lanham et al., 2014). Both of these modeling approaches use a set of stoichiometric and kinetic equations to describe the transformation steps of the EBPR process (Oehmen et al., 2007). Metabolic models use biochemistry knowledge of the active metabolic pathways to explain the cells' biochemical transformations (Oehmen et al., 2007). Metabolic models have been used to investigate the much-debated GAO-PAO competition in EBPR and reveals that the role of GAOs is negatively impacting the P-removal. However, the yield coefficients for PAOs and GAOs in metabolic models are determined theoretically based upon the reaction stoichiometry for the assumed pathways. Indeed GAOs and PAOs are challenging to be obtained in pure culture. This lack of experimental data is therefore, the major limitation of these models. As compared to

Table 3
Considerations in applying ASMs to the MBRs for the EBPR process.

Parameter/factor	Conventional activated sludge	Membrane bioreactor
Microbial composition	CASPs are operated at lower SRTs ranging between 4 and 15 days (Hai et al., 2018; Judd, 2010)	SRT of MBRs ranges between the same to three-time of the CASP (Hai et al., 2018). MBR promotes slow-growing micro-organisms such as nitrifiers and micro-organisms that are usually washed out in a CASP system while the membrane retains 100%. Specific stoichiometric and kinetic parameters adjustments are required while applying ASM in order to model MBRs (Fenu et al., 2010; Naessens et al., 2012a).
MLSS	CASP is operated at MLSS concentration ranging between 1500 and 3000 $g \cdot m^{-3}$ (Hai et al., 2018)	MBRs are operated at higher MLSS concentrations ranging between 4000 and 15,000 $g \cdot m^{-3}$ (Hai et al., 2018) and, therefore, lower FM ratio. Higher MLSS in combination with higher SRT cause stress to the micro-organisms in an MBR, which requires more energy for cell maintenance and therefore leaves less energy for cell production. Higher MLSS may induce the competitive advantage of GAOs over PAOs.
EPS/SMP	EPS/SMP produces in CASP are washed away and/or removed through sludge. EPS/SMPs are not considered in unmodified ASMs	Accumulation of the EPS/SMPs onto the membrane surface may affect the fouling and the biological process. As discussed earlier, EPS also affects the P-removal. EPS/SMP concentration in MBR sludge may be different from the CASP sludge due to different microbial community and F/M ratio.
Fine bubble aeration	Aeration is used for carbon matter degradation and the nitrification conversion.	Aeration is used for carbon matter degradation and nitrification. However, due to higher MLSS concentration (unfavorable) and smaller floc size, (favorable) mass transfer limitations have been reported different in MBRs than in CAPs (Fenu et al., 2010).
Coarse bubble aeration	Coarse bubble aeration is not involved	In addition to fine bubble aeration, coarse bubble aeration aims at scrubbing the membrane surface to mitigate the membrane fouling. It creates turbulence and affects the floc size and mass transfer processes.
Separation	separation is carried out by the clarifiers (secondary) and the phenomenon is modeled through clarifier/settling models (Hai et al., 2018; Henze et al., 2008)	Separation is carried out by physical media (membrane). With this, MBR requires a sub-model to simulate filtration–fouling phenomenon and retention of the soluble/dissolved fraction of COD and nutrient (Di Bella et al., 2008; Mannina et al., 2018). Due to complete retention, the microbial composition in MBR may vary.

metabolic models, ASMs use a global "mechanistic approach" to characterize the energy, redox, and mass balances of cell processes within CASP/MBR to describe the EBPR process. These are focused on macroscopic phenomena and depend on biochemical transformation pathways of soluble and particulate compounds in sludge and metabolic activities (Baetens, 2001; Santos et al., 2020; Seviour et al., 2019). The role of GAOs is mainly neglected in the original ASMs. However, some modified ASMs consider the glycogen as a storage polymer in addition to PHA, taking into account the growth and activity of the GAOs (Baetens, 2001; Gernaey et al., 2004; Hauduc et al., 2013; Oehmen et al., 2007). The effect of temperature, pH, and carbon source on the competition between PAO and GAO populations has been discussed in modified ASM (Lopez-Vazquez et al., 2009). The yield coefficient is measured experimentally, making ASMs distinguished from metabolic models (Baetens, 2001).

During the last two decades, a couple of detailed reviews have been published focused on comparing the model structures, limitations, and differences of the processes such as hydrolysis, growth, and decay of organisms, including their limitations for P-removal. The first detailed review was conducted by (Baetens, 2001) considering all the published models, metabolic and ASM (original and modified) and combinations till 2000. Following this, (Gernaey et al., 2004) published a review on the white box models (ASM1, ASM2, ASM2/ASM2d, ASM3 TUDP, Barker & Dold's model, and ASM3-BioP) and discussed that how the objective of the modeling exercise influences the model selection from the available range, data gathering, and model calibration. The authors further discussed the gray box (statistical), black-box (stochastic), and hybrid models and their potential applications in WWTPs, such as supervisory control system development. Following this, Hauduc et al. (2013) compared seven published models, including ASM1 (Henze et al., 1987), ASM2d (Henze et al., 1999), ASM3 (Gujer et al., 1999), ASM3-BioP (Rieger et al., 2001), ASM2d-TUD (Meijer, 2004), Barker & Dold's model (Barker and Dold, 1997), and UCTPHO+ (Hu et al., 2007) using a structured approach and dealt with the difficulties in comparing models as highlighted by Baetens (2001). These models are compared based upon several standard processes among the range of models, including i) hydrolysis, ii) fermentation iii) growth and decay of OHOs iv) growth and decay of ANOs v) growth and decay of PAOs vi) storage of PHA and vii) storage of polyphosphate. Following the works of Gernaey et al. (2004) and of Hauduc et al. (2013), the mini-review of Zuthi et al. (2013) compared the five models (ASM2, ASM2d, TUDP, UCTPHO+, and ASM3-BioP) that takes into account the P-removal for the CASP and MBR along with the advantages and disadvantages of these models. All these reviews had limited discussions related to the applications of these models to the full-scale WWTP and in particular to MBR and their corresponding adjustments and challenges faced during their adaptations to the MBRs.

P-removal from the wastewater can be mathematically described using several models derived from models of COD removal (Dold et al., 1981, van Haandel et al., 1981, Henze et al., 1987, Gujer et al. 1999), including i) ASM2 (Gujer et al., 1995) ii) ASM2d (Henze et al., 1999), iii) SIPHOR kinetic model (Johansson, 1996), iv) Dold's mechanistic model (Barker and Dold, 1997), v) Wentzel's model (Wentzel, 1989), vi) UCTPH model (Wentzel et al., 1992) vii) ASM2/ASM2d-TUDP model (Wentzel et al., 1988; Meijer, 2004), viii) New UCTPH (Hu et al., 2007), ix) EAWAG's ASM3-BioP (Rieger et al., 2001), x) FCASM-1 (Sun and Song, 2009), and xi) modified ASM3-BioP-N2 (Ni et al., 2010). A new bio-kinetic model (modified Barker and Dold's model) was developed considering the roles of GAOs and incorporating the new process concerning the GAOs (Varga et al., 2018) and validated at lab scale as well at full-scale CASP.

All these models can be studied under three groups i) models with considering the role of denitrifying PAOs, ii) models without considering the role of denitrifying PAOs, and iii) Models with the incorporation of the PAO and GAOs (Fig. 4).

2.5.1. Calibration of models

Metabolic models can be easily calibrated due to the limited number of parameters, and kinetic parameters are calibrated only when stoichiometric and kinetic reactions are changed to accommodate new process understanding (Lanham et al., 2014). Meanwhile, ASMs required intensive stoichiometric and kinetic parameters adjustments that compromise their predictive power and limit their practical applications for long-term EBPR process evaluations (Santos et al., 2020). Although it has been observed during the literature survey that most of the modeling studies involved calibration of the stoichiometric and kinetic parameters, albeit adjustment of the stoichiometric parameters is not considered as a good modeling practice (Rieger et al., 2012). The ASM's calibration process is time-consuming and complex. Therefore, several protocols have been developed recently to cope with this complexity and perform a systematic calibration of the model parameters, including BioMATH, STOWA, HSG, WERF, and sensitivity analysis

based approach (Gernaey and Sin, 2008; Mannina et al., 2011; Sin et al., 2005).

2.5.2. MBR simulation studies

This review is voluntarily limited to the ASM models (modified/unmodified) applied to the MBRs for P-removal. As per the Scopus data, there are 18 publications related to MBR modeling, and ASM2d is found to be widely used model (13 studies) while ASM3-BioP (1 study), TUDP (1 study), New General Model (3 studies) has rarely been used for MBR modeling. Table 4 summarizes selected papers related to MBR modeling. The details related to operational conditions and influent characteristics of the modeling studies are provided as supplementary material (Appendix C). The modeling and simulations case studies are discussed below.

A six-chambered pilot MBR plant was modeled using ASM2d (Fleischer et al., 2005). The authors concluded that the model was able to successfully predict the BNR performance of the MBR and was found capable to predict the phosphorus concentration below 0.1 $mgP_{tot}\ L^{-1}$. Although, no information has been provided about the model structure, calibration, and validation procedures. Similarly, Daigger et al. (2010) successfully modeled the Traverse City full-scale MBR plant with a capacity of 32,000 m^3d^1 and Broad Run pilot plant using ASM2d. The publication provides no details about the model structure calibration and validation process as of Fleischer et al. (2005). In the study of Monclús et al. (2010), a UCT-type pilot MBR is modeled using ASM2d with a special focus on biological P-removal. The model could simulate the P-removal performance without any change in the stoichiometric and kinetic parameters. Furthermore, the authors found that the decrease in the recirculation flow from the anoxic to anaerobic zone negatively impacted the P-removal.

A pilot plant receiving high strength wastewater from toilet flushing has been used for dynamic modeling using ASM2d (Verrecht et al., 2010). The model was first calibrated with steady-state, where it was required to have a correct representation of MLSS concentrations. The model parameters including μPAO_Max (2 d^{-1} vs default value of 1 d^{-1}), bPAO (0.1 d^{-1} vs default value of 0.2 d^{-1}) and YPP_Stor_PAO (0.2 $gP(gCOD)^{-1}$ vs default value of 0.4 $gP(gCOD)^{-1}$) were calibrated through heuristic approach without batch tests. However, the modeling of the removal of other nutrients could not be completely validated. While, with the dynamic simulation, PAO concentration increased without the adjustments to μPAO_Max, bPAO, and YPO and MLSS concentration were representative as the dynamic equilibrium was reached. The values of the parameters including mPAO, bPAO, and YPP_Stor_PAO, were then reverted to defaults.

The SMPs and ESP now has an established role in membrane fouling (Meng et al., 2009) and it has been proved that higher concentration of EPS deteriorates the P-removal performance (Ichihashi et al., 2006; Jiang et al., 2009). Keeping this in view, Jiang et al. (2008) extended ASM2d with SMP module (ASM2d-SMP) considering the soluble utilization associated products (SUAP) and soluble biomass related products to investigate the role of SMPs onto the membrane fouling. The introduction of SMP modules increased the model complexity and the additional parameters required calibration. Nevertheless, the ASM2d-SMP model successfully simulated the BNR behavior of a lab-scale MBR under steady-state conditions and was validated by the experimental data. The authors concluded that if the objective is to remove nutrients, an optimum SRT (17 days) agrees with published studies as discussed in Section 2.3.4. Following their previous research, Jiang et al. (2009) investigated ASMs' (unmodified) applicability and required adjustments to meet the MBR system biomass kinetics. Again, a lab-scale, MBR

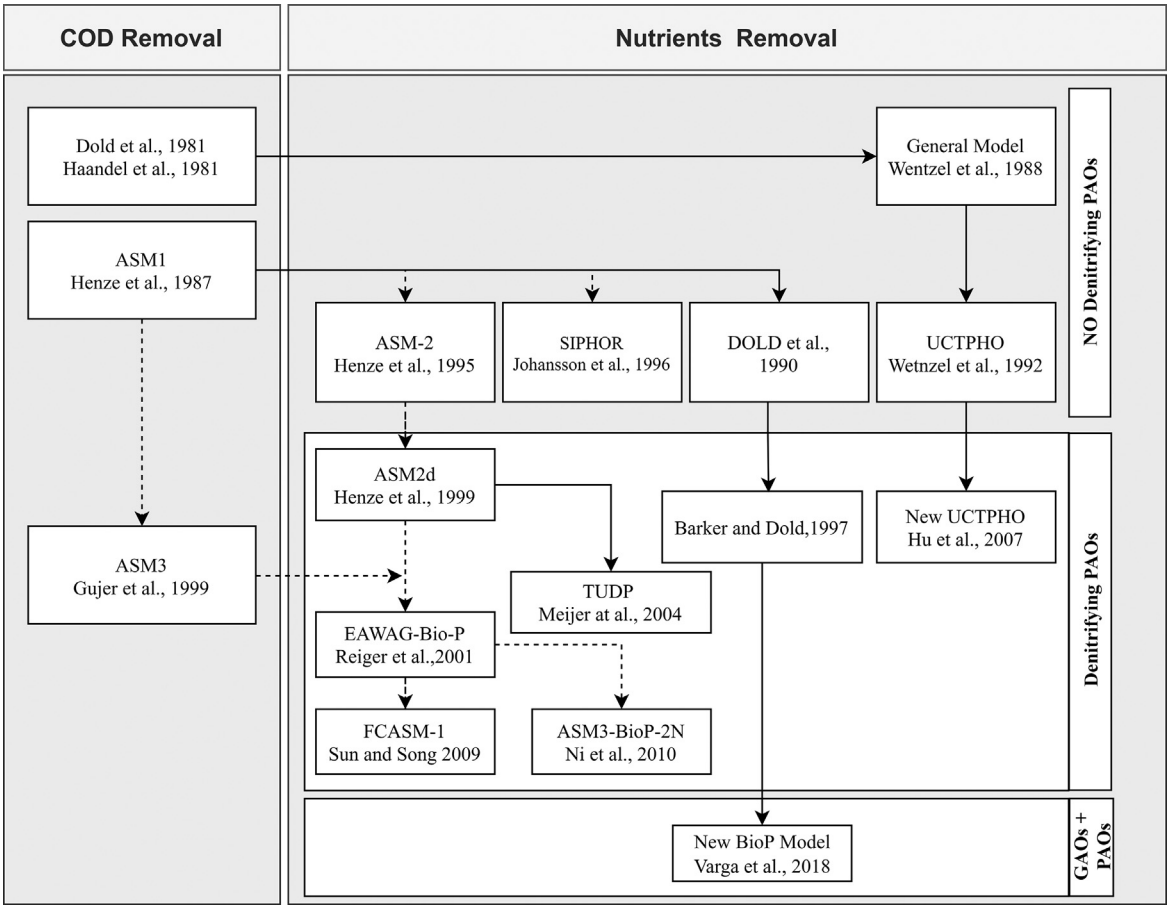

Fig. 4. Evolution and classification of the ASMs concerning GAOs and PAOs.

Table 4
Summary of the key information and process conditions used in reviewed MBR modeling studies.

Reference	Model features									Operating conditions					TP	PO_4^{3-}
	Model used	Wastewater	MBR scale	Configuration	precipitation	calibration protocol	Simulation environment	COD/TP	COD/TN	HRT (h)	SRT (d)	MLSS ($g \cdot L^{-1}$)	DO ($(g \cdot m^{-3})$)	Temp. (^0C)	Predicted effluent traits (mgL^{-1})	
								influent ratios								
Fleischer et al., 2005	ASM2d	R	P	Bardenpho	Al	–	–	24.2[a]	3.8[b]	8.4–8.8	13–19	4–9	8	–	0.1	
Al-Atar, 2007	TUDP	R	P	UCT		STOWA	AQUASIM	88.8	10.6	7–10	12–20	7.4	3	16–24		0.15
Nopens et al., 2007	ASM2d	S	P	MUCT		heuristic	–	–	9.91	6.4	17.55	10	2	15		6.58*
Ersu et al., 2008	NGM	S	L	AO/A2O		heuristic	BioWin	45.3	12	14	25	8	2	22.3	1.37	
Jiang et al., 2008	ASM2d-SMP	S	L	$AO_{sequencing}$		STOWA	–	36.2	7.29	17	7.2	10.9	0–2.5	15	2.2	
Abegglen et al., 2008	ASM3-BioP	R	P	AO		heuristic	SIMBA	75	5.6	24–72	30–50	–	–	–	1.2	
Jiang et al., 2009	ASM2d-SMP	S	P	$AO_{sequencing}$		STOWA	–	36.2	7.29	17	7.2	8.86	0–2.5	15	2.2	
Monclús et al., 2010	ASM2d	R	P	UCT		heuristic	WEST	114	9.09	14–18	23	9.8	1.5	16.4		0.32
Verrecht et al., 2010	ASM2d	R	P	MLE		heuristic	WEST	51.67[c]	5.88	26	47	8	2	15–20		4.35
Daigger et al., 2010	ASM2d	R	F	VIP	Al	–	–	58.22	5.95	8.4	19–23	1.5–9	–	16.1	0.33	
Ersu et al., 2010	NGM	S	L	UCT		heuristic	BioWin	40.8	12.81	8	10–75	7.5	2	22–23	3.4	
Liu et al., 2011	NGM	R	P	UCT	Al	WERF	BioWin	61.7	8.83	–	51	9–10	2	20		0.025
Gholikandi and Khosravi, 2012	ASM2d	S	L	$AO_{sequencing}$		STOWA	WEST	–	–	7	15–40	10–12.4	–	10–23		5.8*
Cosenza et al., 2013	ASM2d-SMP	R	P	UCT		GLUE	–	81.75	3.59	–	36	3.5–8	–	19–26		0.63
Cosenza et al., 2014	ASM2d-SMP	R	P	UCT		GLUE	–	81.75	3.59	–	36	3.5–8	–	19–26		0.63
Sarioglu et al., 2017	DND-GP	R	P	UCT		heuristic	AQUASIM	79.3	12	7.7	12	10–12	4	33.6	0.2	
Mannina et al., 2018	ASM2d-SMP	R	P	UCT		Novel	–	–	10	–	–	–	–	–		0.4–3
Bis et al., 2019	ASM2d	R	F	UCT		heuristic	GPS-X	27.1[a]	12.64	3.6	10.4	9.8	2		0.5	0.45

Notes: NGM: new general model, P: pilot scale, L: lab-scale, F: full-scale, R: real wastewater, S: synthetic, Al- Aluminum coagulant, a-BOD/TP; b-BOD/TKN, c-COD/PO_4^{3-}, * PO_4^{3-} could not be simulated.

system was modeled using ASM2d, and the model parameters were calibrated using the same approach as the previous study. By and large, the ASM2d model could characterize the EPBR removal performance of sMBRs after substantially modifying the rate constant for S_{VFA} uptake rate (q_{PAO,VFA_Stor}) and rate constant for storage of $X_{PAO,PP}$ ($q_{PAO,PO4,PP}$) and taking into account the differences discussed in Table 3 (Jiang et al., 2009).

In continuation to previous research, Gholikandi and Khosravi (2012) modeled a side stream MBR using ASM2d and expanded with an SMP module to improve the nitrification prediction capabilities of the MBR as suggested by Jiang et al. (2009). The default ASM2d parameters had to modify in order to increase the anaerobic VFA up-take and aerobic phosphorus up-take with the same protocol (Jiang et al., 2009). However, in the current ASM2d-SMP model, the development of UAP delayed the fermentation process and allowed the restoration of specific PAO-related parameters (nμPAO, and qSF_VFA_max) to their default ASM2d values (Table 5).

It is established to some extent that higher SRT in MBRs change the biomass kinetics. Therefore, ASMs may require calibration of the kinetic parameters before their applications to the MBR. In order to investigate the impact of SRT on model calibration, Ersu et al. (2010) used BioWin's General Model (AS/AD) to mimic the nutrient removal behavior of a lab-scale MBR at SRTs ranging between 19 and 75 days. The model was calibrated with the measured data using the heuristic approach based on sensitivity analysis. Compared to the default values, the calibrated model based on adjusted kinetic parameters at SRT of 35 days accurately predicted effluent characteristics. A sensitivity analysis revealed that effluent phosphorus concentrations were impacted by i) heterotrophic anoxic yield, ii) anaerobic hydrolysis factors of heterotrophs, iii) heterotrophic maximum growth rate iv) hydrolysis rate v) oxic endogenous decay rate for heterotrophs, and vi) oxic endogenous decay rate of PAOs. The model simulated results for COD, TN, and TP matched the experimental data reasonably well at SRT of 35 days.

An integrated new general model (Liu et al., 2011) was implemented on a UCT type MBR system to characterize its P-removal performance with/without the addition of coagulant. This integrated version couples activated sludge anaerobic digestion models and is complemented with sub-models for pH, gas transfer, and chemical precipitation. The authors calibrated the model against the measured data using the WERF protocol (Melcer, 2004). The kinetic and stoichiometric parameters related to PAOs were set to default. The model accurately predicted PO_4^{3-} with/without the addition of coagulant. The authors observed BioP-removal though it was severely impacted by the nitrates recycled from the anoxic zone to the anaerobic zone (in addition to influent nitrates). Similar results were obtained in another study where an extension to standard ASM2d was proposed to accommodate the nitrates' inhibition (Sin et al., 2008). Authors further found that adding excessive coagulant induced nitrates much more than required and negatively impacted the BioP-removal due to the limited availability of readily available COD (starvation conditions) for PAOs. The model could predict the combined biological and chemical P-removal up to a concentration of 0.025 $mgPL^{-1}$.

In the study presented by Cosenza et al. (2013), a UCT type, pilot-scale MBR is characterized using an integrated and complex model with 17 state variables and 79 kinetic parameters using domestic wastewater. The authors had to calibrate the rate constant for storage of poly-P (qPAO, PO4_PP) at a much higher value than previous studies reported in the literature (Gholikandi and Khosravi, 2012; Jiang et al., 2009). This higher qPAO and PO4_PP, was demonstrated by the fact that PO_4^{3-} was assimilated not only in the aerobic zone but also in the anoxic zone. The model simulation accounted for the increasing storage rate during the K_2PO_4 addition and un-modeled phosphorus release due to potential anaerobic conditions occurring within the cake layer on the membrane surface, explaining the higher qPAO_PO4_PP value. In addition to qPAO_PO4_PP, several other kinetic and stoichiometric parameters were calibrated (Table 5) to improve the fit.

Table 5
Default and modified parameters related to P-modeling in reviewed studies (modified within parenthesis).

Reference	Model											
	Al-Atar, 2007	Nopens et al., 2007	Jiang et al., 2008	Abegglen et al., 2008	Ersu et al., 2008	Jiang et al., 2009	Verrecht et al., 2010	Gholikandi and Khosravi, 2012	Cosenza et al., 2013	Cosenza et al., 2014	Mannina et al., 2018	Calibration range (ASM2d/ASM2d-SMP)
Bio-kinetic model	ASM2d + TUDP	ASM2d	ASM2d SMP	ASM3-BioP	New general model	ASM2d SMP	ASM2d SMP	ASM2d SMP	ASM2d SMP	ASM2d SMP	ASM2d SMP	–
P-related processes	11	8	8	11	19	8	8	8	8	8	8	–
P-related kinetic parameters	27	18	18	21	11	18	18	18	18	18	18	–
P-related stoichiometric parameters	11	3	3	4	8	3	3	3	3	3	3	–
A. Calibration of stoichiometric parameters												
Y_{PAO}		0.625	0.625 (0.57)		0.639	0.625 (**0.57**)	0.625	0.625	0.625	0.625	0.625 (**0.61**)	**0.57–0.61**
$Y_{PP,Stor,PAO}$		0.4	0.4		0.52	0.4	0.4 (**0.2**)	0.4	0.4 (**0.442**)	0.4 (**0.442**)	0.4 (**0.58**)	**0.20–0.58**
$Y_{Stor,PP,\ Ox}$					0.95 (**1.50**)							
B. Calibration of kinetic parameters												
$q_{PAO,VFA,Stor}$		3 (**1**)	3 (**1**)		2	3 (**1**)	3	3 (**5.5**)	3 (**3.699**)	3 (**3.699**)	3 (**4.36**)	**1–5.5**
$q_{PAO,PO4,PP}$	0.1	1.5 (**1.1**)	1.5 (**1.1**)	1.5		1.5 (**1.1**)	1.5	1.5 (**1.0**)	1.5 (**2.431**)	1.5 (**2.431**)	1.5 (**2.01**)	**1.1–2.43**
$K_{S,fPP,PAO}$		0.01	0.01	0.05		0.01	0.01	0.01	0.01	0.01	0.01 (**0.008**)	**0.008–0.01**
$K_{PP,PAO}$	0.01 (**0.2**)				0.01							**0.01–0.2**
$f_{PP\_PAO,Max}$	0.35	0.34	0.34	0.20		0.34	0.34	0.34	0.34	0.34	0.34 (**0.71**)	**0.34–0.71**
$f_{Gly\_PAO,Max}$	0.50											
$\mu_{PAO,Max}$		1	1	1	0.95	1	1	1	1 (**0.716**)	1 (**0.716**)	1	**0.716–1.0**
$\mu_{PAO,Max,lim}$		1	1		0.42	1	1 (**2**)	1	1	1	1	**1.0–2.0**
$n_{\mu PAO}$		0.60	0.60	0.60	0.40	0.60	0.60	0.60 (**0.45**)	0.60	0.60	0.60	**0.45–0.60**
m_{PAO}				0.20 (**0.15**)	0.04							
b_{PAO}		0.20				0.20	0.20 (**0.1**)	0.20	0.20 (**0.235**)	0.20 (**0.235**)	0.20	**0.1–0.235**
no.of kinetic processes impacted due to changes in kinetic parameters	3	6	6	2	0	6	6	6	6	6	6	

Notes: Complete set of stoichiometric and kinetic parameters (Table C.3) along with their default values can be accessed in Appendix C. In addition the kinetic rates equation/processes impacted are also highlighted (Table C.4).

However, It is generally not considered as a good modeling practice (Rieger et al., 2001). A novel calibration protocol developed by Mannina et al. (2011) based on global sensitivity analysis (GSA) helped in identifying the most influent parameters and reduce the calibration effort (65% reduction in number of candidate parameters chosen for calibration).

In the study of Mannina et al. (2018), a UCT-type pilot-scale MBR was modeled using an integrated approach employing ASM2d-SMP-GHG modules. The rate constant for storage of Poly-P (PAO, PO4_PP) was calibrated and the final value (2.01 $gX_{PP}gX_{PAO}^{-1}d^{-1}$) was higher than the default (1.5 $gX_{PP}gX_{PAO}^{-1}d^{-1}$) because, during aerobic and anoxic environments, an increase in PAO, PO4_PP contributed to an increase in the rate of polyphosphate storage and thus limited the possibility of the accumulating nitrification related intermediate compounds. Despite high values of the kinetic parameters i.e. PAO, PO4_PP, the model simulation fitted well with the experimental data. This model has further been used to propose ways to reduce the MBR's environmental footprint using the multi-criteria optimization and estimation of greenhouse gases (GHGs) emissions (Mannina et al., 2020).

DNN-GP model (Sarioglu et al., 2017) describes the BNR process of a pilot-scale UCT type MBR, receiving real municipal waste through the coupling of two sub-models: a) GAOs-PAOs competition and b) two step N/DN process. The GAOs-PAOs competition is modeled by adjusting their endogenous decay and substrate storage rates. Relative sensitivity analysis was used to calibrate the model parameters using the heuristic approach. Initial parameter values were selected from the published literature, and then calibrated ones were used for dynamic simulations. The authors found that temperature-dependent substrate storage and endogenous decay rates were the critical determinants of GAOs-PAOs completion. As compared to PAOs, the GAOs had a lower decay rate while PAOs had much higher maximum substrate storage rates than GAOs. Besides, GAOs remained activated even at a higher temperature and substrate, although phosphorus uptake rate was considerably reduced. The model successfully simulated the EBPR process. The P-removal performance was found around 98% even with elevated influent VFA/COD ratio. The P-removal revealed to be sensitive to DO concentrations in the aerobic/MBR tanks which is in agreement with the findings of the study presented by Sayi-Ucar et al. (2015). In a recent theoretical study (Bis et al., 2019), the CASP and MBR modeling approaches were compared. Plants were configured in a virtual environment using the GSP-X simulation tool and were characterized using ASM2d, and for MBR, an additional filtration module in submerged

membrane configuration was added. The authors found a higher concentration of PAOs in MBR than CASP, marginally higher P-removal was observed in MBR. The authors, however did not provide any detail about the calibration and validation of the model used for simulations.

A lab-scale MBR (Ersu et al., 2008) with anaerobic, anoxic zones followed by oxic plate and frame membrane zone was considered for modeling with five different recirculation arrangements (Fig. B.2). The model was built in a BIOWIN environment using "New General Model" targeting carbon and nutrient removal. The model was calibrated using the experimental data. The model could predict well effluent TN, TP, and NO_3^- N but over-predicted CODs and NH_4^+. Based on sensitivity analysis, two kinetic parameters (μ_{PAOmax}, mPAO) were calibrated. The calibrated values against the default values can be seen in Table 5.

In another study (Al-Atar, 2007), a UCT-type MBR pilot plant was modeled in the AQUASIM environment. The calibrated model was able to predict the EBPR process reasonably. The simulation reasonably fitted well with the experimental data. However, the exact concentrations for anoxic nitrate and effluent PO_4^{3-} were not predicted well. The model was slightly calibrated by adjusting the rate of poly-phosphate formation, KPP_PAO, which was increased from 0.01 to 0.2 $gP(gCOD)^{-1}$ to better predict the anoxic PO_4^{3-} concentrations results showed that the sludge distribution within the anaerobic and anoxic zones is critical for P-removal.

In the study conducted by Abegglen et al. (2008), a small-scale MBR receiving toilet wastewater is modeled using the ASM3-BioP model in the SIMBA simulation platform. The MBR modeled in this study is subject to extreme load fluctuation. The EAWAG BioP module was implemented, and the decay rate of PAO (mPAO) was adjusted only by changing its value from 0.2 to 0.15 d^{-1}. The implementation of the model allows to adjust the MBR return sludge ratio to 1.2 times the influent to achieve a stable EBPR with efficiency above 90%. Theoretically, PAOs concentration was found to be in the range of 300–1500 mgCOD L^{-1} for sludge recirculation ratio of 0.6–1.7 and there was no increase in the PAO concentration above 1.2.

As presented in Table 4, ASM2d (with and with EPS/SMP consideration) is a widely used model for simulation of BioP-removal in MBRs, for lab-scale as well as pilot systems, and very limited (5) studies have been published for full-scale systems (10–100 m^3d^{-1}). No study has been published for super-large scale MBR (≥ 100,000 m^3d^{-1}). Perceived competitive advantage of GAOs over PAOs under the longer SRTs (thus higher MLSS and MLVSS) is countered by modifying the design configurations of the MBRs to control the SRT and feed composition (e.g., step feed configuration). ASMs can successfully simulate the BioP-removal in MBRs when fundamental differences in MBR functioning (Table 3) compared to CASP are considered. However, due to complete biomass retention in MBRs and especially the PAOs due to their increased size, several PAOs related model parameters required adjustments (Table 4) through calibration approaches. The majority of the studies considered calibrating the kinetic parameters, while few studies even calibrated the stoichiometric parameters as well, which seems necessary to accommodate the effects due to different stoichiometric rates induced by the GAOs and PAOs competition for phosphorous uptake.

2.5.3. Wastewater simulation software

Table 4 shows that the modelers have used various special-purpose simulation software, which is far less straightforward and easy to use than the general-purpose simulation environments such as MATLAB/SIMULINK or spreadsheets. The most frequently used simulation software in simulation studies in academia and the industry are; BioWin, GPS-X, SIMBA, WEST (previously EFOR), SUMO, and EAWAG's AQUASIM. Simulators like ASIM, STOAT, lynx, and JASS are primarily used in academia for research and teaching purposes. The wastewater treatment industry is also using relatively new simulators like DESASS (design and simulation of activated sludge systems) and EPD (EnviroProDesigner) to design and optimize the WWTPs. A summary of the simulators' features based on the information available in each product's description by its respective supplier is provided as supplementary material as Appendix D.

3. Chemical P-removal modeling and control

3.1. Phosphorus precipitation process

Chemical phosphorus removal, also called "removal by a salt addition," can be applied in combination with BioP-removal as i) pre-precipitation, ii) simultaneous iii) post-precipitation and iv) sometimes side stream precipitation, which is usually adopted when P-recovery is intended (Van Haandel and Van Der Lubbe, 2007). Sometimes in one plant, metal salts are added in different points or locations along the treatment chain resulting in two or more "places" of precipitation. The metal salt is used to convert the dissolved inorganic phosphorus compounds in the wastewater into a low solubility metal phosphate, which can be removed in the process's subsequent stages. Among the various pathways; i) adsorption of phosphate onto hydrous ferric oxides (HFO) ii) co-precipitation of phosphate into the HFO structure iii) Precipitation of metal phosphate and iv) precipitation of mixed cation phosphates (i.e., calcium, magnesium, iron, or aluminum phosphates, or hydroxy phosphate) are the most commonly considered processes for removing phosphorus (Smith et al., 2008). In addition, these processes also improve the sludge properties via neutralizing the floc charge and improving the filterability by the changing the settling properties of the sludge (Lee et al., 2001; Asensi et al., 2019). Metal ions can bond with negatively charged groups within EPS and increase floc size, packing density (Asensi et al., 2019), and shearing resistance (Zhang et al., 2008).

Chemical P-removal in MBR is relatively different than CASP due to i) limited or no soluble phosphorus in case of MBR effluent and metal carryover is comparatively less than CASP ii) operation of MBRs at higher SRT and thus higher MLSS which improved the flocculation and coagulation potential of phosphorus iii) addition of the coagulant at the downstream of the process in case of MBR, and iv) interaction of metal ions with EPS and membrane surface to cause/reduce fouling (a controversial in the literature). Chemical P-removal in the following sections is discussed in details keeping in view all these aspects of MBR functioning. Furthermore, a brief discussion on the fundamentals of the chemical precipitation is dedicated keeping in view the metal and hypothetical phosphate complexes assumed in chemical precipitation models.

Chemical P-removal depends upon effective coagulation and flocculation processes. Multivalent metals salts, e.g., ferric chloride ($FeCl_3$), ferric sulfate ($Fe_2(SO4)_3$), ferrous sulfate($FeSO_4$), ferrous chloride ($FeCl_2$), alum chloride ($AlCl_3$), and lime, are generally used as a coagulant (Van Haandel and Van Der Lubbe, 2007) in wastewater treatment to improve P-removal and the removal of higher molecular weight organics such as EPS and SMPs (Sun et al., 2019; Wang et al., 2014). The coagulation is then followed by flocculation process, which helps to form neutralized larger-sized flocs due to collision and electrostatic attraction of the sludge particles under slow mixing (Takács et al., 2005; Zhang et al., 2015). Afterwards, the larger-sized flocs formation (Asensi et al., 2019), along with phosphorus entrapped into, is removed via separation process or sludge extraction (Tchobanoglous et al., 2002). Ideally, 1 mol of the trivalent metal salt is required to remove 1 mol of phosphorus (Me/P of 1:1) as described by the theoretical stoichiometric expression (Eq. (3.1)).

$$Me^{3+}\ (aq) + PO_4{}^{3-}\ (aq) \rightarrow MePO_4\ (s) \tag{3.1}$$

$$Me^{3+}\ (aq) + H_2PO_4{}^{-}\ (aq) \rightarrow MePO_4(s) + 2H^+ \tag{3.2}$$

For example, when $FeCl_3$ is used as a metal salt, the weight ratio of Fe^{3+} to phosphorus is 1.8. Similarly, 1 mol of aluminum is required to

remove one mole of phosphorus. The weight ratio for Al/P is thus 0.87.

$$FeCl_3\ (aq) + PO_4^{3-}\ (aq) \rightarrow FePO_4\ (\downarrow) + 3Cl^- \quad (3.3)$$

$$Al_2\ (SO_4)_3 + 2PO_4^{3-}\ (aq) \rightarrow 2AlPO_4 + 3SO_4^{2-} + 14\ H_2O \quad (3.4)$$

The use of ferrous sulfate (divalent metal) in full-scale MBRs is also preferred over ferric salts due to low cost (Wu et al., 2015) and comparable efficiency to ferric salts (Wang et al., 2014). When $FeSO_4$ is used as metal salts, it is first oxidized to trivalent metal ions (Me^{3+}) from divalent (Me^{2+}) as described by Eq. (3.5) or precipitate as vivianite ($Fe_3(PO_4)_2.8H_2O$). Prediction of the chemical precipitation in MBRs is difficult because of oxidation of ferrous to ferric combined with several interactions between iron, phosphorus, and other ligands (Wu et al., 2015). Furthermore, among several factors that may impact the oxidation process including; i) DO concentration ii) the catalytic response by the microbes or influent constituents like sulphur and iii) inhibition by the water matrices such as carbonate and pH (Thistleton et al., 2001). It has been investigated that in-situ production of Fe^{3+} by oxidation (Eq. (3.5)) from the Fe^{2+} is a more efficient phosphate precipitant than the external addition of Fe^{3+} (Thistleton et al., 2002).

$$Fe^{2+}\ (aq) + H^+ + 0.5\ O_2 \rightarrow Fe^{3+}\ (aq) + 0.5\ H_2O \quad (3.5)$$

For example, when ferrous chloride is used, the weight ratio of Fe^{2+}/P is 2.7 (three moles of ferrous required to remove two moles of phosphorus) as described by the stoichiometric reaction (Eq. (3.6)).

$$FeCl_2\ (aq) + 2\ PO_4^{3-}\ (aq) \rightarrow Fe_3\ (PO_4)_2(\downarrow) + 6\ Cl^- \quad (3.6)$$

The trace amount of sulfide coming from the sewer system due to longer retention times is also present in the influent, which may react with the divalent/trivalent metal ions and form metal sulfides (and thus remove the rotten eggs like odor) as described by the stoichiometric reactions (see Eqs. (3.7) & (3.8)). The sulfide is usually removed by the chemical precipitation process as demonstrated in the study (Gutierrez et al., 2010) wherein sulfide concentration were reduced from 7.6 $mgSL^{-1}$ to 0.1 $mgSL^{-1}$.

$$Me^{2+}\ (aq) + S^{2-} \rightarrow MeS\ (s) \quad (3.7)$$

$$Me^{3+}\ (aq) + 3\ s^{2-} \rightarrow Me_2S_3(s) \quad (3.8)$$

For practical applications, metal salts (inorganic coagulants) are normally dosed with higher Me/P ratios (molar ratio ranges between 1 and 4) than the theoretical stoichiometric ratio (i.e. Me/P: 1). It is presumably due to the higher pH of the sludge than the theoretical (between 5 and 6) required for precipitation of metal phosphate complexes (De Haas et al., 2000; Van Haandel and Van Der Lubbe, 2007). Secondly, a higher dose is also required because the metal ions react with water to produce hardly soluble metal hydrated complexes, e.g., Me $(H_2O)_6^{3+}$ as described by Eq. (3.9). Thirdly, this excess dose is most likely explained by the competition between OH^- and PO_4^{3-} and the need of excess Fe^{3+} to destabilize $FePO_4$ and other colloids, and this can be examined through estimating the equilibrium log constants of the reactions (Thistleton et al., 2002). Furthermore, P-removal efficiency is affected by the influent characteristics, the discharge limit, and operating conditions (Tchobanoglous et al., 2002). The factors affecting the P-removal are discussed in Section 3.2.

$$Me^{3+}\ (aq) + 3H_2O \rightarrow Me\ (OH)_3\ (s) + 3\ H^+ \quad (3.9)$$

In addition to the precipitation as insoluble metal phosphate ($MePO_4$), adsorption of positively charged hydrated metal complexes (insoluble metal hydroxide such as unbound HFO with high sorption or amorphous ferric oxyhydroxide (AFO) helps to remove phosphorus from wastewater. If the PO_4^{3-} concentration is lower in the influent and higher metal salt is dosed owing to the competition between the formation of metal phosphate and metal hydroxides, additional metal ions will react with water (Eq. (3.9)) or OH^- present in the wastewater. As a result, an increased solids production in MBRs or increased concentrations of metal salts in CASP effluents are noticed (De Haas et al., 2000; Gnirss et al., 2003; Thistleton et al., 2002; Zhang et al., 2015).

The precipitation of phosphate as calcium hydroxyapatite ($Ca_5(PO_4)_3OH$) is the primary removal process when lime $Ca(OH)_2$ is used for simultaneous P-removal (see Eqs. (3.10)–(3.12)). Since lime reacts with bicarbonate alkalinity present in wastewater to form $CaCO_3$ and raising the pH above 8. The concentration of lime required for P-removal is determined by the wastewater's alkalinity. The chemical reactions involved in P-removal through lime are:

$$Ca(OH)_2\ (aq) + H_2PO_4^- \rightarrow CaHPO_4\ (s) + H_2O + OH^- \quad (3.10)$$

$$Ca^{2+}\ (aq) + 3\ PO_4^{3-} + OH^- \rightarrow Ca_5(PO_4)_3OH\ (s) \quad (3.11)$$

$$Ca^{2+}\ (aq) + CO_3^{2-} \rightarrow CaCO_3\ (s)\ (\text{at pH} \geq 9.5) \quad (3.12)$$

Lime is not used in simultaneous P-removal applications as the pH must be raised to a value ≥10 for calcium to react and precipitate as phosphate and therefore not compatible for biological treatment. It increases the complexities involved in handling the process and storage of the lime in addition to complexities associated with pH handling (Tchobanoglous et al., 2002). The usage of different salts provides different results and associated problems. Therefore, a careful selection of the right kind of metal salts or coagulants is essential. Ferric salts are widely used and are more advantageous due to their low costs, least handling complexities and are slightly more effective than aluminum salts (Mishima and Nakajima, 2009).

3.2. Factors affecting chemical precipitation for phosphorous

Performance of chemical P-removal is linked to several factors, including i) influent chemistry and composition ii) operational conditions such as DO, zeta potential and pH control iii) type of coagulant, coagulant/P molar ratio and dosing location and v) mixing conditions of the coagulant with the sludge (Kim and Chung, 2014; Zhang et al., 2015). These factors can influence the types of Fe and P species present in the influent/sludge and the degree and magnitude of transition between these species (Fleischer et al., 2005; Wang and Waite, 2010). For example, when an inorganic ferric (Fe^{3+}) salt is first added to the mixed liquor, it can form AFO precipitates, which can then adsorb phosphate, organic compounds like SMP, and other dissolved constituents and may influence the membrane fouling. The precise pH conditions and local concentrations of sorbing species decide whether this process involves successive or simultaneous precipitation/adsorption phenomena between iron and phosphate. The factors influencing the chemical precipitation are briefly discussed in the following paragraphs and a summary is given in Table 6.

3.2.1. Influent chemistry and composition

The majority of early studies on chemical P-removal used simple water matrices composition (i.e., hydrogen (H), metal (Me), oxygen (DO), hydroxides, carbonates and phosphorus. Understanding the influence of more complex water chemistry is expected to enhance precipitation models' ability to predict chemical P-removal in wastewater. Chemical P-removal is affected by influent constituents, such as alkalinity, soluble and total COD, and TSS concentrations. The extent of their influence on P-removal is discussed in the following sections regardless of the technology (CASP or MBR).

Table 6
Summary of the factors influencing the chemical precipitation in MBR.

Factor	Description of the influence	References
Alkalinity	Lower influent alkalinity reduced the P-removal due to sudden changes in the pH after addition of the coagulant The alkalinity of wastewater between 98 and 120 mg $CaCO_3L^{-1}$ is sufficient to maintain the sludge pH close to circumneutral level (6–6.5) during the $FeCl_3$ dosing and flocculation and achieving ≥98% of TP-removal	Banu et al., 2009; Kim and Chung, 2014; Li et al., 2018
Dissolved oxygen	Higher DO (1 5–2.5 $g \cdot m^{-3}$) concentration helps in better P-precipitation, mainly when ferrous (iron) is used as a coagulant.	Kim and Chung, 2014; Ren et al., 2019; Wu et al., 2019; Zhang et al., 2015
Basicity/pH	Change in pH of the sludge in MBR did not affect the P-removal though significantly higher fouling was observed at a pH range of 4–5.The optimal pH for chemical precipitation in MBR was found in the range of 6.5–7.	Li et al., 2017; Meng et al., 2009
Type of coagulant	The P-removal performance of each of the coagulants is above 85%, depending upon several other factors discussed in Section 2.3. The coagulant should be selected based on its price, regulatory acceptance and toxicity risk for the receiving bodies (in case of carryover).	Alibardi et al., 2021; Holba et al., 2012; Li et al., 2017; Ren et al., 2019; Song et al., 2008; Sun et al., 2019; Wang et al., 2014; Wu et al., 2015; Yang et al., 2011; Zhang et al., 2015
Molar ratio	Based on several studies presented Table 8 the optimum molar ratio varies between 1.5 and 4. Higher molar ratios can lead to breach of regulatory iron concentration due to carryover. Carryover in MBR is limited to soluble fraction (due to 100% solid retention) of phosphorus which do participate in floc formation. This aspect requires further study.	
Dosing location and numbers of dosing points	The coagulant's addition in the aerobic zone of the MBR provided the best results or P-removal. Two points (upstream and downstream before the filtration process/secondary clarifiers) coagulant dosing is common in full-scale plants.	Mbamba et al., 2019; Wu et al., 2015
	Single point dosing (12–14 mgL^{-1}) can also achieved 95 ± 3% of the TP removal.	Alibardi et al., 2021
Mixing	Mixing had little to no effect on P-removal in MBRs.	Kim and Chung, 2014
	Rapid mixing improved the P-removal in both MBR and CASP. It risks to damage the microorganisms when provided with greater shear with values greater than 425 s^{-1} and therefor shear induced by coarse bubble aeration is sufficient for mixing of coagulant in MBR.	Autin et al., 2016; Li et al., 2019

3.2.1.1. Alkalinity. An optimum alkalinity of the influent is essential for the adequate precipitation of phosphorus. In low alkalinity (≤ 50 mgL^{-1}) influent, the addition of coagulant induced sudden pH changes, creating a challenging environment and resulting in lower P-removal (Banu et al., 2009). In an MBR study (Zhang et al., 2015), it was observed that the addition of metal salt in excess resulted in consumption of the alkalinity at unprecedented rates and thus decreased the pH of the sludge (≤ 4) and slowed the hydrolysis rate of the metal. Therefore, the nitrification was substantially impaired at these low pH values. Nevertheless, nitrogen reduction can be restored by adjusting the pH to neutral levels via control system. Two other studies (Clark et al., 2000; Philips et al., 2003) investigated the iron salts' toxicity for the microbial community (AOB and Nitrobacter) responsible for nitrification process. The authors found that the metal's toxicity negatively impacted the nitrification rate contrary to the findings of previous study presented by Sun et al. (2019).

The study presented by Szabó et al. (2008) explored the influence of the P-precipitation in wastewater in the presence of excessive alkalinity (0–600 $mgCaCO_3L^{-1}$). The authors found that the higher alkalinity resulted in significantly higher residual soluble P (PO_4^{3-}), but this phenomenon remained unexplained. A hypothesis was that the metal hydroxide (MeOH) formation occurs more rapidly in higher alkalinity waters because the hydrogen ion (H^+) trapping potential is greater, resulting in a kinetic advantage for fast MeOH precipitation and a less likelihood of metal phosphate (MeP) and MeOH co-precipitation. The same authors also tried to explain this phenomenon by assumed competition between bicarbonate ions (HCO_3^-) and monohydrogen phosphate (HPO_4^{2-}) for active sites. This phenomenon, however, necessitates further study and confirmation. While two other studies reported contradictory findings, wherein changes in alkalinity (i.e., from 0 to 400 $mgCaCO_3L^{-1}$) had a negligible effect on P-precipitation (Kang et al., 2003; Newcombe et al., 2008). A relatively recent model-based study (Hauduc et al., 2015), with influent alkalinity of 125 $mgCaCO_3L^{-1}$ (controlled pH at 6.5 and higher mixing) resulted in more than 95% P-removal. Phosphorus precipitation with metal salts consumes alkalinity and demands supplemental addition of $CaCO_3$ (or $NaHCO_3$) to avoid dramatic pH drop to acidic range and is not suitable for the microbiology. It is therefore essential to control the pH of the wastewater treatment process (especially with alum and iron salts) and therefore must be studied along with the alkalinity.

In the absence of a sufficient number of studies and contradiction in the published literature, it is hard to establish the role of alkalinity in P-removal. Therefore, more research is needed to determine the impact of alkalinity on chemical P-removal, especially for the MBR, which is almost non-existent within the last two decades.

3.2.1.2. Initial phosphorus load. The P-removal efficiency is determined by the raw wastewater's soluble phosphorus concentration. As discussed previously, higher the initial concentration of phosphorus, lower is the Me/P ratio. The relative efficiency of the P-removal increased with the increased concentration of initial soluble phosphorus since low concentration of PO_4^{3-} are more difficult to remove than higher ones. Although, with increasing coagulant dosing P concentration decreases down to certain level (0.01 gPm^{-3}), higher coagulant concentration did not help to reduce any further the residual P concentration (Smith et al., 2008; Szabó et al., 2008).

3.2.1.3. Presence/absence of colloidal organic matter. Several studies have reported the influence of organic matter on P-removal (Aleta et al., 2018; Mao et al., 2012; Szabó et al., 2008). The presence of citrate (50, 100, and 200uM) decreased P-adsorption onto the fresh HFO (Mao et al., 2012). According to Szabó et al. (2008), increasing the influent COD and TSS concentrations resulted in lower chemical P-removal. The authors assumed that the corresponding decrease in the P-removal rate may be due to the competition to fill the binding sites available onto the metal hydroxide surface between phosphate ions and carboxylic-phenolic groups present in the organic matter.

3.2.2. Influence of operational conditions

3.2.2.1. Dissolved oxygen concentrations. Optimum DO concentration become essential with the use of ferrous salts required for Fe^{2+} oxidation to ferric (Fe^{3+}) and subsequent precipitation of vivianite ($Fe_3(PO_4)_2.8H_2O$). These processes are limited by the oxygenation rate and sludge pH (Wu et al., 2019) specially in the anoxic chamber where DO <0.1 mgL^{-1} and the oxidation is slow (Zhang et al., 2015).

3.2.2.2. Basicity/pH. Phosphate and metal reactions commonly used to remove phosphate have been reported to be pH-dependent. The effect of pH on P-removal has been studied extensively (Caravelli et al., 2012, 2010; Kim and Chung, 2014; Mao et al., 2012; Smith et al.,

2008; Szabó et al., 2008). According to Smith et al. (2008), effective P-removal occurred between pH range of 5.5–7.0 for CASP. Due to other chemical reactions in the wastewater, the optimum pH range is situation-dependent. To fully remove phosphorus, the exact coagulant dose must also be calculated as function of pH and this may vary from case to case depending upon factors discussed in Section 2.3 as well as other factors discussed in the current section. On the other hand, some other studies (Caravelli et al., 2012; Szabó et al., 2008) found low precipitation of MeOH at lower pH (< 4) and formation of soluble P-complexes and phosphate precipitates with Mg^{2+} and Ca^{2+} ions at higher rates at pH greater than 10 (Szabó et al., 2008). The study of Zhang et al. (2015) investigated the effect of pH on P-removal and membrane fouling. Although the pH of the mixed liquor in MBR was within circumneutral region (6–7) and therefor the P-removal performance was not compromised, it did have an impact on the nature of membrane fouling, which was possibly due to the relative rates of formation of Fe^{3+}-SMP complexes and amorphous ferric oxyhydroxides. AFO formation was especially favored at neutral pH value (6–7), and it resulted in successful EPS removal from solution, but at the expense of filtration results, either through the formation of a Fe^{3+}-polysaccharide gel layer or pore blocking. Higher pH values (8–9) have been reported to increases the precipitation of $CaCO_3$ and results in inorganic fouling of the membrane (Meng et al., 2009). In another MBR study (Li et al., 2017) where the pH after adding the coagulant was controlled between 6.5 and 7, it was possible to achieve the P-removal above 80% with ferric and aluminum salts.

There is no general agreement on the optimum pH range for P-removal based on the reviewed literature. However, it can be inferred that successful removal occurs in the circumneutral pH range typical of WWTP.

3.2.2.3. Biomass concentration. Caravelli et al. (2012) investigated the impact of biomass concentration on chemical P-removal. For pH values below 5 and 6, biomass presence had little to no effect on P-removal. For higher pH values (7–8), biomass population significantly increased P-removal, presumably due to sweep flocculation favoring phosphate anions' retention under the alkaline conditions. Further research is needed to explore if biomass concentrations reduce P-removal due to competition mechanisms (for MeP and MeOH production) and smaller floc sizes which is the case for MBRs.

3.2.3. Type of coagulant, molar ratio, and dosing location

3.2.3.1. Type of coagulant. As discussed in Section 3.1, multivalent salts (such as ferric chloride ($FeCl_3$), ferric sulfate ($Fe_2(SO4)_3$), ferrous sulfate($FeSO_4$), ferrous chloride ($FeCl_2$) and alum chloride ($AlCl_3$)), lime, and polymers are used to co-precipitate phosphorus in wastewater treatment. A careful selection of the coagulant is essential to achieve the maximum P-removal efficiency in MBR while keeping the fouling low. There is a dearth of full-scale MBR studies focusing on performance assessment of different coagulants and fouling development. Ferric chloride is a widely used coagulant for P-removal and odor control via sulfide precipitation (Tchobanoglous et al., 2002). In a lab-scale MBR study, it was found that the ferric salt performs better (97%) as compared to ferrous (95%), which is comparatively cheaper than ferric with the same Fe/P molar ratio (i.e. 2) (Wu et al., 2015). Meanwhile the study presented by Song et al. (2008) evaluated the aluminum and ferric salts and found the same P-removal (98%) for both but with a 15% higher aluminum concentration (Me/P ratio < 1.5). Several MBR studies listed in Table 7 summarizes the type of coagulant used and their respective P-removal efficiency. Irrespective of the type of coagulant, above 85% P-removal could be achieved. However, this performance must not be studied in isolation from the cost of sludge production, toxicity induction, and inorganic fouling, as reported in few studies.

3.2.3.2. Molar ratio. In practice, metal dosages are usually determined based on the bench, and full-scale tests as current chemical precipitation models do not consider competing reactions (Tchobanoglous et al., 2002). MBR requires higher doses of metal salts than CASP due to higher SRT, as reported by Conidi and Parker (2015). The Fe/P molar ratio of 2–4 is optimum to achieve P-removal above 85%. P-removal achieved with different coagulant/P molar ratio in several MBR studies is given in Table 7. However, most of these studies have considered coagulant addition (low molar ratio) as fouling abatement and P-removal achieved as their secondary objective. The effect of coagulant addition on the fouling development/fouling removal, in addition to P-removal, is discussed in Section 3.3.

3.2.3.3. Dosing location. The right place for adding the precipitant to the influent or the effluent channel of the activated sludge/MBR tanks must be tested in each case, particularly regarding the essential intensive and rapid mixing with sewage flow to the treatment lane. The coagulant's addition in the aerobic zone of the A/O MBR was found to be the most effective, with P-removal efficiency over 85% (Zhang et al., 2015). A pilot-scale CASP study (Mbamba et al., 2019) analyzed the dosing of $FeSO_4$ at three different locations: aerobic, anoxic, and RAS/DEOX tanks. Feeding at the aerobic tank had a slightly higher effect on the chemical P-removal; consequently, this location is preferable due to high DO and good mixing conditions that could maximize HFO particulates and iron phosphate formation.

3.2.4. Mixing conditions

Apart from the coagulant type and dosage, mixing speed is the most critical aspect from the engineering point, given the slow P-removal kinetics. Understanding the role of mixing in P-removal kinetics is essential as almost all equilibrium-based precipitation models are based upon the assumption of ideal mixing and instant reactions (De Haas et al., 2000; Smith et al., 2008; Takács et al., 2011). Several studies have reported the importance of providing sufficient mixing for efficient P-removal, and the literature review revealed diverse results.

(Szabó et al., 2008) carried out studies with pre-polymerized metal salts rather than freshly formed salts to mimic conditions of inadequate mixing under which metal hydroxides form in the absence of phosphorus. Pre-polymerized salt removal was found to be less effective. Thus, a greater likelihood of interaction between P molecules and HFO flocs is provided by adequate mixing due to increased co-precipitation and adsorption. Mixing with a G value of 425 s^{-1} achieved almost 90% P-removal in 10–20 min, while coagulant addition during low mixing rate (20 rpm, G = 6 $s^{-1)}$ hampered P-removal (Smith et al., 2008). G value of 425 s^{-1} in a wastewater treatment facility is normally undesirable since the strong shear can break up flocs. The earlier studies with higher mixing rates had little to zero influence on P-removal performance (Thistleton et al., 2002; Kim and Chung, 2014). A recent MBR study (Li et al., 2019) documented the impact of mixing on P-removal. $FeCl_3$ was dosed into the MBR with rapid mixing (200 rpm) for around 5 min. It was possible to achieve over 95% P-removal with rapid mixing.

Keeping view the literature discussed, it is hard to establish the role of mixing in P-removal effectiveness. However, it can inferred that the mixing speed of 20–200 rpm is an optimum depending upon the time span of mixing which vary between with an inverse relationship with the rpm.

3.3. Chemical P-removal and membrane fouling

The precipitant is usually added downstream of the CASP, while in the case of MBR systems, it is added in the mixed liquor and before the filtration process or sometimes directly into the membrane tank (Gómez et al., 2013; Song et al., 2008). Therefore, the logistics and control of chemical addition and the dynamics and reliability of chemical P-removal are all more complicated in the MBR process than CASP (Zhang et al., 2015). It is now well established that the colloidal and SMPs found

Table 7
Chemical P-removal in MBR, SMP/EPS production and fouling development and/or mitigation.

Sr. no.	Reference	Wastewater	Scale	Configuration	Influent wastewater characteristics (mgL^{-1})						Coagulant information			Total P-removal %	Effluent P mgL^{-1}	EPS/SMP/macro molecules Concentration	Fouling
					COD	TN	NH_4	NO_3-N	PO_4^{3-}	TP	Coagulant	Molar Ratio	Optimum dose (mgL^{-1})				
1	Gnirss et al.,2003	RW	Lab	A/O	998	70	41	0.4		10.5	GFH	2.12	40	99.0%	0.1	NC	NE
		RW	Pilot	A/O	740	61	43	~~		9.1	GFH	2.45	40	98.9%	0.1	NC	NE
2	Adam et al., 2003	RW	Lab	UCT	998	69.7	41.3	0.42		10.5	$FeCl_3$	1.3	25	99.5%	0.05	NC	NC
3	Song et al., 2008	SW	Lab		45	35.4				11.1	$AlCl_3$	1.51	30	98.0%	0.05	NC	↓
		SW	Lab		27	30.8				13.1	$FeCl_3$	1.28	30	98.0%		NC	↓
4	Mishima and Nakajima, 2009	SW	Lab	A/O	560						$FeCl_3$	1.0	2260	92.5%		↓	↓
		SW	Lab	A/O	25						$FeCl_3$	2.0	4520	99.7%		↓	↓
5	Gómez et al., 2013	RW	Pilot	A/O	250		49	1.4	4.6	4.7	$FeCl_3$	2.0	12.4	84.7%	0.7	↓	NC
6	Yang et al., 2011	RW	Pilot	A/O	196	20.5	18.5	1.2		2.9	PFC	2.4	12.5	91.0%	0.26	↓	↑
7	Holba et al., 2012	RW	Pilot	MLE	724		40.8		4.2	4.3	$FeSO_4$	0.5	3.5	84.7%		↓	NC
		RW	Full	MLE	1140		105			8.7	$FeSO_4$	0.2	3.5	85%		↓	NC
		RW	Full	MLE	655		73.4			14.5	$FeSO_4$	0.1	3.5			↓	NC
8	Wang et al., 2014	RW	Pilot	UCT	400	50	25			9	FeCl3	2		>96%	0.05	↓	↑
		RW	Pilot								$FeSO_4$	2		>96%	0.05	↓	↑
9	Zhang et al., 2015	SW	Lab	UCT	400	60	25			10	$FeCl_3$	4		99.8%	0.02	↓	↑
											$Fe_2(SO_4)_3$	2		99.6%	0.03	↓	↑
10	Wu et al., 2015	SW	Pilot	A/O	400	50				8	$AlCl_3$	2		95.2%	0.38	NC	NC
			Pilot								$FeCl_3$	2		96.7%	0.26	NC	NC
11	Li et al., 2017	RW	Lab		50	17	15			2	Ferric	5.6	20	80.3%	0.29	↓	↓
											$AlCl_3$	17.2	30	80.3%	0.33	↓	↓
12	Lee et al., 2017	SW	Lab	UCT	293	24.3	20.7	0.4		4.25	PAC	3.4		85.5%	0.62	↑	↑
13	Li et al., 2018	RW	Lab		360	28.5				6.35	$FeCl_3$	1.8	20	95.6%	0.28	↓	↓
14	Wu et al., 2019	RW	Pilot	UCT					3.05		$Fe2(SO_{4)3}$	2				↓	↓
15	Sun et al., 2019	RW	Lab	UCT	268.1	40.4	38.6			4.97	$AlCl_3$	2.3	10	85.4%	0.73	↓	↓
16	Ren et al., 2019	SW	Lab	A/O	425	45	27.5			10	$Fe2(SO4)_3$	2		96.9%	0.31	NC	↓
												1		96.2%	0.38	NC	↓
17	Alibardi et al., 2021	RW	Full	A/O	579		26.9			9.18	$Fe2(SO_{4)3}$	3.75	14	95%	0.46	NC	NC

SM-synthetic wastewater; RM-real wastewater; NC- not confirmed; NE- no effect; PAC- Poly-aluminum chloride, GHF- granular ferric.

in mixed liquor are mainly responsible for membrane fouling (Gao et al., 2013). These products have a similar size to membrane pores and often appear to form impermeable gels on the membrane surface (Meng et al., 2017). The addition of precipitant (if not dosed optimally) into the MBR is assumed to be influential for organic, inorganic, and biofouling in addition to the P-removal (Hai et al., 2018; Meng et al., 2017).

As extensively discussed in the MBR fouling literature, inorganic fouling in MBRs is caused by biological and/or chemical precipitation of the metal cations (e.g., $Fe^{3+}$and Al^{3+}) and anions of ionizable biopolymers (e.g., as PO_4^{3-} and SO_4^{2-}) onto the membrane (Iorhemen et al., 2017; Wang et al., 2008). Several studies investigated the addition of a small concentration of coagulant into the MBR with the intention to control membrane fouling. It reduced the extent of the TMP evolution, which is assumed to be attributed to the large-sized floc formation (formed due to neutralization) and reduced organics concentration in the supernatant (reduction of organic fouling), limiting the pore blockage (Fan et al., 2007; Fleischer et al., 2005; Koseoglu et al., 2008; Wu et al., 2006; Zhang et al., 2008). In addition, it has been perceived that an optimum coagulant addition decreases the compressibility of the sludge flocs, changes the particle size distribution (PSD), reduces the concentration of EPS (and thus the reduction in the biofouling), increases the porosity of the membrane, and increases the MLSS filterability (Gómez et al., 2013; Song et al., 2008; Sun et al., 2019). Finally, it is assumed to pose an unknown risks to the membrane life when operated over more extended periods (Gnirss et al., 2003) and requires further research.

As described by Song et al. (2008), the hydraulic resistance of the cake is influenced by the coagulant addition, and a noticeable reduction was observed with the addition of coagulant above 200 mgL^{-1}. Usually, higher concentrations (*Fe/P in the range of 2–4*) are used for P-removal, and therefore results of these studies might be irreverent to understand the trade-off between the P-removal and membrane fouling. If the objective is complete P-removal, the Fe/P ratio is adjusted in the range of 1.5 and 4 (Sun et al., 2019; Takács et al., 2011; Zhang et al., 2015). Thus, an in-depth analysis of various studies focused on P-removal and membrane fouling is essential to derive the conclusions.

In addition to P-removal, coagulant (alum) addition enhanced membrane filtration performance and reduced the membrane fouling due to incorporation of the colloidal solids into the flocs (later removed with sludge) rather than sticking onto the membrane surface (Fleischer et al., 2005). Effect of ferric chloride and alum addition was investigated on P-removal, and on membrane fouling in a lab-scale study (Song et al., 2008). The authors found that the alum addition (13.3 mgAlum/mgP) resulted in 98% P-removal and reduced the specific cake resistance due to increased sludge particle size (from 45 μm to 57 μm). It was further found that the nitrification process was not impacted by the addition of the $FeCl_3$, while the phosphorus was removed and the membrane fouling effectively controlled. However, it reduced the pH to almost half (≈ 3.4) of its initial value as the concentration increased from 0 to 500 mgL^{-1}.

In another lab-scale study, the addition of $FeCl_3$ (Fe/P ratio = 2) successfully removed 99.7% of the phosphorus from the synthetic wastewater and decreased the fraction of SMPs (having protein and carbohydrates sizes falling between 0.1 and 0.4 μm) by 50% and thus reduced the membrane fouling propensity due to increased floc size (Mishima and Nakajima, 2009). Another pilot-scale study (Yang et al., 2011) employing polymeric ferric chloride (PFC) revealed an increase in membrane fouling. The authors conducted cake layer analysis using a three-dimensional excitation-emission matrix (EEM) and gel filtration chromatography (GFC). The analysis indicated that higher molecular weight organics (> 1000 kDa) were the main contributors of the membrane biofouling. Fourier transform infrared spectrum (FTIR) analysis further confirmed that these higher molecular weight organics were mostly protein and polysaccharides. The same authors also observed the formation of a dense and nonporous gel layer onto the membrane surface with clusters of bacteria and bio-polymers with help of a scanning electron microscope (SEM). Besides, X-ray elemental diffractometric analysis elucidated that ferric metal was the most prominent foulants responsible for inorganic fouling of the membrane.

The study of Holba et al. (2012) investigated the effect of lower coagulant concentration on P-removal and SMP production at pilot and full-scale. A fixed coagulant dose of 3.5 $mgFeSO_4L^{-1}$ was used for all three systems (one pilot and two full-scales). A better P-removal efficiency (84.7%) with a 68% reduction of SMPs was observed in pilot-scale plant. However, large load fluctuations and constant coagulant dosing in the full-scale plant caused in unsatisfactory P-removal. In another pilot-scale MBR study (Wang et al., 2014), similar effects have been documented where the coagulant dosing required optimization to balance the enhanced P-removal and coagulant-driven membrane fouling. The addition of metal salt (i.e. $FeCl_3$) resulted in 89%–97% P-removal efficiency and produced more sludge (Chae et al., 2015). In a lab-scale investigation (Sun et al., 2019), the addition of metal salt (20 mgL^{-1} of $Al_2(SO_4)_2$) resulted in achieving over 90% P-removal and reduced TMP (from 11.3$kPad^{-1}$ to 0,57$kPad^{-1}$) due to a decline in EPS concentrations and accumulation of particles on the membrane surface and increase in the particle size. The study of Asensi et al. (2019) revealed that the addition of $FeCl_3$ (in neutralized condition) linearly increased the floc size and resulted in more compact floc structure. This increases the settling properties of the sludge to an extent where the coagulant concentration reaches to an optimum level and beyond that floc is not able to retain the coagulant and the settling properties are then negatively impacted. This suggest that while modeling the membrane fouling using phenomenological models, changes in the settling properties of the sludge due to addition of coagulant should not be ignored. In another pilot-scale study (Gómez et al., 2013), the addition of 12.4 $mgFeCl_3L^{-1}$ improved the P-removal efficiency from 54.7% to 84.7%. The authors observed reduction in SMP concentration with the addition of the coagulant. The X-ray elemental diffractometric analysis of the cake layer found a significant increase in the Fe^{3+} concentration and a substantial contribution to inorganic fouling. The same authors further noticed that, at lower coagulant concentrations, it was not easy to ascertain the trade-off between the fouling reduced by the SMP removal and Fe^{3+} deposition and resulting inorganic fouling. The higher coagulant doses resulted in significant pH decrease and precipitated TP present in the sludge, resulting in a lack of available phosphorus for PAO to grow on and participate in the EBPR process. This becomes pertinent for MBR systems, which are operated at higher biomass concentrations as compared to CASP.

As phosphorus is essential for microbial communities other than PAOs, participating in nitrification and denitrification processes (Daigger et al., 2010). Similarly, Zhang et al. (2015) found that the precipitant dosing lowered the membrane fouling when with Fe/P molar ratios <1. However, P-removal was compromised and severe fouling (due to Fe-rich gel layer) was observed with higher molar ratios due to the formation of Fe-SMP complexes and amorphous ferric hydroxides ($Fe/P > 2$). The severity of the membrane fouling was observed when coagulant was dosed in the anoxic zone compared to dosing in the aerobic zone (much closer to membrane). The authors further found that molar ratio of 2 for Fe^{3+}/P successfully removed 99% phosphorus without impeding the nitrification/denitrification. However, it impacted the nitrification process significantly with a higher dose (molar ratio of 4) due to increased consumption of alkalinity associated with a decrease of pH value to almost 4 and thus required the pH adjustment. Minimizing overall iron dosage is also important, not only for cost reasons but also to avoid unwanted side effects like membrane fouling. Furthermore, the same authors found that lowering the phosphorus concentrations to 0.1–0.2 $mgPL^{-1}$ using higher coagulant doses did not inhibit nitrification. Instead, the harmful effects of the chemical precipitants (Fe^{2+} and Fe^{3+}) were blamed for suppressing nitrification and denitrification due to toxicity induced by the metals as reported by Philips et al. (2003).

Some studies used flotation (DAF) and biologically aerated filters (BAF) as post/pre-treatment to membrane filtration to improve the P-removal performance and as well as to counter the inorganic fouling caused by the metal deposition onto the membrane surface (Lee et al., 2016; Li et al., 2017). Similarly, Ren et al. (2019) reported the change in the microbial composition due to addition of ferrous in a ceramic MBR with a molar ratio of 2. The authors found that the relative abundance of the aerobic denitrifying bacterial community "Zoogolea" increased consistently. While the population of other bacterial community including "Dechloromonas, Hyphomicrobium and Thauera (anoxic denitrifying bacteria), Nitrospira (NOB) and Candidatus Accumulibacter (PAO) which is responsible for BioP-removal reduced sharply due to toxic effects of iron dose on bacterial physiology.

A trade-off between precipitant dose, fouling, and P-removal is reported differently for different studies, and hence further research is needed to explore the relationship between the type (cake formation, pore blocking, etc.) and quantum of the fouling induced (Loderer et al., 2015; Zhang et al., 2015). Majority of the MBR studies summarized in Table 7 are either lab-scale or pilot scale units while experiences of the P-removal and fouling abatement/fouling increase is limited and therefore more research is needed in this direction.

3.4. Modeling chemical precipitation of phosphorous

Several chemical precipitation models were developed for P-removal in wastewater systems, and very few of them have been adopted for precipitation modeling in CASP and MBRs. The precipitation model commonly used in combination with ASM models has been discussed briefly regarding its conceptualization and processes involved, application in MBR modeling, and the P-removal limitations. Mainly ASM2d is being used for modeling chemical P-removal in MBRs. Chemical precipitation models employ three main approaches i) chemical equilibrium approach, ii) kinetic model approach, iii) combined chemical equilibrium-kinetic approach and geo-chemical complexation (De Haas et al., 2000; Smith et al., 2008). These precipitation models are briefly reviewed for quick comparison in terms of processes considered, limitations, and their usefulness for coupling with the biological and filtration model in the MBR case. Although this review's scope is limited to the last two decades, it is still worth encompassing the modeling knowledge briefly beyond two decades.

3.4.1. Equilibrium-based models

Chemical precipitation modeling gained importance in the late 1970s, and Ferguson and King (1977) introduced the first equilibrium-based model using empirically derived solubility products. The model employed co-precipitation as the sole mechanism for removing PO_4^{3-}. It did not consider the removal of TP or even removal of precipitated orthophosphate. The molar ratio for Al/P in the precipitate is deemed to be constant at all pH values. The model was sufficient to describe the effects of alum dosage qualitatively and pH observed in several experimental studies. However, the model is based on a solubility equilibrium of a fictitious precipitate, i.e., $Al_{1.4}PO_4(OH)_{1.2,}$ and solubility products are empirically derived. Furthermore, the model did not consider pathways other than co-precipitation for the P-removal. It also did not included the effect of the competition of ions such as calcium, magnesium, iron, or hydroxy phosphate.

The previous model's limitation led to the development of an improved P-removal equilibrium model with ferric salt employing simultaneous precipitation and adsorption mechanisms (Luedecke et al., 1988). The model consists of i) mass balance equations (based on equilibrium) describing the acid-base reactions for dissociation (by hydrolysis) of PO_4^{3-} species and ferric ion-pair complexation with phosphate or OH^- ii) mass balance equations for phosphate and ferric iii) equations defining the split between the type of precipitate formed ($Fe_rPO_4(OH)_{3r\text{-}3}$ and FeOOH) at given pH and iv) adsorption equilibrium. The model has four parameters (Stoichiometric coefficient, solubility product, equilibrium constants ferric phosphate, and adsorption coefficient) with unknown values, estimated from the jar test under aerobic conditions and pH control. The model is again based on fictitious precipitates ($Fe_rPO_4(OH)_{3r\text{-}3}$ and FeOOH), and the solubility products are thus empirically derived. The adsorption coefficient is modified to each experimental condition over a wide range, inferring that the hypothetical adsorption mechanism is over-simplified and does not fully describe the actual adsorption phenomenon (De Haas et al., 2000; Hauduc et al., 2015).

The Water Environment Federation (WEF) suggested a chemical equilibrium-based precipitation model that took into account the amount of PO_4^{3-} removed as well as the pH sensitivity and is based on hypothetical ferric phosphate precipitate, i.e., $Fe_{1.6}H_2PO_4(OH)_{3.8,}$ which has been verified to be non-existent (Smith et al., 2008). The model is provided for both ferric and aluminum salts. Stoichiometric reactions are used to measure iron/alum dose close to a residual of 1.6 $mgPO_4L^{-1}$, at which point the equilibrium is reached, and the competition reaction starts. Additional metal salt is needed to achieve effluent P-removal below 1 $mgPL^{-1}$ since stoichiometric estimations are no longer reliable. In addition to metal phosphate precipitate, metal hydroxide is formed. The model predicts a minimum of 35 μgPO_4L^{-1} at an optimum pH of 6.95 (Takács et al., 2005). The model was then recalibrated by Takács et al. (2005) by combining it with equilibrium-based pH calculations, enabling the solution's ionic composition and termed as 'enhanced WEF.' The model was later implemented in BioWin to mimic the P-removal in full-scale facilities as a sub-module to the bio-kinetic model. The current version of the WEF model available in BioWin has improved the limitation caused by the fixed Fe/P molar ratio. The model is sufficient to estimate the pH, iron dose, and sludge production. Although it does not takes into account the P-removal pathways other than co-precipitation.

3.4.2. Models based on empirical kinetics

The bio-kinetic model (ASM2d) was extended with two chemical processes (precipitation and re-dissolution) to simulate two hypothetical compounds, namely metal hydroxide (X_{MeOH}) and metal phosphate (X_{MeP}). The model assumed that these two processes are opposite of each other and are in equilibrium at steady state conditions (Gujer et al., 1995). The precipitation and re-dissolution are modeled as simple first-order reactions using process kinetic rate (K_{pre}, and K_{red}). The authors used the example of ferric ion dosing in an activated sludge environment. MeOH is assumed to be $Fe(OH)_3$ in this situation, and MeP is considered $FePO_4$. The model does not account for the loss of hydroxide ions (a reduction in alkalinity) from the bulk process during the formation of $Fe(OH)_3$, but pH is assumed to be near neutral. The model does not provide any guidance for the estimation of the kinetic rates. Neither gives any indication for the model applicability with alum salts or other coagulants. It is mostly used in WEST software as standalone as well as with the bio-kinetic model (ASMs).

3.4.3. Models based on combined chemical equilibrium-kinetic approaches

Based on the steady-state equilibrium model of Luedecke et al. (1988), a dynamic model employing processes including i) co-precipitation, ii) dissociation, iii) hydrolysis, iv) adsorption, and v) biological nutrient requirements; was proposed by Briggs (1996). The model's basis is almost the same as inherent one with further addition of rate expressions for the precipitation/dissolution and adsorption/desorption. The Elovich equation (Manchado et al., 1989) is used to model P-adsorption, with switching functions for the residual phosphorus and full-adsorption potential. Besides, it considers the release of the adsorbed phosphorus during the dissociation process. The model further considered the biological components affecting the chemical phosphorus removal. Since the model is based on the same assumptions as of Luedecke et al. (1988), it inherited the same limitations. Furthermore, the mode was found unable to simulate the effluent's solids concentrations and thus its impacts on effluent total P concentrations.

Table 8
Comparative assessment of the chemical P-removal models.

Model reference	Model characteristics							
	Ferguson and King, 1977	Luedecke et al.,1989	Briggs et al.,1996	WEF Model,1998	IWA-ASM2d Model, 1999	Smith et al., 2008	Hauduc et al., 2015	Giwa and Hasan, 2015
Modeling approach								
Kinetic					√			
Chemical equilibrium	√	√		√		√	√	
Combined kinetic-equilibrium			√					
Geo-chemical reaction						√	√	
Electro-coagulation								√
System behavior (change in concentration over time)								
Steady state	√	√		√		√	√	
Dynamic			√	√		√	√	√
Removal mechanisms considered								
Hydrolysis		√	√					
Dissociation		√	√					√
Precipitation		√			√		√	
Co-precipitation	√		√	√		√	√	
Adsorption		√	√			√		
De-sorption			√					
Surface complexation/aging							√	
Biological nutrient requirements			√					
Dissolution			√					
Coagulants considered								
Aluminum	√		√	√				√
Ferric		√	√	√	√		√	
Type of model with respects to calculations								
Empirical	√	√	√					
Mechanistic					√	√	√	√
pH dependence	√	√	√					
Alkalinity dependence						√		
Influence of aging/surface consolidation						√		
Ability to predict low P-concentration			√	√	√	√	√	√
Limited	√	√	√					
Excellent				√	√		√	
P-species considered								
Ortho-phosphate	√		√	√	√		√	
Total phosphorus		√						
Influent P-fractionation			√					

3.4.4. Models based surface complexation and chemical equilibrium

Current equilibrium models are based on dissociation and solubility principles and cannot account for variable precipitate stoichiometry and time dynamics. The model proposed by Smith et al. (2008) employs geochemical principles in combination with chemical equilibrium. This model takes into account the interactions between amorphous HFO and P (i.e. adsorption and co-precipitation). The model uses an active site factor (ASF) to describe the availability of reactive oxygen atoms or "surface sites" for P complexation before, after, and during precipitation. The value of the ASF was found to be a function of parameters i.e. dosing, mixing, pH and aging conditions already discussed in detail in Section 3.2. The surface complexation model (SCM) has many benefits over previously used equilibrium and kinetics based models, including the fact that it is based on known chemical elements, as opposed to equilibrium or kinetic models which are based on fictitious precipitates. It also incorporates surface geochemical interactions, which were neglected in previous equilibrium and kinetic models. The SCM is best suitable to predicting behavior in systems with low effluent P limits. The model is based on simple hydrogen–iron-P system and completely ignores the variable water chemistry. Furthermore this model is not capable to describe the kinetic behavior of P-removal i.e. initial fast removal followed by the slow removal and the influence of HFO aging as observed by Szabó et al. (2008).

A recent study proposed a mechanistic chemical P-removal modeling method that explains HFO precipitation and flocculation, as well as P-adsorption onto HFO particulates and co-precipitation (Hauduc et al., 2015). All process reactions are described using kinetic rate expressions. The aging aspect of the model described by Hauduc et al. (2015) is one of the main modifications to the model by Smith et al. (2008), and therefore the model can provide more details than the previous version. There are still some limitations to address: i) HFO aging was calibrated to experimental data with a maximum age of 30 min and does not account for solid ages typical of wastewater treatment and ii) The effects of pH, TSS, and COD were not investigated.

Table 8 presents a comparative summary of the briefly presented models. The literature review has revealed that models now have improved the ability to predict the effluent P-removal for low concentrations. However, these are still unable to reliably describe the removal kinetics and impacts of the metal complex aging with higher SRTs. Not even a single study has been reported for their application and validation with the system operating at higher SRTs such as MBR. The recently developed model (Hauduc et al., 2015) yet requires validation at full-scale. Furthermore, the models have not been tested for their ability to predict chemical P-removal behavior in complex waters, where organics and other organisms could obstruct removal mechanisms. Improving the models' ability to explain these processes would result in more stable effluent P-levels and chemical sludge output at lower dose rates, resulting in cost savings in chemical and sludge treatment.

3.5. Application of chemical precipitation models to MBRs

There is a shortage of studies reporting the chemical precipitation model's application to MBRs operated at higher SRTs, and floc size is already smaller and sticky due to the higher concentration of EPS/SMPs.

Two of the reported MBR studies used ASM2d's kinetic precipitation model (Daigger et al., 2010; Fleischer et al., 2005) and did not provide any details about the kinetic and stoichiometric parameters and their adjustments. Meanwhile (Liu et al., 2011) used an enhanced WEF model available in BioWin simulation software with its default kinetic and stoichiometric parameters.

4. Control systems for P-removal

The conventional controllers (e.g., P, PI, PID) and advanced controllers (e.g., predictive, robust adaptive, sliding, and multi-model) have successfully been adopted in wastewater for process improvement and optimization. Artificial intelligence-based model controls such as artificial neural networks (ANN), deep learning neural networks (DNN), fuzzy techniques, and hybrid controls (neuro-fuzzy) are adapted in wastewater (Garikiparthy et al., 2016). However, their success is not satisfactory for complex phenomena such as P-removal (Sin and Al, 2021). Logarithm-based phosphorus control systems are deployed and are automated using SCADA to reduce consumption of the precipitants (to reduce cost) and maintain effluent compliance. The control systems used for precipitant addition are based on: i) continuous fixed dosing, ii) scheduled dosing, iii) influent proportional flow dosing-feed ratio controller, iv) phosphorus load proportional, and v) feedback control or PI controller (Garikiparthy et al., 2016; Kern, 2016). The chemical precipitation control system can be implemented with CASP and the MBRs or with any other technology requiring additional P-removal to meet the discharge limits (Shiek et al., 2020). The majority of the published studies in the precipitant dosing control domain are related to CASPs, while few studies have been found related to the MBR (Alibardi et al., 2021; Mbamba et al., 2019).

The most straightforward dosage controls have historically been based on flow rate and turbidity measurements. Still, a primary feedback controller was used to achieve outstanding control efficiency and substantial chemical savings with an online in situ phosphorus sensor in place (Ingildsen, 2002). The sensor was mounted in the flocculation chamber located near the effluent discharge point. The sensor-based online phosphorus measurements enabled (Devisscher et al., 2002) to monitor the chemical dose required to remove the phosphorous as per the set-point. The study of Craig et al. (2014) evaluated the application of a feedback-based "off the shelf" control system for precipitant dosing on full-scale extended aeration-based CASP. The system monitored the PO_4^{3-} concentration at the secondary clarifier's exit and controlled the ferric feeding upstream. The controller used an advanced algorithm capable of calculating the P-load and the required ferric dose, taking into account the stoichiometric relationship. This automated chemical P-removal system resulted in a 56% reduction in ferric consumption and fully recovered the investment in just 6.8 months. Another study (Garikiparthy et al., 2016) evaluated the application of four different controllers, i.e., feedback, feedforward and feed-ratio, and fixed-rate dosing, for a CASP to control the effluent phosphorus concentration by regulating the coagulant dosing and saving the chemical costs. The authors found that the feedback controller improved the P-removal by 52.54% and performed better than others. However, the same authors also found that the phosphorous removal (EQI) and the P-removal (OCI) cost are conflicting and, therefore, suggested further research of the plant-wide dosing control. In a most recent full-scale MBR study (Alibardi et al., 2021), application of feed-forward control based on PO_4^{3-} load proportional, reduced the iron consumption from 14 mgL^{-1} to 12 mgL^{-1}. The schematics of various control systems discussed in this section are given in Appendix E.

5. Knowledge gaps and future research directions

This review is dedicated to summarize the current 'state of the art' in progress toward understanding of the P-removal in MBR, and application of existing bio-kinetic and chemical precipitation models. Keeping in view the findings from large number of scientific publications considered, identified research gaps and speculations about the future research are presented in this section.

The review of the global regulations (Appendix A), revealed that the majority of the countries have based their discharge regulations considering TP concentrations while eutrophication is mainly caused by bioavailable fraction of the phosphorus (Preisner et al., 2020) which mainly included PO_4^{3-}. Therefore, it is recommended to revisit the phosphorus discharge limits and should be ideally based on PO_4^{3-} concentrations. However, literature review revealed that there is no standardized and globally accepted approach for classifying the phosphorus fractions and this presents an urgent need to address this issue along with the standardized notation of each fraction and corresponding testing method (Rosario et al., 2021). Despite overall effectiveness of different wastewater treatment technologies for TPremoval is well known, there is a dearth of studies documenting the effectiveness of various technologies for removal of specific fractions of phosphorus. Most of the full scale application use EBPR and chemical precipitation in conjunction to maximize the P-removal and therefore sufficient data is not available to quantitatively describe how much of the P-removal is due to EBPR or chemical precipitation. Further research is required to assess the degree of BioP-removal that can be achieved in full scale MBRs that requires chemical addition to reliably meet the discharge limits.

EBPR is well established and yet poorly understood process for P-removal from wastewater (Bunce et al., 2018). Full-scale facilities are still being challenged by the process instability of EBPR process due to lack of understanding of the role of microbial communities, especially PAOs and their selection in anaerobic zone in comparison to GAOs. Over the last five decades, primary PAO responsible for EBPR has been changing from *Acinetobacter* to *Accumulibacter* and most recently *Tetrasphaera* have been found in large number of full scale CASP facilities (Hauduc et al., 2015; Mielczarek et al., 2013; Stokholm-Bjerregaard et al., 2017). This is probably because of the fact that PAOs responsible for EBPR have not been identified in pure culture neither GAOs responsible for deterioration of EBPR. Theoretically, anaerobic zone is compelling requirements for proliferation of PAOs and their selection for P-removal, while some full-scale studies without having an anaerobic zone have demonstrated 50–68% removal efficiencies with operating conditions not suitable to EBPR process (Gabarrón et al., 2014; Itokawa et al., 2014). Future research should be dedicated to enhance the EBPR process stability in MBRs by improving the MBR design configurations and optimizing operational conditions without compromising its capabilities to remove carbon and nitrogen. Majority of the full-scale MBR facilities are anoxic-aerobic or MLE configurations while UCT and MUCT are widely in research at bench and pilot scales. To the best of authors' knowledge, no full-scale study is dedicated to assess the BioP-removal in relation to the microbial composition involved in each MBR configuration and unit cost of biological and chemical precipitation should be investigated to present a fair comparison.

The bio-kinetic models appeared to be successful in simulating the P-removal in MBRs, provided fundamental differences in CASP and MBR functioning (Table 3) are considered in the modeling approach. It has been found that ASMs when applied to MBR require substantial modifications of the stoichiometric and kinetic parameters (Table 5) to adjust the lack of understanding in details and dynamics of the process as a generalized EBPR model. Efforts dedicated to develop systematic calibration procedures have resulted in decreasing the required calibration efforts. However, the calibration processes lacks identification of bio-kinetics involved in parametric adjustments and results in diverse range of parameters values. Moreover, the existing model consider only one PAO community i.e. *Accumulibacter* while literature suggested a number of PAOs communities are responsible for EBPR and therefore bio-kinetic models require improvements to accommodate the role of other microbial communities as well. A combination of metabolic and kinetic models can be helpful in apprehension of the complex

biological interactions in relation with their population dynamics and thus improving the EBPR modeling (Al-Atar, 2007; Hauduc et al., 2015). Some experimental studies have investigated that the EPS/SMP play a positive role in BioP-removal (Adoonsook et al., 2019; Ichihashi et al., 2006; Jiang et al., 2009; Zhang et al., 2013) while the current ASMs do not consider this phenomenon. It is therefore proposed to undertake full-scale studies to rule out the difference in lab-scale to full-scale models' applications.

Chemically enhanced P-removal (CEP) is a well-established yet again poorly understood because of formation of unknown metal complexes and multiple pathways involved. P-removal in MBR is different than CASP due to specificities involved in its functioning and risk of fouling development (Mbamba et al., 2019; Sun et al., 2019). Moreover, the effect of MLSS concentration, floc size (which is smaller in MBRs) on CEP performance should be investigated considering the competing mechanism for MeP and MeOH production. Diverse results have been reported for fouling development/abatement and P-removal trends in various bench-pilot scale studies, while experiences from the full scale facilities are yet required to be explored. A dedicated research is therefore needed to explore the effect of coagulant addition on membrane fouling in addition to P-removal along with clear description of type and quantum of the fouling induced. Precipitation models have now good prediction capabilities yet unable to reliably describe the removal kinetics and impacts of metal complex aging at higher SRTs which is the case in the MBRs. Further research is need to explore the applicability of these precipitation models at full-scale MBRs operating at higher SRTs and with smaller floc size, generally undesirable for effective coagulation and operating under higher shear induced by the coarse bubble aerations.

The control of coagulant and carbon dosing, recirculation rates and DO concentration are key factors in achieving maximum P-removal in MBRs. There is a shortage of studies documenting the role of the automatic controls for chemical dosing in MBRs and techno-economic assessment of the proposed control systems. Future research should be dedicated to apply the various instrumentation and control systems for advanced automated controls for enhanced and cost effective P-removal.

6. Conclusion

MBRs are successful in P-removal below regulatory limits by employing combined EBPR and chemical precipitation mechanisms. P-removal in MBR is a complex and poorly understood phenomenon which is sensitive to design configurations (MLE, A/O, UCT, A^2/O, VIP and Bardenpho), influent characteristics and several operating parameters related to EBPR (Microbial composition, MLSS, SRT, HRT, temperature and DO) and chemical precipitation (influent chemistry and composition, DO, pH, MLSS, Me/P molar ratio, dosing location and number of dosing points and mixing conditions). It is hard to establish the role of EBPR and chemical precipitation methods when used in conjunction. The bench and pilot scale UCT and MUCT configurations provide excellent control over nitrates interference in the anaerobic zone resulting in higher BioP-removal efficiencies (up to 90%). However, MLE and Bardenpho are widely used configurations at full-scale facilities. MBR can provide enhanced Bio-P removal, if:

- The influent COD/TP, BOD/TP, COD/TN ratio are provided in the ranges of 2.9–45, 12.33–45, and 5.3–7.3 respectively. Furthermore, influent nitrate are kept lower than 1 $g \cdot m^{-3}$ to keep the anaerobic zone efficiency intact with PAOs proliferation.
- The MLSS concentration is controlled under 7 $g \cdot m^{-3}$ with SRT in the range of 15–40 days. Anaerobic and aerobic HRT are controlled in the range of 2–2.9 h and 3–6 h respectively, while total HRT is kept around 10 h.
- 7–10% of the sludge biomass are PAOs.
- The DO concentration of 0.4–2.5 $g \cdot m^{-3}$ is maintained in the aerobic zone

Similarly, chemically precipitation in MBR can provide excellent results, if:

- Alkalinity of the influent wastewater is within 98–123 $CaCO_3$ $g \cdot m^{-3}$
- The pH of the sludge is controlled near circumneutral level (6.5–7)
- Relatively higher DO concentration (1.5–2.5 $g \cdot m^{-3}$) are maintained in the aerobic zone
- Metal to Phosphorus molar ratio is adjusted in the range 1.5–4 with an optimum ratio of 2.5.
- Two point dosing is practiced, first dosing at the inlet or at 3/4th of the anoxic reactor and 2nd dosing in the aerobic zone.
- Rapid mixing is provided with G values ranging between 100 and 200 s^{-1}

Several bio-kinetic, precipitation, filtration as well as integrated models are available to simulate the MBR process including P-removal. The addition of the precipitant affects the relative abundance of microbial community sludge composition and fouling phenomenon. Therefore, integrated models should have provision to adjust the stoichiometric changes induced due to change in the microbial composition and competition among them as well as the reduction in EPS concentration. Filtration model must be adjusted to take into account the influence of floc size reduction, role of coagulant (metal ions e.g. Fe^{2+}) in inorganic fouling and reduction in the stickiness between the membrane and sludge particles due to reduced deposition of EPS onto membrane. Majority of the modeling studies are focused on pilot-scale units and lab-scale units and there is dire shortage of the full-scale MBR systems. It is therefore suggested to undertake full-scale integrated modeling studies in future taking into account the bio-chemical P-removal and fouling development as well as the influence of the precipitant addition on microbial communities.

IWA standard nomenclature for model parameters

$q_{XCB\_SB,hyd}$ maximum specific hydrolyis rate
$n_{qhyd,An}$ corrction factor for hydrolyis
$K_{NHx,OHO}$ half saturation coefficient for S_{NHx}
b_{OHO} decay rate of X_{OHO}
q_{PAO,VFA_Stor} rate constant for X_{PAO} storage
$q_{PAO,PO4\_PP}$ rate constant for storage of X_{PAO_PP}
$K_{PP,PAO}$ half saturation coefficient for X_{PAO_PP}
$\mu_{PAO,Max}$ maximum growth rate of X_{PAO}
μ_{PAO,Max_lim} maximum growth rate of X_{PAO} (when P is limiting)
$n_{\mu PAO}$ reduction factor for anoxic growth rate of X_{PAO}
m_{PAO}/b_{PAO} decay rate of X_{PAO}
$\mu_{ANO,Max}$ maximum growth rate of X_{ANO}
b_{ANO} decay rate of X_{ANO}
$K_{O2,ANO}$ half saturation coefficient for S_{O2}
$K_{NHx,ANO}$ half saturation coefficient for S_{NHx}
$K_{O2,hyd}$ inhibitation coefficient for S_{NHx}
$q_{SF\_VFA,Max}$ Maxmum specific fermentation growth rate
$\mu_{OHO,Max}$ Max. growth rate of X_{OHO}
$n_{\mu OHO,Ax}$ reduction factor for anoxic growth rate
Y_{OHO} Yield for X_{OHO} growth
$Y_{OHO,Ax}$ Yield for X_{OHO} growth (anoxic)
$Y_{Stor\_OHO,Ax}$ Yield for X_{OHO} growth per $X_{OHO,\ stor}$ (anoxic)
$f_{XU\_Bio,lys}$ fraction of X_U generated in X_{OHO} decay
Y_{PAO} Yield for X_{PAO} growth
$Y_{PP\_Stor,PAO}$ Yield for $X_{PAO,PP}$ requirement
i_{N_XU} N content of X_U
i_{N_XCB} N content of X_{CB}
i_{P_XU} P content X_U
i_{P_XBio} P content of biomass
i_{P_XCB} P content of X_{CB}

Supplementary data to this article can be found online at https://doi.org/10.1016/j.scitotenv.2021.151109.

Credit authorship contribution statement

Kashif NADEEM, Data collection, Data analysis and interpretation, Drafting the article, Final approval of the version to be published.

Marion ALLIET Conception or design of the work, Data analysis and interpretation, Drafting the article, Final approval of the version to be published.

Queralt PLANA Drafting the article, Critical revision of the article, Final approval of the version to be published.

Jean BERNIER Drafting the article, Critical revision of the article, Final approval of the version to be published.

Sam AZIMI Managing the global project, Final approval of the version to be published.

Vincent ROCHER Managing the global project, Final approval of the version to be published.

Claire ALBASI Conception or design of the work, Data analysis and interpretation, Critical revision of the article, Final approval of the version to be published.

Declaration of competing interest

The authors declare that they have no known competing financial interests or personal relationships that could have appeared to influence the work reported in this paper.

Acknowledgments

The authors gratefully acknowledge the financial support of Higher Education Commission of Pakistan and Parisian Sanitation Public Service (SIAAP) for this project. Furthermore, the technical support of the SIAAP is greatly acknowledged in structuring and reviewing the manuscript.

References

Abegglen, C., Ospelt, M., Siegrist, H., 2008. Biological nutrient removal in a small-scale MBR treating household wastewater. Water Res. 42, 338–346. https://doi.org/10.1016/j.watres.2007.07.020.

Adam, C., Gnirss, R., Lesjean, B., Buisson, H., Kraume, M., 2002. Enhanced biological phosphorus removal in membrane bioreactors. Water Sci. Technol. 46, 281–286. https://doi.org/10.2166/wst.2002.0606.

Adam, C., Kraume, M., Gnirss, R., Lesjean, B., 2003. Membrane bioreactor configurations for enhanced biological phosphorus removal. Water Sci. Technol. Water Supply 3, 237–244.

Adoonsook, D., Chia-Yuan, C., Wongrueng, A., Pumas, C., 2019. A simple way to improve a conventional A/O-MBR for high simultaneous carbon and nutrient removal from synthetic municipal wastewater. PLOS ONE 14, e0214976. https://doi.org/10.1371/journal.pone.0214976.

Ahmed, Z., 2012. Microbial communities in nutrient-removing membrane bioreactors: a review. J. Environ. Sci. Technol. 5, 16–28.

Ahmed, Z., Lim, B.-R., Cho, J., Ahn, K.-H., 2007. Effects of the internal recycling rate on biological nutrient removal and microbial community structure in a sequential anoxic/anaerobic membrane bioreactor. Bioprocess Biosyst. Eng. 30, 61–69. https://doi.org/10.1007/s00449-006-0098-4.

Ahn, K.-H., Song, K.-G., Choa, E., Cho, J., Yun, H., Lee, S., Me, J., 2003. Enhanced biological phosphorus and nitrogen removal using a sequencing anoxic/anaerobic membrane bioreactor (SAM) process. Desalination, Desalination and the Environment: Fresh Water for All. 157, pp. 345–352. https://doi.org/10.1016/S0011-9164(03)00415-6.

Al-Atar, E., 2007. Dynamic Modeling and Process Design of a Membrane Enhanced Biological Phosphorus Removal Process. University of British Columbia, Canada https://doi.org/10.14288/1.0228857 PhD dissertation.

Aleta, P., Parikh, S.J., Silchuk, A.P., Scow, K.M., Park, M., Kim, S., 2018. The effect of organic matter on the removal of phosphorus through precipitation as struvite and calcium phosphate in synthetic dairy wastewater. Membr. Water Treat. 9, 163–172. https://doi.org/10.12989/mwt.2018.9.3.163.

Al-Hashimia, M.A.I., Abbas, T.R., Jasema, Y.I., 2013. Performance of sequencing anoxic/anaerobic membrane bioreactor (SAM) system in hospital wastewater treatment and reuse. Eur. Sci. J. 9 (15) ISSN: 1857 – 7881 (Print) e - ISSN 1857- 7431.

Alibardi, L., Vale, P., Bajón Fernández, Y., 2021. Full-scale trials to achieve low total phosphorus in effluents from sewage treatment works. 40, 101981. https://doi.org/10.1016/j.jwpe.2021.101981.

Arif, A.U.A., Sorour, M.T., Aly, S.A., 2020. Cost analysis of activated sludge and membrane bioreactor WWTPs using CapdetWorks simulation program: case study of Tikrit WWTP (middle Iraq). 59 (6), 4659–4667. https://doi.org/10.1016/j.aej.2020.08.023.

Asensi, E., Zambrano, D., Alemany, E., Aguado, D., 2019. Effect of the addition of precipitated ferric chloride on the morphology and settling characteristics of activated sludge flocs. Sep. Purif. Technol. 227, 115711. https://doi.org/10.1016/j.seppur.2019.115711.

Autin, O., Hai, F., Judd, S., McAdam, E.J., 2016. Investigating the significance of coagulation kinetics on maintaining membrane permeability in an MBR following reactive coagulant dosing. J. Membr. Sci. 516, 64–73. https://doi.org/10.1016/j.memsci.2016.06.008.

Azizi, J., 2018. Management of Non-renewable Resources: Market Equilibrium, Socio-economic Impacts and Potential Channels of Resource Curse-An Application to Phosphate Rock. Ph.D. DissertationCERNA at Ecole des Mines, Paris, France 2018PSLEM030_archivage.pdf.

Baetens, D., 2001. Enhanced Biological Phosphorus Removal: Modelling and Experimental Design Gestimuleerde Biologische Fosfaatverwijdering: Modelbouw en Experimenteel Ontwerp. Ph.D. DissertationUniversity of Ghen, Belgium.

Banu, J.R., Uan, D.K., Chung, I.-J., Kaliappan, S., Yeom, I.-T., 2009. A study on the performance of a pilot scale A2/0-MBR system in treating domestic wastewater. J. Environ. Biol. 30, 959–963.

Barker, P.S., Dold, P.L., 1997. General model for biological nutrient removal activated-sludge systems: model presentation. 69, 969–984. https://doi.org/10.2175/106143097X125669.

Barnard, J.L., Dunlap, P., Steichen, M., 2017. Rethinking the mechanisms of biological phosphorus removal. 89, 2043–2054. https://doi.org/10.2175/106143017X15051465919010.

Bashar, R., Gungor, K., Karthikeyan, K.G., Barak, P., 2018. Cost effectiveness of phosphorus removal processes in municipal wastewater treatment. Chemosphere 197, 280–290. https://doi.org/10.1016/j.chemosphere.2017.12.169.

Bis, M., Montusiewicz, A., Piotrowicz, A., Łagód, G., 2019. Modeling of wastewater treatment processes in membrane bioreactors compared to conventional activated sludge systems. Processes 7, 285. https://doi.org/10.3390/pr7050285.

Briggs, T.A., 1996. Dynamic Modelling of Chemical Phosphorus Removal in the Activated Sludge Process. School of Graduate Studies, McMaster Univ, Hamilton, Ontario, Canada M. Sc. Thesis.

Brown, P., Ong, S.K., Lee, Y.-W., 2011. Influence of anoxic and anaerobic hydraulic retention time on biological nitrogen and phosphorus removal in a membrane bioreactor. Desalination 270, 227–232. https://doi.org/10.1016/j.desal.2010.12.001.

Bunce, J.T., Ndam, E., Ofiteru, I.D., Moore, A., Graham, D.W., 2018. A review of phosphorus removal technologies and their applicability to small-scale domestic wastewater treatment systems. Front. Environ. Sci. 6. https://doi.org/10.3389/fenvs.2018.00008.

Burman, I., Sinha, A., 2018. A review on membrane fouling in membrane bioreactors: control and mitigation. In: Gupta, T., Agarwal, A.K., Agarwal, R.A., Labhsetwar, N.K. (Eds.), Environmental Contaminants: Measurement, Modelling and Control, Energy, Environment, and Sustainability. Springer, Singapore, pp. 281–315 https://doi.org/10.1007/978-981-10-7332-8_13.

Caravelli, A.H., Contreras, E.M., Zaritzky, N.E., 2010. Phosphorous removal in batch systems using ferric chloride in the presence of activated sludges. J. Hazard. Mater. 177, 199–208. https://doi.org/10.1016/j.jhazmat.2009.12.018.

Caravelli, A.H., De Gregorio, C., Zaritzky, N.E., 2012. Effect of operating conditions on the chemical phosphorus removal using ferric chloride by evaluating orthophosphate precipitation and sedimentation of formed precipitates in batch and continuous systems. Chem. Eng. J. 209, 469–477. https://doi.org/10.1016/j.cej.2012.08.039.

Chae, S.-R., Chung, J.-H., Heo, Y.-R., Kang, S.-T., Lee, S.-M., Shin, H.-S., 2015. Full-scale implementation of a vertical membrane bioreactor for simultaneous removal of organic matter and nutrients from municipal wastewater. Water 7, 1164–1172. https://doi.org/10.3390/w7031164.

Cho, J., Song, K.-G., Hyup Lee, S., Ahn, K.-H., 2005. Sequencing anoxic/anaerobic membrane bioreactor (SAM) pilot plant for advanced wastewater treatment. Desalination, Membranes in Drinking and Industrial Water Production. 178, pp. 219–225. https://doi.org/10.1016/j.desal.2004.12.018.

Choi, H.-J., Lee, H., Lee, S.-M., 2011. Effect of phosphorus concentration on phosphorus removal and biomass. Water Sci. Technol. 64, 887–891. https://doi.org/10.2166/wst.2011.656.

Clark, T., Burgess, J.E., Stephenson, T., Arnold-Smith, A.K., 2000. The influence of iron-based co-precipitants on activated sludge biomass. Process Saf. Environ. Prot. 78, 405–410. https://doi.org/10.1205/095758200530916.

Cloete, T.E., Oosthuizen, D.J., 2001. The role of extracellular exopolymers in the removal of phosphorus from activated sludge. Water Res. 35, 3595–3598. https://doi.org/10.1016/S0043-1354(01)00093-8.

Conidi, D., Parker, W.J., 2015. The effect of solids residence time on phosphorus adsorption to hydrous ferric oxide floc. Water Res. 84, 323–332. https://doi.org/10.1016/j.watres.2015.07.046.

Cordell, D., Drangert, J.-O., White, S., 2009. The story of phosphorus: global food security and food for thought. Global Environmental Change, Traditional Peoples and Climate Change. 19, pp. 292–305. https://doi.org/10.1016/j.gloenvcha.2008.10.009.

Corsino, S.F., de Oliveira, T.S., Di Trapani, D., Torregrossa, M., Viviani, G., 2020. Simultaneous sludge minimization, biological phosphorous removal and membrane fouling mitigation in a novel plant layout for MBR. J. Environ. Manag. 259, 109826. https://doi.org/10.1016/j.jenvman.2019.109826.

Cosenza, A., Mannina, G., Neumann, M.B., Viviani, G., Vanrolleghem, P.A., 2013. Biological nitrogen and phosphorus removal in membrane bioreactors: model development and parameter estimation. Bioprocess Biosyst. Eng. 36, 499–514. https://doi.org/10.1007/s00449-012-0806-1.

Cosenza, A., Mannina, G., Vanrolleghem, P.A., Neumann, M.B., 2014. Variance-based sensitivity analysis for wastewater treatment plant modelling. Sci. Total Environ. 470, 1068–1077. https://doi.org/10.1016/j.scitotenv.2013.10.069.

Craig, K., Minnema, R., Dabkowski, B., Gironi, M.S., 2014. Evaluation of an "Off the Shelf" automated chemical phosphorus removal system. Procedia Engineering, 12th International Conference on Computing and Control for the Water Industry, CCWI2013. 70, pp. 363–368. https://doi.org/10.1016/j.proeng.2014.02.041.

Daigger, G.T., Crawford, G.V., Johnson, B.R., 2010. Full-scale assessment of the nutrient removal capabilities of membrane bioreactors. 82, 806–818.
De Haas, D.W., Wentzel, M.C., Ekama, G.A., 2000. The use of simultaneous chemical precipitation in modified activated sludge systems exhibiting biological excess phosphate removal-part 1: literature review. Water SA 26, 439–452.
de-Bashan, L.E., Bashan, Y., 2004. Recent advances in removing phosphorus from wastewater and its future use as fertilizer (1997–2003). Water Res. 38, 4222–4246. https://doi.org/10.1016/j.watres.2004.07.014.
Delrue, F., Choubert, J.M., Stricker, A.E., Spérandio, M., Mietton-Peuchot, M., Racault, Y., 2010. Modelling a full scale membrane bioreactor using activated sludge model no.1: challenges and solutions. Water Sci. Technol. 62, 2205–2217. https://doi.org/10.2166/wst.2010.383.
Denisova, V., Tihomirova, K., Neilands, J., Gruskevica, K., Mezule, L., Juhna, T., 2020. Comparison of Phosphorus Removal Efficiency of Conventional Activated Sludge System and Sequencing Batch Reactors in a Wastewater Treatment Plant. https://doi.org/10.15159/ar.20.049.
Devisscher, M., Bogaert, H., Bixio, D., Van de Velde, J., Thoeye, C., 2002. Feasibility of automatic chemicals dosage control–a full-scale evaluation. Water Sci. Technol. 45, 445–452.
Di Bella, G., Mannina, G., Viviani, G., 2008. An integrated model for physical-biological wastewater organic removal in a submerged membrane bioreactor: model development and parameter estimation. J. Membr. Sci. 322, 1–12.
Dold, P.L., Ekama, G.A., Marais, G.vR., 1981. A general model for the activated sludge process. Water Pollution Research and Development. Elsevier, pp. 47–-77 https://doi.org/10.1016/B978-1-4832-8438-5.50010-8.
Dold, P.L., Bye, C.M., Hu, Z., 2010. Nutrient Removal MBR Systems: Factors in Design and Operation, Nutrient Removal MBR Systems: Factors in Design and Operation. Water Environment Federation.
Downing, L., Young, M., Cramer, J., Nerenberg, R., Bruce, S., 2014. Low level DO operation: impacts on energy, nutrients, and ecology. Proc. Water Environ. Fed. 2014, 6771–6783.
du Toit, G.J.G., Ramphao, M.C., Parco, V., Wentzel, M.C., Ekama, G.A., 2007. Design and performance of BNR activated sludge systems with flat sheet membranes for solid-liquid separation. Water Sci. Technol. 56, 105–113. https://doi.org/10.2166/wst.2007.643.
Emergen, R., 2021. Membrane Bioreactor Market by system configuration (external, submerged), by membrane type (flat sheet, hollow fiber, multi-tubular), by application (industrial wastewater treatment, municipal wastewater treatment), and by region, forecasts to 2027. https://www.emergenresearch.com/industry-report/membrane-bioreactor-market received 6th September 2021.
Ersu, C., 2006. Biological Nutrient Removal in Bench-scale Membrane Bioreactor and Full-scale Sequencing Batch Reactor Under Various Configurations and Conditions. Iowa State University, USA https://doi.org/10.31274/rtd-180813-8752 Ph.D. Dissertation.
Ersu, C., Ong, S.K., Arslankaya, E., Brown, P., 2008. Comparison of recirculation configurations for biological nutrient removal in a membrane bioreactor. Water Res. 42, 1651–1663. https://doi.org/10.1016/j.watres.2007.10.022.
Ersu, C.B., Ong, S.K., Arslankaya, E., Lee, Y.-W., 2010. Impact of solids residence time on biological nutrient removal performance of membrane bioreactor. Water Res. 44, 3192–3202. https://doi.org/10.1016/j.watres.2010.02.036.
Falahati-Marvast, H., Karimi-Jashni, A., 2020. A new modified anoxic-anaerobic-membrane bioreactor for treatment of real wastewater with a low carbon/nutrient ratio and high nitrate. 33, 101054. https://doi.org/10.1016/j.jwpe.2019.101054.
Fan, F., Zhou, H., Husain, H., 2007. Use of chemical coagulants to control fouling potential for wastewater membrane bioreactor processes. 79, 952–957. https://doi.org/10.2175/106143007X194329.
Fenu, A., Guglielmi, G., Jimenez, J., Spèrandio, M., Saroj, D., Lesjean, B., Brepols, C., Thoeye, C., Nopens, I., 2010. Activated sludge model (ASM) based modelling of membrane bioreactor (MBR) processes: a critical review with special regard to MBR specificities. Water Res. 44, 4272–4294. https://doi.org/10.1016/j.watres.2010.06.007.
Ferguson, J.F., King, T., 1977. A model for aluminum phosphate precipitation. J. Water Pollut. Control Fed. 646–658.
Ferrero, G., Monclús, H., Buttiglieri, G., Gabarron, S., Comas, J., Rodríguez-Roda, I., 2011. Development of a control algorithm for air-scour reduction in membrane bioreactors for wastewater treatment. J. Chem. Technol. Biotechnol. 86, 784–789. https://doi.org/10.1002/jctb.2587.
Fleischer, E.J., Broderick, T.A., Daigger, G.T., Fonseca, A.D., Holbrook, R.D., Murthy, S.N., 2005. Evaluation of membrane bioreactor process capabilities to meet stringent effluent nutrient discharge requirements. 77, 162–178. https://doi.org/10.2175/106143005X41735.
Fu, Z., Yang, F., An, Y., Xue, Y., 2009. Simultaneous nitrification and denitrification coupled with phosphorus removal in an modified anoxic/oxic-membrane bioreactor (A/O-MBR). Biochem. Eng. J. 43, 191–196. https://doi.org/10.1016/j.bej.2008.09.021.
Gabarrón, S., Ferrero, G., Dalmau, M., Comas, J., Rodriguez-Roda, I., 2014. Assessment of energy-saving strategies and operational costs in full-scale membrane bioreactors. J. Environ. Manag. 134, 8–14. https://doi.org/10.1016/j.jenvman.2013.12.023.
Gabarrón, S., Dalmau, M., Porro, J., Rodriguez-Roda, I., Comas, J., 2015. Optimization of full-scale membrane bioreactors for wastewater treatment through a model-based approach. Chem. Eng. J. 267, 34–42. https://doi.org/10.1016/j.cej.2014.12.097.
Gao, M., Yang, M., Li, H., Yang, Q., Zhang, Y., 2004. Comparison between a submerged membrane bioreactor and a conventional activated sludge system on treating ammonia-bearing inorganic wastewater. J. Biotechnol. 108, 265–269. https://doi.org/10.1016/j.jbiotec.2003.12.002.
Gao, W.J., Han, M.N., Qu, X., Xu, C., Liao, B.Q., 2013. Characteristics of wastewater and mixed liquor and their role in membrane fouling. Bioresour. Technol. 128, 207–214. https://doi.org/10.1016/j.biortech.2012.10.075.
Garikiparthy, P.S.N., Lee, S.C., Liu, H., Kolluri, S.S., Esfahani, I.J., Yoo, C.K., 2016. Evaluation of multiloop chemical dosage control strategies for total phosphorus removal of enhanced biological nutrient removal process. Korean J. Chem. Eng. 33, 14–24. https://doi.org/10.1007/s11814-015-0132-9.
Germain, E., Nelles, F., Drews, A., Pearce, P., Kraume, M., Reid, E., Judd, S.J., Stephenson, T., 2007. Biomass effects on oxygen transfer in membrane bioreactors. Water Res. 41, 1038–1044. https://doi.org/10.1016/j.watres.2006.10.020.
Gernaey, K., Sin, G., 2008. Wastewater treatment models. Encyclopedia of Ecology, pp. 3707–3718 https://doi.org/10.1016/b978-008045405-4.00828-4.
Gernaey, K.V., van Loosdrecht, M.C.M., Henze, M., Lind, M., Jørgensen, S.B., 2004. Activated sludge wastewater treatment plant modelling and simulation: state of the art. 19, 763–783. https://doi.org/10.1016/j.envsoft.2003.03.005.
Gholikandi, G.B., Khosravi, M., 2012. Upgrading of submerged membrane bioreactor operation with regard to soluble microbial products and mathematical modeling for optimisation of critical flux. Desalin. Water Treat. 39, 199–208. https://doi.org/10.1080/19443994.2012.669176.
Giwa, A., Hasan, S.W., 2015. Numerical modeling of an electrically enhanced membrane bioreactor (MBER) treating medium-strength wastewater. J. Environ. Manag. 164, 1–9. https://doi.org/10.1016/j.jenvman.2015.08.031.
Gnirss, R., Lesjean, B., Adam, C., Buisson, H., 2003. Cost effective and advanced phosphorus removal in membrane bioreactors for a decentralised wastewater technology. Water Sci. Technol. 47, 133–139. https://doi.org/10.2166/wst.2003.0638.
Gomes de Quevedo, C.M., da Silva Paganini, W., 2016. Detergents as a source of phosphorus in sewage: the current situation in Brazil. Water Air Soil Pollut. 227 (1), 14. https://doi.org/10.1007/s11270-015-2700-3.
Gómez, M., Dvořák, L., Růžičková, I., Wanner, J., Holba, M., Sýkorová, E., 2013. Influence of phosphorus precipitation on permeability and soluble microbial product concentration in a membrane bioreactor. Bioresour. Technol. 129, 164–169. https://doi.org/10.1016/j.biortech.2012.11.052.
Gray, N.F., 2004. Biology of Wastewater Treatment. 2nd edition. World Scientific, Singapore https://doi.org/10.1142/p266.
Gu, A.Z., Liu, L., Neethling, J.B., Stensel, H.D., Murthy, S., 2011. Treatability and fate of various phosphorus fractions in different wastewater treatment processes. Water Sci. Technol. 63, 804–810.
Gujer, W., Henze, M., Mino, T., Matsuo, T., Wentzel, M.C., Marais, G.V.R., 1995. The activated sludge model no. 2: biological phosphorus removal. Water Sci. Technol. 31, 1–11.
Gujer, W., Henze, M., Mino, T., van Loosdrecht, M., 1999. Activated sludge model no. 3. Water Sci. Technol. 39 (1), 183–193. https://doi.org/10.1016/S0273-1223(98)00785-9.
Guo, W.Q., Luo, H.C., Yang, S.S., Wu, Q.L., Peng, S.M., 2014. Emerging technologies for phosphorus removal and recovery: a review. in: Applied Mechanics and Materials. Trans Tech Publ, pp. 702–706.
Gutierrez, O., Park, D., Sharma, K.R., Yuan, Z., 2010. Iron salts dosage for sulfide control in sewers induces chemical phosphorus removal during wastewater treatment. Water Res. 44, 3467–3475. https://doi.org/10.1016/j.watres.2010.03.023.
Hai, F.I., Yamamoto, K., Lee, C.-H., 2018. Membrane Biological Reactors: Theory, Modeling, Design, Management and Applications to Wastewater Reuse. Iwa Publishing https://doi.org/10.2166/9781780409177.
Han, X., Wang, Z., Ma, J., Zhu, C., Li, Y., Wu, Z., 2015. Membrane bioreactors fed with different COD/N ratio wastewater: impacts on microbial community, microbial products, and membrane fouling. Environ. Sci. Pollut. Res. 22, 11436–11445. https://doi.org/10.1007/s11356-015-4376-z.
Hauduc, H., Rieger, L., Oehmen, A., van Loosdrecht, M.C.M., Comeau, Y., Héduit, A., Vanrolleghem, P.A., Gillot, S., 2013. Critical review of activated sludge modeling: state of process knowledge, modeling concepts, and limitations. Biotechnol. Bioeng. 110, 24–46. https://doi.org/10.1002/bit.24624.
Hauduc, H., Takács, I., Smith, S., Szabo, A., Murthy, S., Daigger, G.T., Spérandio, M., 2015. A dynamic physicochemical model for chemical phosphorus removal. Water Res. 73, 157–170. https://doi.org/10.1016/j.watres.2014.12.053.
Henze, M., Leslie Grady, C.P., Gujer, W., Marais, G.V.R., Matsuo, T., 1987. A general model for single-sludge wastewater treatment systems. Water Res. 21 (5), 505–515. https://doi.org/10.1016/0043-1354(87)90058-3.
Henze, M., Gujer, W., Mino, T., Matsuo, T., Wentzel, M.C., Marais, G.V.R., Van Loosdrecht, M.C.M., 1999. Activated sludge model no.2d, ASM2D. Water Sci. Technol. 39, 165–182. https://doi.org/10.2166/wst.1999.0036.
Henze, M., van Loosdrecht, M.C., Ekama, G.A., Brdjanovic, D., 2008. Biological Wastewater Treatment. https://doi.org/10.2166/9781780401867.
Hocaoglu, S.M., Insel, G., Ubay Cokgor, E., Orhon, D., 2011. Effect of sludge age on simultaneous nitrification and denitrification in membrane bioreactor. Bioresour. Technol. 102, 6665–6672. https://doi.org/10.1016/j.biortech.2011.03.096.
Holakoo, L., Nakhla, G., Yanful, E.K., Bassi, A.S., 2005. Simultaneous nitrogen and phosphorus removal in a continuously fed and aerated membrane bioreactor. J. Environ. Eng. 131 (10), 1469–1472. https://doi.org/10.1061/(ASCE)0733-9372(2005)131:10(1469).
Holba, M., Plotěný, K., Dvořák, L., Gómez, M., Růžičková, I., 2012. Full-scale applications of membrane filtration in municipal wastewater treatment plants. CLEAN – Soil,Air, Water 40, 479–486. https://doi.org/10.1002/clen.201000398.
Hu, Z., Wentzel, M.C., Ekama, G.A., 2007. A general kinetic model for biological nutrient removal activated sludge systems: model development. Biotechnol. Bioeng. 98, 1242–1258. https://doi.org/10.1002/bit.21508.
Hu, X., Xie, L., Shim, H., Zhang, S., Yang, D., 2014. Biological nutrient removal in a full scale anoxic/anaerobic/aerobic/pre-anoxic-MBR plant for low C/N ratio municipal wastewater treatment. Chin. J. Chem. Eng. 22, 447–454. https://doi.org/10.1016/S1004-9541(14)60064-1.
Ichihashi, O., Satoh, H., Mino, T., 2006. Effect of soluble microbial products on microbial metabolisms related to nutrient removal. Water Res. 40, 1627–1633. https://doi.org/10.1016/j.watres.2006.01.047.

Iglesias, R., Simón, P., Moragas, L., Arce, A., Rodriguez-Roda, I., 2017. Cost comparison of full-scale water reclamation technologies with an emphasis on membrane bioreactors. Water Sci. Technol. 75 (11), 2562–2570.
Ingildsen, P., 2002. Realising Full-scale Control in Wastewater Treatment Systems Using In Situ Nutrient Sensors PhD. Dissertation in Industrial Electrical Engineering and Automation of Lund University, Sweden.
Insel, G., Hocaoğlu, S.M., Cokgor, E.U., Orhon, D., 2011. Modelling the effect of biomass induced oxygen transfer limitations on the nitrogen removal performance of membrane bioreactor. J. Membr. Sci. 368, 54–63. https://doi.org/10.1016/j.memsci.2010.11.003.
Insel, G., Erol, S., Övez, S., 2014. Effect of simultaneous nitrification and denitrification on nitrogen removal performance and filamentous microorganism diversity of a full-scale MBR plant. Bioprocess Biosyst. Eng. 37, 2163–2173. https://doi.org/10.1007/s00449-014-1193-6.
Iorhemen, O.T., Hamza, R.A., Tay, J.H., 2017. Membrane fouling control in membrane bioreactors (MBRs) using granular materials. Bioresource Technology. Special Issue on Challenges in Environmental Science and Engineering, CESE-2016240, pp. 9–24. https://doi.org/10.1016/j.biortech.2017.03.005.
Itokawa, H., Tsuji, K., Yamashita, K., Hashimoto, T., 2014. Design and operating experiences of full-scale municipal membrane bioreactors in Japan. Water Sci. Technol. 69 (5), 1088–1093. https://doi.org/10.2166/wst.2014.020.
Jadhao, R.K., Dawande, S.D., 2012. Modeling of biological phosphorus removal using membrane bioreactor- part-1. Int. J. Chem. Sci. Appl. 3 (2), 276–282.
Janssen, P.M.J., Meinema, K., Van der Roest, H.F., 2002. Biological Phosphorus Removal. IWA publishing ISBN13: 9781843390121.
Janus, T., 2014. Integrated mathematical model of a MBR reactor including biopolymer kinetics and membrane fouling. Procedia Engineering. 12th International Conference on Computing and Control for the Water Industry, CCWI201370, pp. 882–891. https://doi.org/10.1016/j.proeng.2014.02.098.
Jiang, T., Myngheer, S., De Pauw, D.J.W., Spanjers, H., Nopens, I., Kennedy, M.D., Amy, G., Vanrolleghem, P.A., 2008. Modelling the production and degradation of soluble microbial products (SMP) in membrane bioreactors (MBR). Water Res. 42, 4955–4964. https://doi.org/10.1016/j.watres.2008.09.037.
Jiang, T., Sin, G., Spanjers, H., Nopens, I., Kennedy, M.D., van der Meer, W., Futselaar, H., Amy, G., Vanrolleghem, P.A., 2009. Comparison of the modeling approach between membrane bioreactor and conventional activated sludge processes. 81, 432–440.
Johansson, P.N.O., 1996. SIPHOR: A Kinetic Model for Simulation of Biological Phosphate Removal. Department of Water and Environmental Engineering, Lund University, Sweden PhD dissertation.
Judd, S., 2010. The MBR Book: Principles and Applications of Membrane Bioreactors for Water and Wastewater Treatment. Elsevier.
Kang, S.-K., Choo, K.-H., Lim, K.-H., 2003. Use of iron oxide particles as adsorbents to enhance phosphorus removal from secondary wastewater effluent. Sep. Sci. Technol. 38, 3853–3874. https://doi.org/10.1081/SS-120024236.
Kapagiannidis, A.G., Zafiriadis, I., Aivasidis, A., 2012. Effect of basic operating parameters on biological phosphorus removal in a continuous-flow anaerobic–anoxic activated sludge system. Bioprocess Biosyst. Eng. 35, 371–382. https://doi.org/10.1007/s00449-011-0575-2.
Kern, P., 2016. Computational Intelligence Techniques for Control and Optimization of Wastewater Treatment Plants. Ph.D. DissertationNational University of Ireland Maynooth, Ireland.
Kim, J.-O., Chung, J., 2014. Implementing chemical precipitation as a pretreatment for phosphorus removal in membrane bioreactor-based municipal wastewater treatment plants. KSCE J. Civ. Eng. 18, 956–963. https://doi.org/10.1007/s12205-014-0070-9.
Kishida, N., Kim, J., Tsuneda, S., Sudo, R., 2006. Anaerobic/oxic/anoxic granular sludge process as an effective nutrient removal process utilizing denitrifying polyphosphate-accumulating organisms. Water Res. 40, 2303–2310. https://doi.org/10.1016/j.watres.2006.04.037.
Koseoglu, H., Yigit, N.O., Iversen, V., Drews, A., Kitis, M., Lesjean, B., Kraume, M., 2008. Effects of several different flux enhancing chemicals on filterability and fouling reduction of membrane bioreactor (MBR) mixed liquors. J. Membr. Sci. 320, 57–64. https://doi.org/10.1016/j.memsci.2008.03.053.
Krzeminski, P., Leverette, L., Malamis, S., Katsou, E., 2017. Membrane bioreactors–a review on recent developments in energy reduction, fouling control, novel configurations, LCA and market prospects. J. Membr. Sci. 527, 207–227.
Lanham, A.B., Oehmen, A., Saunders, A.M., Carvalho, G., Nielsen, P.H., Reis, M.A.M., 2014. Metabolic modelling of full-scale enhanced biological phosphorus removal sludge. Water Res. 66, 283–295. https://doi.org/10.1016/j.watres.2014.08.036.
Lee, J.C., Kim, J.S., Kang, I.J., Cho, M.H., Park, P.K., Lee, C.H., 2001. Potential and limitations of alum or zeolite addition to improve the performance of a submerged membrane bioreactor. Water Sci. Technol. 43, 59–66.
Lee, H., Han, J., Yun, Z., 2009. Biological nitrogen and phosphorus removal in UCT-type MBR process. Water Sci. Technol. 59, 2093–2099. https://doi.org/10.2166/wst.2009.242.
Lee, H., Yun, G.H., Kim, S., Yun, Z., 2015. The 4-stage anoxic membrane bioreactor for simultaneous nitrogen and phosphorus removal, and its strengths and weaknesses. Desalin. Water Treat. 54, 3616–3624. https://doi.org/10.1080/19443994.2014.923214.
Lee, E.-J., Kim, H.-S., Jang, A., 2016. Application of dissolved air flotation (DAF) with coagulation process for treatment of phosphorus within permeate of membrane bioreactor (MBR). Desalin. Water Treat. 57, 9043–9050. https://doi.org/10.1080/19443994.2015.1057034.
Lee, E.-J., An, A.K., Kim, H.-S., 2017. Effects of coagulant with different basicity on membrane-based biological treatment for removing phosphorus. J. Coast. Res. 79 (sp1), 65–69. https://doi.org/10.2112/SI79-014.1.
Lesjean, B., Gnirss, R., Adam, C., Kraume, M., Luck, F., 2003. Enhanced biological phosphorus removal process implemented in membrane bioreactors to improve phosphorous recovery and recycling. Water Sci. Technol. 48, 87–94.
Lesjean, B., Gnirss, R., Buisson, H., Keller, S., Tazi-Pain, A., Luck, F., 2005. Outcomes of a 2-year investigation on enhanced biological nutrients removal and trace organics elimination in membrane bioreactor (MBR). Water Sci. Technol. 52 (10-11), 453–460.
Lesjean, B., Ferre, V., Vonghia, E., Moeslang, H., 2009. Market and design considerations of the 37 larger MBR plants in Europe. Desalin. Water Treat. 6, 227–233. https://doi.org/10.5004/dwt.2009.648.
Li, X., Liu, Y., Liu, F., Liu, A., Feng, Q., 2017. Comparison of ferric chloride and aluminum sulfate on phosphorus removal and membrane fouling in MBR treating BAF effluent of municipal wastewater. 7, 442–448. https://doi.org/10.2166/wrd.2016.151.
Li, R., Wang, X., Li, X., 2018. A membrane bioreactor with iron dosing and acidogenic cofermentation for enhanced phosphorus removal and recovery in wastewater treatment. Water Res. 129, 402–412. https://doi.org/10.1016/j.watres.2017.11.035.
Li, R., Wang, W., Li, B., Zhang, J., Liu, J., Zhang, G., Guo, X., Zhang, X., Li, X., 2019. Acidogenic phosphorus recovery from the wastewater sludge of the membrane bioreactor systems with different iron-dosing modes. Bioresour. Technol. 280, 360–370. https://doi.org/10.1016/j.biortech.2019.02.060.
Liau, K.F., Shoji, T., Ong, Y.H., Chua, A.S.M., Yeoh, H.K., Ho, P.Y., 2015. Kinetic and stoichiometric characterization for efficient enhanced biological phosphorus removal (EBPR) process at high temperatures. Bioprocess Biosyst. Eng. 38, 729–737. https://doi.org/10.1007/s00449-014-1313-3.
Liu, W., Hu, Z., Walker, R.L., Dold, P.L., 2011. Enhanced nutrient removal MBR system with chemical addition for low effluent TP. Water Sci. Technol. 64, 1298–1306. https://doi.org/10.2166/wst.2011.145.
Liu, C., Chen, L., Zhu, L., Wu, Z., Hu, Q., Pan, M., 2019. The effect of feed temperature on biofouling development on the MD membrane and its relationship with membrane performance: an especial attention to the microbial community succession. J. Membr. Sci. 573, 377–392. https://doi.org/10.1016/j.memsci.2018.12.003.
Loderer, C., Gahleitner, B., Woerle, A., Fuchs, W., 2015. Dynamic filtration––influence of different precipitation agents on the filtration performance using an inside-out filtration module. Desalin. Water Treat. 53, 940–950. https://doi.org/10.1080/19443994.2013.846235.
Lopez-Vazquez, C.M., Oehmen, A., Hooijmans, C.M., Brdjanovic, D., Gijzen, H.J., Yuan, Z., van Loosdrecht, M.C.M., 2009. Modeling the PAO–GAO competition: effects of carbon source, pH and temperature. Water Res. 43, 450–462. https://doi.org/10.1016/j.watres.2008.10.032.
Luedecke, C., Hermanowicz, S.W., Jenkins, David, 1988. In: Lijklema, L., Imhoff, K.R., Ives, K.J., Jenkins, D., Ludwig, R.G., Suzuki, M., Toerien, D.F., Wheatland, A.B., Milburn, A., Izod, E.J. (Eds.), Water Pollution Research and Control Brighton. Pergamon, pp. 325–337 https://doi.org/10.1016/B978-1-4832-8439-2.50035-3.
Maere, T., Verrecht, B., Moerenhout, S., Judd, S., Nopens, I., 2011. BSM-MBR: a benchmark simulation model to compare control and operational strategies for membrane bioreactors. Water Res. 45, 2181–2190. https://doi.org/10.1016/j.watres.2011.01.006.
Manchado, M.C., Guil, J.M., Paniego, A.R., 1989. The elovich differential equation. Hydrogen and oxygen adsorption on supported iridium. 85, 1775–1786.
Mannina, G., Cosenza, A., Vanrolleghem, P.A., Viviani, G., 2011. A practical protocol for calibration of nutrient removal wastewater treatment models. J. Hydroinf. 13, 575–595. https://doi.org/10.2166/hydro.2011.041.
Mannina, G., Cosenza, A., Ekama, G.A., 2018. A comprehensive integrated membrane bioreactor model for greenhouse gas emissions. Chem. Eng. J. 334, 1563–1572. https://doi.org/10.1016/j.cej.2017.11.061.
Mannina, G., Ni, B.-J., Ferreira Rebouças, T., Cosenza, A., Olsson, G., 2020. Minimizing membrane bioreactor environmental footprint by multiple objective optimization. Bioresour. Technol. 302, 122824. https://doi.org/10.1016/j.biortech.2020.122824.
Mannina, G., Alliet, M., Brepols, C., Comas, J., Harmand, J., Heran, M., Kalboussi, N., Makinia, J., Robles, Á., Rebouças, T.F., Ni, B.-J., Rodriguez-Roda, I., Victoria Ruano, M., Bertanza, G., Smets, I., 2021. Integrated membrane bioreactors modelling: a review on new comprehensive modelling framework. Bioresour. Technol. 329, 124828. https://doi.org/10.1016/j.biortech.2021.124828.
Mao, Y., Ninh Pham, A., Xin, Y., David Waite, T., 2012. Effects of pH, floc age and organic compounds on the removal of phosphate by pre-polymerized hydrous ferric oxides. Sep. Purif. Technol. 91, 38–45. https://doi.org/10.1016/j.seppur.2011.09.045 Special issue In honor of Professor Xiang-zhong Li.
Mao, Y., Graham, D.W., Tamaki, H., Zhang, T., 2015. Dominant and novel clades of candidatus accumulibacter phosphatis in 18 globally distributed full-scale wastewater treatment plants. Sci. Rep. 5, 11857. https://doi.org/10.1038/srep11857.
Mbamba, C.K., Lindblom, E., Flores-Alsina, X., Tait, S., Anderson, S., Saagi, R., Batstone, D.J., Gernaey, K.V., Jeppsson, U., 2019. Plant-wide model-based analysis of iron dosage strategies for chemical phosphorus removal in wastewater treatment systems. Water Res. 155, 12–25.
Meijer, S.C.F., 2004. Theoretical and Practical Aspects of Modelling Activated Sludge Processes. Delft University of Technology, The Netherlands PhD Dissertations.
Melcer, H., 2004. Methods for Wastewater Characterization in Activated Sludge Modelling ISBN13: 9781843396628.
Meng, F., Chae, S.-R., Drews, A., Kraume, M., Shin, H.-S., Yang, F., 2009. Recent advances in membrane bioreactors (MBRs): membrane fouling and membrane material. Water Res. 43, 1489–1512. https://doi.org/10.1016/j.watres.2008.12.044.
Meng, F., Chae, S.R., Shin, H.S., Yang, F., Zhou, Z., 2012. Recent advances in membrane bioreactors: configuration development, pollutant elimination, and sludge reduction. Environ. Eng. Sci. 29 (3), 139–160. https://doi.org/10.1089/ees.2010.0420.
Meng, F., Zhang, S., Oh, Y., Zhou, Z., Shin, H.-S., Chae, S.-R., 2017. Fouling in membrane bioreactors: an updated review. Water Res. 114, 151–180. https://doi.org/10.1016/j.watres.2017.02.006.

Mielczarek, A.T., Nguyen, H.T.T., Nielsen, J.L., Nielsen, P.H., 2013. Population dynamics of bacteria involved in enhanced biological phosphorus removal in danish wastewater treatment plants. 47, 1529–1544. https://doi.org/10.1016/j.watres.2012.12.003.
Mishima, I., Nakajima, J., 2009. Control of membrane fouling in membrane bioreactor process by coagulant addition. Water Sci. Technol. 59, 1255–1262. https://doi.org/10.2166/wst.2009.090.
Monclús, H., Sipma, J., Ferrero, G., Comas, J., Rodriguez-Roda, I., 2010. Optimization of biological nutrient removal in a pilot plant UCT-MBR treating municipal wastewater during start-up. Desalination 250, 592–597. https://doi.org/10.1016/j.desal.2009.09.030.
Monti, A., Hall, E.R., Dawson, R.N., Husain, H., Kelly, H.G., 2006. Comparative study of biological nutrient removal (BNR) processes with sedimentation and membrane-based separation. Biotechnol. Bioeng. 94, 740–752. https://doi.org/10.1002/bit.20896.
Monti, A., Hall, E.R., Koch, F.A., Dawson, R.N., Husain, H., Kelly, H.G., 2007. Toward a high-rate enhanced biological phosphorus removal process in a membrane-assisted bioreactor. 79, 675–686. https://doi.org/10.2175/106143007X156790.
Mulkerrins, D., Dobson, A.D.W., Colleran, E., 2004. Parameters affecting biological phosphate removal from wastewaters. Environ. Int. 30, 249–259.
Naessens, W., Maere, T., Nopens, I., 2012a. Critical review of membrane bioreactor models – part 1: biokinetic and filtration models. Bioresource Technology. 122, pp. 95–106. https://doi.org/10.1016/j.biortech.2012.05.070.
Naessens, W., Maere, T., Ratkovich, N., Vedantam, S., Nopens, I., 2012b. Critical review of membrane bioreactor models – part 2: hydrodynamic and integrated models. Bioresource Technology. 122, pp. 107–118. https://doi.org/10.1016/j.biortech.2012.05.071.
Newcombe, R.L., Strawn, D.G., Grant, T.M., Childers, S.E., Möller, G., 2008. Phosphorus removal from municipal wastewater by hydrous ferric oxide reactive filtration and coupled chemically enhanced secondary treatment: part II—mechanism. Water Environ. Res. 80, 248–256. https://doi.org/10.2175/106143007X220987.
Ng, A.N.L., Kim, A.S., 2007. A mini-review of modeling studies on membrane bioreactor (MBR) treatment for municipal wastewaters. Desalination 212, 261–281. https://doi.org/10.1016/j.desal.2006.10.013.
Ni, B.-J., Xie, W.-M., Liu, S.-G., Yu, H.-Q., Gan, Y.-P., Zhou, J., Hao, E.-C., 2010. Development of a mechanistic model for biological nutrient removal activated sludge systems and application to a full-scale WWTP. 56, 1626–1638.
Nielsen, P.H., McIlroy, S.J., Albertsen, M., Nierychlo, M., 2019. Re-evaluating the microbiology of the enhanced biological phosphorus removal process. Current Opinion in Biotechnology. Energy Biotechnology • EnvironmentalBiotechnology57, pp. 111–118. https://doi.org/10.1016/j.copbio.2019.03.008.
van Nieuwenhuijzen, A.F., van der Graaf, J.H.J.M, Kampschreur, M.J., Mels, A.R, 2004. Particle related fractionation and characterisation of municipal wastewater. Water Sci. Technol. 50 (12), 125–132. https://doi.org/10.2166/wst.2004.0704.
Nopens, I., Sin, G., Jiang, T., d'Antonio, L., Stama, S., Zhao, J., Vanrolleghem, P.A., 2007. Model-based optimisation of the biological performance of a sidestream MBR. Water Sci. Technol. 56, 135–143. https://doi.org/10.2166/wst.2007.640.
Oehmen, A., Lemos, P.C., Carvalho, G., Yuan, Z., Keller, J., Blackall, L.L., Reis, M.A.M., 2007. Advances in enhanced biological phosphorus removal: from micro to macro scale. Water Res. 41, 2271–2300. https://doi.org/10.1016/j.watres.2007.02.030.
Omwene, P.I., Kobya, M., Can, O.T., 2018. Phosphorus removal from domestic wastewater in electrocoagulation reactor using aluminium and iron plate hybrid anodes. Ecol. Eng. 123, 65–73. https://doi.org/10.1016/j.ecoleng.2018.08.025.
Onnis-Hayden, A., Majed, N., Schramm, A., Gu, A.Z., 2011. Process optimization by decoupled control of key microbial populations: distribution of activity and abundance of polyphosphate-accumulating organisms and nitrifying populations in a full-scale IFAS-EBPR plant. Water Res. 45, 3845–3854. https://doi.org/10.1016/j.watres.2011.04.039.
Panswad, T., Doungchai, A., Anotai, J., 2003. Temperature effect on microbial community of enhanced biological phosphorus removal system. Water Res. 37, 409–415. https://doi.org/10.1016/S0043-1354(02)00286-5.
Parco, V., du Toit, G., Wentzel, M., Ekama, G., 2007. Biological nutrient removal in membrane bioreactors: denitrification and phosphorus removal kinetics. Water Sci. Technol. 56, 125–134. https://doi.org/10.2166/wst.2007.642.
Park, J.-H., Kang, H.-J., Kim, H.-S., Wells, G.F., Park, H.-D., 2019. Effects of alkali-treated sludge supplementation for enhanced biological phosphorus removal in a membrane bioreactor. Fuel 254, 115588. https://doi.org/10.1016/j.fuel.2019.05.171.
Pellegrin, M.L., Neethling, J.B., Menniti, A., Sandino, J., Stensel, D., 2015. Application of Membrane Bioreactor Processes for Achieving Low Effluent Nutrient Concentrations. IWA Publishing https://doi.org/10.2166/9781780406756.
Philips, S., Rabaey, K., Verstraete, W., 2003. Impact of iron salts on activated sludge and interaction with nitrite or nitrate. Bioresour. Technol. 88, 229–239. https://doi.org/10.1016/S0960-8524(02)00314-0.
Preisner, M., Neverova-Dziopak, E., Kowalewski, Z., 2020. An analytical review of different approaches to wastewater discharge standards with particular emphasis on nutrients. Environ. Manag. 66, 694–708. https://doi.org/10.1007/s00267-020-01344-y.
Rahman, S.M., Eckelman, M.J., Onnis-Hayden, A., Gu, A.Z., 2016. Life-cycle assessment of advanced nutrient removal technologies for wastewater treatment. Environ. Sci. Technol. 50, 3020–3030. https://doi.org/10.1021/acs.est.5b05070.
Ramasahayam, S.K., Guzman, L., Gunawan, G., Viswanathan, T., 2014. A comprehensive review of phosphorus removal technologies and processes. J. Macromol. Sci. A 51, 538–545.
Ramphao, M., Wentzel, M.C., Merritt, R., Ekama, G.A., Young, T., Buckley, C.A., 2005. Impact of membrane solid–liquid separation on design of biological nutrient removal activated sludge systems. Biotechnol. Bioeng. 89, 630–646. https://doi.org/10.1002/bit.20311.
Ren, B., Li, C., Zhang, X., Zhang, Z., 2019. Fe(II)-dosed ceramic membrane bioreactor for wastewater treatment: nutrient removal, microbial community and membrane fouling analysis. Sci. Total Environ. 664, 116–126. https://doi.org/10.1016/j.scitotenv.2019.02.019.
Reynolds, C.S., Davies, P.S., 2001. Sources and bioavailability of phosphorus fractions in freshwaters: a British perspective. Biol. Rev. 76 (1), 27–64. https://doi.org/10.1111/j.1469-185X.2000.tb00058.x.
Rieger, L., Koch, G., Kühni, M., Gujer, W., Siegrist, H., 2001. The EAWAG bio-P module for activated sludge model no. 3. Water Res. 35, 3887–3903.
Rieger, L., Gillot, S., Langergraber, G., Ohtsuki, T., Shaw, A., Takacs, I., Winkler, S., 2012. Guidelines for Using Activated Sludge Models. IWA publishing.
Roberts, R., 2020. Mapping Spontaneous Biological Phosphorus Removal in a Membrane Bioreactor Process Without the Anaerobic Condition: Investigating the Effect of Alternative External Carbon Sources. Master ThesisKTH, Sweden. https://kth.diva-portal.org/smash/get/diva2:1509979/FULLTEXT01.pdf.
Rosario, P., Viswash, R., Seenivasan, T., Ramalingam, S., Sellgren, K.L., Grego, S., Trotochaud, L., 2021. Potential pitfalls in wastewater phosphorus analysis and how to avoid them. 15. https://doi.org/10.1177/11786302211019218.
Rosenberger, S., Witzig, R., Manz, W., Szewzyk, U., Kraume, M., 2000. Operation of different membrane bioreactors: experimental results and physiological state of the microorganisms. Water Sci. Technol. 41, 269–277. https://doi.org/10.2166/wst.2000.0659.
Rossle, W.H., Pretorius, W.A., 2001. A review of characterisation requirements for in-line prefermenters: paper 2: process characterisation. Water SA 27 (3), 413–422. https://doi.org/10.4314/wsa.v27i3.4986.
Saito, T., Brdjanovic, D., van Loosdrecht, M.C.M., 2004. Effect of nitrite on phosphate uptake by phosphate accumulating organisms. Water Res. 38, 3760–3768. https://doi.org/10.1016/j.watres.2004.05.023.
Santos, J.M.M., Rieger, L., Lanham, A.B., Carvalheira, M., Reis, M.A.M., Oehmen, A., 2020. A novel metabolic-ASM model for full-scale biological nutrient removal systems. Water Res. 171, 115373. https://doi.org/10.1016/j.watres.2019.115373.
Sarioglu, M., Sayi-Ucar, N., Cokgor, E., Orhon, D., Van Loosdrecht, M.C.M., Insel, G., 2017. Dynamic modeling of nutrient removal by a MBR operated at elevated temperatures. Water Res. 123, 420–428.
Sayi-Ucar, N., Sarioglu, M., Insel, G., Cokgor, E.U., Orhon, D., van Loosdrecht, M.C.M., 2015. Long-term study on the impact of temperature on enhanced biological phosphorus and nitrogen removal in membrane bioreactor. Water Res. 84, 8–17. https://doi.org/10.1016/j.watres.2015.06.054.
Seviour, T., Derlon, N., Dueholm, M.S., Flemming, H.-C., Girbal-Neuhauser, E., Horn, H., Kjelleberg, S., van Loosdrecht, M.C.M., Lotti, T., Malpei, M.F., Nerenberg, R., Neu, T.R., Paul, E., Yu, H., Lin, Y., 2019. Extracellular polymeric substances of biofilms: suffering from an identity crisis. Water Res. 151, 1–7. https://doi.org/10.1016/j.watres.2018.11.020.
Shiek, A.G., Machavolu, V.R.K., Seepana, M.M., Ambati, S.R., 2020. Design of control strategies for nutrient removal in a biological wastewater treatment process. Environ. Sci. Pollut. Res. https://doi.org/10.1007/s11356-020-09347-2.
Silva, A.F., Carvalho, G., Lousada Ferreira, M., van Nieuwenhuijzen, A., Guglielmi, G., Crespo, J., Reis, M.A., Crespo, M.T.B., 2009. Microbial population structure of pilot and full scale membrane bioreactors. Proceedings of Final MBR Network Workshop 31 March–1 April, Berlin, Germany.
Silva, A.F., Carvalho, G., Oehmen, A., Lousada-Ferreira, M., van Nieuwenhuijzen, A., Reis, M.A., Crespo, M.T.B., 2012. Microbial population analysis of nutrient removal-related organisms in membrane bioreactors. Appl. Microbiol. Biotechnol. 93, 2171–2180.
Sin, G., Al, R., 2021. Activated sludge models at the crossroad of artificial intelligence—a perspective on advancing process modeling. NPJ CleanWater 4, 1–7. https://doi.org/10.1038/s41545-021-00106-5.
Sin, G., Van Hulle, S.W.H., De Pauw, D.J.W., van Griensven, A., Vanrolleghem, P.A., 2005. A critical comparison of systematic calibration protocols for activated sludge models: a SWOT analysis. Water Res. 39, 2459–2474. https://doi.org/10.1016/j.watres.2005.05.006.
Sin, G., Niville, K., Bachis, G., Jiang, T., Nopens, I., van Hulle, S., Vanrolleghem, P.A., 2008. Nitrite effect on the phosphorus uptake activity of phosphate accumulating organisms (PAOs) in pilot-scale SBR and MBR reactors. Water SA 34, 249–260. https://doi.org/10.4314/wsa.v34i2.
Smith, S., Takacs, I., Murthy, S., Daigger, G.T., Szabo, A., 2008. Phosphate complexation model and its implications for chemical phosphorus removal. 80, 428–438.
Smith, S., Kim, G., Doan, L., Roh, H., 2014. Improving biological phosphorus removal in membrane bioreactors–a pilot study. 4, 25–33.
Song, K.-G., Kim, Y., Ahn, K.-H., 2008. Effect of coagulant addition on membrane fouling and nutrient removal in a submerged membrane bioreactor. Desalination 221, 467–474.
Sözüdoğru, O., Massara, T.M., Çalık, S., Yılmaz, A.E., Bakırdere, S., Katsou, E., Komesli, O.T., 2021. Influence of hydraulic retention time (HRT) upon the treatment of wastewater by a laboratory-scale membrane bioreactor (MBR). Anal. Lett. 54, 1578–1587. https://doi.org/10.1080/00032719.2020.1815756.
Stokholm-Bjerregaard, M., McIlroy, S.J., Nierychlo, M., Karst, S.M., Albertsen, M., Nielsen, P.H., 2017. A critical assessment of the microorganisms proposed to be important to enhanced biological phosphorus removal in full-scale wastewater treatment systems. Front. Microbiol. 8. https://doi.org/10.3389/fmicb.2017.00718.
Suh, C., Lee, S., Cho, J., 2013. Investigation of the effects of membrane fouling control strategies with the integrated membrane bioreactor model. J. Membr. Sci. 429, 268–281. https://doi.org/10.1016/j.memsci.2012.11.042.
Sun, P.-D., Song, Y.-Q., 2009. Study on fully coupled activated sludge model no. 1 (FCASM1) for wastewater treatment biological processes. Int. J. Environ. Pollut. 38, 88–99.
Sun, F., Wang, X., Li, X., 2013. An innovative membrane bioreactor (MBR) system for simultaneous nitrogen and phosphorus removal. Process Biochem. 48, 1749–1756. https://doi.org/10.1016/j.procbio.2013.08.009.

Sun, G., Zhang, C., Li, W., Yuan, L., He, S., Wang, L., 2019. Effect of chemical dose on phosphorus removal and membrane fouling control in a UCT-MBR. 13, 1–11.
Szabó, A., Takács, I., Murthy, S., Daigger, G.T., Licskó, I., Smith, S., 2008. Significance of design and operational variables in chemical phosphorus removal. 80, 407–416. https://doi.org/10.2175/106143008X268498.
Takács, I., Murthy, S., Fairlamb, P.M., 2005. Chemical phosphorus removal model based on equilibrium chemistry. Water Sci. Technol. 52, 549–555.
Takács, I., Johnson, B.R., Smith, S., Szabó, A., Murthy, S., 2011. Chemical P removal–from lab tests through model understanding to full-scale demonstration. Proceedings of the 11th IWA Specialised Conference on Design, Operation and Economics of Large Wastewater Treatment Plants, pp. 101–108.
Tchobanoglous, G., Burton, F.L., Stensel, H.D., 2002. Wastewater Engineering: Treatment and Reuse, International edition4, pp. 361–411 ISBN13 9780070418783.
Thistleton, J., Clark, T., Pearce, P., Parsons, S.A., 2001. Mechanisms of chemical phosphorus removal: 1—iron (II) salts. Process Saf. Environ. Prot. 79, 339–344. https://doi.org/10.1205/095758201753373104.
Thistleton, J., Berry, T.-A., Pearce, P., Parsons, S.A., 2002. Mechanisms of chemical phosphorus removal II: iron (III) salts. Process Saf. Environ. Prot. 80, 265–269. https://doi.org/10.1205/095758202762277623.
Vaiopoulou, E., Melidis, P., Aivasidis, A., 2007. An activated sludge treatment plant for integrated removal of carbon, nitrogen and phosphorus. 211, 192–199. https://doi.org/10.1016/j.desal.2006.02.092.
Van Haandel, A., van der Lubbe, J., 2007. Handbook Biological Waste Water Treatment-design and Optimisation of Activated Sludge Systems. Webshop Wastewater Handbook ISBN: 9789077983225.
van Haandel, A.C., Ekama, G., Marais, G., 1981. The activated sludge Process-3 single sludge denitrification. Water Res. 15 (10), 1135–1152. https://doi.org/10.1016/0043-1354(81)90089-0.
van Puijenbroek, P.J.T.M., Beusen, A.H.W., Bouwman, A.F., 2019. Global nitrogen and phosphorus in urban waste water based on the shared socio-economic pathways. J. Environ. Manag. 231, 446–456. https://doi.org/10.1016/j.jenvman.2018.10.048.
Van Vuuren, D.P., Bouwman, A.F., Beusen, A.H.W., 2010. Phosphorus demand for the 1970–2100 period: a scenario analysis of resource depletion. 20, 428–439. https://doi.org/10.1016/j.gloenvcha.2010.04.004.
Varga, E., Hauduc, H., Barnard, J., Dunlap, P., Jimenez, J., Menniti, A., Schauer, P., Lopez Vazquez, C.M., Gu, A.Z., Sperandio, M., Takács, I., 2018. Recent advances in bio-P modelling – a new approach verified by full-scale observations. Water Sci. Technol. 78, 2119–2130. https://doi.org/10.2166/wst.2018.490.
Verrecht, B., Judd, S., Guglielmi, G., Brepols, C., Mulder, J.W., 2008. An aeration energy model for an immersed membrane bioreactor. Water Res. 42, 4761–4770.
Verrecht, B., Maere, T., Benedetti, L., Nopens, I., Judd, S., 2010. Model-based energy optimisation of a small-scale decentralised membrane bioreactor for urban reuse, 2010. Water Res. 44, 4047–4056. https://doi.org/10.1016/j.watres.2010.05.015.
Vohla, C., Kõiv, M., Bavor, H.J., Chazarenc, F., Mander, Ü., 2011. 37, 70–89. https://doi.org/10.1016/j.ecoleng.2009.08.003.
Wadood, T.M., Sarmad, A.R., 2012. Phosphorus removal from wastewater using oven-dried alum sludge. Int. J. Chem. Eng., 125296 https://doi.org/10.1155/2012/125296 11 pages.
Wan, C.-Y., De Wever, H., Diels, L., Thoeye, C., Liang, J.-B., Huang, L.-N., 2011. Biodiversity and population dynamics of microorganisms in a full-scale membrane bioreactor for municipal wastewater treatment. Water Res. 45 (3), 1129–1138. https://doi.org/10.1016/j.watres.2010.11.008.
Wang, Y., 2020. Intermittently aerated MBR for nutrients removal and phosphorus recovery. In: Wang, Y. (Ed.), Development of Novel Bioelectrochemical Membrane Separation Technologies for Wastewater Treatment and Resource Recovery. Springer, Singapore, pp. 43–79 https://doi.org/10.1007/978-981-15-3078-4_3 ISBN13: 9781843390121.
Wang, X.-M., Waite, T.D., 2010. Iron speciation and iron species transformation in activated sludge membrane bioreactors. Water Res. 44, 3511–3521. https://doi.org/10.1016/j.watres.2010.03.031.
Wang, Z., Wu, Z., Yin, X., Tian, L., 2008. Membrane fouling in a submerged membrane bioreactor (MBR) under sub-critical flux operation: membrane foulant and gel layer characterization. J. Membr. Sci. 325, 238–244. https://doi.org/10.1016/j.memsci.2008.07.035.
Wang, Y., Tng, K.H., Wu, H., Leslie, G., Waite, T.D., 2014. Removal of phosphorus from wastewaters using ferrous salts – a pilot scale membrane bioreactor study. Water Res. 57, 140–150. https://doi.org/10.1016/j.watres.2014.03.029.
Wang, Y.-K., Pan, X.-R., Geng, Y.-K., Sheng, G.-P., 2015. Simultaneous effective carbon and nitrogen removals and phosphorus recovery in an intermittently aerated membrane bioreactor integrated system. Sci. Rep. 5, 16281. https://doi.org/10.1038/srep16281.
Wang, D., Wu, Y., Guo, F., Li, Z., Wu, G., 2018. Comprehensive assessment of system performance in a full-scale wastewater treatment plant with an anaerobic/anoxic/aerobic membrane bioreactor combined with the ozonation process. Water Sci. Technol. 78 (3), 690–698. https://doi.org/10.2166/wst.2018.344.
Wei, V., Elektorowicz, M., Oleszkiewicz, J.A., 2012. Electrically enhanced MBR system for total nutrient removal in remote northern applications. Water Sci. Technol. 65, 737–742. https://doi.org/10.2166/wst.2012.908.
Wentzel, M., 1989. Enhanced polyphosphate organism cultures in activated sludge systems.Part III: kinetic model. 15, 89–102.
Wentzel, G.E., Ekama, G.A., Dold, P.L., Loewenthal, R.E., Marias, G.R., 1988. Biological excess phosphorus removal, WRC REPORT NO 148/1/88. http://www.wrc.org.za/wp-content/uploads/mdocs/148-1-882.pdf.
Wentzel, M.C., Ekama, G.A., Marais, G.v.R., 1992. Kinetics of nitrification denitrification biological excess phosphorus removal systems–a review. Water Sci. Technol. 23, 555–565. https://doi.org/10.2166/wst.1991.0505.
Wilfert, P., Kumar, P.S., Korving, L., Witkamp, G.-J., van Loosdrecht, M.C.M., 2015. The relevance of phosphorus and iron chemistry to the recovery of phosphorus from wastewater: a review. Environ. Sci. Technol. 49, 9400–9414. https://doi.org/10.1021/acs.est.5b00150.
Wu, J., Chen, F., Huang, X., Geng, W., Wen, X., 2006. Using inorganic coagulants to control membrane fouling in a submerged membrane bioreactor. Desalination 197, 124–136. https://doi.org/10.1016/j.desal.2005.11.026.
Wu, H., Ikeda-Ohno, A., Wang, Y., Waite, T.D., 2015. Iron and phosphorus speciation in fe-conditioned membrane bioreactor activated sludge. Water Res. 76, 213–226. https://doi.org/10.1016/j.watres.2015.02.020.
Wu, H., Wang, Y., Ikeda-Ohno, A., Miller, C.J., Waite, T.D., 2019. Impact of ferrous iron dosing on iron and phosphorus solids speciation and transformation in a pilot scale membrane bioreactor. Environ. Sci. Water Res.Technol. 5, 1400–1411. https://doi.org/10.1039/C9EW00225A.
Xiao, K., Liang, S., Wang, X., Chen, C., Huang, X., 2019. Current state and challenges of full-scale membrane bioreactor applications: a critical review. Bioresour. Technol. 271, 473–481. https://doi.org/10.1016/j.biortech.2018.09.061.
Yang, X.-L., Song, H.-L., Chen, M., Cheng, B., 2011. Characterizing membrane foulants in MBR with addition of polyferric chloride to enhance phosphorus removal. Bioresour. Technol. 102, 9490–9496. https://doi.org/10.1016/j.biortech.2011.07.105.
Yilmaz, G., Lemaire, R., Keller, J., Yuan, Z., 2007. Effectiveness of an alternating aerobic, anoxic/anaerobic strategy for maintaining biomass activity of BNR sludge during long-term starvation. Water Res. 41, 2590–2598. https://doi.org/10.1016/j.watres.2007.02.011.
Yılmaz, F., Otuzaltı, M.M., Perendeci, N.A., Karatay, M., Ünşar, E.K., Ateş, M., Akin, R., Yıldız, O., Orhon, D., 2020. Potential of aerobic membrane bioreactor for recycling and reuse of domestic wastewater for irrigation. Environ. Earth Sci. 79 (11), 260. https://doi.org/10.1007/s12665-020-09006-2.
Yu, B., Luo, J., Xie, H., Yang, H., Chen, S., Liu, J., Zhang, R., Li, Y.Y., 2021. Species, fractions, and characterization of phosphorus in sewage sludge: a critical review from the perspective of recovery. Sci. Total Environ., 147437 https://doi.org/10.1016/j.scitotenv.2021.147437.
Yuan, L.-M., Zhang, C.-Y., Zhang, Y.-Q., Ding, Y., Xi, D.-L., 2008. Biological nutrient removal using an alternating of anoxic and anaerobic membrane bioreactor (AAAM) process. Desalination, European Desalination Society and Center for Research and Technology Hellas (CERTH), Sani Resort 22 –25 April 2007, Halkidiki, Greece 221, pp. 566–575 https://doi.org/10.1016/j.desal.2007.01.118.
Yuan, L.M., Zhang, C.Y., Yan, R., Zhao, G.Z., Tian, L.J., He, Z.X., Liu, H., Zhang, Y.Q., 2012. Advanced wastewater treatment under different dissolved oxygen conditions in an innovative step-feed process [WWW Document]. Adv. Mater. Res. https://doi.org/10.4028/www.scientific.net/AMR.383-390.3707.
Zarragoitia-González, A., Schetrite, S., Alliet, M., Jáuregui-Haza, U., Albasi, C., 2008. Modelling of submerged membrane bioreactor: conceptual study about link between activated sludge biokinetics, aeration and fouling process. J. Membr. Sci. 325, 612–624.
Zhang, Z., 2020. 8 - nutrients removal in membrane bioreactors for wastewater treatment. In: Ng, H.Y., Ng, T.C.A., Ngo, H.H., Mannina, G., Pandey, A. (Eds.), Current Developments in Biotechnology and Bioengineering. Elsevier, pp. 163–180 https://doi.org/10.1016/B978-0-12-819809-4.00008-5.
Zhang, H.-M., Xiao, J.-N., Cheng, Y.-J., Liu, L.-F., Zhang, X.-W., Yang, F.-L., 2006. Comparison between a sequencing batch membrane bioreactor and a conventional membrane bioreactor. Process Biochem. 41, 87–95. https://doi.org/10.1016/j.procbio.2005.03.072.
Zhang, H., Sun, B., Zhao, X., Gao, Z., 2008. Effect of ferric chloride on fouling in membrane bioreactor. Sep. Purif. Technol. 63, 341–347.
Zhang, H., Wang, X., Xiao, J., Yang, F., Zhang, J., 2009. Enhanced biological nutrient removal using MUCT–MBR system. Bioresour. Technol. 100 (3), 1048–1054. https://doi.org/10.1016/j.biortech.2008.07.045.
Zhang, Z., Li, H., Zhu, J., Weiping, L., Xin, X., 2011. Improvement strategy on enhanced biological phosphorus removal for municipal wastewater treatment plants: full-scale operating parameters, sludge activities, and microbial features. Bioresour. Technol. 102 (7), 4646–4653. https://doi.org/10.1016/j.biortech.2011.01.017.
Zhang, H.-L., Fang, W., Wang, Y.-P., Sheng, G.-P., Zeng, R.J., Li, W.-W., Yu, H.-Q., 2013. Phosphorus removal in an enhanced biological phosphorus removal process: roles of extracellular polymeric substances. Environ. Sci. Technol. 47, 11482–11489. https://doi.org/10.1021/es403227p.
Zhang, Z., Wang, Y., Leslie, G.L., Waite, T.D., 2015. Effect of ferric and ferrous iron addition on phosphorus removal and fouling in submerged membrane bioreactors. Water Res. 69, 210–222. https://doi.org/10.1016/j.watres.2014.11.011.
Zhang, C., Xu, X., Zhao, K., Tang, L., Zou, S., Yuan, L., 2018. Novel MBR_based main stream biological nutrient removal process: high performance and microbial community. Biodegradation 29, 11–22.
Zuthi, M.F.R., Guo, W.S., Ngo, H.H., Nghiem, L.D., Hai, F.I., 2013. Enhanced biological phosphorus removal and its modeling for the activated sludge and membrane bioreactor processes. Bioresour. Technol. 139, 363–374. https://doi.org/10.1016/j.biortech.2013.04.038.

APPENDIX-A

Modeling, simulation and control of biological and chemical P-removal processes for membrane bioreactors (MBRs) from lab to full-scale applications: state of the art

Kashif NADEEM[a], Marion ALLIET[a] Queralt PLANA[b], Jean BERNIER[b], Sam AZIMI[b], Vincent ROCHER[b], Claire ALBASI[a*]

[a] Laboratory of Chemical Engineering, University of Toulouse, CNRS, INPT, UPS, 31000 Toulouse, France

[b] Parisian Sanitation Public Service (SIAAP), Direction Innovation, 92700 Colombes-France

*corresponding author

Table A.1: Globally adopted regulations concerning phosphorus discharges from WWTPs

Country/Geographic Region	Total phosphorus (TP) mgL^{-1}	PO_4^{3-} mgL^{-1}	Population Equivalent	Other bases for standard	Reference
EU/France/ Germany	*2*		*<100,000*		*Directive E.U.W., 1991*
	1		*>100,000*	*receiver oriented*	
Australia	*0.5-3*		*>50,000*	*Region specific and receiver oriented*	*DPIWE, 2001*
UK	*0.2-2*	*0.01*		*Daily average*	*House of Parliment, UK, 2014*
Denmark	*1.5*		*>5,000*		*Brix & Arias, 2005*
	0.4			*Sensitive area*	*Vind, 2017*
Sweden	*0.3*		*<100,000*	*Receiver oriented*	*Mbamba et al., 2019; Morling, 2019*
	0.3		*>100,000*		
Belarus	*4.5*		*<100,000*		*Preisner et al., 2020*
	4.5		*>100,000*		
Switzerland		*0.8*	*<100,000*	*Receiver oriented*	*Preisner et al., 2020*
		0.8	*>100,000*		
USA	*1-0.1*			*Monthly average*	*Gu et al., 2011*
Canada, British Colombia	*1*	*0.5*	*states are using their own guidelines*		*BCOLCMAG 2005*
Japan	*8-16*			*Daily average: 8 mgL^{-1} for the discharge of 50m^3 or more of effluent per day on average.*	*MOE, 2015*
China	*0.5*			*Effluent /day on average and receiver oriented*	*Sun et al., 2019*
Dubai	*2*			*Daily average*	*Preisner et al., 2020*

References

BCOLCMAG - British Columbia Office of Legislative Counsel Ministry of Attorney General 2005. Environmental Management Act Municipal Wastewater Regulation B.C. Reg. 87/2012. https://www.canlii.org/en/bc/laws/regu/bc-reg-87-2012/137521/bc-reg-87-2012.html#document (accessed 21 July 2020)

Brix, H., & Arias, C. A. 2005. The use of vertical flow constructed wetlands for on-site treatment of domestic wastewater: New Danish guidelines. Ecological Engineering, 25(5), 491–500. https://doi.org/10.1016/j.ecoleng.2005.07.009

Directive, E. U. W. 1991. Council Directive of 21. May 1991 concerning urban waste water treatment (91/271/EEC). J. Eur. Commun, 34, 40. https://www.era-comm.eu/EU_water_law/stand_alone/part_4/index.html (accessed 15 Aug 2020)

DPIWE, Department of Primary Industries, Water and Environment. 2001. Emission Limit Guidelines: Sewage Treatment Plants, Asutralia, https://epa.tas.gov.au/Documents/Emission_Limit_Guidelines_June_2001.pdf (accessed 15 Aug 2020)

Gu, A. Z., Liu, L., Neethling, J. B., Stensel, H. D., & Murthy, S. 2011. Treatability and fate of various phosphorus fractions in different wastewater treatment processes. Water Science and Technology, 63(4), 804–810.

House of Parliment, UK. 2014. Phosphate resources, Houses of parliament http://researchbriefings.files.parliament.uk/documents/POST-PN-477/POST-PN-477.pdf, (Accessed 5th March 2021).

Mbamba, C. K., Lindblom, E., Flores-Alsina, X., Tait, S., Anderson, S., Saagi, R., Batstone, D. J., Gernaey, K. V., & Jeppsson, U. 2019. Plant-wide model-based analysis of iron dosage strategies for chemical phosphorus removal in wastewater treatment systems. Water Research, 155, 12–25.

MOE, J. 2015. National Effluent Standards. https://www.env.go.jp/en/water/wq/nes.html, retrieved on 12th May 2021.

Morling, S. 2019. Swedish Experience and Excellence in Wastewater Treatment Demonstrated Especially in Phosphorus Removal. Journal of Water Resource and Protection, 11(3), 333–347. https://doi.org/10.4236/jwarp.2019.113019

Preisner, M., Neverova-Dziopak, E., & Kowalewski, Z. 2020. An Analytical Review of Different Approaches to Wastewater Discharge Standards with Particular Emphasis on Nutrients. Environmental Management, 66(4), 694–708. https://doi.org/10.1007/s00267-020-01344-y

Sun, G., Zhang, C., Li, W., Yuan, L., He, S., & Wang, L. 2019. Effect of chemical dose on phosphorus removal and membrane fouling control in a UCT-MBR. Frontiers of Environmental Science & Engineering, 13(1), 1–11.

Vind, J. 2017. Wastewater innovation in Denmark—Water technology alliance a report by the ministry of foreign affairs of Denmark, Copenhagen , Denmark. https://bacwa.org/wp-content/uploads/2017/06/Wastewater-Innovation-in-Denmark.pdf

APPENDIX-B

Modeling, simulation and control of biological and chemical P-removal processes for membrane bioreactors (MBRs) from lab to full-scale applications: state of the art

Kashif NADEEM[a], Marion ALLIET[a] Queralt PLANA[b], Jean BERNIER[b], Sam AZIMI[b], Vincent ROCHER[b], Claire ALBASI[a*]

[a] Laboratory of Chemical Engineering, University of Toulouse, CNRS, INPT, UPS, 31000 Toulouse, France

[b] Parisian Sanitation Public Service (SIAAP), Direction Innovation, 92700 Colombes-France

B.1. Bioreactor configuration

This section provided detailed elaboration on several configurations available at full scale as well as pilot scales for effective nutrient removal and in particular phosphorus removal.

Table B1: Various configuration of the biological reactors used in MBR for enhanced BioP-removal

Configuration	Description	Advantages and disadvantages
modified Ludzack-Ettinger (MLE) with direct recycle to anoxic reactor (2-stage)	MLE is a simple process for nitrification and denitrification. The nitrates produced in the aeration zone are used as a source of oxygen for facultative bacteria in the event of the breakdown of raw wastewater in the anoxic reactor. In this configuration, the Influent is received by the anoxic zone followed by an aerobic zone and the sludge from the MBR tank is recirculated back to anoxic reactor in the range of 200 -500 % of the influent flow (Chae et al., 2015; Holba et al., 2012; Itokawa et al., 2014).	- Require low recycle rate - Good for C-BOD and ammonia removal. - *Not suitable for P-removal, though it could be coupled with chemically enhanced P-removal* - *Oxygen carryover from aeration zone to anoxic zone may terminate the denitrification process, especially with low readily available COD in the influent*
modified Ludzack-Ettinger (MLE) with cascaded recycle to anoxic reactor (2-stage)	In this configuration, highly oxygenated sludge from the MBR tank is recycling to anoxic zone via aerobic zone (cascaded). The recirculation ration for recirculation from MBR tank to aerobic tank is maintained in the range of 200-500% of the influent flow, while the recirculation from aerobic to anoxic is maintained at 100% of the influent. (Fenu et al., 2010; Holba et al., 2012; Oleszkiewicz et al., 2015; Van Haandel & Van Der Lubbe, 2007)	- Provide partial denitrification - Good P-removal performance - *Maintaining higher MLSS in cascaded configuration is more difficult than conventional MLE thus more difficult to control.* - *Require higher recirculation between MBR tank and aerobic tank to avoid MLSS accumulation and fouling.*
Sequencing anoxic-anaerobic modified Ludzack-Ettinger (MLE)	In this configuration, the influent is also received by intermittently changing anoxic/anaerobic zone followed by an aerobic zone and the sludge from the MBR tank is recirculated back to anoxic reactor. For denitrification, anoxic conditions are provided for 1 hour after every 3 hours with active recirculation. While anaerobic conditions are provided for 2 hour after every 3 hours without recirculation. Hydraulic retention time of this modified configuration is 2-3 times less than conventional MLE (Ahn et al., 2003).	- Enhanced P-removal owing to strict anaerobic conditions and simultaneous phosphate uptake and denitrification. - Enhanced denitrification due to enhanced availability of PHBs in the anoxic zone as substrate for denitrifiers. - *Higher recirculation ratio* - *Lowe TN removal efficiency*

Two stage Phoredox and A/O	These configuration have been designed for both carbon and nitrogen removal. These are based on two reactors in series. First, receiving the influent is anaerobic while the other is aerobic for P-uptake. The sludge is recirculated from the final clarifier tank to the anaerobic reactor (1-1.5*Q) and there is no other recirculation stream between the two reactors. These configuration was developed for P-removal in CASP with lower SRT and to provide optimal conditions required for EBPR. Based on the configuration, Phoredox and AO processes are same with anaerobic and aerobic reactors in series. The only difference between these two processes is that the anaerobic and aerobic reactors in A/O configuration compartments to induce plug flow regime (Chan Pacheco, 2018; Linden et al., 2001; Rossle & Pretorius, 2001; Van Haandel & Van Der Lubbe, 2007).	- Most simple configuration - Simple operations with least reactor volume - Good phosphorus removal efficiency when the nitrates inhibitation is limited (i.e. true anaerobic conditions) - Can be operated at lower SRT when nitrification is not intended - *Not suitable when nitrogen removal is required* - *Operations at lower SRTs make it unsuitable for MBR* - *Not suitable for hot regions due to favorable conditions for nitrification.*
Alternating A/O/Phoredox	This is the modified configuration of the A/O/Phoredox. The reticulation from the aerobic to either anaerobic or anoxic is controlled by a valve. Conditions for denitrification and P-release are marinated for 1 hour alternatively with recirculation ration of 200 % of the influent flow. The nitrobacteria and PAOs could make full use of the organic substrate present in the wastewater due to alternating anoxic and anaerobic conditions. (Yuan et al., 2008; Ahmed et al., 2007)	- Improved P-removal with efficiency above 90% - *Adjusting the duration of the recirculation recycle and recirculation rate is crucial and may vary according to the influent quality.* - *TN removal is limited*
Three stage Phoredox and A^2/O	In order to accommodate the nitrification process, these configurations were introduced with anoxic reactor in between the anaerobic (receiving influent) and aerobic reactors. The external recirculation (from clarifier) is same as of two stage Phoredox/A/O process (100-200% of the influent flow) while additional recirculation stream from aerobic to anoxic reactor (400% of the influent flow) is introduced. 3-stage Phoredox is identical to A^2/O but not the same as the latter is tightly compartmentalized. (Ersu et al., 2008; Rajesh Banu et al., 2009)	- Provided partial denitrification - Moderate to high P-removal efficiency due to limited nitrate interference - Reduced aeration requirements - Although recycle to the anoxic zone results in substantial removal of nitrate, complete removal is not possible, and some nitrate is recycled to the anaerobic zone.
University Cape Town (UCT)	This is the modified version of A2/O process. In the configuration, the recirculation stream from the MBR tank is directed towards the anoxic zone and then from anoxic to anaerobic zone, hereby eliminating the introduction of nitrate to the anaerobic stage and improving the uptake of phosphorus. The anaerobic detention time should be 1-2 h in this configuration. (Jiang et al., 2005; Lesjean et al., 2003; Oleszkiewicz et al., 2015; Smith et al., 2008; Sun et al., 2019; Van Haandel & Van Der Lubbe, 2007)	- Prevents recirculation of nitrate - Provide flexibility to control the nitrate concentration in the anaerobic zone by controlling the recirculation rate from anoxic to anaerobic zone. - *Denitrification capacity is underutilized.* - *influent flows directly into the anaerobic zone, which can result in unstable conditions when high flow rates occur, or when the wastewater contains high levels of dissolved oxygen or low substrate levels*
Modified UCT with additional anoxic zone	Modified UCT is designed to ensure that the introduction of nitrates to anaerobic zone is impossible even with a variable nitrate	- Complete denitrification and no nitrates in the anaerobic zone. - Simple and easy to control

	concentration in excess of the denitrification capacity. In this configuration, additional anoxic zone (2) is added after the first anoxic zone and nitrate rich MLSS stream from the aerobic zone is first directed to anoxic zone (2). (Oleszkiewicz et al., 2015; Sun et al., 2019; Van Haandel & Van Der Lubbe, 2007)	configuration for MLSS recirculation and denitrification - *In this configuration, anoxic zone as a whole is under-loaded with nitrate and therefore larger anoxic volume to bear this shock-load.* - *influent flows directly into the anaerobic zone, which can result in unstable conditions when high flow rates occur, or when the wastewater contains high levels of dissolved oxygen or low substrate levels*
Modified UCT with A/O sequencing	In this configuration, the influent receiving reactor is operator as both anoxic and anaerobic reactors intermittently. While the aerobic tank is intermittently operated and aerobic and anoxic reactor. The sludge flow the aerobic MBR tank is recirculated to anoxic/anaerobic reactor intermittently also. The cycle time of anoxic /anaerobic functioning is controlled along with the recirculation ratio. (Zhang et al., 2006)	- Higher NH4-N removal efficiency (>95%) due to presence of sufficient nitrifying bacteria - Higher BioP-removal efficiency with increase organic loading rate
Step-feed UCT	In this configuration, portion of the influent (40-50%) is directed fed to anoxic zone aiming to optimize the COD allocation to enhanced nitrogen removal. The supply of influent COD to anoxic zone removed the nitrates thereby reduced the nitrate recycle to anaerobic zone. (Lee et al., 2009)	- Improved nitrogen and phosphorus removal performance of the UCT system. - Require additional energy to pump influent to anoxic zone and may offer complexities for MLSS control.
Virginia institute process (VIP)	In this configuration, the influent is received by the anaerobic zone followed by anoxic, aerobic, post-anoxic, aerobic process zones with a 4xQ internal recycle (aerobic → anoxic), a 1xQ internal recycle (anoxic → anaerobic), and a 1 to 1.5xQ RAS rate (external recirculation from MBR/clarifier → aerobic). This configuration is described as a high-rate system, operating with much shorter SRT, maximizing the BPR efficiency.	- The process requires low BOD/P ratio - *Operates at much lower SRT* - *it is more complex and requires additional capital costs*
Bardenpho Process (Four-Stage)	Influent is received by the anoxic zone followed by anaerobic, anoxic, aerobic and post-anoxic process zones with a side stream anaerobic zone (RAS → anaerobic), a 400% is internally recycled (aerobic → anoxic), and a 100% to 150% of the influent is externally recirculated.	- Limited on no phosphorus removal due to absence of the anaerobic zone - Complete denitrification is possible for low TKN/COD - Excellent nitrogen removal (<3 gm^{-3}) - *Large reactor volumes are required as bulk sludge is produced* - *The best combination of reactor sizes is complex*
Modified Bardenpho (5-stage)	In this modified Bardenpho, the Influent is received by the anaerobic reactor followed by anoxic, aerobic, aerobic and post-anoxic process zones with a 400% internal recycle (aerobic → anoxic) and a 100 to 150% of the MBR sludge to aerobic and a 2nd internal recirculation of 100-300% from anoxic to anaerobic reactor. The overall process SRTs and HRTs in the anoxic and aerobic zones are similar to the corresponding SRTs and HRTs in the four-stage process	- Excellent P-removal - Excellent denitrification and can achieve effluent TN below < 3 gm^{-3} -

B.2. Role of Various Zones in the MBR Configurations

This section provide a detailed information on role of various zone in the reactor configuration of the MBR technology.

Table B.2: Functions of various zones in MBR configurations

Zone	Functions	Mediating Organisms
Pre-Anoxic Zone	- Nitrates coming from the anoxic re-circulation stream are denitrified before the mixed liquor enters the anaerobic zone - Readily available organics in the primary effluent undergo rapid de-nitrification - This zone protects the anaerobic zone from nitrates which are known to impede BioP- removal.	Heterotrophs (Non-PAOs) Autotrophs - Nitrite-oxidizing bacteria (NOB) - Ammonia oxidizing bacteria (AOB)
Anaerobic Zone	- This zone provides an enabling environment for the proliferation of PAOs - PAOs can use energy stored in the form of polyphosphate to absorb simple carbon sources (principally volatile fatty acids- VFAs), which are metabolized in subsequent anoxic and aerobic zones. - PAOs absorb carbon in this zone and have a competitive edge over non-PAOs (heterotrophs), especially denitrifying PAOs (DPAOs)	Heterotrophs (PAOs) And sometimes glycogen accumulating Organisms (GAOs)
Anoxic Zone	- Available nitrates in this zone become the oxygen source (electron acceptor) and thus converted into water and N_2 released to the environment in the subsequent zone. - Use of stored poly-β-hydroxybutyrate (PHB) or polyhydroxyalkanoates (PHA) for phosphorus uptake through DPAOs.	Heterotrophs (Non-PAOs) Heterotrophs (DPAOs)
Aerobic Zone	- Degradation of the residual organic matter and completion of the BOD/COD removal process - Ammonification - Nitrification - PHB degradation and uptake of excess phosphorus	Heterotrophs (Non-PAOs) Autotrophs (AOB & NOB) Heterotrophs (PAOs)

B.3. Bioreactor configuration used in various MBR studies in a bid to improve P-removal

In this section, the schematics of configuration used in several studies dedicated to improve the P-removal capabilities of the MBR is presented.

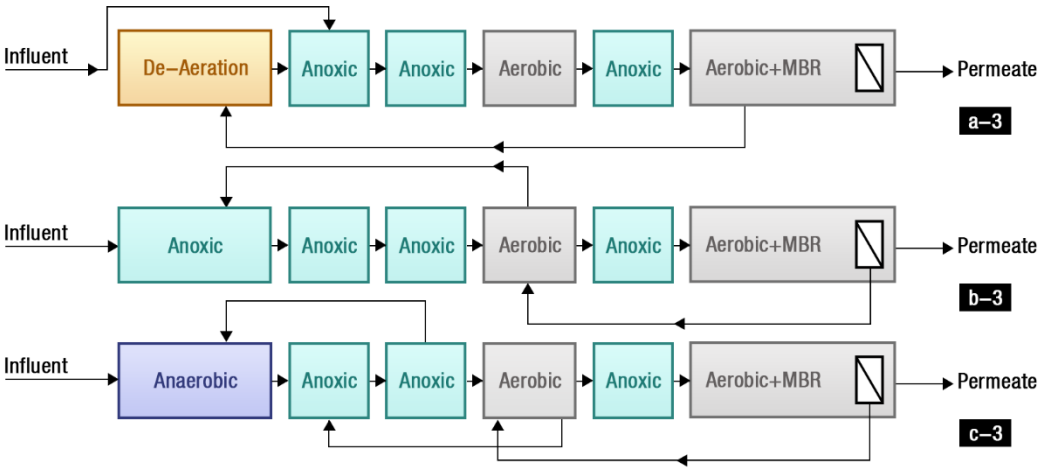

Figure B.1: Re-circulation configurations for P-removal adopted from (Fleischer et al., 2005)

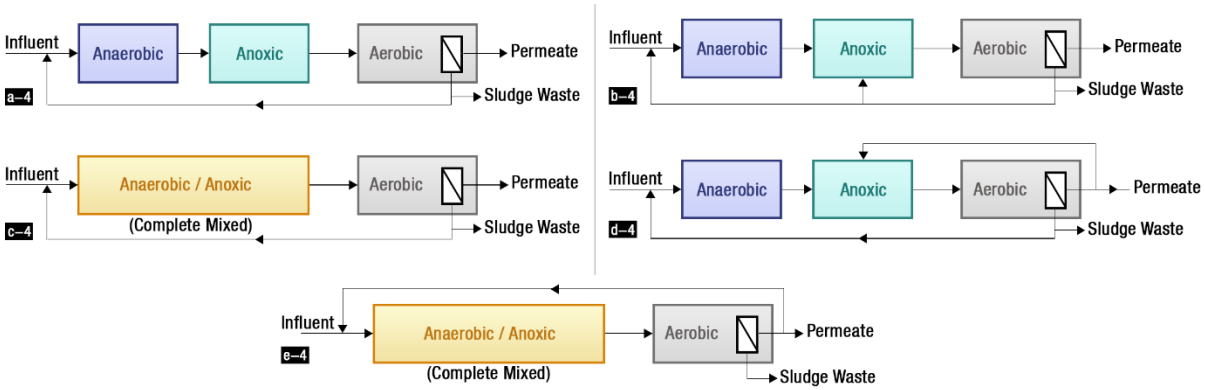

Figure B.2: Different re-circulation configurations for P-removal (Ersu et al., 2008)

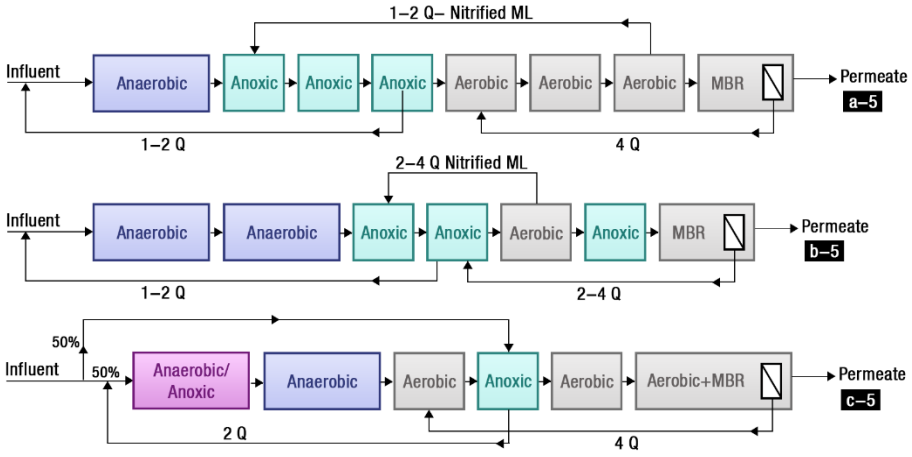

Figure B.3: Various design configuration for P-removal (Daigger et al., 2010)

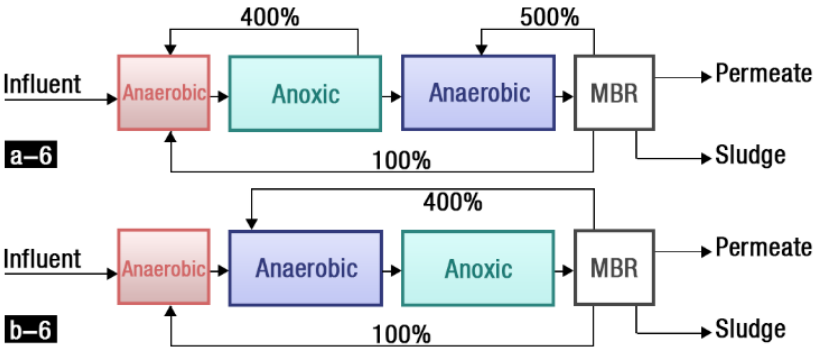

Figure B.4: MBR configuration for P-removal (Lesjean et al., 2003)

References

Ahmed, Z., Lim, B.-R., Cho, J., & Ahn, K.-H. 2007. Effects of the internal recycling rate on biological nutrient removal and microbial community structure in a sequential anoxic/anaerobic membrane bioreactor. *Bioprocess and Biosystems Engineering*, *30*(1), 61–69. https://doi.org/10.1007/s00449-006-0098-4

Ahn, K.-H., Song, K.-G., Choa, E., Cho, J., Yun, H., Lee, S., & Me, J. 2003. Enhanced biological phosphorus and nitrogen removal using a sequencing anoxic/anaerobic membrane bioreactor (SAM) process. *Desalination*, *157*(1), 345–352. https://doi.org/10.1016/S0011-9164 (03)00415-6

Chae, S.-R., Chung, J.-H., Heo, Y.-R., Kang, S.-T., Lee, S.-M., & Shin, H.-S. 2015. Full-Scale Implementation of a Vertical Membrane Bioreactor for Simultaneous Removal of Organic Matter and Nutrients from Municipal Wastewater. *Water*, *7*(3), 1164–1172. https://doi.org/10.3390/w7031164

Chan Pacheco, C. R. 2018. *Integrating enhanced biological phosphorus removal (EBPR) in a resource recovery scenario*. PhD thesis. Universitat Autònoma de Barcelona.

Daigger, G. T., Crawford, G. V., & Johnson, B. R. 2010. Full-Scale Assessment of the Nutrient Removal Capabilities of Membrane Bioreactors. *Water Environment Research*, *82*(9), 806–818. JSTOR. https://www.jstor.org/stable/27870381

Ersu, C., Ong, S. K., Arslankaya, E., & Brown, P. 2008. Comparison of recirculation configurations for biological nutrient removal in a membrane bioreactor. *Water Research*, *42*(6), 1651–1663. https://doi.org/10.1016/j.watres.2007.10.022

Fenu, A., Roels, J., Wambecq, T., De Gussem, K., Thoeye, C., De Gueldre, G., & Van De Steene, B. 2010. Energy audit of a full scale MBR system. *Desalination*, *262*(1), 121–128. https://doi.org/10.1016/j.desal.2010.05.057

Fleischer, E. J., Broderick, T. A., Daigger, G. T., Fonseca, A. D., Holbrook, R. D., & Murthy, S. N. 2005. Evaluation of Membrane Bioreactor Process Capabilities to Meet Stringent Effluent Nutrient Discharge Requirements. *Water Environment Research*, *77*(2), 162–178. https://doi.org/10.2175/106143005X41735

Holba, M., Plotěný, K., Dvořák, L., Gómez, M., & Růžičková, I. 2012. Full-scale Applications of Membrane Filtration in Municipal Wastewater Treatment Plants. *CLEAN – Soil, Air, Water*, *40*(5), 479–486. https://doi.org/10.1002/clen.201000398

Itokawa, H., Tsuji, K., Yamashita, K., & Hashimoto, T. 2014. Design and operating experiences of full-scale municipal membrane bioreactors in Japan. *Water Science and Technology*, *69*(5), 1088–1093. https://doi.org/10.2166/wst.2014.020

Jiang, F., Beck, M. B., Cummings, R. G., Rowles, K., & Russell, D. 2005. Estimation of costs of phosphorus removal in wastewater treatment facilities: Adaptation of existing facilities. *Water Policy Working Paper*, *11*, 2005.

Lee, H., Han, J., & Yun, Z. 2009. Biological nitrogen and phosphorus removal in UCT-type MBR process. *Water Science and Technology*, *59*(11), 2093–2099. https://doi.org/10.2166/wst.2009.242

Lesjean, B., Gnirss, R., Adam, C., Kraume, M., & Luck, F. 2003. Enhanced biological phosphorus removal process implemented in membrane bioreactors to improve phosphorous recovery and recycling. *Water Science and Technology*, *48*(1), 87–94.

Linden, K. G., Hawkins, J. M., & Bonislawsky, M. P. 2001. *Evaluation of Performance and Operatonal Costs for Three Biological Nutrient Removal Schemes At a Full-Scale Wastewater Treatment Plant*. Water Resources Research Institute of the University of North Carolina.

Oleszkiewicz, J., Kruk, D. J., Devlin, T., Lashkarizadeh, M., & Yuan, Q. 2015. Options for improved nutrient removal and recovery from municipal wastewater in the Canadian context. *Environ. Technol*, *20*, 132.

Rajesh Banu, J., Uan, D. K., & Yeom, I.-T. 2009. Nutrient removal in an A2O-MBR reactor with sludge reduction. *Bioresource Technology*, *100*(16), 3820–3824. https://doi.org/10.1016/j.biortech.2008.12.054

Rossle, W. H., & Pretorius, W. A. 2001. A review of characterisation requirements for in-line prefermenters: Paper 2: Process characterisation. *Water Sa*, *27*(3), 413–422.

Smith, S., Takacs, I., Murthy, S., Daigger, G. T., & Szabo, A. 2008. Phosphate complexation model and its implications for chemical phosphorus removal. *Water Environment Research*, *80*(5), 428–438.

Sun, G., Zhang, C., Li, W., Yuan, L., He, S., & Wang, L. 2019. Effect of chemical dose on phosphorus removal and membrane fouling control in a UCT-MBR. *Frontiers of Environmental Science & Engineering*, *13*(1), 1–11.

Van Haandel, A., & Van Der Lubbe, J. 2007. *Handbook biological waste water treatment-design and optimisation of activated sludge systems*. Webshop Wastewater Handbook.

Yuan, L.-M., Zhang, C.-Y., Zhang, Y.-Q., Ding, Y., & Xi, D.-L. 2008. Biological nutrient removal using an alternating of anoxic and anaerobic membrane bioreactor (AAAM) process. *Desalination*, *221*(1), 566–575. https://doi.org/10.1016/j.desal.2007.01.118

Zhang, H.-M., Xiao, J.-N., Cheng, Y.-J., Liu, L.-F., Zhang, X.-W., & Yang, F.-L. 2006. Comparison between a sequencing batch membrane bioreactor and a conventional membrane bioreactor. *Process Biochemistry*, *41*(1), 87–95. https://doi.org/10.1016/j.procbio.2005.03.072

APPENDIX-C

Modeling, simulation and control of biological and chemical P-removal processes for membrane bioreactors (MBRs) from lab to full-scale applications: state of the art

Kashif NADEEM[a], Marion ALLIET[a] Queralt PLANA[b], Jean BERNIER[b], Sam AZIMI[b], Vincent ROCHER[b], Claire ALBASI[a*]

[a] Laboratory of Chemical Engineering, University of Toulouse, CNRS, INPT, UPS, 31000 Toulouse, France

[b] Parisian Sanitation Public Service (SIAAP), Direction Innovation, 92700 Colombes-France

*corresponding author

Table C1: influent composition and operational conditions of the system modeled in the reviewed papers

Type of Process	Scale	Membrane type and pore size	Inflow (m^3d^{-1})	Influent type	Influent C: N:P	Process conditions		Flow quality (mgL^{-1}) Effluent> Model output			Reference
								Parameter	Influent	Effluent	
A1-A2-O-A2-O-MBR (Modified Bardenpho) (Pre-denitrification)	Pilot	Zenon-ZeeWeed Immersed hollow fiber (0.04µm)	166	domestic	40:6.5:1	**Volume of reactor (m^3):**	27.225	**TSS**	82		Fleischer et al., 2005
						Temperature (C°):	--	**BOD_5**	133		
						SRT (days)	19--23	**COD_t**	NA		
						HRT (hours)	8.8	**pH**	--		
						MLSS (gL^{-1})	7	**TKN**	36	10	
						DO (mgL^{-1})	- -	**NH_4**	21		
						Flux (Lm^{-2} h^{-1})	34	**NOx**			
						TMP (kPa)	7--55	**P_{tot}**	5.5	0.01	
						Membrane area (m^2)	46.5	**PO_4**	--		
						Filtration/relaxation/backwashing cycle	--	**EPS mg/gTSS**	--		
						Coagulant	Alum	**Turbidity NTU**	--	0.1	
						Coagulant dose ($mg(mgTP)^{-1}$)	27				
Anaerobic-Anoxic-Aerobic-MBR (UCT)	Pilot	Zenon ZeeWeed Immersed hollow fiber (0.04µm)	5.12	domestic	84:7.98:1	**Volume of reactor (m^3):**	2.130	**TSS**	--		Al-Atar, 2007
						Temperature (C°):	16-24	**BOD_5**	--		
						SRT (days)	12-20	**COD_t**	357	27	
						HRT (hours)	10	**CODs**	113	27	
						MLSS (gL^{-1})	--	**pH**	6.3-7.3	--	
						DO (mgL^{-1})	3	**TKN**	33.9	0.4	
						Flux (Lm^{-2} h^{-1})	---	**NH_4**	26.7	0.1	
						TMP (kPa)	--	**NOx**	0.057	8	
						Membrane area (m^2)	12.2	**P_{tot}**	4.26	0.1	
						Filtration/relaxation/backwashing cycle	--	**PO_4**	2.61	0.1	
						Coagulant	--	**EPS mg / gTSS**	--	--	

Type of Process	Scale	Membrane type and pore size	Inflow (m^3d^{-1})	Influent type	Influent C: N:P	Process conditions		Flow quality (mgL^{-1}) Effluent> Model output			Reference
								Parameter	Influent	Effluent	
						Coagulant dose ($mg(mgTP)^{-1}$)	--	**Turbidity NTU**	--	--	
								VFA	22.8	--	
A1-A2-MBR (MUCT)	Pilot	PVDF Membrane (Norit, XF Membrane)-(0.03µm)	0.10800	Synthetic	100:13.7:2.76	**Volume of reactor (m^3):**	0.0288	**TSS**	Synthetic wastewater with known composition		Nopens et al., 2007
						Temperature (C°):	15	**BOD_5**			
						SRT (days)	17.55	**COD_t**		11	
						HRT (hours)		**CODs**			
						MLSS (gL^{-1})	10	**pH**			
						DO (mgL^{-1})	2	**TKN**		10.2	
						Flux (Lm^{-2} h^{-1})	31.8	**NH_4**		0.18	
						TMP (kPa)		**NOx**		7.30	
						Membrane area (m^2)	0.17	**P_{tot}**			
						Filtration/relaxation/backwashing cycle time (sec)	475	**PO_4**		5.63	
Anaerobic-Anoxic –Oxic-MBR (AO/A^2O)	Lab-scale	Plate frame Cellulose 0.2 µm	0.001	Synthetic	100:8.4:2.2	**Volume of reactor (m^3):**	0.012	**TSS**	75.4±8.4		Ersu et al., 2008
						Temperature (C°):	≤85	**BOD_5**	295±10.9		
						SRT (days)		**COD_t**	510±9.1		
						HRT (hours)		**CODs**	396±8	33.38	
						MLSS (gL^{-1})	8	**pH**	7.7±0.2		
						DO (mgL^{-1})		**TKN**			
						Flux (Lm^{-2} h^{-1})		**TN**	42.6±2	13.04	
						TMP (kPa)	15-25	**NH_4**	22.9±1.8	0.24	
						Membrane area (m^2)	0.15	**NOx**	0.3±0.1	11.60	
						Filtration/relaxation/backwashing cycle time (sec)		**P_{tot}**	11.4±0.9	3.29	
						Coagulant	--	**PO_4**			
Anoxic /oxic-MBR (AO	Lab-scale	PVDF Membrane (Norit, XF Flow Membrane)-	0.1080 0	Synthetic	100:13 .7:2.76	**Volume of reactor (m^3):**	0.0288	**TSS**	waste water with known		Jiang et al., 2008
						Temperature (C°):	15	**BOD_5**			
						SRT (days)	17.55	**COD_t**		11	

Type of Process	Scale	Membrane type and pore size	Inflow (m^3d^{-1})	Influent type	Influent C: N:P	Process conditions		Flow quality (mgL^{-1}) Effluent> Model output			Reference
								Parameter	Influent	Effluent	
		(0.03µm)				**HRT (hours)**	6.4	**CODs**			
						MLSS (gL^{-1})	10	**pH**			
						DO (mgL^{-1})	1.5-2.5	**TKN**		10.2	
						Alternating aeration [ON:OFF] minutes	23:17	**NH_4**		0.18	
						Flux (Lm^{-2} h^{-1})	31.8	**NOx**		7.30	
						TMP (kPa)	475	**P_{tot}**			
						Membrane area (m^2)	0.17	**PO_4**		5.64	
						Coagulant	None				
Anaerobic/Anoxic-oxic-MBR (A/O)	Small Scale Plant	A flat sheet membrane (0.04µm)	0.34-0.36		75:1 (COD:P)	**Volume of reactor (m^3):**	3	**COD_t**	562 ±120	38±6.8	Abegglen et al., 2008
						Temperature (C°):	-	**pH**	7.8-7.9		
						SRT (days)	30-50	**NH_4**	84.3±12.9	1.04±1.08	
						HRT (hours)	-	**NOx**		45±6.7	
						F/M ratio (kgCOD(kgVSSday)$^{-1}$)	0.06-0.11	**P_{tot}**	23.9±2		
						Membrane area (m^2)	4	**PO_4**		17±2.8	
Anaerobic-Anoxic/oxic-MBR (AO sequencing)	Lab-scale	PVDF Membrane (Norit, XF Flow Membrane)-(0.03µm)	0.10800	Synthetic	100:13.7:2.76	**Volume of reactor (m^3):**	0.0288	**TSS**	Synthetic wastewater with known composition		Jiang et al., 2009
						Temperature (C°):	15	**BOD_5**			
						SRT (days)	17.55	**COD_t**		11	
						HRT (hours)	6.4	**CODs**			
						MLSS (gL^{-1})	10	**pH**			
						DO (mgL^{-1})	1.5-2.5	**TKN**		10.2	
						Alternating aeration [ON:OFF] minutes	23:17	**NH_4**		0.18	
						Flux (Lm^{-2} h^{-1})	31.8	**NOx**		7.30	
						TMP (kPa)	475	**P_{tot}**			
						Membrane area (m^2)	0.17	**PO_4**		5.64	
xic/q	-sc	Double sided, plate frame	.0	th	0::	**Volume of reactor (m^3):**	0.016	**TSS**	71.7±6,4		al

Type of Process	Scale	Membrane type and pore size	Inflow (m^3d^{-1})	Influent type	Influent C: N:P	Process conditions		Flow quality (mgL^{-1}) Effluent> Model output			Reference
								Parameter	Influent	Effluent	
		cellulose membrane (Kubita,Co.,Osaka, Japan) with nominal pore size of 0.2 µm				**Temperature (C°):**	22.5±1	**BOD_5**	342±11		
						pH control	7-8	**COD_t**	555±9.1		
						Anaerobic ORP (mV)	-340	**CODs**	502±11.1	34	
						Anoxic ORP (mV)	-235	**pH**	7.7±0.2		
						Aerobic ORP (mV)	100	**TKN**			
						SRT (days)	≥25	**TN**	43.3±1.9	8.8	
						HRT (hours)	2,2,8	**NH_4**	22.7±1.8	0.3	
						MLSS (gL^{-1})	7.5	**NOx**	0.7±0.1	7.3	
						DO (mgL^{-1})	>2	**P_{tot}**	20±1.5	3.7	
						Flux ($Lm^{-2}\ h^{-1}$)	8-28	**PO_4**			
						Filtration –relaxation (sec)	540:60				
						Backwashing	None				
						TMP (kPa)	<15				
						Membrane area (m^2)	0.15				
Anaerobic-Anoxic/oxic-MBR (UCT Configuration) Distribution by Volume: (14%-14%-23%-49%)	Pilot	Submerged hollow fiber membrane with pore size of 0.1 µm	0.125-1.5	Domestic	100:11:0.8	**Volume of reactor (m^3):**	2.26	**TSS**	--		Monclús et al., 2010
						Temperature (C°):	--	**BOD_5**	293		
						pH control	yes	**COD_t**	459	19.68	
						Anaerobic recirculation ratio	1-1.29	**CODs**			
						Anoxic recirculation ratio	0.8-0.92	**pH**			
						Membrane to anoxic recirculation ratio	1.10-1.36	**TKN**	50.6	5.88	
						SRT (days)	23	**TN**			
						HRT (hours)		**NH_4**			
						MLSS (gL^{-1})	1.1-12	**NOx**	0.3		
						DO (mgL^{-1})	1.5	**P_{tot}**			
						Flux ($Lm^{-2}\ h^{-1}$)	6-12.2	**PO_4**	4	0.48	
						Membrane area (m^2)	12.5				

Type of Process	Scale	Membrane type and pore size	Inflow (m^3d^{-1})	Influent type	Influent C: N:P	Process conditions		Flow quality (mgL^{-1}) Effluent> Model output			Reference
								Parameter	Influent	Effluent	
						Filtration –relaxation (sec)	540:60				
						Backwashing	yes				
						TMP (kPa)					
Anoxic-Oxic/MBR Distribution by Volume: (55%-45%) (MLE)	Pilot	Zeno ZeeWeed (ZW500c) (anoxic tank intermittently work as anaerobic tank)		Domestic	114:12/65:1	**Volume of reactor (m^3):**	22.78	**TSS**			Verrecht et al., 2010
						Temperature (C°):		**BOD_5**			
						pH control		**COD_t**	480.5		
						SRT (days)	45-47	**TN**	81.58		
						Aerobic-anoxic recirculation (%)	2.27-4.25	**TKN**	81		
						HRT (hours)		**NH_4**	69.10	0.338	
						MLSS (gL^{-1})	8	**NOx**		21.68	
						DO (mgL^{-1})	1.25-2	**P_{tot}**	11		
						Flux (Lm^{-2} h^{-1})		**PO_4**	9.29	5.18	
						Filtration –relaxation-backwash time (sec)	600:30:30	**Organic nitrogen**	12.21		
						Membrane area (m^2)	139				
						SADm ($Nm^3m^{-2}h^{-1}$)	0.128-0.2				
						Membrane aeration (Nm^3h^{-1})	84-42				
MBR (modified VIP process) Distribution by Volume: (10%-35-55%)	Full	Zenon ZW 500C	32,000	domestic	59:06:01	**Volume of reactor (m^3):**		**TSS**	104		Daigger et al., 2010
						Temperature (C°):	16.1	**BOD_5**	179	0.5	
						pH control		**COD_t**	361	21.1	
						SRT (days)	7.8	**TN**			
						Aerobic-anoxic recirculation (%)		**TKN**	35		
						HRT (hours)		**NH_4**	27	0.1	
						MLSS (gL^{-1})	1.5-9	**NOx**			
						DO (mgL^{-1})		**P_{tot}**	6.2	0.33	
						Flux (Lm^{-2} h^{-1})		**PO_4**			

Type of Process	Scale	Membrane type and pore size	Inflow (m^3d^{-1})	Influent type	Influent C: N:P	Process conditions		Flow quality (mgL^{-1}) Effluent> Model output			Reference
								Parameter	Influent	Effluent	
						Coagulant Addition	yes	**Organic nitrogen**			
						Coagulant	$FeCl_3$				
						Coagulant dose (mg(mg P)$^{-1}$)	38				
Anaerobic-anoxic-aerobic-Anoxic-MBR (modified VIP process) Distribution by Volume: (13%-13-51%-9%)	Full	Zenon ZW 500C	42,000	domestic	51:1 (COD:TP)	**Volume of reactor (m^3):**	42,000	**TSS**	82		Daigger et al., 2010
						Temperature (C^o):		**BOD_5**	133		
						pH control		**COD_t**	283	11.3	
						SRT (days)	14-21	**TN**	36	3.6	
						Aerobic-anoxic recirculation %		**TKN**			
						HRT (hours)		**NH_4**	21	0.03	
						MLSS (gL^{-1})	6.7	**NOx**			
						DO (mgL^{-1})	1.5-2	**P_{tot}**	5.5	0.05	
						Flux (Lm^{-2} h^{-1})		**PO_4**		0.04	
						Coagulant Addition	Yes	**Organic nitrogen**			
						Coagulant	Alum				
						Coagulant dose (mg(mgP)$^{-1}$)	87				
Anaerobic-anoxic-aerobic- -MBR Distribution by Volume: (18%-35-44%-3%) (modified UCT process)	pilot	AEN-MBR system developed by the Siemen Water Technologies with PVDF hollow fibre membrane with nominal pore size of 0.1 µm	21.8	Domestic	69.69:6.9:1	**Volume of reactor (m^3):**	10	**TSS**	84		Liu et al., 2011
						Temperature (C^o):	20	**COD_t**	327	12.7	
						pH control	Yes	**VSS**	109		
						SRT (days)	51	**TKN**	37		
						Aerobic-anoxic recirculation ratio	5	**NH_3-N**		0.61	
						Anoxic-Anaerobic recirculation ratio	2	**NOx**	4.9	6.2	
						HRT (hours)		**P_{tot}**	5.3	0.032	
						MLSS (gL^{-1})	9-10	pH	7.2		
						DO (mgL^{-1})	2	Alkalinity (mmol/L)	3		

Type of Process	Scale	Membrane type and pore size	Inflow (m^3d^{-1})	Influent type	Influent C: N:P	Process conditions		Flow quality (mgL^{-1}) Effluent> Model output			Reference
								Parameter	Influent	Effluent	
						Flux (Lm^{-2} h^{-1})	24				
						Filtration –relaxation (sec)	720:60				
						Membrane aeration (Nm^3h^{-1})	9				
						Coagulant Addition	Yes				
						Coagulant	Alum				
						Coagulant dose (mg(L of influent)$^{-1}$)	17.5				
Anaerobic-anoxic/aerobic- -MBR (A)-sequencing)	Lab -scale	Hollow fiber MF membrane modules from Mistubishi Rayon, Japan. The membrane is made of polyethylene with hydrophilic coating and have a nominal pore size of 0.3 µm				**Volume of reactor (m^3):**	--	**TSS**	Synthetic wastewater with known composition		Gholikandi & Khosravi, 2012
						Membrane area (m^2)	1.8	**BOD_5**			
						Temperature (C°):	10.9-23.1	**COD_t**		14.2	
						pH control	7.6±0.3	**VSS**			
						SRT (days)	15-40	**TN**		9.45	
						HRT (hours)		**NH_3-N**		0.5	
						MLSS (gL^{-1})		**NOx**		8.6	
						Alternate aeration [ON/OFF]- minutes	50:71	**PO_4**		5.8	
						DO (mgL^{-1})	1.5-2	**SUAP**		0.85	
								SBAP		7.1	
Anaerobic-anoxic-aerobic- - Oxic-MBR (UCT process) Distribution by Volume: (12%-27-54%-8%)	Pilot	Zenon ZeeWeed System (ZW10) equipped with hollow fibre membranes having nominal pore size of 0.04 µm	0.96	domestic	106.75:22.75:1	**Volume of reactor (m^3):**	0.616	**TSS**	282		Cosenza et al., 2013
						Membrane area (m^2)	0.93	**BOD_5**	176		
						MLSS (gL^{-1})	3-6.5	**COD_t**	327		
						Volatile fraction of MLSS (%)	70	**VSS**	177		
						F/M ratio (kgCOD(kgVSSday)$^{-1}$)	0.13	**TKN**	91		
						Temperature (C°):	21	**NH_3-N**	16		
						pH control	7.6	**NOx**	2		
						SRT (days)	37	**PO_4**	1.5		

Type of Process	Scale	Membrane type and pore size	Inflow (m^3d^{-1})	Influent type	Influent C: N:P	Process conditions		Flow quality (mgL^{-1}) Effluent> Model output			Reference
								Parameter	Influent	Effluent	
						Flux (LHH)	42	**P_{tot}**	4		
						TMP (kPa)	50				
						Filtration –relaxation (sec)	540:60				
						Backwash	yes				
						Chemical cleaning	yes				
Anaerobic-anoxic-aerobic- -Oxic-MBR (UCT process) Distribution by Volume: (12%-27-54%-8%)	Pilot	Zenon ZeeWeed System (ZW10) equipped with hollow fibre membranes having nominal pore size of 0.04 µm	0.96	domestic	106.75:22.75:1	**Volume of reactor (m^3):**	0.616	**TSS**	282		Cosenza et al., 2014
						Anaerobic recirculation ratio	5-6	**BOD_5**	176		
						Anoxic recirculation ratio	6	**COD_t**	327		
						Anaerobic recirculation	3	**VSS**	177		
						Membrane area (m^2)	0.93	**TKN**	91		
						MLSS (gL^{-1})	3-6.5	**NH_3-N**	16		
						Volatile fraction of MLSS (%)	70	**NOx**	2		
						F/M ratio ($kgCOD(kgVSSday)^{-1}$)	0.13	**PO_4**	1.5		
						Temperature (C^o):	21	**P_{tot}**	4		
						pH control	7.6				
						SRT (days)	37				
						Flux (LHH)	42				
						TMP (kPa)	50				
						Filtration –relaxation (sec)	540:60				
						Backwash	yes				
Anaerobic-anoxic-aerobic- -Oxic-MBR (UCT process) Distribution by Volume: (12%-17-	Pilot	Flat sheet System form Hitachi, Japan.; with membrane cut of size of 0.2 µm	17	Domestic	79.29:6.5:1	**Volume of reactor (m^3):**	5.16	**COD_t**	785		Sarioglu et al., 2017
						Anoxic recirculation ratio	4	**TKN**	65		
						Anaerobic recirculation	1	**PO_4**	0.4-7.7		
						ORP (anoxic)-(mV)	-200	**P_{tot}**	9.9		
						Membrane area (m^2)	18	**VFA**	75-120		
						MLSS (gL^{-1})	10-16				
						Temperature (*C):	24-38				

Type of Process	Scale	Membrane type and pore size	Inflow (m^3d^{-1})	Influent type	Influent C: N:P	Process conditions		Flow quality (mgL^{-1}) Effluent> Model output			Reference
								Parameter	Influent	Effluent	
						pH control					
						Biological aeration (m^3h^{-1}) Aerobic Tank	30				
						Biological aeration (m^3h^{-1}) Membrane Tank	10				
						Flux (Lm^{-2} h^{-1})	43				
						TMP (kPa)	50				
						Filtration –relaxation (sec)					
						Backwash	Yes				
						Chemical cleaning	Yes				
	Pilot	UF hollow fibre membrane with nominal pore size of 0.03 µm	0.48	Domestic	Not provided	**Volume of reactor (m^3):**	0.421	**TSS**	Not provided	Not provided	Mannina et al. 2018
						Membrane area (m^2)	1.4	**BOD_5**			
						Anaerobic recirculation ratio	1	**COD_t**			
						Anoxic recirculation ratio	3	**TKN**			
						ORP (anoxic)-(mV)	--	**NH_3-N**			
						MLSS (gL^{-1})	--	**NOx**			
						Volatile fraction of MLSS (%)	--	**PO_4**			
						F/M ratio ($kgCOD(kgVSSday)^{-1}$)	--	**P_{tot}**			
						Temperature (C°):	--				
						pH control	--				
						Biological aeration (m^3d^{-1}) Aerobic Tank	22.45				
						SRT (days)	--				
						Flux (Lm^{-2} h^{-1})	21				
						TMP (kPa)	--				
						Filtration –backwashing (sec)	540:60				
						Backwash	yes				

Type of Process	Scale	Membrane type and pore size	Inflow (m^3d^{-1})	Influent type	Influent C: N:P	Process conditions		Flow quality (mgL^{-1}) Effluent> Model output			Reference
								Parameter	Influent	Effluent	
						Chemical cleaning	Yes				
Anaerobic-Anoxic- Aerobic-MBR (UCT Process)	Full-scale	No information provided	9800	domestic		**Volume of reactor (m^3):**	4525	**TSS**	390	10.3	Bis et al., 2019
						Membrane area (m^2)	--	**BOD_5**	428	3.3	
						Anaerobic recirculation ratio	1.50	**COD_t**	810	82.3	
						Anoxic recirculation ratio	2.50	**TN**	64.5	16.1	
						DO mg/L	2	**TKN**		2	
						MLSS (gL^{-1})	9.8	**NH_3-N**	51	0.88	
						SRT (days)	10	**NOx**	0.5	14.1	
						F/M ratio ($kgCOD(kgVSSday)^{-1}$)	0.16	**P_{tot}**	15.8	0.67	
						Temperature (C^o):		**PO_4**	11.9	0.09	

Table C2: Default Stoichiometric Parameters of the various models applied for P-removal modeling in MBRs

	Al-Atar, 2007	**Nopens et al., 2007**	**Jiang et al., 2008**	**(Abegglen et al., 2008)**	**Ersu et al., 2008**	**Jiang et al., 2009**	**Verrecht et al., 2010**	**Gholikandi & Khosravi, 2012**	**Cosenza et al. 2013**	**Cosenza et al. ,2014**	**Mannina et al, 2018**
Bio-kinetic model	TUDP	ASM2d	ASM2d SMP	ASM3-BioP	New general model	ASM2d SMP	ASM2d SMP	ASM2d SMP	ASM2d SMP	ASM2d SMP	ASM2d SMP
P-related processes	11	8	8	11	19	8	8	8	8	8	8
Y_{PAO}		0.625	0.625		0.639	0.625	0.625	0.625	0.625	0.625	0.625
$1/Y_{Stor,PP}$		0.2	0.2			0.2	0.2	0.2	0.2	0.2	0.2
$Y_{PP,Stor,PAO}$		0.4	0.4		0.52	0.4	0.4	0.4	0.4	0.4	0.4
$Y_{PAO,Ox}$				0.60							
$Y_{PAO,Ax}$				0.50							
$Y_{Stor,PP}$				0.20							
$Y_{PP,Stor,PAO}$				0.35							
$Y_{Stor,PP,\ Ox}$					0.95						
$Y_{Stor,PP,\ Ax}$					0.55						
$Y_{VFA,Stor,PAO}$					0.889						
$Y_{PHA,PAO,Ox}$	1.39										
$Y_{PHA,PAO,Ax}$	1.72										
$Y_{PAO,PP,Ax}$	3.02										
$Y_{PAO,PP,Ox}$	4.42										
$Y_{VFA,PHA,PAO,An}$	1.5										
$Y_{VFA,PHA,PAO,Ax}$	0.71										
$Y_{PP,PHA,PAO,An}/\ Y_{PO4}$	0.35										
$Y_{PP\_PHA,PAO,Ax}$	0.23										
$Y_{PAO,Gly,Ax}$	1.18										
$Y_{PAO,Gly,Ox}$	1.11										
$Y_{NADH,ATP}$	1.85										

Table C3: Default kinetic Parameters of the various models applied for P-removal modeling in MBRs

	Al-Atar, 2007	Nopens et al., 2007	Jiang et al., 2008	Abegglen et al., 2008)	Ersu et al., 2008	Jiang et al., 2009	Verrecht et al., 2010	Gholikandi & Khosravi, 2012	Cosenza et al. 2013	Cosenza et al. ,2014	Mannina et al, 2018
Bio-kinetic model	TUDP	ASM2d	ASM2d SMP	ASM3-BioP	New general model	ASM2d SMP	ASM2d SMP	ASM2d SMP	ASM2d SMP	ASM2d SMP	ASM2d SMP
$q_{PAO,VFA,Stor}$		3	3		2	3	3	3	3	3	3
$q_{PAO,PO4,PP}$	0.1	1.5	1.5	1.5		1.5	1.5	1.5	1.5	1.5	1.5
$q_{PAO,VFA,PHA,An}$	8										
$q_{PAO,VFA,PHA,Ax}$	1.2										
$q_{PAO,SB,Stor}$				6							
q_{Gly}	0.93										
$q_{PHA,PAO}$	5.51										
$K_{S,fPP,PAO}$		0.01	0.01	0.05		0.01	0.01	0.01	0.01	0.01	0.01
$K_{fGly,PAO}$	0.01										
$K_{I,fPP,PAO}$	0.01	0.02	0.02	0.05		0.02	0.02	0.02	0.02	0.02	0.02
$K_{fGly,PAO}$	0.01										
$K_{fPHA,PAO}$											
$K_{fStor,PAO}$		0.01	0.01	0.10	0.10	0.01	0.01	0.01	0.01	0.01	0.01
$K_{fStor,PAO,Plim}$					0.05						
$K_{VFA,PAO}$	4	4	4		2.5	4	4	4	4	4	4
$K_{O2,PAO}$	0.20	0.20	0.20	0.20		0.20	0.20	0.20	0.20	0.20	0.20
$K_{NOx,PAO}$	0.50	0.50	0.50	0.50		0.5	0.50	0.50	0.50	0.50	0.50
$K_{NHx,PAO}$	0.05	0.05	0.05	0.05		0.05	0.05	0.05	0.05	0.05	0.05
$K_{PO4,PAO,upt}$	1	0.20	0.20	0.20	0.25	0.20	0.20	0.20	0.20	0.20	0.20
$K_{PO4,PAO,nut}$	0.02	0.01	0.01	0.01		0.01	0.01	0.01	0.01	0.01	0.01
$K_{PHA,PAO}$	0.01										
$K_{Gly,PAO}$	0.01										
$K_{Alk,PAO}$	0.01	0.10	0.10	0.10		0.10	0.10	0.10	0.10	0.10	0.10
$K_{PP,PAO}$	0.01				0.01						
$K_{PO4,PAO,lys}$											
$K_{SB,PAO}$											10
$f_{PP\_PAO,Max}$	0.35	0.34	0.34	0.20		0.34	0.34	0.34	0.34	0.34	0.34
$f_{Gly\_PAO,Max}$	0.50										
$\mu_{PAO,Max}$		1	1	1	0.95	1	1	1	1	1	1
μ_{PAO,Max_lim}		1	1		0.42	1	1	1	1	1	1
$n_{\mu PAO}$		0.60	0.60	0.60	0.40	0.60	0.60	0.60	0.60	0.60	0.60
n_{qPAO}	0.8										
n_{mPAO}				0.33							
$n_{bPP,PO4}$				0.33							
$n_{mPAO,Stor}$				0.33							
$m_{PAO,Stor}$				0.20							
m_{PAO}				0.20	0.04						
$m_{PAO,O2}$	0.096										
$m_{PAO,Ox}$	0.06										
$m_{PAO,Ax}$	0.09										
$m_{PAO,An}$	0.05										
b_{PAO}		0.20				0.20	0.20	0.20	0.20	0.20	
$b_{PP,PO4}$		0.20		0.20	0.03	0.20	0.20	0.20	0.20	0.20	
$b_{Stor,VFA}$		0.20				0.20	0.20	0.20	0.20	0.20	

Table C4. Kinetic rate equation for Phosphorus modeling in various models used in reviewed studies (adapted and modified from Hauduc et al., 2013)

Model	Kinetic Process	Impacted with change of kinetic parameters	P-related kinetic rate equations
ASM3-BioP	**Storage of X_{PHA}**		$q_{PAO,SB\_Stor} \times [S_B/(K_{SB,PAO}+S_B)] \times [S_{Alk}/(K_{Alk,PAO}+S_{Alk})] \times [(X_{PAO,PP}/X_{PAO})/(K_{S,fPP\_PAO}+X_{PAO,PP}/X_{PAO})] \times X_{PAO}$
	Aerobic storage of X_{PP}		$q_{PAO,PO4\_PP} \times [S_{O2}/(K_{O2,PAO}+S_{O2})] \times [S_{PO4}/(K_{PO4,PAO,upt}+S_{PO4})] \times [S_{Alk}/(K_{Alk,PAO}+S_{Alk})] \times [(X_{PAO,Stor}/X_{PAO})/(K_{fStor\_PAO}+X_{PAO,Stor}/X_{PAO})] \times [(f_{PP\_PAO,Max}-(X_{PAO,PP}/X_{PAO}))/(K_{I,fPP\_PAO}+f_{PP\_PAO,Max}-(X_{PAO,PP}/X_{PAO}))] \times X_{PAO}$
	Anoxic storage of X_{PP}		$q_{PAO,PO4\_PP} \times n_{\mu PAO} \times [K_{O2,PAO}/(K_{O2,PAO}+S_{O2})] \times [S_{NOx}/(K_{NOx,PAO}+S_{NOx})] \times [S_{PO4}/(K_{PO4,PAO,upt}+S_{PO4})] \times [S_{Alk}/(K_{Alk,PAO}+S_{Alk})] \times [(X_{PAO,Stor}/X_{PAO})/(f_{PP\_PAO,Max}+X_{PAO,Stor}/X_{PAO})] \times [(K_{S,fPP\_PAO}-(X_{PAO,PP}/X_{PAO}))/(K_{I,fPP\_PAO}+f_{PP\_PAO,Max}-(X_{PAO,PP}/X_{PAO}))] \times X_{PAO}$
	Aerobic growth of X_{PAO}		$\mu_{PAO,Max} \times [S_{O2}/(K_{O2,PAO}+S_{O2})] \times [S_{NHX}/(K_{NHx,PAO}+S_{NHX})] \times [S_{PO4}/(K_{PO4,PAO,nut}+S_{PO4})] \times [S_{Alk}/(K_{Alk,PAO}+S_{Alk})] \times [(X_{PAO,Stor}/X_{PAO})/(K_{fStor\_PAO}+X_{PAO,Stor}/X_{PAO})] \times X_{PAO}$
	Anoxic growth of X_{PAO}		$\mu_{PAO,Max} \times n_{\mu PAO} \times [K_{O2,PAO}/(K_{O2,PAO}+S_{O2})] \times [S_{NOx}/(K_{NOx,PAO}+S_{NOx})] \times [S_{NHX}/(K_{NHx,PAO}+S_{NHX})] \times [S_{PO4}/(K_{PO4,PAO,nut}+S_{PO4})] \times [S_{Alk}/(K_{Alk,PAO}+S_{Alk})] \times [(X_{PAO,Stor}/X_{PAO})/(K_{fStor\_PAO}+X_{PAO,Stor}/X_{PAO})] \times X_{PAO}$
	Aerobic endogenous respiration of X_{PAO}	*Yes, due to change in values of mPAO*	$m_{PAO} \times [S_{O2}/(K_{O2,PAO}+S_{O2})] \times X_{PAO}$
	Anoxic endogenous respiration of X_{PAO}	*Yes, due to change in values of mPAO*	$m_{PAO} \times n_{mPAO} \times [K_{O2,PAO}/(K_{O2,PAO}+S_{O2})] \times [S_{NOx}/(K_{NOx,PAO}+S_{NOx})] \times X_{PAO}$
	Aerobic lysis of X_{PP}		$b_{PP\_PO4} \times [S_{O2}/(K_{O2,PAO}+S_{O2})] \times X_{PAO,PP}$
	Anoxic lysis of X_{PP}		$b_{PP\_PO4} \times n_{bPP\_PO4} \times [K_{O2,PAO}/(K_{O2,PAO}+S_{O2})] \times [S_{NOx}/(K_{NOx,PAO}+S_{NOx})] \times X_{PAO,PP}$
	Aerobic respiration of X_{PHA}		$m_{PAO,Stor} \times [S_{O2}/(K_{O2,PAO}+S_{O2})] \times X_{PAO,Stor}$
	Anoxic respiration of X_{PHA}		$m_{PAO,Stor} \times n_{mPAO,Stor} \times [K_{O2,PAO}/(K_{O2,PAO}+S_{O2})] \times [S_{NOx}/(K_{NOx,PAO}+S_{NOx})] \times X_{PAO,Stor}$
ASM2d/ASM2d-SMP	**Storage of X_{Stor}**	*Yes, due to change in values of $q_{PAO,VFA,Stor}$ and K_{S,fPP_PAO}*	$q_{PAO,VFA,Stor} \times [S_{VFA}/(K_{VFA,PAO}+S_{VFA})] \times [S_{Alk}/(K_{Alk,PAO}+S_{Alk})] \times [(X_{PAO,PP}/X_{PAO})/(K_{S,fPP\_PAO}+(X_{PAO,PP}/X_{PAO}))] \times X_{PAO}$
	Aerobic Storage of X_{PP}	*Yes, due to change in values of $q_{PAO,PO4\_PP}$, K_{fStor_PAO} and $f_{PP\_PAO,Max}$*	$q_{PAO,PO4\_PP} \times [S_{O2}/(K_{O2,PAO}+S_{O2})] \times [S_{PO4}/(K_{PO4,PAO,upt}+S_{PO4})] \times [S_{Alk}/(K_{Alk,PAO}+S_{Alk})] \times [(X_{PAO,Stor}/X_{PAO})/(K_{fStor\_PAO}+(X_{PAO,Stor}/X_{PAO}))] \times [(f_{PP\_PAO,Max}-X_{PAO,PP}/X_{PAO})/(K_{I,fPP\_PAO}+f_{PP\_PAO,Max}-(X_{PAO,PP}/X_{PAO}))] \times X_{PAO}$
	Anoxic Storage of X_{PP}	*Yes, due to change in values of $q_{PAO,PO4\_PP}$, $n_{\mu PAO}$ and $f_{PP\_PAO,Max}$*	$q_{PAO,PO4\_PP} \times n_{\mu PAO} \times [S_{NOx}/(K_{NOx,PAO}+S_{NOx})] \times [K_{O2,PAO}/(K_{O2,PAO}+S_{O2})] \times [S_{PO4}/(K_{PO4,PAO,upt}+S_{PO4})] \times [S_{Alk}/(K_{Alk,PAO}+S_{Alk})] \times [(X_{PAO,Stor}/X_{PAO})/(K_{fStor\_PAO}+(X_{PAO,Stor}/X_{PAO}))] \times [(f_{PP\_PAO,Max}-X_{PAO,PP}/X_{PAO})/(K_{I,fPP\_PAO}+f_{PP\_PAO,Max}-(X_{PAO,PP}/X_{PAO}))] \times X_{PAO}$
	Aerobic growth of X_{PAO}	*Yes, due to change in value of $\mu_{PAO,Max}$*	$\mu_{PAO,Max} \times [S_{O2}/(K_{O2,PAO}+S_{O2})] \times [S_{NHx}/(K_{NHx,PAO}+S_{NHx})] \times [S_{PO4}/(K_{PO4,PAO,nut}+S_{PO4})] \times [S_{Alk}/(K_{Alk,PAO}+S_{Alk})] \times [(X_{PAO,Stor}/X_{PAO})/(K_{fStor\_PAO}+(X_{PAO,Stor}/X_{PAO}))] \times X_{PAO}$
	Anoxic growth of	*Yes, due to*	$\mu_{PAO,Max} \times n_{\mu PAO} \times [K_{O2,PAO}/(K_{O2,PAO}+S_{O2})] \times [S_{NOx}/(K_{NOx,PAO}+S_{NOx})] \times$

Model	Kinetic Process	Impacted with change of kinetic parameters	P-related kinetic rate equations
	X_{PAO}	*change in values of* $\mu_{PAO,Max}$ and $n_{\mu PAO}$	$[S_{NHx}/(K_{NHx,PAO}+S_{NHx})]_x [S_{PO4}/(K_{PO4,PAO,nut}+S_{PO4})]_x [S_{Alk}/(K_{Alk,PAO}+S_{Alk})]_x [(X_{PAO,Stor}/X_{PAO})/(K_{fStor\_PAO}+(X_{PAO,Stor}/X_{PAO}))]_x X_{PAO}$
	Lysis of X_{PAO}	*Yes, due to change in value of* b_{PAO}	$b_{PAO}{}_x X_{PAO}{}_x [S_{Alk}/(K_{Alk,PAO}+S_{Alk})]$
	Lysis of X_{PP}		$b_{PP\_PO4}{}_x [S_{Alk}/(K_{Alk,PAO}+S_{Alk})]_x [X_{PAO,PP}/X_{PAO}]_x X_{PAO}$
	Lysis of X_{Stor}		$b_{Stor\_VFA}{}_x [S_{Alk}/(K_{Alk,PAO}+S_{Alk})]_x [X_{PAO,Stor}/X_{PAO}]_x X_{PAO}$
ASM2+TUDP	**Anaerobic Storage of S_A**	*Yes, due to change in value of* $K_{PP,PAO}$	$q_{PAO,VFA\_PHA,An}{}_x [S_{VFA}/(K_{VFA,PAO}+S_{VFA})]_x [K_{O2,PAO}/(K_{O2,PAO}+S_{O2})]_x [K_{NOx,PAO}/(K_{NOx,PAO}+S_{NOx})]_x [X_{PAO,Gly}/(K_{Gly,PAO}+X_{PAO,Gly})]_x [X_{PAO,PP}/(K_{PP,PAO}+X_{PAO,PP})]_x X_{PAO}$
	Anaerobic Maintenance	*Yes, due to change in value of* $K_{PP,PAO}$	$m_{PAO,An}*[K_{O2,PAO}/(K_{O2,PAO}+S_{O2})]*[K_{NOx,PAO}/(K_{NOx,PAO}+S_{NOx})]*[X_{PAO,PP}/(K_{PP,PAO}+X_{PAO,PP})]*X_{PAO}$
	Anoxic storage of S_A	*Yes, due to change in value of* $K_{PP,PAO}$	$q_{PAO,VFA\_PHA,Ax}{}_x [S_{VFA}/(K_{VFA,PAO}+S_{VFA})]_x [K_{O2,PAO}/(K_{O2,PAO}+S_{O2})]_x [S_{NOx}/(K_{NOx,PAO}+S_{NOx})]_x [X_{PAO,PP}/(K_{PP,PAO}+X_{PAO,PP})]_x X_{PAO}$
	Anoxic PHA consumption		$q_{PHA\_PAO}{}_x n_{qPAO_x} [K_{O2,PAO}/(K_{O2,PAO}+S_{O2})]_x [S_{NHx}/(K_{NHx,PAO}+S_{NHx})]_x [S_{NOx}/(K_{NOx,PAO}+S_{NOx})]_x [S_{PO4}/(K_{PO4,PAO,nut}+S_{PO4})]_x [S_{Alk}/(K_{Alk,PAO}+S_{Alk})]_x [(X_{PAO,PHA}/X_{PAO})/(K_{fPHA\_PAO}+(X_{PAO,PHA}/X_{PAO}))]_x X_{PAO}$
	Anoxic Storage of X_{PP}		$q_{PAO,PO4\_PP}{}_x n_{qPAO}{}_x [X_{PAO}/X_{PAO,PP}]_x [K_{O2,PAO}/(K_{O2,PAO}+S_{O2})]_x [S_{NOx}/(n_{KO2}{}_x K_{NOx,PAO}+S_{NOx})]_x [S_{PO4}/(K_{PO4,PAO,nut}+S_{PO4})]_x [X_{PAO,PHA}/(K_{PHA,PAO}+X_{PAO,PHA})]_x [(f_{PP\_PAO,Max}-(X_{PAO,PP}/X_{PAO}))/(K_{I,fPP\_PAO}+(f_{PP\_PAO,Max}-X_{PAO,PP}/X_{PAO}))]_x X_{PAO}$
	Anoxic glycogen formation		$q_{Gly}{}_x n_{qPAO}{}_x [X_{PAO,PHA}/X_{PAO,Gly}]_x [K_{O2,PAO}/(K_{O2,PAO}+S_{O2})]_x [S_{NOx}/(K_{NOx,PAO}+S_{NOx})]_x [X_{PAO,PHA}/(K_{PHA,PAO}+X_{PAO,PHA})]_x [(f_{Gly\_PAO,Max}-(X_{PAO,Gly}/X_{PAO}))/(K_{fGly\_PAO}+(f_{Gly\_PAO,Max}-X_{PAO,Gly}/X_{PAO}))]_x [S_{Alk}/(K_{Alk,PAO}+S_{Alk})]_x X_{PAO}$
	Anoxic maintenance		$m_{PAO,Ax}{}_x [K_{O2,PAO}/(K_{O2,PAO}+S_{O2})]_x [S_{NOx}/(K_{NOx,PAO}+S_{NOx})]_x X_{PAO}$
	Aerobic PHA consumption		$q_{PHA\_PAO}{}_x [S_{O2}/(K_{O2,PAO}+S_{O2})]_x [S_{NHx}/(K_{NHx,PAO}+S_{NHx})]_x [S_{PO4}/(K_{PO4,PAO,nut}+S_{PO4})]_x [S_{Alk}/(K_{Alk,PAO}+S_{Alk})]_x [(X_{PAO,PHA}/X_{PAO})/(K_{fPHA\_PAO}+(X_{PAO,PHA}/X_{PAO}))]_x X_{PAO}$
	Aerobic Storage of X_{PP}		$q_{PAO,PO4\_PP}{}_x [X_{PAO}/X_{PAO,PP}]_x [S_{O2}/(n_{KO2x}K_{O2,PAO}+S_{O2})]_x [S_{PO4}/(K_{PO4,PAO,nut}+S_{PO4})]_x [X_{PAO,PHA}/(K_{PHA,PAO}+X_{PAO,PHA})]_x [(f_{PP\_PAO,Max}-(X_{PAO,PP}/X_{PAO}))/(K_{I,fPP\_PAO}+(f_{PP\_PAO,Max}-X_{PAO,PP}/X_{PAO}))]_x X_{PAO}$
	Aerobic glycogen formation		$q_{Gly}{}_x [X_{PAO,PHA}/X_{PAO,Gly}]_x [S_{O2}/(K_{O2,PAO}+S_{O2})]_x [X_{PAO,PHA}/(K_{PHA,PAO}+X_{PAO,PHA})]_x [(f_{Gly\_PAO,Max}-(X_{PAO,Gly}/X_{PAO}))/(K_{fGly\_PAO}+(f_{Gly\_PAO,Max}-X_{PAO,Gly}/X_{PAO}))]_x X_{PAO}$
	Aerobic maintenance		$m_{PAO,Ox}{}_x [S_{O2}/(K_{O2,PAO}+S_{O2})]_x X_{PAO}$
New General Model	**Aerobic growth of Z_P with N_{H3}**		$\mu_{PAO,Max}{}_x [S_{O2}/(K_{O2,OHO}+S_{O2})]_x [(X_{PAO,Stor}/X_{PAO})/(K_{fStor\_PAO}+(X_{PAO,Stor}/X_{PAO}))]_x [S_{NHx}/(K_{NHx,OHO}+S_{NHx})]_x [S_{PO4}/(K_{PO4,PAO,upt}+S_{PO4})]_x X_{PAO}$
	Aerobic growth of Z_P with N_{O3}		$\mu_{PAO,Max}{}_x [S_{O2}/(K_{O2,OHO}+S_{O2})]_x$

Model	Kinetic Process	Impacted with change of kinetic parameters	P-related kinetic rate equations
			$[(X_{PAO,Stor}/X_{PAO})/(K_{fStor\_PAO}+(X_{PAO,Stor}/X_{PAO}))]$ x $[S_{NOx}/(K_{NOx,OHO}+S_{NOx})]$*$[K_{NHx,OHO}/(K_{NHx,OHO}+S_{NHx})]$ x $[S_{PO4}/(K_{PO4,PAO,upt}+S_{PO4})]$ x X_{PAO}
	Aerobic growth of Z_P with N_{H3} / P_{O4} limited		$\mu_{PAO,Max,Plim}$ x$[S_{O2}/(K_{O2,OHO}+S_{O2})]$ x $[(X_{PAO,Stor}/X_{PAO})/(K_{fStor\_PAO,Plim}+(X_{PAO,Stor}/X_{PAO}))]$ x $[S_{NHx}/(K_{NHx,OHO}+S_{NHx})]$ x $[K_{PO4,PAO,upt}/(K_{PO4,PAO,upt}+S_{PO4})]$ x $[X_{PAO,PP,Lo}/(K_{PP,PAO}+X_{PAO,PP,Lo})]$ x X_{PAO}
	Aerobic growth of Z_P with N_{O3} / P_{O4} limited		$\mu_{PAO,Max,Plim}$ x $[S_{O2}/(K_{O2,OHO}+S_{O2})]$ x $[(X_{PAO,Stor}/X_{PAO})/(K_{fStor\_PAO,Plim}+(X_{PAO,Stor}/X_{PAO}))]$ x $[S_{NOx}/(K_{NOx,OHO}+S_{NOx})]$ x $[K_{NHx,OHO}/(K_{NHx,OHO}+S_{NHx})]$ x $[K_{PO4,PAO,upt}/(K_{PO4,PAO,upt}+S_{PO4})]$ x $[X_{PAO,PP,Lo}/(K_{PP,PAO}+X_{PAO,PP,Lo})]$ x X_{PAO}
	Anoxic growth of Z_P with N_{H3}		$\mu_{PAO,Max}$ x $\eta_{\mu PAO}$x $[K_{O2,OHO}/(K_{O2,OHO}+S_{O2})]$ x $[(X_{PAO,Stor}/X_{PAO})/(K_{fStor\_PAO}+(X_{PAO,Stor}/X_{PAO}))]$ x $[S_{NOx}/(K_{NOx,OHO}+S_{NOx})]$ x $[S_{NHx}/(K_{NHx,OHO}+S_{NHx})]$ x $[S_{PO4}/(K_{PO4,PAO,upt}+S_{PO4})]$ x X_{PAO}
	Aerobic decay of Z_P		m_{PAO} x $[S_{O2}/(K_{O2,OHO}+S_{O2})]$ x X_{PAO}
	$P_{PP\text{-}LO}$ lysis on aerobic decay		m_{PAO} x $[S_{O2}/(K_{O2,OHO}+S_{O2})]$ x $[X_{PAO,PP,Lo}/X_{PAO}]$ x X_{PAO}
	$P_{PP\text{-}HI}$ lysis on aerobic decay		m_{PAO} x $[S_{O2}/(K_{O2,OHO}+S_{O2})]$ x $[X_{PAO,PP,Hi}/X_{PAO}]$ x X_{PAO}
	S_{PHB} lysis on aerobic decay		m_{PAO} x $[S_{O2}/(K_{O2,OHO}+S_{O2})]$ x $[X_{PAO,Stor}/X_{PAO}]$ xX_{PAO}
	Anoxic decay of Z_P		m_{PAO} x $[K_{O2,OHO}/(K_{O2,OHO}+S_{O2})]$*$[S_{NOx}/(K_{NOx,OHO}+S_{NOx})]$ x X_{PAO}
	$P_{PP\text{-}LO}$ lysis on anoxic decay		m_{PAO} x $[K_{O2,OHO}/(K_{O2,OHO}+S_{O2})]$ x $[S_{NOx}/(K_{NOx,OHO}+S_{NOx})]$ x $[X_{PAO,PP,Lo}/X_{PAO}]$ xX_{PAO}
	$P_{PP\text{-}HI}$ lysis on anoxic decay		m_{PAO}x $[K_{O2,OHO}/(K_{O2,OHO}+S_{O2})]$ x $[S_{NOx}/(K_{NOx,OHO}+S_{NOx})]$ x $[X_{PAO,PP,Hi}/X_{PAO}]$ x X_{PAO}
	S_{PHB} lysis on anoxic decay		m_{PAO}x $[K_{O2,OHO}/(K_{O2,OHO}+S_{O2})]$ x $[S_{NOx}/(K_{NOx,OHO}+S_{NOx})]$ x $[X_{PAO,Stor}/X_{PAO}]$ xX_{PAO}
	Anaerobic decay of Z_P		m_{PAO}x $[K_{O2,OHO}/(K_{O2,OHO}+S_{O2})]$ x $[K_{NOx,OHO}/(K_{NOx,OHO}+S_{NOx})]$ xX_{PAO}
	$P_{PP\text{-}LO}$ lysis on anaerobic decay		m_{PAO}*$[K_{O2,OHO}/(K_{O2,OHO}+S_{O2})]$*$[K_{NOx,OHO}/(K_{NOx,OHO}+S_{NOx})]$*$[X_{PAO,PP,Lo}/X_{PAO}]$*$X_{PAO}$
	$P_{PP\text{-}HI}$ lysis on anaerobic decay		m_{PAO}*$[K_{O2,OHO}/(K_{O2,OHO}+S_{O2})]$*$[K_{NOx,OHO}/(K_{NOx,OHO}+S_{NOx})]$*$[X_{PAO,PP,Hi}/X_{PAO}]$*$X_{PAO}$
	S_{PHB} lysis on anaerobic decay		m_{PAO}*$[K_{O2,OHO}/(K_{O2,OHO}+S_{O2})]$*$[K_{NOx,OHO}/(K_{NOx,OHO}+S_{NOx})]$*$[X_{PAO,Stor}/X_{PAO}]$*$X_{PAO}$

Model	Kinetic Process	Impacted with change of kinetic parameters	P-related kinetic rate equations
	Cleavage of poly_P for anaerobic maintenance		$b_{PP\_PO4}*[K_{O2,OHO}/(K_{O2,OHO}+S_{O2})]*[X_{PAO,PP,Lo}/(K_{PP,PAO}+X_{PAO,PP,Lo})]*X_{PAO}$
	Sequestration of S_{CFA} by Z_P		$q_{PAO,VFA\_Stor}*[S_{VFA}/(K_{VFA,PAO}+S_{VFA})]*[X_{PAO,PP,Lo}/(K_{PP,PAO}+X_{PAO,PP,Lo})]*X_{PAO}$

Nomenclature:

Notation	**Description**
S_B	Soluble biodegradable organics
S_{Alk}	Alkalinity (HCO_3^-)
S_{VFA}	Fermentation product (Volatil Fatty Acids)
S_{O2}	Dissolved oxygen
S_{PO4}	Inorganic soluble phosphorus
$X_{PAO,\ stor}$	Stored poly-β-hydroxyalkanoate in PAOs
X_{PAO}	Phosphorus accumulating organisms
$X_{PAO,PP}$	Stored polyphosphates in PAOs
$X_{PAO,\ Gly}$	Stored glycogen in PAOs
S_{NOX}	Nitrate and nitrite (NO3 + NO2) (considered to be NO3 only for stoichiometry)
S_{NHX}	Ammonia (NH_4^+ + NH_3)
q_{PAO,SB_Stor}	Rate constant for S_B uptake rate ($X_{PAO,Stor}$ storage)
$q_{PAO,PO4\_PP}$	Rate constant for storage of $X_{PAO,PP}$
K_{S,fPP_PAO}	Maximum ratio of $X_{PAO,PP}/X_{PAO}$
$f_{PP\_PAO,Max}$	Half-saturation coefficient for $X_{PAO,PP}/X_{PAO}$
K_{I,fPP_PAO}	Half-inhibition coefficient for $X_{PAO,PP}/X_{PAO}$
$\mu_{PAO,Max}$	Maximum growth rate of X_{PAO}
$n_{\mu PAO}$	Reduction factor for anoxic growth of X_{PAO}
K_{fStor_PAO}	Saturation constant for $X_{PAO,Stor}/X_{PAO}$
m_{PAO}	Endogenous respiration rate of X_{PAO}
n_{mPAO}	Reduction factor for anoxic endogenous respiration of X_{PAO}
b_{PP_PO4}	Rate constant for Lysis of $X_{PAO,PP}$
n_{bPP_PO4}	Reduction factor for anoxic lysis of $X_{PAO,PP}$
$m_{PAO,Stor}$	Rate constant for respiration of $X_{PAO,Stor}$
$n_{mPAO,Stor}$	Reduction factor for anoxic respiration of $X_{PAO,Stor}$
$K_{SB,PAO}$	Half-saturation coefficient for S_B
$K_{O2,PAO}$	Half-saturation coefficient for S_{O2}
$K_{NOx,PAO}$	Half-saturation coefficient for S_{NOx}
$K_{NHx,PAO}$	Half-saturation coefficient for S_{NHx}

Notation	**Description**
S_B	Soluble biodegradable organics
S_{Alk}	Alkalinity (HCO_3^-)
S_{VFA}	Fermentation product (Volatil Fatty Acids)
S_{O2}	Dissolved oxygen
S_{PO4}	Inorganic soluble phosphorus
$X_{PAO,\ stor}$	Stored poly-β-hydroxyalkanoate in PAOs
X_{PAO}	Phosphorus accumulating organisms
$X_{PAO,PP}$	Stored polyphosphates in PAOs
$X_{PAO,\ Gly}$	Stored glycogen in PAOs
S_{NOX}	Nitrate and nitrite (NO3 + NO2) (considered to be NO3 only for stoichiometry)
S_{NHX}	Ammonia ($NH_4^+ + NH_3$)
$K_{PO4,PAO,upt}$	Half-saturation coefficient for S_{PO4} uptake ($X_{PAO,PP}$ storage)
$K_{PO4,PAO,nut}$	Half-saturation coefficient for S_{PO4} as nutrient (X_{PAO} growth)
$K_{Alk,PAO}$	Half-saturation coefficient for S_{Alk}
b_{PAO}	Endogenous respiration rate of X_{PAO}
b_{Stor_VFA}	Rate constant for respiration of $X_{PAO,Stor}$
$K_{VFA,PAO}$	Half-saturation coefficient for S_{VFA}
$q_{PAO,VFA\_PHA,An}$	Rate constant for S_{VFA} uptake rate ($X_{PAO,PHA}$ storage) (anaerobic)
$q_{PAO,VFA\_PHA,Ax}$	Rate constant for S_{VFA} uptake rate ($X_{PAO,PHA}$ storage) (anoxic)
n_{KO2}	Reduction factor for K_{O2} for $X_{PAO,PP}$ formation
n_{KNOx}	Reduction factor for K_{NOx} for $X_{PAO,PP}$ formation
q_{Gly}	Rate constant for formation of $X_{PAO,Gly}$
$f_{Gly\_PAO,Max}$	Maximum ratio of $X_{PAO,Gly}/X_{PAO}$
K_{fGly_PAO}	Half-saturation coefficient for $X_{PAO,Gly}/X_{PAO}$
q_{PHA_PAO}	Rate for $X_{PAO,PHA}$ consumption (X_{PAO} growth)
$K_{PHA,PAO}$	Half-saturation coefficient for $X_{PAO,PHA}$
$K_{Gly,PAO}$	Half-saturation coefficient for $X_{PAO,Gly}$
$K_{Alk,PAO}$	Half-saturation coefficient for S_{Alk}
$\mu_{PAO,Max,Plim}$	Maximum growth rate of X_{PAO} (when P is limiting)
$K_{fStor\_PAO,Plim}$	Half-saturation coefficient for $X_{PAO,Stor}/X_{PAO}$ (P limit)
$K_{O2,OHO}$	Half-saturation coefficient for S_{O2}
$K_{NOx,OHO}$	Half-saturation coefficient for S_{NOx}
$K_{NHx,OHO}$	Half-saturation coefficient for S_{NHx}

References

Abegglen, C., Ospelt, M., & Siegrist, H. 2008. Biological nutrient removal in a small-scale MBR treating household wastewater. *Water Research*, *42*(1), 338–346. https://doi.org/10.1016/j.watres.2007.07.020

Al-Atar, E. 2007. *Dynamic modeling and process design of a membrane enhanced biological phosphorus removal process* Ph.D. Dissertation. University of British Columbia, Canada. https://doi.org/10.14288/1.0228857

Bis, M., Montusiewicz, A., Piotrowicz, A., & Łagód, G. 2019. Modeling of Wastewater Treatment Processes in Membrane Bioreactors Compared to Conventional Activated Sludge Systems. *Processes*, *7*(5), 285. https://doi.org/10.3390/pr7050285

Cosenza, A., Mannina, G., Vanrolleghem, P. A., & Neumann, M. B. 2014. Variance-based sensitivity analysis for wastewater treatment plant modelling. *Science of the Total Environment*, *470–471*, 1068–1077. https://doi.org/10.1016/j.scitotenv.2013.10.069

Cosenza A., Bella G. Di, Mannina G., Torregrossa M., & Viviani G.. 2013. Biological Nutrient Removal and Fouling Phenomena in a University of Cape Town Membrane Bioreactor Treating High Nitrogen Loads. *Journal of Environmental Engineering*, *139*(6), 773–780. https://doi.org/10.1061/(ASCE)EE.1943-7870.0000667

Daigger, G. T., Crawford, G. V., & Johnson, B. R. 2010. Full-Scale Assessment of the Nutrient Removal Capabilities of Membrane Bioreactors. *Water Environment Research*, *82*(9), 806–818. JSTOR. https://www.jstor.org/stable/27870381

Ersu, C. B., Ong, S. K., Arslankaya, E., & Lee, Y.-W. 2010. Impact of solids residence time on biological nutrient removal performance of membrane bioreactor. *Water Research*, *44*(10), 3192–3202. https://doi.org/10.1016/j.watres.2010.02.036

Ersu, C., Ong, S. K., Arslankaya, E., & Brown, P. 2008. Comparison of recirculation configurations for biological nutrient removal in a membrane bioreactor. *Water Research*, *42*(6), 1651–1663. https://doi.org/10.1016/j.watres.2007.10.022

Fleischer, E. J., Broderick, T. A., Daigger, G. T., Fonseca, A. D., Holbrook, R. D., & Murthy, S. N. 2005. Evaluation of Membrane Bioreactor Process Capabilities to Meet Stringent Effluent Nutrient Discharge Requirements. *Water Environment Research*, *77*(2), 162–178. https://doi.org/10.2175/106143005X41735

Gholikandi, G. B., & Khosravi, M. 2012. Upgrading of submerged membrane bioreactor operation with regard to soluble microbial products and mathematical modeling for optimisation of critical flux. *Desalination and Water Treatment*, *39*(1–3), 199–208. https://doi.org/10.1080/19443994.2012.669176

Hauduc, H., Rieger, L., Oehmen, A., Loosdrecht, M. C. M. van, Comeau, Y., Héduit, A., Vanrolleghem, P. A., & Gillot, S. 2013. Critical review of activated sludge modeling: State of process knowledge, modeling concepts, and limitations. *Biotechnology and Bioengineering*, *110*(1), 24–46. https://doi.org/10.1002/bit.24624

Jiang, T., Myngheer, S., De Pauw, D. J. W., Spanjers, H., Nopens, I., Kennedy, M. D., Amy, G., & Vanrolleghem, P. A. 2008. Modelling the production and degradation of soluble microbial products (SMP) in membrane bioreactors (MBR). *Water Research*, *42*(20), 4955–4964. https://doi.org/10.1016/j.watres.2008.09.037

Jiang, T., Sin, G., Spanjers, H., Nopens, I., Kennedy, M. D., van der Meer, W., Futselaar, H., Amy, G., & Vanrolleghem, P. A. 2009. Comparison of the modeling approach between membrane bioreactor and conventional activated sludge processes. *Water Environment Research: A Research Publication of the Water Environment Federation*, *81*(4), 432–440. https://doi.org/10.2175/106143008x370377

Liu, W., Hu, Z., Walker, R. L., & Dold, P. L. 2011. Enhanced nutrient removal MBR system with chemical addition for low effluent TP. *Water Science and Technology*, *64*(6), 1298–1306. https://doi.org/10.2166/wst.2011.145

Mannina, G., Cosenza, A., & Ekama, G. A. 2018. A comprehensive integrated membrane bioreactor model for greenhouse gas emissions. *Chemical Engineering Journal*, *334*, 1563–1572. https://doi.org/10.1016/j.cej.2017.11.061

Monclús, H., Sipma, J., Ferrero, G., Rodriguez-Roda, I., & Comas, J. 2010. Biological nutrient removal in an MBR treating municipal wastewater with special focus on biological phosphorus removal. *Bioresource Technology*, *101*(11), 3984–3991. https://doi.org/10.1016/j.biortech.2010.01.038

Nopens, I., Sin, G., Jiang, T., d'Antonio, L., Stama, S., Zhao, J., & Vanrolleghem, P. A. 2007. Model-based optimisation of the biological performance of a sidestream MBR. *Water Science and Technology*, *56*(6), 135–143. https://doi.org/10.2166/wst.2007.640

Sarioglu, M., Sayi-Ucar, N., Cokgor, E., Orhon, D., Van Loosdrecht, M. C. M., & Insel, G. 2017. Dynamic modeling of nutrient removal by a MBR operated at elevated temperatures. *Water Research*, *123*, 420–428.

Verrecht, B., Maere, T., Benedetti, L., Nopens, I., & Judd, S. 2010. Model-based energy optimisation of a small-scale decentralised membrane bioreactor for urban reuse. *Water Research*, *44*(14), 4047–4056. https://doi.org/10.1016/j.watres.2010.05.015

APPENDIX-D

Modeling, simulation and control of biological and chemical P-removal processes for membrane bioreactors (MBRs) from lab to full-scale applications: state of the art

Kashif NADEEM[a], Marion ALLIET[a] Queralt PLANA[b], Jean BERNIER[b], Sam AZIMI[b], Vincent ROCHER[b], Claire ALBASI[a*]

[a] Laboratory of Chemical Engineering, University of Toulouse, CNRS, INPT, UPS, 31000 Toulouse, France

[b] Parisian Sanitation Public Service (SIAAP), Direction Innovation, 92700 Colombes-France

[*] Corresponding author

Table D.1: Comparative Assessment of the commercially available simulation software

Simulation Software/ environment / Model's features	SUMO	BioWin	WEST	GPS-X	SIMBA	AquaSim	EFOR	JASS	ASIM	Lynix	STOAT	DESASS	EnviroProDesigner
A-Model Library													
ASM Family													
ASM1	☑	☑	☑	☑	☑	☑	☑	☑	☑	☑	☑		
ASM2							☑		☑				
ASM2d	☑	☑	☑	☑				☑			☑		
ASM3	☑	☑	☑	☑	☑		☑				☑		
ASM2d_TUDBioP	☑												
ASM3-BioP	☑		☑		☑								
UCTPHO+ (UCT)	☑												
Extended bio-P (PAO-GAO)	☑												
New General Model (Barker and Dold's Model)	☑			☑									
ASM based on BOD Balance											☑		
Dual Nitrification Denitrification e GAO PAO (DND-GP)						☑							
BNRM1												☑	
BNRM2												☑	
Anaerobic Digestion													
General Bio kinetic Model		☑											
ADM1	☑	☑	☑	☑									
Mesophilic Digestion Model											☑		
Settlers/Secondary													
Flux Theory													
Teckas-Reactive	☑	☑		☑									
Teckas Non-Reactive	☑				☑						☑		
Settlers/Primary													
Teckas- Reactive	☑			☑									

Simulation Software/ environment / Model's features	SUMO	BioWin	WEST	GPS-X	SIMBA	AquaSim	EFOR	JASS	ASIM	Lynix	STOAT	DESASS	EnviroProDesigner
Teckas- Non-Reactive	☑	☑											
Otterpohl and Freund					☑								
Lessard and Beck			☑								☑		
Biochemical Process			☑								☑		
MBR Models													
Membrane filtration model (simple)			☑	☑									
Fouling Model			☑	☑									
B-Sub-Models													
EPS/SMP			☑										
Aeration Model	☑		☑	☑	☑								
Chemical Precipitation Model (Equilibrium)		☑											
Chemical Equilibrium with ASM2 Kinetics	☑		☑	☑									
Adsorption models				☑	☑								
Methanol Addition	☑			☑									
GHG	☑			☑	☑								
Odour Model	☑												
pH, alkalinity	☑												
Energy	☑		☑	☑									
Operating Cost	☑		☑	☑									
C-Reactor/Processes /Unit Operations													
Activated Sludge Processes(fixed film and suspended growth)	☑	☑	☑	☑	☑	☑		☑	☑	☑	☑		☑
Membrane Processes/Bioreactor	☑	☑	☑	☑	☑	☑							
Filters (including trickling filters)	☑	☑	☑	☑	☑								
Advanced Oxidation Processes (AOPs)	☑	☑	☑	☑	☑								
Sludge Drying	☑	☑	☑	☑	☑								
Anaerobic Digesters	☑	☑	☑	☑	☑								
Fermentation	☑	☑	☑	☑	☑								
Chlorination/Disinfection	☑	☑	☑	☑	☑								
Flow control devices	☑	☑	☑	☑	☑								
Phase separators	☑	☑	☑	☑	☑								
Process configurations (MLE, UCT, VIP, Phoredox, Bardenpho)	☑	☑	☑	☑	☑								
Flexibility to modify/unlimited	☑	☑	☑	☑	☑								
D-Control System													
Timer Based Controllers	☑	☑	☑	☑	☑				☑		☑		
ON/OFF controller	☑	☑	☑	☑	☑				☑		☑		
Feed Forward-Feedback control	☑		☑	☑	☑								
P-Controller	☑		☑	☑	☑						☑		
PI Controller	☑		☑	☑	☑								
PID controller	☑	☑	☑	☑	☑								

Simulation Software/ environment / Model's features	SUMO	BioWin	WEST	GPS-X	SIMBA	AquaSim	EFOR	JASS	ASIM	Lynix	STOAT	DESASS	EnviroProDesigner
Cascade	☑	☑	☑	☑	☑								
E-Optimisation & Sensitivity analysis													
Parameters Estimation & Calibration			☑	☑	☑	☑							
Sensitivity Analysis			☑	☑		☑							
Scenario Analysis			☑	☑						☑			
Multi-Criteria Optimisation			☑	☑	☑					☑			
F-Other Features													
Graphical User Interface (GUI)	☑	☑	☑	☑	☑		☑	☑		☑			
Model Building													
Simple	☑	☑	☑	☑						☑	☑		
Intermediate Level of Complexity					☑	☑							
Complicated													
Model Editor/Automatic Balance Check	☑			☑					☑				
Peterson Matrix Editor	☑	☑	☑	☑	☑			☑	☑				
Simulations													
Steady State	☑	☑	☑	☑	☑				☑				
Dynamic	☑	☑	☑	☑	☑				☑				
Simulation Speed													
Limited									☑		☑		
Unlimited	☑	☑	☑	☑	☑	☑		☑		☑			
Input data (upload as)													
Excel file	☑	☑	☑		☑								
Text File (.csv /.txt)			☑	☑									
Copy input data to input data module				☑									
Results Analysis and Report Generation													
Word report			☑	☑									
Data Export in Excel/text	☑		☑	☑									
Statistical Analysis of the simulation Results			☑	☑									
Comparison with Measured data				☑									
Flexibility to build Indigenous Model	☑												
Model source code													
Open	☑					☑		☑	☑	☑		☑	☑
Hidden		☑	☑	☑	☑								
Free Access						☑		☑	☑		☑		

APPENDIX-E

Modeling, simulation and control of biological and chemical P-removal processes for membrane bioreactors (MBRs) from lab to full-scale applications: state of the art

Kashif NADEEM[a], Marion ALLIET[a] Queralt PLANA[b], Jean BERNIER[b], Sam AZIMI[b], Vincent ROCHER[b], Claire ALBASI[a*]

[a] Laboratory of Chemical Engineering, University of Toulouse, CNRS, INPT, UPS, 31000 Toulouse, France

[b] Parisian Sanitation Public Service (SIAAP), Direction Innovation, 92700 Colombes-France

* Corresponding author

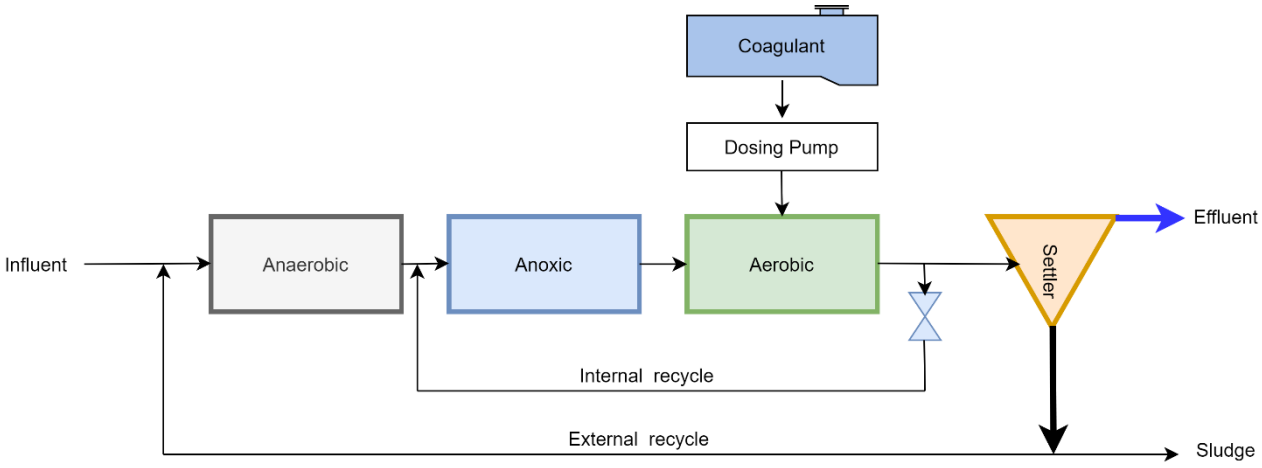

Figure E.1(a): fixed coagulant dosing strategy (adopted and modified from Garikiparthy et al., 2016)

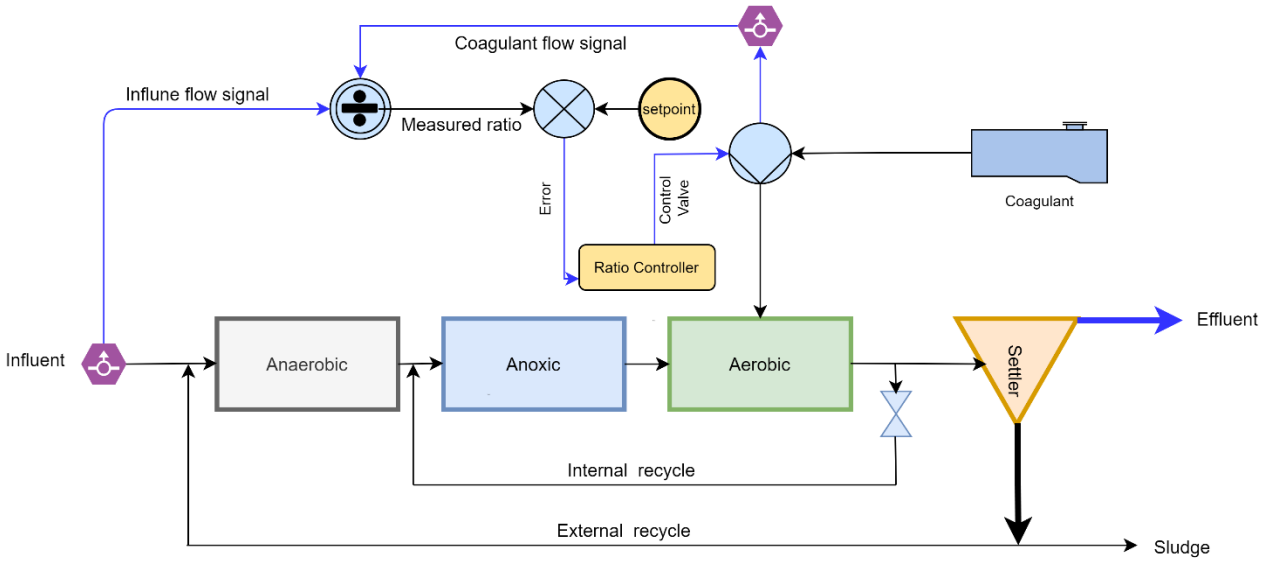

Figure E.1(b): ratio based coagulant dosing controller (adopted and modified from Garikiparthy et al., 2016)

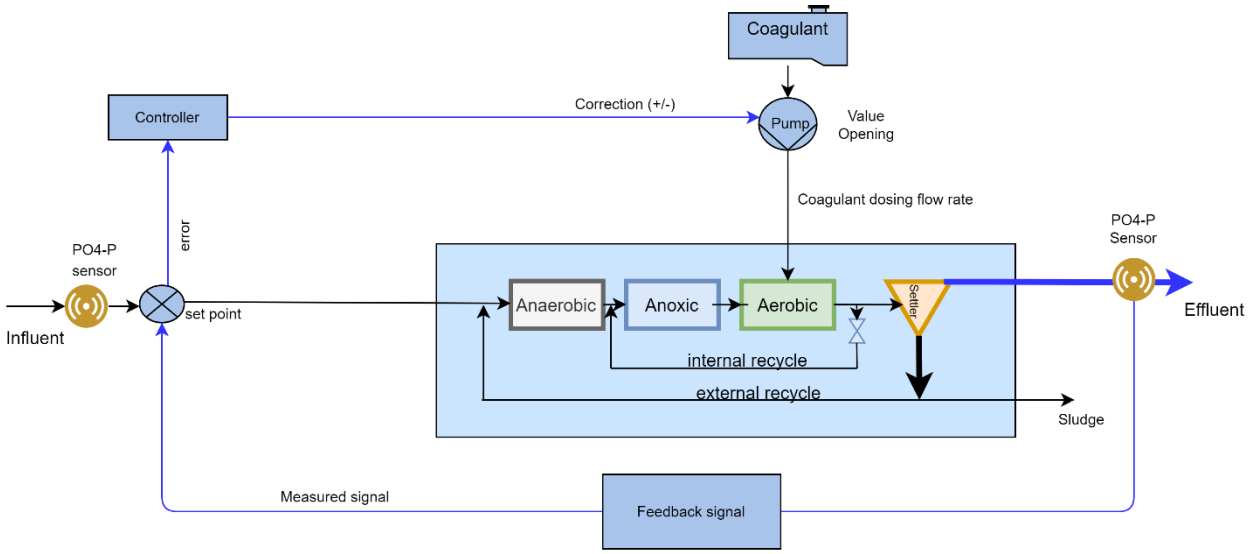

Figure E.1(c): ratio based coagulant dosing controller (adopted and modified from Garikiparthy et al., 2016)

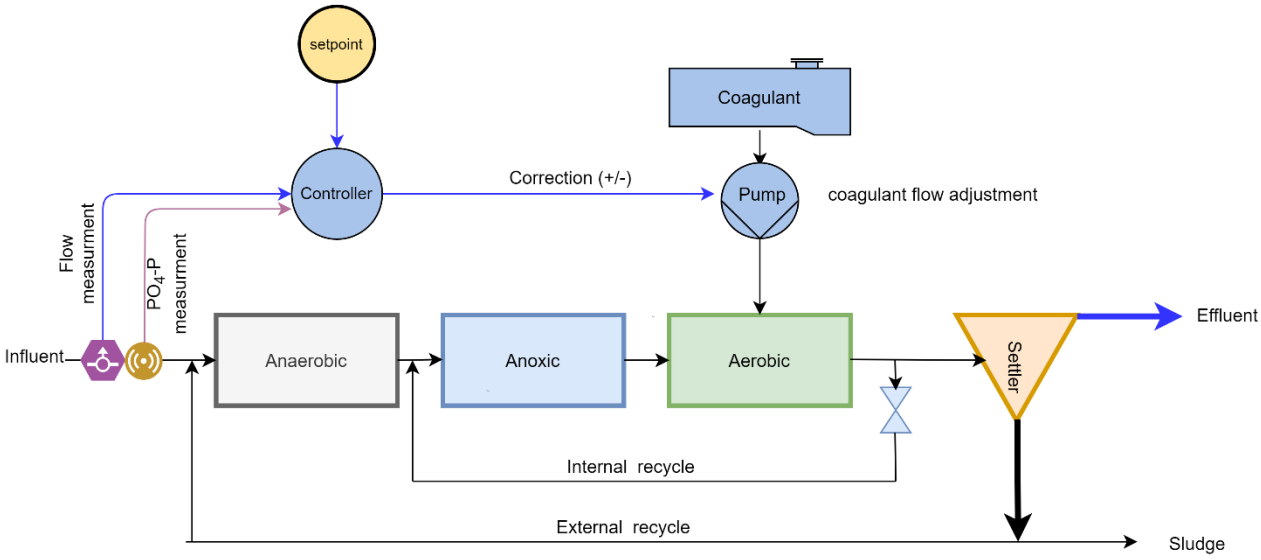

Figure E.1(d): load proportional feedforward PI controller (adopted and modified from Garikiparthy et al., 2016)

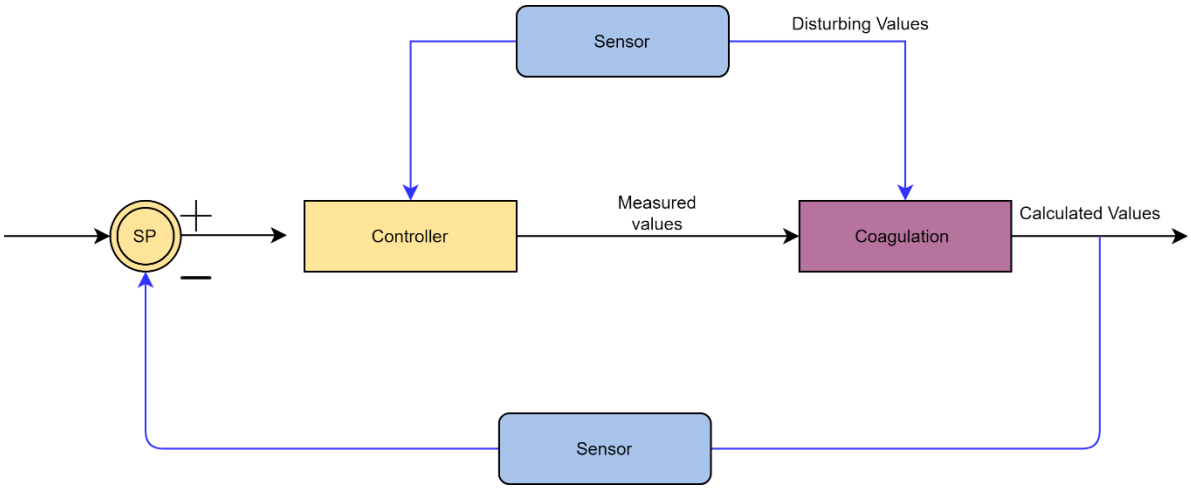

Figure E.2: Control strategy of combining FF and FB (Liu & Ratnaweera, 2016)

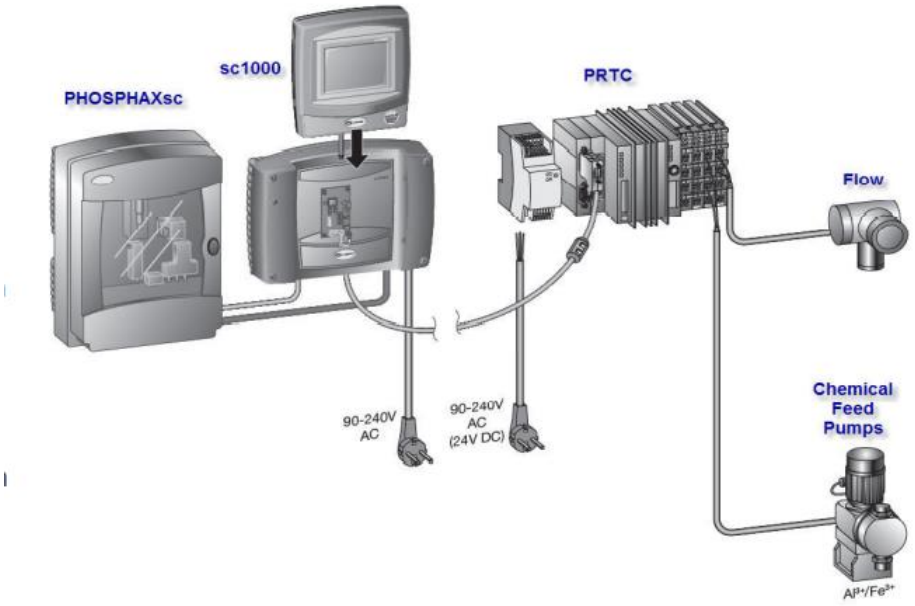

Figure E.3: Load proportional feedforward "off the shelf" automated dosing system by HACH (Craig et al., 2014)

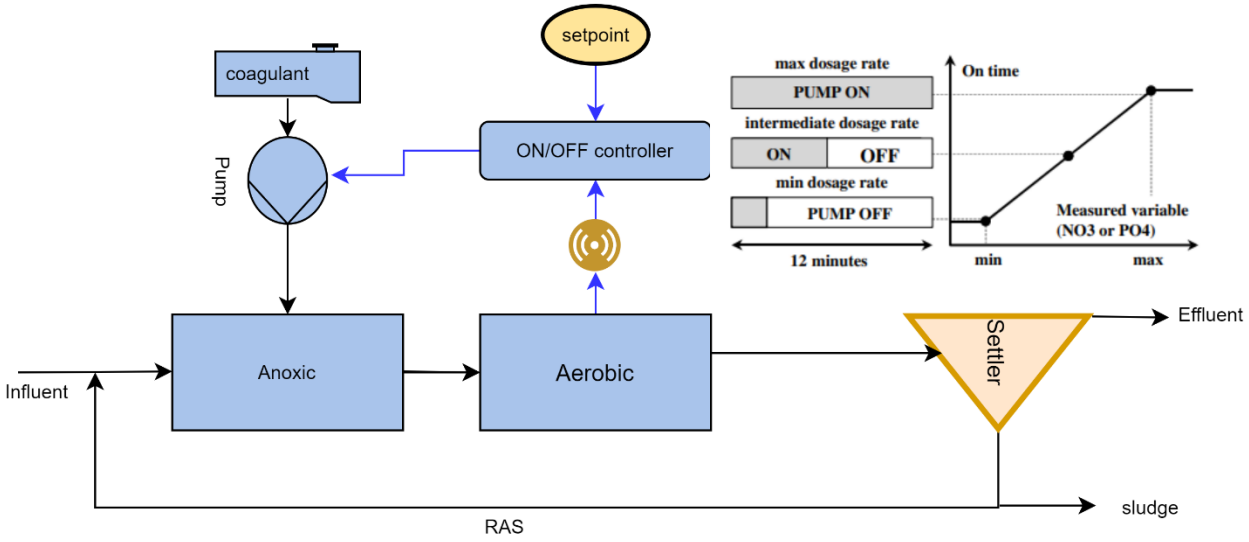

Figure 4: 12 Minute cycle ON-OFF automated dosing system (Devisscher et al., 2002)

References

Craig, K., Minnema, R., Dabkowski, B., Gironi, M.S., 2014. Evaluation of an "Off the Shelf" Automated Chemical Phosphorus Removal System. Procedia Engineering, 12th International Conference on Computing and Control for the Water Industry, CCWI2013 70, 363–368. https://doi.org/10.1016/j.proeng.2014.02.041

Devisscher, M., Bogaert, H., Bixio, D., Van de Velde, J., Thoeye, C., 2002. Feasibility of automatic chemicals dosage control–a full-scale evaluation. Water science and technology 45, 445–452.

Garikiparthy, P.S.N., Lee, S.C., Liu, H., Kolluri, S.S., Esfahani, I.J., Yoo, C.K., 2016. Evaluation of multiloop chemical dosage control strategies for total phosphorus removal of enhanced biological nutrient removal process. Korean J. Chem. Eng. 33, 14–24. https://doi.org/10.1007/s11814-015-0132-9

Liu, W., & Ratnaweera, H. (2016). Improvement of multi-parameter-based feed-forward coagulant dosing control systems with feed-back functionalities. Water Science and Technology, 74(2), 491–499. https://doi.org/10.2166/wst.2016.180

ANNEXURE-B

Full expression of the stoichiometric parameters used in Peterson matrix and their default and calibrated values

Annexure-B

FULL EXPRESSION OF THE STOICHIOMETRIC PARAMETERS USED IN PETERSON MATRIX AND THEIR DEFAULT AND CALIBRATED VALUES

Table -1: Full expression of the stoichiometric parameters used in the Peterson matrix

Para.	Expression	Para.	Expression
a_2	$-(1-Y_{SB\_Stor\_Ox})$	m_5	$Y_{SB\_Stor\_Ax}$
a_3	$-(1-Y_{SUAP\_Stor\_Ox})$	m_6	$Y_{SUAP\_Stor\_Ax}$
a_4	$-(1-Y_{SBAP\_Stor\_Ox})$	m_7	$Y_{SBAP\_Stor\_Ax}$
a_8	$-(1-Y_{SB\_OHO\_Ox}-\gamma_{SB\_SUAP\_Ox})/Y_{SB\_OHO\_Ox}$	m_{11}	$-1/Y_{Stor\_OHO\_Ox}$
a_9	$-(1-Y_{SUAP\_OHO\_Ox})/Y_{SUAP\_OHO\_Ox}$	m_{15}	$-1/Y_{Stor\_OHO\_Ax}$
a_{10}	$-(1-Y_{SBAP\_OHO\_Ox})/Y_{SBAP\_OHO\_Ox}$	n_{16}	$1-\gamma_{ANO\_XEPS\_G\_Ox}$
a_{11}	$-(1-Y_{Stor\_OHO\_Ox}-\gamma_{Stor\_SUAP\_Ox})/Y_{Stor\_OHO\_Ox}$	p_1	$-(1-f_{SU\_XCB\_hyd})*i_{P\_SB}-f_{SU\_XCB\_hyd}*i_{P\_SU}+i_{P\_XCB}$
a_{16}	$-(-i_{COD\_NO3}-Y_{ANO}-\gamma_{SNHx\_SUAP\_Ox})/Y_{ANO}$	p_8 -p_{16}	$-i_{P\_XBio}+i_{P\_XBio}*\gamma_{OHO\_XEPS\_G\_Ox}$
a_{20}	$-(1-f_{XU\_Bio\_lys}-\gamma_{OHO\_SBAP\_Ox}-\gamma_{OHO\_XEPS\_D\_Ox})$	p_{20}-p_{23}	$i_{P\_XBio}-(f\_{XU}*i_{PXU})$
a_{22}	$-(1-f_{XU\_Bio\_lys}-\gamma_{ANO\_SBAP\_Ox}-\gamma_{ANO\_XEPS\_D\_Ox})$	p_{25}	$Y_{PP\_Stor\_PAO}+i_{P\_SB}$
a_{26}	$-Y_{Stor\_PP}$	p_{30}-p_{31}	$-f_{XU\_Bio\_lys}*i_{P\_XU}+i_{P\_XBio}$
a_{28}	$-(1-Y_{PAO\_Ox})/Y_{PAO\_Ox}$	w_{25}	$-Y_{PP\_Stor\_PAO}$
a_{30}	$-(1-f_{XU\_Bio\_lys})$	x_{26}-x_{27}	$-Y_{Stor\_PP}$
c_1	$1-f_{SU\_XCB\_hyd}$	x_{28}	$-1/Y_{PAO\_Ox}$
c_8	$-1/Y_{SB\_OHO\_Ox}$	x_{29}	$-1/Y_{PAO\_Ax}$
c_{12}	$-1/Y_{SB\_OHO\_Ax}$	y_1	$g_1*i_{Charge\_SNHx}+u_1*i_{Charge\_SPO4}$
c_{17}	$f_{SB\_XEPS\_hyd}$	y_2	$i_{N\_SB}*i_{Charge\_SNHx}+i_{P\_SB}*i_{Charge\_SPO4}$
d_8	$\gamma_{SB\_SUAP\_Ox}/Y_{SB\_OHO\_Ox}$	y_3	$i_{N\_SUAP}*i_{Charge\_SNHx}+i_{P\_SB}*i_{Charge\_SPO4}$
d_9	$-1/Y_{SUAP\_OHO\_Ox}$	y_4	$i_{N\_SBAP}*i_{Charge\_SNHx}+i_{P\_SB}*i_{Charge\_SPO4}$
d_{11}	$\gamma_{Stor\_SUAP\_Ox}/Y_{Stor\_OHO\_Ox}$	y_5	$i_{N\_SB}*i_{Charge\_SNHx}+h_5*i_{Charge\_SNOx}+i_{P\_SB}*i_{Charge\_SPO4}$
d_{12}	$\gamma_{SB\_SUAP\_Ax}/Y_{SB\_OHO\_Ax}$	y_6	$i_{N\_SUAP}*i_{Charge\_SNHx}+h_6*i_{Charge\_SNOx}+i_{P\_SB}*i_{Charge\_SPO4}$
d_{13}	$-1/Y_{SUAP\_OHO\_Ax}$	y_7	$i_{N\_SBAP}*i_{Charge\_SNHx}+h_7*i_{Charge\_SNOx}+i_{P\_SB}*i_{Charge\_SPO4}$
d_{15}	$\gamma_{Stor\_SUAP\_Ax}/Y_{Stor\_OHO\_Ax}$	y_8	$g_8*i_{Charge\_SNHx}+u_8*i_{Charge\_SPO4}$
d_{16}	$\gamma_{SNHx\_SUAP\_Ox}/Y_{ANO}$	y_9	$(i_{N\_SUAP}/Y_{SUAP\_OHO\_Ox}-i_{N\_XBio}*(1-\gamma_{OHO\_XEPS\_G\_Ox})-i_{N\_XEPS}*\gamma_{OHO\_XEPS\_G\_Ox})*i_{Charge\_SNHx}+(i_{P\_XBio}+i_{P\_XBio}*\gamma_{OHO\_XEPS\_G\_Ox})*iCharge\_SPO4$
e_{10}	$-1/Y_{SBAP\_OHO\_Ox}$	y_{10}	$((i_{N\_SBAP}/Y_{SBAP\_OHO\_Ox}-i_{N\_XBio}*(1-\gamma_{OHO\_XEPS\_G\_Ox})-i_{N\_XEPS}*\gamma_{OHO\_XEPS\_G\_Ox}))*i_{Charge\_SNHx}+(-i_{P\_XBio}+i_{P\_XBio}*\gamma_{OHO\_XEPS\_G\_Ox})*i_{Charge\_SPO4}$
e_{14}	$-1/Y_{SBAP\_OHO\_Ax}$	y_{11}	$(-i_{N\_XBio}*(1-\gamma_{OHO\_XEPS\_G\_Ox})-i_{N\_XEPS}*\gamma_{OHO\_XEPS\_G\_Ox}-\gamma_{Stor\_SUAP\_Ox}*i_{N\_SUAP}/Y_{Stor\_OHO\_Ox})*i_{Charge\_SNHx}+(-i_{P\_XBio}+i_{P\_XBio}*\gamma_{OHO\_XEPS\_G\_Ox})*i_{Charge\_SPO4}$
e_{17}	$1-f_{SB\_XEPS\_hyd}$	y_{12}	$g_{12}*i_{Charge\_SNHx}+h_{12}*i_{Charge\_SNOx}+u_{12}*i_{Charge\_SPO4}$
e_{20}	$\gamma_{OHO\_SBAP\_Ox}$	y_{13}	$g_{13}*i_{Charge\_SNHx}+h_{13}*i_{Charge\_SNOx}+u_{13}*i_{Charge\_SPO4}$
e_{21}	$\gamma_{OHO\_SBAP\_Ax}$	y_{14}	$g_{14}*i_{Charge\_SNHx}+h_{14}*i_{Charge\_SNOx}+u_{14}*i_{Charge\_SPO4}$
e_{22}	$\gamma_{ANO\_SBAP\_Ox}$	y_{15}	$g_{15}*i_{Charge\_SNHx}+h_{15}*i_{Charge\_SNOx}+u_{15}*i_{Charge\_SPO4}$
e_{23}	$\gamma_{ANO\_SBAP\_Ax}$	y_{16}	$g_{16}*i_{Charge\_SNHx}+h_{16}*i_{Charge\_SNOx}+u_{16}*i_{Charge\_SPO4}$

Para.	Expression	Para.	Expression
f_1	$f_{SU\_XCB\_hyd}$	y_{17}	$g_8*i_{Charge\_SNHx}$
g_1	$i_{N\_XCB}-(1-f_{SU\_XCB\_hyd})*i_{N\_SB}-f_{SU\_XCB\_hyd}*i_{N\_SU}$	y_{19}	$-1/i_{NO3\_N2}*i_{Charge\_SNOx}$
g_8	$i_{N\_SB}/Y_{SB\_OHO\_Ox}-i_{N\_XBio}*(1-\gamma_{OHO\_XEPS\_G\_Ox})-i_{N\_XEPS}*\gamma_{OHO\_XEPS\_G\_Ox}-i_{N\_SUAP}*\gamma_{SB\_SUAP\_Ox}/Y_{SB\_OHO\_Ox}$	y_{20}	$g_{20}*i_{Charge\_SNHx}+u_{22}*i_{Charge\_SPO4}$
g_9	$i_{N\_SUAP}/Y_{SUAP\_OHO\_Ox}-i_{N\_XBio}*(1-\gamma_{OHO\_XEPS\_G\_Ox})-i_{N\_XEPS}*\gamma_{OHO\_XEPS\_G\_Ox}$	y_{21}	$g_{21}*i_{Charge\_SNHx}+h_{21}*i_{Charge\_SNOx}+u_{21}*i_{Charge\_SPO4}$
g_{10}	$(i_{N\_SBAP}/Y_{SBAP\_OHO\_Ox}-i_{N\_XBio}*(1-\gamma_{OHO\_XEPS\_G\_Ox})-i_{N\_XEPS}*\gamma_{OHO\_XEPS\_G\_Ox})$	y_{22}	$g_8*i_{Charge\_SNHx}+u_8*i_{Charge\_SPO4}$
g_{11}	$-i_{N\_XBio}*(1-\gamma_{OHO\_XEPS\_G\_Ox})-i_{N\_XEPS}*\gamma_{OHO\_XEPS\_G\_Ox}-\gamma_{Stor\_SUAP\_Ox}*i_{N\_SUAP}/Y_{Stor\_OHO\_Ox}$	y_{23}	$g_{23}*i_{Charge\_SNHx}+h_{23}*i_{Charge\_SNOx}+u_{23}*i_{Charge\_SPO4}$
g_{12}	$i_{N\_SB}/Y_{SB\_OHO\_Ax}-i_{N\_XBio}*(1-\gamma_{OHO\_XEPS\_G\_Ax})-i_{N\_XEPS}*\gamma_{OHO\_XEPS\_G\_Ax}-i_{N\_SUAP}*\gamma_{SB\_SUAP\_Ax}/Y_{SB\_OHO\_Ax}$	y_{25}	$i_{N\_SB}*i_{Charge\_SNHx}+u_{25}*i_{Charge\_SPO4}+w_{25}*i_{Charge\_XPAO\_PP}$
g_{13}	$i_{N\_SUAP}/Y_{SUAP\_OHO\_Ax}-i_{N\_XBio}*(1-\gamma_{OHO\_XEPS\_G\_Ax})-i_{N\_XEPS}*\gamma_{OHO\_XEPS\_G\_Ax}$	y_{26}	$-1*i_{Charge\_SPO4}+1*i_{Charge\_XPAO\_PP}$
g_{14}	$i_{N\_SBAP}/Y_{SBAP\_OHO\_Ax}-i_{N\_XBio}*(1-\gamma_{OHO\_XEPS\_G\_Ax})-i_{N\_XEPS}*\gamma_{OHO\_XEPS\_G\_Ax}$	y_{27}	$h_{27}*i_{Charge\_SNOx}-i_{Charge\_SPO4}+i_{Charge\_XPAO\_PP}$
g_{15}	$-i_{N\_XBio}*(1-\gamma_{OHO\_XEPS\_G\_Ax})-i_{N\_XEPS}*\gamma_{OHO\_XEPS\_G\_Ax}-\gamma_{Stor\_SUAP\_Ax}*i_{N\_SUAP}/Y_{Stor\_OHO\_Ax}$	y_{28}	$-i_{N\_XBio}*i_{Charge\_SNHx}+(-i_{P\_XBio})*i_{Charge\_SPO4}$
g_{16}	$-1/Y_{ANO}-i_{N\_XBio}*(1-\gamma_{ANO\_XEPS\_G\_Ox})-i_{N\_XEPS}*\gamma_{ANO\_XEPS\_G\_Ox}-i_{N\_SUAP}*\gamma_{SNHx\_SUAP\_Ox}/Y_{ANO}$	y_{29}	$-i_{N\_XBio}*i_{Charge\_SNHx}+h_{29}*i_{Charge\_SNOx}-i_{P\_XBio}*i_{Charge\_SPO4}$
g_{17}	$-(1-f_{SB\_XEPS\_hyd})*i_{N\_SBAP}-f_{SB\_XEPS\_hyd}*i_{N\_SB}+i_{N\_XEPS}$	y_{30}	$g_{30}*i_{Charge\_SNHx}+u_{30}*i_{Charge\_SPO4}$
g_{20}	$i_{N\_XBio}-f_{XU\_Bio\_lys}*i_{N\_XU}-\gamma_{OHO\_SBAP\_Ox}*i_{N\_SBAP}-i_{N\_XEPS}*\gamma_{OHO\_XEPS\_D\_Ox}$	y_{31}	$g_{31}*i_{Charge\_SNHx}+h_{31}*i_{Charge\_SNOx}+u_{31}*i_{Charge\_SPO4}$
g_{21}	$i_{N\_XBio}-f_{XU\_Bio\_lys}*i_{N\_XU}-\gamma_{OHO\_SBAP\_Ax}*i_{N\_SBAP}-i_{N\_XEPS}*\gamma_{OHO\_XEPS\_D\_Ax}$	y_{32}-y_{33}	$i_{Charge\_SPO4}-i_{Charge\_XPAO\_PP}$
g_{22}	$i_{N\_XBio}-f_{XU\_Bio\_lys}*i_{N\_XU}-\gamma_{ANO\_SBAP\_Ox}*i_{N\_SBAP}-i_{N\_XEPS}*\gamma_{ANO\_XEPS\_D\_Ox}$	y_{35}	$h_{35}*i_{Charge\_SNOx}$
g_{23}	$i_{N\_XBio}-f_{XU\_Bio\_lys}*i_{N\_XU}-\gamma_{ANO\_SBAP\_Ax}*i_{N\_SBAP}-i_{N\_XEPS}*\gamma_{ANO\_XEPS\_D\_Ax}$	y_{36}	$-i_{Charge\_SPO4}$
g_{30}	$-f_{XU\_Bio\_lys}*i_{N\_XU}+i_{N\_XBio}$	y_{37}	i_{Charge_SPO4}
g_{31}	$-f_{XU\_Bio\_lys}*i_{N\_XU}+i_{N\_XBio}$	z_1	$-i_{TSS\_XCB}$
h_5	$-(1-Y_{SB\_Stor\_Ax})/i_{NO3\_N2}$	z_2	$Y_{SB\_Stor\_Ox}*i_{TSS\_XOHO\_Stor}$
h_6	$-(1-Y_{SUAP\_Stor\_Ax})/i_{NO3\_N2}$	z_3- z_4	$Y_{SBAP\_Stor\_Ax}*i_{TSS\_XOHO\_Stor}$
h_7	$-(1-Y_{SBAP\_Stor\_Ax})/i_{NO3\_N2}$	z_5	$Y_{SB\_Stor\_Ax}*i_{TSS\_XOHO\_Stor}$
h_{12}	$-(1-Y_{SB\_OHO\_Ax}-\gamma_{SB\_SUAP\_Ax})/(Y_{SB\_OHO\_Ax}*i_{NO3\_N2})$	z_6- z_7	$Y_{SBAP\_Stor\_Ax}*i_{TSS\_XOHO\_Stor}$
h_{13}	$-(1-Y_{SUAP\_OHO\_Ax})/(Y_{SUAP\_OHO\_Ax}*i_{NO3\_N2})$	z_8- z_{10}	$i_{TSS\_XBio}-\gamma_{OHO\_XEPS\_G\_Ox}*i_{TSS\_XBio}+\gamma_{OHO\_XEPS\_G\_Ox}*i_{TSS\_EPS}$
h_{14}	$-(1-Y_{SBAP\_OHO\_Ax})/(Y_{SBAP\_OHO\_Ax}*i_{NO3\_N2})$	z_{11}	$(-1/Y_{Stor\_OHO\_Ox})*(i_{TSS\_XOHO\_Stor})+i_{TSS\_XBio}-\gamma_{OHO\_XEPS\_G\_Ox}*i_{TSS\_XBio}+\gamma_{OHO\_XEPS\_G\_Ox}*i_{TSS\_EPS}$

Para.	Expression	Para.	Expression
h_{15}	$-(1-Y_{Stor\_OHO\_Ax}-\gamma_{Stor\_SUAP\_Ax})/(Y_{Stor\_OHO\_Ax}*i_{NO3\_N2})$	z_{12}	$i_{TSS\_XBio}-\gamma_{OHO\_XEPS\_G\_Ax}*i_{TSS\_XBio}+\gamma_{OHO\_XEPS\_G\_Ax}*i_{TSS\_EPS}$
h_{19}	$-1/i_{NO3\_N2}$	z_{13}	$i_{TSS\_XBio}-\gamma_{OHO\_XEPS\_G\_Ax}*i_{TSS\_XBio}+\gamma_{OHO\_XEPS\_G\_Ax}*i_{TSS\_EPS}$
h_{21}	$-(1-f_{XU\_Bio\_lys}-\gamma_{OHO\_SBAP\_Ax}-\gamma_{OHO\_XEPS\_D\_Ax})/i_{NO3\_N2}$	z_{14}	$i_{TSS\_XBio}-\gamma_{OHO\_XEPS\_G\_Ax}*i_{TSS\_XBio+}\gamma_{OHO\_XEPS\_G\_Ax}*i_{TSS\_EPS}$
h_{22}	$-(1-f_{XU\_Bio\_lys}-\gamma_{ANO\_SBAP\_Ax}-\gamma_{ANO\_XEPS\_D\_Ax})/i_{NO3\_N2}$	z_{15}	$i_{TSS\_XBio}+i_{TSS\_EPS}*\gamma_{OHO\_XEPS\_G\_Ax}-(1/Y_{Stor\_OHO\_Ax})*i_{TSS\_XOHO\_Stor}-\gamma_{OHO\_XEPS\_G\_Ox}*i_{TSS\_XBio}$
h_{27}	$-(Y_{Stor\_PP})/i_{NO3\_N2}$	z_{16}	$i_{TSS\_XBio}-\gamma_{ANO\_XEPS\_G\_Ox}*i_{TSS\_XBio}+\gamma_{ANO\_XEPS\_G\_Ox}*i_{TSS\_EPS}$
h_{29}	$-(1-Y_{PAO\_Ax})/Y_{PAO\_Ax}*1/i_{NO3\_N2}$	z_{17}	$-i_{TSS\_EPS}$
h_{31}	$-(1-f_{XU\_Bio\_lys})/i_{NO3\_N2}$	z_{18}- z_{19}	$-i_{TSS\_XOHO\_Stor}$
h_{35}	$-1/i_{NO3\_N2}$	z_{20}	$(f_{XU\_Bio\_lys}*i_{TSS\_XU})-i_{TSS\_XBio}+(\gamma_{ANO\_XEPS\_D\_Ox}*i_{TSS\_EPS})$
i_{20}-i_{23}	$f_{XU\_Bio\_lys}$	z_{21}	$f_{XU\_Bio\_lys}*i_{TSS\_XU}-i_{TSS\_XBio}+(\gamma_{OHO\_XEPS\_D\_Ax}*i_{TSS\_EPS})$
i_{30}-i_{31}	$f_{XU\_Bio\_lys}$	z_{22}	$(f_{XU\_Bio\_lys}*i_{TSS\_XU})-i_{TSS\_XBio}+(\gamma_{ANO\_XEPS\_D\_Ox}*i_{TSS\_EPS})$
j_8-j_{11}	$\gamma_{OHO\_XEPS\_G\_Ox}$	z_{23}	$-i_{TSS\_XBio}+f_{XU\_Bio\_lys}*i_{TSS\_XU}+\gamma_{ANO\_XEPS\_D\_Ax}*i_{TSS\_EPS}$
j_{12}-j_{15}	$\gamma_{OHO\_XEPS\_G\_Ax}$	z_{25}	$i_{TSS\_XOHO\_Stor}-i_{TSS\_XPAO\_PP}*Y_{PP\_Stor\_PAO}$
j_{16}	$\gamma_{ANO\_XEPS\_G\_Ox}$	z_{26}- z_{27}	$-Y_{Stor\_PP}*i_{TSS\_XOHO\_Stor}+i_{TSS\_XPAO\_PP}$
j_{20}	$\gamma_{OHO\_XEPS\_D\_Ox}$	z_{28}	$-(1/Y_{PAO\_Ox})*i_{TSS\_XOHO\_Stor}+i_{TSS\_XBio}$
j_{21}	$\gamma_{OHO\_XEPS\_D\_Ax}$	z_{29}	$-(1/Y_{PAO\_Ax})*i_{TSS\_XOHO\_Stor}+i_{TSS\_XBio}$
j_{22}	$\gamma_{ANO\_XEPS\_D\_Ox}$	z_{30}- z_{31}	$-i_{TSS\_XBio}+f_{XU\_Bio\_lys}*i_{TSS\_XU}$
j_{23}	$\gamma_{ANO\_XEPS\_D\_Ax}$	z_{32}- z_{33}	$-i_{TSS\_XPAO\_PP}$
k_8-k_{15}	$1-\gamma_{OHO\_XEPS\_G\_Ox}$	z_{34}-z_{35}	$-i_{TSS\_XOHO\_Stor}$
m_2	$Y_{SB\_Stor\_Ox}$		
m_3	$Y_{SBAP\_Stor\_Ox}$		
m_4	$Y_{SUAP\_Stor\_Ox}$		

Table -2: Stoichiometric and kinetic parameters values for biokinetic model

Parameters	Notation	Units	Value at 20 C
Fraction of inert COD generated in hydrolysis	$f_{SU\_XCB,\ hyd}$	-	0.0
Yield for X_{OHO} growth per S_B (Aerobic)	$Y_{SB\_OHO\_OX}$	-	0.681
Yield for X_{OHO} growth per S_B(Anoxic)	$Y_{SB\_OHO\_Ax}$	-	0.59
Yield of X_{OHO_Stor} formation per S_B (Aerobic)	$Y_{SB\_Stor\_OX}$	-	0.85
Yield of X_{OHO_Stor} formation per S_B (Anoxic)	$Y_{SB\_Stor\_Ax}$	-	0.85
Yield of X_{OHO} growth per X_{OHO_Stor} (Aerobic)	$Y_{stor\_OHO\_OX}$	-	0.80
Yield of X_{OHO} growth per $X_{OHO,\ Stor}$ (Anoxic)	$Y_{stor\_OHO\_AX}$	-	0.65
Aerobic yield of X_{OHO_sto} per S_{UAP} (Anoxic)	$Y_{SUAP\_Stor\_Ax}$	-	0.8

Parameters	Notation	Units	Value at 20 C
Aerobic yield of X_{OHO_sto} per S_{UAP} (Aerobic)	$Y_{SUAP\_Stor\_Ox}$	-	0.85
Yield of X_{OHO_Stor} formation per S_{BAP} (Anoxic)	$Y_{SBAP\_Stor\_Ax}$	-	0.8
Yield of X_{OHO_Stor} formation per S_{BAP} (Aerobic)	$Y_{SBAP\_Stor\_ox}$	-	0.8
Yield of X_{OHO} growth per S_{UAP} (Anoxic)	$Y_{SUAP\_OHO\_Ax}$	-	0.8
Yield of X_{OHO} growth per S_{UAP} (Aerobic)	$Y_{SUAP\_OHO\_Ox}$	-	0.67
Yield of X_{OHO} growth per S_{BAP} (Anoxic)	$Y_{SBAP\_OHO\_Ax}$	-	0.59
Yield of X_{OHO} growth per S_{BAP} (Aerobic)	$Y_{SBAP\_OHO\_Ox}$	-	0.67
Yield of X_{ANO} growth per S_{NO3}	Y_{ANO}	g COD.gN^{-1}	0.24
Yield of X_{PAO} growth per X_{PAO_Stor} (Aerobic)	Y_{PAO_Ox}	-	0.6
Yield of X_{PAO} growth per X_{PAO_Stor} (Anoxic)	Y_{PAO_Ax}	-	0.5
Yield for X_{PAO_PP} storage (S_{PO4} uptake) per X_{PAO_Stor} utilized	Y_{Stor_PP}	gP.g COD^{-1}	0.2
Yield for X_{PAO_PP} requirement (S_{PO4} release) per X_{PAO_Stor} stored (S_B utilized)	$Y_{PP\_Stor\_PAO}$	gCOD X_{PO4}.$gCODSB^{-1}$	0.35
UAP formation constant per X_{OHO_Stor} (Anoxic)	$\gamma_{Stor\_SUAP\_Ax}$		0.2
UAP formation constant per $X_{OHO,\ Stor}$ (Aerobic)	$\gamma_{Stor\_SUAP\_Ox}$		0.2
UAP formation constant per S_B (Anoxic)	$\gamma_{SB\_SUAP\_Ax}$		0.3
UAP formation constant per S_B (Aerobic)	$\gamma_{SB\_SUAP\_Ox}$		0.3
EPS formation fraction during X_{OHO} growth decay (Anoxic)	$\gamma_{OHO\_XEPS\_G\_Ax}$		0.12
EPS formation fraction during X_{OHO} growth decay (Aerobic)	$\gamma_{OHO\_XEPS\_G\_Ox}$		0.12
EPS formation fraction during X_{OHO} decay (Anoxic)	$\gamma_{OHO\_XEPS\_D\_Ax}$		0.05
EPS formation fraction during XOHO decay (Aerobic)	$\gamma_{OHO\_XEPS\_D\_Ox}$		0.05
EPS formation fraction during XANO growth decay (Aerobic)	$\gamma_{ANO\_XEPS\_G\_Ox}$		0.12
EPS formation fraction during XANO decay (Anoxic)	$\gamma_{ANO\_XEPS\_D\_Ax}$		0.05
EPS formation fraction during X_{ANO} decay (Aerobic)	$\gamma_{ANO\_XEPS\_D\_Ax}$		0.05
BAP formation constant per X_{OHO} (Anoxic)	$\gamma_{OHO\_SBAP\_Ax}$		0.15
UAP formation constant per S_{NHx} (Aerobic)	$\gamma_{SNHx\_SUAP\_Ox}$		0.1
BAP formation constant per X_{OHO} (Aerobic)	$\gamma_{OHO\_SBAP\_Ox}$		0.1
BAP formation constant per X_{ANO}(Anoxic)	$\gamma_{ANO\_SBAP\_Ax}$		0.1
Fraction of X_U generated in heterotrophic biomass decay	$f_{XU\_Bio\_lys}$		0.2
Fraction of S_U generated in X_{PAO} decay	$f_{SU\_PAO\_lys}$		0

Parameters	Notation	Units	Value at 20 C
Fraction of S_B generated in hydrolysis	$f_{SB\_XEPS\_hyd}$		0.4
Fraction of X_{EPS} stored during X_{OHO} growth	f_{EPS_Stor}	gCOD .gCOD^{-1}	0.2
N content of S_B	i_{N_SB}	g N.g COD^{-1}	0.03
N content of S_U	i_{N_SU}	g N.g COD^{-1}	0.01
N content of X_U	i_{N_XU}	g N.g COD^{-1}	0.03
N content of X_B	i_{N_XCB}	g N.g COD^{-1}	0.035
N content of biomass (X_{OHO}, X_{PAO}, X_{ANO})	i_{N_XBio}	g N.g COD^{-1}	0.07
N content of S_{UAP}	i_{N_SUAP}	g N.g COD^{-1}	0.03
N content of S_{BAP}	i_{N_SBAP}	g N.g COD^{-1}	0.02
N content of X_{EPS}	i_{N_XEPS}	g N.g COD^{-1}	0.07
P content of S_B	i_{P_SB}	g P.g COD^{-1}	0
P content of S_U	i_{P_SU}	g P.g COD^{-1}	0
P content of X_U	i_{P_XU}	g P.g COD^{-1}	0.01
P content of X_B	i_{P_XCB}	g P.g COD^{-1}	0.005
P content of biomass (X_{OHO}, X_{PAO}, X_{ANO})	i_{P_XBio}	g P.g COD^{-1}	0.014
Conversion factor X_U in TSS	i_{TSS_XU}	g TSS.g COD^{-1}	0.75
Conversion factor X_B in TSS	i_{TSS_XCB}	g TSS.g COD^{-1}	0.75
Conversion factor X_{OHO_Stor} in TSS	$i_{TSS\_XOHO\_Stor}$	g TSS.g COD^{-1}	0.60
Conversion factor biomass in TSS	i_{TSS_XBio}	g TSS.g COD^{-1}	0.90
Conversion factor X_{PAO_PP} in TSS	$i_{TSS\_XPAO\_PP}$	g TSS.g COD^{-1}	3.23
TSS to COD ratio for X_{EPS}	i_{TSS_EPS}	g TSS.g COD^{-1}	0.66
Conversion factor for NO_3 reduction to N_2	i_{NO3_N2}	g COD.g N^{-1}	2.86
Conversion factor for NO_3 in COD	i_{COD_NO3}	g COD.g N^{-1}	-4.57
Conversion factor for N_2 in COD	i_{COD_N2}	g COD.g N^{-1}	-1.71
Conversion factor for SN_{Hx} in charge	i_{Charge_SNHx}	Charge.g N^{-1}	0.07
Conversion factor for NO_3 in charge	i_{Charge_SNOx}	Charge.g N^{-1}	-0.07
Conversion factor for X_{PAO_PP} $(K_{0.33}Mg_{0.33}PO_3)_n$ in charge	$i_{Charge\_XPAO\_PP}$	Charge.g P^{-1}	-0.03
Conversion factor for PO_4 in charge	i_{Charge_SPO4}	Charge.g P^{-1}	-0.05
Maximum specific hydrolysis rate	$q_{XCB\_SB\_hyd}$	d^{-1}	3
Half-saturation coefficient for X_{CB}/X_{OHO}	K_{XCB_hyd}	-	1
Biomass affinity constant for S_{BAP}	K_{SBAP_OHO}	gCOD m^{-3}	85
Biomass affinity constant for S_{UAP}	K_{SUAP_OHO}	gCOD m^{-3}	100

Parameters	Notation	Units	Value at 20 C
Rate constant for X_{OHO_stor} storage	q_{SB_Stor}	d^{-1}	5
Hydrolysis rate for S_{UAP}	q_{SUAP_stor}	d^{-1}	1.53
Hydrolysis rate for S_{BAP}	q_{SBAP_stor}	d^{-1}	0.057
Max. growth rate of X_{OHO} based on S_{SMP}	$u_{OHO\_SMP\_max}$	d^{-1}	1
Maximum growth rate of X_{OHO}	u_{OHO_Max}	d^{-1}	2
Reduction factor for anoxic growth of X_{OHO}	n_{uOHO_Ax}	----	0.6
Half-saturation coefficient for S_B	K_{SB_OHO}	g COD m^{-3}	10
Half-saturation coefficient for X_{OHO_Stor}/X_{OHO}	K_{Stor_OHO}	-	0.1
Endogenous respiration rate of X_{OHO}	m_{OHO_ox}	d^{-1}	0.2
Reduction factor for Anoxic endogenous respiration of X_{OHO}	m_{OHO_Ax}	-	0.1
Endogenous respiration rate of X_{OHO_Stor} (Anoxic)	m_{Stor_Ax}	d^{-1}	0.2
Endogenous respiration rate of X_{OHO_Stor} (Aerobic)	m_{Stor_Ox}	d^{-1}	0.1
Half-saturation coefficient for S_{O2}	K_{O2_OHO}	g $S_{O2}.m^{-3}$	0.2
Half-saturation coefficient for S_{NOx}	K_{NOx_OHO}	g Nm^{-3}	0.5
Half-saturation coefficient for S_{NHx}	K_{NHx_OHO}	g $N.m^{-3}$	0.01
Half-saturation coefficient for S_{PO4}	K_{PO4_OHO}	g $P.m^{-3}$	0.01
Half-saturation coefficient for S_{Alk}	K_{Alk_OHO}	mol $HCO_3^-.m^{-3}$	0.1
Rate constant for Sa_c uptake rate (X_{PAO_Stor} storage)	$q_{PAO\_SB\_Stor}$	d^{-1}	6
Rate constant for storage of X_{PAO_PP}	$q_{PAO\_PO4\_PP}$	g PX_{PP}.g $CODX_{PAO}^{-1}.d^{-1}$	1.5
Maximum ratio of X_{PAO_PP}/X_{PAO}	$K_{S\_fPP\_PAO}$	g PX_{PP}.g $CODX_{PAO}^{-1}$	0.05
Half-saturation coefficient for X_{PAO_PP}/X_{PAO}	$f_{PP\_PAO\_Max}$	g PX_{PP}.g $CODX_{PAO}^{-1}$	0.2
Half-inhibition coefficient for X_{PAO_PP}/X_{PAO}	$K_{I,\ fPP\_PAO}$	g PX_{PP}.g $CODX_{PAO}^{-1}$	0.05
Maximum growth rate of X_{PAO}	u_{PAO_Max}	d^{-1}	1
Reduction factor for anoxic growth of X_{PAO}	n_{uPAO}	-	0.6
Fraction of substrate used for storage	f_{sto}	d^{-1}	0.67
Saturation constant for X_{PAO_Stor}/X_{PAO}	K_{fStor_PAO}	-	0.1
Endogenous respiration rate of X_{PAO}	m_{PAO}	d^{-1}	0.2
Reduction factor for anoxic endogenous respiration of X_{PAO}	n_{mPAO}	-	0.33
Rate constant for Lysis of X_{PAO_PP}	b_{PP_PO4}	d^{-1}	0.2
Reduction factor for anoxic lysis of X_{PAO_PP}	n_{bPP_PO4}	-	0.33
Rate constant for respiration of X_{PAO_Stor}	m_{PAO_Stor}	d^{-1}	0.2

Parameters	Notation	Units	Value at 20 C
Reduction factor for anoxic respiration of X_{PAO_Stor}	n_{mPAO_Stor}	-	0.33
Half-saturation coefficient for S_B	K_{SB_PAO}	g COD.m^{-3}	10
Half-saturation coefficient for S_{O2}	K_{O2_PAO}	g S_{O2}.m^{-3}	0.2
Half-saturation coefficient for S_{NOx}	K_{NOx_PAO}	g N.m^{-3}	0.5
Half-saturation coefficient for S_{NHx}	K_{NHx_PAO}	g N.m^{-3}	0.05
Half-saturation coefficient for S_{PO4} uptake (X_{PAO_PP} storage)	$K_{PO4\_PAO\_upt}$	gP.m^{-3}	0.2
Half-saturation coefficient for S_{PO4} as nutrient (X_{PAO} growth)	$K_{PO4\_PAO\_nut}$	g P.m^{-3}	0.01
Half-saturation coefficient for S_{Alk}	K_{Alk_PAO}	mol HCO_3^-.m^{-3}	0.1
Maximum growth rate of X_{ANO}	u_{ANO_Max}	d^{-1}	1
Decay rate for X_{ANO} (Aerobic)	m_{ANO_ox}	d^{-1}	0.15
Decay rate for X_{ANO} (Anoxic)	m_{ANO_Ax}	d^{-1}	0.05
Half-saturation coefficient for S_{O2}	K_{O2_ANO}	g S_{O2}.m^{-3}	0.5
Half-saturation coefficient for S_{NHx}	K_{NH_ANO}	g N.m^{-3}	1
Half-saturation coefficient for S_{PO4}	K_{PO4_ANO}	g P.m^{-3}	0.01
Half-saturation coefficient for S_{Alk}	K_{Alk_ANO}	mol HCO_3^-.m^{-3}	0.5
Rate constant for P precipitation	q_{P_pre}	m^3.g $Fe(OH)_3^{-1}$.d^{-1}	1
Rate constant for redissolution	q_{P_red}	d^{-1}	0.6
Half-saturation coefficient for alkalinity	K_{alk_pre}	mol $HCO3^-$.m^{-3}	0.5
X_{MeOH} requirement per S_{PO4} utilized	$f_{MeOH\_PO4\_MW}$	g $TSSX_{MeOH}$. g P^{-1}	-3.45
X_{MeP} formation per S_{PO4} utilized	$f_{MeP\_PO4\_MW}$	g X_{MeP}. g P^{-1}	4.86
Conversion factor for X_{MeP} ($FePO_4$) in P	i_{P_XMeP}	g P.g $TSSX_{MeP}^{-1}$	0.206

ANNEXURE-C

LSTM Models Structure

ANNEXURE-C

Table C.1: Structural details of LSTM used for prediction of effluent quality

Layer (type)	Output Shape	Param #
Input	(None, 10, 400)	377600
Bidirectional (Layer-1)	(None, 10, 200)	400800
Bidirectional (Layer-2)	(None, 100)	100400
Dense	(None, 3)	303
Activation	(None, 3)	0

Total parameters: 879,103
Trainable parameters: 879,103
Non-trainable parameters: 0

Note: (Dimension, batch size, number of neuron units), with return sequence at each time, is set to false. The default is 3D, and "None" means 2 dimensions.

Table C.2: LSTM structure used for TMP prediction

Layer (type)	Output Shape	Param #
Input	(None, 10, 400)	342400
Bidirectional (Layer-1)	(None, 10, 200)	400800
Bidirectional (Layer-2)	(None, 100)	100400
Dense	(None, 1)	101
Activation	(None, 1)	0

Total parameters: 845,301
Trainable parameters: 845,301
Non-trainable parameters: 0

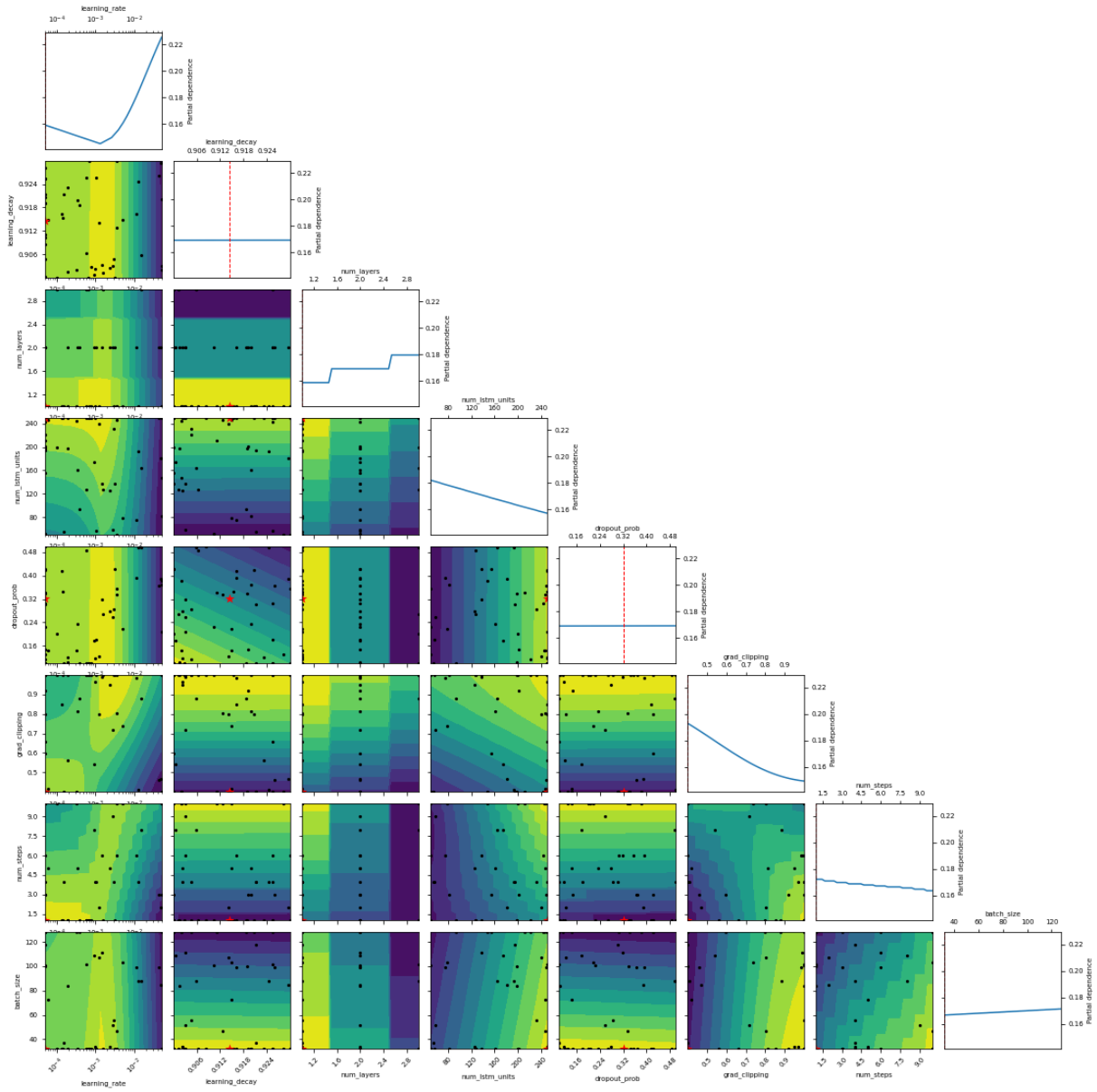

Figure C.1: Hyper parameter Optimisation of LSTM model for effluent quality prediction

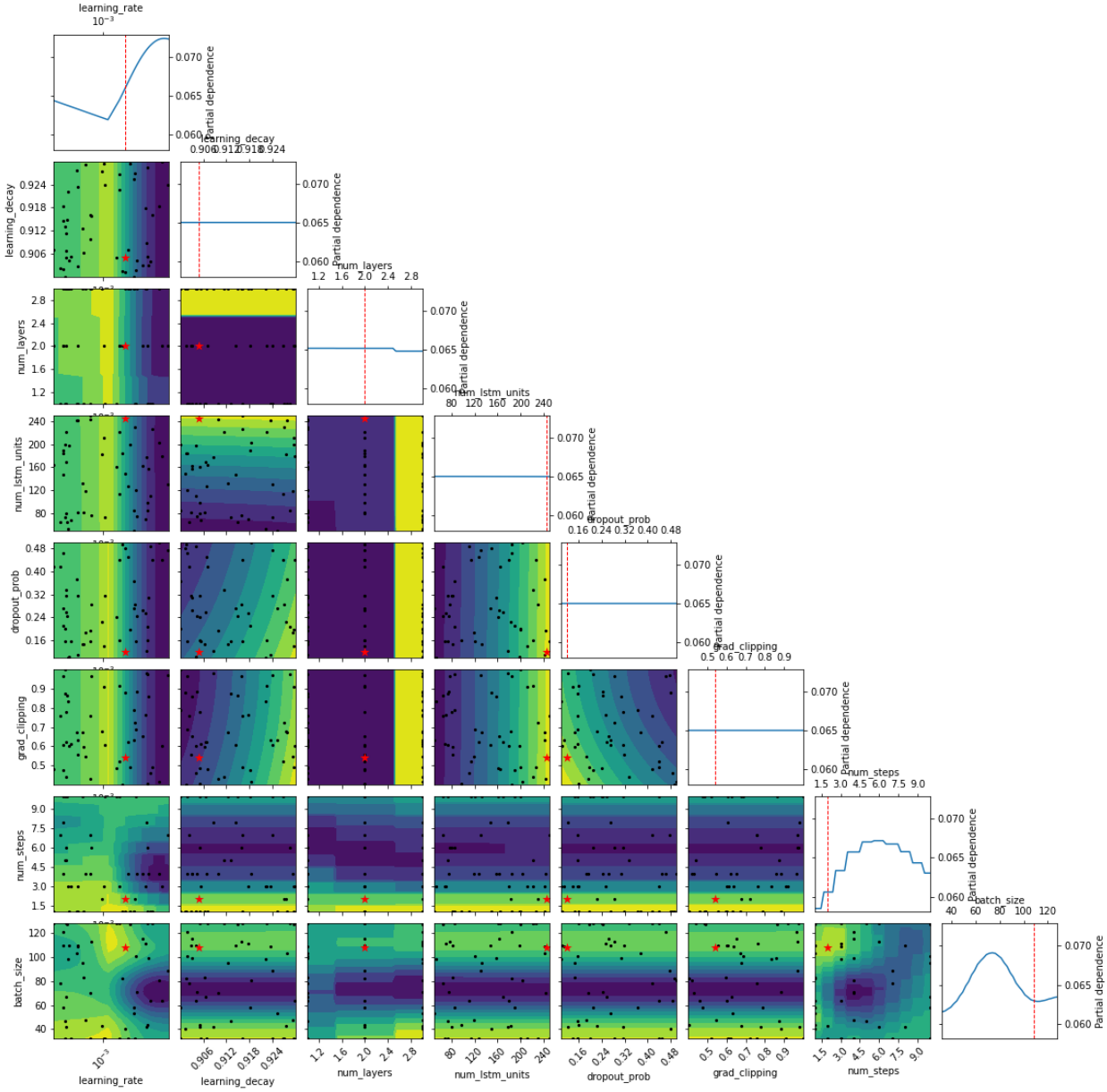

Figure C.2: Hyper parameter Optimisation of LSTM model for effluent TMP prediction